Proceedings of
The Third International Symposium on

GROUND FREEZING

ISGF 82

DTIC
ELECTE
SEP 3 1982

A

82 09 03 058

Proceedings of
The Third International
Symposium on
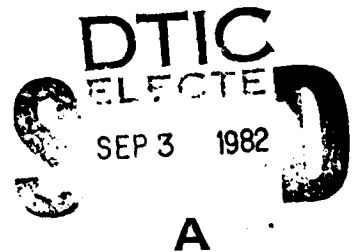# GROUND FREEZING

22-24 June 1982
U.S. Army Corps of Engineers
Cold Regions Research and Engineering Laboratory
Hanover, New Hampshire, U.S.A.

ISGF '82

Special Report 82-16

DTIC
ELECTE
SEP 3 1982

A

PREFACE

Artificial freezing of ground has been used increasingly in the last few decades to stabilize earth materials and to control ground water seepage in geotechnical construction projects. During this period of time there have been many significant advances in ground freezing technology. As a result, artificial ground freezing is becoming more and more attractive as a construction technique.

As application of the ground freezing technique has become more widespread, the need for more accuracy in predicting the effects of freezing on soil properties has grown. Accuracy in predicting refrigeration requirements and placing freezing pipes has also assumed great importance.

Two international symposia have been held to bring ground freezing specialists from all over the world together for discussions on these subjects. The First International Symposium on Ground Freezing, held in March 1978 in Bochum, West Germany, was hosted by the Ruhr University Bochum under the direction of Professor Hans L. Jessberger. This meeting was such a success that it was followed by a second symposium in June 1980 in Trondheim, Norway. At the close of the second symposium, it was decided to continue this type of meeting on a regular basis; a third symposium, to be held in the United States in two years, was planned.

The Third International Symposium on Ground Freezing is being held 22-24 June 1982 at the United States Army Corps of Engineers Cold Regions Research and Engineering Laboratory in Hanover, New Hampshire. At the past two symposia on ground freezing, many excellent theoretical, experimental and case history studies were reported, and several advances in the state of the art were made. However, it is felt that a significant gap between theory and practice still exists. Therefore, the theme of this symposium is to emphasize the relation between theory, design and application in artificial ground freezing. Attendees are particularly encouraged to describe difficulties encountered during construction, and to point to areas where further research is needed to advance the state of the art.

This symposium is divided into four main sessions:

Session I	Mechanical Properties and Processes
Session II	Thermal Properties, Processes and Analysis
Session III	Frost Action
Session IV	Engineering Design and Case Histories

This preprint volume contains the papers accepted for presentation at the Symposium. More than 70 papers are included, representing contributions from 12 countries (Canada, Federal Republic of Germany, Finland, France, Italy, Japan, Norway, People's Republic of China, Sweden, United Kingdom, U.S.A. and U.S.S.R.). Editing of the manuscripts has been kept to a minimum, to preserve the integrity of the contribution of each author. The few papers that were not submitted prior to press time are represented only by their abstracts. These papers are being distributed at the Symposium.

The National Administrative Organizing Committee and the International Organizing committee for the Third International Symposium on Ground Freezing wish to express their appreciation to the U.S. Army Cold Regions Research and Engineering Laboratory in Hanover, New Hampshire, the U.S. Army Research Office in Durham, North Carolina, and the State of Alaska Department of Transportation and Public Facilities for sponsoring and supporting this meeting. The staff support provided by CRREL during all stages of the planning has been particularly valuable. In addition, the State of Alaska Department of Transportation staff has provided valuable assistance in organizing the Alaskan field trip that will follow the Symposium.

The committee chairmen gratefully acknowledge the efforts and cooperation of the members of the committees. Dr. Dean Freitag and Mr. Henry Springer, both of whom have made recent career changes that have resulted in their withdrawing from active participation, should be recognized for their efforts in getting this Symposium under way. Finally, the Organizing Committee wishes to acknowledge the authors of the papers and the staff of the Technical Information Branch at CRREL for their diligence in putting this volume together. The cooperation of so many people has resulted in a very impressive document on the practice of artificial ground freezing.

The National Organizing Committee hopes that this Symposium will provide for a fruitful exchange of ideas and information.

Edwin J. Chamberlain
Francis H. Sayles
Co-Chairmen, ISGF '82

ii

iii

Secretariat

B.S. Yamashita
Public Affairs Officer
USACRREL
Hanover, New Hampshire

D.B. Langlois
Public Affairs Specialist
USACRREL
Hanover, New Hampshire

Technical Editor
Edwin J. Chamberlain
Research Civil Engineer
USACRREL
Hanover, New Hampshire

Proceedings Editor
Donna R. Murphy
Production Editor
USACRREL
Hanover, New Hampshire

CONTENTS:

SESSION I. MECHANICAL PROPERTIES AND PROCESSES

SESSION II. THERMAL PROPERTIES, PROCESSES AND ANALYSIS

B. Thermal Analysis

SESSION III. FROST ACTION

A. Modeling, Mechanism of Heaving

B. Frost Susceptibility Tests and Heave Pressures

C. Movements Due to Frost Action

SESSION IV. ENGINEERING DESIGN AND CASE HISTORIES

Session I
MECHANICAL PROPERTIES AND PROCESSES

Strength, stress–strain
behavior, long-term strength
and creep, change in properties
by freezing and thawing, and
physical properties

SALT CONCENTRATION EFFECTS
ON STRENGTH OF FROZEN SOILS

Nobuhide OGATA
Masayuki YASUDA
Tetsuyuki KATAOKA
(Civil Engineering Laboratory, Central Research Institute of Electric Power Industry, Japan)

Abstract

The influence of salt concentrations on strength of frozen soils is discussed from the experimental point of view. In recent years, a considerable interest has been developed in underground or inground storage of cryogenic liquids. If an LNG storage tank is constructed in the ground with no heating equipment around the tank, the ground will be frozen with the lapse of years. To examine the safety of an LNG inground storage tank, it is required to estimate the phenomenon of frost heave involved in such freezing of ground and the frozen earth pressure acting on the wall of the tank. In this study, the mechanical properties of frozen soils are experimentally obtained. They are required for analyzing the above problems by the finite element method. Since LNG inground storage tanks are often constructed along the coast, tests were made on the frozen soils containing salt, to report the results here.

Introduction

Liquefied natural gas (LNG) is stored by various methods, and recently in Japan, in addition to aboveground LNG storage tanks, inground storage tanks are being constructed increasingly for the reasons of disaster prevention and scenery. In Japan, most LNG storage tanks are constructed in the soft ground reclaimed on the foreshore. In case of inground storage tanks, containers made of concrete are constructed inground to secure sufficient safety against earthquakes.

Meanwhile, if LNG is stored in an inground storage tank with no heating equipment, the ground around the tank becomes frozen in long years, even though the tank is internally provided with a thermal insulator. An analyzed temperature

distribution in the ground around a 60,000 kℓ LNG inground storage tank now constructed in Japan is shown in Fig. 1 as an example
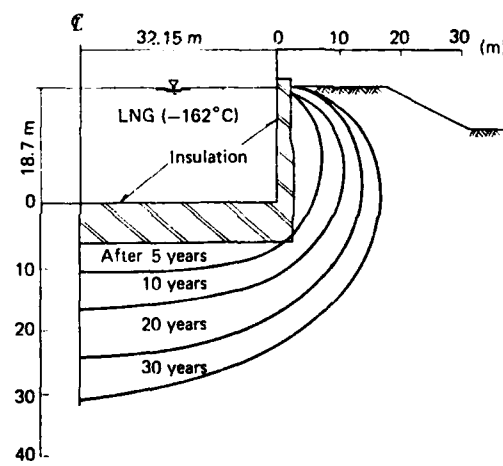
Fig. 1 Growth of the frozen zone around a LNG tank

As can be seen from Fig. 1, 30 years later, the range of frozen ground covers about 25 m directly below the bottom plate of the tank, and maximum about 14 m in the direction of the side wall. If the ground around a tank is frozen widely like this, it is feared that a large frozen earth pressure may act on the tank body, to lower the safety of the tank, that the frost heave caused by frozen soil may raise the inground storage tank, making it unstable, and furthermore that locally uneven frost heave may be caused by uneven frost heave susceptibility of the ground, to raise the tank unequally.

This report describes the results obtained by experimentally examining the mechanical properties of frozen soil, which are required when the

3

change of frozen earth pressure acting on a tank with the lapse of time is analyzed by the finite element method. In particular, it describes the influence of salt concentration on the strength and creep characteristics of frozen soil, since LNG inground storage tanks are very often constructed along the coast. As described in this paper, the influence of salt concentration on the strength and creep characteristics of frozen soil is very large. The salt concentrations actually measured in the ground near the coast are shown in Fig. 2 as an example.
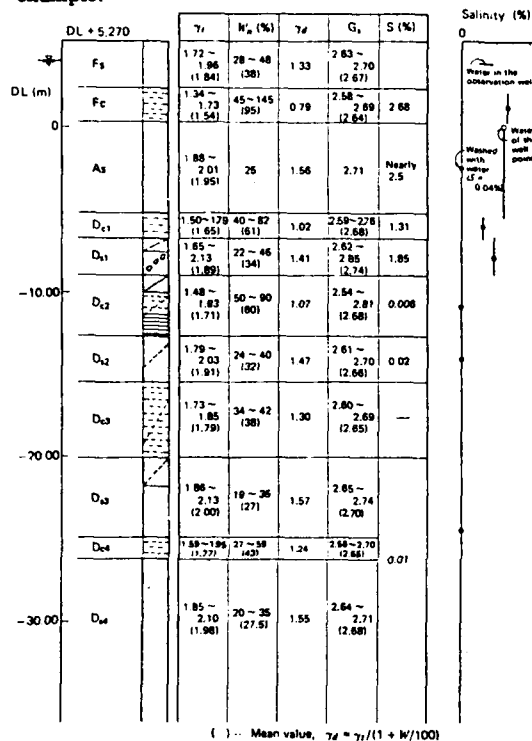
Fig. 2   Soil profile and salinity distribution at the site

Materials and Method

Materials

The materials used in this study were four kinds of sand and three kinds of cohesive soil. Of them, alluvial sand, clayey silt and clay were sampled from the construction site of LNG inground storage tanks. Toyoura sand is widely used as standard sand in Japan. The other materials were purchased in the market. The grain size distribution curves of the materials used for the tests are shown in Fig. 3.

Preparation and Freezing of Specimens

For sand specimens, sand was sufficiently dipped in any of saline solutions respectively prepared by adding sodium chloride to distilled water at predetermined ratios, and was put in 5 cm diameter and 10 cm high steel molds, being tamped, and refrigerated by a refrigerator of –20°C, to make frozen samples.

For cohesive soil specimens, the respective air-dried materials were loosened, and any of saline solutions with predetermined salt concentrations was added to them, making them contain water by not less than the liquid limit. The slurry materials thus made were put in 15 cm inside diameter and 25 cm high cylindrical containers, and consolidated under a pressure load of 0.049 MPa. After consolidation for 2 weeks, the samples were taken out of the cylindrical containers, and cut into 5 cm diameter and 10 cm high cylinders, being put in steel molds and made into frozen samples by a refrigerator of –20°C.

The properties of specimens made like this are collectively shown in Table 1.

Fig. 4 shows distributions of salt concentrations in the specimens prepared as above, taking sand for example. As can be seen from Fig. 4, salt concentrations in specimens cannot be said to be even. Salt concentrations mentioned in this paper refer to the salt concentrations of saline solutions
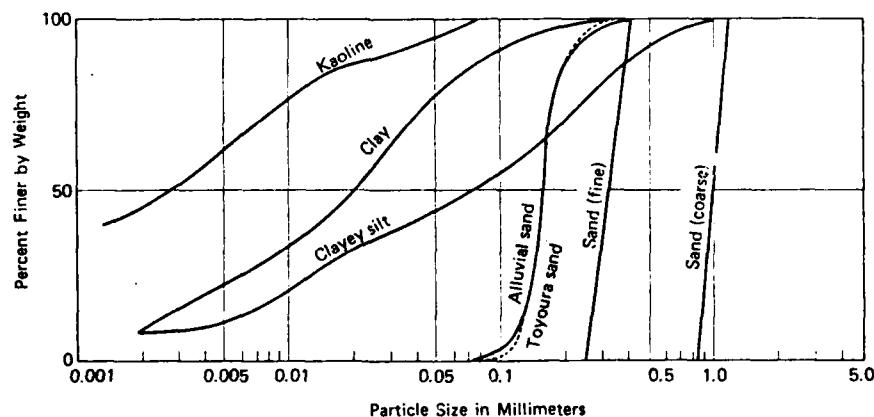
Fig. 3   Grain-size distribution

4

Table 1 Summary of laboratory data for the materials

Material	Wet density γ_t (g/cm^3)	Moisture content W (%)	Dry density γ_d (g/cm^3)	Specific surface area S_s (m^2/g)
Alluvial sand	1.88	28.0	1.47	7.3
Toyoura sand	1.94	22.5	1.58	0.9
Sand (fine)	1.86	28.5	1.45	2.2
Sand (coarse)	1.87	28.8	1.45	2.1
Kaoline	1.67	44.1	1.16	35.7
Clay	1.50	66.1	0.91	63.5
Clayey silt (diluvial deposit)	1.67	47.4	1.13	110.0
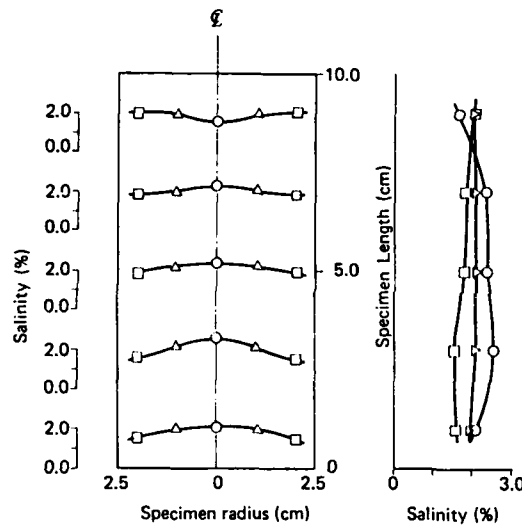
Fig. 4　Example of distribution of salinity in specimen (sand)

used when specimens were prepared, and have nothing to do with any change of salt concentration by freezing, or any unevenness of salt concentration in the specimens, or any change of concentration in the brine.

Tests

All the tests were conducted by the unconfined compression test at a compressive strain rate of 1 %/min. The relation between stress and strain of the frozen soil containing salt is shown in Fig. 5, as an example of test results. Fig. 5 shows the the results of alluvial sand test conducted at a temperature of −20°C.

Results and Discussion

Strength

Fig. 5 shows a phase that the strength of frozen alluvial sand decreased with the increase of salt concentration at a temperature of −20°C. Further tests were conducted in a wide temperature range. How the strength of frozen sandy soil changed with the change of salt concentration is shown in Fig. 6. When the temperature was higher
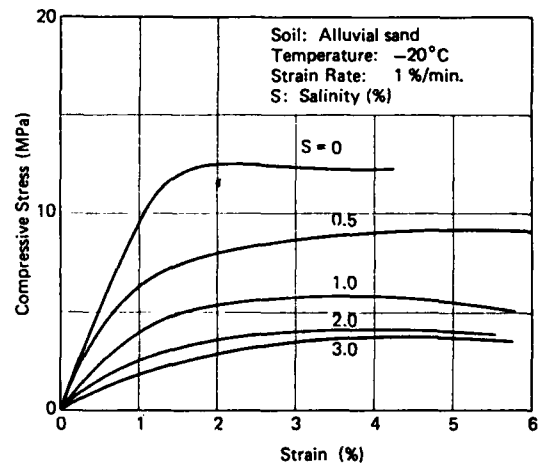
Fig. 5　Relation between stress and strain at various salinity: alluvial sand

than −20°C, the compressive strength of frozen soil decreased with the increase of salt concentration, and especially in a salt concentration range of 1 % or less, the rate of strength decrease was very large. On the other hand, the results of the test conducted at a temperature of −32°C showed

5
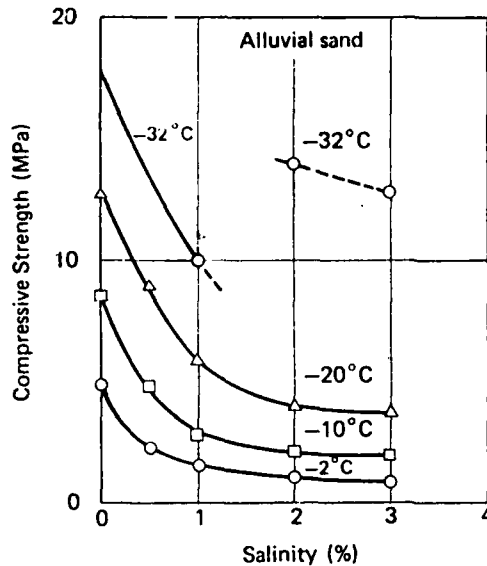
Fig. 6 Relation between compressive
strength and salinity: alluvial sand

Fig. 7 Relation between compressive
strength and salinity: (a) Calyey silt,
(b) Alluvial sand, (c) Kaoline

a trend similar to the results obtained at tempera-
tures higher than −20°C in a salt concentration
range of 1% or less, but when the salt concentra-
tion was 2% or more, larger compressive strengths
were shown on the contrary. The reason is sur-
mised to be that the eutectic point of the sodium
chloride-ice system is about −22°C.

Apart from the above mentioned results on
sand, the relation between compressive strength
and salt concentration was examined also for
cohesive soil, and the results as shown in Fig. 7

could be obtained. Fig. 7 shows the results con-
cerning clayey silt and kaoline at −10°C, and as
indicated there, clayey silt and kaoline were very
different in the trend of strength decrease. In case
of clayey silt, the compressive strength decreased
linearly with the increase of salt concentration. but
in case of kaoline, the rate of strength decrease was
remarkable in a salt concentration range of 1% or
less as in case of alluvial sand. However, it was not
so remarkable as in alluvial sand.

Fig. 8 shows the relation between compressive

Fig. 8 Relation between compressive
strength and temperature at various
salinity for alluvial sand
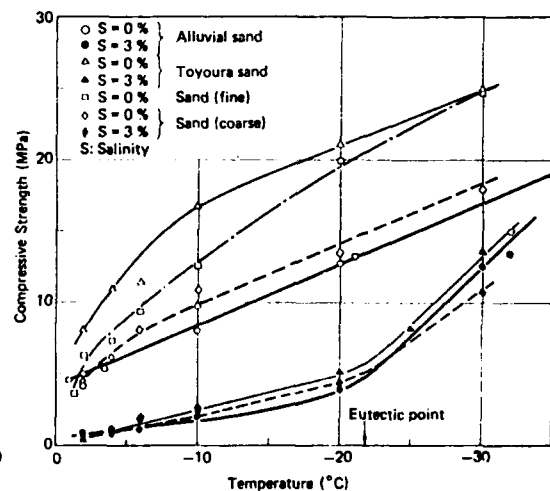
Fig. 9 Relation between compressive
strength and temperature for sands

6

strength and temperature of alluvial sand, examined at the respective salt concentrations. When the salt concentration was 0.5 % or less, the compressive strength increased almost linearly with the drop of temperature, but when the salt concentration was increased, considerably different trends were observed between the temperature range higher than the eutectic point and the temperature range lower. At high salt concentrations and low temperatures, the strength increase for temperature drop was very remarkable. Fig. 9 shows the relation between compressive strength and temperature examined of other kinds of sand at salt concentrations of 0 % and 3 %. At a salt concentration of 0 %, the compressive strengths of respective kinds of sand dispersed in a very wide range, but at a salt concentration of 3 %, all kinds of sand showed almost the same compressive strength. Fig. 10 shows a similar relation examined of cohesive soils.

centration, the larger the amount of unfrozen water.[2,3]
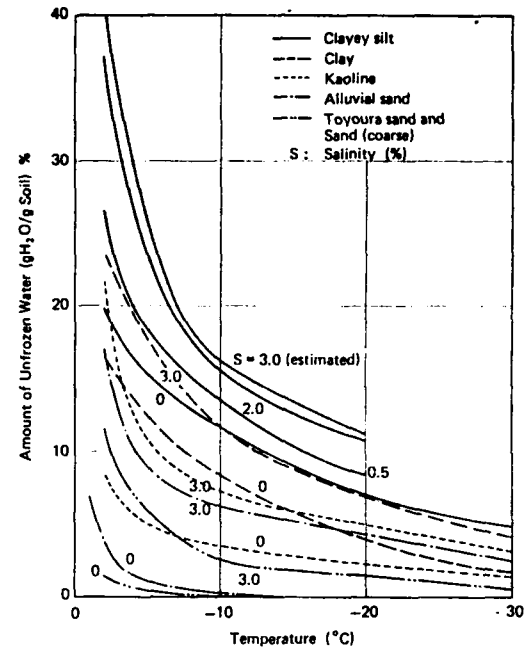
Fig. 11   Relation between unfrozen water content and temperature (Experimental results)

Fig. 10   Relation between compressive strength and temperature at various salinity

The compressive strength of frozen soil is surmised to have a close relation with the amount of unfrozen water in the frozen soil. For this reason, the amount of unfrozen water in frozen soil was measured by the calorimeter method[1], using the samples prepared by quite the same method as adopted for preparing the specimens used for the strength tests of frozen soils. Fig. 11 shows the results. All the values were obtained experimentally, except the value of clayey silt at a salt concentration of 3 %. The curves showing the relation between the amount of unfrozen water and temperature obtained here suggest that the amount of unfrozen water is closely related with the specific surface area of each sample. As generally said, it can be recognized that the larger the specific surface area, the larger the amount of unfrozen water, and that the higher the salt con-

Fig. 12   Relation between compressive strength and amount of unfrozen water for sands

Fig. 12 shows the relation between the amount of unfrozen water and compressive strength of sand, obtained as mentioned above. This graph suggest that the compressive strength of sand is very closely related with the amount of unfrozen

water. That is, the larger the amount of unfrozen water, the lower the compressive strength of frozen sandy soil. Also with regard to the specimens of frozen sand soil containing salt, if the amount of unfrozen water increased by the salt content is found, the relation between compressive strength and the amount of unfrozen water obtained for a case of no salt contained can be surmised to apply directly.

In the above, the compressive strength of frozen sandy soil was examined in reference to the amount of unfrozen water. Fig. 13 shows the relation between ice saturation and compressive strength. The ice saturation was obtained by the following equation.

$$S_i \approx \frac{V_i}{V_v} \qquad (1)$$

where S_i = Ice saturation, V_v = Volume of pores in frozen soil, V_i = Volume occupied by ice in frozen soil.
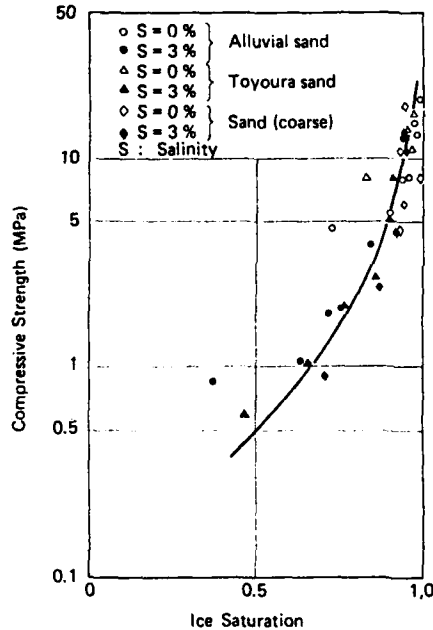
Fig. 13 Relation between compressive strength and ice saturation for sands

In Fig. 13, fairly good coincidence with strength is attained with all the three kinds of samples used in this study, in case of frozen sandy soil, in reference to the concept of ice saturation, without referring to the salt concentration. As for the specific surface area, the sand used in this study showed a maximum value of 7.3 m^2/g with alluvial sand a minimum value of 0.9 m^2/g with Toyoura sand.

The same conception adopted for frozen sandy soil was applied also to the frozen cohesive soil containing salt. However, as shown in Fig. 14 though the relations between compressive strength
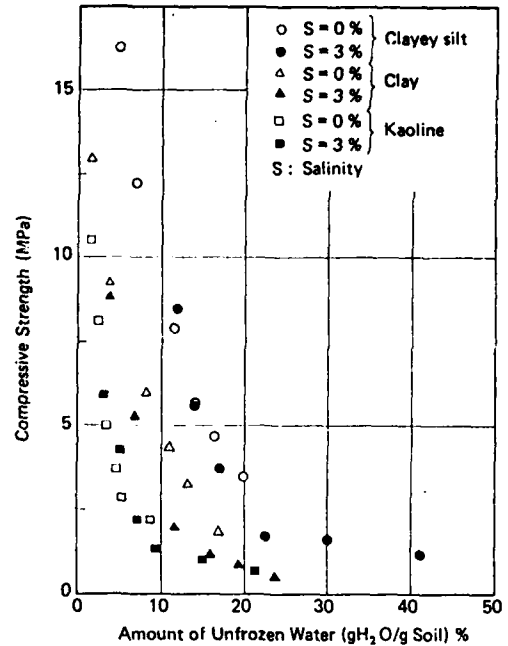
Fig. 14 Relation between compressive strength and amount of unfrozen water for cohesive soils

and the amount of unfrozen water at salt concentrations of 0 % and 3 % can be expressed by almost the same curve, if the materials are the same. the relations between strength and the amount of unfrozen water, of different materials, are different, and cannot be discussed under the same concept. In this case, soil particles were assumed to be surrounded by unfrozen water, and the mean thickness of unfrozen water film was calculated by the following equation.[4] And it was decided to examine the relation between the thickness of unfrozen water film and the compressive strength of frozen cohesive soil.

$$\delta = \frac{W_u}{S_s \times \rho_w} \qquad (2)$$

where δ = Thickness of unfrozen water film, W_n = Amount of unfrozen water, S_s = Specific surface area, ρ_w = Density of water.

Fig. 15 shows the relation between strength and the thickness of unfrozen water film calculated from equation (2). Compared with Fig. 14. it seems possible to explain the trend of the compressive strength of frozen cohesive soil more generally in reference to the thickness of unfrozen water film rather than to the amount of unfrozen water. Fig. 16 shows the same results as Fig. 15, plotted

8
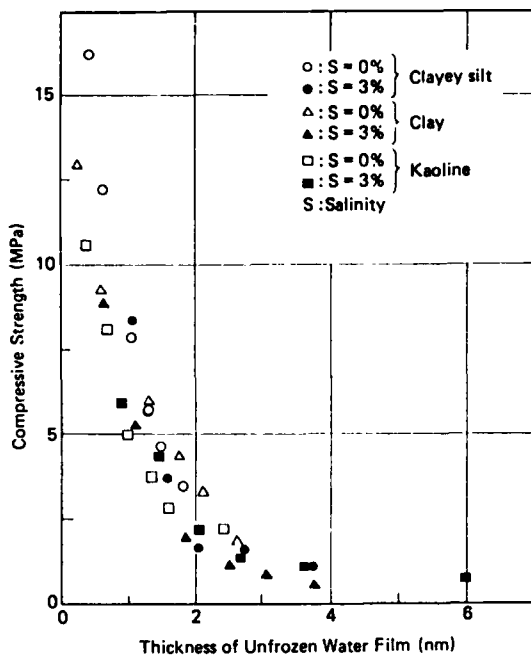
Fig. 15   Relation between compressive
strength and thickness of unfrozen
water film for cohesive soils
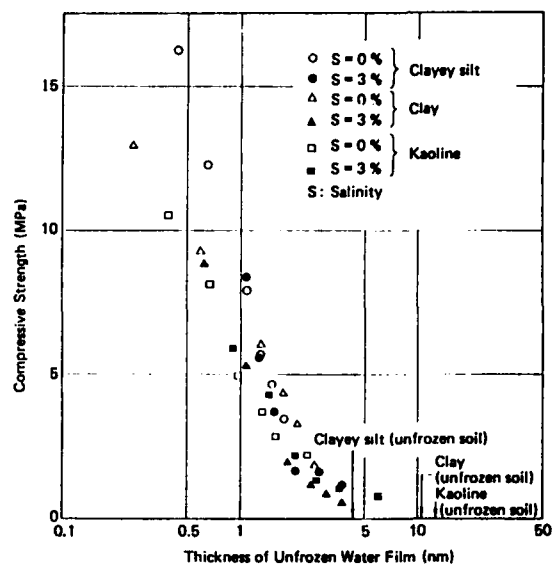
Fig. 16   Relation between compressive
strength and thickness of unfrozen
water film for cohesive soils
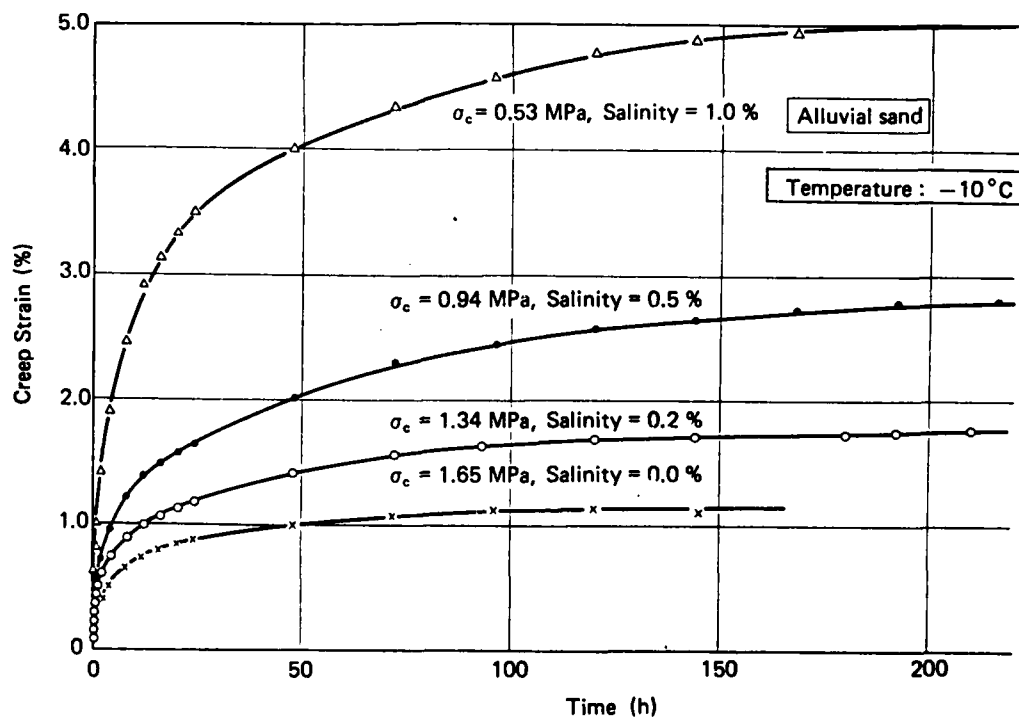
Fig. 17   Example of relation between creep strain and time
(σ_c = 20 % of the unconfined compressive strength of each sample)

9

on semilogrithmic graph paper. It indicates that if the thickness of unfrozen water film becomes less than about 2.5 nm, the compressive strength becomes suddenly high. Since the average diameter of one mc'ecule of water is about 0.25 nm, the thickness of layers of unfrozen water which causes a sudden change of strength corresponds to about 10 molecules of water. Though strict discussion could not be made since equation (2) was used, it was dem. istrated that the compressive strength of frozen cohesive soil could be explained by the mean thickness of unfrozen water film around soil particles. Fig. 16 also shows the values of δ obtained from equation (2) using the water content in unfrozen soil, and it can be seen that clayey silt is small in the thickness of water film even in the state of unfrozen soil.

Creep

In the above, it was demonstrated that the strength of frozen soil was very considerably affected by salt. Now concerning the relation between the creep strain caused with a certain load applied to a specimen of alluvial sand containing salt, and time, tests were conducted, and some of the results are shown in Fig. 17. The tests were conducted at the temperature of $-10°C$ for the four cases of 0, 0.2, 0.5 and 1.0 % salt concentrations. The magnitude of the load was made 20 % of the strength, since the strength depended on the salt concentration of each specimen. Thus, according to the increase of salt concentration, the load was made smaller, and yet the value of creep strain increased with the increase of salt concentration. Thus, it was demonstrated that the frozen soil containing salt was very large in creep deformation.

Conclusions

How the strength characteristics of frozen soil were affected by the concentration of salt contained in soil was experimentally examined, using sand and cohesive soil. Furhermore, with regard to sand, creep characteristics were examined.

The conclusions obtained in this study are as follows:

1) If frozen soil contains salt, the compressive strength of the frozen soil is considerably affected. When temperature is higher than $-20°C$, the compressive strength of frozen soil decreases if the salt content increases, and especially in a range of low salt concentrations, the rate of decrease is large.

2) The compressive strength of frozen sandy soil can be obtained almost correctly, if ice saturation is calculated, considering the amount of unfrozen water increased by salt content.

3) The compressive strength of frozen cohesive soil could be inferred from the concept of the average thickness of unfrozen water film formed around soil particles. However, whether this inference can be applied also to other cohesive soil can be concluded after collecting further data.

4) The creep deformation of frozen soil is considerably affected by salt concentration. If salt concentration increases, the creep deformation, too, becomes large.

5) Compared with the frozen soil not containing salt, the frozen soil containing salt is low in strength and large in creep deformation. Therefore, the conditions of the site concerned must be reproduced correctly in a laboratory. Furthermore, the distribution of salt concentrations in the ground at the site must be known.

References

1) Young, R. N., and B. P. Warkentin, Introduction to soil behavior (translated into Japanese), Kajima Institute Publishing Co., Ltd. 1972.

2) Banin, A., and D. M. Anderson. Effects of salt concentration changes during freezing on the unfrozen water content of porous materials, Water Resources Research. Feb. 1974, 124—128.

3) Young, R.N., C.H. Cheung, and D.E. Sheeran, Prediction of salt influence on unfrozen water content in frozen soils. Proc. Internationl Symposium on Ground Freezing, 87—101, 1978.

4) Anderson. D. M., A. R. Tice, and A. Banin. The water-ice phase composition of clay-water systems: I. The kaolinite-water system, Soil Soc. Amer. Proc. 37: 819—822, 1973.

STRENGTH AND DEFORMATION BEHAVIOR
OF FROZEN SALINE SAND

D.C. Sego,   University of Alberta, Edmonton, Alberta
T. Shultz,   University of Alberta, Edmonton, Alberta
R. Banasch,   The UMA Group, Edmonton, Alberta

SUMMARY

This study presents the results of a laboratory investigation of the strength and deformation behaviour of frozen saline sand. Unconfined compression experiments were conducted at $-7.0°C$ and at various strain rates. The results indicate that the strength and deformation are strain rate dependent and are strongly influenced by the concentration of the saline pore fluid. The behaviour is best analyzed using a power law to indicate the relationship between both the strength and the deformation moduli with the strain rate.

INTRODUCTION

The commitment to hydrocarbon exploration in the Beaufort Sea has required that oil well drilling be designed and constructed that are able to withstand the ice loading. The major type of structure used in water depths up to 8 meters or less has been artifically constructed islands. The design and construction of these islands in shallow water have been discussed in detail by Riley (1975), Garret and Kry (1978), and Croasdale and Marcellus (1978) More recently, as exploration moves into deeper water, a caisson retained island has been designed and constructed for Dome Petroleum Ltd. (Van der Wal, 1982) This island is constructed in 20 meters of water.

These artificial islands require the hydraulic placement of large amounts of sand fill in order to be stable when subjected to ice loading. Therefore, the use of artificial freezing of the sand to reduce the volume of sand required and to increase stability is a possibile design that might be considered. Frozen saline soils are also encountered in other circumstances and therefore it is of interest to determine their properties. This study reports on a preliminary set of experimental results that were conducted to establish the strength and deformation behaviour of an artificially frozen sand with pore fluids of various concentrations of NaCl.

TEST MATERIAL

The fine sand used in the experimental program was a readily available local concrete mortar sand having the grain size distribution shown in Figure 1. The grain size distribution of the sand tested is compared in Figure 1 with the ranges of grain size of marine sands found in the Beaufort Sea as reported by O'Connor, et al. (1979). The test sand is a clean light brown, poorly graded sand with coefficient of uniformity of 2.3 and a Unified Soil Classification of SP. The sand grains are subrounded to angular.
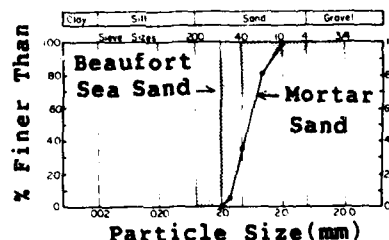
Figure 1: Grain size curves comparing sand used to Beaufort Sea Sand reported by O'Connor et al. (1979).

SAMPLE PREPARATION

Mixtures of mortar sand and saline solution at concentrations of 0, 10, 35, and 100 gm NaCl/liter were prepared at a moisture content of 30%. Each mixture was placed on a vibratory table and thoroughly mixed, while being vibrated. The mixture was covered with a plastic wrap and stored in a moisture room.

The samples were prepared at an essentially constant density by being subjected to consolidation pressure of 80 kPa in a one-dimensional consolidation apparatus. The cell used was constructed of PVC and its design features have been outlined by Mageau (1978). The samples prepared with this device were 100 mm in diameter and 180 mm in length.

The consolidation apparatus was located in an environmentally controlled room that was maintained at +1.0°C. The base plate was connected to a constant temperature circulation bath in which the fluid was maintained at −75.0°C. Upon completion of consolidation the cold fluid was circulated through the base plate and the sample was frozen one-dimensionally from the base upward. During freezing the constant consolidation pressure of 80 kPa was maintained and the sample was allowed to reject fluid through the top load cap. This ensured that, during freezing, there was no buildup of excess pressure at the freezing front. The sample was subjected to the freezing temperature for 24 hours to ensure that it was completely frozen.

The consolidation cell was transferred to a cold room maintained at −20°C and the sample was removed from the apparatus. It was wrapped in saran wrap after being sprayed with water from a mist bottle. The mist was applied to reduce ablation of the pore ice during storage. Each sample was labelled and placed in a freezer chest until required for testing.

In preparation for testing the sample was removed from the freezer chest and placed in the preparation cold room maintained at −20°C. The sample was allowed 24 hours in the cold room to come to temperature equilibrium. The ends of the sample were machined parallel and perpendicular to the sides with a shell mill that contained tungsten carbide tips. The sample was weighed and its dimensions recorded and the density calculated.

The sample was mounted in a triaxial cell that had been modified for testing frozen soil. The modifications to the triaxial cell have been given by Savigny (1980) and a schematic diagram of the testing system is given in Figure 2a. The sample was mounted on the lower platen, the upper platen was centered and a latex rubber membrane was placed around the sample. The cell was assembled and a light parafin oil at −20°C was pumped into the cell to surround the sample. The use of light parafin oil in triaxial testing has been discussed by Iverson and Moum (1974). The platen used were standard aluminum platen without any friction reduction.
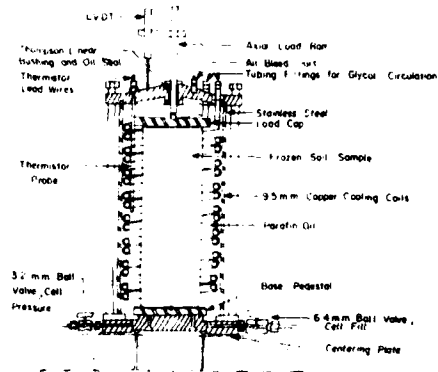
Figure 2 a: Cut away view of modified triaxial cell after Savigny (1980).
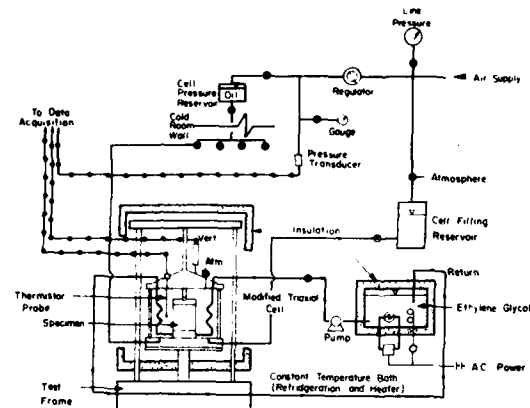
Figure 2 b: Schematic of constant displacement rate loading apparatus.

TEST EQUIPMENT

The tests were performed using a 90 kN capacity Wykeham Farrance constant displacement rate loading press. The displacement rate could be varied between 1.2 mm per minute and 0.00049 mm per minute.

The triaxial cell, which was modified to provide temperature measurements, was selected since it allows a cell fluid to surround the sample hence reducing ablation of the pore ice during testing. This light parafin oil also acted as thermal mass surrounding the sample which helps to maintain a constant temperature in the sample during the experiment.

The temperature of the sample was maintained constant by circulating a mixture of ethyelene glycol through the cooling coils that surround the sample. The cooling coils which act as heat exchangers, are mounted within the triaxial cell. The temperature of the ethylene glycol mixture was maintained constant during the experiment by circulating the fluid through a Hot Pak constant temperature bath. The base of the triaxial cell

12

was isolated from the load frame by a cooling plate mounted between the cell and the movable loading frame platen. The cooling fluid from the Hot Pak apparatus was circulated through this plate. The triaxial cell and measuring equipment were housed in an insulated cabinet which isolated them from the temperature fluctuations of the cold room.

The measuring instruments were a linearly variable displacement transducer (LVDT), thermistor, and temperature compensated strain gauge load cell. The Hewlett Packard 24 DCDT LVDT was capable of measuring deformations to .0013 mm. Load cells of various capacity were used throughout the experimental program, and were chosen to match the expected sample failure load. The temperature of the triaxial cell fluid was measured using a temperature measuring probe located at the mid-height of the sample between the sample and the copper cooling coil. This probe was constructed using a stainless steel tube and an Atkins No. 3 thermistor bead (Roggensack, 1977). The thermistor was calibrated using a quartz thermometer to ± 0.001°C; and therefore, measured a temperature to 0.01°C ± .005°C. A schematic diagram of the constant displacement rate loading and measuring system is shown in Figure 2b.

TEST PROCEDURE

The cell and sample were transferred from the soil preparation room to the cold room that contained the constant displacement rate loading frame. The cooling coils were connected to the constant temperature circulation system. The ethyelene gylcol at a temperature of −7°C was circulated through the cell for 24 hours to bring the sample to test temperature. The temperature measuring probe was inserted into the cell between the cooling coil and the sample and the temperature was monitored.

Once the sample temperature had stabilized the LVDT, and load cell were adjusted to their zero reading. The gearing system of the constant displacement rate press was adjusted to the desired rate, a small seating load was applied and the electronic recording system was started. Throughout the application of constant deformation rate the load, the vertical deformation, and the temperature were monitored at regular time intervals. The electronic output data was recorded on a magnetic tape and subsequently transferred to a central computer for data reduction and plotting.

EXPERIMENTAL RESULTS

During the experimental program a total of 26 samples were tested using average strain rate between 0.03%/hour and 24%/hour. All the experiments were conducted at an average test temperature of −7.0°C, but in the initial program the temperature deviated by up to +1.5° from this value. Figures 3, 4, 5, 6, and 7 record the

stress-strain curves of the samples tested. Each Figure contains the results for a different pore water salinity. The stress-strain curve is identified with the average strain rate applied during testing.
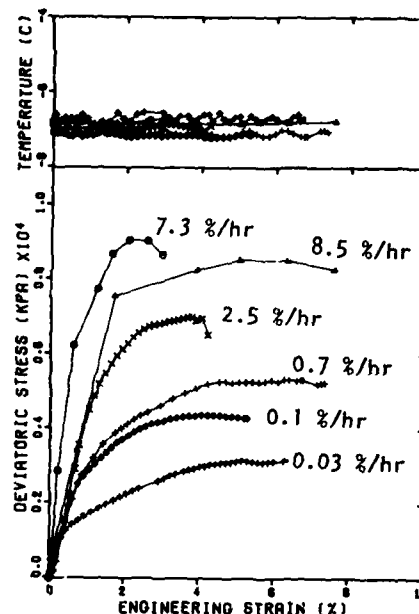
Figure 3: Stress and temperature verse strain for salinity of 0 gm NaCl/1.
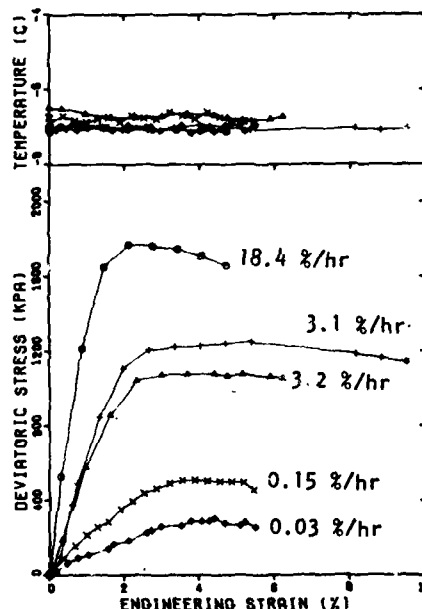
Figure 4: Stress and temperature verse strain for salinity of 10 gm NaCl/1.

13
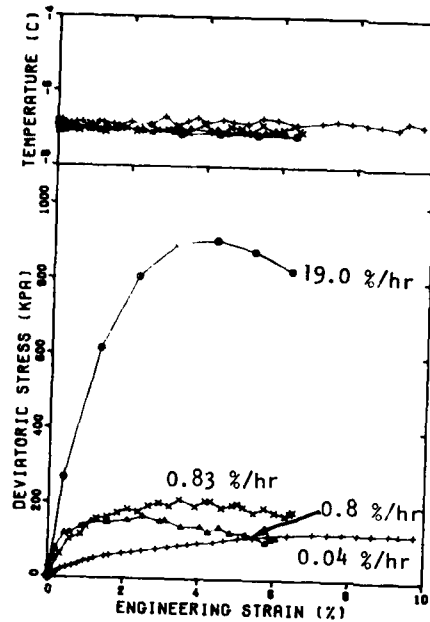
Figure 5: Stress and temperature
verse strain for salinity
of 35 gm NaCl/l.
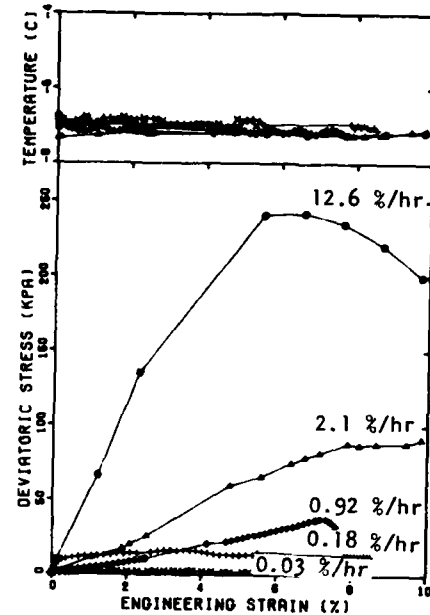
Figure 7: Stress and temperature
verse strain for salinity
of 100 gm NaCl/l.
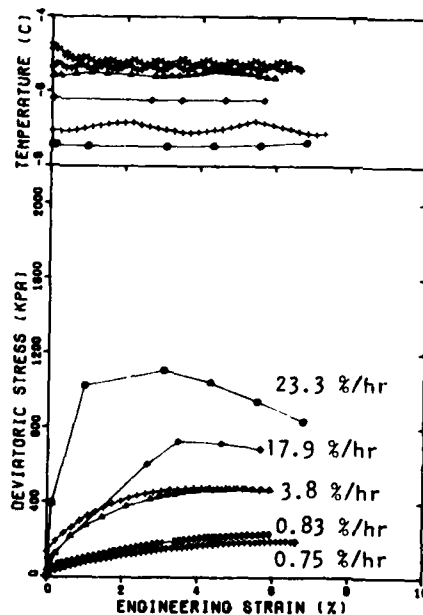
Figure 6: Stress and temperature
verse strain for salinity
of 35 gm NaCl/l.

Table 1 contains a summary of the sample properties, the test conditions, and the measured failure results for each sample. The data illustrates that all the artificial samples were uniform in density and moisture content. The failure results show that the peak deviator stress at failure varies with both the salinity of the pore fluid and the strain rate. The strain to failure is influenced slightly by strain rate and by salinity. The Secant Young's Modulus varies with both strain rate and salinity

DISCUSSION OF RESULTS

Failure Stress

The experiments conducted on the fine sand with and without a saline pore fluid illustrate a dependence of the peak failure stress on the concentration of the pore fluid at the test temperature of −7.0°C Figure 8 is a plot of the peak failure stress versus strain rate data from this investigation, the experimental data on unconfined compressive strength of sand reported by Ladanyi and Paquin (1978) at a temperature of −6.0°C, and the data reported by Ruedrich and Perkins (1974) at a temperature of −7.7°C.

The data of Ladanyi and Paquin at −6.0°C compares well with the data from this experimental program when there was no salt in the pore fluid. Ruedrich and Perkins' data for Prudhoe Bay sand at −7.7°C and a salinity of 9.7 gm of NaCl/l shows a slightly higher strength at different strain rates than the experiments conducted at −7.0°C and a salinity of 10 gm/l in this program. These two comparisons indicate that the experimental results are consistent with previous studies of strength and deformation of frozen sand.

14

Table I Summary of Unconfined Compression Experiments

Sample Characteristic				Test Conditions		Failure Conditions		
Sample Number	Salt Content (gm/l)	Total Density (Mg/m³)	Moisture Content (%)	Test Temp (°C)	Average Strain Rate (%/hour)	Peak Stress (kPa)	Failure Strain (%)	Young's Modulus (mPa)
TS-11	0.0	2.02	18.8	-6.8	7.310	9067.4	2.07	438.0
TS-12	0.0	1.99	19.7	-6.8	8.576	8642.8	5.02	170.2
TS-13	0.0	1.97	21.0	-7.0	0.717	5334.7	6.27	85.1
TS-14	0.0	2.00	18.9	-7.0	2.535	7006.5	3.76	186.3
TS-15	0.0	1.99	19.0	-7.2	0.128	4379.3	4.20	104.3
TS-27	0.0	1.98	19.0	-6.8	0.033	3150.5	6.24	50.5
TS-21	10.0	1.97	20.9	-6.7	3.167	1079.8	4.41	24.5
TS-22	10.0	1.98	20.3	-7.0	18.431	1772.3	2.11	84.0
TS-23	10.0	1.99	20.5	-6.8	0.152	510.4	3.62	14.5
TS-26	10.0	1.98	20.3	-7.1	0.034	304.9	4.41	8.9
TS-31	10.0	1.97	20.2	-7.0	3.119	1250.1	5.38	23.2
TS-1	35.0	2.02	17.9	-7.1	0.789	166.4	2.50	6.7
TS-2	35.0	2.01	17.8	-6.9	0.037	127.0	9.07	1.4
TS-4	35.0	2.02	17.3	-7.1	0.829	213.6	3.47	6.2
TS-6	35.0	1.99	17.7	-7.1	18.955	915.2	3.29	27.8
RB-1	35.0	1.97	12.4	-7.5	23.278	1106.2	3.06	38.2
RB-2	35.0	1.97	16.6	-5.5	3.819	475.9	5.06	9.4
RB-3	35.0	2.00	16.5	-7.0	3.932	479.5	4.53	10.6
RB-4	35.0	1.98	16.0	-5.2	0.827	236.4	6.25	3.8
RB-5	35.0	1.99	16.7	-6.2	17.907	728.1	3.45	21.1
RB-6	35.0	1.99	16.7	-5.4	0.748	191.0	8.38	3.0
TS-9	100.0	2.00	19.4	-7.2	1.264	241.9	6.63	3.6
TS-16	100.0	1.99	18.6	-6.9	0.176	162	3.51	0.47
TS-17	100.0	1.93	19.4	-7.1	0.919	379.4	7.15	0.53
TS-18	100.0	1.93	18.6	-7.1	2.167	91.2	9.75	0.94
TS-30	100.0	1.97	19.3	-7.0	0.029	261	3.77	0.07
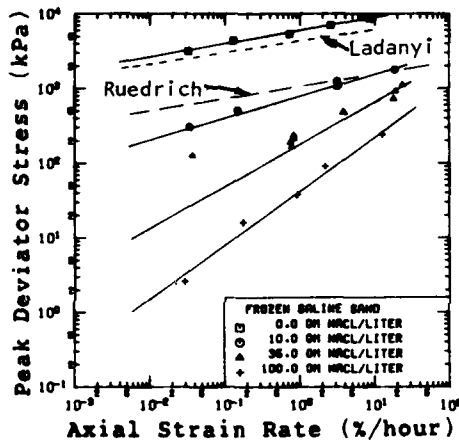
Figure 8: Peak deviator stress versus strain rate.
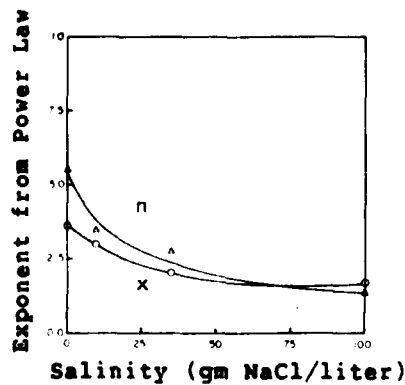
Figure 9: Exponent of power law relationship versus salinity.
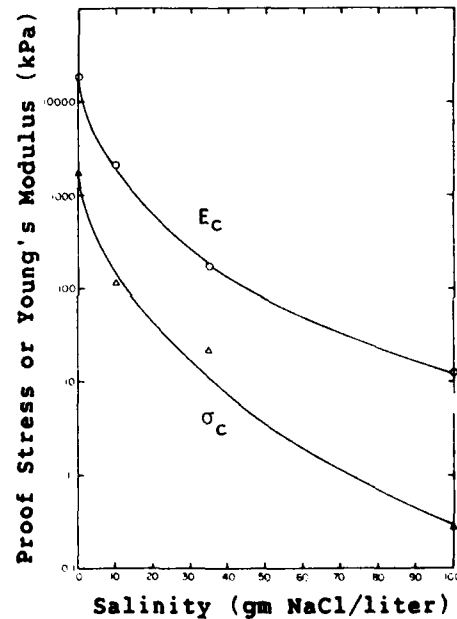
Figure 10: Proof stress and Modulus versus salinity.

15

The data plotted in Figure 8 shows the variation of the peak failure stress with strain rate and salinity. The effect of salinity is most pronounced at the lower strain rates. At each salinity the variation of peak failure stress with strain rate were represented by the simple power law relationship advocated by

Ladanyi (1972):

$$\left[\frac{\dot{\varepsilon}}{\dot{\varepsilon}_c}\right] = \left[\frac{\sigma}{\sigma_c}\right]^n \qquad (1)$$

where

$\dot{\varepsilon}$ denotes the strain rate
$\dot{\varepsilon}_c$ denotes the proof strain rate
σ^c denotes the axial stress
σ_c denotes the proof stress
n^c denotes the power law exponent

The proof strain rate is a convenient strain rate used to normalize the data and Ladanyi (1972) suggests using 0.001%/hour. The proof stress is that required to maintain the proof strain rate.

The data from Table 1 at each salinity has been fitted with the power law relationship to establish the proof stress and the exponent n. These results are summarized in Table 2 for the different salinities. The data illustrates that both the proof stress and the exponent n are dependent on the salinities. Figure 9 shows the variation of the exponent n the power law relationship with salinity. At low salt contents the exponent is highly dependent on the value of the salinity but this dependence decreases as the salinity increases. No data is available to establish the influence of temperature on the exponent.

Table 2: Parameters relating Stress to strain rate

Salt Content (gm/l)	Proof Stress (kPa)	n
0	1709.20	5.52
10	119.80	3.58
35	22.10	2.75
100	0.27	1.36

The variation of the exponent n with salinity is explained by the changing characteristic of sand-ice bond in the frozen sand. With no salt in the pore fluid, the exponent obtained was 5.52 compared to 7.03 obtained by Ladanyi and Paquin (1978). These exponents are higher than those measured for pure ice and are explained by the softening effect that the sand has on ice which bonds the particles together. The exponent measured for polycrystalline ice is 3.0 (Sego, 980). The decrease in the exponent with increasing salinity shows that properties of the ice and ice-particle interaction is changing. At high salinity the exponent will decrease to 0.0, since the strength of a granular material is independent of strain rate over the range of strain-rates examined in this research program.

Figure 10 shows the variation of the proof stress with salinity. The decrease of the proof stress with salinity is explained by the increase of unfrozen water at −7.0 C and the decrease in the strength of the ice bonding the sand grains together. The unfrozen water content increases with increasing salinity. Ions are rejected from the water during the ice forming process to a hull surrounding the soil particles. At very high salinity and a temperature of −7.0°C the soil could have all the water phase in an unfrozen state and the unconfined strength would approach that of unfrozen sand. In this instance, the power law relationship between strain rate and stress would no longer be valid.

Secant Young's Modulus

The Secant Young's Modulus determined for each sample is in Table 1. The Secant Modulus is defined as the peak stress divided by the strain accumulated to reach the peak stress. The Secant Young's Modulus versus strain rate for this research is presented in Figure 11. The results show a linear variation of Young's Modulus with strain rate in the log-log plot.
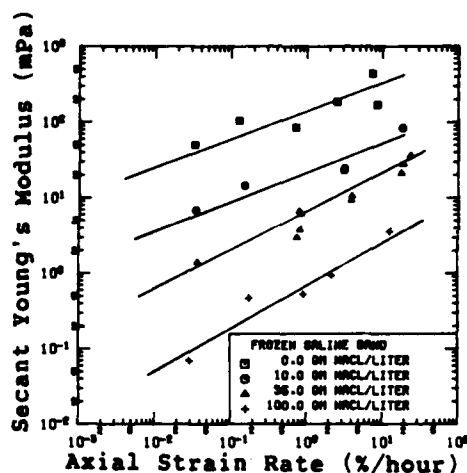
Figure 11: Secant Youngs' Modulus versus strain rate.

The relationship between strain rate and Young's Modulus can be represented by a power law relationship similar to Equation 1 having the following form:

$$\left[\frac{\dot{\varepsilon}}{\dot{\varepsilon}_c}\right] = \left[\frac{E}{E_c}\right]^x \qquad (2)$$

where

Ec   denotes the proof Modulus at a strain rate of 0.001%/hour.
x   denotes the exponent

The best fit linear relationship through the data plotted in Figure 11 is given in Table 3. The exponent and proof Young's Modulus (Ec) at each pore fluid salinity is tabulated and indicates that both these parameters are related to the salinity of the pore fluid. The

16

variation of the exponent x with salinity is given in Figure 9; and the variation in the proof Young's Modulus is contained in Figure 10. The explanation for the variation of each of these parameters with salinity is similar to the variation of the calculated parameter of the flow law given previously. The exponent x evaluated in Equation 2 does not vary as much as the exponent n evaluated from Equation 1. This suggests that the stiffness of the material is not as strain rate dependent as the failure strength of the frozen sand. The proof Young's Modulus shown in Figure 10 has a similar variation with salinity to that of the proof stress obtained from Equation 1.

Table 3: Parameters relating Secant Moduli to strain rate

Salt Content (gm/l)	Proof Modulus (kPa)	x
0	19,800.0	3.53
10	2,120.0	2.97
35	184.0	2.02
100	12.0	1.70

Strain at Failure

The strain at failure in the experiments is tabulated in Table 1. There is no significant dependence on either the salinity or strain rate that can be evaluated. On average, the strain to failure is about 4.5% with the average strain to failure increasing to 6.0% for the sample with a salinity of 100 gm NaCl/l. No relationship between strain to failure as a function of strain rate is discernible from the data.

CONCLUSIONS

The results of this experimental study on the strength and deformation behaviour of frozen sand with a saline pore fluid indicate the following:
1. The flow law parameters of the frozen sand vary with salinity.
2. The Young's Modulus varies with strain rate and salinity in a similar manner.

ACKNOWLEDGEMENT

REFERENCES

1. Croasdale, K.R., and Marcellus, R.W., 1978. "Ice and wave action on artificial islands in the Beaufort Sea." Canadian Journal of Civil Engineering, Vol. 5, pp. 98-113.

2. Garratt, D.H., and Kry, P.R., 1978. "Construction of artificial islands as Beaufort Sea drilling platforms." Journal of Canadian Petroleum Technology, April.

3. Iverson, K., and Moum, J. 1974. "The paraffin method-triaxial testing without rubber membranes." Geotechnique, Vol. 24. pp 665-670.

4. Ladanyi, B. 1972. "An Engineering theory of creep of frozen soils." Canadian Geotechnical Journal, Vol 9., pp 63-80.

5. Ladanyi, B. and Paquin, J. 1978. "Creep behaviour of frozen sand under a deep circular load." Proceedings: Third International Conference on Permafrost, Edmonton, Canada, Vol. 1, pp 679-686.

6. Mageau, D.W., 1978. "Moisture Migration in Frozen Soil." Unpublished M.Sc. thesis. University of Alberta, 146 p.

7. O'Connor, M., MacLeod, N., and Blasco, S. 1979. "Surficial Geology of the Southern Beaufort Sea." Proceedings: First Canadian Conference on Marine Geotechnical Engineering, Calgary, Alberta, pp. 67-78.

8. Ruedrich, R.A. and Perkins, T.K. 1974. "A study of factors influencing the mechanical properties of deep permafrost." Journal of Petroleum Technology, Vol. 26, pp 1167-1177.

9. Roggensack, W.D., 1977. "Geotechnical *Properties of Fine-Grained Permafrost* soils." Unpublished Ph.D. thesis, University of Alberta, 449 p.

10. Savigny, K.W., 1980. "Analysis of Creep in Ice-Rich Permafrost Soil." Unpublished Ph.D. thesis, University of Alberta, 439 p.

11. Sego, D.C., 1980. "Deformation of Ice under Low Stresses." Unpublished Ph.D. thesis, University of Alberta, 429 p.

12. Van der Wal, J.U. 1982, "Artificial island construcion in the Beaufort Sea." Presented to Association of Professional Engineers Geologists and Geophysicists Luncheon Meeting in Calgary.

FROZEN SALINE SAND SUBJECTED
TO DYNAMIC LOADS

Hans L. Jessberger, Prof.   Dep. of Civil Engineering
Peter Jordan, Dipl.-Ing.   Ruhr-Universität Bochum
                              Federal Republic of Germany

Little is known about the behaviour of frozen ground subjected to dynamic loads whereas since a long time the strength and the creep of frozen soil subjected to static loads were investigated. In this paper the test method, the equipment including the stress or strain control-system, and the measurement devices for cyclic loaded triaxial tests are described. A similar method is used succesfully to investigate the dynamic behaviour of unfrozen soils in offshore and earthquake engineering. The sample preparation providing a constant density and a certain salinity is also described. Test results showing the influence of temperature and frequency on the elastic and plastic deformation caused by cyclic triaxial loadings are reported and discussed.

INTRODUCTION

Since 1973 17 artificial islands made of gravel, sand and even silt have been constructed in the offshore waters of the Canadian Arctic. Artificial islands are also planned to be built in the Alaskan Beaufort Sea and in New Foundland waters. Artificial islands in the Beaufort Sea are built in water depths down to 19,5 m. The latest development goes in the direction of building an island in water depth of 60 m at Kopanoar (Anonymus 1981).

The increasing water depth in which artificial islands should be built requires increasing masses of sand fill. To withstand a collision with an ice island the underwater side slopes of the island in deep water are designed as sacrificed beach (Croasdale and Marcellus 1981). Special structures are used and developed to hold the ice loads of packice, ice ridges etc. in the wave zone. The Tarsiut prototype island is topped with concret caissons which should resist the ice forces. These caissons are filled with sand or gravel. Another possibility is to freeze the soil inside the island under the protection of construction elements in order to reduce the dimensions of the structures.

The frozen soil mass within the sand island has to be stable against high ice loads for many years. The ice will fail in crushing the contact face of the retaining structure. Therefore it is to be assumed that the frozen soil mass is loaded dynamically by the ice loads. In order to investigate the time dependent deformation behaviour of the frozen soil body loaded by ice, dynamic triaxial tests where performed on water saturated soil samples with 3 % salinity.

KIND AND MAGNITUDE OF ICE LOADS

Some considerations and full scale ice force measurements (Kry 1979, Metge et al. 1981 and Matlock et al. 1969) show that the ice loads forcing against wide structures lead to local stress variations instead of permanent load on the total contact area. It was found that the total stress effective against the total interaction width is smaller than the maximum local stress (Fig. 1).
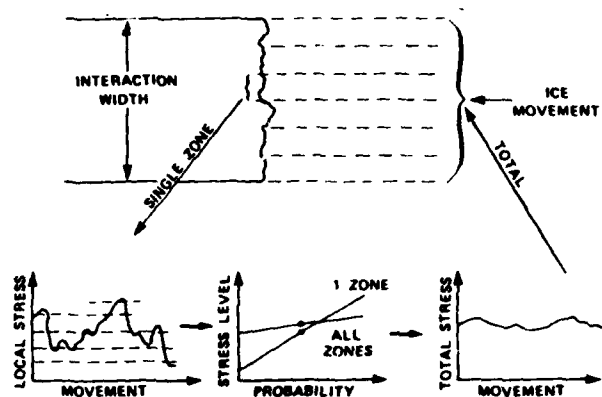
Fig. 1: Statistical influence on peak expected stress as a function of structure width (Kry 1979)

To analyse the stability of the sand island as a whole, the reduced stress related to the total interaction width is to be used; according to Kry (1979) the maximum ice load which equals the maximum ice strength can be reduced by 50 %. But the design of single parts or zones of the sand island should be based on dynamic ice loads. In this study it is assumed that the ice load reaches 2,8 MN/m² as peak value.

These dynamic ice loads working against the protected frozen soil body are simulated in a triaxial shear apparatus. The constant cell pressure σ_c is equal to the vertical in situ stress; in the triaxial test the dynamic axial stress is simulating the horizontal in situ stress caused by the dynamic ice load and the overburden pressure. The stress conditions shown in Fig. 2 represent the stresses in an element of the frozen soil near the water line. The cyclicly changing axial stresses $\sigma_{v\ min}$ and $\sigma_{v\ max}$ are leading to the dynamic stress path which loads the frozen soil samples. It is obvious that in a shear plane of 45° a changing shear stress is produced. But the amount of the positive shear stress is much higher than that of the negative one.

TEST CONDITIONS

Soil-Sample Preparation

In the dynamic triaxial shear tests a fine sand is used with properties given in Table 1.
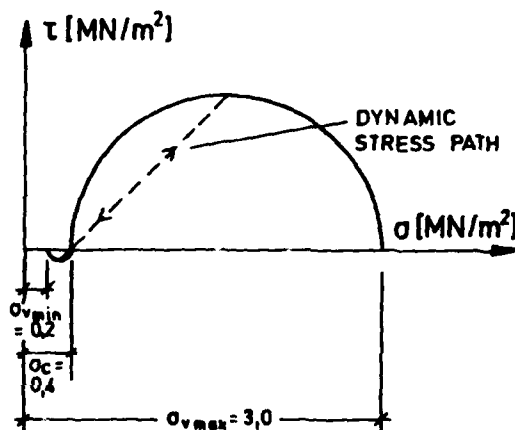
Fig. 2: Stress conditions for dynamic shear tests

Property	Value
Specific Gravity	2.65
Minimum Density	1.33 t/m³
Maximum Density	1.61 t/m³
Average Grain Size	0.19 mm
Coeff. of Uniformity $C_u = D_{60}/D_{10}$	1.43

Table 1: Properties of Fine Sand

The samples were prepared by pluvial deposition of the dry sand from a hopper hanging in constant distance above the just reached sand level in the mould. By this way a constant sample density I_D was reached. After this the sand sample (h/d = 20/10 cm) was saturated with saline water of 3 % salinity. Before saturation the air in the pore space was replaced by CO_2 to avoid air conclusions in the water. Finally the sample including the preparation mould was chilled down to -20°C.

Dynamic Shear Apparatus

For the tests for simulating the above described in situ conditions the special triaxial shear apparatus "TSW-Apparatus IIb" is used. In Figure 3 this apparatus is shown schematically together with the periferal modules. The servohydraulic actuator operates in a closed loop system which recently is introduced into materials testing. The actuator (4) is loading the frozen sample (5) vertically, and the system works in the following way:

High pressure oil from the power pack (9) is delivered through a servo valve (3) to the hydropulse actuator (4) which in return loads the soil sample (5). The test force is measured in the form of a voltage by a load cell (6) and its associated signal conditioner (7). The output of the displacement transducer (6a) installed in the base of the actuator is used as controll parameter. In the servo controller (2) the feedback
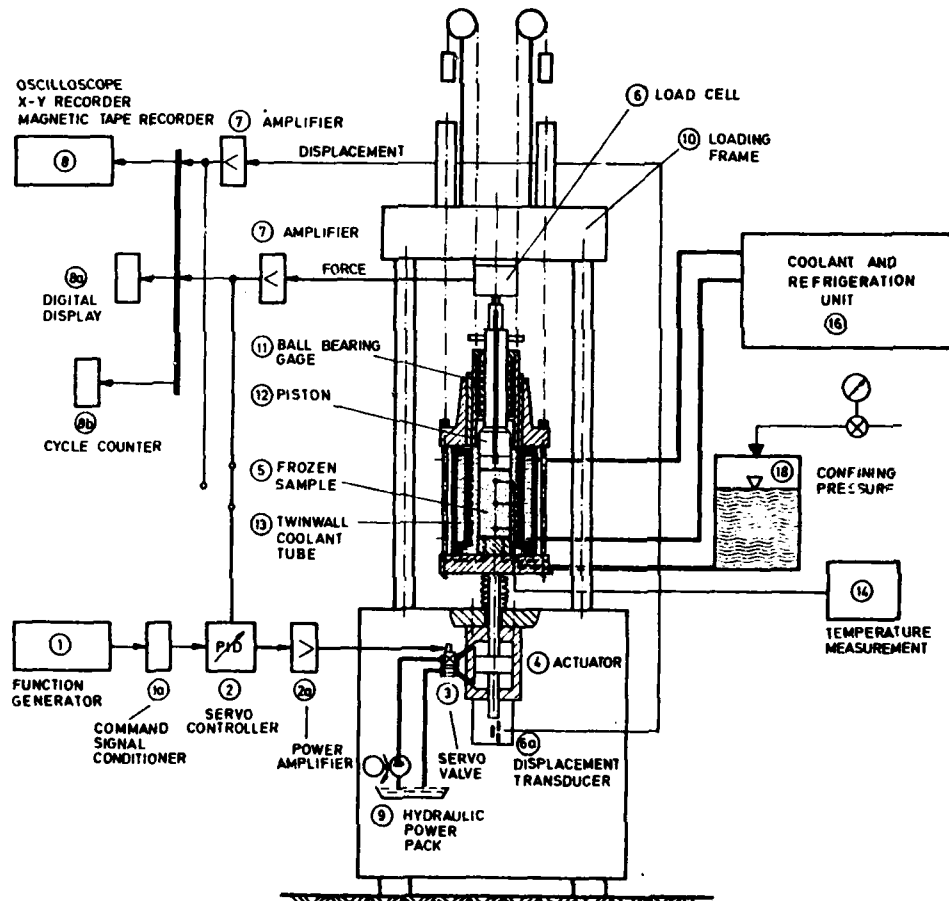
Fig. 3: Dynamic triaxial shear apparatus (TSW IIb) with signal flow diagram

21

signal is continuously compared with a command signal which is produced by the function generator (1). The power amplifier (2a) converts the resulting difference into the controll signal for the servo valve (3). The function generator (1) produces sine , triangular and square wave forms.

The system is connected with parameter readout and recording units. The data of displacements are recorded by multichannel recorder or by tape (8).With periodic signals the peak values are stored and displayed at the digital display unit (8a).

The frozen soil sample with 10 cm diameter and 20 cm length can be loaded vertically by a maximum stress (static or dynamic) of 5 MPa and horizontally by a static cell pressure of max. 1 MPa. The limit frequency of the system depends on the magnitude of the dynamic load and of the piston amplitude. Testing frozen soil the limiting frequency can reach at the most 60 to 80 Hz.

The sample is frozen with the help of a twinwall tube (13). In the space between the two tube walls the coolant is circulating. To make the heat transfer from the twinwall tube to the cell fluid easier, at the inside of the wall many carves are cut to increase the contact surface. It was found in preliminary tests that this system leads to constant temperature fields around the frozen soil sample. At three points outside the soil sample the temperature was measured using thermistors with the result that the requested temperature is constant within a tolerance of $\pm$ 0,2°C.

Test Method

The saline soil sample already in frozen conditions is placed into the triaxial shear apparatus and subjected to a sinoidal dynamic axial loading. Figure 4 shows schematically a triaxial test result. The dynamic stress leads to a cyclic vertical strain ε. $\Delta\varepsilon_{el}$ as the difference between the maximum ε_{max} and minimum ε_{min} vertical strain is called the elastic strain. The Modulus of dynamic deformation is given by the following relation:

$$\tilde{E} = \frac{\Delta\sigma_v}{\Delta\varepsilon_{el}}$$
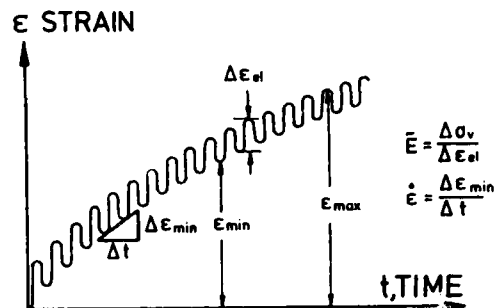
Fig. 4: Typical test result of the dynamic triaxial shear test, schematically

TEST RESULTS

The stress and time dependent deformation behaviour of frozen soil is usually investigated by creep tests. In the literature many papers are dealing with this characteristic behaviour of frozen soil, s.e. Vyalov (1962) and Klein (1978). Creep tests with statically loaded samples should be nominated as static creep tests, while the tests for investigation of the vertical deformation of frozen soil samples subjected to dynamically acting vertical stress should be nominated as dynamic creep tests. It is assumed that the creep behaviour of frozen soil is influenced by dynamic stresses in similar way as by static stresses. Therefore this paper is concentrated on the influence of frequency and temperature on the creep behaviour of dynamically loaded saline soil.

The test results presented in Fig.5 and 6 are received from tests with the stress path of Fig. 2. Fig. 5 shows the increase of minimum vertical sample deformation with time.These dynamic creep curves are strongly frequency dependent. While the data of Fig. 5 are related to a sample temperature of T = -10°C, in Fig. 6 the temperature dependency of the dynamic creep behaviour of the frozen soil is shown. Again this curves are typical creep curves with continuously decreasing strain rate. The time hardening effect is obvious on the Figures 5 and 6. Strong influence of frequency and temperature on the remaining time dependent vertical strain is also clearly shown.

22
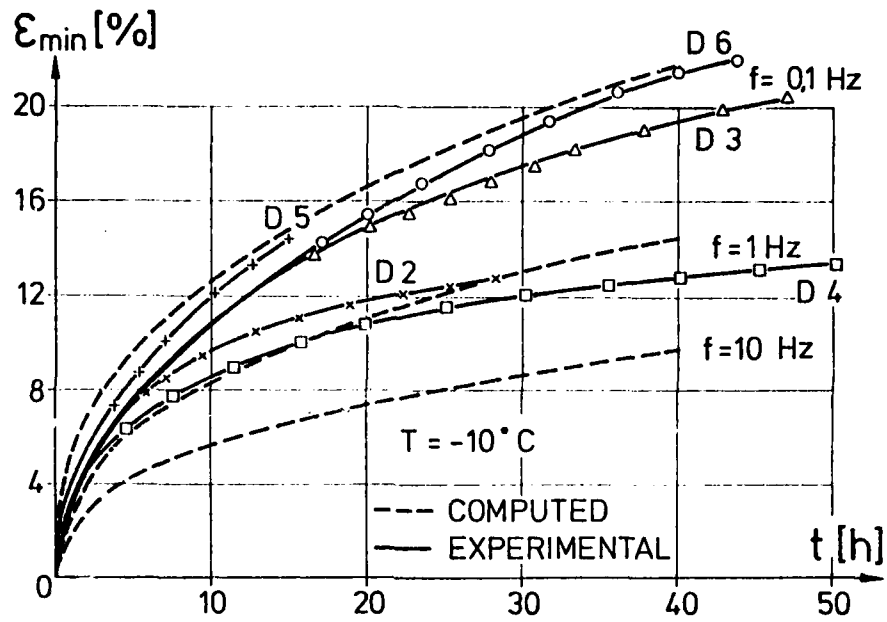
Fig. 5: Effect of frequency on the creep behaviour
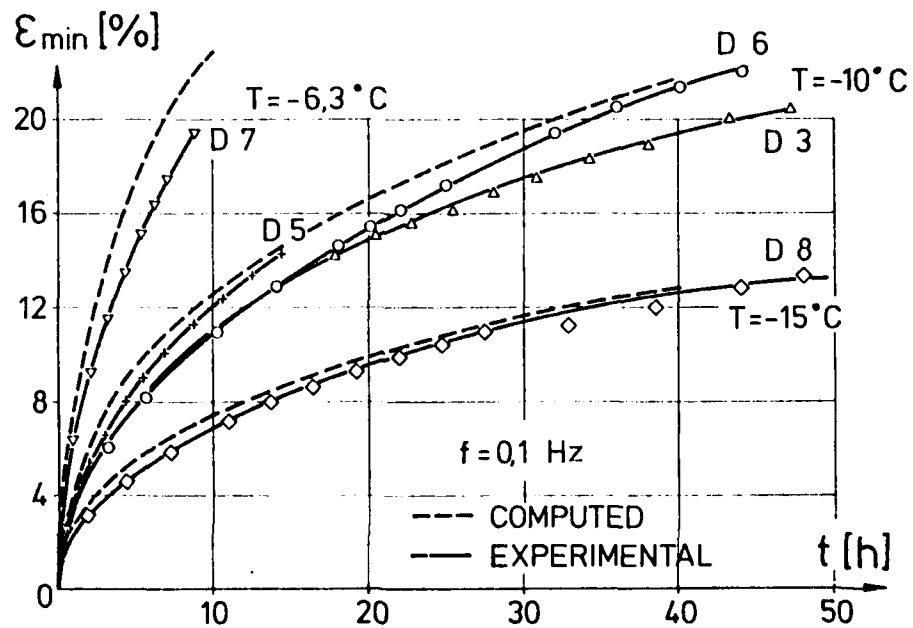
Fig. 6: Effect of temperature on the creep behaviour

In extension of Norton's power law developed for high temperature metallurgy the test results are taken to formulate the following empirical relation.

$$\varepsilon_{min} = D \cdot |T|^G \cdot (\tfrac{1}{f})^E \cdot t^F$$

ε_{min} : minimal vertical strain

T : temperature in °C

f : frequency in Hz

t : time in hours

The following material parameters are found from the test results:

$$D = 0,6698 \left[(°C)^{-G} \cdot (Hz)^E \cdot h^{-F} \right]$$

$$G = -1,9266$$

$$E = 0,176$$

$$F = 0,395$$

The relationship given above is only valid for f > 0 Hz, T < 0°C.

The dotted lines of Fig. 5 and 6 are representing the application of the above given relationship to the investigated saline frozen soil. Obviously there is a very good correlation between test results and calculation.

The Modulus of dynamic deformation characterizes the deformation behaviour of the frozen soil under investigation. From Fig. 7 the strong influence of frequency on the Modulus of dynamic deformation is obvious. It should be emphasized that these curves are valid for specimen temperature of -10°C and also for the test conditions of Fig. 2. The tests also showed that temperature which is in the range of -5 to -15°C has a minor influence on the Modulus of dynamic deformation $\tilde{E}$. But with increasing load frequency the deformation Modulus $\tilde{E}$ increases. This finding is in good agreement with the results reported by Vinson et al. (1978).

CONCLUSION

A series of dynamic triaxial tests was performed to study the deformation behaviour of frozen soil samples loaded dynamically. Fine sand samples of 3 % salinity with 10 cm diameter and 20 cm height were tested at temperatures between -6,3 and -15°C. The dynamic stress path was chosen with respect to stress conditions within a frozen soil mass loaded by dynamic ice forces.
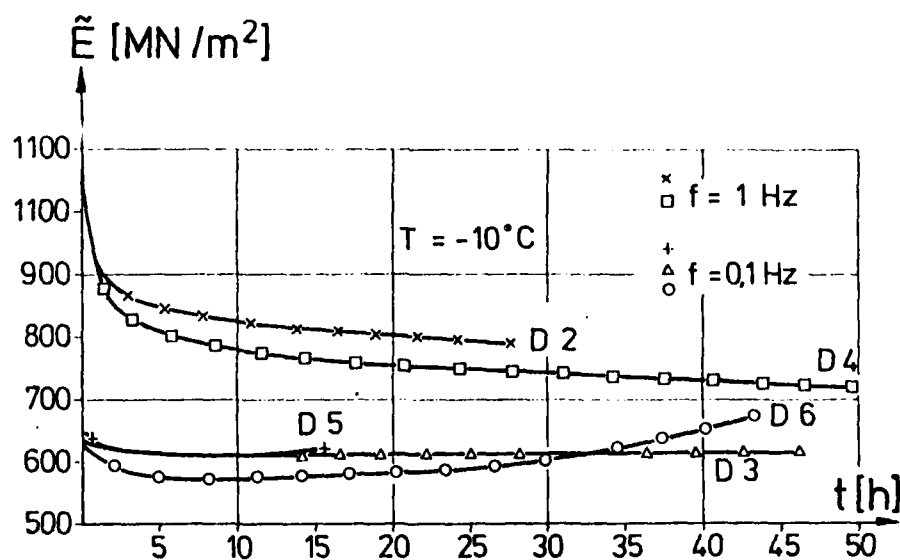
Fig. 7:Modulus of dynamic deformation versus time

24

It was found that the load frequency has strong influence on the deformation behaviour of the material under investigation in that way, that with increasing frequency the Modulus of dynamic deformation increases while the time dependent remaining deformation is decreasing. Within the test period of 50 hours all samples show a decreasing strain rate which means that the tertiary phase was not reached.

ACKNOWLEDGEMENT

REFERENCES

Anonymus (1981), Offshore Engineer Arctic Supplement, August, p. 17

Croasdale, K.R., Marcellus, R.W. (1981), Ice Forces on Large Marine Structures, IAHR, International Symposium on Ice, July 27-31, Québec, Canada, pp. 607-617

Klein, J. (1978), Nichtlineares Kriechen von künstlich gefrorenem Emscher Mergel, Schriftenreihe Institut für Grundbau, Wasser- und Verkehrswesen, Serie Grundbau, Ruhr-Universität Bochum, Heft 2

Kry, P.R. (1979), Implications of Structure Width for Design Ice Forces, IUTAM Symposium "Physics and Mechanics of Ice", Copenhagen

Matlock, H., Dawkins, W.P., Panak, J.J. (1969), A Model for the Prediction of Ice-Structure Interaction, Offshore Technology Conference, Dallas, OTC 1066, pp. 687-694

Metge, M., Danielewicz, B., Hoare, R. (1981), On Measuring Large Scale Ice Forces; Hans Island 1980, The 6th International Conference on Port and Ocean Engineering under Arctic Conditions, Vd. II, July 27-31, Québec, Canada, pp. 629-642

Vinson, T.S., Chaichanavong, T. and Czajkowski (1978), Behaviour of Frozen Clay under Cyclic Axial Loading, Journal of the Geotechnical Engineering Division, ASCE, GT7, July, pp. 779-800

BOND AND SLIP OF STEEL BARS
IN FROZEN SAND

O. B. Andersland, Professor of Civil Engineering, Michigan State University,
                   East Lansing, Michigan, USA
M. R. M. Alwahhab, Graduate Research Assistant, Michigan State University,
                   East Lansing, Michigan, USA

ABSTRACT

A frozen soil mass (beam) subjected to an external bending moment may fail because of a weakness in tensile strength. Use of tension reinforcement members introduces questions relative to load transfer at the interface with frozen soil. Bond at the interface can be described as the shearing stress or force between the reinforcement member and surrounding frozen sand. This experimental study involved measurement of three bond components — ice adhesion, friction, and mechanical interaction between frozen sand and bar surface roughness. Initially, adhesion combined with friction prevents slip. After adhesion is broken and partial slip has occurred, a small residual value for adhesion and friction controls the pull-out load. Introduction of bearing action of frozen sand on a single lug greatly increased the pull-out load. This load can be estimated using a steady displacement rate equation based on cavity expansion theory. Data presented include the effects of loading and displacement rates, temperature, bar size, and lug size on the pull-out load.

INTRODUCTION

Design of frozen soil structures requires that suitable criteria be available for selection of allowable stresses in the frozen earth. A frozen soil mass (beam) subjected to an external bending moment may fail because of a weakness in tensile strength. Introduction of tension reinforcement, either rods or structural members, leads to questions relative to load transfer at the interface with frozen soil. Bond at the interface can be described as the shearing stress or force between the reinforcement member and surrounding soil. Bond includes three components: (a) ice adhesion, (b) friction, and (c) mechanical interaction between frozen soil and surface roughness of the reinforcement member. Bond of plain bars depends primarily on the first two components. Bond with deformed bars depends primarily on mechanical interlocking.

This experimental study involved measurement of ice adhesion, friction and mechanical interaction between frozen sand and surface roughness of steel bars. Test variables affecting results of pull-out tests included bar displacement or loading rate, temperature, bar size, and lug size. Initially, adhesion of ice to the steel bar prevents slip. As displacement increased, friction and mechanical interaction contributed to the pull-out load. When a single lug was added to the bar, bearing action of frozen sand on the lug restrained bar movement giving rise to a much larger pull-out load. Comparisons are made between observed pull-out loads and predicted lug bearing on frozen sand based on cavity expansion theory. Experimental data are summarized in terms of the test variables.

SPECIMENS AND PROCEDURES

Pull-out Specimens. The frozen sand pull-out sample shown in Figure 1 was 152 mm in diameter by 152 mm high and consisted of Wedron sand frozen around a steel bar centered vertically in the mold. The sand consisted of subangular quartz particles with a uniform gradation (size range of 105 μm to 595 μm)

and a coefficient of uniformity equal to 1.50. All samples were prepared in split steel molds with a sand volume fraction close to 64 percent based on preweighed sand quantities. This density was comparable to values normally encountered in the field and insured the development of dilatancy and interparticle friction in front of the lugs. To insure a high degree of ice saturation (about 97 %), molds were partially filled with distilled water and sand was slowly poured into the water permitting air bubbles to escape to the surface. The sample was tamped to give the desired packing. All samples were frozen at close to -20 °C for about 12 hours. After removal from the mold, rubber membranes (double thickness) were placed, as shown in Figure 1, to protect the frozen sample during immersion in the circulating anti-freeze/water coolant mixture. Data read-out from the thermistor embedded in the frozen sample told when sample temperatures were ready for testing.

Smooth cold rolled steel bars with diameters of 2.38, 4.76, 9.52, and 15.87 mm were frozen into the sand samples. A threaded portion at both bar ends permitted easy hook-up to a reaction hook at the bottom of the coolant tank and mounting of a displacement transducer at the upper bar end (Figure 1). Lugs welded to the 9.52 mm diameter bar, shown in Figure 2b, included heights, h, of 1.59, 3.17, and 4.76 mm and a length, L, of 12.7 mm. Lug heights were limited to 4.76 mm so as to avoid failure in the 9.52 mm steel bar. Clearance between the bar and reaction plate was maintained at close to 1.6 mm for all bar diameters by use of a removeable steel washer in the reaction plate.

Test Procedure. Both constant displacement rate and constant load (creep) pull-out tests were conducted using the loading frame shown in Figure 1. During the pull-out test a constant displacement rate was maintained by a Graham variable speed gear box mounted on a 44.5 kN (10 kip) capacity Soiltest load frame. The same Soiltest load frame with a lever system and dead weights was used for the constant load (creep) pull-out tests. Movement of the bar relative to the lower reaction plate and soil sample was monitored using a displacement transducer mounted on the bar above the coolant liquid with the core mounted on a rod extending down to the reaction plate. Loads were monitored by the force transducer attached to the top of the loading frame
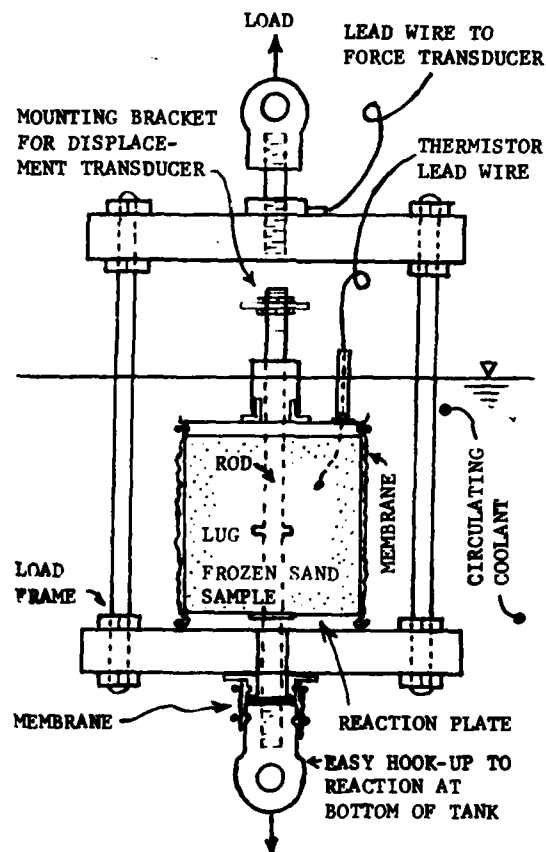
Figure 1. Equipment for pull-out tests including sample, steel rod with lug, and loading frame immersed in the circulating coolant.

shown in Figure 1. Sample temperatures were controlled by circulating an anti-freeze/water coolant mixture from an external refrigerated bath around the protected sample and loading frame.

EXPERIMENTAL RESULTS

Pull-out tests included two types, (1) constant displacement rate and (2) constant load (creep), on a frozen Wedron sand with ice saturation close to 97 percent. Load displacement curves for smooth 15.87 mm bars at several temperatures and a displacement rate of 11.4 um/min are shown in Figure 3. In all cases the maximum load developed at very small displacements, about 20 to 50 μm. At rupture a small bar displacement occurred and the load may drop to zero before development of a residual load. Colder temperatures increased both the maximum and residual loads. Experimental data from tests on smooth bars at other loading rates and

28

38 mm | 305 mm | 38 mm

(a) BAR DIAMETER

(b) LUG LENGTH, L | LUG HEIGHT, h
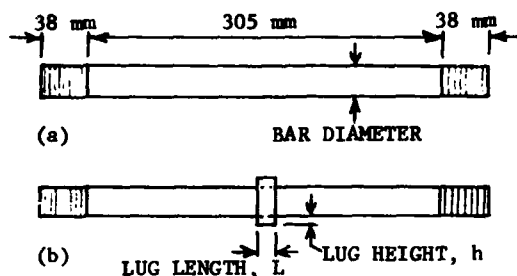
Figure 2. Bar configuration. a) Smooth bar. b) Smooth bar with 90-degree lug.

bar sizes are included later in the discussion section. Data for constant load (creep) tests on smooth bars were not available when this paper was written.

For smooth bars adhesion and friction are primarily responsible for development of the pull-out load. To increase mechanical interaction a single 3.17 mm lug was welded to the 9.52 mm bar as

shown in Figure 2b. Load displacement curves for this bar and lug combination are summarized in Figure 4. Colder temperatures again increased the pull-out loads. The displacement curves show the same initial behavior characteristic of smooth bars followed by a drop or reduced rate of load increase. Additional lug displacement mobilizes frictional and dilatancy strength components of the frozen sand in front of the lugs leading to increased pull-out loads. The ultimate load developed at displacements close to 5 mm followed by a relatively constant load. Bar slip with lugs can occur in two ways: (1) the lugs can push frozen soil away from the bar (wedging action), and (2) densification can occur in front of the lugs. For the sample size shown in Figure 1, 152 mm diameter by 152 mm height, only densification was observed with pressures at higher pull-out loads sufficient to crush the quartz sand in a small zone in front of the lugs. Data for other lug sizes are given in the discussion section.

Constant load (creep) pull-out tests conducted on the frozen sand using a smooth 9.52 mm bar with a single 3.17 mm lug (Figure 2b) provided the data summarized in Figure 5. A step loading procedure with time intervals sufficient to permit development of steady state creep provided more data per soil sample. More time was usually required on the first load increment to insure development of steady state creep. Increased densification of frozen sand in front of the lug along with some redistribution of ice through pressure melting, water flow to adjacent regions of lower stress, and refreezing explains
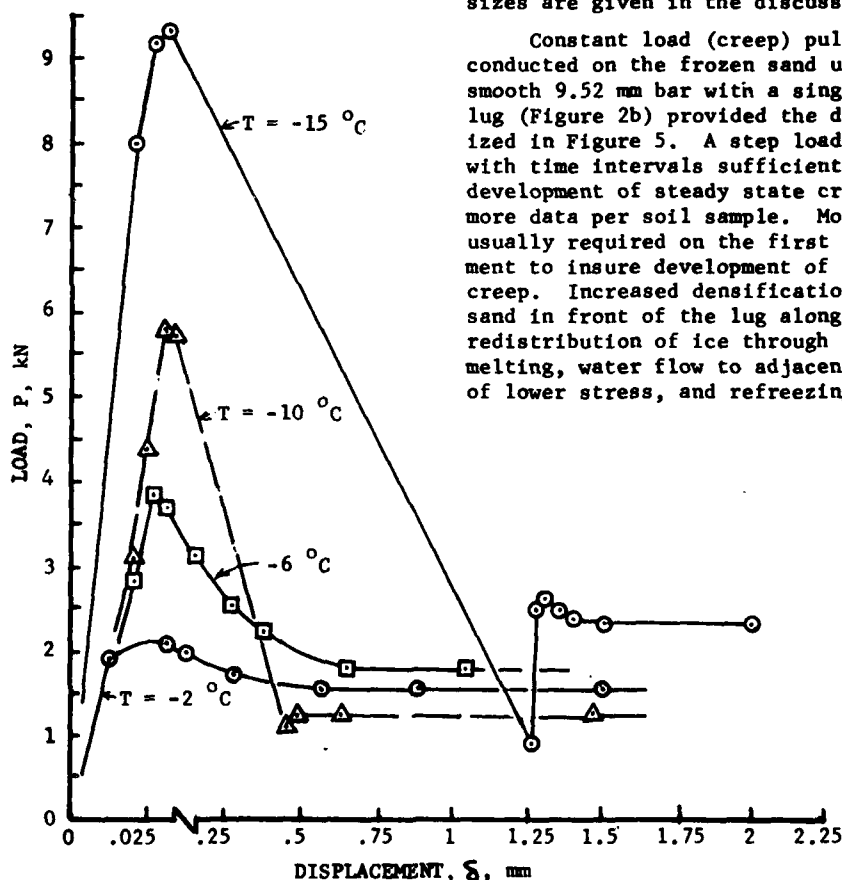
Figure 3. Load-displacement curves for smooth 15.9-mm bars in frozen sand at several temperatures and a displacement rate of 11.4 μm/min (data from Alwahhab, 1982).

29
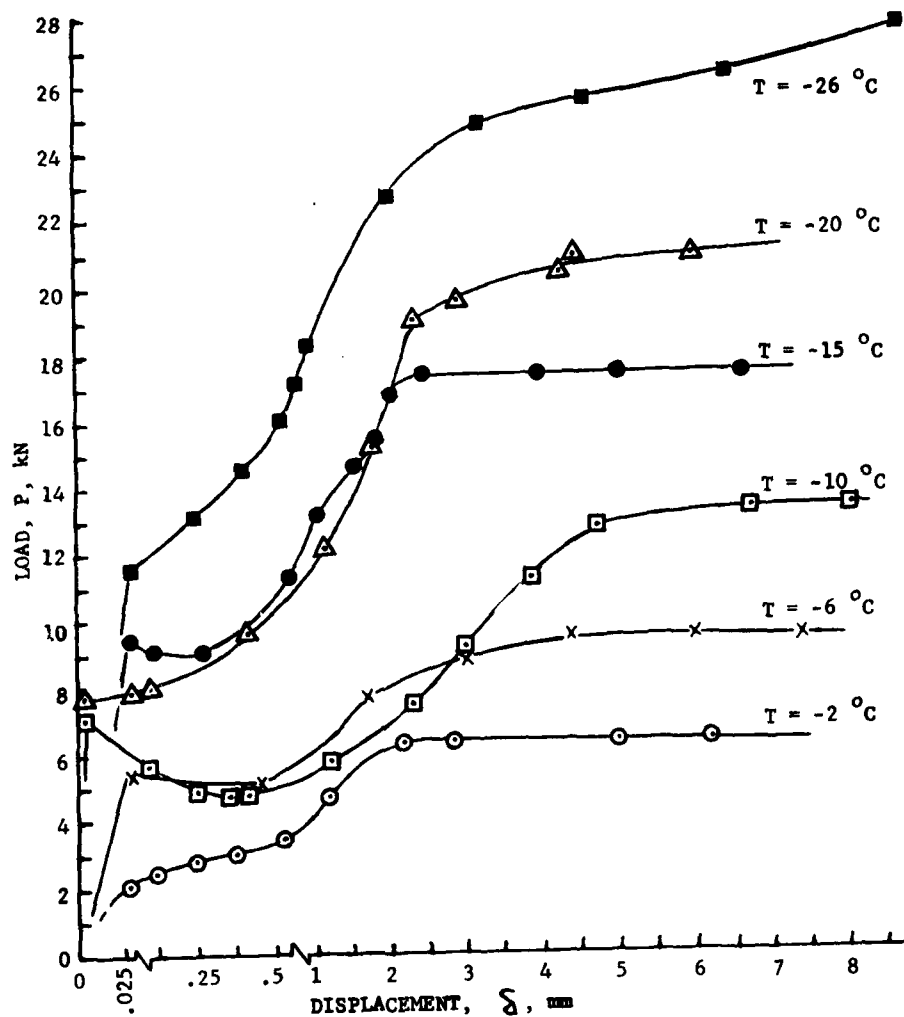
Figure 4. Load-displacement curves for smooth 9.52-mm bars with a 3.17-mm lug in frozen sand at several temperatures and a displacement rate of 11.4 μm/min. (data from Alwahhab, 1982).

some of the mechanisms operating during the creep pull-out test. At higher creep loads sand particles in front of the lug were crushed giving a small zone containing quartz powder. A failure strain (start of tertiary creep) was not observed within the displacement limits (about 35 mm) of the loading frame (Figure 1). Creep pull-out test data are summarized in the discussion section.

DISCUSSION

Bond Components. Load transfer at the interface between tension reinforcement members and frozen sand includes three components: (1) adhesion of ice to the steel bar, (2) friction between sand particles and steel, and (3) mechanical

interaction between frozen sand and roughness of the bar surface. Single lugs were welded to smooth bars to increase mechanical interaction. A comparison of load displacement curves (Figure 6) for a 9.52 mm smooth bar in polycrystalline ice and frozen sand and a duplicate bar with a 3.17 mm lug height in frozen sand provides information on the contribution by each bond component. Ice adhesion tolerates very little bar displacement with rupture occurring for displacements less than 50 μm. A residual adhesion develops after rupture and equals less than 5 percent of the initial value in Figure 6. Friction between sand particles and the bar adds to the pull-out load at all displacements. The rigid quartz particles embedded in

30
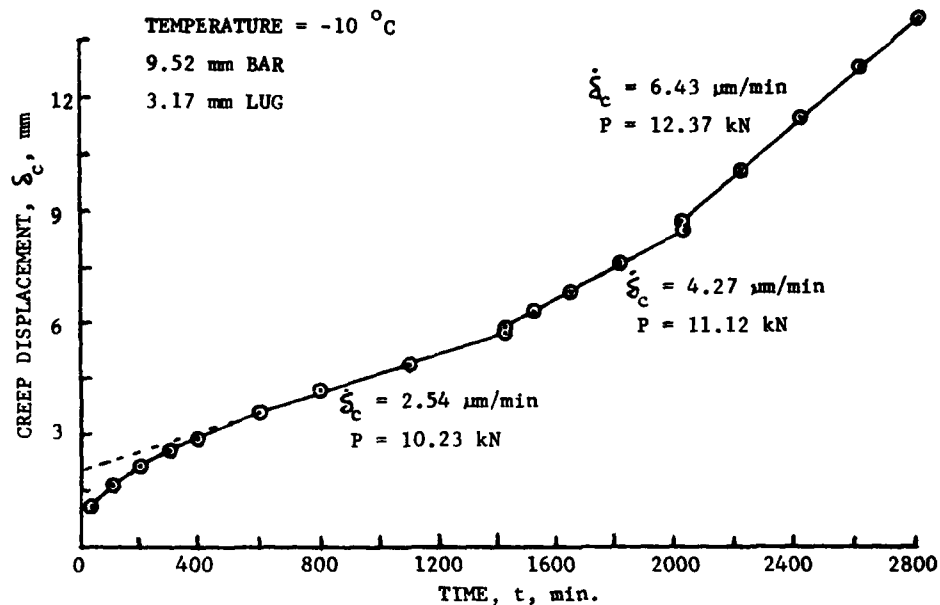
Figure 5. Constant load (creep) curves for step loading on a smooth 9.52-mm bar with a 3.2-mm lug in frozen sand at -10°C (data from Alwahhab, 1982).

the ice matrix appeared to add to the initial adhesion and after rupture added to the residual pull-out load. It appears reasonable to separate ice adhesion and sand friction as shown in Figure 6

Introduction of the single lug on the smooth bar increased both the initial and ultimate pull-out loads for the frozen sand. The lug requires that a larger por-

tion of ice matrix and embedded sand particles be disturbed before the initial rupture will occur. This increase over the load with no lug, shown in Figure 6, was close to 75 percent. After rupture the load decreased until friction and dilatancy components of sand in front of the lug were mobilized by lug displacement. The pull-out load increased to an
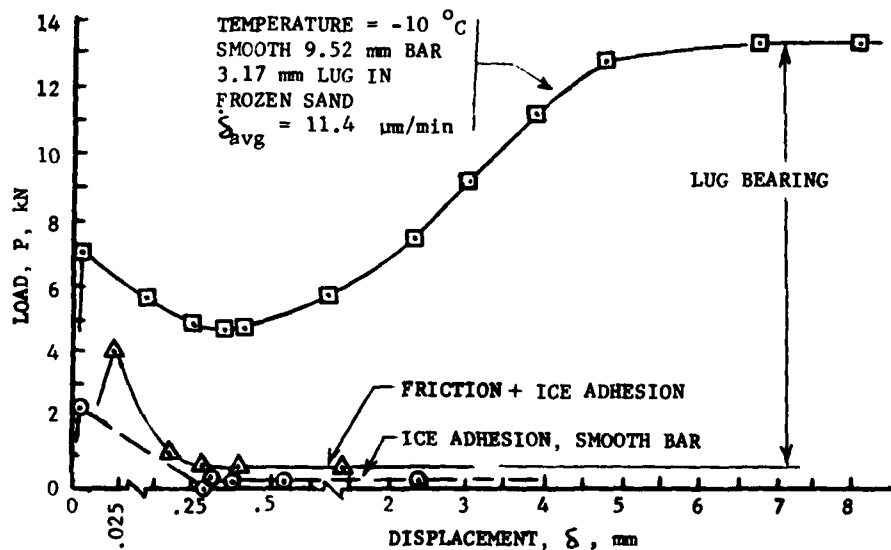
Figure 6. Load-displacement curves showing the contribution of ice adhesion, friction, and lug bearing to the ultimate pull-out capacity (data from Alwahhab, 1982).

31

ultimate value close to 5 mm displacement followed by a relatively constant load. The mechanical interaction (lug bearing) appeared to be the contribution after adhesion and friction were subtracted from the ultimate load. For this sample at -10 °C the pressure on the lug at the ultimate pull-out load was about 102.5 MPa (14,871 psi).

Temperature and Loading Rate Effects. The bond components — adhesion, friction, and mechanical interaction — all increased with colder temperatures and increasing loading rates as shown in Figures 3, 4, and 7. The ultimate bond strengths reported in Figure 7 are average values with individual data points interpolated to the given loading rate on the basis of strength versus loading rate curves. A uniform stress was assumed along the entire embedded portion of the bar at the ultimate pull-out load. The bond strength for the smooth bars (Figure 7) shows a linear relationship with temperature at the slow 25 N/min loading rate. At higher loading rates strength increased more rapidly with decrease in temperature down to -5 °C. At colder temperatures the increase in strength was similar to that for the slower loading rates. Preliminary data for constant load (creep) pull-out

tests on smooth bars with lugs suggest a temperature dependence similar to that observed for uniaxial compression tests on frozen sand.

Lug Size. The influence of lug size on pull-out loads for frozen sand was determined using three 9.52 mm smooth bars, each with lug heights of 1.59, 3.17, and 4.76 mm, respectively. Constant displacement rate (δ_{avg}= 12.5 μm/min) pull-out tests provided the data summarized in Figure 8 showing ultimate loads as a function of the ratio of lug area divided by bar area. The curves do not pass thru the origin because total loads plotted include ice adhesion, surface friction, and mechanical interaction with bar surface roughness. The lug contribution equals the ultimate load less the residual adhesion and friction developed at larger displacements. The curves show that the ultimate loads do not increase in a linear proportion to increase in lug area. A temperature decrease from -10 °C to -20°C significantly increased the lug contribution to the ultimate pull-out load.

Data for constant load (creep) pull-out tests are summarized in Figure 9 with load and displacement (creep) rates both plotted on logarithmic scales. A step
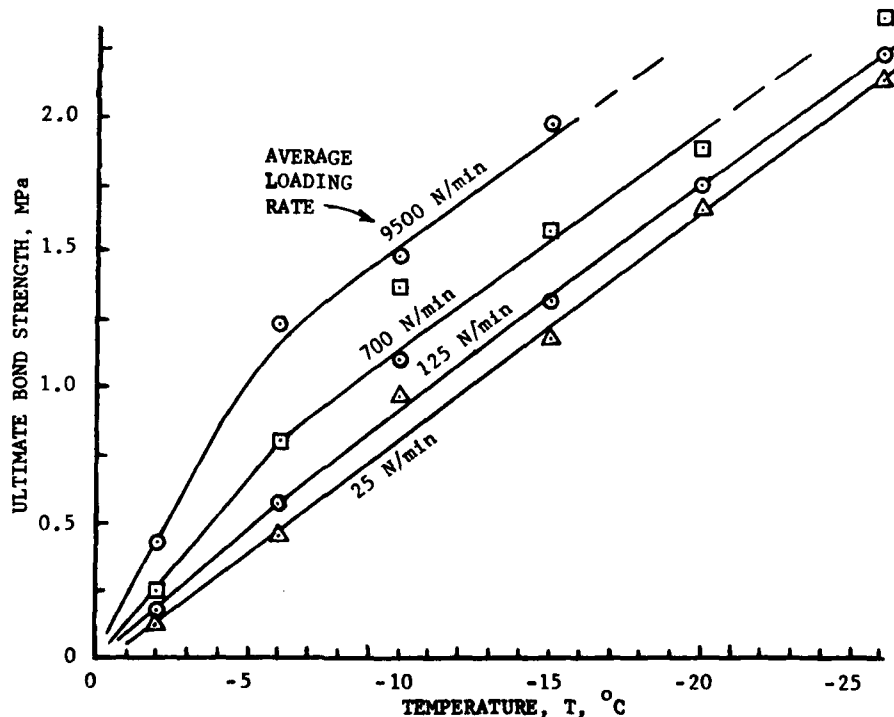
Figure 7. Temperature and loading rate effects on the bond strength of frozen sand to a smooth 15.87-mm steel bar (data from Alwahhab, 1982).

32
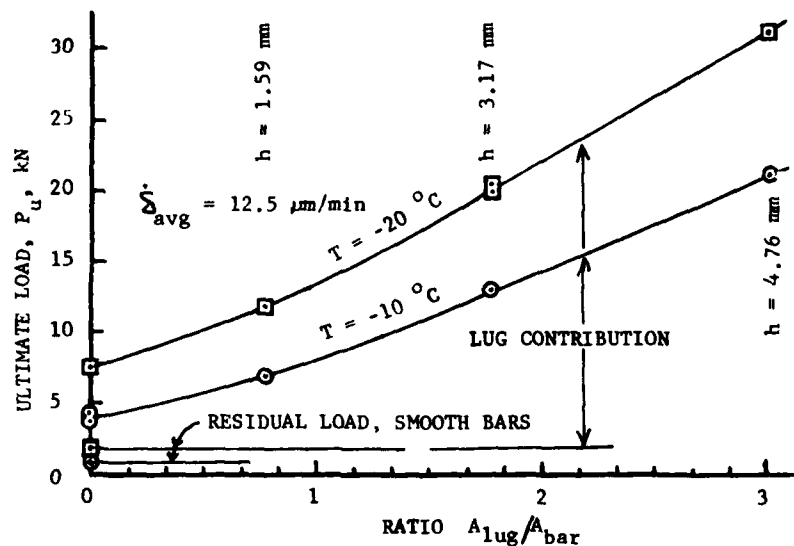
Figure 8. Lug size (height) effect on the ultimate pull-out load of smooth 9.52-mm bars with 90-degree lugs in frozen sand (data from Alwahhab, 1982).

loading procedure permitted several data points to be obtained for each test. The data suggested a straight line relationship for each lug size, and since the displacement mechanisms in the frozen soil should be similar, it appeared reasonable that the lines would be parallel. The dark data points in Figure 9 represent the first load increment for the step loading procedure illustrated in Figure 3. Straight line relationships indicate that the data points from additional load increments are equivalent to single step load creep tests. Some data scatter, especially for the first step load, appears to be due to insufficient time for

steady state creep to develop. This would cause observed creep rates to fall to the right of the correct creep rates which appears to be the case for several data points in Figure 9. A comparison of pull-out loads for a displacement rate of 12.5 μm/min shows 12.81 kN for the constant displacement rate test and 14.23 kN for the constant load (creep) test. This difference, about 1.42 kN, appears to develop because of greater sand densification in front of the lug with the creep type of pull-out test.

Pull-out Load Prediction. The pull-out load for a smooth bar and single lug
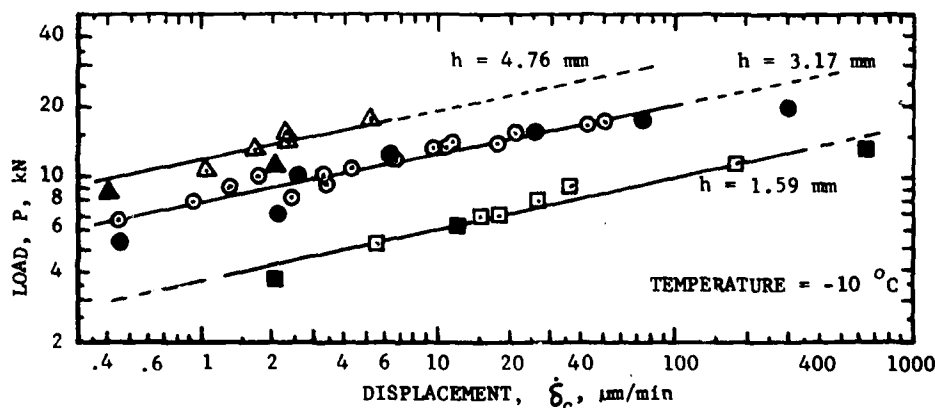
Figure 9. Lug size (height) effect on load displacement rate curves for creep tests with smooth 9.52-mm bars and 90-degree lugs in frozen sand at -10°C (data from Alwahhab, 1982).

33

can be estimated using cavity expansion theory (Ladanyi and Johnston, 1974). Visualize the pull-out load (lug bearing) as the difference in bearing capacity of two concentric circular footings with radius of the smaller footing r_1 equal to that of the bar and radius of the larger footing r_2 equal to that of the bar plus lug height. Neglect the small residual ice adhesion and friction between the smooth bar and sand particles. Consider, for example, a displacement (creep) rate $\dot{\delta}_c =$ 25.4 μm/min corresponding to a 3.17 mm lug and observed pull-out load on Figure 9. Mechanical properties for the quartz sand (Bragg, 1980) include a proof stress in uniaxial compression $\sigma_{cu\theta}$ = 12.928 MPa (1875 psi) at -10 $^\circ$C, arbitrary strain rate $\dot{\varepsilon}_c$ = 6 x 10^{-5} min^{-1}, creep parameter n = 11.765, a failure strain ε_f = 0.06 observed to be independent of temperature and strain rate, and an angle of internal friction ϕ = 30 degrees with flow value $N_\phi = (1 + \sin\phi)(1 - \sin\phi)^{-1}$ equal to 3.0. The footing (lug) pressure q may be computed by substituting values into the steady settlement rate equation:

$$\dot{\varepsilon}_c = \frac{A}{2}\left[\frac{3}{2\,n}\ (q - p_o - \eta c)\right]^n \qquad (1)$$

where the term $A = \dot{\varepsilon}_c/\sigma_{cu\theta}^n$ = 5.023x10^{-18}, degree of friction mobilization η = 1, confining pressure p_o = 0, and cohesion

$c = \left(\sigma_{cu\theta}/2N_\phi\right)\left(\varepsilon_f / t_f\ \dot{\varepsilon}_c\right)^{1/n}$ equals

4.454 MPa. The time to failure $t_f = \delta_f/\dot{\delta}_c$ = 0.2 (2 r_2)/$\dot{\delta}_c$ = 125 min. Compute the lug pressure q = 134 MPa. Using the lug area (1.267 x 10^{-4} m^2) gives the pull-out load P = (1.267 x 10^{-4}) 134 = 17 kN. Comparing 17 kN with the measured value of 15.84 kN indicates reasonable agreement. The difference between predicted and observed pull-out loads may be due to (1) inaccuracies in measurement of the steady displacement rate for the lug, (2) differences in shape factor for a circular footing versus the ring lug bearing, and (3) the assumed failure displacement equal to 20 percent of the lug (footing) diameter. Additional studies are currently in progress.

CONCLUSIONS

1. Bond between frozen sand and steel bars includes ice adhesion, surface friction between sand particles and the steel bar, and mechanical interaction between sand and lugs welded to the bar. Ice adhesion ruptures for bar displacements approaching 50 μm or less. About 5 mm bar displacement was required to mobilize particle friction and dilatancy in front of the lugs.

2. Colder temperatures and larger displacement or loading rates both increased the bond components — ice adhesion, friction, and mechanical interaction. Experimental relationships were determined for temperatures of -2 $^\circ$C to -20 $^\circ$C and constant loading rates ranging from 25 N/min to 9500 N/min.

3. Observed ultimate pull-out loads for smooth bars with lugs was greater for constant load (creep) tests as compared to constant displacement rate tests. The difference appears to be a result of greater sand densification in front of the lugs during the creep process.

4. Mechanical interaction between frozen sand and lugs on smooth steel bars produces a pull-out load which can be estimated using a steady displacement rate relationship based on cavity expansion theory. Comparisons of predicted and observed pull-out loads were in reasonable agreement.

REFERENCES

1. Alwahhab, M.R.M., "Bond and slip of steel bars in frozen sand," unpublished Ph.D. thesis, Michigan State University, East Lansing (in preparation, 1982).

2. Bragg, Richard A., "Material properties for sand-ice structural systems," unpublished Ph.D. thesis, Michigan State University, East Lansing, 1980.

3. Ladanyi, B., and Johnston, G.H., "Behavior of circular footings and plate anchors in permafrost," Canadian Geotechnical Journal, Vol. 11, No. 4, 531-553, 1974.

EXCAVATION RESISTANCE OF
ARTIFICIALLY FROZEN SOILS

Arvind Phukan, Assoc. Professor
Civil Engineering, University of Alaska
Shinji Takasugi, Graduate Research
Student, University of Alaska

ABSTRACT

The ground freezing techniques which are often used to stabilize "troublesome" earth materials may be involved in the excavation of artificially frozen soils. It is very important to determine the excavation resistance of these soils at different temperatures so that an appropriate excavation cutting machine may be built to handle such civil engineering construction problems.

This paper presents the results of a systematic laboratory study on the excavation resistance of artificially frozen sand and silt. An apparatus is developed to simulate the field excavation technique in the laboratory. Frozen sand and silt soil samples at different temperatures, -3°C to -14.5°C (5.9°F to 26.6°F) are tested at different rake angles, cutting depths and cutting tool widths. Relationships are found for the cutting resistance against rake angles and cutting depths at different freezing temperatures.

The studies show that a critical rake angle approximately 35° at which the tangential resistance is minimal, exists for frozen silt at a particular freezing temperature. This tangential resistance increases with lower temperatures of frozen silt. The testing of frozen Ottawa sand and concrete sand did not show such a relationship. The failure characteristics of frozen sand and silt were also different during the cutting process. Triaxial tests were also carried out on the artificially frozen sands and silts at different temperatures. These results are compared with the failure criteria obtained during the cutting process. The results of this study may be used efficiently to design machine cutting tools for the excavation of artificially frozen soils.

1.0 INTRODUCTION

Various investigators (Ref. 1,2,3,4 and 5) reported the results of theoretical as well as experimental studies on the mechanics of cutting soils and rocks under different parameters such as width of tool, rake angle, cutting depth, speed and so on. However, little data is available on the cutting characteristics of frozen soils. As the artificially freezing technique is becoming popular to stabilize many "troublesome" earth materials, the excavation or cutting of frozen soils is of great importance to designers and construction engineers.

Based on failure characteristics of frozen soils under different temperatures it will be useful to examine excavation techniques which will face least resistance to frozen soils.

This paper presents the results of a systematic laboratory study on the excavation resistance of artificially frozen sand and silt with temperatures varying from -3°C to -14.5°C. Relationships are obtained between rake angle, resistance and cutting depth for these soils at different freezing temperatures. The failure characteristics of frozen silts and sands under the simulated excavation technique are evaluated. Shear strength parameters obtained from the standard triaxial tests are compared with the cutting process.

Based on laboratory studies, it is envisioned that effective cutting tools may be designed to excavate frozen soils.

2.0 LABORATORY STUDY

2.1 Apparatus and Test Procedure

The laboratory studies were carried out with an apparatus which was designed by the authors and built at the Geophysical Institute's workshop. A photographic picture of the apparatus is shown in Fig. 1. The apparatus consists of a box 8"x 10"x4" resting on two screw-driven tracks and a cutting tool which is mounted on bolts and plate frame arrangements. Samples are placed in the box which is insulated except for the top and the cutting side of the sample. A variable speed motor is mounted to drive the sample box toward the cutting tool, whose orientation may be changed to meet the required cutting depth.
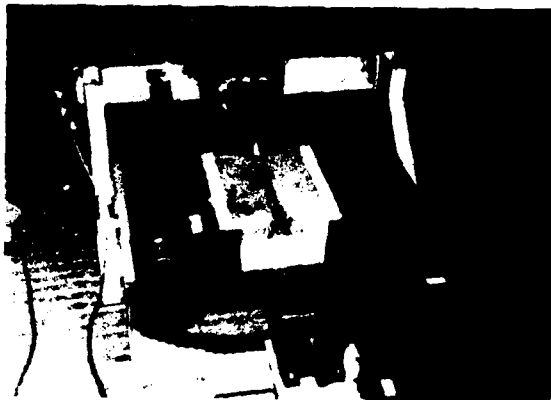
Figure 1.
Photographic View
of Apparatus

Initially, the sample is placed in the cold room for 24 hours to attain the required test temperature. The temperature of the cold room is monitored until a constant desired temperature (±0.5°C) is obtained. After a duration of 8 hours constant temperature, the prepared sample is tested at a speed of around 0.1"/sec. An automatic chart recorder is used to monitor the tangential (RH) and normal resistance (R_v) of frozen soil as the sample was moved against the cutting tool.

Cutting depths and rake angles were varied to test different samples at different freezing temperatures varying from -3° to -14.5°C.

After the test, the failure characteristics of the tested sample were noted and photographed. The test duration varies from 2 to 4 hours. Four different tools were used and their descriptions are illustrated in Fig. 2(a). Also, the tool widths were varied and a relationship between the resistance the the tool width was obtained (Ref. Fig. 2(b)) to determine the desired cutting width of the tool for the experimental studies.

a) CUTTING TOOL DESCRIPTION

b) CUTTING TOOL WIDTH
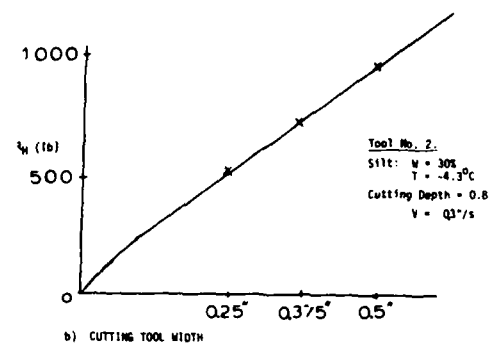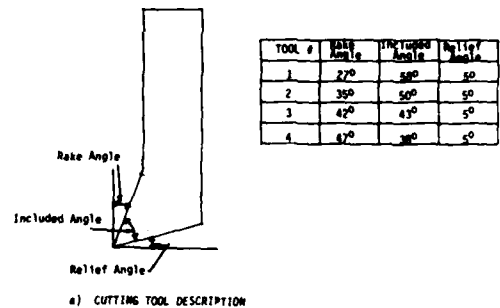
FIG. 2

2.2 TEST RESULTS

Two types of sands, Ottawa sand and concrete sand, were tested at the freezing temperature of -10.1°C. The gradation of tested sands is given in Table 1. The resistance obtained at different cutting depths with varying tools for the tested sands is presented in Fig. 3(a). Figure 3(b) illustrates the relationship between the rake angle, the tangential resistance (R_H) and normal resistance (R_v) of Ottawa sand at a cutting depth of 0.6 inch. Experimental results on silt samples tested at temperatures of -3.0°C, -8.3°C and -14.5°C are shown in Figures 4 through 9. Figures 4, 6 and 8 show the relationship between the resistance and the cutting depth with varying cutting tools at different temperatures. The critical relationship between the rake angle and the re-

36
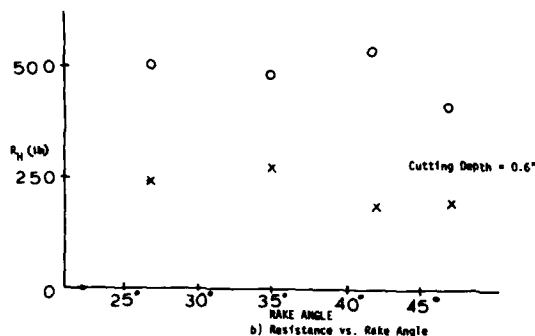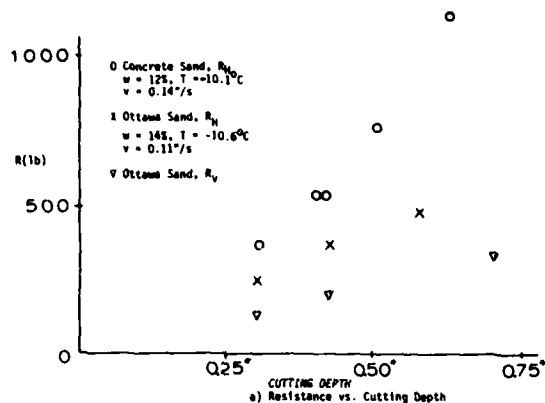
Figure 3.

Figure 4.

sistance at a particular cutting depth (around 0.6 inch) for the tested silt samples is presented in Figures 5, 7, 9.

Typical resistances of frozen samples during a cutting travel are illustrated in Fig. 10.

Table 1. Gradation of Sands

Particle Size(mm)	Concrete Sand	Ottawa Sand
	% Passing	
2	74	100
1.19	66	100
0.42	50	36
0.177	7	1.8
0.075	0.2	-

Figure 5.

Figure 6.

37
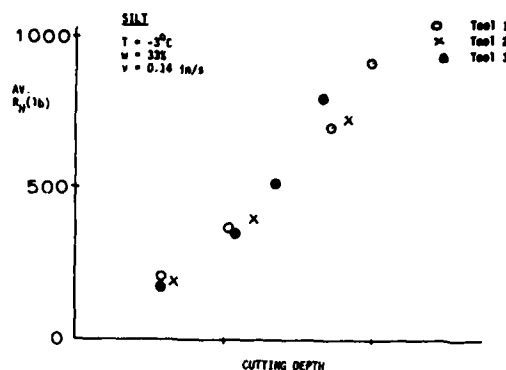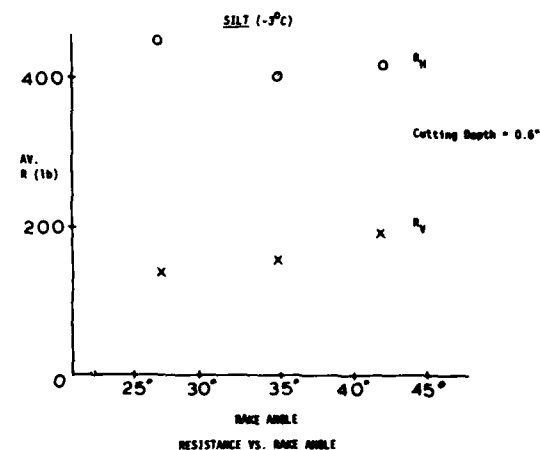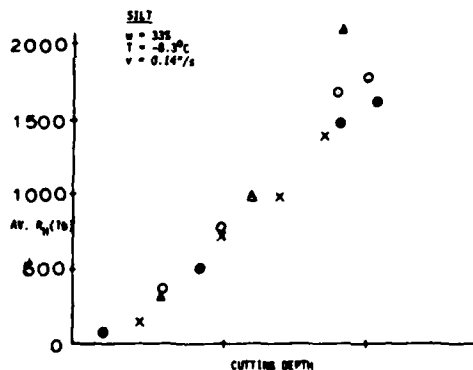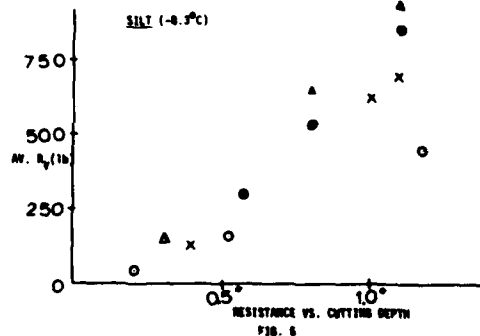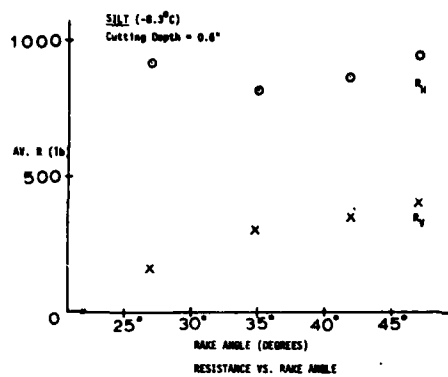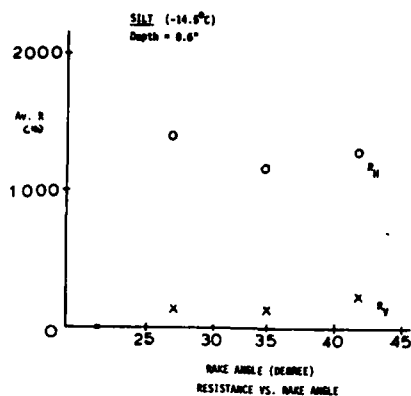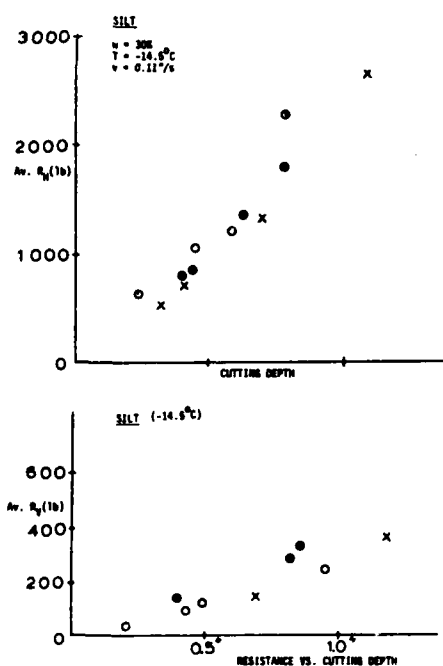
Figure 7.

Figure 9.

Figure 8.
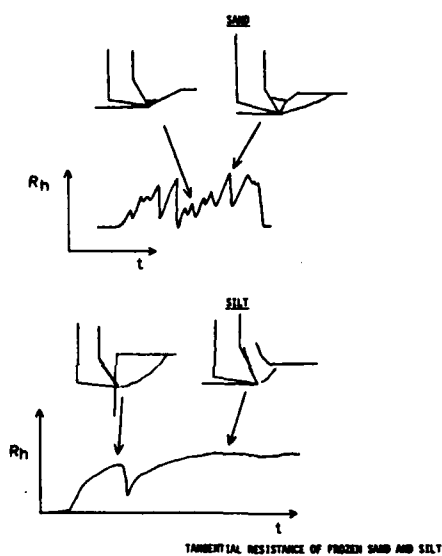
Figure 10.

3.0 DISCUSSION AND CONCLUSIONS

Excavation resistances of artificially frozen sands and silts at different freezing temperatures show a unique pattern. It appeared from the tested results of Ottawa sand that the rake angle is independent of cutting resistance at a particular cutting depth (Ref. Fig. 3(b)). Obviously, the cutting resistance of concrete sand is much higher than Ottawa sand as illustrated in Fig. 3(a). This primarily is due to higher frictional resistance of concrete sand.

The tangential and normal resistance of silt vary with the temperature and cutting depth with different cutting tools. However, there is a critical rake angle at which the tangential resistance is minimum for a particular depth of cutting. This critical rake angle for stilt at temperatures of -3°C, -8.3°C and -14.5°C is found to be around 35° at a cutting depth of 0.6". The tangential resistance varies with the freezing temperature at this critical rake angle.

As illustrated in Fig. 10, cutting resistances offered by frozen sand and

38

Sand   Silt

Figure 11.   Failure Characteristics.

silt are different and consequently, the failure characteristics of tested frozen sand and silt are shown in Fig. 11.

Triaxial tests were carried out on frozen Ottawa sands and silts and the failure criteria obtained at different freezing temperatures were evaluated. These criteria are found to be inadequate to predict the failure conditions during the cutting process. As such, theoretical works are being carried out to formulate a failure predictive model during the cutting process in frozen soils. This theoretical evaluation is not included as it is beyond the scope of the paper.

It is concluded from this experimental study that:

(a) A unique excavation failure pattern exists for frozen sand and silt. Failure characteristics in sands appeared to be piece by piece, whereas in silts a progressive failure is generated.

(b) The cutting tool rake angle is a predominant factor for the excavation resistance of frozen silt and a critical rake angle may be obtained for a particular cutting depth. This critical rake angle is found to be approximately 35° for the tested silt samples at temperatures of -3°C, -8.3°C and -14.5°C.

(c) The failure criteria obtained from the triaxial tests on frozen sands and silts at different freezing temperatures show a much higher strength parameters than the cutting process. This is due to complex state of stress configuration generated during the cutting process.

(d) Last but not least, excavation tools may be designed to offer least resistance for excavations in frozen soils.

REFERENCES

1. Mellor, M., 1977. Mechanics of Cutting and Boring, Part IV: Dynamics and Energetics of Parallel Motion Tools, CRREL Report 77-7
2. Nishimatsu, Y., 1972. The Mechanics of Rock Cutting. Int. Journal of Rock Mechanics and Mining Sciences, Vol. 9, p. 261-270.
3. Roxborough, F.F., 1969. Rock Cutting Research, Tunnels and Tunnelling, Vol. 1, No. 3, p. 125
4. McKyes, E. and Ali, O.S., 1977. The Cutting of Soil by Narrow Blades, Journal of Terramechanics, Vol. 14, No. 2, pp. 43.
5. Harrison, W.L., 1972. Soil Failure Under Inclined Loads. CRREL Research Report 303, pp. 93.

CREEP BEHAVIOR AND STRENGTH
OF AN ARTIFICIALLY FROZEN SILT
UNDER TRIAXIAL STRESS STATE

Norbert Diekmann, Dipl. Ing., Department of Civil Engineering
Hans L. Jessberger, Prof.   Ruhr University Bochum
                              Federal Republic of Germany

ABSTRACT

Triaxial creep tests were performed with four different confining pressures and at three different soil temperatures to study the time and temperature-dependent stress-strain behavior and the strength of an artificially frozen sandy silt under triaxial stress state. The test equipment, the procedure for specimen preparation and testing is described. Creep and isochronic stress-strain curves are presented. The test data are inter- preted in relation to confining pressure, loading time, and soil temperature. The results show a strong effect of the con- finement on creep deformation and stress and strain at failure. A constitutive creep equation is proposed taking into consideration the effect of the confin- ing pressure on the non-linear time and temperature-dependent stress-strain be- havior of frozen soil.

HEAVING DEFORMATION AND THERMAL CREEP OF FROZEN, ICE-SATURATED, COARSE-GRAINED SOILS

N.A.Tsytovich,
Y.A.Kronik,
A.N.Gavrilov
Branch Research Laboratory
for Engineering Cryopedology
in Power-Plant Construction,
Kuibyshev Civil Engineering
Institute, Moscow, USSR

ANNOTATION. The present paper deals with the results of laboratory and field experimental investigations of heaving deformation and thermal creep of water-saturated gravelly gruss soils and rock fill in their freezing and thawing. These results were obtained by the authors in the period 1978-80 in the Branch Research Laboratory for Engineering Cryopedology in Power-Plant Construction of the USSR Ministry of Energy and the USSR Ministry of Higher Education. This laboratory is at the Kuibyshev Civil Engineering Institute and is under the general scientific supervision of Prof.N.A.Tsytovich, Corresponding Member of USSR Academy of Sciences.

A comparison is made between the deformative properties of artificially and naturally frozen ice-saturated coarse-grained soils having no fine-grained filler.

A description of the established laws of deformability of the soils being investigated is given on the basis of the thermal creep theory. Formulas are given for calculating the course of settlement of ice-saturated coarse-grained frozen soils with time. Also given are practical recommendations for determining the reference deformation and thermorheological characteristics of the soil being considered,and of rock-fill materials. Certain of the most important problems are formulated for further research in the fields of thermorheology and thermomechanics of frozen soils.

Under definite conditions,the freezing of water-saturated coarse-grained soils is accompanied by the heaving of the soil skeleton by the ice that is formed. As a result,the porosity of the soil is increased and its density is reduced. Such processes have frequently been observed,both in naturally freezing soils,as well as when they are artificially frozen [Kalabin, 1957; Gasanov,1969; Aidla,1961 and others]. There exists,at the same time,another widely held opinion,according to which such soils are not at all to be dealt with as heaving soils. These contradictory opinions indicate that the given problem has not yet been sufficiently investigated.

In this connection,experiments were conducted in the Branch Research Laboratory for Engineering Cryopedology in Power-Plant Construction,located at the Kuibyshev Civil Engineering Institute. The experiments,under the gene-

ral supervision of Prof. N. A. Tsytovich, Corresponding Member of the USSR Academy of Sciences, investigated the heaving deformation of moist coarse-grained soils in freezing, as well as their creep under load and under variable temperature conditions. The first results of this research are dealt with in the present paper.

The experiments were conducted under laboratory conditions on homogeneous gruss soils, consisting of fractions from 2 to 5mm in diameter and obtained by crushing larger cleaved pieces of Kolyma biotite granite, with the density (unit weight) γ_s=2.69 g/cm^3. The procedure for preparing the specimens consisted in layer-by-layer stacking of the material being investigated into the working chamber of an oedometer designed by the Research Sector of the Hydroproject Institute. The cross-sectional area of the chamber was 60 cm^2. The bottom of the instrument was hermetically sealed and the specimens were covered on top by a polythene film. The soil in the instruments was not compacted beforehand so that its porosity averaged about 0.47. The variation of porosity in various specimens did not exceed 10%. The degree of water saturation S_r of the specimens varied in a wide range from 0.38 to 0.99. This enabled the effect of the moisture content of coarse-grained soil with no silt filler on its heaving in freezing to be assessed. The freezing temperature in the experiments varied in the range from -2.9°C to -20.9°C.

In carrying out the experiments, the temperature in the cooling chamber was recorded, as well as the vertical deformation of the specimens. The latter was measured by dial-type indicators reading to 0.01mm.

The heaving of the coarse-grained soil was evaluated by the value of the heaving factor (F_h), which is the ratio of the absolute heaving deformation to the thickness of the freezing layer [Tsytovich and Kronik, 1970].

The obtained dependence of F_h on S_r is shown in Fig.1a, which
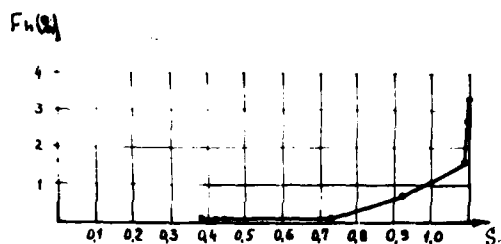
Fig.1. Dependence of the heaving factor on the degree of water saturation of gruss soils

indicates that the value of F_h in the range of variation of S_r from 0.38 to 0.9 is slight and does not exceed 0.5%. However, upon a further increase in S_r, above 0.9, the value of F_h increases sharply and, at a degree of water saturation close to unity (0.99), F_h reaches 3.2%. This puts the soils in the heaving category, according to the classification of Tsytovich and Kronik [1970] and requires that heaving be taken into account in assessing the deformation of surface and underground structures erected on such or similar soils subject to freezing. Taking into account the nonlinear nature of the relationship $F_h=f(S_r)$, the dependence being considered in the intervals S_r=0.38 to 0.74, 0.74 to 0.8, 0.8 to 0.99 and 0.99 to 1.0 can be approximated by piecewise-linear functions.

Owing to the small heaving deformation in the degree of water saturation ranging from 0.38 to 0.9, it can be neglected in this range in engineering practice.

Field investigations of the heaving process on coarse-grained soils, subject to wetting by meltwater and rain with subsequent natural freezing, were carried out on an experimental embankment of rock debris and lump granite material (rock fill). The granulometric composition of the embankment soil is listed in Table 1. The unit mass of the soil was 2.2 tonnes/m^3, and the porosity varied from 0.182 to 0.219. The initial height of the experimental embankment was about 11m.

44

Table 1

Size, cm	0 to 5	5 to 10	10 to 20	20 to 30	30 to 40	40 to 50	50 to 60	60 to 70	70 to 80	80 to 100	100 to 140
Percentage	17.2	6.3	10.3	10.9	8.2	10.5	9.7	4.3	9.8	7.2	6.6

Field observations were made during two seasons from September 1978 to September 1980. Recorded in these observations were the vertical deformation of the embankment and its soil base by taking readings on six depth marks, three of which (DM-I, II and III) being installed on the base and three on the first level of the embankment (see Fig.2a). Moreover, observations were recorded during the whole period of the temperatures and the rain and meltwater infiltrating the body of the structure. It should be pointed out that in erecting the embankment, which took from September 1978 to March 1979, two overcompacted soil layers were formed in its body at the elevations 7.0 and 9.5m (Fig.2a) due to interruptions in the stage-by-stage filling and frequent trips made by automobile in installing the instrumentation. After freezing and ice saturation, these overcompacted layers could serve as water-resisting barriers and prevent uniform penetration of moisture into the soil.

(a)

(b)

(c)

Fig.2. Diagram showing the location of depth marks in the body of the experimental embankment (a); its absolute amounts of settlement (b); and thermal conditions (c) at the depth marks II (1) and III (2). Depth marks are designated by Roman numerals.

The results of field observations of the behaviour of the structure are shown in Fig.2b and c. In considering the course of deformation of the embankment with time, in conjunction with the variations in its thermal conditions, the following stages of its development can be distinguished:

Stage I, from September 1978 through March 1979, in which the settlements were due to the stage-by-stage erection of the structure. From 77 to 86% of the maximum amounts of settlement of the first level of the rock fill occurred during this time.

Stage 2, from April through May 1979, was a period of relatively complete stabilization

of the settlement in the embankment's rock mass,whereas the settlement of its base continued to develop. This latter suggests that in the given situation the stabilization of vertical deformation of the coarse-grained soil was due to its heaving at its moisture froze. This moisture entered the body of the embankment from the melting of the snow cover. In April and May the temperature in the body of the embankment varied from -17°C to -10°C.

Stage 3, from June through August 1979,consisted in the development of thermal settlement due to the melting out of the infiltration ice,formed temporarily in the embankment,as well as snow buried during the construction period.

Stage 4, from September 1979 through April 1980,is distinguished by settlement due to completion of compaction of the thawed soil. The magnitude of this settlement,together with the thermal settlement,constituted from 13.9 to 27.4% of the maximum measured deformation. The settlement of the base,at this time, was already close to stabilization.

Stage 5,in May 1980,consisted of heaving of the soils in the base and the coarse-grained soil of the first level in the embankment,which was recorded by all six depth marks installed in the structure. The absolute value of heaving of the base,also composed of coarse-grained soil,amounted to 11 or 12cm, or from 38.7 to 80% of the maximum measured settlement. It should be noted that previously,in May 1979,the same amount of heaving was recorded according to depth mark I (DM-1).

To assess the heaving of the material itself in the embankment,it is necessary to subtract from the amounts of deformation recorded by means of DM-IV,DM-V and DM-VI,the deformation of DM-I,DM-II and DM-III,which were installed on the base. Then the absolute amount of heaving of the first level of the embankment is from 2 to 9cm or,respectively,from 0.32 to 1.37% of the

thickness of the layer of rock fill as recorded before the beginning of heaving. Qualitatively,this agrees with the data obtained in laboratory investigations.

As the temperature of the soil in the body of the structure passed through 0°C in June 1980, thermal settlement of the embankment begain again.

The formation of a basal cryogenic texture, which may be produced in through freezing and subsequent heaving of water-saturated coarse-grained soils,promotes an improvement in the rheological properties of such materials and also makes their deformability dependent on the temperature.

The time,temperature and stress factors can be simultaneously taken into account by the thermal creep equation [Meschyan, 1974] in the form

$$\mathcal{E}(t,\theta) = C_{\kappa}(t,\theta) \cdot F(\sigma,\theta) \qquad (1)$$

where $\mathcal{E}(t,\theta)$ is the strain, $C_k(t,\theta)$ is the measure of the creep that is due to the temperature,and $F(\sigma,\theta)$ is a function of the stress,also depending upon the temperature in the general case.

It has previously been shown [Kronik and Gavrilov,1980; Tsytovich et al,1980] that in application to the conditions of damped creep of frozen coarse-grained soils,equation (1) can be written in the form

$$\mathcal{E}(t,\theta) = \mathcal{E}_{\infty}(\theta) \frac{t}{T^{*}(\theta)+t} \cdot \sigma^{\beta'(\theta)} \qquad (2)$$

where $\mathcal{E}_{\infty}, T^{*}$ and β' are peremeters determined experimentally and depending on the temperature (θ), t is the time and σ is the stress.

It was here established that in a considerable range of minus temperatures (-2.9 to -20.9°C), the relations $\mathcal{E}_{\infty} = f(\theta)$ and $T^{*} = f(\theta)$ are of a linear nature. But,if the temperature range is extended up to 0°C and down to -21°C, these relations become nonlinear,as is evident in Fig. 3a and b. In view of the afore-

46
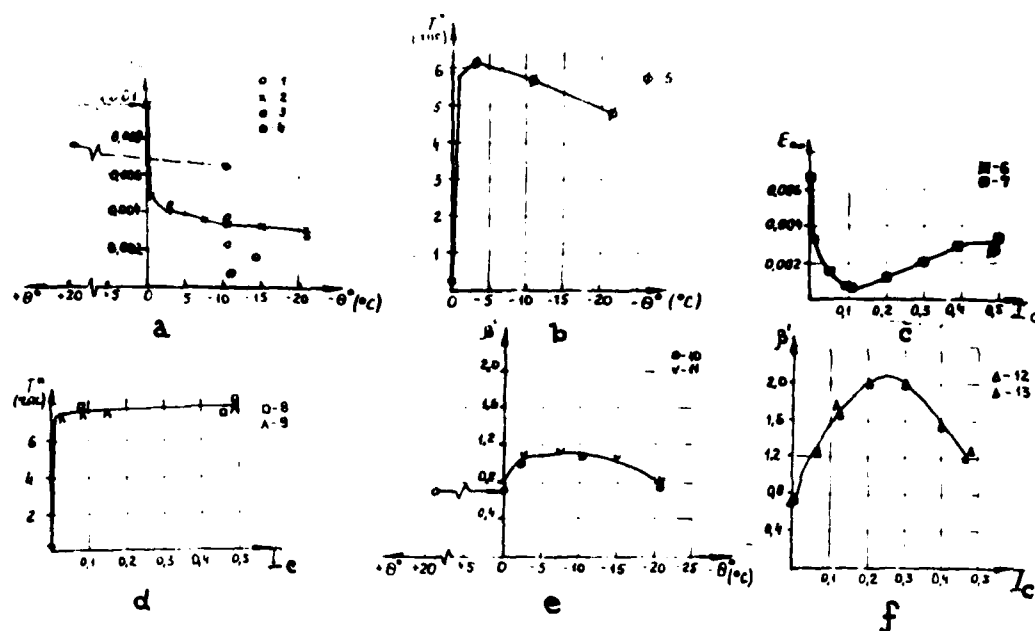
Fig.3. Dependence of the rheological parameters of frozen and below-zero-temperature dry gruss soils on the temperature (a,b and e) and on the ice content I_c (c,d and f); 1 -experimental data (I_c 0.4), 2 - their relevant curve plotted according to equation (3), 3 - experimental data (I_c=0.12), 4 - experimental data (I_c=0), 5 - experimental data and their relevant curve plotted according to equation (4), 6 - experimental data, 7 - their relevant curve plotted according to equation (5), 8 - experimental data, 9 - their relevant curve plotted according to equation (6), 10 - experimental data, 11 - their relevant curve plotted according to equation (7), 12 - experimental data, 13 - their relevant curve plotted according to equation (8).

said, $\varepsilon_\infty = f(\theta)$ for ice-saturated soils can be approximate by a more exact expression:

$$\varepsilon_\infty = K - \beta \cdot \theta^f \qquad (3)$$

where k, β and ρ are parameters determined experimentally; for investigating granite gruss at complete ice saturation they are equal to 9.94×10^{-3}, 542×10^{-3} and 7.6×10^{-2}, respectively, and θ is the absolute value of the temperature in °C.

The dependence of T* on the temperature increases by more than an order of magnitude (by 49.7 times) at the beginning (in the temperature range from 0 to -2.9°C). Then parameter T* slowly decreases (by only a factor

of 1.35) as the temperature drops to θ =-20.9°C. The law of the variation of T* with the temperature, described above, can be expressed by the equation

$$T^* = T_o^* + K \cdot \theta^N \cdot e^{\theta \cdot D} \qquad (4)$$

where T_o^* is the value of T* for unfrozen water-saturated soil; k,N and D are empirical parameters equal to 5.652, 0.117 and -0.0295 for the soil being investigated; e is the base of natural logarithms; and θ is the temperature in °C without the minus (-) sign.

Besides the temperature, the rheological parameters of an ice-saturated coarse-grained soil are considerably influenced by a

47

change in its ice content (I_c). The effect of I_c on the magnitude of the parameter ε_∞ is not single-valued (Fig.3c). First, with an increase of ice content from 0 to 0.12, there is a substantial reduction (by a factor of 6.72) in ε_∞. Upon a further increase in the ice saturation of the specimens, the value of ε_∞ increases again, but still remains less (by a factor of 1.67) than the value of ε_∞ for below-zero-temperature dry coarse-grained soil. This nature of the relation $\varepsilon_\infty = f(I_c)$ is evidently due to the effect of the cryogenic texture of the specimens. In the freezing of incompletely water-saturated coarse-grained soil having no filler, a film (bread-crust) texture is mainly formed due to the freezing of the loosely bound moisture. No essential violation of the contacts between the pieces of the material are observed in this case. This is indicated by the low values of F_h, which do not exceed 0.1 to 0.15% (see Fig.1). At the same time, the formation of ice-cementing bonds prevents the repacking of the coarse-grained particles. This leads to reduced deformability of such material, as compared to unfrozen or below-zero-temperature (air-dry) soil. In the freezing of water-saturated soil, a basal texture is evidently formed, as mentioned above. The contacts between the lumps are ruptured and in this case the mechanical properties of the ice and rock material are due primarily to the deformability of the ice. This, evidently, is what leads to an increase in parameter in completely ice-saturated coarse-grained soil.

The relation $\varepsilon_\infty = f(I_c)$ can be described with sufficient accuracy by the equation

$$\varepsilon_\infty = \varepsilon_{0i} - K_i I_c^{N_i} \cdot e^{zI_c} \qquad (5)$$

where ε_{01} is the value of ε_∞ for below-zero-temperature dry soil; K_1, N_1 and z are empirical parameters, equal to 0.0184, 0.375 and -3.125, respectively, for Kolyma gruss soil; $\varepsilon_{01} = 0.00667$; I_c is the ice content in a fraction of

unity; and e is the base of natural logarithms.

The relation $T^* = f(I_c)$ in the range of I_c values from 0.0 to 0.12 is of a nature close to the relation $T^* = f(\theta)$, i.e. it increases by more than one order of magnitude (by 65.1 times). But any further increase in ice content has no appreciable effect on the value of parameter T^*. Taking into account the aforesaid, $T^* = f(I_c)$ can be approximated by an expression of the form

$$T^* = T_0^* + T_\infty \frac{I_c}{J + I_c} \qquad (6)$$

where T_0^* is the value of T^* at $I_c = 0.0$ and T_∞ and J are experimentally determined parameters equal, in our case, to 7.74 and 0.0039, respectively.

The effect of the temperature and ice content on the nonlinearity parameter β' is shown in Fig.3e and f, and is evidently due to the change in the mechanical properties of the intrapore ice as the temperature drops. This effect is also due to the influence of the cryogenic texture, which is formed in specimens of various initial moisture content when they are frozen. These effect are due, in particular, to the increase in the elasticity of material with a massive bread-crust texture and its decrease in the formation of the basal texture.

Attention is drawn by the fact that in many cases $\beta' > 1$. This last is oviously a result of the fact that under laboratory conditions, frozen coarse-grained soils were tested in oedometers at maximum stresses not exceeding 0.8 MPa. At this stress, the nonlinearity of the dependence of the stabilized strain (ε_{st}) on the stress is not yet so strongly manifested for low-ice-content soils. Moreover, at low levels of acting stresses (about 0.1 to 0.2 MPa) nonlinearity of function $\varepsilon_{st} = f(\sigma)$ is observed. This is due to the structural strength of the material being investigated and the curve is of a convex shape. It may be supposed that with an increase in stresses, the nature of functions $\beta' = f(\theta)$ and $\beta' = f(I_c)$ should change and that, in particular, β' will be less than unity

and will depend less on $\theta°$. Hence, the obtained relationships are to be regarded as qualitative ones.

At the same time in the investigated range of stresses, ice content and temperatures, the dependences $\beta'=f(\theta)$ and $\beta'=f(I_c)$ can be described by uniform equations of the type:

$$\beta'= V\cdot\theta^2 + F\cdot\theta + R \qquad (7)$$

$$\beta'= V_i\cdot\theta^2 + F_i\cdot\theta + R_i \qquad (8)$$

where V,F,R,V_i,F_i and R_i are empirical parameters, θ is the temperature without the minus (-) sign, and I_c is the ice content in a fraction of unity. For the soils being investigated, the above-mentioned empirical parameters equal: -0.0029, 0.0564, 0.861, -21.08, 10.36 and 0.82, respectively.

Then, taking into account expressions (3),(4) and (7) for high-ice-content ($I_c=0.4$ to 0.5) coarse-grained soils, equation (2) is written in the form

$$\epsilon(t,\theta)=(K-\beta\theta^\rho)\frac{t}{(T_o^*+K\cdot\theta^\nu e^{\beta\vartheta})+t}\,\sigma^{V\cdot\theta^2+F\cdot\theta+R} \qquad (9)$$

It should be noted that in engineering practice, in order to simplify calculations of settlement of high-ice-content coarse-grained soils as their temperature varies from 0.0° to -21.0°C, the relations $\epsilon_\infty=f(\theta)$ and $T*=f(\theta)$ can be taken as being linear in the ranges of minus temperatures from 0.0 to -1.0°C and -1.0° to -21.0°C. Then equation (9) is simplified and, for the indicated temperature ranges, takes the form

$$\epsilon(t,\theta)=(M_\epsilon+L_\epsilon\cdot\theta)\frac{t}{(M_T+L_T\theta)+t}\,\sigma^{V\cdot\theta^2+F\cdot\theta+R} \qquad (10)$$

where M, L, M_T and $\pm L_T$ are empirical parameters. The plus (+) sign is put before L_T in the temperature range $\theta=0.0$ to -1.0°C and the minus (-) sign in the range $\theta=-1.0$ to -21.0°C.

In erecting such structures as earth dams, rock fills are used in which the diameters od the lumps frequently reach a diameter from 50 to 100cm and even larger, thereby leading to technical difficulties in their laboratory investigation. In this connection, it proves expedient to determine the rheological parameters of such

soils by employing the results of field observations of the settlement and temperature conditions of either the whole structure or some fragment of it.

It is necessary first to obtain a rheological equation relating the deformation and time at a given acting stress σ_i. This equation should be of the form

$$\epsilon(t) = \Phi(t) \qquad (11)$$

where $\Phi(t)$ is a function of time

Then, if σ_i is not equal to unity, it is necessary to determine the measure of creep $C(t)$ for which the following expression [Meschyan,1974] can be applied:

$$C(t)=\frac{\epsilon(t)}{F(\sigma_i)} \qquad (12)$$

where $F(\sigma_i)$ is a function of the stress at σ_i.

The form of the stress function is found by a known procedure [Meschyan,1974] and, if it proves impossible to load the fragment of the structure, $F(\sigma_i)$ is determined by trial and error, as was done in our case. The resulting expression enables the development of settlement with time to be predicted, taking into account the factor of static loading, for air-dry unfrozen and below-zero-temperature coarse-grained soil of the granulometric composition indicated in Table 1.

Since the temperature factor is manifested mainly only in deforming ice-saturated coarse-grained soils, it can be neglected for a below-zero-temperature (air-dry) material. Then expression (10) takes the form

$$\epsilon(t)= M_\epsilon\frac{t}{M_T+t}\,\sigma^R \qquad (13)$$

The empirical parameters of equation (13), characterizing the deformability of both an unfrozen and a below-zero-temperature rock fill, are listed in Table 2.

However, upon the water saturation of such a material and its subsequent freezing, its rheological parameters change as has been shown by laboratory experiments. Assuming that this process is similar to that con-

Table 2

Values of Rheological Characteristics in Equation (10) for Below-Zero-Temperature Dry and for Frozen Rock Fill of Kolyma Biotite Granite in the Temperature Ranges from 0.0 to -1.0°C and from -1.0 to -21.0°C

Type of soil	Rheological parameters										
	M_ε		L_ε		M_T		L_T		V	F	R
	0 to -1.0°	-1.0 to -21.0°	0 to -1.0°	-1.0 to -21.0°	0 to -1.0°	-1.0 to -21.0°	0 to -1.0°	-1.0 to -21.0°	0 to -21.0°	0 to -21.0°	0 to -21.0°
Rock fill $I_c=0$	0.0657		–		0.150 year		–		–	–	0.396
Rock fill I=0.4 t8 0.5	0.0657	0.0315	-0.035	-0.0006	0.150 year	9.5 years	9.3 years/°C	0.11 years/°C	-0.00157	0.0331	0.396

50

ducted under laboratory conditions, the recorded experimental data enable the values of the characteristics in expression (10) to be determined. These values are also listed in Table 2.

The obtained parameters can be used for a tentative prediction of the deformation of a frozen rock fill by means of equation (10) for variable thermal conditions and coarse-grained ice-saturated material.

REFERENCES

1. Aidla T.A. 1961, On the Formation of Heaved Permafrost Coarse-Skeleton Soils, Proc. VNII-1, vol.XX, Magadan.
2. Gasanov Sh.Sh. 1969, Structure and Formation History of the Frozen Soils of Eastern Chukotka, Nauka Publishers, Moscow.
3. Kalabin A.I. 1957, Certain Results of Cryopedological Research, J.Kolyma, No.10.
4. Kronik Y.A. and Gavrilov A.N. 1980, Rheological Properties of Rock-Ice Materials, in "Proc.of USSR Symposium on Soil Rheology", Erivan State University Publishers, Erivan, p.238-241.
5. Meschyan S.R. 1974, Mechanical Properties of Soils and Laboratory Methods for Their Determination, Nedra Publishers, Moscow.
6. Tsytovich N.A. and Kronik Y.A. 1970, Geocryological Research in Dam Construction under Severe Climatic Conditions, in "Collection of Papers on Hydraulic Engineering and Hydroelectric Construction", Nauka Publishers, Moscow, p.11-22.
7. Tsytovich N.A., Kronik Y.A., Gavrilov A.N. and Vorobyov E.A. 1980, Mechanical Properties of Frozen Coarse-Grained Soils, Proc.of 2nd International Symposium on Ground Freezing, University of Trondheim, Norwegian Institute of Technology, p.65-74.

STRENGTH AND CREEP TESTING
OF FROZEN SOILS

A.R. GARDNER   University of Nottingham, U.K.
R.H. JONES   University of Nottingham, U.K.
J.S. HARRIS   Foraky Limited, Nottingham, U.K.

ABSTRACT

A purpose-built microcomputer-controlled triaxial apparatus for testing frozen soils is described. Either constant strain rate strength tests or constant stress creep tests can be performed. The steel cell, which also acts as a reaction frame, is refrigerated by circulating coolant to temperatures down to -20°C. The maximum cell pressure is 1.8 MPa and the load capacity is 35 kN which corresponds to a uniaxial stress of 31 MPa on a 38 mm diameter specimen. The use of a standard microcomputer for data acquisition and feedback control, in conjunction with other design features, has resulted in a compact, self-contained apparatus at appreciably lower cost than alternatives.

Laboratory specimens of an unsaturated medium to fine sand have been prepared by uniaxial freezing in an open system, and insitu frozen samples have been recovered from a trial freezing site. Comparisons to date indicate that similar creep behaviour is obtained for both types of specimen. This would suggest that the method of uniaxial freezing in an open system gives specimens similar to those obtained in the field, and consideration should be given to adopting this freezing method for reference testing.

INTRODUCTION

The structural design of an artificial ground freezing (AGF) project requires knowledge of the mechanical behaviour of the frozen soil. The creep behaviour of the material is important when this design takes the form of time-dependent finite element analysis.

To determine the mechanical behaviour of specimens of frozen soil in the laboratory, facilities for both strength and creep testing at various temperatures and confining pressures are required. Separate testing rigs are typically used for this purpose.

At Nottingham, careful consideration of the merits of existing testing rigs has led to the design and manufacture of a multi-purpose triaxial testing apparatus. The use of a standard microcomputer for data acquisition and feedback control has resulted in a compact apparatus at appreciably lower cost than alternatives.

This paper describes the testing apparatus and presents the results of triaxial strength and uniaxial creep tests on insitu frozen Brussels sand. Some preliminary uniaxial creep tests on laboratory frozen specimens (which can be prepared and tested at the design stage) are also presented. The creep behaviour of laboratory and insitu frozen specimens is compared on the basis of a creep power law and the implications with respect to reference testing are briefly discussed.

TESTING APPARATUS

General Description

The apparatus is used for strength

and creep tests on 38 mm diameter by 76 mm high specimens of frozen soil at temperatures down to -20°C. Load capacity is 35 kN with a maximum confining pressure, limited by the ram seal, of 1.8 MPa.

Fig. 1 shows a schematic of the testing apparatus and Fig. 2 a block diagram of the main components.
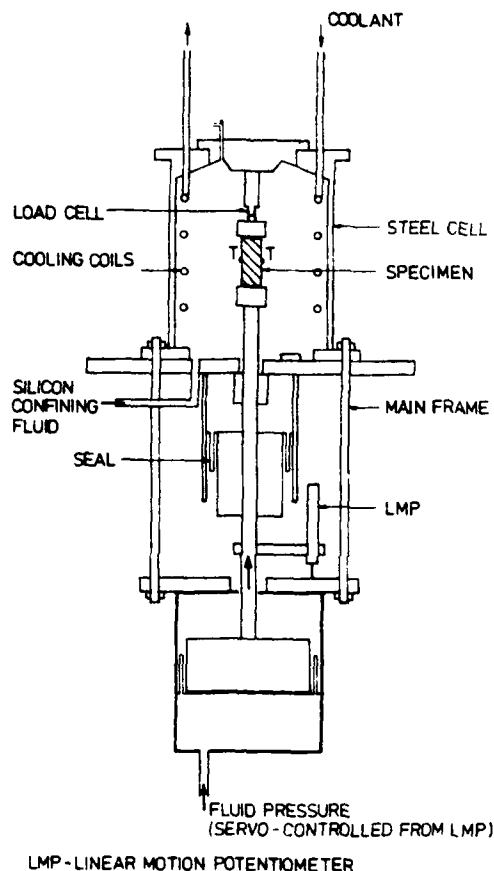
Figure 1. Schematic of testing apparatus.

LMP - LINEAR MOTION POTENTIOMETER

The specimen, surrounded by two neoprene membranes, is held between two platens in the cylindrical steel triaxial cell (internal dimensions 200 mm diameter by 270 mm high), which also acts as the reaction frame. Load is applied through the bottom platen by a ram, travelling through a low friction Rolofram seal, driven by an hydraulic piston. Confining pressure is applied by pressurising silicon fluid inside the cell. This fluid is cooled by circulating a methanol/water mixture from a refrigeration unit through a copper coil

inside the cell. The whole apparatus is mounted on legs, with a total height of 1.5 m.
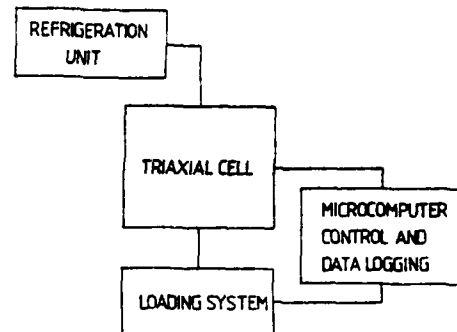
Figure 2. Block diagram of main components.

Load, deformation, temperature and confining pressure are monitored through transducers and an analogue-to-digital convertor by the microcomputer, which in turn controls specimen load through a digital-to-analogue convertor and motor driven regulator in the piston supply. In calculating specimen deformation, due account is taken of system stiffness, and system deformation is subtracted from the measured value.

The test data is displayed on the microcomputer screen, with up-dates of averaged values (from sets of ten) of each reading every second. Data is also recorded on a printer at selected time intervals and, if required, on an X-Y plotter. In the event of system malfunction a failsafe pressure shut-down device is incorporated.

Constant Strain Rate (Strength) Testing

Constant strain rate testing is performed by the microcomputer monitoring the deformation of the specimen and comparing it with the set strain rate at small time intervals. Any significant difference in the value is then corrected by adjusting the load on the specimen through the motor driven regulator.

Simple constant load rate tests can also be performed by increasing the load at a constant rate until failure occurs.

Constant Stress (Creep) Testing

For constant stress testing, the load applied to the specimen is converted to a stress using the assumption that the specimen remains a right cylinder of constant volume. If the

54

stress differs significantly from the
set stress value, then adjustments are
made to the load through the motor
driven regulator.

TESTING OF FROZEN BRUSSELS SAND

Introduction

Two sets of triaxial strength tests
(at -5°C and -10°C) and one set of uni-
axial creep tests (-10°C) have been
completed on insitu frozen specimens of
Brussels sand recovered from a trial
AGF site. In addition, some uniaxial
creep tests (-10°C) on laboratory frozen
Brussels sand and an unfrozen shear box
test have been carried out. For the
frozen tests, all specimens were
tempered at the test temperature for
24 hours prior to loading.
The long term purpose of the test
program is to characterise the
mechanical behaviour of frozen Brussels
sand, to compare results from insitu and
laboratory frozen specimens, and to
compare the laboratory creep results
with insitu tests performed at the site.

Brussels Sand

Brussels sand is a yellow uniform
medium to fine sand with a specific
gravity of 2.63. Fig. 3 gives the
grading curve. The insitu frozen
specimens had dry densities of approx-
imately 1.70 Mg/m³ and low moisture
contents in the range 3.2-5.5% with an
average of 4.2%, corresponding to a
degree of saturation of 21%.

Figure 3. Grading curve for Brussels sand.

*Insitu Frozen Specimens - Recovery,
Transportation, Storage and Preparation*

Core samples (76 mm diameter) and a
block sample (250 mm x 380 mm x 300 mm)
were recovered from the trial AGF site
in Brussels. The samples were trans-
ported by air in an insulated container
to Nottingham, where they are stored in
a cold room (average temperature -14°C).
In addition 65 kg of unfrozen sand was
recovered.
Immediately prior to temperature
tempering and testing, specimens were
individually reduced to 38 mm diameter
by 76 mm high cylinders in the cold room
using a manual soils lathe and a variety
of files and saws. At all times, the
specimens were only trimmed with pre-
cooled equipment. Trimming also has the
added advantage of removing any outer
part which may have been subject to
sublimation. A purpose made jig was
used to ensure that specimen ends were
plane.
The prepared specimens were then
surrounded with two neoprene membranes
and sealed with O-rings to the removable
top and bottom platens. These platens
consist of stainless steel holders with
perspex inserts, although experimenta-
tion with other designs (particularly
friction reducers and compliant platens)
is envisaged.
Although the low moisture contents
of the specimens meant that they were
relatively fragile, the preparation
phase proved easier than expected.
However, for stronger frozen soils,
preparation may require the use of a
powered lathe operating in a cold room.

Preparation of Laboratory Frozen
Specimens

Laboratory frozen specimens were
prepared by first mixing oven-dried sand
with de-aired distilled water to the
required moisture content of 4.2% by
weight. The moist sand was left to
equilibrate for at least 24 hours in a
sealed jar, and then compacted by
rodding and using a vibrating table in
layers of 15 mm depth into a 38 mm
diameter perspex split mould to a height
of 160 mm. This extra height was to
reduce the effects of sublimation during
freezing and to provide surplus for
moisture content samples.
Freezing was carried out uniaxially
in an open system (Fig. 4) with the
freezing temperature at the top and
drainage at the bottom.

FREEZING TEMPERATURE

Figure 4. Uniaxial freezing.

Table 1. Strength tests on in situ frozen specimens.

Temperature °C	Moisture Content %	Dry Density Mg/m³	Cohesion MPa	Friction Angle deg	Remarks
20	3.8	1.58	0.008	36	Shear box test
-5	4.1	1.70	0.07	44	UCS = 0.4 MPa
-10	4.2	1.70	0.38	49	UCS = 2.6 MPa

UCS = Unconfined compressive strength

Previous experience had indicated that freezing in an open system avoided cracking of specimens, which is sometimes observed when they are frozen from the outside towards the centre. After freezing, the specimens were stored in their moulds in sealed plastic bags prior to tempering and testing, this storage period being less than one week.

Before tempering, the specimens were carefully extruded from their split moulds in the cold room, and were end-trimmed and sealed to the platens in the same manner as the insitu frozen specimens.

Tests on Insitu Frozen Specimens

Two sets of triaxial strength tests at a strain rate of 4%/min and -5°C and -10°C have been completed on insitu frozen specimens. A $q = (\sigma_1-\sigma_3)/2$ versus $p = (\sigma_1+\sigma_3)/2$ plot for both tests and the unfrozen shear box test is given in Fig. 5 and the results summarised in Table 1.

Results of uniaxial creep tests at different stress levels on insitu frozen specimens are summarised in Table 2. All the tests were conducted at -10°C, as the stress levels for testing at -5°C would be impractically low.

Table 2. Uniaxial creep tests of in situ frozen specimens (-10°C).

Uniaxial Stress MPa	Moisture Content %	Dry Density Mg/m³	t_f hours	Remarks
1.30	4.4	1.60	-	failed on load application
1.00	4.3	1.68	-	failed on load application
0.90	4.4	1.68	9	
0.70	4.0	1.64	13	
0.64	4.6	1.62	36	
0.40	4.2	1.68	14	low t_f value

t_f = time to onset of tertiary creep stage (taken as failure)

Figure 5. q-p plots for Brussels sand.
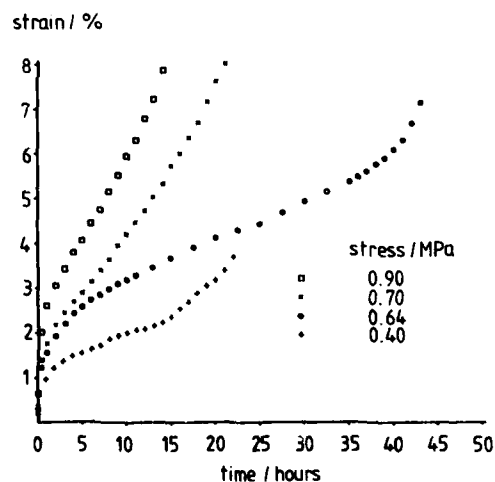
Figure 6. Creep curves for in situ frozen Brussels sand (-10°C).

56

The resulting strain versus time curves are plotted with representative points in Fig. 6. All the curves exhibit the expected behaviour of an instantaneous initial strain and three stages of creep.

The low strength and sensitivity of the material has so far prevented the production of well-defined creep curves at stresses above 0.9 MPa.

Tests on Laboratory Frozen Specimens

Results of uniaxial creep tests on laboratory frozen specimens are summarised in Table 3. The test temperature for these tests was also -10°C.

Table 3. Uniaxial creep tests of laboratory frozen specimens (-10°C).

Uniaxial Stress MPa	Moisture Content %	Dry Density Mg/m³	t_f hours	Remarks
0.90	4.4	1.64	-	failed on load application
0.80	4.2	1.59	4.5	
0.70	4.2	1.58	8	

t_f = time to onset of tertiary creep stage (taken as failure)

Fig. 7 is a plot of the strain versus time curves with representative points, all the curves exhibiting similar behaviour to the insitu frozen specimens, though with correspondingly lower t_f values.

The low strength and sensitivity of the material has prevented the production of creep curves above 0.8 MPa.
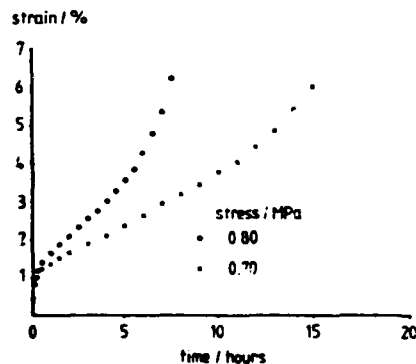
Figure 7. Creep curves for laboratory frozen Brussels sand (-10°C).

CREEP EQUATION

Introduction

When stressed, frozen ground typically undergoes an instantaneous initial strain and then three stages of creep strain: a primary stage with a decreasing creep rate, a constant creep rate secondary stage and a tertiary stage with a rapidly increasing creep rate leading to failure. The onset of the tertiary creep stage is usually taken as failure, and so for design purposes only the strain until the end of the secondary stage needs to be modelled.

Vyalov (1962) proposed a power law to characterise the primary and secondary creep strains for uniaxial loading, based on non-linear hereditary creep. Assur (1963) has slightly modified the original law to give

$$\varepsilon_{c_{1,2}} = [\frac{\sigma t^\lambda}{\omega(\theta+\theta_o)^\kappa}]^{1/m} \qquad (1)$$

where $\varepsilon_{c_{1,2}}$ is the strain in the primary and secondary creep stages, σ is the applied uniaxial stress, t is the time since load application, θ is the temperature in degrees below freezing, θ_o is a reference temperature (1°C when θ is in centigrade) and ω, κ, λ, m are experimentally defined creep parameters. Vyalov (1962) and Sanger (1968) found good agreement with experimental data for this type of equation.

A simplified version of Eqn (1) is

$$\varepsilon_{c_{1,2}} = A \sigma^B t^C \qquad (2)$$

where A is a material and temperature dependent modulus with units of stress^{-B} time^{-C}, B is an exponent greater than unity describing the stress dependence of creep, and C is an exponent less than unity describing the time dependence.

Adding the effect of the initial strain to Eqn (2) gives an expression for the total uniaxial strain up to the onset of the tertiary creep stage

$$\varepsilon = \frac{\sigma}{E_T} + A \sigma^B t^C \qquad (3)$$

where ε is the total strain, E_T is a temperature dependent modulus and the other symbols are as before. Eqn (3)

57

can be successfully used in time-depend-
ent finite element analysis of the defor-
mations and stresses in AGF excavations
(Klein 1979, Gardner 1982). In the
analysis, to relate uniaxial test results
to the multi-axial stress state in the
excavation, the concept of an equivalent
stress based on the second invariant
(Von Mises material) is typically used.
Although this con. ept may be valid for
frictionless frozen materials (e.g.
clays), the decrease in creep strain
that is observed when confining pressure
is increased for frictional materials
(e.g. frozen sands), is not modelled.
Accordingly, research is now proceeding
into modifying Eqn (3) and the finite
element analysis to take any friction
angle effect into account.

For the purpose of this paper,
Eqn (3) serves as providing a comparison
between the uniaxial creep behaviour of
the insitu and laboratory frozen speci-
mens of Brussels sand, and with the
results of other investigators.

Calculation of Creep Parameters

For each set of uniaxial creep
tests (insitu frozen and laboratory
frozen specimens) the experimental
results have been fitted to Eqn (3)
using the method of least squares. The
resulting values of A,B,C (and average
values of E_T) are given in Table 4,
along with some results for frozen
sand from other investigators.

The values for the insitu frozen
specimens were obtained using the results
of the tests at 0.90, 0.70 and 0.64 MPa:
the results from the test at 0.40 MPa
were not used as this specimen suffered
premature failure. For the laboratory
frozen specimens, both the tests at 0.80
and 0.70 MPa were used.

Plots of Eqn (3) for the insitu and
laboratory frozen specimens with the
appropriate values inserted from Table 4
are given in Figs 8 and 9 respectively.
Representative experimental points are
also plotted on these figures.

Figure 8. Experimental and calculated
creep curves--in situ frozen Brussels
sand.
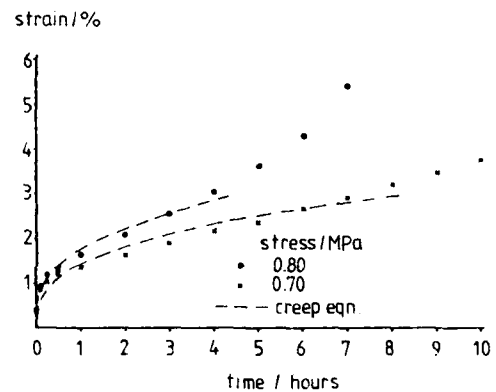
Figure 9. Experimental and calculated
creep cruves--laboratory frozen fro-
zen Brussels sand.

DISCUSSION

Strength Testing

The results of the triaxial
strength tests on insitu frozen speci-
mens illustrate the increase in strength
with decreasing temperature, which is
mainly due to the increase in cohesion.
The large increase in friction angle
from the unfrozen to   frozen tests is
thought to be mainly due to the higher
density of the frozen material.

The strength of the frozen sand is
low by typical AGF standards (Andersland
and Anderson 1978), this being due to
the low moisture content (average 4.2%)

Table 4. Creep parameters for frozen
sand (-10°C).

Material	A MPa^{-B} hr^{-C}	B -	C -	E_T MPa
Brussels sand - insitu frozen	2.3 x 10^{-2}	1.40	0.38	195
laboratory frozen	1.9 x 10^{-2}	1.40	0.40	203
Ottawa sand (Sayles 1968)	3.5 x 10^{-4}	1.28	0.45	
Manchester fine sand (Sayles 1968)	1.9 x 10^{-4}	2.63	0.63	
Karlsruhe sand (Klein 1979)	1.3 x 10^{-3}	2.00	0.40	

of the specimens resulting in a weak ice-poor material. This has also caused the frozen material to be very sensitive to any variations in moisture content, which is shown in the difficulty of creep testing at stress levels near the UCS.

Creep Testing - Insitu Frozen Specimens

The results of the uniaxial creep tests on the insitu frozen specimens show the expected creep behaviour of a frozen soil. The low t_f values illustrate the relative weakness of the sample and the difficulty in testing above 0.9 MPa (although the UCS was found to be 2.6 MPa) illustrates the sensitivity of the material at this low moisture content.

The comparison of the calculated (from Eqn (3)) and experimental results plotted in Fig. 8 shows good agreement. This is true even for the test at 0.4 MPa, which was not used in the calculation of the creep parameters.

Creep Testing - Laboratory Frozen Specimens

The results of the two uniaxial creep tests on laboratory frozen specimens also show the expected creep behaviour, although the t_f values are lower than those for the insitu frozen specimens. This is probably due to the lower dry densities of the laboratory frozen specimens: research is now underway into improving compaction methods.

The low moisture contents of the specimens again resulted in a weak, sensitive material: successful testing above creep stress levels of 0.8 MPa has still to be achieved.

The result of the curve fit of Eqn (3) has given promising results, as the comparison of calculated and experimental values plotted in Fig. 9 shows. However, more tests are required to define the creep parameters with confidence.

Comparison of Creep Test Results

To date, comparison of the creep parameters obtained for the two types of specimen (Table 4) shows good agreement, although many more tests are required on the Brussels sand and other soils to confirm that this agreement is generally applicable. The results suggest that uniaxial freezing in an open system gives laboratory specimens with similar creep

behaviour to those obtained in the field, and serious consideration should be given to adopting this freezing method for reference testing.

Comparison of the creep parameters with those of other investigators (Table 4) shows that the B and C values are in the same range, although the A values are much larger. These larger values are thought to be due to the low moisture content of the Brussel sand specimens when compared to the other sands (which were saturated).

CONCLUSIONS

(1) An economic and compact triaxial testing system for the strength and creep testing of frozen ground has been designed and built.
(2) The recovery, transportation, preparation and testing of insitu frozen samples of an unsaturated medium to fine sand (Brussels sand) has been achieved successfully.
(3) The preparation and testing of laboratory frozen specimens of Brussels sand at the required moisture content of 4.2% has been achieved successfully.
(4) The low moisture content (4.2%) of the insitu frozen specimens has resulted in a weak ice-poor material with a cohesion of only 0.38 MPa at -10°C and a corresponding friction angle of 49°.
(5) The creep equation

$$\varepsilon = \frac{\sigma}{E_T} + A \, \sigma^B \, t^C$$

successfully models the creep behaviour of both the insitu frozen and laboratory frozen specimens up to the onset of the tertiary creep stage.
(6) Very close agreement was obtained between respective B and C values calculated for both types of specimen, whilst there was a variation of 20% between the A values.
(7) The method of preparing laboratory specimens of Brussels sand by uniaxial freezing in an open system appears satisfactory, as similar creep behaviour has been obtained between these and insitu frozen specimens. Although more tests are required on this and other soils to confirm that this agreement is generally applicable, serious consideration should be given to adopting uniaxial freezing for reference testing.

59

REFERENCES

ANDERSLAND, O.B. & ANDERSON, D.M. (Ed.) (1978) 'Geotechnical Engineering for Cold Regions', McGraw-Hill.

ASSUR, A. (1963) 'Creep of frozen soil' (discussion). Proc. 1st Permafrost Int. Conf., Building Research Advisory Board, National Academy of Sciences, Publ. 1287, p. 339.

GARDNER, A.R. (1982) 'The creep behaviour of frozen ground in relation to artificial ground freezing', Ph.D. thesis in preparation, Univ. of Nottingham.

KLEIN, J. (1979) 'The application of finite elements to creep problems in ground freezing', 3rd Int. Conf. on Num. Methods in Geomechanics, Aachen, April.

SANGER, F.J. (1968) 'Ground freezing in construction', Proc. Amer. Soc. Civil Eng., 94, (SM1), pp. 131-158.

SAYLES, F.H. (1968) 'Creep of frozen sands', U.S. Army Cold Reg. Res. Eng. Lab. Tech. Rep. 190, Hanover, N.H.

VYALOV, S.S. (1962) 'The strength and creep of frozen soils and calculations for ice-soil retaining structures', U.S. Army Cold Reg. Res. Eng. Lab. Trans. 76, Hanover, N.H. 1965.

PERMAFROST CREEP MEASUREMENTS IN THE CRREL TUNNEL

Nils I. Johansen, P. E.*
Associate Professor, University of
Alaska
John W. Ryer**
Field Engineer, Dresser-Atlas Oil
Field Service Group, Prudhoe Bay,
Alaska

*At present, on sabbatical leave
and with Shannon & Wilson, Inc., Geotech-
nical Consultants, Fairbanks, Alaska.

**Former student, geological engi-
neering, Univeristy of Alaska.

Abstract: Over the last decade, there has been significant creep of the permafrost soils in the U. S. Army Cold Regions Research and Engineering Laboratory (USA CRREL) permafrost tunnel at Fox, Alaska. This study supplements previous creep measurements in the tunnel and also investigates probable links between the significant settlement in the back portion of the tunnel and the tunnel geometry in this area and also parameters such as soil type, ground temperature, ice content and thickness of overburden. The studies have been ongoing intermittently since 1980. The instrumentation used was designed by the junior author as part of an independent study project when he was an undergraduate engineering student at the University of Alaska. The simple instrument has been in operation for tow years and measurements show a constant creep rate of approximately 0.002"/day (0.05mm/day). The creep data obtained will be helpful in predicting future behavior of the tunnel and also assist in design of roof support system in frozen ground in areas subjected to constant creep.

General Setting, Statement of Problem

The USACRREL permafrost tunnel at Fox, Alaska was constructed in the mid 1960's for the purposes of exploring excavation techniques for frozen silts and gravels. The tunnel geology and the engineering properties of the materials exposed in the tunnel are discussed in two CRREL reports by Sellman (Sellman 1967, 1972). A summary of the engineering properties of the exposed soils as well as a general discussion of the formation of permafrost is found in a School of Mineral Industry, University of Alaska in house field guide to the permafrost tunnel. (Johansen, 1976).

Since the excavation of the tunnel, it has been used for additional research projects in permafrost, but the tunnel opening itself shows two engineering problems. 1. Sublimation of the ice matrix in the frozen soil creates a significant amount of dust in the tunnel. This was the subject of a paper by Johansen, Chalich and Wellen (1980, 1981). 2. Soil Creep is apparent in the tunnel, especially away

from the opening near station 3 + 60. This is an area of the tunnel where the temperature remains fairly constant -1.5°C at all times.

At this temperature, permafrost silt is a very soft material and is easily deformed. Early in situ creep investigations in the CRREL tunnel was reported by Thompson and Sayles, (1972). Phukan (1980) on permafrost silts in the tunnel showed a bimodel strength, soil temperatures above 29°F (or -1.5°C) showed a marked reduction in the compressive strength of the silt; 200 psi at 29°F a compressive strength of 450 psi was reported. Over the years, soil creep has been observed from the excavated areas, especially where temperatures are close to the freezing point. Near the end of the main adit at station 3 +60 CRREL installed an insulated room in the late 60's and today the door frame, made from 2" x 4" lumber, has broken from soil creep. Measurements of the frame gives settlement figures of about 4" for the 10 years since the installation. The tunnel roof in the same vicinity show evidence of soil creep, the headroom has been reduced significantly over the last dozen or 20 years, the senior author has had the opportunity to visit the CRREL tunnel. There is however no creep data for the unsupported roof portion near Station 3 +60. In order to obtain creep data and also make an assessment of the urgency for installing some means of roof support should this be needed, the present investigation was carried out.

Equipment

With the help of the Alaska project office of CRREL, the junior author constructed as part of an individual study course at the School of Mineral Industry, University of Alaska, two instruments capable of directly recording settlement. Basically they are spring loaded rods exerting pressure on the roof and floor but not enough to restrict the movement of soil. The movement of the rod is measured by dial gages, one of which reads to .0001 inch, the other to .001 inch. The design of these instruments was further constrained by availability of supplies.

Data Gathering

The gages were installed by Mr. Ryer in late May 1980 and readings were taken almost daily starting 3 June 1980. The readings are shown on Figure 1.

The gages recorded a creep rate of about 0.0002"/day. Some small variations were encountered. The readings are temperature sensitive, that is, an increase in the air temperature from -1.5° to 0°C, as was readily observed with a large group of visitors in the tunnel, would cause the gages to show continuous movement. A reading like this is shown on the attached graph. However, as also can be seen, when the temperature anamoly is removed, the data again cluster on the same line.

To explain the observed data, the following model is proposed. It should be noted that the conclusions are tentative at this time and may be modified as more data is obtained, especially data related to strength, creep and sublimation properties of the actual soil at installation.

The overburden at the site is about 50-55', and the weight is about 100 $\#/ft^3$ giving a soil pressure of about 5000 $\#/ft^2$. This is close to observed strength of multicrystalline lake ice at -1 to -2°C. So, the creep could then be explained as creep of the pore-ice, the pore-ice and free water in the permafrost acting as a lubricant for the soil particles.

The motion could be thought of as that of a glacier. This may also explain the much higher creep rates obtained by CRREL in the gravel section of the tunnel (Thompson and Sayles 1972). The creep increases exponentially with depth, not linearly.

Conclusions

The creep rate of about 0.002"/day seems to be constant, no acceleration has been observed. The safety of the section of the tunnel is unknown at this time. As far as a possible support is concerned, a system must be designed to carry the total weight of the system, should this kind of support be desirable in this portion of the tunnel.

Acknowledgements

62
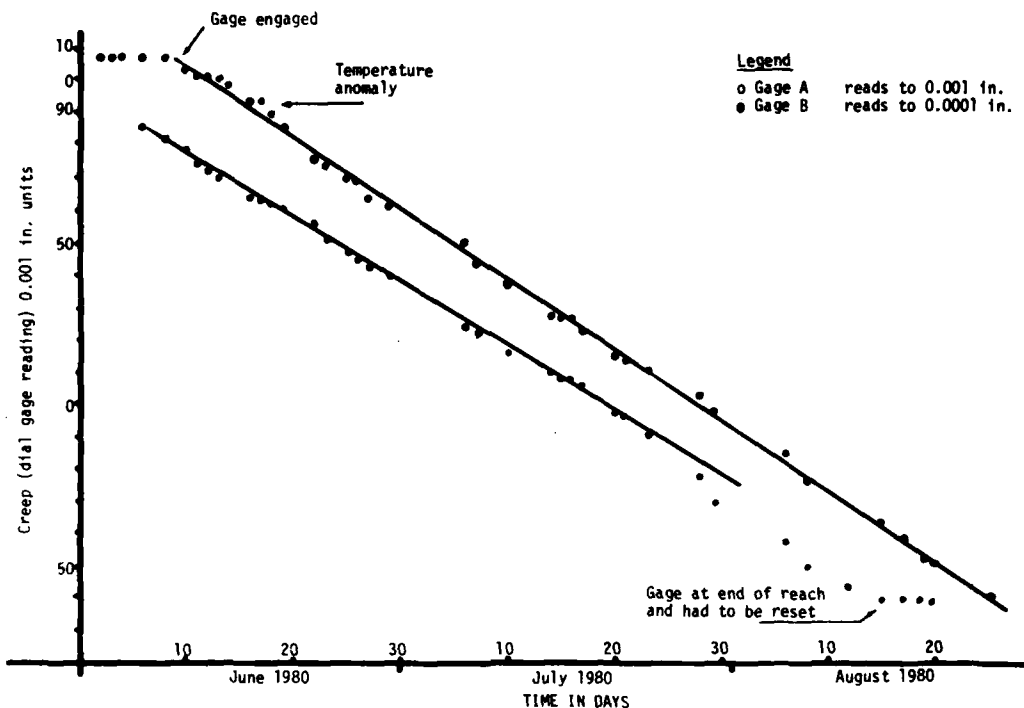
Figure 1. Roof creep vs time in the CRREL permafrost tunnel.

USACRREL provided the materials for the deformation instruments and of course the CRREL permafrost tunnel at Fox.

References

Johansen, Nils I., "The USACRREL Permafrost Tunnel", in house field guide (unpublished) School of Mineral Industry, University of Alaska, 1976.

Johansen, Nils I., Chalich, Peter C., and Wellen, Earl W., "Sublimation and Sublimation Control in the CRREL Tunnel" 2nd Sumposium on Ground Freezing, Trondheim, Norway, 1980.

Johansen, Nils I., Chalich, P. C. and Wellen, E. W., "Sublimation and Its Control in the CRREL Permafrost Tunnel CRREL Special Report 81-8 USACRREL, Hanover, N. H., 1981.

Phukan, Arvind, Oliver, James and Lambert, Chris, "Excavation of Failure Mechanism of Frozen Material II." Submitted to Mining and Mineral Resources Research Institute. Office of Surface Mining, U. S. Department of Interior, Washington, D.C., March 1980

Sellmann, Paul V., "Geology of the USA CRREL Permafrost Tunnel Fairbanks, Alaska", USA CRREL Technical Report 199, July 1967.

Sellmann, Paul V., "Geology and Properties of Materials exposed in the USA CRREL Permafrost Tunnel", USA CRREL Special Report 177, July 1972.

Thompson, Erik G., and Sayles, Francis H. "In Situ Creep Analysis of Room in Frozen Soil", Journal of the Soil Mechanics and Foundation Division, ASCE, Vol. 98, No. SM9, Proc. Paper 9202, September, 1972, pp. 899-915.

ELASTIC AND COMPRESSIVE DEFORMATION OF FROZEN SOILS

Zhu Yuanlin   Lanzhou Institute of Glaciology and
Zhang Jiayi   Cryopedology, Academia Sinica,
Wu Ziwang   Lanzhou, PRC

ABSTRACT

The paper mainly discusses the results of compression laboratory tests on frozen soils (with lateral spreading of the soil prevented) at a constant negative temperature. In this paper the authors not only state the general behaviors of elastic and compressive deformation of frozen soils, but also list some of the experimentally obtained values of their characteristics, the normal elastic modulus E and the summary relative compressibility coefficient a^{Σ}_r of frozen soils. Furthermore, on the basis of analyzing the influence of some factors (such as negative temperature, moisture, soil composition and external pressure) on the above two characteristics, the authors present two equations for estimating the normal elastic modulus and summary relative compressibility coefficient of frozen soils respectively, according to negative temperatures of the soils, and also give the values of corresponding parameters for the equations here.

INTRODUCTION

The study on the deformability of frozen soils at negative temperatures is of great theoretical and practical importance. When designing foundations to be built on permafrost, many design engineers totally took the frozen subsoils at negative temperatures as a practically incompressible body. Engineering practice in permafrost area has proved that this point of view is incorrect, and at least, incomplete. As a matter of fact, the compacting deformations will invariably occur in the frozen subsoils subjected to loading even if its negative temperature remains constant, and, especially, for the high-temperature plastically frozen subsoils, the amount of compressive deformation will be in the order of considerable magnitudes, being one of the decisive factors of foundation design on permafrost (6). The authors, therefore, quite agree with the opinion that in designing structures to be built on frozen ground it is necessary to consider the compressibility of plastically frozen soils, which governs their settling under load, even when the negative ground temperatures are preserved (1).

To get a deep understanding of the compressibility of frozen soils so as to offer engineers the necessary characteristics and methods for predicting the foundation settling on plastic frozen ground with maintenance of its negative temperature, the authors have pursued the compression laboratory tests on about 200 samples of frozen Fenghou Shan loam, frozen Lanzhou medium-grained sand and laboratory-made pure ice for the past two years, and meanwhile, we have also investigated the elastic (reversible) deformations of the frozen soils.
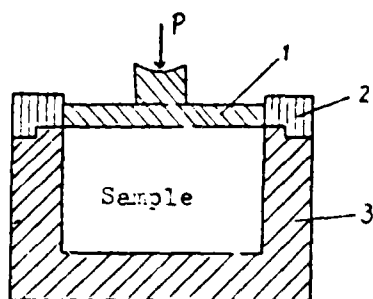
Figure 1. Cross section of sample container. 1-steel bearing plate; 2-leaded ring; 3-sample container.
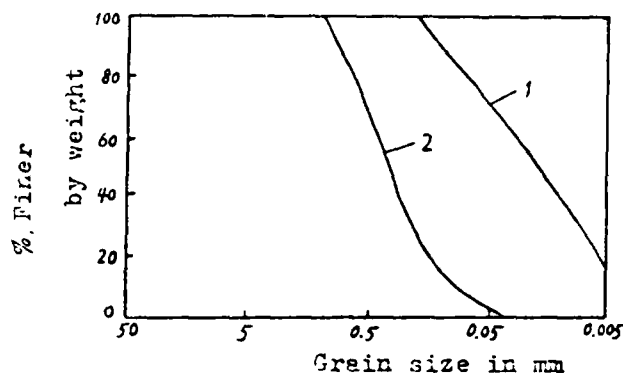
Figure 2. Gradations of soil samples tested.

EXPERIMENT

Test Method

The experiments were carried out on a modified soil consolidation test apparatus set in a small low-temperature room equipped with a thermostat, by which the fluctuation of temperatures of samples could be controlled not more than ±0.1°C. The frozen disturbed soil samples were put into a self-made steel container (see Fig. 1) with a cross-section area of 45 cm^2 and a height of 4 cm. The pressed unfrozen water was allowed to flow out from the top of the container during compression. The testing load was mechanically applied with a same load increment, and therefore the compressive pressures applied to samples remained ideally constant during the whole period of experiment. The compressive deformation of tested samples was measured by the dial gauges with a distinguishability of 0.001 cm, and it was considered to have come to a steady state if the strain rate has

lowered to the following values: 2.08×10^{-5} hr^{-1} for the sample temperature being higher than -1.0°C, and 1.04×10^{-5} hr^{-1} for that being lower than -1.0°C.

Tested Materials

The experiments were carried out on the two types of soils, the Fenghou Shan loam from Qinghai-Xizang Plateau and the Lanzhou medium-grained sand. Their gradations are shown in Figure 2, and part of their physical indicators are listed in Table I.

ANALYSIS AND DISCUSSION

Elastic Deformation of Frozen Soils

The elastic deformations of frozen soils are closely responsible for the effects of dynamic load (explosion, impact, vibration, seismic oscillation, etc.) on frozen bases under structures and buildings; thus, it is absolutely necessary, for pre-

Table I. Physical indicators of soil samples tested.

Soil type	Liquid limit W_l, %	Plastic limit W_p, %	Plastic index I_p, %	Freezing tem.* θ_f, °C	Saltness** Z, %
Fenghou Shan loam	23.6	14.5	9.1	-0.27	0.082
Lanzhou medium-grained sand	--	--	--	-0.36	0.096

* After Tao Zaozian's experiments.
** After Chang Xiaoxia's experiments.

66

dicting the behaviors of structures and buildings and their foundations under dynamic load, to master the knowledge of elastic-property characteristics of frozen subsoils. In addition, mastering the knowledge is also very significant for the applications of seismological, ultrasonic and optical methods to the investigations of frozen soils.

As far as authors know, there is no definite conception on the elasticity of frozen soils up to now, but it seems to be certain that the so-called elastic behavior of frozen soils is quite different from that of common elastic materials, i.e., much of the elastic strain of the former cannot repeat at each different cycle of loading-unloading because the frozen soil is a polyphase compound body, but not a homogeneous elastic body. (Most researchers consider it as a viscous-elastic body or a viscous-plastic-elastic body.) Therefore, the so-called elasticity of frozen soil is actually a kind of "quasi-elasticity."

The so-called elastic deformation discussed here refers to the resultant (steady) reversible deformation of frozen soil samples occurring after the first time of unloading at any load level. Experiments show that the amount of the reversible deformation of frozen soils is little, and, generally only consititutes 10-30% of that of the total compaction deformation, and especially for ice-rich plastic frozen soils, this percentage is lesser, even less than 10%.

As is known to all, in the case of a continuous, uniformly distributed load (one-dimensional problem), the normal elastic modulus of frozen soil E (kg/cm^2) can be calculated by the expression

$$E = p \cdot h/s \qquad (1)$$

where p is the compressive stress; h is the height of sample, and s is the gauged resultant elastic (reversible) deformation of the samples for the first time of unloading.

Some of the values of elastic modulus E for frozen Fenghou Shan loam and Lanzhou medium-grained sand calculated by eq. (1) according to test data are presented in Tables II and III, respectively.

We can see on inspection of the above data that the elastic modulus of frozen soils is variable and depends upon the soil temperature and moisture, soil composition, and the range of external pressure; among which, the negative temperature serves the governing one--the lower the negative temperature of frozen soil, the greater does the value of its elastic modulus become. If we take no account of the effects of water content of frozen soil on its elastic modulus (i.e., take the averaged value of several elastic moduli of the same soil material for various water content at a certain negative temperature as an average normal elastic modulus of the soil, $\bar{E}$, at the temperature), then we can draw Figure 3 according to our experimental results.

Apparently, from Figure 3 the average elastic modulus of frozen
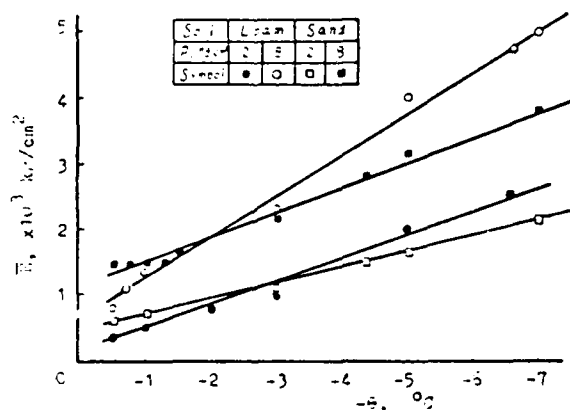
Figure 3. Average normal elastic modulus of frozen soils as a function of negative temperature $-\theta$.

67

soils $\bar{E}$ (kg/cm^2) as a function of the temperature $-\theta$ can be approximately described by the following linear relation at not too low temperatures (above -5 to -7°C):

$$\bar{E} = a + b \cdot \theta \qquad (2)$$

where θ is the absolute value of the negative temperature of frozen soils in °C; a and b are the experimental factors dependent on soil composition and applied pressure, and their calculated values from Figure 3 are presented in Table IV.

It can be also seen from Figure 3 or Tables II and III that the elastic modulus of frozen soils is closely related to the external pressure: the elastic modulus increases with the increase in external pressure. And

Table II. Values of normal elastic modulus E for frozen Fengou Shan loam.

θ, °C	w, %	E, kg/cm^2 in the following pressures, kg/cm^2 2	8	θ, °C	w, %	E, kg/cm^2, in the following pressures, kg/cm^2 2	8
-0.5	18.3	200	604		21.1	678	1,649
	34.7	258	571	-3.0	33.3	850	1,720
	98.7	533	1,103		48.3	1,026	3,137
-0.7	13.8	—	1,176		20.0	2,758	5,614
				-5.0	22.8	2,105	5.926
	18.4	678	762		24.6	1,356	2,500
-1.0	32.6	426	1,231				
	69.0	374	2,000	-6.6	18.3	2,667	4,700
	21.0	291	988		22.0	--	4,571
-2.0	33.3	1,081	2,645	-7.0	31.0	—	4,556
	48.3	777	2,162		84.0	--	6,400

Table III. Values of normal elastic modulus E for frozen Fenghou medium-grained sand.

θ, °C	w, %	E, kg/cm^2 in the following pressures, kg/cm^2 2	8	θ, °C	w, %	E, kg/cm^2, in the following pressures, kg/cm^2 2	8
-0.5	6.0	419	1,087		13.5	—	1,600
	13.4	900	1,580	-1.5	19.8	—	1,524
	19.5	667	1,208				
					7.4	—	2,000
-0.7	6.0	—	1,461	-3.0	12.3	1,460	2,130
	10.9	—	1,524		15.5	800	2,286
	19.8	—	1,481				
				-4.3	12.3	1,600	2,909
	4.0	544	1,448				
-1.0	5.5	615	1,524		6.6	1,194	2,581
	13.4	1,181	1,583	-5.0	12.6	3,211	5,531
					18.4	530	1,468
	7.8	—	2,280				
-1.2	11.7	—	1,067		6.6	2,222	2,406
	16.8	—	810	-7.0	12.6	2,500	5,000
					18.4	2,060	3,404

68

Table IV. Values of a and b in equation 2.

Soil type	a, kg/cm^2		b, kg/cm^2	
	p=2 kg/cm^2	p=8 kg/cm^2	p=2 kg/cm^2	p=8 kg/cm^2
Fenghou Shan loam	200	700	350	600
Lanzhou medium-grained sand	470	1,200	210	300

Table V. Values of elastic modulus E_1 for ice samples.

θ, °C	E_1, kg/cm^2	
	p=2 kg/cm^2	p=8 kg/cm^2
−0.5	889	2,462
−1.1	—	3,450
−1.5	—	3,050
−4.3	2,667	5,333
−7.0	4,000	6,400

this just stands the opinion that the elastic behavior of frozen soils is quite different from that of common elastic materials.

Additionally, experimental results indicate that the moisture of frozen soils also has a certain influence on elastic modulus. But, the available test data is not enough to analyze this influence quantitatively. However, on inspection of the data listed in Tables II and III it seems that there is such a law; i.e., for frozen sand the values of elastic modulus rank the maximum in the case of water saturation or around, while for frozen loam they increase with increasing moisture content, finally being close to that for ice samples with the averaged density of about 0.9 g/cm^3 (see Table V).

Generally, the value of elastic modulus of frozen sand is greater than that of frozen clayey soils, and that of ice is between them both [1]. However, our test results indicate that there is no significant difference between the value of elastic modulus for frozen Lanzhou medium-grained sand and that of frozen Fenghou Shan loam, and both of them are considerably less

than that of ice. This is probably because the Lanzhou medium sand contains more fine mineral particles.

We note that the values of elastic modulus of frozen soil obtained by the method employed here are in good agreement with those calculated from the results of the field load-test on frozen ground and ground ice [2,3] and of the unaxial compressive test on frozen soils [4] performed by the authors.

Compressive Deformation of Frozen Soils

Time variation of compressive deformation during compacting

The compacting of high-temperature frozen soils is a highly complex physicomechanical process governed by the deformability and displacements of al components—gaseous, liquid (unfrozen water), viscoplastic (ice), and solid (mineral particles) [1]. Among these, both the liquid and solid phases of water behave most actively, invariably undergoing phase transitions with each other during the whole compacting process so as to keep the dynamic equilibrium between them. The pre-

69

vailing process is the thawing of ice at the heavily stressed points of contact between mineral particles and the subsequent migrating, filtrating and refreezing of the melting water, together with the compacting and displacement of ice crystal and soil particles under pressure, resulting in the changes in volume and structure of the frozen soils during compression.

Experiments showed that the time variation of compressive deformation of frozen soils was different at different test conditions (temperature, moisture, soil composition and external pressure). Figures 4 and 5 show the increase in the measured compacting deformations with the passage of time t under stepped load with the same load increment of 2 kg/cm^2 for frozen Fenghou Shan loam and Lanzhou medium-grained sand, respectively. Obviously, these curves are different in their patterns. For example, for frozen loam the compacting deformation

$$S_t = S_o \left(\frac{t}{T_o} \right)^K$$
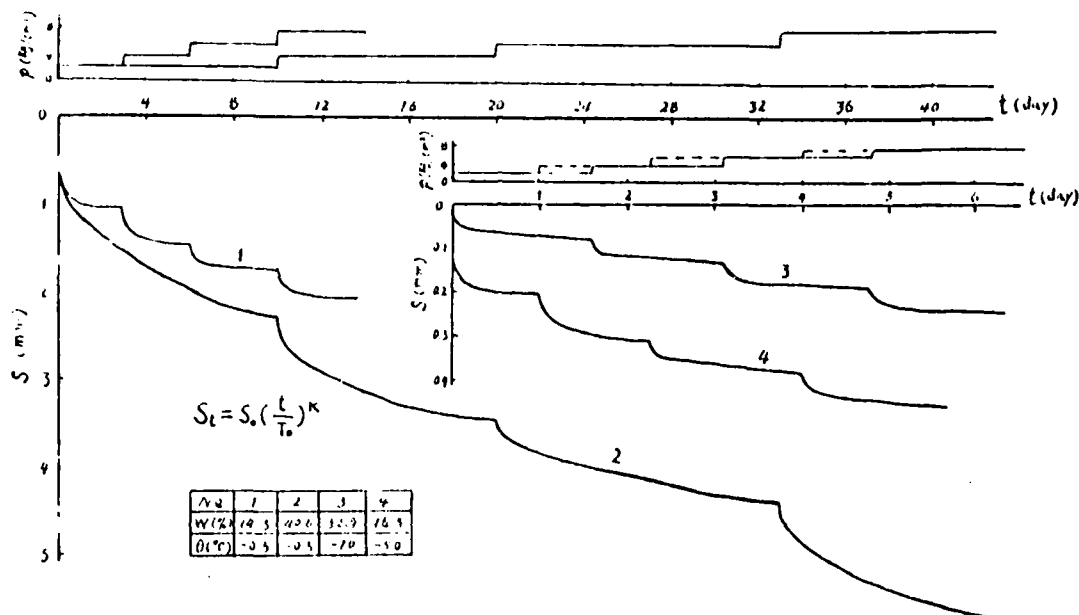
Figure 4. Time variation of compacting deformation (s) in frozen Fenghou Shan loam under stepped load.
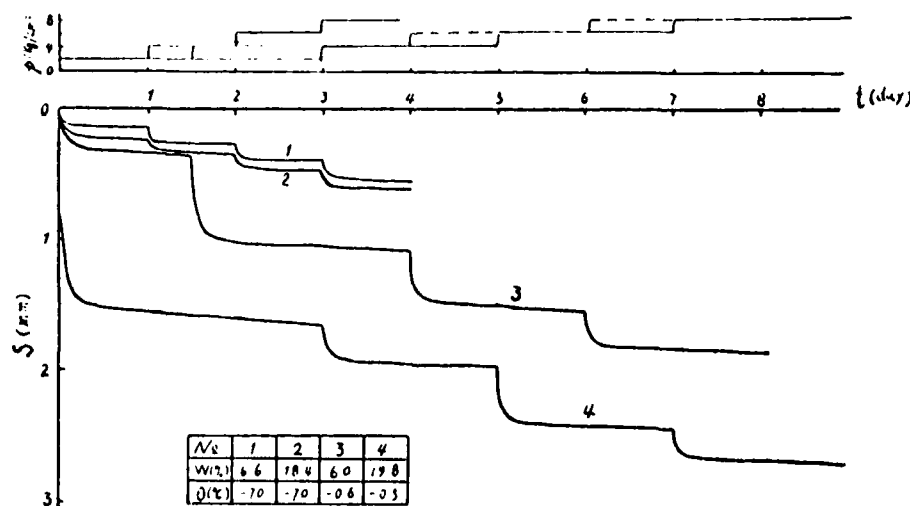
Figure 5. Time variation of compacting deformation (s) in frozen Lanzhou medium-grained sand under stepped load.

70
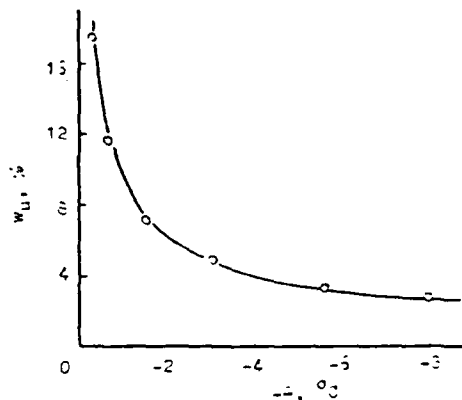
Figure 6. Unfrozen water content w_u of frozen Fenghou Shan loam as a function of its temperature $-\theta$. (After Zhang Jingshen et al., 1981.)

proceeded very slowly with the passage of time; in other words, it took a long time to come to a steady strain state, especially for the high-temperature, ice-rich frozen loam (see the curve 2 in Fig. 4). We call this long-term deformability of frozen clayey soils the "secondary consolidation" (secondary creep), and the authors consider that it is caused by the existence of a considerable amount of unfrozen water in the frozen soils (see Fig. 6), and that it must be taken into account in engineering practice concerned with the high-temperature plastic frozen ground in permafrost areas.

However, as the temperature of frozen loam is low enough (say lower than -5°C, the limit of substantial water-to-ice phase transitions), its compacting deformation can reach a steady state within a short time (a few days), and the amount of deformation is very small. This is due to the significant decrease in unfrozen water content of the frozen loam in this case.

But, for frozen sand, the compression s-t curve is of a quite different pattern. From Fig. 5 it can be clearly seen that the most amount of deformation of samples occurred within a very short time after loading and it quickly came to steady state, whether the soil-tested temperature was high or low. For example, the compacting deformations of frozen sand samples could come to steady state in a few days under an applied pressure of 8 kg/cm^2 even as the negative temperature of the samples is close to their thaw point. This could be explained by the fact that the unfrozen water content of frozen sand is very small and the "excessive" unfrozen water can flow away from the samples very quickly under pressure.

According to the s-t curves mentioned above, the compacting deformations of frozen soils can be divided into three stages—those of instantaneous, nonsteady and steady compaction. Their corresponding deformations are called the instantaneous, filtration-migrational (or primary creep) and decaying creep (or secondary creep) deformation, respectively (1). Obviously, the filtration-migration deformation occurs primarily within a very short time interval after loading because it mainly results from the seepage of unfrozen water and compression of soil pores, while the decaying creep deformation invariably lasts a long time because it is related to the local melting of ice, recyrstallization and rearrangement of mineral articles.

Experiments show that for the high ice content plastic-frozen soils the filtration-migrational deformation composes only a small fraction (about 1/5 to 1/3) of the total compacting deformation, and the compacting deformation is always attenuating (of course, in the case of without lateral spreading of the soil), having the similar pattern of the s-t cuve to that of the decaying creep curve obtained from a typical creep test on frozen soil (5). Therefore, if the filtration-migrational deformation is not taken into account, then the total compacting deformation s_t of frozen soils at any time t can be approximately predicted by the hereditary creep theory (using the hyperbolic creep coefficient) (1), or by the following power-law equation presented by authors

$$s_t = s_o (t/T_o)^k \qquad (3)$$

where s_o is the referring creep deformation corresponding to an arbitrary T_o after the beginning of creep, and k is the nonlinearity parameter dependent upon the temperature, moisture and applied pressure for frozen soils. Experiments found that for frozen loam with $\theta = -0.5°C$ and $w = 40.6\%$, $k = 0.35$ as $p = 2$ kg/cm^2, and $k = 0.44$ as $p = 4$ kg/cm^2.

71
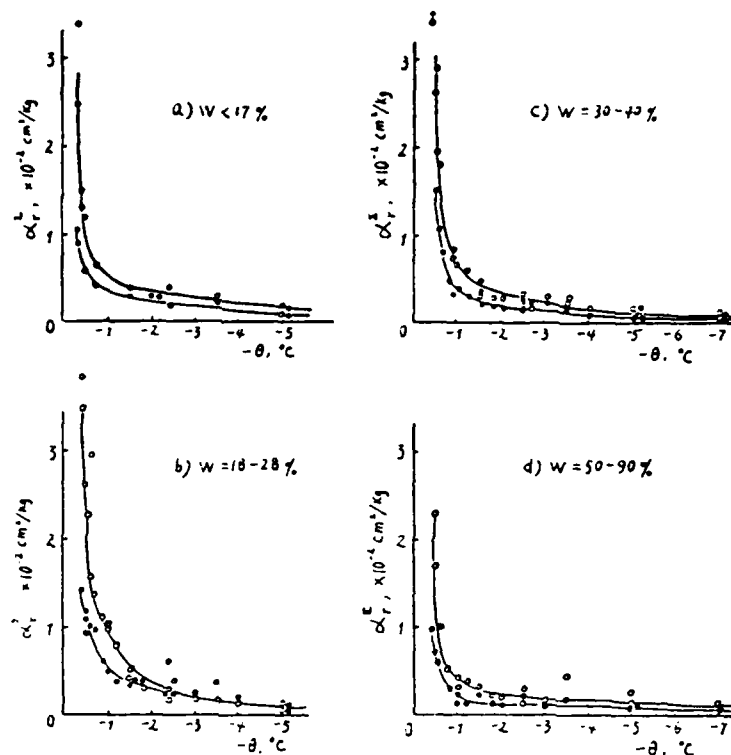
Figure 7. Compressibility coefficient α^{Σ}_r as a function of $-\theta$ for frozen Fenghou Shan loam. p: o—0 to 2 kg/cm²; ●—0 to 8 kg/cm².

In constrast, for frozen sand, especially for the high-temperature frozen sand, the filtration-migration deforation composes the most part (near 70-90%) of the total compaction deformation

Compressibility coefficient of frozen soils

The compressibility of frozen soils is a conventionally used characteristic describing the compressive deformability of frozen soils under load, and also a basic factor for predicting foundation settling on plastic frozen subbases with maintenance of negative temperature, so that it is one of the most important mechanical characteristics of frozen soils.

The compressibility coefficient of frozen soils discussed here refers to the summary relative compressiblity coefficient as the strain of frozen samples comes to steady, and is marked with the symbol of α^{Σ}_r.

Experiments showed that the compressibility coefficient of frozen soil: was mainly governed by the temperature and moisture of frozen soils, its composition and the range of external pres-

sure. The temperature of frozen soils was found to have a substantial influence on its compressibility coefficient. According to our test data, a series of graphs of the summary relative compressibility coefficient α^{Σ}_r against the negative temperature $-\theta$ were drawn up respectively for frozen Fenghou Shan loam (Fig. 7) and frozen Lanzhou medium-grained sand (Fig. 8) at various water contents and different external pressures. Evidently, these curves indicate that α^{Σ}_r invariably increases with increasing temperature, and the relations between them can be well described by the following power-law equation (except for Fig. 8a and b)

$$\alpha^{\Sigma}_r = A \cdot e^{B/\theta} \qquad (4)$$

where θ is the absolute value of the negative temperature of frozen soils in °C, and A and B are experimentally determined parameters dependent upon the water content of frozen soils and external pressure. Some of the values of A and B, which are calculated by authors from test data with the re-

72
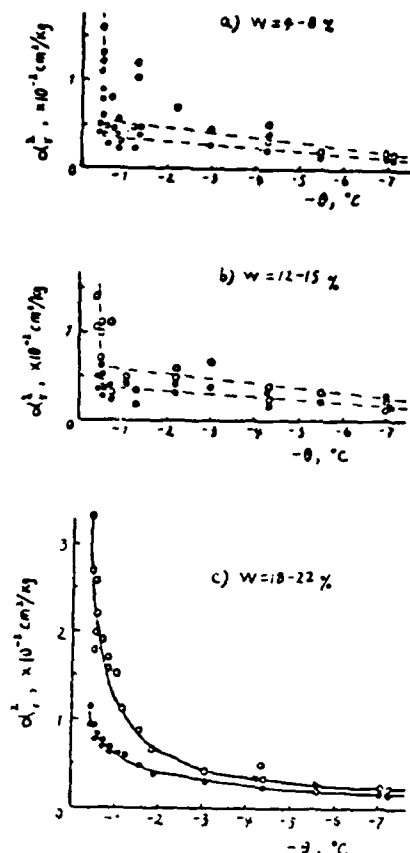
Figure 8. Compressibility coefficient α^{Σ}_r as a function of $-\theta$ for frozen Lanzhou medium-grained sand.
p: o – 0 to 2 kg/cm^2; ● – 0 to 8 kg/cm^2

gressive statistical method, are listed in Table VI.

We note that the compressibility coefficient of frozen soils varies very rapidly with their temperature within the range of higher temperatures (say, for frozen loam, above $-1.0°C$). It means that in this case a very little change in temperature of frozen soils would result in a great variation of magnitude of their compressibility coefficient. From this point of view, thus, when a structure is to be built on warm permafrost, it might be very important and signficicant for engineers to try to make the ground temperature of the working high-temperature frozen subgrade as low as possible, at least lower than the limit of rapid change of its compressiblity coefficient, and to choose the design temperature of the subgrade carefully and reasonably.

Water content of frozen soils also has a certain influence on its compressibility coefficient. For example, from examination of the data given in Figure 7 or Table VIII we can see that for frozen loam with higher temperature the coefficient α^{Σ}_r is greater at the range of water content of 18-40%, and smaller at that of <17% or >50%. But, at lower temperature this difference seems to be insignificant. And, it might be inferred that the coefficient α^{Σ}_r of frozen loam may decrease with further increase in its moisture content, and finally become close to the value of α^{Σ}_{ri} of ice (see Table VII).

Table VI. Values of a and b in equation 4.

Soil type	p, kg/cm^2	W, %	A, kg/cm^2	B, °C
Fenghou Shan loam	0-2	<17	0.0019	0.8
		18-28	0.0015	1.6
		30-40	0.0012	1.5
		50-90	0.0013	1.3
	0-8	<17	0.0022	0.5
		18-28	0.0015	1.1
		30-40	0.0011	1.2
		50-90	0.0010	0.8
Lanzhou medium-grained sand	0-2	18-23	0.0030	1.2
	0-8	18-23	0.0027	1.6

Table VII. Values of α^Σ_r of polycrystalline ice under the pressure of 2 kg/cm².

θ, °C	-0.4	-0.6	-1.1	-1.5	-4.0	-7.0
α^Σ_{ri}, cm²/kg	0.0160	0.0090	0.0050	0.0040	0.0030	0.0019

Note: 1. Density of the ice samples tested averaged above about 0.9 g/cm³;
2. Standard for considering the strain of the ice samples to be steady was 2.08×10^{-5} hr^{-1}.

Another factor that also has a strong influence on the compressibility coefficient of frozen soils is the applied pressure. Some of the experimental values of α^Σ_r for frozen Fenghou Shan loam and Lanzhou medium-grained sand at different ranges of pressure are listed in Tables VIII and IX, respectively. These data clearly indicate that the coefficient α^Σ_r of frozen soils is closely related to the applied pressure, especially fo their negative temperature being higher. Just as unfrozen soils, the coefficient α^Σ_r of frozen sand invariably decreased with the increase in the range of applied pressure. However, there appeared to be a different case for frozen loam with high negative temperature, i.e., the value of α^Σ_r at the range of middle pressure (6-8 kg/cm²) is frequently greater than that at the range of lower pressure (2-4 or 4-6 kg/cm²).

In both Figures 7 and 8, we have drawn the curves of α^Σ_r-θ at the pressures of 2 and 8 kg/cm², respectively. Obviously, the value of α^Σ_r for the former is always greater than that for the latter at the same temperature, and the difference is closely associated with the soil temperature: the higher the soil temperatures the greater does the difference become.

In addition, experiment has shown that the compressibility of frozen soil depends upon the soil composition itself. According to our test data, the coefficient α^Σ_r of frozen Fenghou Shan loam is generally greater than that of frozen Lanzhou medium-grained sand at higher temperature (say above -1.5°C), while there seems to be an insignificant difference between them, and sometimes, the latter becomes even greater than the former at lower temperature. This

might result from the fact that, as is mentioned above, the sand tested contains more fine mineral particles and has lower compressive resistance.

CONCLUSIONS

The results lead to the following conclusions:
1. The values of normal elastic modulus of frozen Fenghou Shan loam and frozen Lanzhou medium-grained sand obtained by the method employed here varied from 1,000 to 5,000 kg/cm² under the pressure of 8 kg/cm² and from 350 to 2,600 kg/cm² under that of 2 kg/cm², respectively, at the temperature not lower than -7°C, and is in good agreement with that calculated from the results of the field load-test and and laboratory uniaxial compression test done by authors. Within this range of negative temperature, the elastic modulus of frozen soils as a function of their temperatures can be well described by the linear equation $E = a + b\theta$.
2. The compacting deformation with lateral spreading of the frozen soils prevented will always be attenuating, and for the high-temperature frozen cohesive soils the decaying creep deformation constitutes most parts (70-90%) of the total compaction deformation, so that the time variations of compacting deformations of the frozen soils can be predicted by the hereditary creep theory or by the power-law expression

$$s_t = s_o (t/T_o)^k$$

presented by the authors.
3. The values of summary compressibility coefficient α^Σ_r of high-temperature plastic frozen soils rank a considerably order, and there-

74

Table VIII. Values of summary relative compressibility coefficient α^Σ_r for frozen Fenghou Shan loam.

Soil temperature θ, °C	Physical indicators		Values of $\alpha^\Sigma_r \times 10^{-4}$, cm²/kg, in the following pressure ranges, kg/cm²			
	Water content w, %	Dry density r_d, g/cm³	0-2	2-4	4-6	6-8
-0.3	14.2	—	263	62	28	20
	20.2	—	444	110	44	21
	35.8	—	1009	284	126	65
-0.5	14.3	—	130	41	33	34
	23.1	1.56	305	21	13	74
	26.4	—	230	55	37	138
	34.0	1.31	293	27	21	91
	40.6	—	320	112	93	175
	52.5	1.06	168	26	17	61
-0.6	18.3	1.72	203	44	34	90
	23.7	—	160	74	73	171
	34.7	1.29	195	33	27	61
	98.6	0.68	101	28	24	48
-0.9	31.5	1.38	73	48	18	22
	20.7	1.63	108	75	30	26
	65.3	0.93	46	34	10	12
-1.0	18.4	1.72	105	37	27	34
	32.6	1.34	75	22	14	24
	69.0	0.86	33	14	8	24
-1.2	18.9	1.68	88	42	34	5
	31.4	1.39	60	29	23	4
	54.0	1.06	39	18	10	4
-1.5	16.5	1.85	40	30	40	28
	38.0	1.31	22	3	25	23
	50.2	1.12	30	20	23	30
-2.0	16.5	1.70	31	36	40	46
	33.0	1.34	25	13	17	14
	66.0	0.91	23	11	13	10
-2.5	17.6	1.76	14	43	45	83
	21.7	1.59	30	65	64	14
	25.6	1.52	18	32	43	50
	31.9	1.35	19	22	43	25
	37.6	1.30	19	9	17	9
	50.6	1.07	17	12	22	17
-3.0	18.1	1.69	19	26	28	46
	31.1	1.33	25	33	27	30
	73.6	0.85	16	9	12	10
-3.4	17.6	1.74	34	90	80	73
	21.7	1.56	19	50	51	47
	25.6	1.53	20	33	48	58
	31.9	1.39	20	6	9	13
	37.6	1.26	26	11	20	20
	50.6	1.07	46	9	17	20
-5.0	16.5	1.85	25	15	8	—
	20.9	1.70	14	14	13	15
	27.3	1.51	18	16	11	12
	30.4	1.43	9	9	8	9
	38.0	1.31	16	10	5	—
	50.2	1.12	28	4	3	--
-7.0	32.9	1.41	9	6	8	—
	41.2	1.18	16	10	12	--
	51.6	1.06	14	11	16	—

75

Table IX. Values of summary relative compressibility coefficient α^{Σ}_r for frozen Lanzhou medium-grained sand.

Soil temperature θ, °C	Physical indicators		Values of $\alpha^{\Sigma}_r \times 10^{-4}$, cm^2/kg, in the following pressure ranges, kg/cm^2			
	Water content w, %	Dry density r_d, g/cm^2	0-2	2-4	4-6	6-8
-0.4	7.6	1.71	37	29	23	33
	14.2	1.74	63	28	20	15
	23.6	1.55	410	52	30	24
-0.5	4.0	1.66	120	19	25	32
	5.5	1.75	113	11	11	19
	6.0	1.57	148	109	58	43
	10.9	1.68	45	29	22	19
	13.4	1.73	320	15	8	16
	19.8	1.57	205	42	57	34
-0.7	5.0	1.63	78	45	38	20
	10.9	1.73	32	28	24	21
	12.3	1.74	116	25	15	13
	20.4	1.59	200	65	35	28
-0.8	6.0	1.57	40	95	54	41
-0.9	9.5	1.72	35	30	22	19
-1.1	7.8	1.70	50	20	11	11
	11.7	1.75	50	116	25	15
	16.8	1.62	162	72	28	18
-1.3	4.0	1.66	120	19	25	32
	5.5	1.75	113	11	11	19
	13.4	1.73	320	15	8	16
-2.2	7.7	1.57	67	—	—	—
	12.3	1.69	65	43	26	23
	15.5	1.73	50	48	36	38
-3.0	7.4	1.69	45	24	24	14
	13.0	1.75	68	34	30	26
	19.8	1.61	41	27	31	60
-4.3	4.5	1.60	55	35	35	35
	6.6	1.69	35	17	12	14
	12.6	1.80	26	24	30	15
	15.2	1.76	40	50	40	25
	18.4	1.64	57	26	28	29
	20.4	1.59	40	35	40	40
-7.0	6.5	1.67	20	20	15	13
	6.6	1.63	19	17	14	13
	12.6	1.85	19	14	16	22
	14.7	1.73	25	25	30	50
	18.4	1.65	27	14	19	12
	22.7	1.54	27	16	17	15

fore, the compressibility of plastic frozen soils must be taken into account in prediction of foundation settling on the plastic frozen sub-grade with maintenance of negative ground temperature.

4. The compressibility coefficient of frozen soils is substantially governed by the soil temperature, and its varying with temperature can be expressed by the power-law equation:

$$\alpha^{\Sigma}_r = A \cdot e^{B/\theta}.$$

5. In view of the fact that there is a considerable difference between the limiting temperature for differentiating the hard frozen soils and plastic frozen soils obtained from our test data and that used in common (the former is lower than the latter), the authors therefore consider that it is necessary for researchers system-

76

atically to investigate the compressibility of various typical frozen soils at negative temperatures so as to rationally determine the limiting temperature for differentiating the hard frozen soil and plastic one in China.

ACKNOWLEDGMENT

The authors wish to thank their colleagues, Zhang Changqing and Fong Cunyao for many of the observations, and Zhang Jingsheng, Tao Zhaoxang, et al., for participating in the test on physical properties of the soils tested.

REFERENCES

1. Tsytovich, N.A.: The mechanics of frozen ground. Scripta Book Co., Washington, D.C., 1975.
2. Wu Ziwang, Liu Yongzhi and Xie Xiede: Load-test on frozen ground in situ. Collections of Permafrost Research, Chinese Science Press (to be published).
3. Zhu Yuanlin, Liu Yongzhi and Xie Xieda. Field test on creep of ground ice. Collections of Permafrost Research, Chinese Science Press (to be published).
4. Zhang Jiayi, Wu Ziwang and Zhu Yuanlin: Strength of frozen soils and their failure behaviours. The Proceedings of First National Conference on Permafrost, Chinese Science Press, 1981.
5. Wu Ziwang, Zhang Jiayi and Zhu Yuanlin: Experimental research on rheology of frozen soils. The Proceedings of First National Conference on Glacier and Permafrost, Chinese Science Press (to be published).
6. Nixon, J.F.: Foundation design approaches in permafrost area, Can. Geotech. J., 15, 96-112 (1978).

FROZEN SHAFTS UNDER
TIME-DEPENDENT LOADING

H. Winter   Institute of Soil Mechanics and Rock Mechanics,
              University of Karlsruhe, D-7500 Karlsruhe, Germany

ABSTRACT

A semi-analytical solution for the creep convergence of a frozen shaft is discussed. A frozen shaft is considered as a rotationally symmetric, thick-walled cylinder under internal and external load with negligible gradients in vertical direction.

A power law is used for the description of the material behavior during the primary and secondary phase of creep. This creep law reflects explicitly the influence of time, temperature, and stress on the creep deformation whereas stress and temperature history are contained implicitly in the parameters of the material law. Taking into account the radial variation of temperature reference solutions, i.e. solutions for unit time, load and temperature variation can be worked out.

The material behavior for time-dependent loading is modeled by a piece-wise power law which admits the use of the reference solutions to construct solutions for the shaft problem under time-dependent loading. The creep deformation and the stresses of the shaft for varying load as an explicit function of time, load, and temperature variation can be used in failure criteria against stress failure and excessive deformation.

Examples from actual shafts and proposals for optimal design are given in this paper.

LONG-TERM CREEP OF FROZEN SOIL
IN UNIAXIAL AND TRIAXIAL TESTS

Wolfgang Orth, Dipl.-Ing. Institute for Soil Mechanics
Helmut Meißner, Dr.-Ing.   and Rock Mechanics
                           University of Karlsruhe
                           D-7500 Karlsruhe, Germany

ABSTRACT

Samples of frozen, fine grained, silty sand are tested in uniaxial and triaxial tests. Sampling took place in situ from frozen subsoil in shafts of up to 300 m depth. Additional samples were prepared and frozen under laboratory conditions. Stresses and temperatures in the laboratory simulated the ones in situ.

The creep behaviour is tested in triaxial compression and extension tests as well as in uniaxial creep tests of about 1000 hours duration. All samples had lubricated and enlarged end platens and a height to diameter ratio of 1.3 or less.

The tests show that the creep behaviour depends on the direction of the stress path in the deviatoric stress plane. The creep rate was never constant, i.e. a so-called secondary creep phase was not observed. A creep law is proposed, which describes the observed creep behaviour.

1. INTRODUCTION

For the calculation of buildings in frozen soil (e.g. tunnels, shafts, excavations) it is necessary to predict strength and deformations prior to the construction. Testing procedures and calculation methods should be available which enable reliable predictions. To develop such methods a research program is promoted in Germany by the Minister of Economics under the name "Tiefe Gefrierschächte", which consists of laboratory tests on undisturbed frozen soil samples and additional in situ measurements of deformations in frozen shafts. To find out the influence of the temperature and stress history, the specimens are taken from deep frozen shafts with registration of the sample orientation. The tests are run under different states of stress according to those in situ.

Test results obtained from cores are usually influenced by inhomogeneities such as fissures etc. Therefore, tests were performed on cores from shafts as well as on artificially frozen samples. The artificially frozen samples were subjected to the same stress and temperature history as those suggested for the cores. In this paper preliminary test results are reported. The influence of different stress states on the creep is shown.

2. SAMPLING

The undisturbed samples of frozen soil have been taken from the bottom of the shafts in blocks having a size of about 40 x 40 x 40 cm. The location of the blocks was precisely registered, and immediately after sampling the blocks were transported to the laboratory. To avoid a disturbance of the cores by sublimation drilling took place just prior to beginning the tests. (Drilling in the laboratory is much easier than in a shaft, so it can be done more carefully, leaving the cores more nearly in their original condition.)

The artificially frozen specimens were prepared in dry state to dense

packing and then saturated with air-free water. Freezing then took place under a load of 0,5 kN/cm^2 at a rate of 3,0 degrees per hour.

3. LABORATORY TESTS

3.1 Testing equipment

All tests are carried out in cooled rooms, so that the temperature is constant throughout the testing equipment. In creep tests a constant load is applied over a duration of 1000 hours or more unless failure occurs before.

The sample diameter is 10 cm; to ensure homogeneous deformation the samples are fitted with lubricated and enlarged end platens and have a height to diameter ratio of 1.3 or less. A rubber sleeve preserves the water content of the specimens.

A load cell controls the hydraulic load system. Axial strain is measured by dial gauges and inductive measuring devices; the radial strain by paper scale-strips used as a gauge. Simulation of the state of stress in deep shafts requires a high confining pressure in the triaxial tests. The triaxial cell used allows confining pressures of 100 bar and a specimen diameter of up to 20 cm. A very stiff load cell for measuring the axial stress σ_1 outside the triaxial cell and a sealing of the piston by a bellow of stainless steel leads to an accuracy of better than 0,06 % of σ_1.

Observation of the specimen and reading of the radial strain scale-strip is made possible by a newly developed optical system.

3.2 Testing conditions

In order to simulate the stress path the frozen soil is subjected to in situ, three types of tests are carried out with a different ratio of axial stress (σ_1) to radial stress (σ_3): (compressive stress is defined as positive)

Uniaxial tests: $\sigma_1 > 0$, $\sigma_3 = 0$
Triaxial compression tests:
$0 < \sigma_3 < \sigma_1$, $\sigma_1 + 2\sigma_3 = $ const
Triaxial extension tests:
$0 < \sigma_1 < \sigma_3$, $\sigma_1 + 2\sigma_3 = $ const.

In triaxial tests the samples are subjected first to an isotropic stress ($\sigma_1 = \sigma_3$) and, after 20 hours, additionally to a deviatoric stress. In this way the settling of the end platens is damped out before the deviatoric deformation starts.

The temperatures during the tests are -20°C and -10°C, respectively.

The three different test series are named:
- Series A: artificially frozen sand samples; uniaxial and triaxial compression tests.
- Series B Cores from coal mine shafts; and C: uniaxial, compression and extension tests.

4. TEST RESULTS

The grain size distributions of the materials used in the three test series are shown in fig. 1.
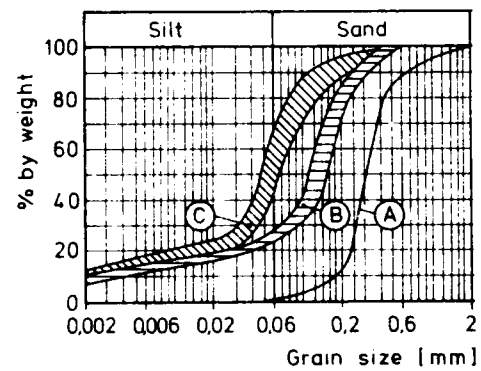
Fig. 1: Grain size distribution of the three tested soils

All soils are nearly water saturated. The dry unit weight γ_d and the water content are given in table 1.

Test series	A	B	C
γ_d [kN/m^3]	17,8	16,8-17,7	16,8-17,6
w [%]	20,0	14,6-17,5	19,2-22,2

Table 1: Dry weight and water content of the specimens

The axes of the cores coincided with the radial directions of the shafts.

In figs. 2, 3 and 4 the creep strains $\varepsilon_1 = -\ln(h/h_0)$ are plotted versus time.

In figs. 3 and 4 results are represented of both compression and extension tests. The axial deformations of samples in extension tests are denoted as negative.

Fig. 2: Axial strain versus time, series A, test results and calculated curves. $T = -20°$
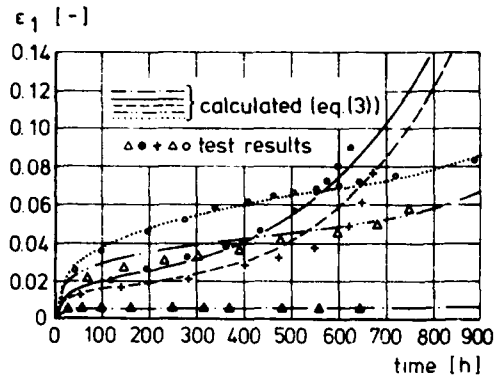
	No	σ_1 [kN/cm²]	σ_3 [kN/cm²]
▲—··—▲	A 175	0.5	—
•——•	A 179	0.9	—
+----+	A 180	0.8	—
△—·—△	A 214	1.3	0.3
•·······•	A 215	1.6	0.4

Fig. 3: Axial strain versus time, series B, test results $T = -10°$
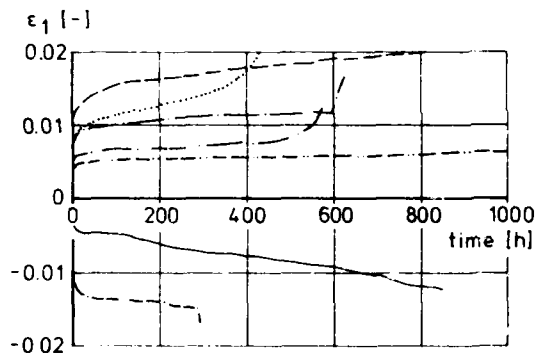
	No	σ_1 [kN/cm²]	σ_3 [kN/cm²]
----	B 5	0.42	—
—··—	B 10	0.285	—
— —	B 100	0.52	0.1
········	B 101	0.62	0.05
— —	B 102	0.45	0.03
—··—	B 104	0.05	0.335
——	B 106	0.05	0.23

Fig. 4: Axial strain versus time, series C, test results $T = -10°$
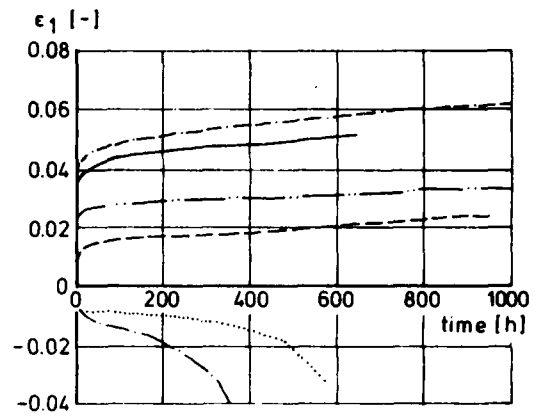
	No	σ_1 [kN/cm²]	σ_3 [kN/cm²]
—··—	C 11	0.207	—
—·—·—	C 15	0.184	—
-----	C 100	0.29	0.166
——	C 101	0.345	0.138
·········	C 103	0.1242	0.2484
—·—·—	C 104	0.1242	0.311

From figs. 2 to 4 it can be seen that the slope of the creep curves (i.e. the creep rate) is never constant. It decreases up to the point of inflection at a time called t_m and a strain ε_m, and then increases again. As some creep curves are rather flat this transition is more easily visible with the aid of
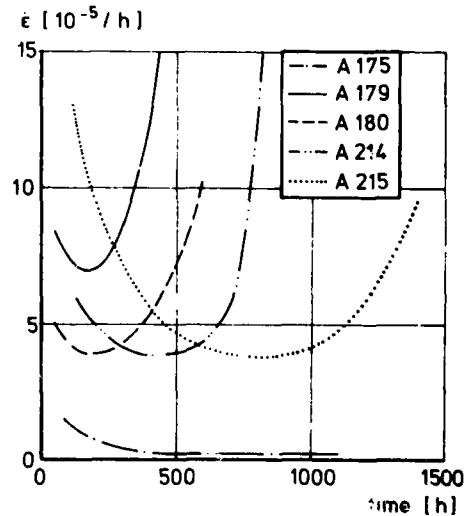
Fig. 5: Axial strain rates versus time, series A, test results

83

strain rates which are plotted versus
time in figs. 5, 6, 7a, 7b.

The strain rate curves are obtained
by graphical differentiation of the creep
curves.

It can be seen that the tests of
all three test series do not yield a so-
called secondary creep phase.

Fig. 7b: Axial strain rate versus time,
test results of series C, uni-
axial tests

tests with the same parameters. This
means, that the failure surface in prin-
cipal stress space is asymmetric besides
a 60°-symmetry as shown in fig. 8.
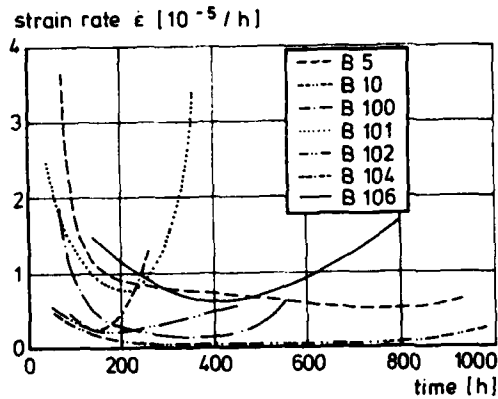
Fig. 6: Axial strain rate versus time,
test results cf series B
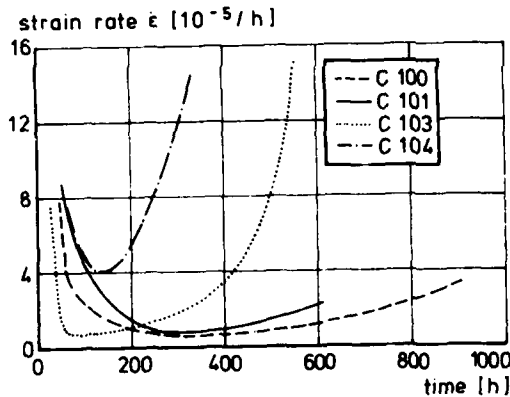
Fig. 7a: Axial strain rate versus time,
triaxial test results of series C

The symbols I_σ and II_s used in the follow-
ing are defined in chapter 5. With α_σ an
angle in the deviatoric plane is denoted
(fig. 8).

The comparison of compression and
extension tests having the same values of
I_σ and $II_s^{1/2}$ yields a different deforma-
tion behaviour. In all cases the exten-
sions lead to higher creep rates and
earlier failure than do the compression

Fig. 8: Trace of failure surfaces in
octahedral plane for a given time

The tests with the same deviatoric
stress $II_s^{1/2}$ but different isotropic
stress I_σ yield a dependence of the creep
behaviour from I_σ also. For frozen sand
an increasing isotropic stress leads to
an increasing creep rate and earlier fail-
ure. Therefore, a creep law has to include
both α_σ and I_σ.

For practical purposes this has the
consequence, that a plasticity rule like
that of v. MISES or TRESCA cannot describe
the frozen material, and it is not certain
whether the parameters taken from com-
pression tests should be used for states
of stress different from those in com-
pression tests.

84

5. CREEP LAW

In this chapter a creep law is proposed, which describes the observed creep curves of frozen soil with decreasin,, and increasing strain rates.

The creep deformations at the times t_m are about 1% to 6% as can be seen from fig. 2 to 4.

Because in all tests only principal strains and stresses have been considered only these are used in the proposed creep law. The principal strain components ε_i, $i = 1, 2 = 3$ and the stress components σ_i are observed to be co-axial. The creep law has to be independent of the used co-ordinate system. Furthermore, the creep law has to describe the creep behaviour independently of dimensions.

In the following a set of parameters are listed which are assumed to influence the creep behaviour of frozen soil. Most of these parameters are common to creep laws of frozen soils and their influence can be observed in tests directly. Here the thermal conductivity and the coefficient of permeability are used in addition for the following reasons.

Vyalov and Tsytovich (1955) explain the physical process of creep in frozen soil by stress concentrations between the soil particles and their points of contact with the ice. These stress concentrations cause pressure-melting of the ice: the water moves to regions of lower stress where it refreezes. Other concepts to describe the creep process in frozen soil are based on the adhesion between the sand particles and the ice (Goughnour and Andersland, 1968). Furthermore, the magnitude of creep depends on the type of soil (as sand, silt or clay) as well as on the density of the soil (Eckardt, 1979, Andersland and Al Nouri, 1970, Sanger, 1968). In these creep concepts the basic idea is a transportation process of water and/or ice through a porous medium which depends on the permeability of the soil. On the other hand, refreezing is influenced by the heat flow. Therefore, the coefficients of permeability and heat conductivity are introduced as parameters in the proposed creep law.

Symbols used for the evaluation of the test results and the representation of the creep law are:

ε_i : principal strain components

s_i : principal deviatoric stress omponents

$\underline{\sigma}$: ,tress tensor

t : time

t_m: time at the point of inflection of the creep curve

ε_m: creep deformation at the time t_m

T : temperature

γ_s: unit weight of solid constituent

e_o: initial void ratio

λ : thermal conductivity

c_s: volumetric heat capacity

k : permeability of the soil

The creep deformations ε_i are assumed to be functions of the parameters listed above, i.e.

$$\varepsilon_i = f_i(\underline{\sigma}, t, T, \gamma_s, e_o, \lambda, c_s, k) \qquad (1)$$

holds with a function f_i.

The following stress invariants are used:

$$I_\sigma = \sigma_1 + \sigma_2 + \sigma_3$$

$$II_s = s_1^2 + s_2^2 + s_3^2$$

In order to make the creep law independent of dimensions a characteristic stress, a characteristic time value and a relative temperature must be introduced. These values exist for each frozen soil, and if they are determined in a physically correct manner a creep law using them can be transferred to any frozen soil.

From parameters listed above we obtain, by means of dimensional analysis (GOERTLER, 1975):

characteristic stress:

$$\sigma_c = \frac{\gamma_s \cdot \lambda}{k \cdot c_s} \quad [\frac{kN}{m^2}]$$

characteristic time:

$$t_c = \frac{\lambda}{c_s \cdot k^2} \quad [sek]$$

related temperature:

$$\theta = \frac{T}{T_s} \qquad T_s = 273,2 \quad [^\circ K]$$

It is noted that the subsequent creep law can also be used with values of σ_c and t_c defined in a different manner.

85

According to VYALOV (1962) the temperature influence can be described by a factor. Then eq. (1) in dimensionless form reads:

$$\varepsilon_i = h_1(\cdot)g_i\left(\frac{t}{t_c}, \frac{I_\sigma}{\sigma_c}, \frac{II_s^{1/2}}{\sigma_c}, \right.$$

$$\left. \cos 3\alpha_\sigma, e_\sigma\right)\frac{s_i}{II_s^{1/2}} \qquad (2)$$

Volumetric strains are defined as

$$I_\varepsilon: = \varepsilon_1 + \varepsilon_2 + \varepsilon_3$$

Volumetric strains obtained by tests are time dependent only in the first creep phase of about 100 hours. During the subsequent creep phase the volumetric strains remain nearly constant. As was found from preliminary tests the volumetric strains can be approximated by

$$I_\varepsilon = h_2\left(\frac{t}{t_c}, \frac{I_\sigma}{\sigma_c}, \cos\alpha_\sigma, e_o\right) \qquad (3)$$

For compression and extension tests the deformations ε_2 and ε_3 become

$$\varepsilon_2 = \varepsilon_3 = I_\varepsilon^- \varepsilon_1.$$

In the following a functional form for g_i is proposed. To reduce the number of parameters in eq. (2), tests with only one temperature and one material are considered. Furthermore, only compression tests are taken into consideration and only for ε_1 a representation is proposed as follows:

$$\varepsilon_1 = \varepsilon_m\left[a\left(\frac{t}{t_m}\right)^{\lambda_1} + b\left(\frac{t}{t_m}\right)^{\lambda_2}\right]\frac{\sigma_1-\sigma_2}{II_s^{1/2}} \qquad (4)$$

The parameters a and b are found to be constant for all test series:

a = 0,97
b = 0,03

The other auxiliary coefficients can be approximated as follows:

$$t_m = t_c\, a_1 \exp\left(a_2 \cdot \left(\frac{II_s^{1/2}}{\sigma_c}\right)^{a_3}\right) \cdot \left(\frac{I_\sigma}{\sigma_c}\right)^{a_4} \qquad (5)$$

$$\varepsilon_m = b_1\left(\frac{II_s^{1/2}}{I_\sigma}\right)^{b_2} \cdot \left(\frac{I_\sigma}{\sigma_c}\right)^{b_3} \qquad (6)$$

$$\lambda_1 = c_{11}\left(\frac{II_s^{1/2}}{\sigma_c}\right)^{c_{12}} \exp\left(c_{13} \cdot \frac{I_\sigma}{\sigma_c}\right)$$

$$\lambda_2 = c_{21}\left(\frac{II_s^{1/2}}{\sigma_c}\right)^{c_{22}} \exp\left(c_{23} \cdot \frac{I_\sigma}{\sigma_c}\right) \qquad (7)$$

As b = 0 leads to an only negligible difference for $t < t_m$ it can be seen that for uniaxial tests eq. (4) is equivalent to the well-known VYALOV creep law.

For tests of series A the following values of the parameters were determined by the method of least squares:

k = 1,3 10^{-3} m/sec (after TERZAGHI)
λ = 3,47 W/m$^\circ$K (after ANDERS-
c_s = 1,89 MJ/m $\cdot ^\circ$K   LAND/ANDERSON)

σ_c = 3,71$\cdot 10^{-6}$ [kN/cm^2]
t_c = 1,088 [sec]
θ = 0,93

The coefficients of equations (5), (6) and (7) then are

$$t_m = 8,51\cdot 10^{-10}\exp\left[\left(\frac{II_s^{1/2}}{\sigma_c}\right)^{-1,85} \cdot 7,8\cdot 10^9\right]$$

$$\left(\frac{I_\sigma}{\sigma_c}\right)^2$$

$$\varepsilon_m = 5,8\cdot 10^{-14}\left(\frac{II_s^{1/2}}{I_\sigma}\right)^{1,5} \left(\frac{I_\sigma}{\sigma_c}\right)^{2,2}$$

$$\lambda_1 = 1,3\cdot 10^{-12}\left(\frac{II_s^{1/2}}{\sigma_c}\right)^{2,18}\exp\left(-1,47\cdot 10^6\frac{I_\sigma}{\sigma_c}\right)$$

$$\lambda_2 = 1,53\cdot 10^7\left(\frac{II_s^{1/2}}{\sigma_c}\right)^{-1,31}\exp\left(2,69\cdot 10^6\frac{I_\sigma}{\sigma_c}\right)$$

The creep curves calculated with these equations (4), (5), (6), (7) and with the determined parameters are shown in fig. 2.

ACKNOWLEDGEMENTS

86

REFERENCES

ANDERSLAND, O.B. and ALNOURI, I., Time-dependent strength behaviour of frozen soils, Journal of the Soil Mechanics and Foundations Division, ASCE, Vol. 96, No. SM4, July 1970

ANDERSLAND, O.B. and ANDERSON, D.W., Geotechnical engineering for cold regions, McGraw-Hill Inc., 1978

ECKARDT, H., Tragverhalten gefrorener Erdkörper, Veröffentlichungen des Instituts für Bodenmechanik und Fels-mechanik, Universität Karlsruhe, Heft 81, 1979

GÖRTLER, H., Dimensionsanalyse, Springer-Verlag, 1975

GOUGHNOUR, R.R. and ANDERSLAND, O.B., Mechanical properties of a sand-ice system, Journal of the Soil Mechanics and Foundations Division, ASCE, Vol. 94, No. SM4, July 1968

SANGER, F.J., Ground freezing in construction, Journal of the Soil Mechanics and Foundations Division, ASCE, Vol. 94, No. SM1, Jan. 1968

VYALOV, S.S., The strength and creep of frozen soil and calculations for soil-ice retaining structures, U.S.Army CRREL, Trans. 76, Hanover, N.H., 1962

VYALOV, S.S. and TSYTOVICH, N.A., An estimate of bearing power of frozen soils, Dokl. Akad. Nank, S.S.S.R., 1955

COMPARATIVE RESPONSE OF SOILS TO FREEZE-THAW AND REPEATED LOADING

Bernard D. Alkire, Michigan
  Technological University, USA
James A. Morrison, Michigan
  Technological University, USA

The shear strength and pore pressures at failure from a laboratory test program are obtained from consolidated undrained triaxial tests. Tests were conducted using unfrozen monotonic, unfrozen, repeated, freeze-thaw monotonic, and freeze-thaw repeated loading. All tests were loaded to failure. In addition to the various types of load and temperature conditioning, the effect of density and soil type are studied. Samples compacted at 1.5 Mg/m^3 and 1.6 Mg/m^3 are used to provide information related to behavior of soils that are "dense" and "loose". Tests on samples of Elo clay and Manchester silt provide the results for determining the effect of soil type. Results are explained by considering the effect of the various tests on the structure of the soil. It is shown that a soil subject to freeze-thaw may be more sensitive to repeated loading than a soil that has not been subjected to freeze-thaw.

INTRODUCTION

Stress cycling has been shown to effect both the strength and deformation characteristics of soils. Stress cycling can occur by different means such as temperature cycling, (freeze-thaw) or repeated axial load cycling. In either case changes in structure brought about by the stress cycling can be used to predict the behavior of soil subject to stress cycling.

It is the purpose of the research presented in this paper to investigate the effects of freeze-thaw and repeated load cycling as they affect the strength and deformation characteristics of soils. To do this, series of four types of triaxial tests were conducted on two soil types compacted to various densities. The unfrozen monotonic (UF-M) tests served as a control series to which the other tests were compared. To isolate the effect of a single freeze-thaw cycle, the frozen monotonic tests (F-M) were conducted and the results compared to the unfrozen series. To isolate the effects of repeated loading (UF-RL), samples were subject to 600 cycles of load between approximately 75% and 25% of the estimated failure load, and the results then compared to the UF-M series. Tests were also conducted with both freeze-thaw and repeated loading (F-RL) to investigate the combined effect of temperature and stress conditioning.

SOILS INVESTIGATED

Manchester Silt: The primary soil in this investigation is Manchester silt obtained from New Hampshire. The soil is light brown in color with sub-rounded to sub-angular particles. The liquid limit is 25% and the plastic limit is 23%, with a specific gravity of 2.72. The Unified classification is ML. 95% of the soil particles are smaller than 0.074 mm and 10% are smaller than 0.002 mm.

Elo Clay: The second soil investigated was an Elo clay obtained from the western upper peninsula of Michigan. The soil is reddish brown in color. The

liquid limit is 38% and the plastic limit is 25% with a specific gravity of 2.79. The Unified classification is CL. 95% of the soil particles were less than 0.074 mm and 30% are less than 0.002 mm.

SAMPLE PREPARATION

Manchester Silt: Samples were compacted to a density of either 1.6 Mg/m^3 or 1.5 Mg/m^3 at a water content of 20%. After compaction the samples were removed from the compaction mold, weighed, measured, placed in a triaxial cell and saturated before testing.

Elo Clay: Elo clay samples were formed by accelerated sedimentation from a clay-water slurry in plexiglass cylinders. All samples came out to a saturated density of 1.77 Mg/m^3 $\pm$ 1% and a void ratio of 1.3 $\pm$ 1%.

LOADING SYSTEM

Several conventional loading systems were used for the unfrozen monotonic tests. However, the repeated load tests and the freeze-thaw tests were run on the system shown in Fig. 1. Cell pressures were generated by compressed air acting through a backpressure panel. The panel independently regulates both confining fluid and pore pressure. The air-driven loading ram is connected to an electro pneumatic regulator and opens to house air through a controlling valve which is used to increase or decrease the load. For the case of repeated loading, the pneumatic regulator is controlled by a function generator. Pore pressure was monitored with a pressure transducers mounted on the backpressure panel and the bottom drainage line of the freeze-thaw triaxial cell. Both transducers gave identical results.

Samples subjected to freeze-thaw cycling were frozen in a modified triaxial cell; see Fig. 1. The cell has 9.52 mm copper tubing coil mounted around its inside perimeter. A cooling fluid (ethelene glycol) is circulated through the coil via a refrigerated circulating bath. The confining fluid used inside the triaxial cell is also a solution of ethelene glycol and water.

RESULTS

Shear Strength at Failure: Perhaps the most important parameter to observe is the effect of freeze-thaw and repeated loading on the shear strength at failure. For dense Manchester silt, the maximum shear strength at failure is seen plotted against consolidation stress in Fig. 2. The values shown here are the average of all tests for the given type. As seen here, the effect of a single freeze-thaw cycle is to increase the shear stress at failure from that of the UF-M
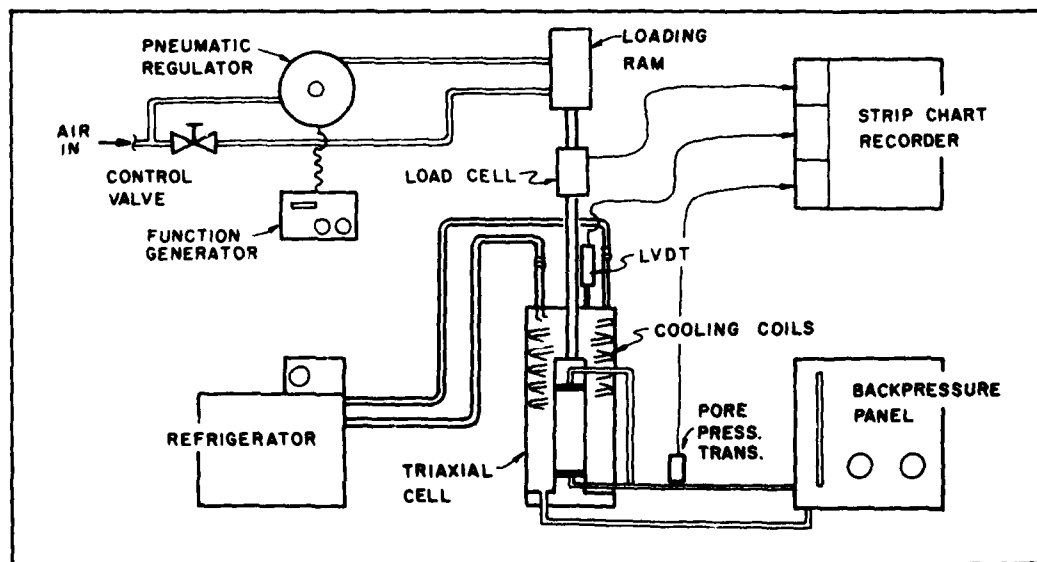
Fig. 1 Test Equipment for Freeze-Thaw and Repeated Load Test.
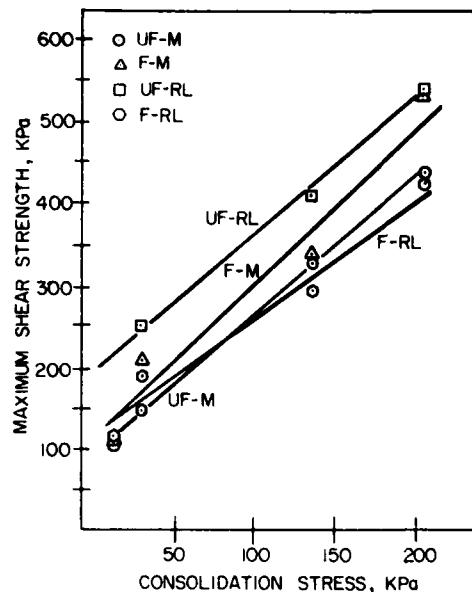
Fig. 2 Shear Strength versus Consolidation Stress for Dense Manchester Silt.
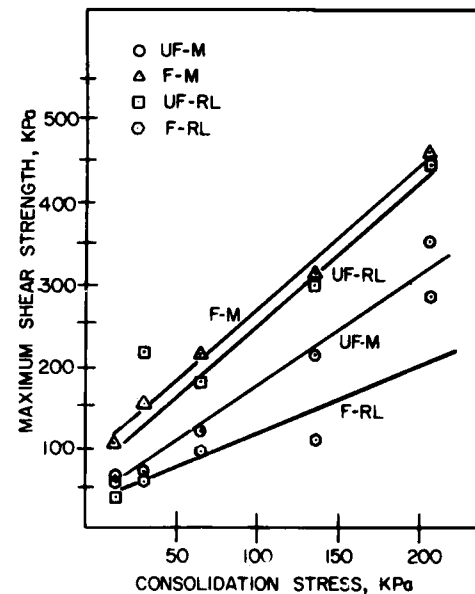
Fig. 3 Shear Strength versus Consolidation Stress for Loose Manchester Silt.

control series.

The effect of repeated loading is also seen to increase the shear strength at failure significantly (20% to 35%). The effect of both freeze-thaw and repeated loading is to increase the shear strength at low consolidation stresses and decrease the shear strength at higher consolidation stress from that of the control series.

For loose Manchester silt, the trend observed for shear strength at failure is similar to that observed for dense silt, for samples subjected to freeze-thaw or repeated load as can be seen in Fig. 3. However, the samples subject to repeated loading produced higher shear strength than those observed in the freeze-thaw tests series. The results for the freeze-thaw and repeated loading tests are the same as for the dense silt but with greater difference when compared to the UF-M samples.

For Elo clay, the shear strength at failure was again higher for samples subject to a freeze-thaw or repeated load cycle than for the unfrozen UF-M control series as seen in Fig. 4.
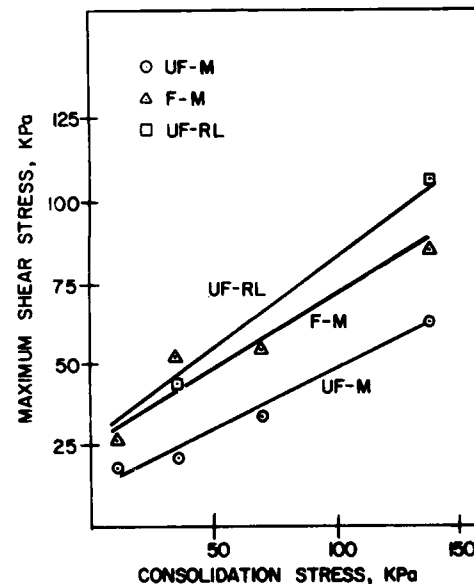
Pore Pressure Development: Pore pressure measurements were observed versus time during all freeze-thaw cycles. A typical response for all tests on Manchester silt is shown in Fig. 5. All

Fig. 4 Shear Strength versus Consolidation Stress for Elo Clay.

samples showed an initial drop in pressure of approximately 13.8 kPa as the temperature neared freezing. As the pore fluid began to freeze, a characteristic jump in pore pressure was observed. The magnitude of this observed jump is
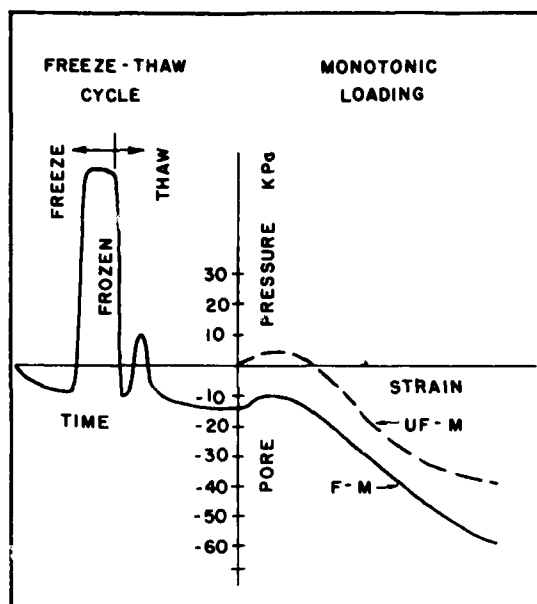
Fig. 5   Pore Pressure Response During
Freeze-Thaw and Monotonic Loading
for Manchester Silt.

Fig. 6   Pore pressure Response During
Freeze-Thaw and Monotonic Loading
for Elo clay.

not considered typical of the pore pres-
sure at the interior of the sample be-
cause the observed reading includes the
freezing and blockage of the drainage
lines leading from the sample. Freezing
was continued for approximately two hours
after the initial jump in pore pressure
to insure complete freezing of the sample.
When freezing was stopped and thawing
commenced, a rapid drop in pore pressure
was observed, followed by a second small
rise which slowly dissapated over a per-
iod of approximately 16 hours, leaving a
net decrease in pore pressure of approxi-
mately 13.8 kPa. This net decrease in
pore pressure corresponds to a net in-
crease in the effective stress state of
the sample after freeze-thaw condition-
ing.

Samples of Elo clay that were sub-
ject to freeze-thaw conditioning showed
similar pore pressure response to that of
Manchester silt during the pre-freeze and
frozen portions of the freeze-thaw cycle.
However, the residual pore pressure and
consequentially the effective stress
state after thawing were quite different
and appear to be dependent on the conso-
lidation stress as shown in Fig. 6. A
net increase in pore pressure and cor-
respondingly a decrease in the effective
stress state was observed for all samples
of Elo clay subject to a single freeze-

thaw cycle. Those samples consolidated
at low stress levels showed a net rise of
6.89 kPa or less after thaw while those
consolidated at 68.9 kPa showed a net
rise of 34.5 kPa and those consolidated
at 138 kPa showed a net rise of 68.9 kPa.
Following the end of thaw the samples
were either loaded monotonically to fail-
ure or had a repeated load applied fol-
lowed by monotonic loading to failure.
Typical examples of the pore pressure
change during monotonic loading for Man-
chester silt and Elo clay are shown in
Fig. 5 and 6 respectively.

Pore Pressures at Failure: A parameter
of interest in determining the effects of
freeze-thaw or repeated loading on soils
is the pore pressure observed at failure.
The final pore pressure for samples of
dense Manchester silt (1.6 Mg/m^3) are
shown in Fig. 7. As seen here, all tests
showed negative pore pressure at failure.
The pore pressure for the UF-M control
series is seen to be a uniform -30 kPa.
The effect of both a single freeze-thaw
cycle and repeated loading is a decrease
in pore pressure at failure. The freeze-
thaw cycle is seen to rise from -70 kPa
at low consolidation pressures to -50 kPa
at a consolidation stress of 138 kPa.
Samples subject to repeated loading pro-
duced pore pressures at failure as low as
-100 kPa. A different result was ob-
served for samples subject to both

92
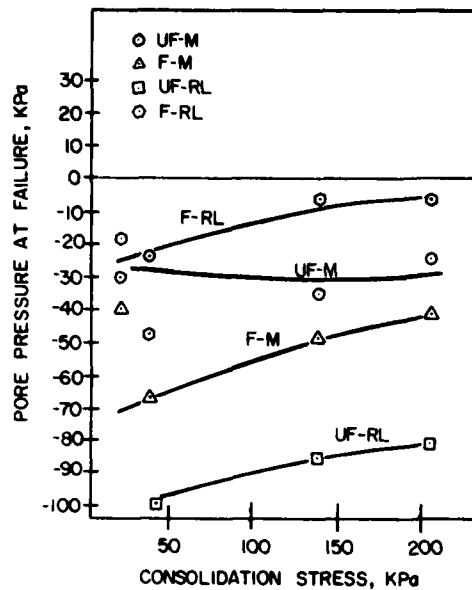
Fig. 7 Pore Pressure at Failure versus
Consolidation Stress for Dense
Manchester Silt.
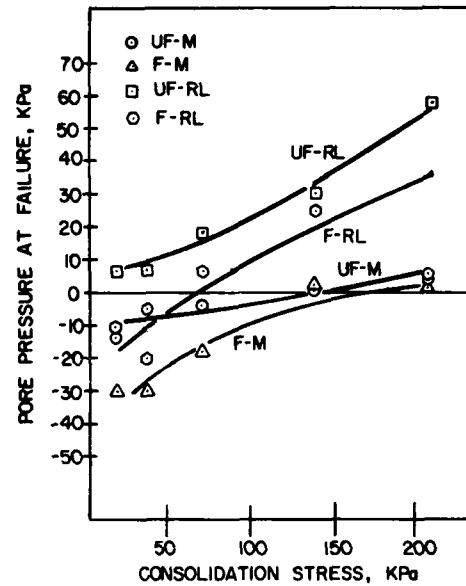
Fig. 8 Pore Pressure at Failure ver-
sus Consolidation Stress for
Loose Manchester Silt.

freeze-thaw and repeated loading. In
this case, the pore pressures at fail-
ure were approximately the same as those
for the unfrozen control series at low
consolidated stress and increasing to
-5 kPa at 138 kPa consolidation stress.
In all cases, the dense Manchester silt
showed pore pressures at failure typi-
cal of a dilative soil.

Pore pressures at failure for loose
Manchester silt (1.5 Mg/m^3) are shown
in Fig. 8. As expected, higher pore
pressures at failure were observed for
the loose silt than for the dense silt.
The effect of a single freeze-thaw cy-
cle was a net decrease in pore pressure
of between 6.9 kPa and 20.7 kPa compared
to the UF-M control series. The results
of a limited number of repeated load
tests indicate a trend of higher pore
pressures at failure than those for the
soil subjected to a freeze-thaw cycle.
Tests on samples subject to both freeze-
thaw and repeated load showed an effect
comparible to what occurred for the
dense samples.

Pore pressures at failure for Elo
clay are shown in Fig. 9. As seen here,
pore pressures at failure are nearly
0 kPa for samples at low consolidation
stress, rising linearly to 75.8 kPa for
samples consolidated to 138 kPa. The
effect of a single freeze-thaw cycle is
seen to produce slightly higher pore
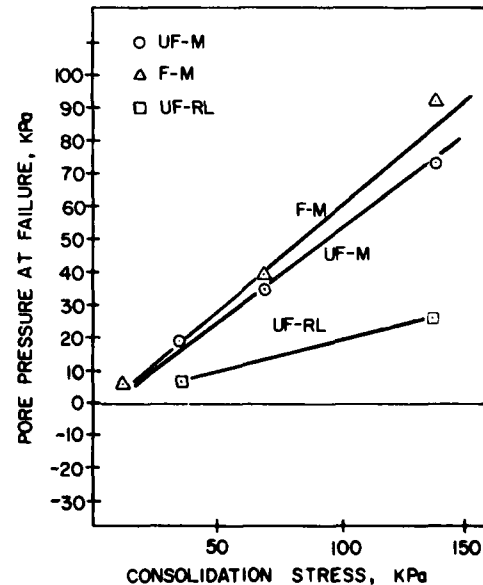
Fig. 9 Pore Pressure at Failure ver-
sus Consolidation Stress for
Elo Clay.

pressure at failure at all consolidated
stresses. However, one must keep in
mind that the residual pore pressure
after the freeze-thaw cycle also in-
creased with increasing consolidation

93

stress. Therefore, the change in pore pressure due to loading was negligible to a modest increase of 13.6 kPa.

INTERPRETATION OF RESULTS

W   samples of Manchester silt are compac.   , it is assumed the initial particle structure is single grained. As soil freezing beings ice crystals will develop along the freezing front. Since drainage lines are closed, the sample will remain at constant volume and as the ice crystals grow soil particles will be displaced into a new structure with the same void ratio but a larger pore network. As thawing commences this "metastable" structure of dense clusters and larger void spaces formed during freezing will remain. This change in soil structure could account for many of the results observed for the soil samples following freeze-thaw. (This is also in agreement with the structural changes observed by Chamberlain (1) on material dredged from waterways subject to freeze-thaw and by Thomson and Lobacz (4) while observing the increased shear strength that develops along a freeze-thaw interface). For example, upon loading it was observed that the loose silt showed an increase in initial tangent modulus when the unconditioned samples were compared to the samples conditioned with a cycle of freeze-thaw. The dense silt also showed the same relationship for the initial tangent modulus as well as an increase in strength at failure for the freeze-thaw treated silt. Both dense and loose silt produced dilative behavior at failure after freeze-thaw as indicated by the more negative pore pressure at failure. To justify the increase in strengtn occurring after freeze-thaw, it is assumed that the "metastable" soil structure mentioned earlier is stiffer than the normal as compacted structure leading to the higher strengths.

Similar to freeze-thaw, repeated load conditioning also produced higher shear strengths at failure. Here it is assumed that a rearrangement or densification of the soil rather than development of structure is responsible for the increases in strength. This explanation has been suggested by Finn, et al. (2) when examining the response of soils to cyclic loads. He explains that for dense soils the pore pressure will increase during the initial stage of a load cycle and then quickly level off or decrease for the remaining of cycles. What

is assumed here is the soil, although initially in a dense state, first becomes liquified and then reorganizes into a denser state.

For loose silt, the soil structure will simply compact into a denser arrangement producing the increase in pore pressure observed during the repeated load sequence of these tests. Thus, for both the dense and loose silt repeated loads produced denser samples with greater strength as noted in the test results.

For samples subject to freeze-thaw followed by repeated loading, a general decrease in strength was observed at failure. An explanation of this can be derived from the observations presented earlier.

After freeze-thaw the soil structure was presumed to be in a metastable state where clumps of densely packed particles are separated by an open pore network. Upon application of a repeated load, the clumps will tend to break apart causing a reduced resistance to shear and lower strengths as noted in the tests.

Therefore, it seems that the strength of a soil after freezing can be explained in terms of structure and changes in structure brought about by the freezing process. This could be a significant finding since it would imply that soils subjected to freeze-thaw would be particularly sensitive to repeated loading. This would make it imparitive that adequate seismic analysis be performed on any structure that passes through a zone of soil subjected to freeze-thaw.

SUMMARY

In order to investigate the effects of freeze-thaw and repeated loading on soils, four series of triaxial tests were conducted. Samples were subject to either one freeze-thaw cycle or 600 cycles of repeated loading or both and then loaded to failure, the results were then compared to those tests without temperature or repeated load conditioning.

The main observations noted were:
1) Freeze-thaw conditioning produced changes in the effective stress state of the samples; a net increase in effective stress for Manchester silt and a net decrease in effective stress for Elo clay.

94

2) Pore pressures at failure were negative for soils conditioned with freeze-thaw and repeated loading in dense silt and for freeze-thaw on loose silt. Repeated loading of loose silt produced higher pore pressure at failure. Freeze-thaw produced high positive pore pressures at failure for Elo clay. The effect of both freeze-thaw and repeated loading on dense silt was generally higher pore pressures at failure than those observed in the unfrozen monotonic case.

3) The shear strength at failure was higher in all cases for samples subject to either freeze-thaw or repeated loading. However, samples of dense silt subject to both freeze-thaw and repeated loading produced lower shear streng⁺h at high consolidation stress than those observed for unfrozen monotonically loaded silt.

ACKNOLWEDGMENT

REFERENCES

1. Chamberlain, Edwin J. and Blouin, Scott E., "Densification by Freezing and Thawing of Fine Material Dredged From Waterways", Third International Conference on Permafrost, Ec onton, Alberta, Canada, 1978.

2. Finn, W. D. L., Lee, K. W., Martin, G. R., "An Effective Stress Model for Liquefaction", Liquefaction Problems in Geotechnical Engineering, ASCE, Preprint 2752, 1976.

3. Sangrey, D. A., Castro, G., Poulos, S. J., and France, J. W., "Cyclic Loading of Sands, Silts, and Clays", Earthquake Engineering, Engineering and Soil Dynamics, Vol. 2, ASCE, 1978.

4. Thomson, S. and Lobacz, E. F., "Shear Strength at a Thaw Interface", Proceedings 2nd International Conference on Permafrost, North American Contribution, Yakutsk, USSR, 1973.

SHORT-TERM CYCLIC FREEZE-THAW EFFECT ON STRENGTH PROPERTIES OF A SENSITIVE CLAY

R.N. Yong[1]
P. Boonsinsuk[2]
D. Murphy[3]

ABSTRACT

The problem of strength changes due to cyclic freeze-thaw effects in freshly cut slopes and surfaces in a sensitive clay soil not previously exposed to frost penetration is examined in this study - using undisturbed natural samples obtained from a field test site. In the tests conducted, the strength and thixotropic strength ratio of the soil samples in the actual unfrozen state were first established - together with initial compositional characteristics. Following this, the samples were subjected to various cycles of freeze-thaw, with strength properties measured after the first and eighth freeze-thaw cycles.

The results will examine the effects obtained in the cyclic freeze-thaw problem, together with compositional influences and control.

[1]Director, Geotechnical Research Centre and William Scott Professor of Civil Engineering and Applied Mechanics, McGill University, Montreal, Quebec, Canada.

[2]Research Associate, Geotechnical Research Centre, McGill University, Montreal

[3]Professional Research Assistant, Geotechnical Research Centre, McGill University, Montreal.

INTRODUCTION

The problem of stability of freshly exposed "never-frozen" clay soils obtained as a result of excavations and cut-slopes subject to initial freezing and subsequent cyclic freeze-thaw is indeed a significant problem. The paramount questions posed relate to changes in the mechanical properties of the soil because of soil freeze/thaw, since standard practice addresses determination of soil properties using core samples obtained in the original "never-frozen" soil. Because of the displacement and stress effects in freeze/thaw, resultant changes in soil structure will occur, thus altering (and generally reducing) the strength of the soil. The nature and extent of these alterations have not been previously modelled or studied.

The soil behaviour after undergoing a number of laboratory simulated freeze-thaw cycles is evaluated in terms of shear strength, liquid limit, pore fluid chemistry and soil suction. The results of this study should reflect the effects of seasonal freeze-thaw on freshly cut slopes and surfaces exposed by excavation or nature (erosion, landslide, etc.) in a sensitive clay which lies below the present frost front.

EXPERIMENTAL PROCEDURE

The soil samples used in this investigation were obtained as undisturbed block samples from Matagami, northern Quebec. Each block sample was 20 cm in

diameter and 7 to 20 cm in height. The
specific blocks employed were recovered
from the depth between 7.72 m and 8.87 m
below the ground surface. The soil is
a sensitive v. rved clay with alternate
light and dark layers of which the exact
boundaries are difficult to locate. The
general properties of the soil in this
depth are summarized in Table 1a and 1b.

Table 1a   Physical Properties of the
           7.72 m to 8.87 m Depth Layer

Plastic limit	24-29%
Liquid limit	65-83%
Natural moisture content	83-94%
Sensitivity (fall-cone method)	4-10
Clay content (less than 2 μm)	70-75%
Silt	16-23%
Sand	0- 2%

Table 1b   Semiquantitative Mineralogical
           Composition of the 7.72 m -
           8.87 m Depth Layer*

Illite	30-40%
Kaolinite	5-10%
Quartz	35-45%
Feldspar	10-15%
Chlorite	0- 5%
Horneblende	0- 5%
Lime	2- 4%
Amorphous	10-12%

*
from X-ray diffractograms and semi-
quantitative analysis - done by peak
height comparison with pure minerals

The overall test program is summa-
rized in Table 2 together with the depths
of the block samples used. Several
blocks from different depths had to be
tested due to the extensive test program
and the limited availability of the
samples. Nevertheless the samples were
located within 1 m from each other. In
general, the physico-chemical properties
of the natural soil were first establi-
shed as references while certain charac-
teristics of interest were evaluated
after the samples underwent the required
number of cyclic freeze-thaw cycles.

Two test conditions were imposed
during thawing, namely: closed system
(i.e. constant moisture content through-
out the freeze-thaw cycles) and open
system (i.e. permitting drainage during
thawing while allowing no water up-take
during freezing). Each sample was
subjected to a freezing temperature of

-12°C for 12 hours after which thawing
was activated at a temperature of +28°C
for another 12 hours, thereby constitu-
ting one cycle of freeze-thaw.

The effects of cyclic freeze-thaw
on the specific properties investigated
will be discussed in the following
sections together with the details of
test procedures involved.

RESULTS AND DISCUSSION

Shear Strength

The undisturbed shear strength of
the natural soil was first determined
by performing the fall-cone test direc-
tly on the horizontal faces of the block
samples. For cyclic freeze-thaw testing
undisturbed samples, each being 4.5 cm
in diameter and 4.5 cm in height, were
carefully trimmed from the block samples
and installed in plastic containers of
similar diameter which were insulated
with thick styrofoam on all sides except
the top to simulate one dimensional
freezing and thawing. Drainage facility
was provided at the bottom of each sam-
ple for the 'open system' series. For
both 'closed system' and 'open system',
the shear strength was determined by the
fall-cone method at the end of the
specified number of freeze-thaw cycles
(at 1 and 8 cycles). Subsequently the
sample was remoulded and tested again
at various aging times to evaluate its
thixotropic strength gain. The aging
times investigated for the closed system
(no drainage) were 1,2,4,8 and 41 days
while those for the open system (with
drainage) were 1,2,4,8 and 32 days. The
moisture content in each sample was kept
constant at all times during the test.
The results of the shear strength at
different numbers of cyclic freeze-thaw
and aging times are shown in Fig. 1.

It is evident from Fig. 1a (no
drainage) that freezing and thawing can
cause a significant degree of disturbance
in the sensitive clay tested. At the
end of thawing, free water usually
appeared on top of the samples, thereby
preventing any meaningful measurement of
shear strength at '0' aging days.
Increasing the number of cycles of
freeze-thaw obviously leads to a decrease
in the shear strength. Note that most
of the strength reduction occurs in the
first freeze-thaw cycle. This observa-
tion is particularly significant since
it dramatizes the problem of first exp-
osure of "never-frozen" clays. Of

particular interest is the observation that the first freezing and thawing cycle results in lower remoulded strengths when compared to that obtained by the manual remoulding process ('0' cycle). Such a phenomenon indicates that freezing a sensitive soil with its natural moisture content higher than the liquid limit produces a relatively high remoulding energy due to stresses generated in volumetric expansion of the pore water during phase changes from water to ice. In addition, the rate of thixotropic strength gain of the soil subjected to cyclic freeze-thaw appears to be slightly less than that of the natural soil.

The effects of cyclic freeze-thaw on shear strength under the 'open' system (with drainage during thawing) cannot be directly compared due to drastic decreases in water content from 91.8% (natural) to 70.7% (1 cycle of freeze-thaw) and 51.5% (8 cycles). The unfrozen water content of the natural soil determined by the calorimetric method is found to be approximately 11% at $-12^\circ C$ (temperature used during freezing). Thus when the soil is first frozen, about 80% of water, primarily free water in the pores becomes ice after which about 20% of the original water content is drained during thawing. This reflects the change in the capability of the soil structure in retaining water while thawing. The rate of thixotropic strength gain (Fig. 1b) of the sample subjected to 8 freeze-thaw cycles is the highest amongst all the tests performed.

Moisture Content Distribution

The distribution of moisture content along the varved soil samples due to cyclic freeze-thaw was investigated by subjecting two soil columns (each being 4.0x4.0x6.3 cm in dimension) to 1 and 8 cycles of one-dimensional freeze-thaw (with drainage during thawing). Upon completion of the specified freeze-thaw cycles, detailed moisture profiles were established as depicted in Fig. 2. It is evident that the light layer, which should be composed of coarser soil particles in comparison to those of the dark layer, retains less water. Cyclic freeze-thaw results in a decrease in water content which in turn leads to a reduction in the overall sample height, thereby changing the positions of the varves. More changes in the water content are noticeable in the

dark layer when compared to the light one. The complex distribution of moisture content would undoubtedly complicate the soil behaviour during freeze-thaw.

Liquid Limit

To determine the influence of cyclic freeze-thaw on the liquid limit, soil samples were subjected to various numbers of freeze-thaw cycles in both systems, i.e. closed system (no drainage) at 10,20,30,40,70,80 and 90 cycles and open system (with drainage) at 1 to 8 cycles. Due to the limited availability of block samples, the samples used in this test series were taken from different blocks (Table 2). Thus comparison between the results from the two systems should be qualitative rather than quantitative.

Each sample, 8.2 cm in diameter by 1.1 cm in thickness, was installed in a plastic container and subjected to one-dimensional freeze-thaw in the same manner as mentioned earlier.

The relationships between the liquid limit and the number of freeze-thaw cycles for both test conditions are shown in Fig. 3. Significant decreases in the liquid limit are evident as the freeze-thaw cycles increase. For the closed system series, the decrease in the liquid limit occurs primarily in the first 30 cycles. The liquid limit drops from 71.4% (natural) to about 54% (30 cycles) after which its value stabilizes around 47% at 90 freeze-thaw cycles. In the case of the open system (with drainage), the liquid limit experiences more change than the closed system value when compared at the same freeze-thaw cycle. The liquid limit drops from 69.2% at the natural state to 56% at 8 cycles of freeze-thaw. The difference between the results from the two test conditions, i.e. with and without drainage, seems to be dependent on the salt concentration of the pore fluid and the amount of frozen water. The decrease in the liquid limit caused by cyclic freeze-thaw should be due to changes in the interparticle forces between the clay fractions which can be verified by pore fluid chemistry, particle size distribution and soil suction as presented in the following discussions.

Pore Fluid Chemistry and Exchangeable Cations

The soluble cation concentration in the pore fluid was analysed through the saturation extract of soil samples subjected to 1 and 8 freeze-thaw cycles together with that of the natural soil for comparison. Each sample was 8.2 cm in diameter and 3.3 cm in height and the freeze-thaw procedure followed the aforementioned technique. Drainage facility was provided during thawing (i.e. open system). At the end of the specified number of cyclic freeze-thaw cycles the four main cations (namely Na^+, K^+, Ca^{+2} and Mg^{+2}) were determined. In addition, the exchangeable cations and the cation exchange capacity were also evaluated using the method proposed by Chhabra et al (1975).

The results accumulated in Table 3 indicate that the soluble salt concentration decreases as the number of freeze-thaw cycles increases. Such behaviour occurs in both monovalent and divalent ions except K^+. The exchangeable cations, however, remain approximately unchanged. It would appear that freezing and thawing cause migration and gravitational drainage of pore water which should carry away some soluble salts. The reduction in soluble salt content in the pore water is evidently not a prime factor affecting the observed decrease in the liquid limit since such a decrease should be associated with an increase in salt concentration (Warkentin, 1961).

Particle Size Distribution

The soil samples subjected to the closed system of cyclic freeze-thaw were used to determine the particle size distribution. Hydrometer analyses were carried out on samples prepared in two conditions - one without dispersing agent and the other using sodium metaphosphate (calgon) to deflocculate clay particles. For the series with no dispersing agent, each sample was soaked with distilled water in the one-litre cylinder for 18 hours. Subsequently it was agitated by shaking the cylinder for 2 minutes followed by turbulent flow in the soil suspension through a perforated disk. This procedure resulted in a breaking up of the unstable soil aggregates and ensured a homogeneous soil suspension for sedimentation. The particle size distribution was then deter-

mined by the hydrometer analysis outlined in the ASTM standard procedure. Once the test was completed, the sample was re-analysed by adding the dispersing agent which was thoroughly mixed with the soil by a high speed mechanical stirrer. The soil samples tested were the natural soil and the soil subjected to 40,50,60,70 and 80 cycles of freeze-thaw (without drainage).

The results shown in Fig. 4 exhibit clearly the effects of cyclic freeze-thaw in causing aggregation in the soil particles. This is demonstrated in the decrease of the percent passing, even when dispersing agent was used. While the series without dispersion show noticeable differences between the samples having undergone different freeze-thaw cycles, such behaviour is not evident in the series with dispersing agent. In other words, the stable fabric units of the soil subjected to cyclic freeze-thaw appear to be independent of the number of freeze-thaw cycles when this is sufficiently large (e.g. more than 40 cycles as investigated herein).

Soil Suction

The water retention capability of the samples subjected to cyclic freeze-thaw (open system with drainage) was established by determining the soil suction - moisture content relationship. Undisturbed soil samples from the same layer were carefully trimmed into small acrylic rings (each being 3.8 cm in diameter and 1.2 cm in height). At the end of the specified freeze-thaw cycles (i.e. 1 and 8), the samples (7-8 samples for each test condition) were installed in the pressure plate for suction test. For the three conditions tested (i.e. natural, 1 and 8 cycles of freeze-thaw), it appears that significant drops in moisture content occur when the suction reaches about pF 3.5. Beyond the value of pF 3.5, the moisture content decreases as the number of freeze-thaw cycles increases. This seems to reflect the smaller pore sizes of the natural soil fabric when compared with the frozen-thawed samples. For the soil suction less than pF 3.5 the changes in moisture content (of the frozen-thawed samples) are comparatively higher than those occurring in the natural soil. This should indicate the larger sizes in macropores of the soils subjected to cyclic freeze-thaw when compared to the

natural undisturbed soil.

CONCLUSIONS

When a sensitive clay with a high initial water content (above its liquid limit) experiences freezing and thawing, the resultant displacement and stresses create remoulding effects to an extent beyond that normally observed in manual remoulding of the soil. Cyclic freeze-thaw causes alterations in the soil structure leading to a decrease in shear strength and liquid limit as the number of freeze-thaw cycles increase. The primary mechanism appears to be the volumetric expansion of water-ice phase change which is more significant as the initial moisture content increases. This appears to destroy the strong bonding of the sensitive clay when it is first frozen. Subsequent freezing forces soil particles to become closer leading to aggregation (Lincoln and Tettenhorst, 1971) thereby reducing the active soil surface area.

Arising from these observations and ongoing work on the study of the fabric of the soils under cyclic freeze-thaw, a model duplicating aggregation of soil units as a result of freezing is being developed. The model should provide the basis for quantitative predictions. More data will need to be accumulated before the quantitative predictions can be successfully developed. This will be reported at a later time.

References

1. Chhabra, R., Pleysier, J. and Cremers, A. (1975), Cation Exchange Capacity and Exchangeable Cation in Soils: A New Method, Proc. Int. Clay Conf., pp. 439-449.

2. Lincoln, J. and Tettenhorst, R. (1971), Freeze-Dried and Thawed Clays, Clays and Clay Minerals, Vol. 19, pp. 103-107.

3. Warkentin, B.P. (1961) Interpretation of the Upper Plastic Limit of Clays, Nature, Vol. 190, pp. 287-288.

Acknowledgements

Table 3 Pore Fluid Chemistry and Exchangeable Cations

No. of Freeze-Thaw Cycles	Cations meq/l					Exchangeable Cations meq/100 g dry soil					Cation Exchange Capacity meq/100 g dry soil
	Na^+	K^+	Ca^{+2}	Mg^{+2}	Total	Na^+	K^+	Ca^{+2}	Mg^{+2}	Total	
0 (natural soil)	2.69	0.60	3.53	1.33	8.15	1.17	1.56	10.11	6.52	19.36	19.07
1	1.94	0.41	3.47	1.02	6.84	0.88	1.34	14.04	1.66	17.92	22.18
8	1.69	0.69	2.16	0.82	5.36	0.87	1.56	9.97	5.79	18.17	19.50

Note: Block No. 61, Drainage provided

101

Table 2. Test program.

Sample Block No.	Depth m	Test Description	Natural Soil (0 freeze-thaw cycles)	No. of freeze-thaw cycles	
				Closed system (no drainage)	Open system (drainage)
56	7.72-7.83	Shear strength (fall-cone method)	✓	1, 8	
61	8.23-8.43		✓		1,8
		Moisture content distribution	✓		1,8
		Pore fluid analysis	✓		1,8
		Soil suction	✓		1,8
		Exchangeable cations	✓		1,8
		Liquid limit	✓		1,8
64	8.79-8.87		✓	10,20,30,50 70,80,90	
		Particle size [*] distribution	✓	40,50,60,70, 80	

Note: ✓ - test performed

          * - with and without dispersing agent

Undisturbed shear strength 10.0 kPa, Block 56

- 1
- 2
- 4   } aging days
- 8
- 41

	w_0·%
natural	95.2
1 cycle	95.5
8 cycles	91.2

w_0 = initial water content

a. Closed system.

Shear strength, kPa

Number of freeze-thaw cycles

Undisturbed shear strength 20.0 kPa, Block 61

- 1
- 2
- 4   } aging days
- 8
- 16
- 32

	w_0·%
natural	91.8
1 cycle	70.7
8 cycles	51.2

b. Open system.

Shear strength, kPa

Number of freeze-thaw cycles
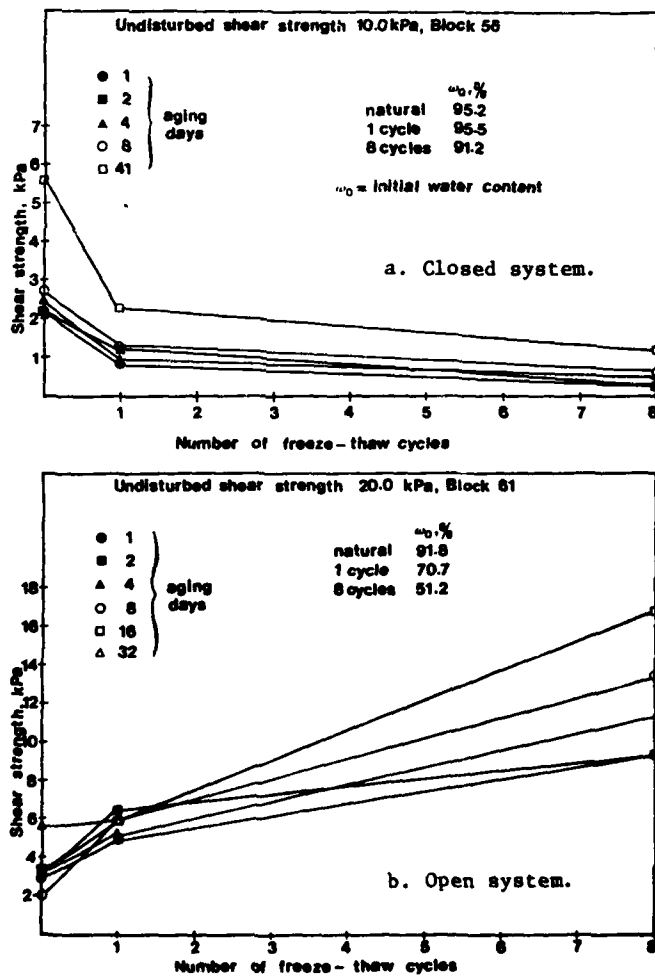
Figure 1.   Thixotropic strength of closed and open systems.
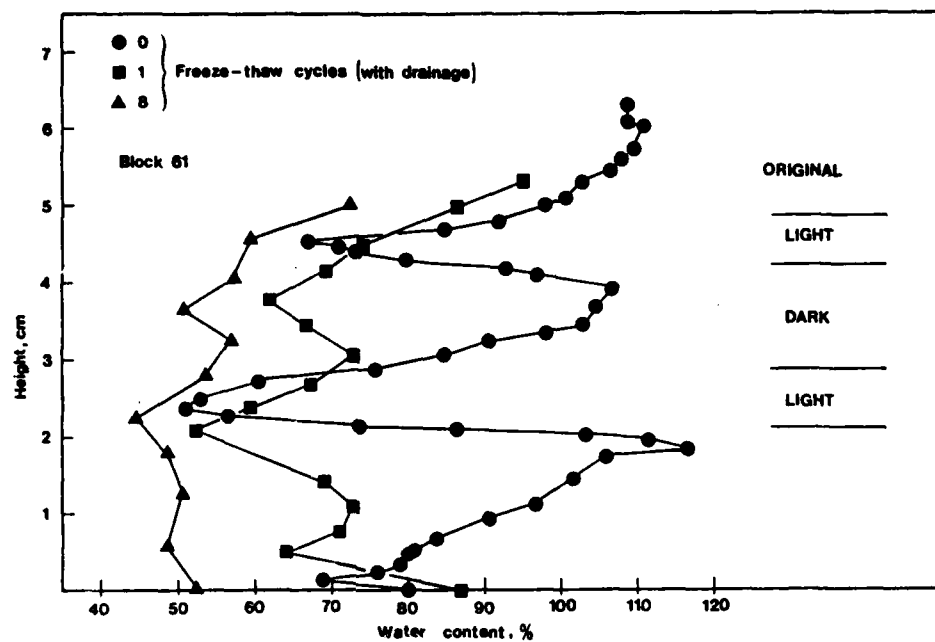
Figure 2.   Moisture content distribution.
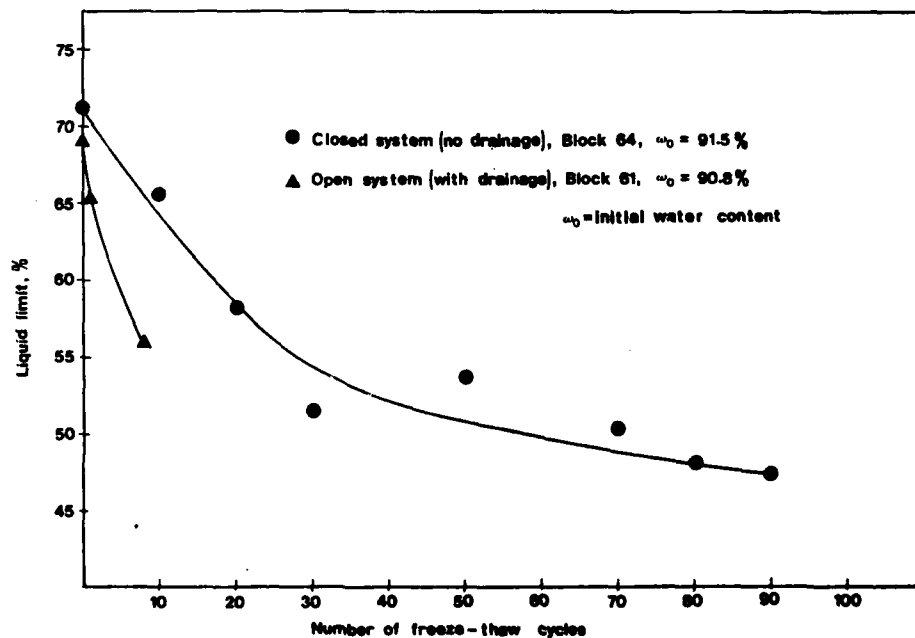
Figure 3.   Liquid limit and freeze-thaw cycle relationships.

103
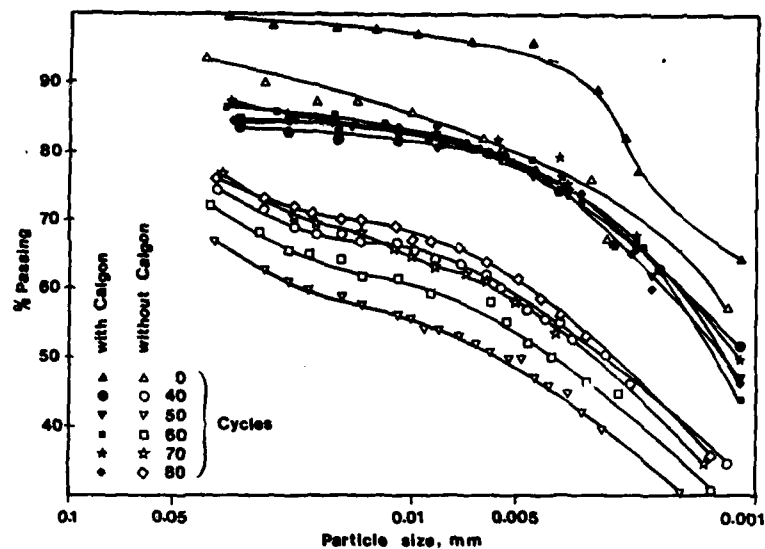
Figure 4. Particle size distribution.
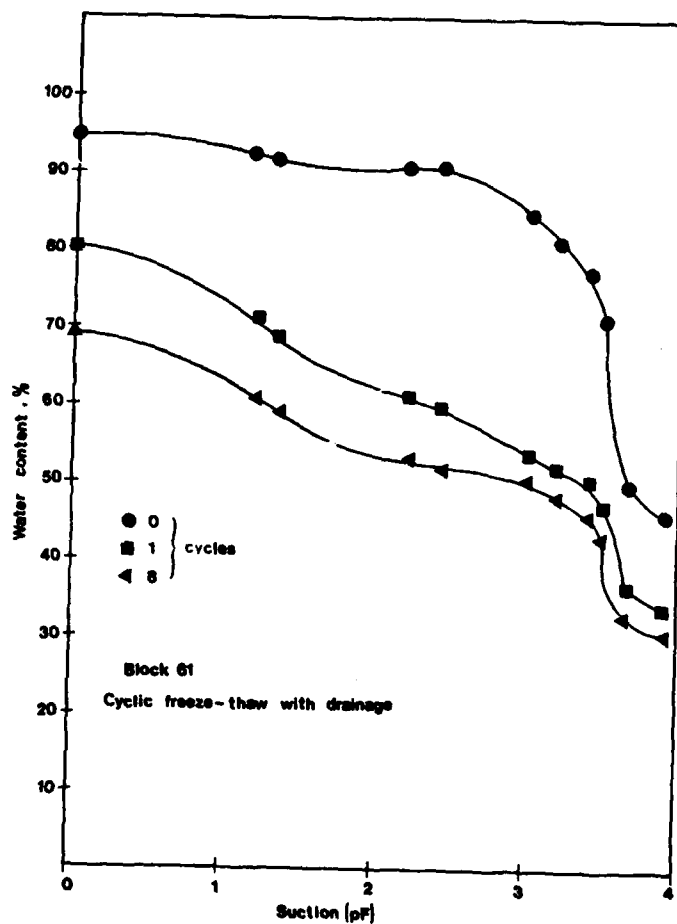
Figure 5. Moisture content and soil suction relationships.

104

MEASUREMENT OF SOIL THAW WEAKENING

J.D. Sage
Worcester Polytechnic Institute
R.A. D'Andrea
Worcester Polytechnic Institute

ABSTRACT

The changes in strength which a soil experiences upon being subjected to frost heave and subsequent thaw are described. It is noted that localized areas of minimal strength occur where thawed water which formerly constituted an ice lens remains perched above soil which remains frozen.

A device which allows study of this phenomenon within the laboratory is described. This unique device permits direct simple shear on a thin sample constituting the upper portion of a large cylindrical specimen which has been frozen from the top downward. Both prior to and during shear, the device remains within a temperature controlled cabinet which initially imparts selected temperature and drainage conditions to the cylindrical specimen. Simple shear testing is performed under undrained conditions after the desired thermal history has been applied. Temperature is controlled during thaw in order that the thin shear sample, whose top and bottom are parallel to the freeze-thaw interface, will be underlain by frozen soil. Successive thawing and shearing of samples taken at various levels within the specimen produces the relationship between strength and depth for the initially imposed thermal conditions.

Results of tests performed on a frost susceptible silty sand are also presented.

INTRODUCTION

In geographical areas which are subject to significant seasonal freezing temperatures, the phenomena of frost heaving and subsequent thawing in soils creates severe engineering problems. The safe, efficient and economical utilization of soil, which has been frozen and thawed, requires explicit knowledge concerning all parameters important to design. Furthermore this knowledge is important in establishing a scientific and engineering definition of the response and behavior of thawed ground in effecting practical solutions to related engineering problems.

A review of the solutions to engineering problems associated with thawed ground emphasizes the need for more detailed knowledge of the strength reduction of soil under varying thermal regimes and applications.

This paper details the design and use of a direct simple shear (DSS) device for measuring in the laboratory the shear strength of a thaw weakened soil. The DSS device described permits an assessment of post-thaw shear strength through localized zones of high moisture content occurring at different elevations in a frozen sample. It also permits an estimation of shear strength recovery accruing as a result of subsequent consolidation of the thawed soil.

SHEAR STRENGTH REDUCTION

Frost heave occurs when a frost

105

susceptible soil which has access to an unfrozen water supply is subjected to a freezing thermal gradient, and crystallization of the least stressed soil water at or near the ground surface is induced. Provided that a sufficient quantity of heat is being continually removed from the soil-water system and that additional water molecules are made available to the newly formed ice crystals, the crystals grow, forming an ice lens. This transfer of water to the zone of ice formation gives rise to progressively greater accumulation of ice in the frozen zone.

On thawing, the accumulation of water which formerly constituted an ice lens remains perched above the soil which is still frozen. Bishop (1) has reviewed abundant evidence regarding the shearing resistance of both undisturbed and remolded cohesionless and cohesive soils which supports the conclusion that shearing resistance will be inversely proportional to water content when all other factors (such as stress history) are equal. Consequently, a fully or partially thawed soil will contain "thaw weakened" zones of markedly lower strength which will reduce the overall continuum of the structure of a soil and

the ability of the soil to resist shear. Skempton (2) has demonstrated that saturated slowly draining soils which are brought to failure under undrained conditions (i.e. constant water content) behave as materials whose strength may be described as consisting solely of a cohesive component. Consequently, an analysis technique which accepts this simplification of material strength representation is referred to as "$\phi=0$" analysis.

Failures of thaw weakened soils are induced, at least in part, by excessive pore water pressures which are slow to dissipate due to the fine material present in any frost susceptible soil. Since the pore pressures temporarily reduce both the effective stress and, as a result, the strength of the soil, a $\phi=0$ analysis would be applicable and the undrained shear strength used to estimate shear strength reduction.

The freeze-thaw-shear process in soils is presently viewed as occurring in four stages. With reference to Figure 1, a soil in the pre-freeze condition with a tight packing possesses a shear strength S_p. Upon freezing and development of an ice lens, a dispersed packing is produced in which the soil
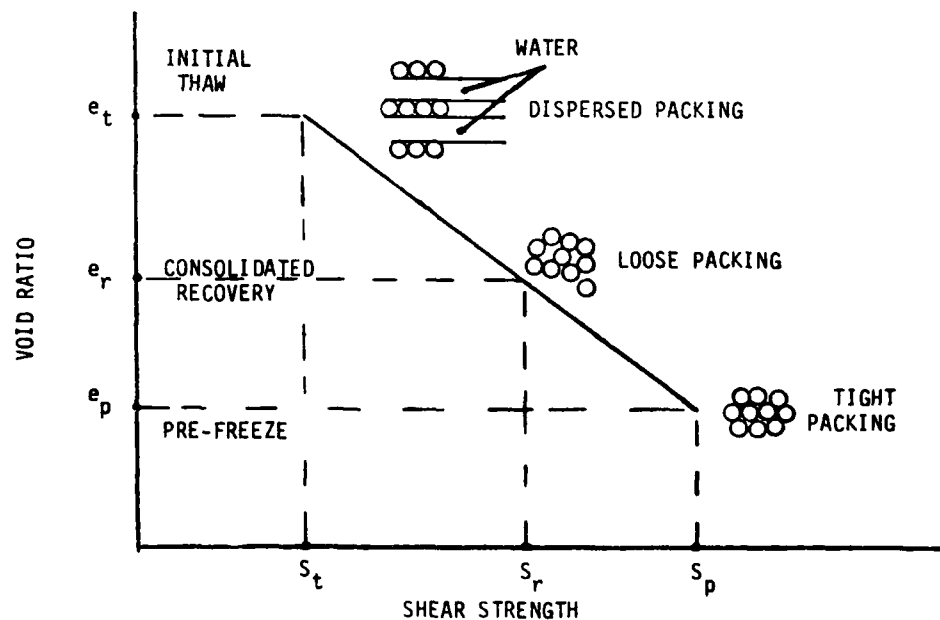
Figure 1. Strength Variation During Freeze-Thaw-Recovery Cycle

particles are separated from adjacent particles by ice. On thawing, this dispersed packing (at a void ratio e_t) is retained and the shear strength of the soil reduced to zero or a low value, S_t. Finally as the sample consolidates under load, the void ratio decreases to e_r at a relatively loose packing compared with the pre-freeze condition and the shear strength recovers to a value S_r. A measure of the shear strength reduction in thawed ground is the thaw weakening ratio defined simply as S_t divided by S_p, where S_t is the shear strength of the sample after thaw.

DIRECT SIMPLE SHEAR DEVICE

The WPI Direct Simple Shear Device (DSS) consists of a tapered interlocking split ring acrylic mold 29.2 centimeters (11.5 inches) in overall length and capable of accepting 15.24 centimeter (6 inch) diameter tapered soil samples. A tapered laterally reinforced rubber membrane provides lateral support to the soil during shear testing. A loading frame built into a freezing cabinet permits application of shear loads through a load cap attached to the DSS device.

Using the DSS device, the direct simple shear of the thaw-weakened soil may be determined on a thin sample at various levels as shown schematically in Figure 2.

(a) Saturate   (b) Freeze-Heave   (c) Freeze-Seal

(d) Initial Thaw   (e) Initial Shear

(f) Next Thaw   (g) Next Shear
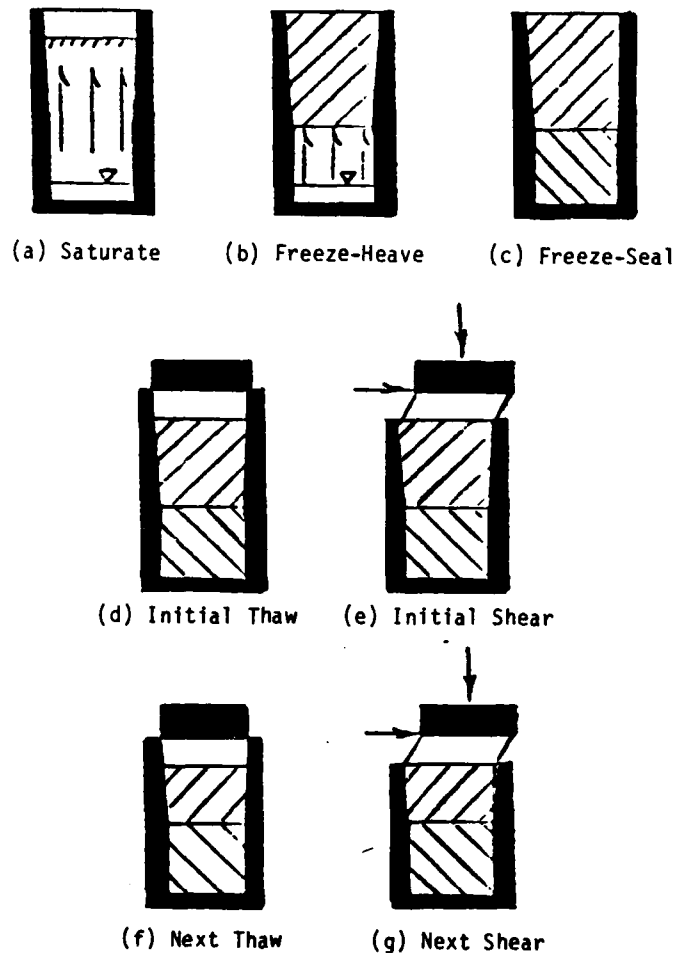
Figure 2. Sequential Steps of Freeze-Thaw-Shear Testing

Figure 3 graphically portrays the essential parts of the WPI device. The features of the device are outlined below within the context of a typical test.

A soil specimen is initially compacted within the tapered acrylic mold containing a reinforced rubber membrane producing a circular cylindrical sample 22.86 centimeters (9 inches) high and approximately 15.24 centimeters (6 inches) diameter. Acrylic was selected since experiments indicated the thermal characteristics of acrylic assist in the generation of horizontal isotherms and subsequent growth of horizontal ice lenses within the soil specimen. The mold and membrane are tapered so that friction between the soil and membrane will not restrict heave during the freezing process. The mold itself is solid throughout its bottom 11.4 centimeters (4.5 inches). The upper 17.8 centimeters (7 inches) of mold consists of interlocking split acrylic discs approximately 0.95 centimeters (0.375 inches) in height. The discs are held together by a vertically adjustable acrylic sleeve. The 22.86 centimeter (9 inch) high soil specimen will be subjected to a thermal environment resulting in freezing of the upper 11.4 centimeters (4.5 inches). Thus, the additional upper 6.35 centimeters (2.5 inches) of the mold is expected to accommodate heaved material upon ice lens generation.

Twelve thermocouples were placed through the split acrylic discs at various depths such that they were in contact with the outer face of the reinforced membrane.

The 15.24 centimeters (or more due to taper) diameter was selected so that the height to diameter ratio of the shear zone is half the upper limit which Shen et al (3) recommend for uniformity of shear strain. In fact, this allows for removal of two discs, if required, prior to shear testing and the strain distribution will still be reasonably uniform.

After the soil is compacted, the protruding upper part of the membrane is secured to a top cap and the mold is attached to a support frame placed within a temperature controlled cabinet.
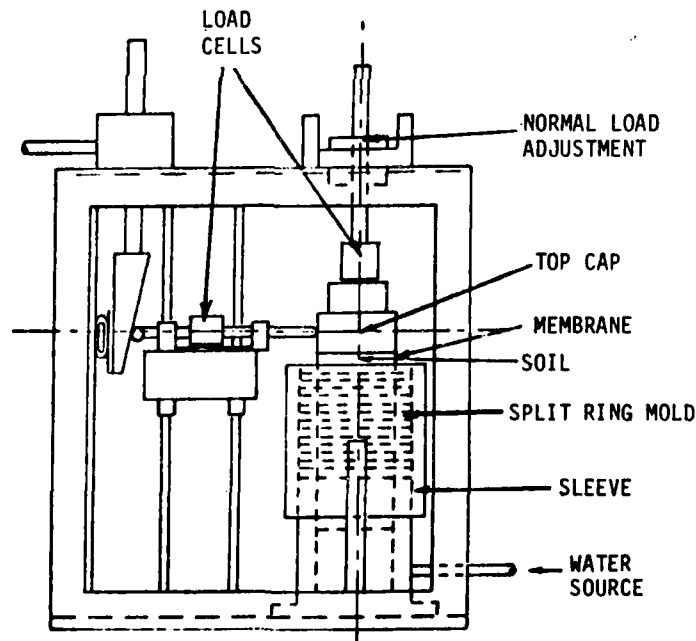
Figure 3. Essential Features of DSS Device

108

A normal load may be applied if desired, and the mold is surrounded by insulating vermiculite. Connections to a monitored temperature controlled water source are made at the base of the mold, and the appropriate thermal environment applied. During the ensuing freeze-heave process, soil temperature is monitored with the thermocouples.

Heave is measured via a vertical deformation gauge and a DC-DT differential gauging transducer. Water migration is measured both manually and by use of a moisture transfer monitoring device. After the desired thermal history has been enacted, and thermal equilibrium established, thawing and shear testing may begin.

Just prior to thaw, the specimen top cap is removed and the upper frozen soil surface shaved level with the top of the highest possible acrylic disc. Since the soil will probably have heaved less than 6.35 centimeters this will require sliding the sleeve down and removing one or more discs.

A specially designed specimen top cap and normal load carriage is placed on the frozen surface. The top cap consists of a porous stone, roughened to prevent slippage during shear, fastened to the top cap base. The top cap base also contains a heating pad which assists the generation of horizontal isotherms during thaw. The top cap is connected to the support shaft with a specially designed carriage consisting of a fixed ball bearing track arrangement. This mechanism permits no rotation but allows horizontal translation along a single axis thus insuring appropriate strain conditions on the upper surface of the shear specimen.

Above the carriage is a load cell used to monitor vertical load during a test. A rod extends vertically from the load cell to a vertical load adjustment mechanism which is attached to the testing frame.

The elevations of this and the horizontal load application mechanism are adjustable in order that a series of shear tests on a single frozen-thawed specimen may be performed.

The membrane is then attached to the top cap and the appropriate vertical load is applied. The outer acrylic sleeve is then lowered so that its top is level with that of the next lowest disc, and the sleeve is secured tightly in that position. The soil within the upper disc is forced to thaw from the top downward by the heating element, under carefully monitored conditions. When it has thawed, but the soil below is still frozen, the disc is removed resulting in a sample of thaw weakened soil, 0.95 centimeters high and slightly more than 15.24 centimeters in diameter. Water movement is prevented laterally by the rubber membrane, upward by the top cap, and downward by the frozen soil. The horizontal load and deformation measuring devices are positioned vertically on their respective supports and attached to the top cap. A horizontal shear force is applied to the top cap by means of a drive shaft forcing a loading wedge downward along a grooved track resulting in simple shear of the specimen. The rate of drive shaft movement is controlled by a variable speed motor and gear box. The shear force and horizontal deformation are measured until failure occurs under a strain controlled testing mode. Since the principal stresses are of unknown direction and magnitude in direct simple shear testing, the major parameter determined is the undrained simple shear strength (the shear force divided by the cross-sectional area of the shear zone). If the 0.95 centimeter high shear specimen has grossly differing strengths on parallel horizontal planes it may not undergo uniform shear strain and will slide horizontally on the weakest plane. Generally, however, a spatial average strength of the 0.95 centimeter specimen will be obtained. Upon completion of shear the top cap is removed, the entire specimen is shaved off level with the top of the lower disc and sleeve, and moisture content is determined.

The sleeve is then lowered to the top of the next lowest disc, thawing permitted through the current upper 0.95 centimeter layer and the shear process repeated. This entire procedure continues until the entire upper part of the soil column (that which has been frozen) has been tested resulting in relationships of both undrained simple shear strength and water content versus depth.

The above steps are schematically shown in Figure 2.

ASSESSMENT OF THAW WEAKENING

The DSS device described above is being used to study and evaluate shear strength reduction and recovery of thaw-weakened soils as part of a continuing

research effort on freeze-thaw phenomena in soils. The results from a typical test on a frost susceptible soil is summarized below.

A capill.ry saturated sample of Ikalanian Sand, having physical properties listed in Table 1, was frozen to a depth of 10.7 centimeters (4.2 inches) in a series of steps in which the thermal gradient was .aried to obtain a frozen sample with different degrees of ice lensing. The quantity of water transported from the base water source to the freezing interface and the resulting heave were measured. Table 2 is a summary of the freeze cycle for this test.

The sample was then thawed from the top of the specimen in steps of approximately 0.95 centimeters and the undrained shear strength determined after each thaw step with results listed in Table 3.

Table 1

Engineering Characteristics of Ikalanian Sand

Specific gravity	2.68

% weight finer than

2.00	mm	99
0.42	mm	88
0.25	mm	77
0.044	mm	36
0.02	mm	9
0.005	mm	2

via ASTM D698:

Maximum dry density (g/cc)	1.73
Optimum water content	13%

Table 2

Summary of Freeze-Test FTS-1

	Maximum	Minimum	Average
Rate frost penetration (cm/sec)	0.19	0.00	0.008
Rate heave (cm/sec)	0.0025	0.0013	0.0021
Rate moisture transfer (cc/sec)	0.072	0.008	0.041

Total frost penetration (cm)................4.16
Total heave (cm)..............................1.10
Total moisture transfer (cc)..................21.14
Duration of test (hours).......520
Density of pre-freeze sample (g/cc).......1.708
Initial water content of pre-freeze sample....15%....(21% after saturation)
Surcharge load (g).......735
Ground water depth (cm).......21.6
Initial void ratio of pre-freeze sample.......0.568

Table 3

Thaw-Shear Test Results for FTS-1

Test No	Level	Height Shear Zone	Initial Normal Stress	Shear Stress @ 20% Strain	Normalized Shear Stress	Thaw Weakening	Moisture Content	Void Ratio
			N_o	S	S/N_o	TWR	w	e
	cm	cm	Pa	Pa			%	
1-2S	-1.30	0.53	3878	909	0.23	0.18	30.0	0.80
1-3S	0.79	0.53	3759	776	0.21	0.16	29.6	0.79
1-4S	2.44	1.45	5161	608	0.12	0.09	23.8	0.64
1-5S	4.95	1.45	3313	780	0.24	0.19	22.1	0.59
1-6S	7.06	0.76	1800	1772	0.98	0.77	21.5	0.58
1-7S	8.71	1.37	4482	5171	1.15	0.90	17.7	0.47

TWR = Normalized shear stress after freezing and thawing divided by the pre-freeze normalized shear stress value of 1.28

The thaw weakening ratio, TWR, defined as the ratio of measured normalized shear strength to the pre-freeze normalized shear strength, was determined. The variation of thaw weakening ratio with depth is shown in Figure 4, from which their dependence is evident.

CONCLUSIONS

A device which permits measurement of the shear strength of soil which has experienced weakening due to freezing and thawing under laboratory controlled conditions has been described. The apparatus utilizes the principle of direct simple shear to measure strength through the localized zones of high water content occurring at different depths in a frozen sample.

The device promises to be useful in pointing out the manner in which various factors influence the strength reduction and recovery of thaw weakened soil.
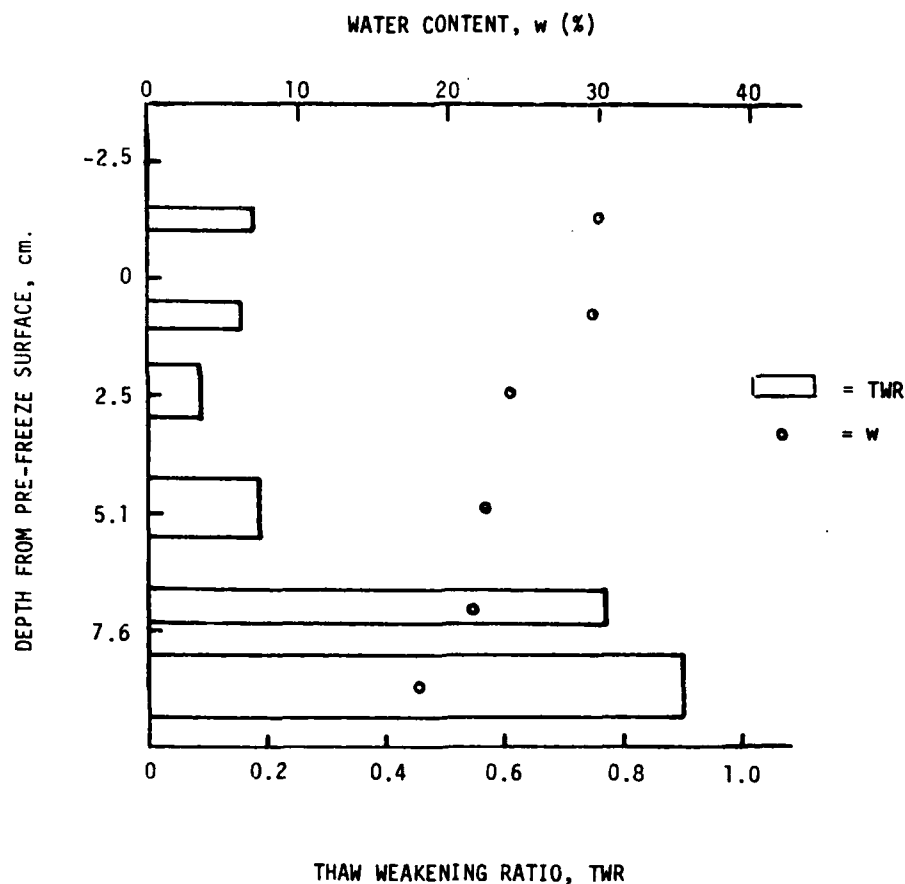
WATER CONTENT, w (%)

Figure 4. Thaw Weakening Ratio and Water Content vs. Depth from Initial Test on Ikalanian Sand

ACKNOWLEDGMENTS

REFERENCES

1. Bishop, Alan W., "Shear Strength Parameters for Undisturbed and Remoulded Soil Specimens", from Stress-Strain Behaviour of Soils, Proceedings of the Roscoe Memorial Symposium, Cambridge University, 1971, pp. 3-58.

2. Skempton, A.W., "The $\phi = 0$ Analysis of Stability and its Theoretical Basis," Proceedings Second International Conference on Soil Mechanics and Foundation Engineering, Rotterdam, 1948, Vol. 1, pp. 72-78.

3. Shen, C. Sadigh, K., and Herrmann, L., "An Analysis of NGI Simple Shear Apparatus for Cyclic Soil Testing," Dynamic Geotechnical Testing, ASTM STP 654, 1978, pp. 148-162.

FREEZING OF TRIAXIAL COMPRESSION TEST SPECIMENS OF COHESIONLESS SOIL TO DETERMINE INTERNAL DENSITY VARIATIONS

P.A. Gilbert   Soil Mechanics Division, Geotechnical Laboratory,
U.S. Army Engineer Waterways Experiment Station,
Vicksburg, Mississippi

ABSTRACT

The cyclic triaxial test is used to evaluate the seismically-induced lique-faction potential of cohesionless soil. Concern that internal density changes due to testing characteristics may render the test inappropriate for dynamic analysis prompted research to investigate such changes. This paper describes equipment and procedures to:

a. Prepare sand specimens of known density uniformity.

b. Cyclically load specimens to various pore pressure and strain responses.

c. Freeze a specimen under test loading conditions in such a manner that the soil skeleton is not disturbed by the freezing process.

d. Dissect a frozen specimen to establish its density distribution.

This research required specimens with a higher degree of density uniform-ity than previously achieved. A complex laboratory study was conducted to develop equipment and procedures to construct the high quality specimens. Additionally, special freezing techniques were required to produce an "undisturbed" frozen speci-men. This freezing process and the be-havior of the soil during freezing will be documented.

Specimens with 100% water saturation were tested in the triaxial chamber, fro-zen, then dissected in an environmental room maintained at 20°F and 90% relative humidity. The density of each segment and, consequently, the density distribu-tion of the specimen were determined from the ice content. Because of the require-ment for precise density determination, errors caused by sublimation and measure-ment uncertainty are discussed in this paper.

COMPARISON OF UNFROZEN WATER CONTENTS MEASURED BY DSC AND NMR

Joseph L. Oliphant, U.S. Army Cold
Regions Research and Engineering Labora-
tory
Allen R. Tice, U.S. Army Cold Regions
Research and Engineering Laboratory

ABSTRACT

Unfrozen water contents of various
sands, silts and clays under partially
frozen conditions have been measured
using Nuclear Magnetic Resonance (NMR).
Apparent specific heats for many of
these soils have been measured as a
function of temperature using Differen-
tial Scanning Calorimetry (DSC). Un-
frozen water contents have been calcu-
lated from the DSC data and compared
with those directly measured with NMR.
Comparisons were made from -20°C to 0°C
with excellent agreement for samples
with low salt contents. For these
samples we conclude that the assumptions
made in calculating the unfrozen water
contents from DSC data are good.

INTRODUCTION

Bouyoucos (1917) first demonstrated
that the volumetric change of frozen
soil due to the freezing of water takes
place over a range of sub-zero tempera-
tures. Since then, it has become
generally accepted that unfrozen water
films exist in frozen soils around the
soil grains down to very low tempera-
tures. The amount of unfrozen water is
a function of the temperature and also
of the soil properties (Anderson and
Tice 1972).

The strength and also the hydraulic
conductivity of a frozen soil are de-
pendent upon the ice content and the un-
frozen water content. Thus, for
construction involving frozen soils and
for modeling water movement and frost
heave in frozen and freezing soils, an
accurate knowledge of the water/ice
phase behavior in the soil is critical.
Unfrozen water contents of frozen soils
have been measured quantitatively using
dilatometry (Bouyoucos 1917, Buehrer and
Aldrich 1946, Hemwall and Low 1955, and
Horiguchi 1978), x-ray diffraction
(Anderson and Hoekstra 1965), some form
of calorimetry (Neresova and Tsytovich
1963, Kolaian and Low 1963, Anderson
1966, and Williams 1963), and more re-
cently, using NMR (Tice, Anderson and
Sterrett 1981, Tice, Burroughs and
Anderson 1978).

Anderson and Tice (1973) have dis-
cussed the assumptions inherent in each
of the above methods of determining un-
frozen water content. For the adiabatic
calorimetry method that has been most
widely used, the assumptions are that
the heat capacities of the sample com-
ponents are known over the entire temp-
erature range of interest, that during
thawing no other process involving heat
takes place except that of the latent
heat of phase change from ice to water,
and that this latent heat of phase
change has the value for pure bulk ice
changing to pure water at 0°C, 79.75
cal/g. With sufficient experimental
effort, heat capacity data on the sample
constituents can be obtained so the
first assumption above can be verified.
The second two assumptions are related
and have been assumed by previous in-
vestigators to be valid close to 0°C but
probably not valid at lower tempera-

tures. In this paper, a computational procedure will be given which does not require the assumptions of constant known latent heat of phase change or the absence of other processes taking place while phase change is occurring.

Anderson and Tice (1973) also discuss three other calorimetric methods they have developed to determine unfrozen water contents: heat capacity, differential thermal analysis and isothermal calorimetry. Each of these methods is based on measuring whether or not ice is present in a series of samples having various water contents at a given temperature. The assumption is made that the unfrozen water content does not depend on the ice content of the sample. With this assumption, the sample having the highest total water content with no ice present has a total water content equal to or less than the unfrozen water content of the soil at the given temperature. This assumption has recenty been verified in this laboratory (Tice et al. 1982) using NMR.

In the experimental section of this paper our method of using NMR to determine unfrozen water contents will be presented. The results of a recent experiment which verifies the accuracy of this method will be briefly reviewed. Our method of using DSC to obtain the apparent specific heats of soil samples as a function of temperature will also be given. In the theory section, a method for calculating unfrozen water contents from apparent specific heat data which has no assumptions that cannot be experimentally verified will be presented. In the results and discussion section the unfrozen water contents of several samples calculated from DSC and NMR data will be compared.

EXPERIMENTAL

A Praxis Model PR-103 pulsed NMR analyzer was operated in the 90° mode with a 0.1 second clock and at a fast scan speed. The first pulse amplitude for each sample was measured at several temperatures above 0°C. Then the sample was frozen and first pulse amplitudes were measured over a range of sub-zero temperatures as the sample was gradually thawed. With the NMR analyzer operated as given above, only protons associated with unfrozen water molecules contribute to the first pulse amplitude.

First pulse amplitude vs. temperature data for a typical sample are shown in Figure 1. It can be seen that the first pulse amplitude increases as temperature decreases for the sample containing no ice, but when water begins to freeze just below 0°C the first pulse amplitude is reduced. Unfrozen water contents are calculated by extending the line drawn through the data points taken with no ice present down to low temperatures by linear regression (Tice et al. 1981). The unfrozen water content is then calculated as the total water content (determined gravimetrically) multiplied by the distance from the regression line to the first pulse amplitude reading (A in the figure) and divided by the distance from the regression line to the background amplitude reading (B in the figure).
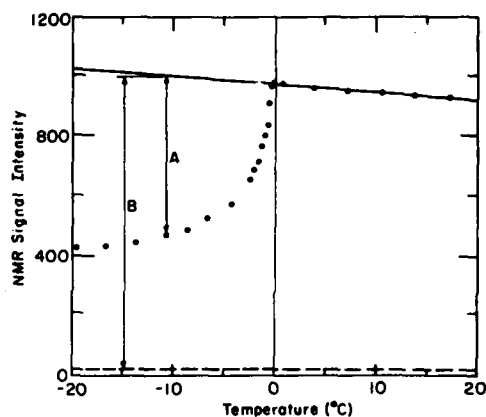
Figure 1. Raw NMR data for Na-bentonite containing 52% total water. ———— Total water regression line. ------ Background signal. • NMR data points. Unfrozen water is equal to total water times length A divided by length B.

That the above procedure gives accurate values of the unfrozen water content was confirmed by a recent experiment (Tice et al. 1982). A soil sample containing about 20% total water was held at -1°C. At this temperature the soil had about 12% unfrozen water as determined by NMR. Water was drawn out of the sample with a dessicant which was periodically weighed. In this way the total weight of ice and water remaining in the soil could be calculated. The unfrozen water was also periodically measured using the NMR as described

116

above. Total water and unfrozen water data as a function of time are shown in Figure 2. It can be seen from the NMR data that the unfrozen water content remained constant for about 100 hrs until all of the ice had been removed. This validates the assumption that the unfrozen water content does not depend on ice content. It can also be seen that after the ice had been removed the unfrozen water content measured with NMR and that measured gravimetrically are in excellent agreement. This helps confirm the accuracy of the NMR unfrozen water content measurements.
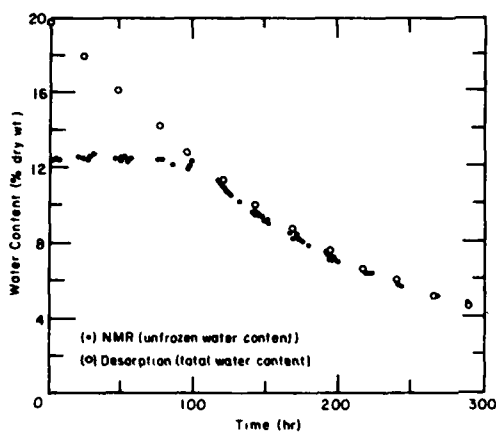
Figure 2. Simultaneous unfrozen water content and desorption data for Morin clay at -1°C.

A Perkin-Elmer Model DSC-2 differential scanning calorimeter was used for the DSC measurements. A laboratory microcomputer was interfaced with the DSC-2 for real time data aquisition and storage. The scanning calorimeter works by changing the temperature of a sample and a reference simultaneously and at a constant rate. The difference between the amount of heat that must be supplied or removed from the sample and the reference to maintain a constant rate of temperature change is converted to a voltage reading by the DSC-2. This voltage is read once each .01 sec by the microcomputer. The readings are averaged over each 0.1°C temperature change and the average values are stored.

The scanning calorimeter runs that we report in this paper were each made at a rate of 10°C/min over a range of 240°K to 290°K. Thus, 500 voltage readings are stored for each run. A total

of three scanning calorimeter runs are used to calculate the apparent specific heat as a function of temperature for each sample. A typical example is shown in Figure 3. First, an empty aluminum sample pan is placed in both the sample and the reference sample holders. A scan is made establishing a baseline. It was found that the absolute position and the slope of the baseline varied slightly from run to run. To avoid any errors due to this, the DSC voltage was monitored and stored both before a scan started and after it finished. These two voltages were used to establish the absolute position and slope of the baseline for each run and corrections were made to all the stored voltages. These corrections have already been made for the scans shown in Figure 3.
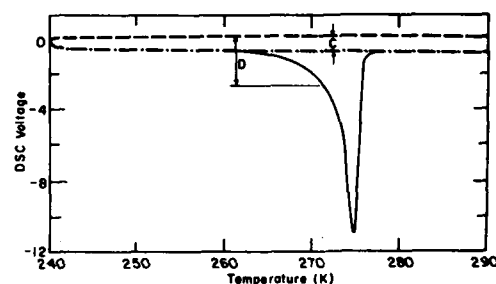
Figure 3. DSC response as a function of temperature scanning at 10°C per minute. ----- Base line. -·-·-·- Sapphire reference signal. ——— Morin clay (containing 21% total water) DSC signal. Distances C and D are used to calculate apparent specific heats.

After the baseline had been established, a scan was made with a pressed sapphire disk in the sample pan. Handbook values for the heat capacity of sapphire as a function of temperature are available and these values were stored in the form of a cubic spline interpolation function in the computer. Thus, at every 0.1°C in the scan, the calorimeter voltage associated with the heat capacity of the sapphire at that temperature can be defined. This is the difference in voltage between the baseline and the sapphire scan line, represented by the distance C in Figure 3.

Finally, a scan with the unknown sample in the sample pan is run. At each 0.1°C the apparent specific heat of

117

the unknown sample is calculated by the equation:

$$C_u = \frac{D}{C} \frac{W_s}{W_u} C_s \qquad (1)$$

where C_u is the apparent specific heat of the unknown sample, W_s and W_u are the weight of the sapphire standard and unknown, respectively, D and C are the differences in voltage between the baseline and the unknown scan line and the baseline and the sapphire scan line, respectively, as shown in Figure 3, and C_s is the handbook value of the heat capacity of sapphire.

The aluminum sample pans used to hold the unknowns and standard varied slightly in weight, weighing 25±0.5 milligrams each. Corrections for these small variations in weight were made by storing handbook values for the heat capacity of aluminum in the form of a cubic spline interpolation function in the computer and then adjusting the heat capacities to account for differences in weight between the sample pans. Sample sizes were about 25 milligrams each. The DSC temperature reading was calibrated using the melting points of pure water at 0°C, and of cyclopentane at -93.88°C. It should be noted that there is an upper limit on the rate that heat

Table 1. Heat capacities of water and ice samples determined by DSC compared with Handbook values *

	Water	
T(°K)	DSC value (cal/g°C)	Handbook Value (cal/g°C)
290	1.01	1.00
280	1.01	1.00
270	1.01	1.01
	Ice	
270	0.50	0.497
260	0.48	0.480
250	0.46	0.462
240	0.44	0.445
230	0.42	0.428
220	0.41	0.410
210	0.39	0.392
200	0.37	0.374

* Handbook values are from Dorsey (1940), p. 258 and 478.

can be transferred to or from the sample pans. Sometimes, when phase changes are taking place the temperature in the sample may lag behind that in the reference pan. Corrections for this phenomena were not made, but it was found not to be important in making the unfrozen water content calculations except at temperatures close to 0°C. Slower scan speeds close to 0°C would help prevent this problem.

The accuracy of the heat capacity values was checked by running pure water and pure ice samples. The heat capacity values obtained are compared with handbook values (Dorsey 1940) in Table I. It can be seen that the agreement is excellent.

THEORY

In this section a method for calculating unfrozen water content values from partial specific heat data will be given. This method depends on the fact that the enthalpy or heat content of a system is a state function and its value does not depend on the previous history of the system. The net enthalpy change in a system going from one state to another is independent of the path that is followed in changing states. Therefore, we can perform the following thought experiment on a wet soil sample going from some temperature, T_i, above 0°C to another temperature, T_f, below 0°C where part of the water is frozen. Let W_T be the total sample water content and W_u and W_f be the unfrozen and frozen water contents at T_f. First, at T_i, separate the sample into two parts, one part being made up of pure water of an amount W_f and the other part containing the remaining water, the soil and any salts or impurities in the soil solution. The heat effect associated with this separation will be of the same magnitude but opposite in sign to the heat associated with mixing an amount of water, W_f, with a soil already containing an amount of water, W_u at T. This heat of wetting, ΔH_w, is experimentally measureable. Now cool the pure water, W_f, from T_i to T_f. This will involve supercooling of the water because T_f is below 0°C, but good heat capacity data are available for supercooled water, so handbook data can be used to calculate the total heat

118

that must be removed for this process. Denote this total heat by

$$W_f \int_{T_f}^{T_1} C_{pw}\, dT$$

where C_{pw} is the heat capacity of pure water. Now take the other part of the sample and cool it from T_1 to T_f. The total heat that must be removed to do this can be measured with an adiabatic or differential scanning calorimeter. Denote this heat by

$$(W_u + M_m) \int_{T_f}^{T_1} C_{pr}\, dT$$

where M_m is the mass of dry soil and C_{pr} is the heat capacity of the soil and remaining water mixture. Now take the pure water at T_f and freeze it to pure bulk ice. The heat that must be removed to do this is easily calculated from handbook data on the heat capacity of supercooled water and pure ice and from the heat of fusion of pure water at 0°C. Denote this heat of fusion of supercooled water by $W_f L_f$. Now mechanically mix the ice and wet soil back together to form a sample having unfrozen water content W_u and ice content W_f. There is no heat associated with this last step if we assume that ice freezes out as pure bulk ice. The total of all the heats added to or removed from the soil sample in the above processes must equal the total heat that would be removed if the sample were cooled from T_1 to T_f in the DSC. This heat value can be obtained by integrating the apparent specific heat of the sample from T_1 to T_f. Let this heat be denoted by

$$(W_T + M_m) \int_{T_f}^{T_1} C_{pT}\, dT$$

where C_{pT} is the apparent specific heat measured by the DSC. Writing this equality out mathematically, we obtain

$$(W_T + M_m) \int_{T_f}^{T_1} C_{pT}\, dT = W_f \int_{T_F}^{T_1} C_{pw}\, dT$$

$$+ (W_u + M_m) \int_{T_f}^{T_1} C_{pr}\, dT - \Delta H_w + W_f L_f \quad (2)$$

Noting that $W_T = W_u + W_f$, this equation can be rearranged to give

$$W_u = \frac{(W_T + M_m)\int_{T_f}^{T_1} C_{pT}\,dT - W_T \int_{T_f}^{T_1} C_{pw}\,dT - M_m \int_{T_f}^{T_1} C_{pr}\,dT + \Delta H_w - W_T L_f}{\int_{T_f}^{T_1} C_{pr}\,dT - L_f - \int_{T_F}^{T_1} C_{pw}\,dT} \quad (3)$$

Equation 3 gives the unfrozen water content of a partially frozen soil sample in terms of handbook data and the results of three experiments. The heat of wetting can be determined either by using isothermal calorimetry or vapor pressure measurements (Oliphant 1980). DSC can be used to determine the two terms

$$\int_{T_f}^{T_1} C_{pT}\, dT \quad \text{and} \quad \int_{T_f}^{T_1} C_{pr}\, dT.$$

Adiabatic calorimetry could also be used to determine these two terms. DSC has the advantage that in one experiment the apparent specific heat of the sample can be determined over the entire range of temperatures that is scanned by the calorimeter. Adiabatic calorimetry gives only the total heat effect in going from one temperature to another so a series of experiments at different subfreezing temperatures is required to obtain the unfrozen water content vs temperature curve. However adiabatic calorimetry has the advantage that there is no possibility of the temperature of the sample lagging behind the reference temperature as may happen in DSC.

RESULTS AND DISCUSSION

In this section unfrozen water content vs temperature curves are presented for three different soil samples determined both by DSC and NMR. Figure 4 shows data for a Na-bentonite from the Avon Lea area, Saskatchewan, having a surface area determined by the ethylene glycol-monoethyl ether method of 566 m^2/g. The total water content for this sample is 52% of the sample dry weight.
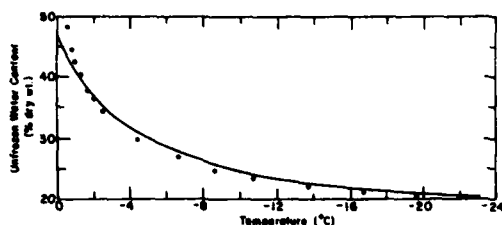
Figure 4. Comparison of DSC and NMR unfrozen water contents for Na-bentonite containing 52% total water. ——— DSC data. ⊡ NMR data.
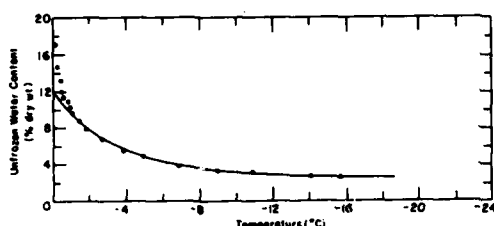
Figure 5. Comparison of DSC and NMR unfrozen water contents for Morin clay containing 21% total water. ——— DSC data. ⊡ NMR data.

Figure 5 shows data for Morin clay, a non-swelling clay from the Morin Brickyard, Auburn, Maine, having a surface area of 60 m^2/g. The total water content of this sample was 21.4% of the dry weight. In Figure 6 data for a geopressured shale having a high salt content and a surface area of 148 m^2/g is shown. The total water content of this sample was 8.6% of the dry weight.
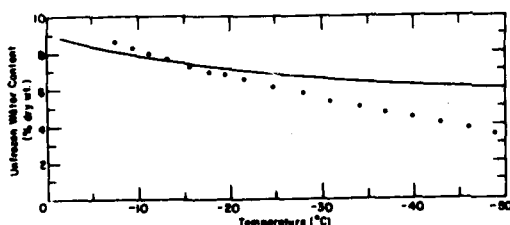
Figure 6. Comparison of DSC and NMR unfrozen water contents for a geopressured shale containing 8.6% total water. ——— DSC data. ⊡ NMR data.

The DSC data in each of these figures was calculated by using apparent specific heat data obtained on the DSC

as explained in the experimental section and by equation 3. There was no heat of wetting data available for these three samples so the term ΔH_w was assumed to be zero. The term

$$\int_{T_f}^{T_i} C_{pr} \, dT$$

was obtained by measuring the apparent specific heats of the dried samples and then assuming that the unfrozen water, W_u, has the same specific heat as pure water. It can be seen in Figures 4 and 5 that the DSC and NMR data match closely with slight deviations close to 0°C caused by the temperature lag in the DSC when a significant amount of ice is melting. In order to avoid supercooling effects, only warming DSC runs were used.

We conclude that the assumptions of zero heat of wetting and the unfrozen water having the same specific heat as pure water are adequate for the bentonite and Morin clay samples. The DSC and NMR data for the geopressured shale sample do not closely agree. There are several possible reasons for this. This sample has a relatively high surface area and a very low water content because the sample was run at natural water content. Therefore, only a small amount of water was frozen (only about 1% of the dry weight at -20°C) and the DSC and NMR are both working at the edge of their respective absolute detection limits to measure this small change in unfrozen water content. Also, it was found that the shale contained a large amount of chloride ion when a sample was being washed and calcium-saturated for surface area determinations. This high salt content probably effects both the heat of wetting and heat capacity of the unfrozen water of this sample.

CONCLUSIONS

In this paper, we have presented a calculational procedure using DSC or adiabatic calorimetry data for obtaining unfrozen water contents as a function of temperature. This approach is based on the fact that the enthalpy of a system is a state function. This approach has the advantage that all necessary data are experimentally obtainable. The only

120

assumption is that water freezes in a soil as pure bulk ice.

We have presented unfrozen water content data for three samples using both DSC and NMR. The DSC and NMR data agree for two of the samples in which a significant amount of water freezes, but the data for the third sample are not in close agreement. In this sample only a very small amount of water freezes.

Results of an experiment which shows the reliability of the NMR data were reviewed. We conclude that, because the NMR and DSC data are in excellent agreement and because we have confidence in the NMR data at least for samples in which a significant amount of water is frozen, the DSC data are also accurate. The theoretical procedure for calculating unfrozen water contents from DSC data allows us, by comparing DSC and NMR data, to determine the importance of heats of wetting and altered heat capacities of the unfrozen water in measuring unfrozen water contents calorimetrically. For the Na-bentonite and Morin clay samples, we conclude that these terms do not contribute significantly to the unfrozen water content calculations down to at least -20°C.

REFERENCES

Anderson, D.M. (1966) Phase composition of frozen montmorillonite-water mixtures from heat capacity measurements. Soil Sci. Soc. Amer. Proc., vol. 30, p. 670-675.

Anderson, D.M. and P. Hoekstra (1965) Migration of interlamellar water during freezing and thawing of Wyoming bentonite. Soil Sci. Soc. Amer. Proc., Vol. 29, p. 498-504.

Anderson, D.M. and A.R. Tice (1972) Predicting unfrozen water contents in frozen soils from surface area measurements. Highway Res. Rec., vol. 373, p. 12-18.

Anderson, D.M. and A.R. Tice (1973) The unfrozen interfacial phase in frozen soil water systems. In: Ecological Studies, 4. Springer, New York, N.Y., p. 107-124.

Buehrer, T.F., and D.G. Aldrich (1946) Studies in soil structure. VI. Water bound by individual soil constituents as influenced by puddling. Univ. Ariz. Tech. Bull, vol. 110.

Bouyoucos, G.J. (1917) Classification and measurement of the different forms of water in soil by means of the dilatometer method. Mich. Agric. Coll. Exp. Sta., Tech. Bull. 36, 48 p.

Dorsey, N.E. (1940) Properties of ordinary water substance in all its phases. Reinhold Publ Corp., New York, N.Y.

Hemwall, J.B. and P.F. Low (1955) The hydrostatic repulsive force in clay swelling. Soil Sci., vol. 82, p. 135-145.

Horiguchi, K. (1978) Studies in the behavior of unfrozen interlamellar water in frozen soil. Contributions from the Institute of Low Temperature Science, Series A, No. 28, p. 55-78.

Nersesova, Z.A. and N.A. Tsytovich (1963) Unfrozen water in frozen soils. Proceedings First Permafrost Intern. Conf., Lafayette, Indiana. NAS -NRC Publ. No. 1287.

Oliphant, J.L.(1980) The thermodynamic properties of mixtures of water and Na-montmorillonite. PhD. Thesis, Purdue Univeristy, Lafayette, Indiana.

Tice, A.R., C.M. Burrous and D.M. Anderson (1978) Phase composition measurements on soil at very high water contents by the pulsed Nuclear Magnetic Resonance technique. Transport. Res. Rec., vol. 675, p. 11-14.

Tice, A.R., D.M. Anderson and K.F. Sterrett (1981) Unfrozen water contents of submarine permafrost determined by nuclear magnetic resonance. Engineering Geology, vol. 18, p. 135-146.

Tice, A.R., J.L. Oliphant, Y. Nakano and T.L. Jenkins (1982) The relationship between the ice phase and the unfrozen water phase in a closed system frozen soil determined by pulsed Nuclear Magnetic Resonance and physcial desorption data. CRREL Report No. 236.

Williams, P.J. (1963) Specific heats and unfrozen water content of frozen soils. In Proc. 1st Can. Conf. Permafrost, Natl. Res. Counc. Canada, Assoc. Cttee. on Soil and Snow Mechs., Tech. Memo 76, p. 104-126.

DETERMINATION OF ICE/WATER CONTENTS
OF FROZEN SOILS BY
TIME DOMAIN REFLECTOMETRY

M.W. Smith   Geotechnical Science Laboratories.
D.E. Patterson   Carleton University,
C.H. Lewis   Ottawa, Canada

ABSTRACT

Previously we have used time domain reflectometry (TDR) to determine the apparent dielectric constant, K_a, of soils from the measurement of propagation time of a step-voltage along a transmission line. This enables us to determine the liquid water content of soils. To determine the ice content, we measure the soil d.c. conductivity, also by TDR. The d.c. conductivity for ice and water differs by several orders of magnitude; thus a measured soil conductivity reflects the ice/water content of the soil. Since the liquid water content is already known (from K_a), the ice content can be determined. Experimental results are presented.

TEMPERATURE DEFORMATIONS OF FROZEN SOILS

Ponomarjov,V.D.,Cand.Sc.,Research Institute for Bases and
Underground Structures,Moscow,USSR

The experimental and theoretical research of the temperature deformation of the permafrost, which is accelerated in the recent years,is caused by the necessity of considering these deformations,when calculating and designing different types of structures,interesting with freezed and frozen soils.It especially refers to the field of highway construction,designing underground storage of crude oil,etc.

Let's mark another field,where the development of temperature deformations may have a substantial meaning.This field refers to studying the strength and defo formative characteristics of the frozen soil and also to the technique of determination of these characteristics.The frozen soil sample during the period from the moment of its selection from the borehole,pit or any other working before starting the test is subjected,as a rule,to numerous temperature effects.These effects may bring to unreparable conditions of the permafrost structure and in the event,on receiving the values of strength or deformative characteristics,not corresponding to the conditions of natural soil bedding,although the temperature during the test of the sample was kept up on the natural level.

Experimental research(I)showed that when cooling frozen soils in the temperature range,cor-responding to the range of intensive phase changes,contraction as well as expansion of the frozen soil is observed.For sand soils at temperatures below -5°C the estimated values of deformation coinside with the experimental ones. For clay soils estimated values not only coinside with the experimental ones but have different signs.It is also seen that the expansion of frozen soil on cooling is observed when the degree of water-saturation is near to I.

In our opinion the most probable reason in sign-changing deformation of frozen soil on its cooling is presence of gaseous component and the possibility of deformation of crystals of pore ice on changing the volume of the gaseous phase in accordance with the changes of the temperature.

Let's consider the offered scheme of deformation process of frozen clay during cooling(Fig.I). The summary deformation of the soil consists of temperature deformation of the mineral particles and ice in accordance with their volume and linear deformation coefficients.Deformation of these soil phases during its cooling will lead to the diminising of volume.

The decrease of temperature of the soil will cause the decrease of the amount of unfrozen water due to its transformation into ice.Thus,the volume of the unfro-

zen water transformed into ice increases by 0.09I. This type of deformation also involves the general increase of the soil volume and appearance of internal pressure.

Fig.I
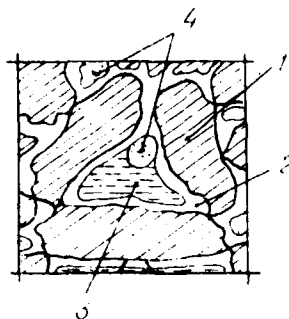
The scheme of the structure of the four-phased clay soil.
1-mineral particles;
2-unfrozen water;
3-pore ice;
4-gaseous phase;

In gaseous phase of the soil, which presents a trapping of gas cavities in the soil pores, occurs a decrease of pressure in accordance with the decrease of temperature.

The ice being a plastic substance of the internal pressure on the ice on one side and the decrease of the gas pressure from the other leads to a possibility of the pore ice deformation and filling the gas cavities, which are decreasing in volume, with this ice.

Thus, the presence of the gaseous phase will compensate the soil volume increase due to transformation of the unfrozen water into ice. The value of this compensation will depend on the initial volume of the gaseous phase.

In accordance with the above-mentioned for the general volume deformation $\mathcal{E}$ of the frozen soil when cooled we may define as:

$$\mathcal{E} = \beta_{sk} V_{sk}(t_2 - t_1) + \beta_i V_i (t_2 - t_1) - \beta_n (V_{n1} - V_{n2}) + \beta_a V_{a1} \quad (I)$$

where β_{sk} and β_i —coefficients of volumetric expansion of the mineral soil skeleton and ice, correspondingly

$$\beta_{sk} \approx 30 \cdot 10^{-6} \ 1/^{\circ}C$$

$$\beta_i \approx 150 \cdot 10^{-6} \ 1/^{\circ}C;$$

β_n — coefficient of volumetric expansion of water transforming into ice= 0.09I;

β_a — coefficient of volumetric contraction of the gaseous phase;

V_{sk}, V_i, V_a — relative volumetric contents in the soil of mineral particles, ice and gaseous phase, correspondingly;

V_{n1} and V_{n2} — relative volumetric contents in the soil of unfrozen water at the initial t_1 and final t_2 soil temperatures, correspondingly.

The relative volumetric contents of separate soil phases may be defined by physical characteristics of the soil as :

$$V_{sk} = \frac{\gamma_{sk}}{\Delta_{sk}} ; \quad (2)$$

$$V_i = \frac{(W_s - W_{n2})\gamma}{\Delta_i} ; \quad (3)$$

$$V_{n1} = \frac{W_{n1} \cdot \gamma_{sk}}{\Delta_n} ; \quad (4)$$

$$V_{n1} = \frac{W_{n2} \cdot \gamma_{sk}}{\Delta_n} ; \quad (5)$$

$$V_a = 1 - (V_{sk} + V_i + V_{n1}); \quad (6)$$

$$or \ V_a = (1 - G)(1 - V_{sk}) \quad (7)$$

where γ_{sk} —volumetric mass of soil skeleton, g/cm^3;

$\Delta_{sk}, \Delta_i, \Delta_n$— density of soil skeleton, ice and unfrozen water, correspondingly, g/cm^3;

W_s — total moisture counted of the soil;

W_{n1} and W_{n2}— moisture content due to unfrozen water at the initial and final soil temperature, correspondingly;

G — degree of water saturation of the soil.

The equation for the coefficient of volumetric contraction of the gaseous phase on cooling the soil may be obtained as defined below.

If the gas pressure in the soil at the temperature T_1 was P_1, then when cooling the soil to the temperature T_2, the pressure will fall to P_2. The pressure on the pore ice, arising in the result of the increase of its volume, when transforming the unfrozen water into ice increases to some extent P_i, apparently close to the value of long-term tensile strength. Filling the part of vo-

lume of gaseous cavities by pore
ice in the result of its deforma-
tion occurs under the effect of
the difference of pressures on
the ice and the pressure in the
gaseous cavity.The deformation of
ice and the decrease of gaseous
phase volume will continue until
the pressure in the gaseous cavi-
ties will become equal to the in-
ternal pressure on the ice.

Using the equation of the
gas condition,may be written as:

$$\frac{P_1 V_{a1}}{T_1} = \frac{P_2 V_{a2}}{T_2} \qquad (8)$$

where P_1 and P_2- pressure in the
gaseous phase of the soil
at the temperatures T_1 and
T_2,correspondingly (T_1 and
T_2- absolute temperatures,
°K);
V_{a1} and V_{a2} - relative volumes
of gaseous component at the
same temperatures.

Taking into account that $V_{a2}=V_{a1}-\Delta V_a$
from (8) we will receive the con-
traction of the relative gaseous
phase volume   on cooling the
soil:

$$\Delta V_a = \left(1 - \frac{P_1}{P_2} \cdot \frac{T_2}{T_1}\right) V_{a1} ; \qquad (9)$$

Thus,the coefficient of the volu-
metric contraction of the gaseous
phase equals;

$$\beta_a = \frac{\Delta V_a}{V_{a1}} = 1 - \frac{P_1}{P_2} \qquad (10)$$

On Fig.2 and 3 we have cur-
ves of linear temperature defor-
mations of the frozen soil,calcu-
lated with the help of formula(I)
considering that linear deforma-
tions $\mathcal{E} = \frac{1}{3}\mathcal{E}_0$.

Soil is the lake-alluvial
loam of massive cryogenic structu
re,volumetric mass γ_m = 0.95 g/cm³,
volumetric mass of the skeleton
γ_{sk} = 0.97 g/cm³,density of mine-
ral particles Δ_{sk} = 2.05 g/cm³,
total moisture content with maxi-
mum water-saturation W_s=60.1% (2).

Contraction of soil on the
curves corresponds to positive
values of $\mathcal{E}$ and expansion to
negative.

Curve (Fig.2)calculated for
cooling condition at initial soil
temperature t_1=-0.5°C and curve
(Fig.3) at the initial temperatu-
re of -2°C.For comparison on Fig4
is given an experimental curve of
development of temperature defor-
mations on cooling frozen soil(2).
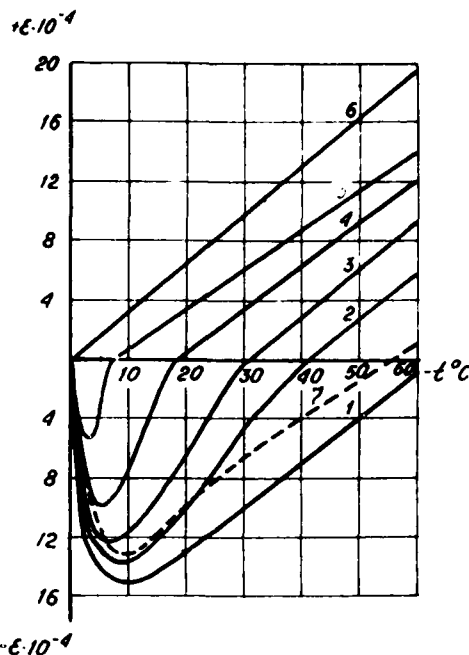
Fig.2. Estimated curve of tempe-
rature deformation of fro-
zen ground on cooling from
-0.5°C.

I-degree of water-saturation G=I;
2.-G=0.98;3.-G=0.96;4.-G=0.90;
5.-G=0.80;6.-without taking into
account the deformation during
the transformation of the unfro-
zen water into ice;7-experimental
curve at G I.
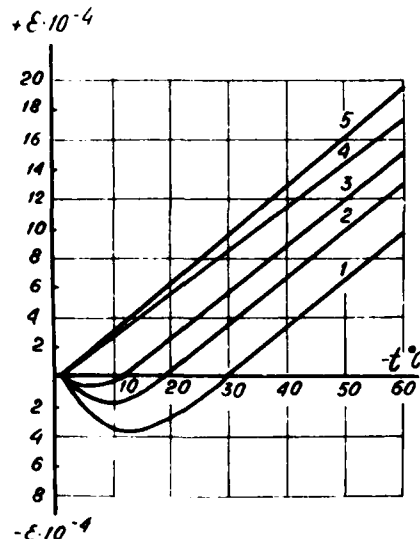
Fig.3.Estimated curve of the tem-
perature deformation of the
frozen soil when cooling

from -2°C.
I-degree of water saturation G=I;
2-G=0.98;3-G=0.96;4-G=0.90;
5-without taking into account the
deformation during the transfor-
mation of the unfrozen water in-
to ice.

By comparing estimated cur-
ves (Fig.2 and 3) and experimen-
tal one (Fig.4)shows the corres-
pondence of the character of the
curves on development of the tem-
perature deformations and appro-
ximately the same absolute values
of deformation in both cases.

Curve (Fig.2)shows a consi-
derable relationship of the cha-
racter of temperature deformati-
on development as well as their
absolute values depending on the
degree of water-saturation.
The degree of water-saturation
being G=I (curve I,Fig.2) we ob-
serve an expansion of soil till
the temperature reaches approxi-
mately -IO°C.Below -IO°C the soil
begins to contract. When degree
of water-saturation reaches G=0.8
the deformation of expansion is
not large.

Comparing curves (Fig.2 and
Fig.3) we find a considerable de-
pendence of the temperature defo-
rmations on the initial cooling
temperature t. During full water-
saturation and $t_I=-0.5°C$ the de-
formations of expansion reach the
value of $\mathcal{E} = 15 \cdot 10^{-4}$,when $t_I=-2°C$
the deformation decrease to $\mathcal{E} \approx 4 \cdot 10^{-4}$
and when the degree of water-sa-
turation G=0.95-0.96 the defor-
mations are practically absent.

The carried out analysis ex-
plains those seemingly paradoxi-
cal results of experimental re-
searches,which were obtained on
the first stage of studying the
temperature deformations of fro-
zen soils(3).Only the contracti-
on of frozen soil obtained in th
these experiments due to cooling
is explained by the small degree
of water-saturation or by the
low initial temperature of fro-
zen soil.

Note,that the calculations
of the temperature deformation
curves of the frozen soil,the re-
sults of which are given on the
curves (Fig.2 and 3) were carri-
ed out with the assumption that
the expression (IO) for the coef-

ficient of volumetric contraction
of the gaseous phase pressure in
the gaseous phase P_I and P_2 at
the temperatures T_I and T_2 are
equal.This assumption is conditio-
nal,because,if the growth rate of
deformations of expansion due to
the transformation of the unfro-
zen water into ice will be fas-
ter than the growth of contrac-
tion of gas cavities due to dec-
rease of pressure of gas in them,
then the effective pressure in
gas cavities will be higher than
the pressure of the corresponding
initial cooling temperature T_I.
This factor will affect the maxi-
mum value of deformation of the
soil expansion to the direction
of its contraction with the deg-
ree of water-saturation G < I and
especially,when the initial tempe
ratures of the soil cooling are
near zero.
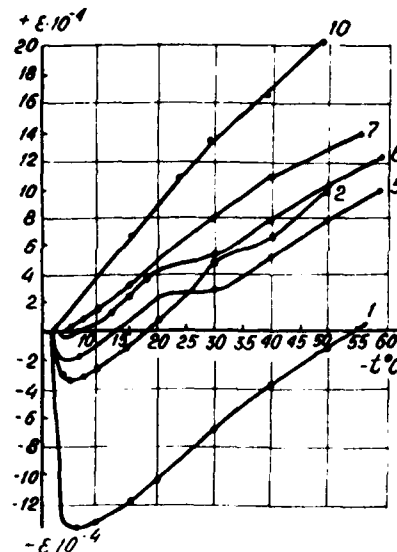
Fig.4. Development of deformati-
ons of the frozen soils at
temperature depression
(experimental data).

Conclusions.

I. The comparison of estimated
and experimental data on the de-
velopment of temperature deforma-
tions in frozen soil showed their
highly satisfactory similarity
which testifies the correctness
of the stated idea of the physi-
cal nature of the temperature
deformation process of the frozen

128

soil.

2.The showed analysis of the mechanism of frozen soil deformation on changing its temperature allows to predict the value of the temperature deformations oy the physical characteristics of the soil and to apply a well-grounded method in studying temperature deformations in accordance with vconcrete aims and soil property.

3.Formula (I) may be used for the estimation of temperature deformation values and their influence on the results of the experiments in studying the strength and deformation characteristics of the frozen soils.

References

I.Snusherina,H.P.,Barkovskaya, H.N.,Revina,L.A.,Sientific research of the dispersed frozen soils in accordance with their substance and temperature in the range of -0.5 to -55°C.Collected Papers "Permafrost Research",vol.XIII, MGU Press,1973.

2.Snusherina,H.P.,Rachevsky,B.S., Otroschenko,O.P.,Scientific research of the dispersed frozen soils.Collected Papers "Permafrost Research",vol.XV, MGU Press,1976.

3.Votyakov,N.G.,Temperature coefficients of expansion of frozen soils.Collected Papers "Strength and Creep of Frozen Soils",Academy of Science Press USSR,1963.

THE HYDRAULIC CONDUCTIVITY OF
SOILS DURING FROST HEAVE

Signe Kjelstrup Ratkje,Laboratory of Physical Chemistry, The Norwegian Insti-
tute of Technology, N-7034 Trondheim - NTH Norway.
Hideo Yamamoto, Tsutomu.Takashi, Takahiro Ohrai and
Jun Okamoto, Research Institute, Seiken Co. Auto-Center Bldg.No.68 Kawarayama-
chi 3-bancho, Minamiku, Osaka, Japan.

ABSTRACT

It is shown that the irreversible
thermodynamic theory of frost heave as
presented by Førland and Ratkje (1980)
is verified by experiments performed by
Takashi et al (1980). This theory pre-
dicts that the essential parameter of
transport during frost heave is the hy-
draulic conductivity of the soil. Using
the data of Takashi et al (1980) the
hydraulic conductivity of Manaita-bridge
clay and Negeshi silt has been calculat-
ed for cooling temperatures as low as
$-29.44^{\circ}C$. The hydraulic conductivity de-
creases in value with decreasig tempera-
ture and is at least one order of magni-
tude smaller than its value predicted
previously.

INTRODUCTION

It is reasonable to look at a trans-
port system using a general thermodyna-
mic framework before introducing models
to describe specific mechanisms of trans-
port. An irreversible thermodynamic
description of transport defines the
overall macroscopic conditions of the
transport system. One description of
this nature has been presented for frost
heave by Førland and Ratkje (1980 a,b).
It predicts the hydrostatic pressure
variation or the overburden pressure in
frost heave and includes conditions for
pressure and temperature variations.
    The purpose of this paper is two-
fold: First to discuss further the con-
ditions and limitations proposed by this
theory, with a verification of the results

by experiments performed by Takashi et al
(1980), and secondly to present calculat-
ions on hydraulic conductivities for
soils during frost heave at a tempera-
ture range extending from $-7^{\circ}C$ to $-30^{\circ}C$.
A study of the temperature range from 0
to $-4^{\circ}C$ will be an extension of this work.

THEORY

The irreversible thermodynamic
theory of frost heave has been described
previously (Førland and Ratkje, 1980 a,
b). The essential points are as follows:
The entropy production of the coup-
led transport of heat and mass in frost
heave is completely described by two in-
dependent fluxes and their conjugate
forces. These are

$$J_q = -\bar{L}_{11} \Delta(\tfrac{1}{T}) - \bar{L}_{12} \frac{1}{T_2} \Delta\mu_{iT} \qquad (1)$$

$$J_w = -\bar{L}_{21}\Delta(\tfrac{1}{T}) - \bar{L}_{22} \frac{1}{T_2} \Delta\mu_{iT} \qquad (2)$$

J_q, is the measureable heat transferred
from the unfrozen water supply to the
ice lens. The coupled transport begins
at $0^{\circ}C$, as negligible coupling between
heat and mass transfer occurs above this
temperature. $\bar{L}_{ij}$ are average transport
coefficients for the finite region of
transport from the $0^{\circ}C$ isotherm to the
ice lens. ΔT for the transport will
always be equal to the temperature at the
ice in $^{\circ}C$. J_w is the water flux across
the soil in kg per area and time. By
choosing a particular reference state
for the transferred heat energy and for
the chemical potential of water, we can

131

use $\Delta\mu_{iT}$ as the chemical force of transport (see Førland and Ratkje, 1980b) $\Delta\mu_{iT}$ is the difference in chemical potential of ice due to concentration and pressure variations in the soil:

$$\Delta\mu_{iT} = \Delta\mu_{iT}^c + V_i(P_2 - P_1) \qquad (3)$$

Usually the soil composition changes very little, so

$$\Delta\mu_{iT}^c = 0 \qquad (4)$$

V_i is the partial molar volume of ice, and $P_2 - P_1 = \Delta P$ is the difference in hydrostatic pressure across the total region of transport.

The transport coefficients, $\bar{L}_{ij}$, are identified by equations that follow. Eqn. 2 is inserted into eqn. 1 go give the heat flow as a function of ΔT and water flow.

$$J_{q'} = -(\bar{L}_{11} - \frac{\bar{L}_{12}\bar{L}_{21}}{\bar{L}_{22}})\Delta(\frac{1}{T}) + \frac{\bar{L}_{12}}{\bar{L}_{22}} J_w \qquad (5)$$

In the case of pure heat conduction ($J_w = 0$) the coefficient parenthesis can be related to the thermal conductivity λ of the soil by Fourier's law. The last part of eqn.5 describes the reversible part of the heat transport. The ratio $\bar{L}_{12}/\bar{L}_{22}$ can be identified as the transported enthalphy per mole of water when going from 0^oC to the ice lens. This is equal to the heat of freezing at T_2 if changes in adsorption enthalpies along the transport path are neglected. This is again close to the heat of freezing at 0^oC. We have:

$$(J_{q'}/J_w)_{\Delta T=0} = -\bar{L}_{12}/\bar{L}_{22} \approx \Delta H_f(0^oC)T<0^oC \qquad (6)$$

The coefficient $\bar{L}_{22}$ may be identified from eqns. 2, 3 and 4:

$$\bar{L}_{22}/T_2 = -(J_w/V_i\Delta P)_{\Delta T=0} \qquad (7)$$

In eqn.7, $\bar{L}_{22}/T_2$ represents the hydraulic conductivity of the soil at constant temperature T_2. Eqn.7 when written in the following manner, is Darcy's law:

$$J = -k\frac{\Delta P}{l_f} \qquad (8)$$

l_f is the length of the sample. J is measured as volume flow per unit area and time (m sec^{-1}), and k is the hydraulic conductivity coefficient. When ΔP is measured in N m^{-2}, k has the dimension sm^{3}kg^{-1}. The relation between $\bar{L}_{22}$ and k is:

$$\bar{L}_{22}/T_2 = \frac{k}{V_i \cdot V_w \cdot l_f} \qquad (9)$$

and J_w is related to J by

$$J = J_w V_w \qquad (10)$$

where V_w is the molar volume of water. Three independent measurements are sufficient for a complete characterization of our transport system. The fourth equation that relates the transport coefficients is Onsager's reciprocal relation: For local transport coefficients $L_{12} = L_{21}$. We will assume that Onsager's relation also holds for average coefficients.

For frost heave only one transport coefficient is essential. This can be seen by combining eqns. 2, 3, 4, 6 and 9.

$$J_w = -\frac{k}{l_f}(\frac{\Delta H_f \cdot \Delta T}{T_2} + V_i\Delta P)\frac{1}{V_i \cdot V_w} \qquad (11)$$

This equation tells us that water is transported to the cold region due to ΔT. It is transported at a speed given by the hydraulic conductivity coefficient until an upper limit of pressure difference, $(\Delta P)_{J_w=0} = \sigma_u$, is obtained. In the frost heave situation it is only eqn.11 that will describe water flow correctly. Darcy's law cannot be used for frost heave, because it is not valid for $\Delta T \neq 0$, as can be seen by comparing eqn. 7 and 8. It should be noted that ΔP in eqn.11 is not the difference in pressure between two different phases, as obtained from Clapeyron's equation (Loch and Kay, 1978). σ_u is independent of soil type but dependent on the temperature at the ice lense as can be seen from the following relation:

$$\sigma_u = \Delta H_f\Delta T/T_2V_i \qquad (12)$$

It should be noted that no assumption about capillary forces are used in the derivation of eqns.11 and 12. Because J is a small quantity in frozen soils, it is difficult to measure J directly and find k through eqn.8. Eqn.11 provides an easier way of finding k during frost heave. In a closed system, J can be related to the heave rate dh/dt and the freezing expansion ratio of water $\Gamma = 0.09$ by:

$$J = dh/(1+\Gamma)dt \qquad (13)$$

When eqns. 10, 11 and 13 are combined we obtain

132

$$k = -\frac{l_f (dh/dt) \, V_i}{(1+\Gamma) \, (\Delta H_f \, \Delta T/T_2 + \Delta P)} \qquad (14)$$

We emphasize that k cannot be determined for an isothermal system when calculated by eqn. 14. k should be regarded as an average coefficient for the temperatures in question. However, at this stage it is valuable to introduce soil parameters that affect microscopic models, such as capillary pore radius; soil water content; viscosity; and others. In practice, k should be determined for different soils, and its value related to important soil parameters. We anticipate that critical range values for k will be found. Soils which are susceptible to frost heave, will have values for k that are below this range. It should be possible to predict susceptibility to frost heave from soil parameters, when a correlation between k and these parameters is developed.

CALCULATIONS

A. The maximum pressure in frost heave.

The maximum theoretically obtainable pressure, σ is independent of soil type. It depends only on ΔT. By inserting physical constants into eqn. 12 we find that $\sigma/\Delta T = -1140$ kN m^{-2} deg^{-1}. The following paramters have been used: $\Delta H_f = 332$ kJ kg^{-1}, $V_i = 1.1 \cdot 10^{-3}$ m^3 kg^{-1} and $T_2 = 263$K.

Takashi et al. paid special attention to the measurement of maximum pressures. They plotted σ against ΔT and found the theoretical value for small values of ΔT. This confirms our assumption for the ratio $\overline{L}_{12}/\overline{L}_{22}$ (eqn. 6).

Two Japanese soils, Manaita-bridge clay and Negishi silt were used in their experiments. Tempereature was measured at the cooling plate Θ_c, and in the unfrozen layer, Θ_{c}. The overburden pressure was registered. This is equal to the total pressure on the system in the region of the ice. The system's total crossectional pressure at the site of a porous plug in the unfrozen layer was also measured. This is the hydrostatic pressure of water at temperature Θ_∞, and it is also equal to the pressure P_1 where water transport begins. The difference, ΔP, was calculated for $J_w = 0$, giving σ. At the upper limit of heaving pressure, equilibrium is obtained between a heat force and the force created by a difference in chemical potential ($V_i\sigma$). By in-

creasing the pressure difference water flow or growth of the ice lens was reversed.

One prerequisite must be satisfied in order that the relationship in eqn. 12 holds true: a continuous path for water flow must be maintained: that is k > 0. The temperature Θ_c on the cooling plate can be so low that ice lens formation occurs in a region with $T_2 < \Theta_c$. This was found experimentally for $\Theta_c < -20°$C for Manaita-bridge clay, and $\Theta_c \lesssim -4°$C for Negishi silt. If Θ_{crit} denotes the lowest temperature at which the network can be uninterrupted while still permitting unfrozen water to flow through a specific soil, then σ (calculated from $\Delta T = \Theta_{crit}$ in eqn. 12) will give the actual maximum heaving pressure for that particular soil.

B. Hydraulic conductivities during frost heave.

The experimental results referred to in the previous section were used to calculate the hydraulic conductivity coefficient k of the Manaita-bridge clay and Negishi silt soils. The hydraulic conductivity coefficient, k, was calculated using eqn. 14. The results are given in Tables 1 and 2.

The hydraulic conductivity coefficients were calculated for parameters obtained after 100 hrs of experiment. At this point in the experiment, the most accurate heave rates were obtained for constant temperature conditions. With the exception of one case given in Table 2, the ice lens always formed at the cooling plate. In the last experiment reported in Table 2, the temperature at the cooling plate was lower than 12°C, and the lens was formed between the freezing front (0°C isotherm) and the cooling plate. The temperature at the ice was the critical temperature ($\Theta_{crit} = -12°$C) for Negishi silt. k is defined as the average value for the specimen at 0°C and the ice lens temperature. Uncertainty in calculated values is ± 20%, which is chiefly due to uncertainty in measurement of heave rate. By comparing the two tables it is seen that k decreases with decreasing temperature. This means that k is temperature dependent. For the same ΔT (-10°C), Manaitabridge clay has a hydraulic conductivity coefficient about 2-3 times greater than that of Negishi

Table 1. Hydraulic conductivity coefficient k for Manaita-bridge clay as calculated from eqn. 14 (see text). The run numbers refer to measurements of Takashi et al. (1980). The heave rate is given by dh/dt, the water flux by J and the temperature difference between the ice lens and the unfrozen water supply by ΔT. ΔP is the pressure difference that developed after 100 hrs. The length of the soil specimen is 9.0 cm.

Run no	dh/dt 10^{-7} mhr^{-1}	J 10^{-10} ms^{-1}	ΔT K	ΔP 10^2 Nm^{-2}	10^{18} k sm^3 kg^{-1}
1	6.19	1.58	-10	75.9	3.5
18	6.86	1.74	-29.4	233.7	1.5

Table 2. Hydraulic conductivity coefficient k for Negishi silt as calculated from eqn. 3.12 (see text). The run numbers refer to measurements of Takashi et al. (1980). The heave rate is given by dh/dt; the water flux by J; and the differences in temperature between the ice lens and the unfrozen eater supply by ΔT. ΔP is the pressure difference that developed after 100 hrs. The length of the specimen is usually 9.0 cm, and ΔT is the temperature Θ_c at the cooling plate. In run 5, $\Theta_c = -14,38^{\circ}$C and the ice lens forms at $\Delta T = \Theta_{crit}$ (at a distance of) 0.5 cm above the cooling plate.

Run no	dh/dt 10^{-7} mhr^{-1}	J 10^{-10} ms^{-1}	ΔT K	ΔP 10^2 Nm^{-2}	10^{18} k sm^3 kg^{-1}
2	6.19	1.58	-7.15	48.3	4.1
3	3.77	0.96	-8.87	53.0	1.7
4	3.64	1.18	-11.98	62.6	1.4
5	5.16	1.31	-12.0	63.3	1.5

silt. A'so, k can be determined for a temperature difference as low as -30°C for Manaita-bridge clay, whereas for Negishi silt $\Delta T = -12^{\circ}$C is the lowest limit for continuous water flow to the ice lens. This difference can be explained in terms of pore size of the two soils. Manaita-bridge clay has a grain size distribution lower than Negishi silt by one order of magnitude (see Takashi et al., 1980). The specific surface area in m^{2}g^{-1} is 136.2 and 27.2 for Manita-bridge clay and Negishi silt respectively. This means that the capillaries in Manita-bridge clay are finer than in Negishi silt, which makes it possible for water to stay in the capillaries at a temperature as low as -30°C as a supercooled water phase.

At present we have not evaluated enough experiments to make good correlations between values of k and soil type.

Eqn.14 permits the calculation of hydraulic conductivity at temperatures below 0°C using experimental data. The values obtained using this procedure are one order of magnitude smaller than the value estimated by Loch and Kay (1978). These same values are two orders of magnitude smaller than those obtained by Burt and Williams (1976) at -0.5°C. The decrease in k below -0.5°C is significant. This was not indicated by the measurements of Burt and Williams. Even if our value of k is comparatively small, the force driving water transport is usually large enough that normal heaves can be adequately modelled.

CONCLUSION

The present results indicate that a useful parameter for the description of frost heave is hydraulic conductivity of various soil types. Further investigations should be carried out in order *to find relationships between this para-meter* and parameters such as grain size and pore size distributions. We believe that predictive models of hydraulic con-ductivities at freezing temperatures can also be used to predict frost heave rates and maximum pressures.

REFERENCES

Førland, T. and Ratkje, S.K., "On the theory of frost heave", Frost i jord 21 (1980 a)45.

Førland, T. and Ratkje, S.K., "Irreversible thermodynamic treatment of frost heave", 2nd Int. Symp. Ground Freezing, Norw. Inst. Technology, June 24 - 26, Trondheim Norway, 1980 b, 611.

Loch, J. and Kay, B. "Water redistribution in partially frozen, saturated silt under several temperature gradients and overburden loads", Soil Sci. Soc. Am. J. 42 (1978)400.

Burt, T. and Williams, P. "Hydraulic conductivity in frozen soils", Earth Surface Process 1 (1976) 349.

Takashi, T., Ohrai, T., Yamamoto, H. and Okamoto, J., "Upper limit of heaving pressure measurements of partially frozen soil". 2nd. Int. Symp. Ground Freezing, Norw. Inst. Technology, June 24 - 26, Trondheim, Norway, 1980, 713.

Session II
THERMAL PROPERTIES,
PROCESSES AND ANALYSIS
Thermal properties and thermal
analysis

THERMAL PROPERTIES OF SOILS
RELEVANT TO GROUND FREEZING
Design Techniques for Their Estimation

Omar T. Farouki, Department of Civil Engineering, Queen's University of Belfast

In ground freezing it is vital to have good estimates of the thermal properties of the soil, both before and after freezing. The Kersten method has so far been generally used for this purpose. The limitations of this method are described in this paper and other methods are proposed that give better estimates when applied to certain types and conditions of soils. In particular, knowledge of the soil quartz content is important as a basis for a more accurate estimate of the thermal conductivity of coarse soil, while for frozen fine soil the unfrozen water content may be important.

Expected ranges of thermal conductivity values are given for fine, and for coarse, soils that may be unfrozen or frozen and have various dry densities and moisture contents. Depending on the volumetric heat capacity of the soil, a calculation can be made of its thermal diffusivity which influences the magnitude and rate of temperature changes.

A discussion is included of the factors which cause changes in the thermal conductivity and other relevant properties of a soil upon freezing.

INTRODUCTION

In ground freezing operations, it is vital to have good estimates of the properties of the soil in the unfrozen and frozen conditions. The relevant properties are the thermal conductivity k, the thermal diffusivity α and the volumetric heat capacity C of the soil, these being connected by the relationship $\alpha = k/C$.

The thermal conductivity determines the rate of heat transfer through the soil and hence the rate at which heat may be extracted from the soil. The thermal diffusivity governs the resulting rate of change of the soil temperature. These properties are required for use in calculations for determining the necessary refrigeration capacity to achieve ground freezing down to a given temperature over the target time period. A further important consideration is that freezing also involves the removal of the latent heat of the soil water as it converts to ice.

In the determination of the thermal conductivity of soils, the method of Kersten (1949) has so far been generally used. Based on this method, Sanger (1968) presented a chart from which the thermal conductivity of saturated soils, unfrozen or frozen, can be found for the purposes of ground freezing in construction. Kersten recognized some of the limitations of his method, noting that it gave thermal conductivity values that were too high for sands containing little quartz. On the other hand for coarse soils with a high quartz content, Johansen (1975) observed that the relevant Kersten equations underpredicted the thermal conductivity, while those equations applicable to silt/clay soils overpredicted. A method was developed by Johansen which would take the quartz content of the soil into account, using this content to derive an average thermal conductivity of the soil solids k_s. Kersten's empirical equations are based on the data of just four or five soils and the equations imply a value of k_s equal to 5 W/mK for coarse soils or to 3 W/mK for fine soils. As the actual

range of variation in k_s may be from about 2 W/mK up to about 8 W/mK, the Kersten method has serious drawbacks.

In a USACRREL research report, Farouki (1981b) evaluated the available methods for calculating the thermal conductivity of soils. There are seven methods which are applicable to unsaturated soils in the unfrozen condition while only four of these apply to the frozen condition. In either condition two more methods may be applied if the soil is saturated. The thermal conductivity values ('predictions') given by these methods were compared with the measured values relating to soils of known composition as reported by various experimenters, an indication of the quartz content being particularly important. A determination was made of the method giving the best agreement between its prediction and the measured value for various types and conditions of soil. A summary is given here of the main conclusions that are relevant to ground freezing. Also stated are some further relevant considerations arising from a study of the thermal properties of soils by Farouki (1981a) in a USACRREL monograph.

RESULTS AND RECOMMENDATIONS

It was found that, where Kersten's method was unreliable, the method of Johansen generally gave the best estimates of thermal conductivity. Particular exceptions were at low degrees of saturation which are unlikely to occur in soils to which the ground freezing technique might be applied. With regard to this technique, special attention is given here to the results applicable to soils with high moisture contents.

Coarse soils

In the case of coarse soils (unfrozen or frozen), the predictions given by the Kersten method are either unacceptably high when the quartz content is low, or unacceptably low when the quartz content is high. The Kersten method, however, gives generally good estimates (within ± 25% of the measured values) at intermediate quartz contents of about 60% of the solids content of the soil (corresponding to $k_s = 4.6$ W/mK).

At a quartz content near 100%, k_s is about 8 W/mK and the Johansen method gives Fig. 1 for unfrozen soils and Fig. 2 for frozen soils. The thermal

Figure 1. Thermal conductivity of unfrozen coarse soil with $k_s = 8$ W/m K (continuous curves at constant dry density γ_d).
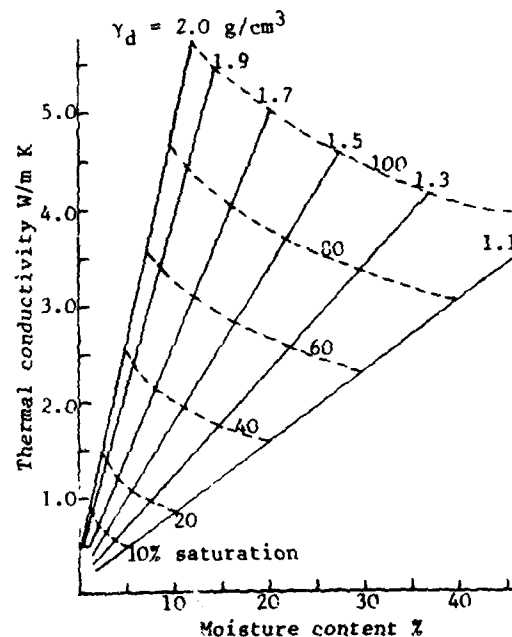
Figure 2. Thermal conductivity of frozen coarse soil with $k_s = 8$ W/m K (continuous curves at constant dry density γ_d).

140

conductivity may be determined from the appropriate figure depending on the moisture content and dry density of the soil.

Drying of a wet coarse soil containing a small amount of clay gave a thermal conductivity value in the nearly dry state that was higher than might have been expected (Farouki 1966). This was considered to result from the binding effect of the clay leading to better heat transfer at the points of contact of the granular skeleton. A similar effect may be expected after freezing since the freezing process is analogous to the drying process. The increase in thermal conductivity after drying was about 160% (as compared with the unbound state) for a clay content of about 8%. If a coarse soil containing such a clay content is subjected to freezing, it is suggested that the thermal conductivity given by the Johansen method should be increased by 160%. The effect would be less if the clay content is different. A greater clay content merely pushes the granular skeleton apart and reduces the effectiveness of heat transfer at the contacts. At clay contents above 15%, no allowance should be made for a binding effect.

At quartz contents near zero, the value of k_s may be around 2 W/mK, the thermal conductivity of feldspar and mica. At this value of k_s, the Johansen method gives the curves in Fig. 3 for unfrozen soils and Fig. 4 for frozen soils.

To find the thermal conductivity of coarse soils with intermediate quartz contents, the value of k_s may first be obtained by interpolation from Fig. 5. This value may then be used to interpolate between the thermal conductivity values corresponding to k_s = 8 W/mK (Fig. 1 or 2) and to k_s = 2 W/mK (Fig. 3 or 4) for the unfrozen or frozen state. Such an interpolation provides sufficient accuracy.

Some coarse soils with quartz contents less than 20% may, in addition to mica, contain minerals such as pyroxene and amphibolite with a thermal conductivity around 4 W/mK. For such soils, it is suggested that the value of k_s may be interpolated between 3.0 and 3.7 W/mK as the quartz content increases from 0 to 20%.

Fine Soils

For fine soils in the unfrozen condition, both the Johansen and Kersten
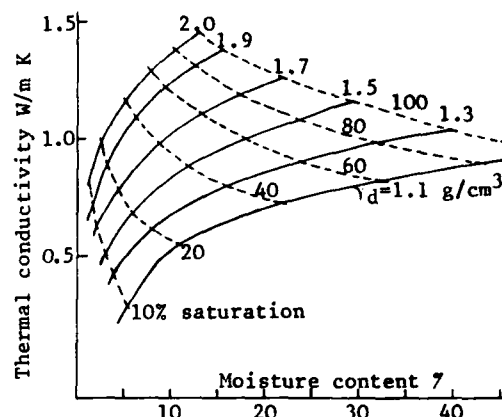
Figure 3. Thermal conductivity of unfrozen coarse soil with k_s = 2 W/m K.
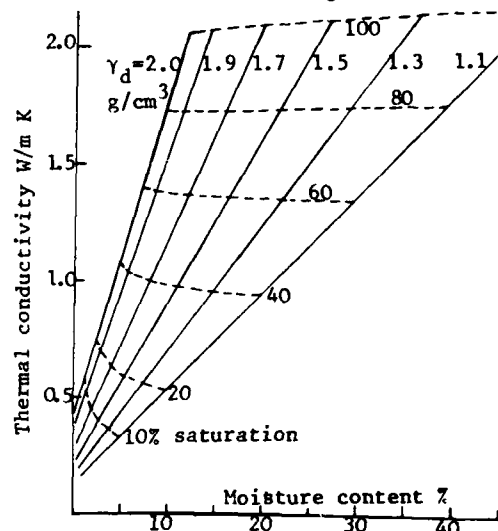
Figure 4. Thermal conductivity of frozen coarse or fine soil (k_s = 2 W/m K) [UWC = 0 for fine soil].
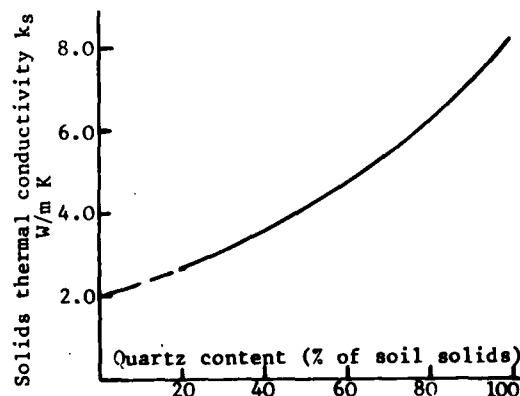
Figure 5. Thermal conductivity of soil solids as a function of their quartz content.

141

methods give good or adequate predictions (within ± 35%) but the latter does so only when the degree of saturation S_r is above 0.3. Fig. 6 is based on the Johansen method setting k_s equal to 2 W/mK. More accurate information is needed on the value of k_s for different clay minerals. When such measurements are available, the thermal conductivity values obtained from Fig. 6 may be adjusted with the aid of the sensitivity coefficients given in Table 1.

In the case of frozen fine soils, the Kersten method generally gave good predictions, so that the thermal conductivity may be determined from Fig. 7. However at S_r above 0.9, the Kersten
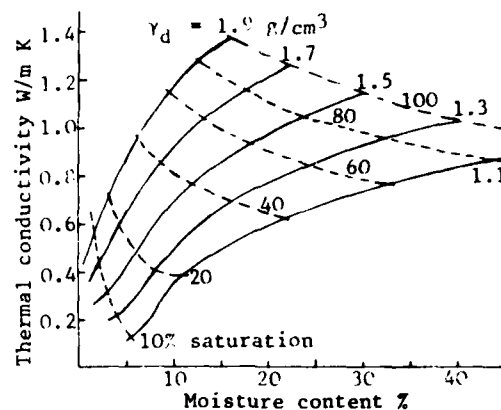
Figure 6. Thermal conductivity of unfrozen fine soil with k_s = 2 W/m K.

Table 1. Sensitivity of soil thermal conductivity to variation in k_s ($\Delta k/\Delta k_s$) W/m K units.

	Coarse soil (k_s range 3 to 8)	Fine soil (k_s range 2 to 3)
Unfrozen S_r = 1.0 S_r = 0.5	0.240 0.189	0.324 0.228
Frozen S_r = 1.0 S_r = 0.5	0.422 0.212	0.572 0.287
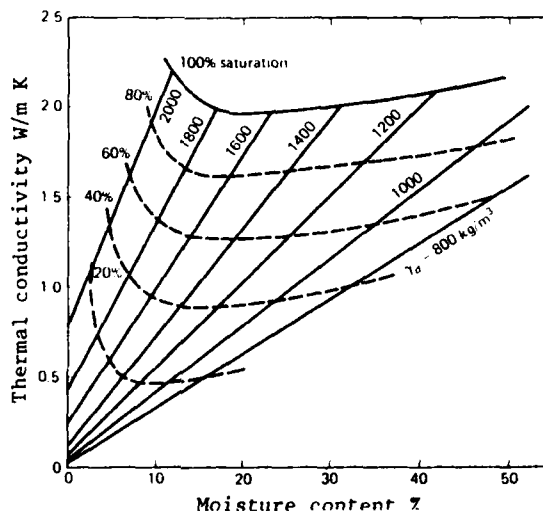
Figure 7. Thermal conductivity of frozen silt/clay soils based on Kersten (1949). After Andersland and Anderson (1978).

method gave some predictions that were too high (up to 60% for Leda clay). It appeared that this was due to the presence of unfrozen water which Kersen's method cannot take into account. Allowance for the unfrozen water content (UWC) was made with the Johansen method resulting in deviations within 10% for UWC values ranging from 0.135 to 0.075 (as a fraction of unit soil volume) at temperatures ranging from -2.5 to -22°C. According to Johansen, the thermal conduct-

ivity of a saturated frozen soil is

$$k_{sat} = k_s^{(1-n)} 2.2^n 0.269^{UWC}$$

where n is the fractional porosity. Table 2 gives an idea of the effect of UWC for a soil with a dry density of 1.4 g/cm^3. (w_u is the percent of unfrozen water content by weight as related to the dry soil weight).

If UWC is set equal to zero in the Johansen method it gives the curves shown in Fig. 4 for frozen fine soils ($k_s = 2$ W/mK) agreeing approximately with Kersten's curves. Table 2 may be used to estimate the effect of UWC in reducing the thermal conductivity values given by Fig. 4 for frozen fine soils that are saturated or unsaturated.

$$\log_e w_u = a + b \log_e S + cS^d \log_e \theta$$

where
a = 0.2618
b = 0.5519
c = -1.449
d = -0.264.

S may be simply determined by multiplying the clay fraction prese. t in the soil by 500 m^2/g which is the average specific surface area of clay minerals (McGaw and Tice 1976).

Sensitivity

To help in assessing the effects of changes in k_s and soil moisture content w, the values in Tables 1 and 3 may be used. These are taken from the sensit-

Table 2. Reduction in frozen saturated soil thermal conductivity due to unfrozen water content.

UWC fraction by volume	w_u % by dry weight	k_{sat} W/mK	% reduction
0	0	2.09	–
0.1	7.1	1.84	12.3
0.2	14.2	1.61	12.3

Unfrozen water content. This has been related to the specific surface area $S(m^2/g)$ of the soil and the temperature $-\theta°C$ by the relationship (Anderson et al 1973):

ivity analysis done by Farouki (1981b). Table 1 gives the change in soil thermal conductivity k due to unit change in k_s. For the higher S_r values, Table 3 gives the sensitivity s_w defined as the percent increase in k per 1% increase in w at constant dry density γ_d.

Table 3. Sensitivity s_w of soil thermal conductivity to moisture content (W/m K units). $k_s = 8$ for coarse or $k_s = 2$ for fine soil.

γ_d g/cm^3	Unfrozen (S_r range 0.5 to 1 approx.)		Frozen (S_r range 0.7 to 1 approx.)	
	Coarse s_w	Fine s_w	Coarse s_w	Fine s_w
1.1	1.2	1.6	2.7	2.6
1.4	1.2	1.6	3.5	3.3
1.7	3.3	2.7	5.4	4.9
2.0	5.1	5.2	12.0	9.6

The effect of changes in γ_d may be expressed by s_γ defined as the percent increase in k per 0.1 g/cm^3 increase in γ_d at constant w. For the higher values of w, rough average values of s_γ are 15% and 12% for unfrozen coarse and fine soils respectively or 18% and 14% for frozen coarse and fine soils respectively. These are based on the Johansen method as are the values given in Tables 1 and 3.

Excessive moisture content

When the water content is so large that the soil grains no longer contact each other, the dry density decreases considerably as water displaces the soil grains. A rapid decrease in the thermal conductivity occurs with increasing water content as shown in Fig. 8 for ocean sed-

iment composed of quartz. The thermal conductivity tends towards the value for water (about 0.57 W/mK) and a like behaviour is expected for marshy conditions.

A similar trend is shown by Fig. 9 where the thermal conductivity of permafrost decreases as the ice content increases excessively. In this case the thermal conductivity tends to a value about 30% below the thermal conductivity of ice (2.2 W/mK). Slusarchuk and Watson (1975) observed that this naturally-occurring ice-rich permafrost contained many small air bubbles and discontinuities which would lower its thermal conductivity.

Thermal diffusivity

The thermal diffusivity of a soil
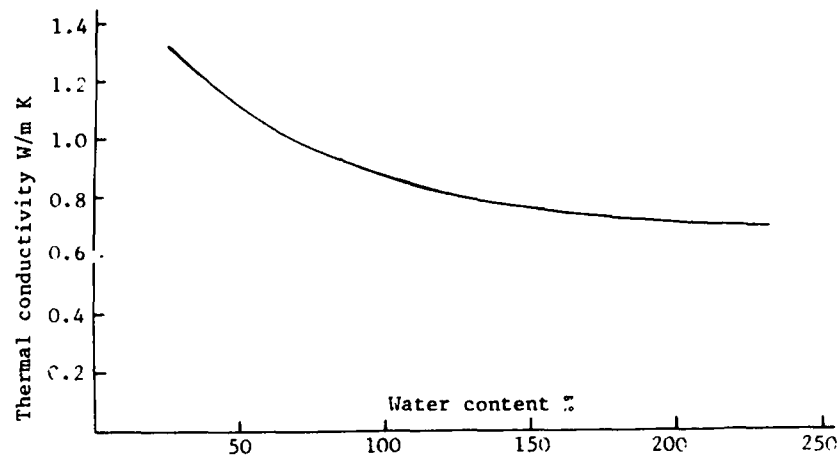
Figure 8. Thermal conductivity of ocean sediment [based on data of Ratcliffe (1960)].
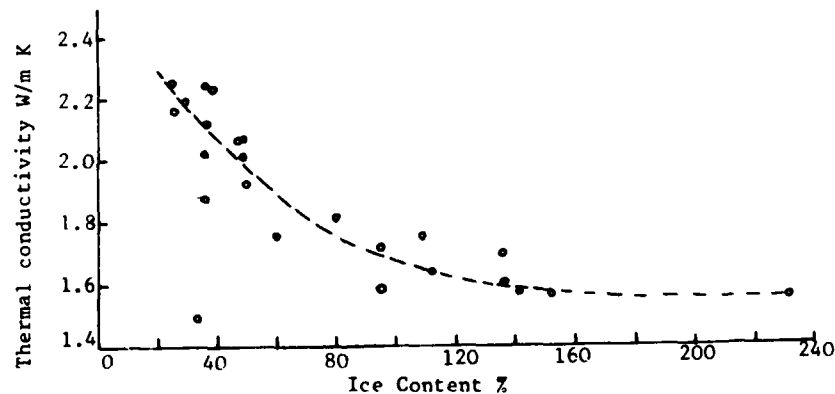
Figure 9. Thermal conductivity of undistrubed permafrost [based on data of Slusarchuk and Watson (1975)].

144

may be calculated from the estimated thermal conductivity value by dividing this by the volumetric heat capacity C of the soil. For unfrozen soils

$$C_u = \frac{\gamma_d}{\gamma_w} (0.18 + 1.0 \frac{w}{100}) C_w$$

while for frozen soil

$$C_f = \frac{\gamma_d}{\gamma_w} (0.18 + 0.5 \frac{w}{100}) C_w$$

where C_w is the volumetric heat capacity of water and γ_w is the density of water.

Factors in soil freezing

Whereas at low S_r values the thermal conductivity of a soil may decrease on freezing, at high S_r values there is a considerable increase in the thermal conductivity when the soil freezes. This results from the fact that the thermal conductivity of ice is about four times that of free water. As the temperature decreases below 0°C the thermal conduct-ivity of a saturated fine soil further increases because its ice content incre-ases and the thermal conductivity of this ice also increases. The gradual conversion of unfrozen water means that the latent heat is released in stages, depending on the relationship of the un-frozen water content to temperature and to specific surface area as given above. This may be taken into account in an expression for the apparent volumetric heat capacity C_a of a freezing soil by including a term dependent on the var-iation of the unfrozen water content with temperature:

$$C_a = C_s x_s + C_i x_w + (C_u - C_i) x_u + \frac{1}{\Delta T} \int_T^{T + \Delta T} L (\frac{\Delta x_u}{\Delta T}) dT$$

where C_s, C_i and C_u are the volumetric heat capacities of the solids, ice and unfrozen water respectively, and x_s, x_i, x_u (=UWC) are their respective volume fractions ($x_w = x_u + x_i$), L is the latent heat of phase change per gram of unfroz-en water and Δx_u is the change in un-frozen water taking place in the temp-erature interval ΔT (Hoekstra 1969). Tsytovich and Khakimov (1961) observed that the soil temperature may be taken to be 2°C higher than the temperature of the coolant in the freezing pipe.

The rate of freeze of a soil de-creases greatly as its moisture content increases. If an external supply of water is available to a silty soil in the field, slow freezing of this soil could lead to formation of ice lenses and surface heaving. To obviate this the freezing should be conducted as rapidly as possible.

CONCLUSIONS

Techniques have been described whereby rational estimates (probably within ± 25% in general) may be obtained for the thermal conductivity (and hence thermal diffusivity) of unfrozen or frozen soils depending on their moisture content and dry density. It is import-ant to know the quartz content of coarse soils or the unfrozen water content of frozen silt/clay materials.

REFERENCES

Andersland, O.B. and D.M. Anderson (1978) (Editors) Geotechnical engineering for cold regions. McGraw-Hill, New York, N.Y.

Anderson, D.M., A.R. Tice and H.L. McKim (1973). The unfrozen water and the apparent specific heat cap-acity of frozen soils, North Am. Contrib. 2nd. Int. Conf. Perma-frost, Yakutsk, USSR. National Academy of Sciences, Washington, D.C., pp. 289-295.

Farouki, O.T. (1966). Physical propert-ies of granular materials with reference to thermal resistivity. Highway Research Record No. 128, pp 25-44. Highway Res. Board, Natl. Ac. of Sc. - Natl. Res. Council, Washington D.C.

Farouki, O.T. (1981a). The thermal pro-perties of soils. U.S. Army Cold Regions Res. and Eng. Lab. mono-graph (in press).

Farouki, O.T. (1981b). Evaluation of the methods for calculating soil thermal conductivity. U.S. Army Cold Regions Res. and Eng. Lab. research report. No.183 (in press).

Hoekstra, P. (1969). The physics and chemistry of frozen soils. High-way Res. Board Special Report 103, Effects of temperature and heat on engineering behavior of soils, pp 78-90. Highway Res. Board, Natl. Ac. of Sc. - Natl. Res. Council, Washington, D.C.

Johansen, O. 1975. Thermal conductivity of soils. Ph.D. thesis, University of Trondheim, Norway. (Available as USACRREL Draft Translation 637, 1977).

Kersten, M.S. 1949. Thermal properties of soils. Univ. of Minnesota Eng. Expt. Station Bulletin No. 28.

McGaw, R. and A.R. Tice 1976. A simple procedure to calculate the volume of water remaining unfrozen in a freezing soil. Proc. 2nd Conf. on Soil-Water Problems in Cold Regions, Edmonton, Alberta, Canada. pp. 114-122. Division of Hydrology, American Geophysical Union, Washington, D.C.

Ratcliffe, E.H. 1960. The thermal conductivities of ocean sediments, J. of Geophy. Res., vol. 65, no. 5, pp. 1535-1541. American Geophysical Union, Washington, D.C.

Sanger, F.J. 1968. Ground freezing in construction. Proc. Am. Soc. of Civil Engrs., J. Soil Mech. and Foundations Div., vol. 94, no. SM1, Proc. Paper 5743, pp. 131-158. Am. Soc. of Civil Engineers, New York, N.Y.

Slusarchuk, W.A. and G.H. Watson 1975. Thermal conductivity of some ice rich permafrost soils. Can. Geotech. J., vol. 12, no. 3, p. 413-424. National Res. Council Ottawa, Canada.

Tsytovich, N.A. and Kh.R. Khakimov 1961. Ground freezing applied to mining and construction. Proc. of 5th Int. Conf. on Soil Mechanics and Foundation Engineering, vol. 2, pp. 737-741. Dunod, Paris, France.

THERMAL PROPERTIES OF FREEZING SOILS

M.W. Smith   Geotechnical Science Laboratories,
D.W. Riseborough   Carleton University,
                    Ottawa, Canada

ABSTRACT

A new needle probe is used to measure the thermal conductivity and diffusivity of soils at freezing temperatures. The design permits use of a very small heat pulse to minimize thermal disturbance of the sample; thus measurements can be made close to 0°C. Corresponding measurements of soil water phase composition are made using time domain reflectometry. The data allow us to derive relationships between thermal conductivity and temperature (i.e. unfrozen water content) and diffusivity versus temperature. Knowledge of the phase composition allows calculation of the volumetric heat capacity, which serves as a check for the thermal probe measurements.

EFFECTS OF SALINITY ON FREEZING
OF GRANULAR SOILS

Larry J. Mahar   Project Engineer, Ertec Western, Inc., Long Beach, California
Ted S. Vinson   Associate Professor, Dept. of Civil Engineering, Oregon
                  State University, Corvallis, Oregon
Ralph Wilson   Graduate Research Assistant, Dept. of Civil Engineering, Oregon
                  State University, Corvallis, Oregon

ABSTRACT

The use of artificial freezing techniques for construction in the marine environment must consider the effects of salinity in the pore water and the consequences of too rapid a rate of freezing on the stability of the resulting frozen soil. To address this problem laboratory model tests were conducted to observe the effects of salinity on the freezing rate of granular soils. Experimental data from laboratory freezing tests are presented which suggest a modification in thermal properties normally used for granular soil to account for salinity in the pore water. The results also demonstrate that, during freezing, salt migrates away from a freezing front causing a zone of high salinity to form at the unfrozen-frozen soil interface. Rapid artificial freezing of soils containing saline pore water may result in the following adverse effects: 1) freezing fronts can skip over zones of high salinity created by migration of salt resulting in development of pockets of unfrozen soil with brine in the pore spaces, and 2) very rapid freezing can restrict the salt migration process resulting in a weakened frozen strength condition.

THERMOPHYSICAL CHARACTERISTICS OF FROZEN, FREEZING-THAWING, AND THAWED ROCKS AND METHODS OF THEIR MEASUREMENT

Philippov P.I. Ins.on Physic.
Stepanov A.V. and Techn.
Timofeev A.M. Problems of
North, USSR

In this paper the evaluation methods of frozen-thawing and thawed rock thermophysical characteristics (volumetric heat capacity,coefficients of heat and temperature conductivities) are described as developed by the authors.

The investigation results concerning the grinded rook heat conductivity coefficient as a function of moisture and the cyclic freezing influence on the clay-and-sand soil thermophysical properties are presented.

heat and temperature conductivity coefficients are

$$\lambda = \frac{(q_2 - q_1)R}{(K+3)\Delta T} \frac{\alpha^2}{(1+\alpha)^2},$$

$$\alpha = \frac{(q_1 - q_2)R^2}{(K+1)(K+3)\Delta \tau} \frac{\alpha}{(1+\alpha)},$$

where $\alpha = \frac{C\rho\pi R^2}{C_n}$ is the sample and heater thermal capacity ratio per unit length; K is the shape factor equal respectively,to 0,1,2 for the plate, the cylinder and the sphere.

I. Methods

Described in [1],a complex method allowing the unfrozen water quantity and thermophysical characteristics evaluation,is used for the study of moist bulk materials.

For hard rocks a stage heating method [2],based on the heat conductivity equation solution at the boundary condition of the second order for bodies of classical forms in the case of two stage sample heating by a heater of stepwise varying power from q_1 to q_2,is elaborated.The experimental curve that characterizes the heat temperature growth with time, is registrated only at one sample (surface) point and has the shape as shown in Fig.I. The formulae for calculating the

Fig.I. The sample surface temperature variation with time.

The next group of rock thermophysical response evaluation

151

methods is based on the heat conductivity equation solution allowing for the finite heat source sizes.

Using in [2] the calculation formula of a short cylindrical sonde heating temperature produced by a constant power heater, proposed by L.R.Ingersoll and al. [3],a simple calculation formula of short pipe surface temperature near the tube middle part has been obtained:

$$\Delta T = \frac{q_e}{4\pi\lambda}\left(4.6\, lg\, \frac{L}{2} - \frac{L}{\sqrt{\pi a \tau}}\right).$$

where L is the sonde length and τ is the sonde radius.

At $a\tau/\tau^2 > 5$, the experimental points of the relationship between ΔT and $1/\sqrt{\tau}$ are located on a straight line. For $1/\sqrt{\tau} = 0$ and $\Delta T = 0$,this line affords,respectively,the calculation formulae of the coefficients of heat and temperature conductivities.

$$\lambda = \frac{q_e}{4\pi\Delta T} \cdot 4.6\, lg\, \frac{L}{\tau},$$

$$a = \frac{L^2}{24.16\, \pi\tau\, \left(lg\, \frac{L}{\tau}\right)^2}.$$

For a flat sonde of limited size,the thermal resistance of a plate located on the bulk rock surface is used [2]

$$R = \frac{1}{\pi A}\, ln\, \frac{4A}{B},$$

where A is the plate length; B is the plate width. Hence,the heat conductivity coefficient is

$$\lambda = \frac{q}{\pi\Delta T A}\, ln\, \frac{4A}{B}$$

The heat loss through the thermal insulator is defined with the help of the preliminary calibration in standard mediums at different heater temperatures.

2. Results

Thermophysical characteristics of grinded rocks are investigated[4]. The diameter of grains did not exceed 4 mm.

The investigation results are given in the form of empirical relationships.For atmospherically dry grinded materials the heat conductivity coefficient is described by the formula

$$\lambda_c = \lambda_r\left[1 + 30\left(\frac{\gamma_{ck}}{\rho_{ck}}\right)^2\right],\ W\cdot m^{-1} K^{-1}$$

where λ_r is the air heat conductivity coefficient; γ_{ck} is the material volume weight; ρ_{ck} is the material unit weight, or

$$\lambda_c = \lambda_{ck}\left[\frac{0.212}{1.257 - \frac{\gamma_{ck}}{\rho_{ck}}} - 0.213\right].$$

The investigations have been carried out for the case when $0.4 \leq \gamma_{ck}/\rho_{ck} \leq 0.9$.
For wet materials at $0° \div +35°C$ the heat conductivity coefficient change as a function of moisture W is expressed by the formula

$$\lambda_{\tau}(W) = \frac{\lambda_c}{1 - 0.74\sqrt{\frac{W}{W_H}}},$$

where $W_H = (1/\gamma_{ck} - 1/\rho_{ck})\,\rho_B, \rho_B$ being the water specific weight.
At negative temperatures, $-15° \div 40°C$

$$\lambda_M(W) = \frac{\lambda_c}{1 - 0.87\sqrt{\frac{W}{W_H}}}.$$

The heat conductivity coefficient change in the temperature range from $-15°$ to $0°C$ is described by the formula

$$\lambda(T) = \frac{\lambda_c}{1 - 0.87\sqrt{\frac{W}{W_H}}}\left[1 - \left(1 - \frac{1 - 0.87\sqrt{\frac{W}{W_H}}}{1 - 0.74\sqrt{\frac{W}{W_H}}}\right)\frac{W_{HB}(T) - W_0}{W - W_0}\right],$$

where $W_{HB}(T)$ is the unfrozen water amount as a function of temperature, W_0 is the unfrozen water amount at $-15°C$.

The cyclic freezing-thawing influence on the thermophysical properties of the South Yakutia clayey soil that did not experience the negative temperature influence is examined in[1].

In the present paper these investigations are developed. By means of the South Yakutia clayey soil washing the sand and the clay were separated. Then, the sand and clay mixtures with the 20%,40%,60%,80% clay weight content were prepared. Using the stage heating method, the thermophysical properties of sand, clay and their mixtures in dry and wet condition were determined. For the dry condition, the empirical formulae of the heat conductivity coefficient as a function of volume weight (Fig.2) and those of mixture specific heat dependence on the clay weight content (Fig.3) are found:

$$\lambda = \frac{0,0774 + 0,0322 \cdot 10^{-3} \gamma_{cк}}{1 - 0,433 \cdot 10^{-3} \gamma_{cк}};$$

$$C_{yg} = (0,875 + 0,421 \cdot \rho) \cdot 10^{3}, \ J \cdot \kappa g^{-1} \cdot K^{-1}$$

where ρ is the clay weight content.

clay content increase the cyclic freezing-thawing influence decreases. The heat conductivity coefficient change of pure clay is comparable to that of 40%clay content mixture.
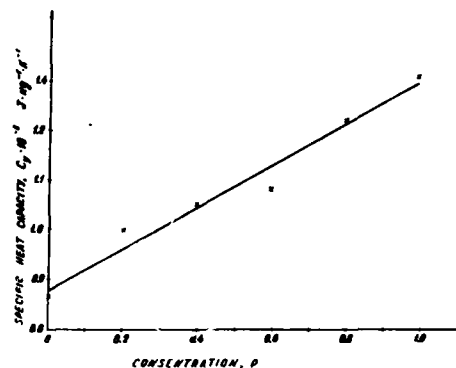
Fig. 3. The specific heat dependence on the clay component concentration in the mixture.

Fig.2 The relationship between the heat conductivity coefficient experimental values of dry sandy-clayey mixtures and the volume weight.

Then, making use of these mixtures, the cyclic freezing-thawing influence on the thermophysical properties of wet clay and sand mixtures is studied.

In sands the cyclic freezing-thawing influence on the heat conductivity coefficient is not observed. With clay component content growth, the cyclic freezing-thawing influence on the thermal conductivity coefficient increases (Fig4). At 60% clay content this influence reaches the maximum value. At further

Fig. 4. The heat conductivity coefficient change produced by the triple freezing-thawing cycle as a function of humidity and of clay component concentration ρ.

According to the moisture and the concentration of mixtures, the following empirical equations for calculating the heat conductivity coefficient change produced by the triple freezing-thawing cycle are established: for the mixture with 40%clay content $\lambda_{3} = \lambda_{e} - 0,25W - 0,147$; 60% clay content $\lambda_{3} = \lambda_{e} - 3,3W + 0,145$; 80% clay content $\lambda_{3} = \lambda_{e} - 2,85W + 0,17$; for the 100% clay content

$$\lambda_{3} = \lambda_{e} - 0,90W,$$

where λ_o, $W \cdot m^{-1} K^{-1}$, is the heat conductivity coefficient of the unfrozen material in thawed state and W is the moisture content in unit fractions.

References

I. Efimov S.S.,Kozhevnikov N.N.,Kurilko A.S.,Nikitina L.M. and Stepanov A.V.Cyclic Freezing-Melting Influence on Heat Mass Transfer Characteristics of Clayey Grounds.The 2nd Internati onal Symposium on Ground Freezing The Norwegian Institute of Technology Preprints.ISGF 80.pp.462-469.

2. Philippov P.I.,Timofeev A.M. Evaluation Methods of Thermophysical Properties of Solids.-Novosibirsk,Nauka,1978,104 p.
3. Ingersoll L.R.,Zobel O.D., Ingersoll A.K.Heat conductivity and its Application in Engineering and Geology,-Moscow,Leningrad Mashgiz,1959,255 p.
4. Ivanov N.S.,Stepanov A.V., Philippov P.I. Thermophysical properties of bulk freiht.- Novosibirsk,Nauka,1974,96 p.

ELECTRICAL POTENTIALS DURING FREEZING OF SOILS

V.R. Parameswaran   National Research Council of Canada

ABSTRACT

Development of electrical potentials during freezing of various kinds of materials such as a saturated quartz sand, a clayey silt, a silty clay, and water, was studied in the laboratory using two different experimental setups. In one setup a hollow cylindrical metallic pile through which a refrigerant could be circulated, was embedded in the material, and the potentials developed during rapid freezing were measured. In the second setup a PVC probe containing copper electrodes at 6-in. intervals was embedded in the material which was allowed to freeze unidirectionally at a very slow rate in a cold room, and the electrical potentials and related currents were measured between the electrodes in the frozen and unfrozen regions.

The magnitude as well as the sign of the freezing potential were found to depend on the characteristics of the mate-rial such as grain size and moisture content, and the rate of freezing. In pure water under rapid cooling (by liquid nitrogen) freezing potentials of up to 12 voltes were measured. In a quartz sand containing 14-20% water the freezing potentials were of the order of 250 mV. Using the second experimental setup, the maximum freezing potential measured under slow cooling in a clayey silt containing 20% water was 230 mV, and in a silty clay the maximum freezing potential measured under the same conditions was 320 mV.

This paper discusses the results of the laboratory measurements of freezing potentials and their implications in the design and construction of foundations, chilled pipelines, etc., in permafrost areas, as well as excavations and construction of underground tunnels by ground freezing.

MODELING THE INTERACTION BETWEEN SOIL FREEZING SYSTEM AND THERMAL REGIME IN SOILS USING FEM

Eugen Makowski, Dipl.-Ing.   Dep. of Civil Engineering
Ruhr-University Bochum
Federal Republic of Germany

ABSTRACT

To design ground freezing systems with difficult and complex conditions numerical methods as the FEM are to be used. Their capability to treat the problem of heat transfer in freezing soils was demonstrated by several authors.

In this paper results of a research project are presented which is related to the development and use of soil freezing system for special conditions such as inhomogeneous soil and rock structure with different thermal properties and unequal locations of freeze pipes.

To investigate these problems a basic FEM-program was extended under following aspects:

- use of models of proved accuracy for the transient heat transfer in soils, the temperature dependent thermal properties, and the release of latent heat

- development of techniques to model the behaviour of the freeze system components

- description of the interaction between soil freezing system and the the thermal regime in soils.

Calculated results are presented and discussed.

THERMAL DESIGN AND INVESTIGATIONS FOR FROZEN SOIL PROJECTS IN LAYERED GROUND

The use of soil freezing is based on an appropriate thermal design which includes a specification of several parameters like size and arrangement of freeze pipes, capacity of the refrigeration system and elapsed time for freezing a certain soil volume. The calculations are usually performed with simplified thermodynamic models, considering only homogeneous soils, idealized freeze pipe arrangements, and constant surrounding temperature.

Dealing with deep frost shafts there is a need of sophisticated thermal investigations to build save and economic frozen soil structures. Especially if significant freeze pipe dislocations exist and no temperature measurements of that area will be available detailed investigations are performed to predict the propagation of the isothermal lines of freeze temperatures. In a layered soil it is essential to know the time when the volume required for stability is frozen in each layer in order to determine a suitable time scheme for shaft sinking.

Basis of a mathematical model is the linking between the performance of refrigeration system as mounted at the construction site including real freeze pipe locations and the thermal regime in different type of soils.

157

The intention of this paper is to present a FEM model suited for these problems due to the implementation of refined boundary conditions. Furthermore results of investigations on deep shafts are given and discussed showing the influence of the real layout of the refrigeration system and layered ground on the propagation of the frozen zone.

GOVERNING EQUATIONS

Transient Heat Conduction in Soils

Providing heat transfer by conduction in water saturated soils the following equations govern the nonlinear problem of transient heat conduction in non-homogeneous and anisotropic soils (Carslaw and Jaeger 1959):

$$\frac{\partial}{\partial x}\left(k_x \frac{\partial T}{\partial x}\right) + \frac{\partial}{\partial y}\left(k_y \frac{\partial T}{\partial y}\right) = c \frac{\partial T}{\partial t} \qquad (1)$$

$$k_{x,y} = k_{x,y}\ (x,y,T,w_u\ (T))$$

$$c = c\ (x,y,T,w_u\ (T))$$

k – thermal conductivity
c – volumetric heat capacity
w_u – unfrozen water content

Continuity at the moving boundary between the two phases of water A and B is given by:

$$\frac{\partial T_f}{\partial x_A} - \frac{\partial T_f}{\partial x_B} = L\rho_d\ w_u\ (T)\ \frac{dx}{dt}$$

$$\frac{\partial T_f}{\partial y_A} - \frac{\partial T_f}{\partial y_B} = L\rho_d\ w_u\ (T)\ \frac{dy}{dt} \qquad (2)$$

$$T_f = T_f(T)$$

T_f – freeze temperature
L – latent heat of fusion

On the boundary curve of the region of interest following conditions can be specified

type I   prescribed temperature (e.g. soil surface temperatures)

$$T = \bar{T}\ (x,y,t) \qquad (3)$$

type II   no flux across the surface

$$\frac{\partial T}{\partial x} + \frac{\partial T}{\partial y} = 0 \qquad (4)$$

type III prescribed flux (e.g. influence of extraction machines)

$$q = \bar{q}\ (x,y,t) \qquad (5)$$

type IV   linear heat transfer (e.g. forced convection)

$$q = b(T\ (x,y,t) - \bar{T}\ (x,y,t)) \qquad (6)$$

type V   nonlinear heat transfer (e.g. radiation)

$$q = c\ (T^4(x,y,t) - \bar{T}^4(x,y,t)) \qquad (7)$$

Initial condition

$$T_o = \bar{T}_o\ (x,y) \qquad (8)$$

Performance of a Mechanical Refrigeration System

Boundary condition of type IV is used if the soil is cooled by a mechanical refrigeration system with a pumped loop secondary coolant because the heat transfer from the soil to the circulating brine is governed by forced convection (Plank 1952, Frivik and Thorbergsen 1980, Jessberger and Makowski 1981). Relating to a unit surface area of a freeze pipe the flux q is

$$q = \alpha_T\ (T_S - T_F) \qquad (9)$$

α_T – heat transfer coefficient at the freeze pipe wall

T_S – soil temperature at the freeze pipe wall

T_F – fluid temperature (brine temperature)

Due to conservation of energy this flux together with an additional flux by losses in the main line has to be transfered to the refrigerant at temperature T_R in the evaporator

$$q = \alpha'_T\ \frac{A_e}{A_p}\ (T'_F - T_R) \qquad (10)$$

α'_T – heat transfer coefficient at the evaporator wall

T'_F – modified brine temperature due to losses in the main lines

T_R – evaporator temperatures

A_e – area of evaporator

A_p – area of freeze pipe

The related capacity Q_e/A_p of the refrigeration system is not constant but strongly influenced by the evaporation temperature

$$q = \frac{Q_e}{A_p} = f(T_R) \qquad (11)$$

The temperatures $T_R(t)$, $T_F(t)$, and therefore $T_S(t)$ will drop in a way that the corresponding flux will always be balanced by the related refrigeration capacity.

The heat transfer coefficients are influenced by the temperature and the velocity v of the brine

$$\alpha_T, \alpha'_T = \alpha_T, \alpha'_T (T_{F,R}, v) \qquad (12)$$

FEM-FORMULATION

Description of the Model

The complete set of equations (1) to (12) cannot be solved by analytical methods. But the FEM can be applied to these transient heat transfer problems involving a change of phase (Lewis, Morgan and Schrefler 1981).

To model the heat transfer in artificially frozen soils the development of some new techniques is required. In a FEM code special subroutines for the freezing process, the change of soil properties, and the simulation of the mechanical refrigeration system are to be implemented (Frivik 1980, Jessberger and Makowski 1981).

Modelling the phase transition has been successfully performed by the heat accumulation technique as well as by the apparent specific heat. Both methods give acceptable results. The change of thermal properties of soils requires special FEM-techniques, because new element properties have to be evaluated when the freeze line divides an element in parts of different properties. A special average procedure is implemented. The temperature change in time direction is calculated by the Crank-Nicholson-method or by a two-time-step interpolation function according to Galerkin. The thermal regimes computed by both methods are close to each other though the Crank-Nicholson method tends more to oscillation if the soil properties are changed in the elements.

Extending and modifiing some ideas of Frivik and Thorbergsen (1980) the basis of the model of the heat remove by a mechanical refrigeration system is a combined heat conduction and convection system. Initial step is the estimation of the brine temperature $T_F{}^t$. With this temperature and the convective boundary condition (9) the thermal regime including $T_S{}^t$ at the freeze pipe surface after one time step Δt is calculated. With $T_F{}^t$ and $T_S{}^t$ the heat flux q_t is given. Providing conservation of energy q_t has to be balanced by the related refrigeration capacity. With the capacity curve over evaporating temperature a new $T_F{}^{t+\Delta t}$ is evaluated.

Both the modelling of the performance of the refrigeration system and the temperature change in soils requires sufficient small time steps. Automatic time-step adjustement can therefore reduce computer time.

To calculate the formation of the frozen zone in a cross-section perpendicular to the freeze pipes a special subroutine is implemented with the capability to prescribe a convective boundary condition at a node in the interiour of the net. At this node brine temperature, freeze pipe diameter, and heat transfer coefficient can be defined separately. The solution of the total system will give the soil temperature at the outer surface of the freeze pipe at this node.

Simulation Test

The analytical solution of Neumann is chosen to control the correspondance of the FEM-model for freezing processes in soils with an exact solution. Figure 1 shows the change of temperature over time in a depth of 15 cm below soil surface. In Figure 2 the propagation of the frost line into the ground calculated by Neumann and the FEM is demonstrated. It is obvious that the FEM-results are more influenced by the chosen time step than by the time-iteration method. The oscillations are less evident for small time-steps.

The capability of the model to calculate the thermal regime in artificially frozen soils is proved with a frost shaft project. For several different soil layers the temperature change in the soil was calculated taking into account the real freeze pipe positions. The accordance of calculated results and measurements was good as Hegemann (1981) reported.
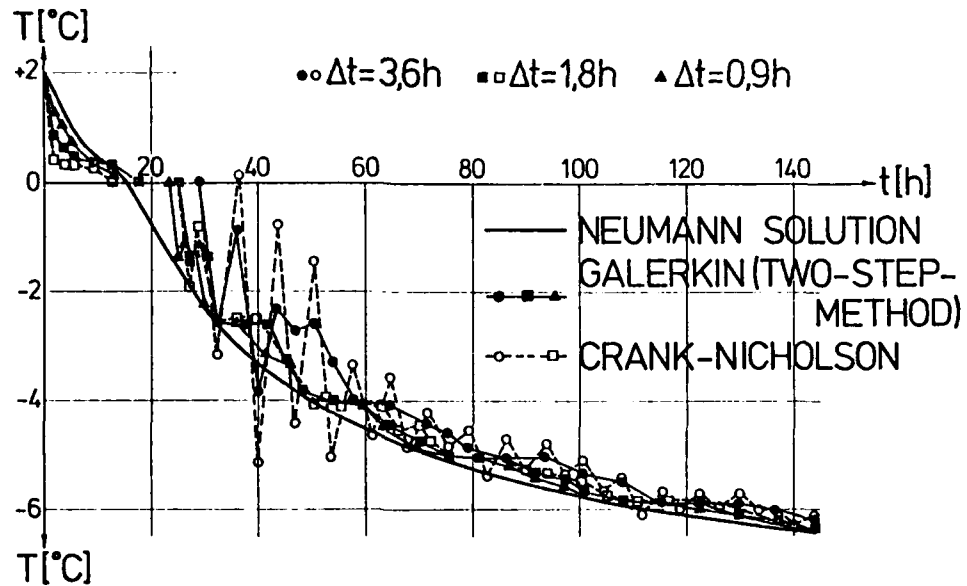
Fig. 1: Simulation test of the FEM code against the exact solution of Neumann - temperature vs. time in a sand underground (depth 15 cm, soil surface temperature -10°C, initial temperature +2°C)
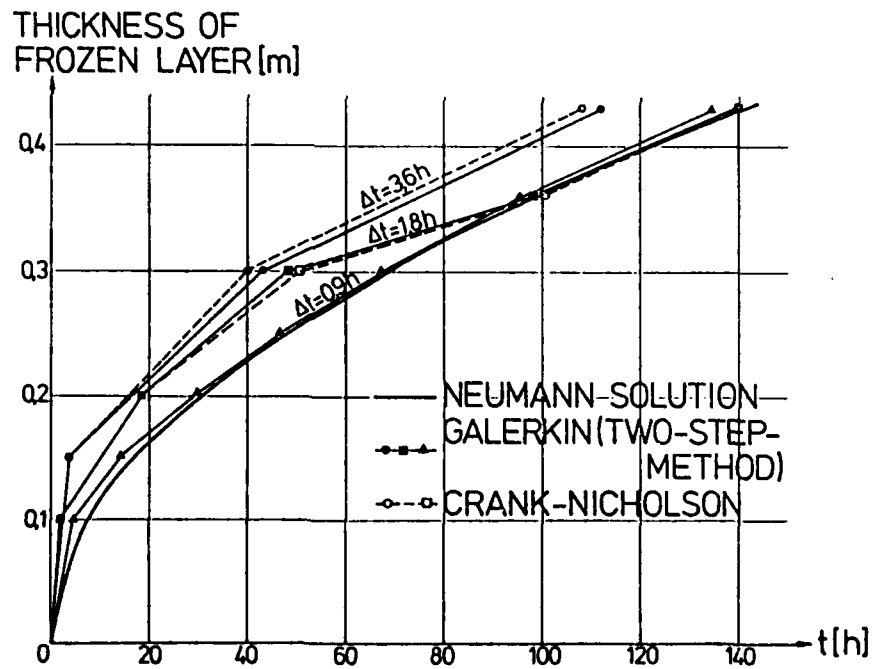
Fig. 2: Simulation test of the FEM code against the exact solution of Neumann - propagation of the frozen soil layer

APPLICATION

The developed FEM code is applied to the systematical investigation of the influence of different factors on the time dependent frost wall thickness of a frost shaft. These factors are

- changes of circulating velocity and refrigeration capacity

- dislocations of freeze pipes

- layered ground

- influence of the extraction sequence.

In this paper some results are presented demonstrating the differing influences of freeze pipe positions and the vertical heat transfer between layers of different soil types.

Influence of Vertical Heat Transfer

In most cases it is reasonable to assume that the underground consists of horizontal layers of different materials. In order to know the horizontal propagation of the frozen zone selected layers with distinct thermal properties are usually investigated by separate horizontal FEM calculations. Then in successive layers different propagation speeds can

be expected. This causes a vertical heat transfer. To investigate to what extend this vertical heat transfer affects the horizontal one, the temperature change around a single freeze pipe is calculated for different underground conditions:

- propagation of the frozen zone in a pure sand or clay

- propagation in a clay layer of a thickness of 5.5 m, embedded in sand and a sand layer of the same thickness embedded in clay

- propagation in a clay or sand layer, 2.75 m thick embedded in sand or clay
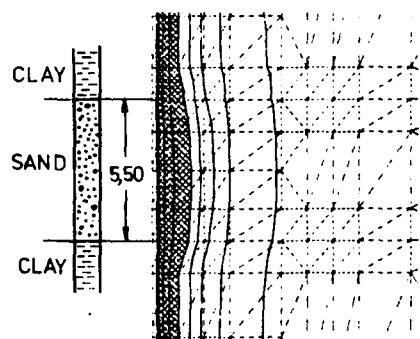
Fig. 4: Thermal regimes of layers with different thermal properties
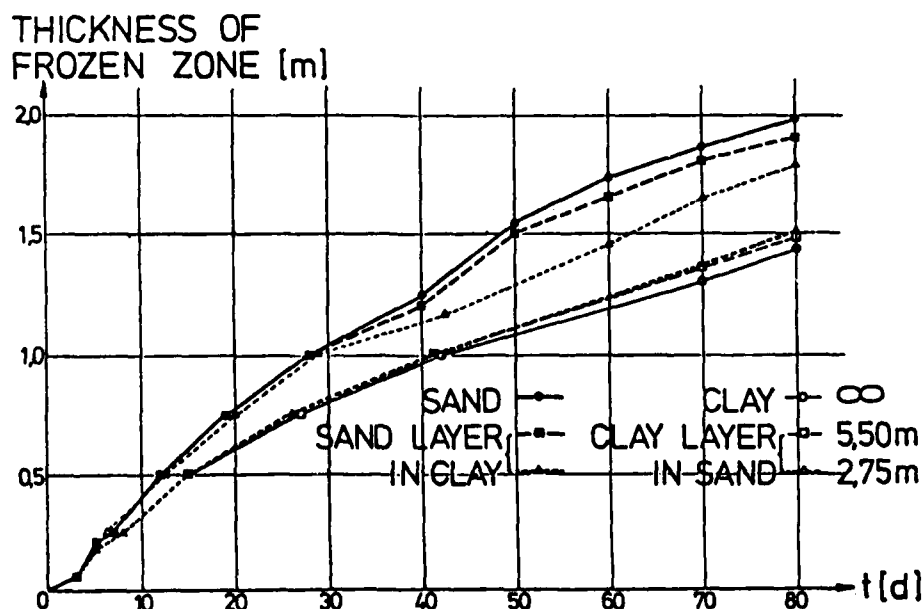
Fig. 3: Influence of vertical heat transfer between horizontal layers of different thermal properties - propagation of the frozen volume

relevant material properties are

	k_u/k_f (W/mK)	c_u/c_f (KJ/m³K)
sand	2.0/3.5	2720/1883
clay	1.5/2.0	2885/2092

Figure 3 displays the results. It shows that the horizontal heat transfer in a clay or sand layer of a thickness of 5.5 m is not influenced by the higher or lower propagation speed in the sand or clay layers. The situation changes in a layer with a thickness of 2.75 m. In this case the propagation speed in the embedded soil is equalized to that of a surrounding type of material.

The transition of a specific thermal regime of a layer to that of another one is limited to narrow zones close to the boundary of the two layers. It is illustrated by the isothermal lines in Figure 4.

Influence of Freeze Pipe Positions

To investigate the influence of freeze pipe deviation it is necessary to integrate the random dislocations in a layer to some basic cases:

case I deviation of one pipe on the freeze pipe cercle

case II deviation of one pipe perpendicular to the freeze pipe cercle

case III deviation of two freeze pipes perpendicular to the freeze pipe cercle but each in opposite directions.

The development of the frozen zone in a layer of silt (k_u/k_f = 1.6/2.35 W/mK, c_u/c_f = 2800/1925 KJ/m³K) is calculated for ideal freeze pipe positions on a cercle with a freeze pipe distance of d = 1.35 m in order to compare these results with those for other positions. Figures 5a to 5c demonstrate the shape of the frozen zone by isothermal lines. The development of the frozen volume over time is shown by Figure 6. In this case the propagation of the minimum frozen volume between two freeze pipes starts after closing and continues with higher speeds till the maximum and minimum frozen volumes are equalized after about twice the elapsed time of closing.

The thermal regimes of the various freeze pipe positions investigated were plotted after specified numbers of time

steps as isothermal lines. They illustrate the shape of the frozen zone in the area of the deviation and allow the determination of the maximum and minimum thickness of the frozen volume in that area. Figure 6 also illustrates the results of case I in comparison with the ideal configuration. Figures 7a to 7c displays the characteristic shape of the frozen zone. It is obvious that this case is the most difficult one. Though two freeze pipes are working together at a close distance the maximum volume do not differ compared to the ideal positions. But the propagation speed of the minimum volume is much lower. The elapsed time of closing doubled and after 100 days of freezing the minimum frozen volume is one half of the
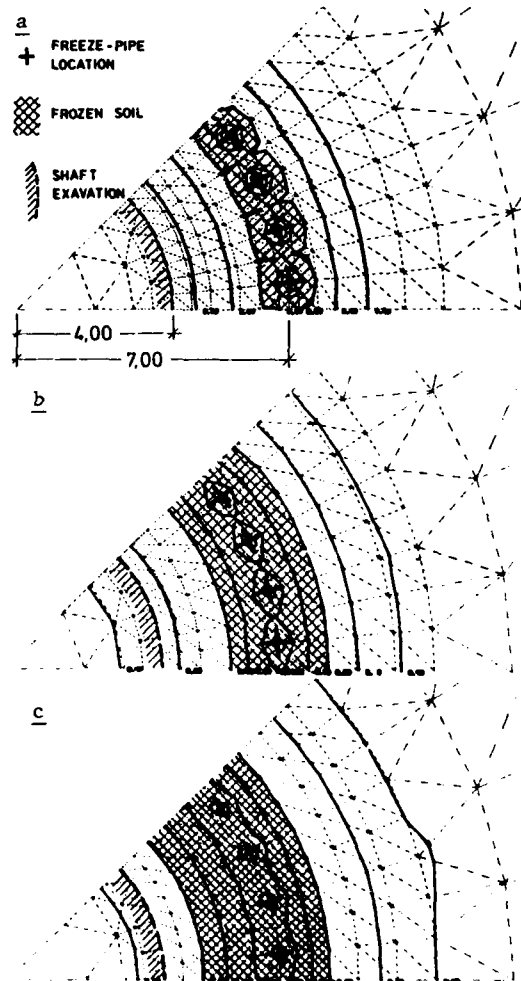
Fig. 5: Isothermal lines for ideal freeze pipe positions after a) 40 b) 80 c) 120 days of freezing

THICKNESS OF
FROZEN ZONE [m]
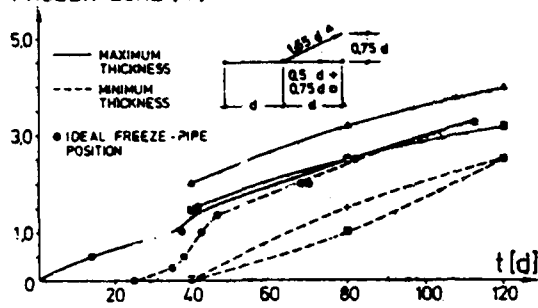
Fig. 6: Comparison between the propagation
of the frozen volume for dislocat-
ed pipes of case I and for ideal
pipe positions

THICKNESS OF
FROZEN ZONE [m]
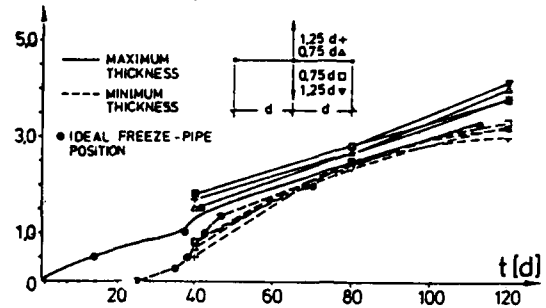
Fig. 8: Comparison between the propagation
of the frozen volume for dislocat-
ed pipes of case II and for ideal
pipe positions
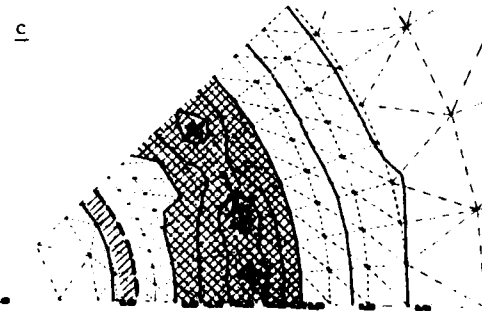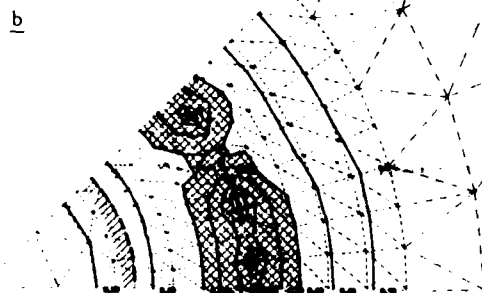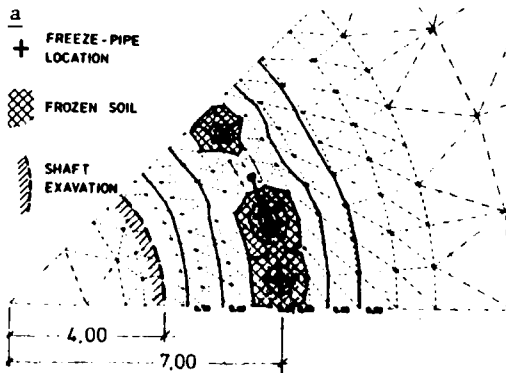
Fig. 7: Isothermal lines for dislocated
pipes of case I after a) 40 b) 80
c) 120 days of freezing
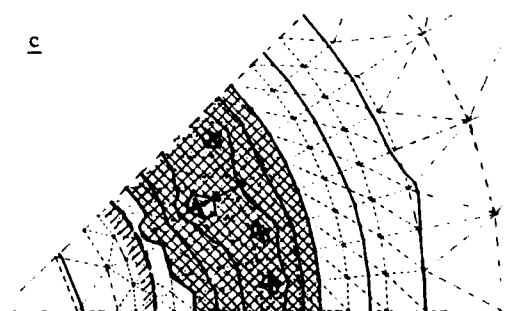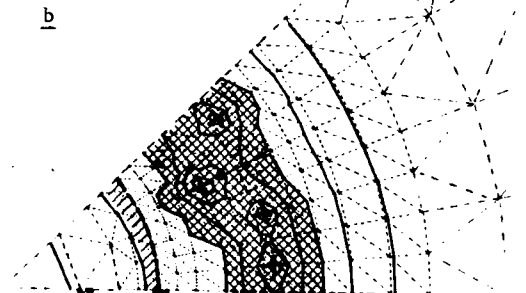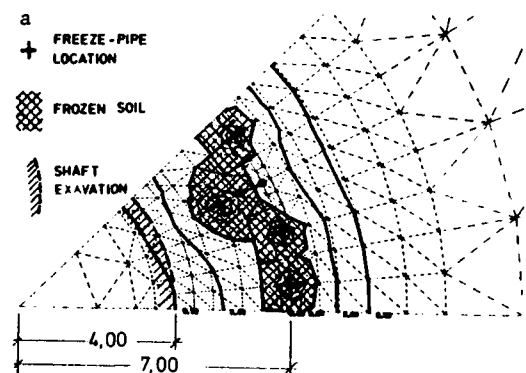
Fig. 9: Isothermal lines for dislocated
pipes of case II after a) 40 b) 80
c) 120 days of freezing

163

THICKNESS OF
FROZEN ZONE (m)
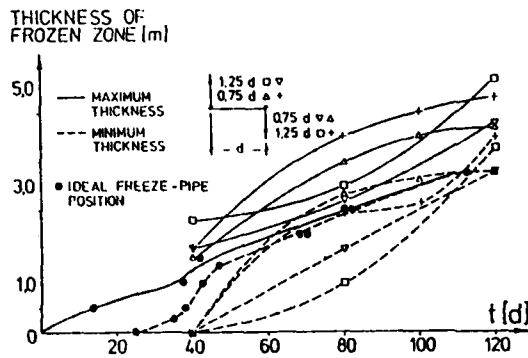
Fig. 10: Comparison between the propaga-
tion of the frozen volume for
dislocated pipes of case III and
for ideal pipe positions

a
FREEZE-PIPE LOCATION

FROZEN SOIL

SHAFT EXAVATION

|———4.00 ———|
|——————— 7.00 ———————|

b

c
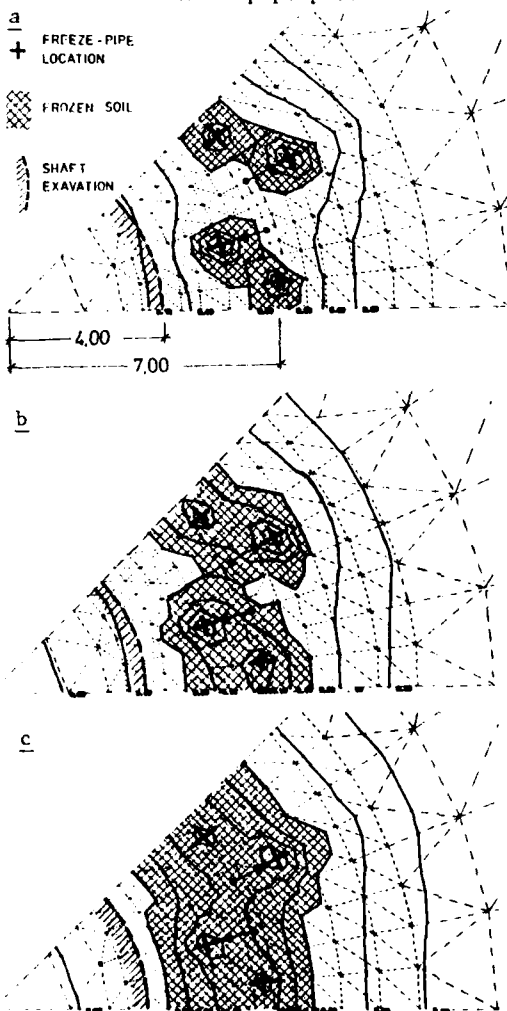
Fig. 11: Isothermal lines for dislocated
pipes of case III after a) 40
b) 80 c) 120 days of freezing

volume for the ideal positions. An exten-
sion of the freeze pipe distance to 1.5 d,
1.75 d or 2.0 d does not change the
minimum volume versus time curve signi-
ficantly.

The results of case II are displayed
in Figure 8 and Figure 9a to 9c. The re-
sults are nearly independent of the di-
rection and of the distance of the de-
viation. The initial higher difference
between the maximum and the minimum vol-
ume disappears after about four times the
elapsed time of closing. Then the frozen
volume is equalized to the ideal case.
Considering larger freezing times case II
does not cause serious problems.

The results of case III Figure 10
and Figures 11a to 11c show an interesting
tendency. While the development of the
minimum volume starts in the same way as
in case I, the propagation accelerates
and after 120 days of freezing the maxi-
mum and minimum volume is at least as
large as the volume related to the ideal
case. Concentrating on freeze shafts the
consequence is that by a regular devia-
tion of freeze pipes in opposite direc-
tions the development of the frozen zone
is positively influenced.

CONCLUSION

For some freeze projects as deep
frozen shafts there is a need of more
realistic calculations of the propaga-
tion of the frozen zone and the energy
consumption.

Basis is the linking between the
thermal regime in soils and the refrige-
ration system. In this paper the main
features of a FEM program capable of
modelling this linkage are given.

The FEM program was used to investi-
gate the influence of vertical heat trans-
fer between soil layers of different
thermal properties. The results presented
show that depending on the thickness of
the layer vertical heat transfer can
affect horizontal heat transfer. A second
investigation of the influence of freeze
pipe deviations on the development of
the frozen zone is reported. While the
deviation of two pipes perpendicular to
the freeze circle each in opposite direc-
tions influences the development of the
frozen volume positively a deviation of
a freeze pipe on the freeze pipe cercle
delays the development of a required
thickness of the frozen volume.

164

REFERENCES

Carslaw, H.S., Jeager, J.C. (1959), Conduction of Heat in Solids / Oxford University Press 2nd edition

Frivik, P.E., Thorbergsen, E. (1980), Thermal Design of Artificial Soil Freezing Systems, 2nd International Symposium on Ground Freezing, The University of Trondheim, Preprints p. 556-567

Frivik, P.E. (1980), Ground Freezing: Thermal Properties, Modelling of Processes and Thermal Design, 2nd Intern. Sympos. on Ground Freezing, The University of Trondheim, Preprints p. 354-373

Hegemann, H. (1981), Konzept und Stand der Arbeiten am tiefen Gefrierschacht Voerde, Berliner Schacht- und Tunnelbaukolloquium, Düsseldorf

Jessberger, H.L., Makowski, E. (1981), Optimization of the Freeze Pipe Arrangement and the Necessary Refrigeration Plant Capacity by a FEM-Computer Program, Engineering Geology, 18, 175-188

Jessberger, H.L., Makowski, E. (1981), Application of Finite Element Methods to the Design of Refrigeration System used in Artificial Ground Freezing, Proc. 2. Int. Conf., Venice, Pineridge Press, Swansea p. 205-217

Lewis, R.W., Morgan, K., Schreffler, B.A., (Ed.) (1981), Numerical Methods in Thermal Problems, Vol. II, Proc. 2. Int. Con., Venice, Pineridge Press Swansea

Plank, R. (1952), Handbuch der Kältetechnik, Springer-Verlag Berlin

THERMOMECHANICAL ENTHALPY MODEL FOR GROUND FREEZING DESIGN

Y.A.Kronik
Branch Research Laboratory
for Engineering Cryopedology
in Power Plant Construction,
Kuibyshev Civil Engineering
Institute, Moscow, USSR

Abstract. The paper deals with research conducted during 1978-80 in the Engineering Cryopedology Laboratory of the Kuibyshev Institute under the general supervision of Prof.N.A.Tsytovich, Corresponding Member of the USSR Academy of Sciences. Existing enthalpy models of ground freezing, proposed by Djuzinber, Buchko and Plotnikov are analyzed. Their shortcomings do not permit calculations of temperature conditions to be carried out for artificial ground freezing, taking into account the alternating initial fields of temperatures and stresses when up-to-date low-temperature cooling media are applied.

A new method of ground freezing design is proposed, based on the author's thermomechanical enthalpy model [3, 8]. It takes into consideration the phase transitions throughout the range of soil temperature variation, from absolute zero to any plus temperature. This new physicomathematical model is based on experimental data and, in a first approximation, takes into account the mechanical and physicochemical processes, the initial state and variability of soil characteristics depending upon changes in their temperatures and stressed-strained states.The model includes four zones of freezing soil, which are specified in ranges of characteristic temperatures established experimentally.

The model has been checked by the finite-element method in calculations and the thermal stressed-strained state of soils.

The extensive application of ground freezing techniques in industrial, mining and water-development construction requires further improvements in the procedures used for calculations of the thermal and mechanical processes that are developed simultaneously in the freezing soil and are correlated into a single thermomechanical process [1,2]. Until recent years, predictions of thermal and mechanical processes in engineering practice were made separately, as a rule, without taking their effects on each other into account. Papers [1,3] proposed the development of a trend in thermomechanics of soils, rock and cryogenic processes that would enable thermal, mechanical and thermomass transfer processes to be dealt with simultaneously.

The basic equations of soil thermomechanics include equations of soil mechanics and thermophysics, whereas in the more general formulation of nonlinear thermomechanics theory, equations of thermodynamics and thermomass transfer are also included. Up to

the present time, changes in the mechanical and physical states of the freezing soil were neglected in solving thermal and thermomass transfer problems. The present paper deals with the new thermomechanical enthalpy model proposed by the author [8,9] of a freezing and thawing soil, taking these changes into account in a first approximation.

In solving thermal and thermomechanical problems as applied to a heterogeneous multiple-component soil medium with phase transitions of the pore moisture taken into account, the most interesting results, especially for complex, two- and three-dimensional problems, have been obtained in employing enthalpy methods and enthalpy models of frozen, freezing and thawing soils [4 through 8]. In his paper Plotnikov deals with the enthalpy models of Djusinber. Buckster and Buchko. Plotnikov analyzes their merits and the shortcomings that do not permit them to be applied to solve many practical problems of soil thermophysics, and proposes a new enthalpy model (Fig.1A). But Plotnikov's model, notwithstanding all its advantages over the enthalpy models of the other authors,also has certain shortcomings that do not allow it to be efficiently applied in many problems of soil thermophysics,especially those involving thermomechanics and artificial ground freezing. The most important of these disadvantages are the following:

1. As in those pf previous authors, the enthalpy model of Plotnikov [5] , rigidly specifies a constant temperature for soil freezing and thawing, equal to 0.0°C. This presents mathematical difficulties in calculations by numerical methods (precisely at the freezing point,which is equal to zero). What is most important, the model does not agree with the actual values of soil and pore moisture freezing temperatures, the pore moisture always being, in essence, a soil solution in the pores, of varied (though low) concentration [6,7 and others].

2.Plotnikov's model does not postulate any relations between mechanical (pressure,compaction, etc.) and physicochemical processes, and the physicomechanical characteristics of real soils. This disagrees with the principle of the equilibrium state of pore water and ice in frozen soils that was established by Tsytovich [7, 9]. The model does not take into account the effect of the actual (natural) physical state of the soils with respect to moisture content and density. It cannot, therefore, be applied to all kinds of soils (including saline, overcompacted and other soils).

3. The introduction of the concept of a "conditional enthalpy of the soil [5], varying from zero at the temperature -50°C and lower to an indefinite quantity at +50°C, is extremely arbitrary and insufficiently substantiated. This concept introduces much indefiniteness into calculations and prectically excludes the treatment of a large class of thermal problems in which the temperatures varies below -50°C (for example, in artificial ground freezing by means of liquid nitrogen, liquid oxygen, air cooled to -100°C, etc.) or above +50°C.

4. The specification of constant values for the volumetric heat capacity C_F and thermal conductivity coefficient λ_F for frozen soil, beginning with the temperature at the end of freezing for the free moisture (or the beginning of freezing of the bound moisture θ_{free}= -0.3°C=const, which is also extremely arbitrary and does not comply with the facts) and lower introduces definite errors into thermal calculations. This is especially true for peaty, clay, course-grained and saline soils, for which the difference between λ_F and λ_U may reach an average of 30 to 40%, and a maximum of 50 to 90%. This is all the more so because, according to experimental data, the values of λ and C at the soil temperature -0.3°C are closer to their values in the unfrozen state (λU and CU) than those

168
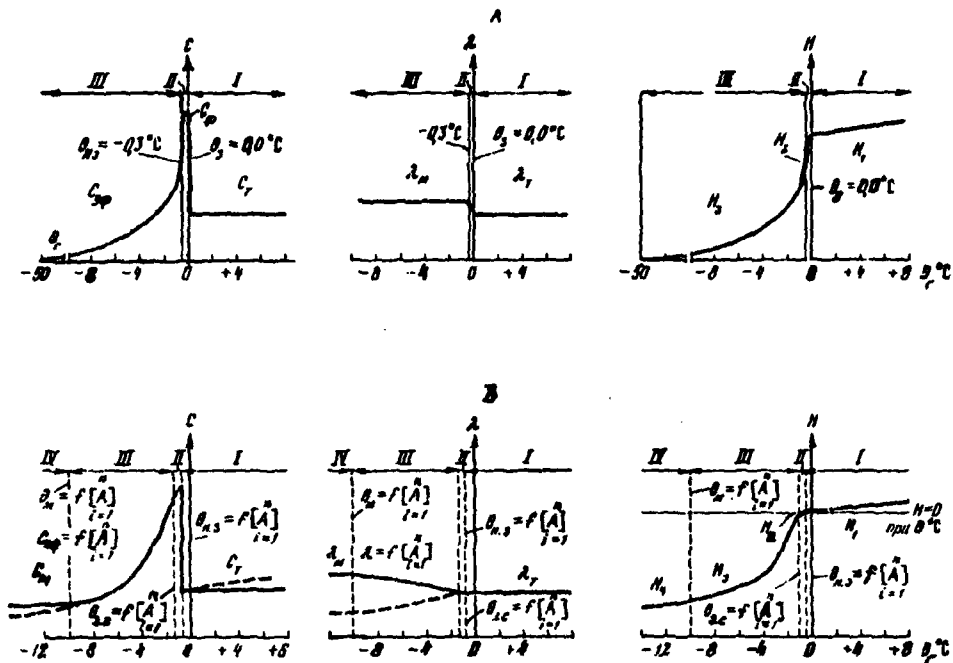
Fig.1 Enthalpy models of frozen, freezing and thawing soils: A - the
Plotnikov model, B - the Kronik thermomechanical model.
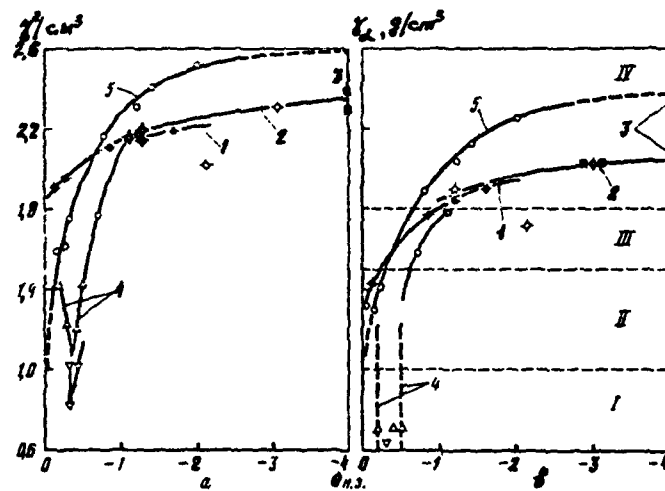
Fig.2 Experimental dependence of the temperature at the beginning
of freezing on the densities: a - unit mass γ and b - unit
mass γ_d of the dry soil for various soils.
I,II,III and IV - dry-density soil zones. Date of: 1 - A.P.
Bozhenova; freezing soils subject to a pressure of $\sigma = 0$ to
6.5 MPa; 2 - Y.A.Kronik;ditto but $\sigma = 0$ to 0.23 MPa;
3 - Yu.P.Akimov, ditto but $\sigma = 22.5$ to 35 MPa; 4 - USSR
Building Code II-18-76;freezing of peaty soils not subject
to pressure; 5 - Y.A.Kronik; freezing of soils not subject
to pressure.

in the frozen state (λ_F and C_F).

There are also other shortcomings that introduce definite errors and a lack of clarity in specifying design characteristics, in calculations and analysis of the dynamics of the temperature fields, in determining the actual interfaces between the frozen, unfrozen, freezing and thawing soils (it is not clear, for instance, what value to take for C_{phase}; there are errors in describing the enthalpy in the freezing zone of the free moisture; the amount of bound water corresponding to the plastic limit w_p is incorrectly specified; etc.).

In connection with the aforesaid, the author has developed (1977-79) a new, more refined enthalpy model of freezing, thawing and frozen soils [8,9], which takes into account, in a first approximation, the mechanical and physicochemical processes, the physicomechanical state and the variability of the characteristics of soils depending upon the changes in their temperature and stressed-strained state. For this reason he has called it a thermomechanical enthalpy model (Fig. 1B).

The proposed model includes four zones (Fig. 1B) with the corresponding temperature ranges in which the thermophysical and thermodynamic parameters of the soil vary according to definite laws.

Zone I is the zone of unfrozen and supercooled (below 0.0°C) soil in a temperature range from a plus value $+\theta_{soil}$ to the temperature θ_{bf} of the beginning of freezing, corresponding to the temperature at which the free pore moisture in the large pores begins to freeze.

Zone II is the freezing (thawing) zone for the free pore water (mainly in the large pores) or the zone of maximal phase transitions in the freezing (thawing) soils with a temperature range from θ_{bf} to the temperature θ_{bfb} of the beginning of freezing of the bound water. For saline soils this zone is characterized by a temperature range from θ_{bfps},

the beginning of freezing (crystallization) of the pore solution (equivalent to the temperature corresponding to the given equilibrium concentration $K_{ps} = K_s$ of the pore solution), to the temperature θ_{fofi} at the end of the freezing-out of clean fresh ice from the solution. This corresponds, for example, to about -8°C for the pore solutions of soils in maritime regions and for seawater.

Zone III is the zone of freezing (thawing) of bound pore water or the zone of freezing (thawing) soil, with a temperature range from θ_{bfb} to the temperature θ_F of the practically frozen state of the soil (according to Tsytovich), which is close to the complete freezing of the loosely bound moisture, when the amount of unfrozen water w_U is extremely close to the amount of adsorbed water w_{ad}, also corresponding to the undissolved volume w_{udv} of pore moisture in saline soils.

Zone IV is the zone of practically frozen soil at a temperature of θ_F and lower.

In contrast to the enthalpy models of other authors, in the proposed model the temperature θ_{bf} of the beginning of freezing of the soils (and the corresponding temperature of the beginning of phase transitions of the free soil moisture), as well as the temperature θ_{bfb} of the beginning of freezing of the bound moisture and that θ_F of the practically frozen state are not constants, equal to zero and to -0.3°C for all soils (as proposed by Buchko, Plotnikov and others), but are variable quantities, in the general case, depending upon the kind of soil, its state with respect to the moisture content and density (unit mass of dry soil γ_d), applied pressure σ, pore solution concentration K_{ps} and soil freezing (thawing) rate $V_f = d\theta_{soil}/dt$ (or the ambient temperature θ_{air}):

$$\theta_{bf} = \overset{N}{\underset{1}{\Phi}}[A] = \Phi[\text{type of soil}$$
$$\text{(plasticity index } I_p, P_c),$$
$$\gamma_{d(w)}, \sigma, K_{ps}(z,w,w_{udv}), V_f(\theta_{air})$$

$$(1)$$

$$\theta_{bfb} = \Phi'[A]_1^{N'} = \Phi'[\text{type of soil}$$

(plasticity index I_p, P_c),
$$\gamma_d(w), G, k_{ps}(z,w,w_{udv}), \theta \text{ soil}$$
(2)

$$\theta_F = \Phi''[A]_1^{N''} = \Phi''[\text{type of soil}$$

(plasticity index I_p, P_c),
$$\gamma_d(w), G, K_{ps}(z,w,w_{udv}), \theta \text{ soil}.$$
(3)

It is advisable to determine the specific values of θ_{bf} directly by experiments in freezing and thawing real soils under conditions as close as possible to natural ones (or in field experiments). These experiments should be performed at a given state with respect to moisture content, density and concentration, under a given load (or without any), at natural freezing rates and temperatures of the cooling medium, all of which are made use of in the specific thermal calculations. Similar experiments are conducted to determine θ_{bfb}, but at a soil moisture content equal to the maximum molecular moisture capacity w_{mmmc}, which more closely corresponds to the bound moisture content than the quantity w_p. This has been confirmed by data obtained in numerous experiments [6,7 10 and others]. If the required experimental data are not available, it is advisable for approximate engineering calculations to apply the reference values of θ_{bf}, θ_{bfb} and θ_F listed in Table 1. These data have been compiled on the basis of experimental research of the author and other investigators [6,7,8,9,10 and others] over a period of many years. It should be noted that the data of Table 1 correspond to reference freezing (thawing) temperatures for soils not subject to load and for typical (average) soil freezing rates. Therefore, they provide a definite margin in engineering calculations toward somewhat increased values (a maximum of 0.3 to 0.5°C) at high cooling rates and low cooling medium temperatures (below -30°C).

An analysis of the experimen-

tal data enabled a general law to be established for practically all kinds of soils, concerning the effects of the densities γ and γ_d on the freezing temperature θ_{bf} (Fig.2a and b), as well as the dependence of θ_{bf} on the normal pressure G (Table 2 and Fig.2), which is especially appreciable for overcompacted soils. The aforesaid enabled the author to classify the soils in their thermomechanical aspect into four classes with respect to density and unit mass of dry soil γ_d as follows: loose (1.0 to 1.49 g/cm^3), dense (1.50 to 1.79 g/cm^3), overcompacted ($\gamma_d \geq 1.80$ g/cm^3) and extremely loose soils with $\gamma_d < 1$ g/cm^3, which include weak and organomineral soils, peat-bog soils and peats. The application of a load above 2kg/cm^2 transforms loose soils into dense ones, and above 10 kg/cm^2, into overcompacted soils. In the latter, the effect of the type of clayey soil is reduced, forces of intermolecular interaction of the clay particles are manifested and strong condensation-cementation structures are formed. Here, for example, the freezing temperature for Beskudniko-, loam is lowered. according to data of Bozhenova[6] (see Table 2 and Fig.2b), by a factor of more than 20 (down to $\theta_{bf} \approx -1.2°C$). For overcompacted soils, the effect of an increase in density and pressure on the freezing temperature θ_{bf} can be tentatively taken into account (with a certain margin) in calculations using the proposed model according to the data listed in Table 3.

For more exact solutions, the values of θ_{bf}, when the soil is under pressure, should be determined by experiments. It should be pointed out that these values of θ_{bf}, obtained by Bozhenova, Akimov and the author (see Table 2) comply with a general law (Fig.2a and b), but substantially differ from the known theoretical laws of Bridgman-Tamman (for ice), Clausius-Clapeyron and Thomson. The coupling factors $k_s = \theta_{bf}/G$ obtained in the above-mentioned experiments vary from 0.2 to 13,

REFERENCE TEMPERATURES FOR THE FREEZING OF SOILS AND PORE MOISTURE

Table 1

Types of soils	Temperature θ_bf of the beginning of freezing of the soil in the moisture content and density states (unit mass of dry soil γ_d, g/cm³):			Temperature θ_bc of the beginning of freezing of bound water, corresponding to w_{mmc}	Temperature θ_eph of the end of intensive phase transitions	Temperature θ_F of the practically frozen state
	High water content, loose	Medium water content, dense	Low water content, overcompacted			
	1.0 to 1.49	1.50 to 1.79	1.80			
Coarse- and medium-grained sand, coarse-grained soil with no filler and with a sand filler	-0,001	-0,005	-0,01	-0,20	-2,0	-3,0
Fine and dust-like sands, sandy loams, coarse-grained soils with sandy-loam fillers	-0,05	-0,10	-0,15	-0,40	-3,0	-5,0
Loams, coarse-grained soils with loamy fillers	-0,10	-0,20	-0,30	-0,50	-5,0	-7,0
Kaolin clays	-0,10	-0,30	-0,50	-0,60	-5,0	-8,0
Polymineral and hydromica clays	-0,20	-0,40	-0,60	-0,70	-7,0	-10,0
Montmorillonite clays	-0,30	-0,50	-0,70	-0,90	-10,0	-13,0

NOTES: 1. The reference temperature for the freezing of water and the melting of ice (triple point) at standard atmospheric pressure is θ = 273.15 K = 0.000°C.

2. Coarse-grained soils with a filler are ones with a content of coarse-grained particles (over 2 mm in size) $P_c \geqslant 10\%$ (by weight); for those without a filler, $P_c \geqslant 90\%$.

172

which is 1,2 or more orders of magnitude greater than the known theoretical values and calls for a more detailed investigation and analysis.

For the proposed model, the thermophysical (λ, C) and thermodynamic (enthalpy $H = f(\theta)$) parameters vary, as shown in Fig.1B, in the following manner:

Zone I - unfrozen soil. The volumetric heat capacity and thermal conductivity coefficient are taken to be constant and equal to the values for unfrozen soil: C_U and λ_U. If it is necessary to investigate a wide range and high plus temperatures, the functional dependence of C_U and λ_U on the temperature can be taken from data established experimentally. Design values for C_U and λ_U for typical soils can be taken approximately, when direct experimental data are unavailable, from building standards [11]; for coarse-grained and saline soils, such data can be taken from the papers [12,13]. Enthalpy values (or, more exactly, increases in enthalpy $\Delta H = H_{soil}$) from $+\theta_{soil}$ to θ_{bf} in this zone ($\theta = \theta_{soil} \geqslant \theta_{bf}$) are determined (expressing θ in $^\circ C$) by the equation

$$H_I = \int_{\theta = \theta_{u.3} + 273.15}^{\theta = \theta_r + 273.15} C_r(\theta)\,d\theta + H_{II}(\theta). \qquad (4)$$

or expressed in the absolute temperature scale ($\theta = T$ in kelvins):

$$H_I = \int_{\theta = T_{u.3}}^{\theta = T_r} C_r(T)\,dT + H_{II}(T). \qquad (5)$$

At $C(\theta) = C_U = const$ and taking into consideration the fact that in $^\circ C$ is a negative quantity, we obtain the same equation for θ in $^\circ C$ and in kelvins (K):

$$H_r = C_r[\theta_r - (-\theta_{u.3})] + H_{II} = C_r\Delta\theta + H_{II} \qquad (4')$$

or

$$H_z = C_r(T_r - T_{u.3}) + H_{II} = C_r\Delta T + H_{II} \qquad (5')$$

where H_{II} is the value of the en-

thalpy at the boundary between zones I and II (at point θ_{bf}).

If the reference point for the increase in enthalpy is $0^\circ C$ ($\theta_0 = 0^\circ C$ or $T_0 = 273.15$ K), $\Delta\theta = \Delta T = \theta_{soil} - \theta_0 = \theta_{soil}$ and the value of the enthalpy in zone I (more exactly, the increase in enthalpy) is equal to

$$\Delta H = H_z = C_r\theta_r = C_r(T_r - 273.15) \qquad (5'')$$

in which case the enthalpy in the region of minus temperatures (in $^\circ C$) takes on negative values, whereas at point $\theta = 0^\circ C$, $H_0 = 0$.

Zone II - freezing (thawing) of the free water. C_{II} and λ_{II} are taken to be variable quantities, depending on the soil temperature θ_{soil} ($\theta_{bf} \leqslant \theta = \theta_{soil} \leqslant \theta_{bfb}$):

$$C_{II} = C_{3\phi}(\theta) = C_{TM}(\theta) + C_{\phi33} = C_r - $$
$$- \frac{(C_r - C_M)(\theta_{u.3} - \theta_r)}{\theta_{u.3} - \theta_M} + \frac{\rho\gamma_{cK}(W_c - W_{cn1})}{\theta_{u.3} - \theta_{3.c}} \qquad (6)$$

where $C_{ef}(\theta)$ is the effective heat capacity, including the heat capacity $C_{UF}(\theta)$ of the freezing (thawing) soil and the latent heat C_{phase} of phase transitions, ρ is the latent heat of crystallization of the free water (latent heat of melting of ice), w_t is the total moisture content of the soil, w_b is the moisture content corresponding to bound water, and approximately equal to w_{mmmc}.

$$\lambda_{II} = \lambda(\theta) = \lambda_r - \frac{(\lambda_r - \lambda_{u1})(\theta_{u.3} - \theta_r)}{\theta_{u.3} - \theta_M}. \qquad (7)$$

Here the ratio λ_F/λ_U can also be less than unity, this being typical for low-moisture content and overcompacted soils [18 and others].

The value of the enthalpy in zone II (with θ expressed in $^\circ C$) is determined by the equation

$$H_{II} = \int_{\theta = \theta_{3.c} + 273.15}^{\theta = \theta_{u.3} + 273.15} C_{3\phi}(\theta)\,d\theta + H_{III}. \qquad (8)$$

or in the absolute temperature scale (with $\theta = T$ in kelvins):

$$H_{II} = \int_{\theta=T_{s.c}}^{\theta=T_{н.з}} C_{эф}(T)\,dT + H_{в} \qquad (8')$$

After substituting the value of C_{ef} and integration from θ_{bf} to $\theta_{soil}(\theta)$, we obtain in the general form at $\theta_{bfb} < \theta = \theta_{soil} - \theta_{bf}$:

$$H_{II} \cong C_{т}(\theta_{н.з} - \theta_{г}) +$$

$$+ \rho\gamma_{ск}(W_{c} - W_{cз3})\,\frac{\theta_{н.з} - \theta_{г}}{\theta_{н.з} - \theta_{з.c}} + H_{III}. \qquad (9)$$

Taking into account the fact that $(\theta_{bf} - \theta_{soil}) < 1$ and the second order of smallness, the second term can be neglected. Then we obtain

$$H_{II} \cong C_{т}(\theta_{н.з} - \theta_{г}) +$$

$$+ \rho\gamma_{ск}(W_{c} - W_{cз3})\frac{(\theta_{н.з} - \theta_{г})}{(\theta_{н.з} - \theta_{з.c})} + H_{III} \qquad (9')$$

For the whole zone II ($\theta_{bfb} < \theta < \theta_{bf}$) we obtain

$$H_{II} = C_{т}(\theta_{н.з} - \theta_{з.c}) + \rho\gamma_{ск}(W_{c} - W_{cз3}) + H_{III}. \qquad (10)$$

Zone III – freezing (thawing) soil and the freezing (thawing) of the bound water ($\theta_{bfb} < \theta = \theta_{soil} < \theta_{F}$); correspondingly:

$$C_{III} = C'_{эф}(\theta) = C_{тм}(\theta) + C_{фз^{-}} \cong C_{м} +$$

$$+ \frac{(C_{т} - C_{м})(\theta - \theta_{м})}{\theta_{н.з} - \theta_{м}} + \rho\gamma_{ск}\frac{\partial W_{н}}{\partial\theta}. \qquad (11)$$

$$\lambda_{III} = \lambda'(\theta) = \lambda_{м} + \frac{(\lambda_{т} - \lambda_{м})(\theta - \theta_{м})}{\theta_{н.з} - \theta_{м}}, \qquad (12)$$

$$H_{III} = H_{IV} + C_{м}(\theta_{з.c} - \theta_{м}) +$$

$$+ \frac{(C_{т} - C_{м})(\theta_{м} - \theta_{з.c})^{2}}{2(\theta_{н.з} - \theta_{м})} + \int_{\theta_{м}}^{\theta_{з.c}}\frac{\partial W_{н}}{\partial\theta}\,d\theta. \qquad (13)$$

After substituting the value of $C_{ef}(\theta)$ into equation (13) and integrating, we obtain

$$H_{III} = H_{IV} + C_{м}(\theta_{з.c} - \theta_{м}) +$$

$$+ \frac{(C_{т} - C_{м})(\theta_{м} - \theta_{з.c})^{2}}{2(\theta_{н.з} - \theta_{м})} + \int_{\theta_{м}}^{\theta_{з.c}}\frac{\partial W_{н}}{\partial\theta}\,d\theta \qquad (13')$$

Zone IV – practically frozen soil. Here

$$C_{IV} = C'_{эф}(\theta) = C_{м} + C_{фз3} \cong C_{м} = \text{const}, \qquad (14)$$

$$\lambda_{IV} = \lambda_{м}(\theta) \approx \lambda_{м} = \text{const}, \qquad (15)$$

$$H_{IV} = \int_{\theta=\theta_{г}+273.15}^{\theta=\theta_{г}+273.15} C'_{эф}(\theta)\,d\theta \approx$$

$$\approx \int_{0}^{} C_{м}\,d\theta = C_{м}(\theta_{г} + 273.15). \qquad (16)$$

or, in the absolute temperature scale:

$$H_{IV} = \int_{0}^{\theta=T_{м}} C_{м}(T)\,dT \cong \int_{0}^{\theta=T_{м}} C_{м}\,dT =$$

$$= C_{м}(T - 0) = C_{м}\cdot T_{м}. \qquad (16')$$

Thus, the solution of the Stefan problem for a four-zone arrangement of freezing (thawing) soil is reduced, in principle, to the solution of a single-layer problem, in which the enthalpy varies continuously from absolute zero to a plus temperature according to the law:

$$H(\theta) = \sum_{i=1}^{n}\Delta H_{i} = C_{м}T_{м} + \int_{0}^{\theta=T_{м}} C_{III\,эф}(T)\,dT +$$

$$+ \int_{\theta=T_{м}}^{\theta=T_{з.c}} C_{II\,эф}(T)\,dT - C_{т}\Delta T, \qquad (17)$$

whereas the second-order differential equation (3) is reduced to a simpler equation of the thermal conductivity in enthalpy form:

$$\frac{\partial H}{\partial t} = \text{div}(\lambda\,\text{grad}\,T). \qquad (18)$$

In the particular case when $\theta_{bf} = 0°C$, the model proposed by the author becomes the approximate enthalpy model of Buchko [6], which is valid for the case of freezing sandy soil at constant values of $\lambda_{F}, C_{F}, \lambda_{U}$ and C_{U}, with $\lambda_{F} > \lambda_{U}$.

The thermomechanical enthalpy model described above was tested in calculations of transient temperature conditions for a frozen dam, making use of the finite-element method. This demonstrated its quite satisfactory usefulness for solving complex problems of the thermophysics and thermomechanics of frozen soils. This model can also find efficient application in calculations for designing artificial ground freezing in shaft and underground construction practice, especially

when the ground is frozen by means of up-to-date low-temperature cooling media.

REFERENCES

1. Kronik Y.A. Certain Principal Engineering Cryopedological Problems of Power Plant Construction in Permafrost Regions,Proc. for Geological Engineering Surveys and Mapping in Permafrost Regions,Siberian Branch of USSR Acad.of Sc.,Issue 3,1977(theses of papers),Yakutsk,1978(papers) p.103-114.
2. Tsytovich N.A.and Kronik Y.A. Interrelationship of the Principal Physicomechanical and Thermophysical Properties of Coarse-Grained Frozen Soils, Proc.1st Intern.Symposium on Ground Freezing,Bochum,19..8;Eng. Geology,v.13,1979,p.163-167.
3. Kronik Y.A. Rheological and Thermomechanical Processes in Soil Dams in the Far North,Proc. III USSR Symposium on Soil Rheology,1980, Erivan State University Press,p.74-87.
4. Buchko N.A. Algorithm for the Numerical Solution of the Stefan Two-Dimensional Problem by the Enthalpy Method According to a Three-Layer Explicit Layout,XIV Intern.Conference on Refrigeration "Refrigeration and Cryogenic Engineering and Techniques", Proc.Leningrad Technical Institute of the Refrigerator Industry, 1975, p.142-154.
5. Plotnikov A.A. Temperature Conditions Design for Permafrost Foundation Bases,J.Power-Plant Construction,1978,No.8,p.70-73.
6. Bozhenova A.P. Temperature Characteristic of the Water Freezing Process in Soils, Collection 3.Data on Laboratory Investigations of Frozen Soils, USSR Acad.Sc.Publishers,1957, Moscow,p.23-27.
7. Tsytovich N.A. Frozen Soil Mechanics,Higher School Publishers,1973,Moscow, p.448.
8. Kronik Y.A. A Thermomechanical Enthalpy Model of Freezing, Thawing and Frozen Soils, in "Investigations of the State, Structure and Properties of Frozen,Freezing and Thawing Soils to Ensure Most Efficient Design and Construction",1981, Moscow,p.161-163.
9. Kronik Y.A. Thermomechanical Models of Frozen Soils and Cryogenic Processes,in "Engineering Cryopedology and Frozen Soil Mechanics",Nauka Publishers,1982,Moscow (in press).
10. Yershov E.D.,Akimov Yu.P.,Cheverev V.G. et al. The Phase Composition of Water in Frozen Soils, Moscow State University Publishers,1979,Moscow,p.188.
11. USSR BUILDING CODE II-18-76, Bases and Foundations on Permafrost,Stroiizdat Publishers, 1977, Moscow, p.48.
12. Tsytovich N.A.,Kronik Y.A. and Loseva S.G. Thermophysical Properties of Soil Mixtures Used in Dam Construction in the Far North,J.Power-Plant Construction, No.4, 1979.
13. Kronik Y.A. and Loseva S.G. Taking the Thermophysical Properties of Artificially Salinized Soil into Account in Earth Dam Construction,J.Power-Plant Construction,No.10,1978,p.74-77.

Table 2

Unit mass of dry soil d, g/cm^3	Freezing temperatures of overcompacted soils subject to pressure σ , MPa			
	0	0.1 to 1	1 to 2	2 to 6
1,80	-0,15-0,7	-1,0	-1,3	-1,7
2,00	-1,0	-1,3	-2,0	-4,0
2,20	-1,6	-2,0	-4,0	
2,30	-2,0	-4,0		
2,40	-4,0			

THERMAL ANALYSIS OF THE POSITION OF THE FREEZING FRONT AROUND AN LNG IN-GROUND STORAGE TANK WITH A HEAT BARRIER

O. Watanabe : Technical Planning Division, Production and
              Engineering Dept., Tokyo Gas Co.,Ltd., Japan

M. Tanaka   : Soil Mech. and Found Division, Kajima Inst.
              of Construction Technology, Japan.

ABSTRACT

In Japan, there have already been completed more than 20 LNG in-ground tanks. It is expected that in the future LNG tanks of such a in-ground type having great structural safety will be ever-increasingly demanded in this country which is very often suffering from earthquakes.

LNG, when stored in-ground, will freeze the surrounding ground with its low temperatures (about $-160°C$). It will therefore become necessary to reduce the influence of the extent of freezing zone on surrounding structures. For this purpose, Tokyo Gas Co., Ltd. has developed a technique of controlling the extent of freezing zone by installing a heat barrier around a in-ground tank, presently actually adopting the heat barrier for its all tanks.

This report describes our experience of controlling the extent of the freezing zone by installing heat barriers based on a comparison of the freezing conditions of the representative three in-ground tanks after operating the bottom heater with their basic designs.

1. Introduction

Tokyo Gas started the operation of its first LNG in-ground tank in 1970, and has constructed and put into operation 16 LNG tanks of reinforced concrete. Further, five tanks are now under construction. We first adopted the heat barrier in March, 1978. Since then, all of our in-ground tanks have been equipped with heat barriers. The heat barrier was first developed and adopted in the United Kingdom for a frozen hole in-ground storage of LNG in which the side wall around the tank is composed of forzen soil completed in 1968 in the Canvey terminals. At the same time, Tokyo Gas carried out our own various analysis and field tests, thus successfully developing a technique applicable to the in-ground tanks of reinforced concrete.

2. Summary of the in-ground LNG tanks and heat barriers

Tokyo Gas has constructed three types of LNG in-ground tanks as shown in Fig. 1[1]. The type of in-ground tank differes with soil characteristics of the tank site, and the method of ground water treatment[2][3]. Type (a) in which uplift pressure due to the ground water acts on the underside of the base. In this type, the base slab resists the uplift pressure by its own deadweight or strength. Type (b) in which the base is constructed on an impermeable layer and, when required, the seeping water is drained, so that no uplift pressure acts on the underside of the base. Type (c) in which the ground water is cut-off by an impermeable layer and a cut-off wall and the seeping water into the cut-off wall is drained so that the uplift pressure on the underside of the base is reduced.

The heat barrier supplies heat from outside to the ground around a tank with a view to controlling the extent of

177

freezing zone. There are two types of heat barriers, which depend on the method of heat supply: a warm-water circulation type and an electric heater type. Tokyo Gas adopts the warm-water circulation type principally using a double pipe system as shown in Fig. 2, in which the warm-water from the header pipe flows into the inner pipe and flows out through the outer pipe. The top of each heat pipe is releasable and it is possible to make certain of airtightness of the system by each block.

3. Heat conduction analysis by F.E.M.

Up to the present, a number of approximate solutions have been proposed to obtain the numerical solution of the termperature distribution in the ground around a LNG in-ground tank. For an analysis which takes into account the complicated sectional form, geological formation, boundary conditions, etc., FEM is considered to be the optimum. A FEM program of heat conduction with latent heat taken into account is outlined below. The equation of three-dimensional heat conduction given by [4]

$$\frac{\partial}{\partial x}(kx\frac{\partial T}{\partial x}) + \frac{\partial}{\partial y}(ky\frac{\partial T}{\partial y}) + \frac{\partial}{\partial z}(kz\frac{\partial T}{\partial z})$$

$$+ Q(x,y,z,t) = C\frac{\partial T}{\partial t} \qquad (1)$$

where T = temperature in arbitrary time (°C)

kx,ky,kz = thermal conductivity in the directions of x, y and z (kcal/mh°C)

Q = internal amount of heat (kcal/m³h)

C = heat capacity (kcal/m³ °C)

t = time (h)

To obtain boundary conditions, the following formulas are conceivable. Temperature specifying

boundary T = Ts   (2)

Heat boundary $kx\frac{\partial T}{\partial x}lx + ky\frac{\partial T}{\partial y}ly + kz\frac{\partial T}{\partial z}lz$

$$= q \qquad (3)$$

Heat transfer boundary $kx\frac{\partial T}{\partial x}lx + ky\frac{\partial T}{\partial y}ly$

$$+ kz\frac{\partial T}{\partial z}lz = h(Th-T) \qquad (4)$$

where Ts = specified temperature (°C)

q = amount of heat flow (kcal/m²h)

h = transfer coefficient (kcal/m²h °C)

Th = external temperature (°C)

lx, ly, lz = cosine in normal direction of boundary

Using the above equations, finite elements are found for regions to be analyzed. Further, by using these finite elements, a balanced equation is established and calculated. Stationary calculation is repetitive calculation of convergence while non-stationary calculation is done by Crank-Nicholson method for the compensation of a non-linear heat conduction matrix and a heat flow vector by each integrated time step.

The following input data and boundary conditions are conceivable.

(1) LNG temperature, and heat transfer (α_1) in the inside wall of tank by LNG

(2) Initial ground temperature, atmospheric temperature, and heat transfer coefficient (α_2) at the ground surface

(3) Thermal constant of soil and concrete (thermal conductivity, specific heat, and latent heat)

(4) Heat transfer coefficient (α_3) of the ground far from the tank

(5) Temperature of heat barrier and bottom heater

The "heat transfer" mentioned above (1) is an equivalent substitute for heat transfer coefficient. This program is capable of analyzing plane, axial symmetry and three-dimensional model.

4. Basic Design of Heat Barrier

4-1. Concept of basic design, and design procedure

In designing the heat barrier, the following items are required to be taken into consideration.

(1) Stopping the extent of freezing zone at a specific point
(2) Economy
(3) Stability

Prior to designing, the thickness of frozen soil and the shape of the frozen soil must be determined as prerequisites. Therefore, it is necessary to determine the following items in the basic design of the heat barrier.

(1) Distance from tank wall (rH)
(2) Depth of installation (ZH)
(3) Interval (ℓ)
(4) Temperature (TH)

In the designing of the heat barrier, a study is performed of various

178

cases with the above four items changed by using the FEM program in order to select the optimum case. Fig. 3 shows the design procedure. The some items in the procedure are as follows.

Thermal constants:

When a heat barrier is installed before the tank is put into operation, thermal constants must be determined by a formula of estimation or on the basis of an actual result of other tanks.

When the heat barrier is to be installed after the tank is put into operation, suitable thermal constants can be selected on the basis of a comparison between the change with time of the progress of the freezing line estimated from the thermocouple readings and a result of heat computation by FEM.

Depth of installation:

The depth in which frozen soil not extending below the heat barrier is to be found by the case study as shown in Fig. 4.

Interval between two heat pipes:

The interval in which the freezing line to be determined must not exceed at least the circle of the heat pipe at the midway of the heat pipe as shown in Fig. 5.

4-2. Example of basic design

Fig. 6 shows the capacities of 95,000 kl LNG in-ground storage tank which is examples of basic design. As the prerequisite of the design, the thickness of the frozen soil was set at about 3.0 meters. The details of the computation are as follows.

Fig. 7 shows a calculation model. Fig. 8 is a partitioned element diagram. Table 2 gives thermal constants. The thermal constants of the soil were determined by the formula of estimation[1] while referring to soil test results. A comparison was made between a change with time of the 0°C line calculated by using this thermal constants and a change with time of the 0°C line estimated from the thermocouple readings. The result of this comparison is shown in Fig.9. The 0°C line estimated from the thermocouple readings, as shown, agrees comparatively well with the calculated value although it shows a slightly faster tendency. Using this thermal constant, therefore, the computation shown in Table 3 was carried out. The heater temperature shown in Table 3(a) is a value obtained from thermal analysis of axial

symmetry model with the thickness of the frozen soil set at 3.0 meters. The computation shown in Table 3(b) was made on the case that the depth of the heat barrier was fixed at 27.6 meters at which the freezing line would not extend below the heat barrier as shown in Fig. 10. The computation result is as described below.

Fig.11 shows a relationship between the interval of heat pipe and the heater temperature. Fig. 12 shows a relationship between the interval and ΔL (Lmax-L min). From this computation results, the basic program was made for the reason of examination that follows.

(1) The heat barrier was set close to the freezing line at a position 4 meters away from the outside wall of the tank.

(2) The depth of heat barrier might be about GL.-28 meters but was set at GL-30 meters considering heat barrier installation accuracy and computation error.

(3) The interval was set at 4 meters in order to reduce the difference (ΔL) between the freezing lines to less than about 10 percent of the overall thickness of frozen soil.

(4) The temperature was set at about 25°C from the computation result.

5. Comparison calculated value with measured value of freezing front line after the operation of heat barrier

The summary of the heat barriers in these three cases are as shown in Table 4. Either tank has a bottom heater and the basic design of the heat barrier was performed after the tank was put into operation.
Case I is the tank described in the example of basic design. The calculation model, the thermal constants and capacity of the tank of Case II are the same as those of the tank of Case I, and the tank of Case III differs in capacity, type of construction and ground. Fig.13 shows the calculation model and the thermal constants.

Case I (Setting the heat barrier at 4m)
Fig. 14 shows the distribution of freezing line. Fig. 15 shows the change with time of the freezing line.
The calculated value agrees comparatively well with the measured value as shown in Figs. 14 and 15.

Case II.(Setting the heat barrier at 3m)

Fig. 16 shows the distribution of freezing line. Fig.17 shows the change with time of the freezing line. The calculated value and measured value agree very well with each other as shown.

Case III.(Setting the heat barrier at 5m)

Fig. 18 shows the distribution of freezing line. Fig. 19 shows the change with time of the freezing line. The freezing line shown is only five months after the operation of heat barrier; the measured value, however, agrees very well with the calculated value, showing that the freezing line is coming closer to a steady state.

A calculated value of the distribution of freezing line ranging from GL-0 meter to about GL-5 meters is slightly greater than the measured value though this is true of all of Cases I, II and III. This is because the computation was made presuming that the LNG tank is full, and practically the liquid level varies, showing a lower value than the calculated value.

6. Conclusion

The foregoing has described the design procedure in the basic design of heat barriers and the comparison between measured values and calculated values. As a result, it has been made clear that the progress of the freezing line can be estimated through thermal analysis and also that the installation of the heat barrier can control the extent of the freezing zone. The cases presented in this report are only partial, but the same result applies to all heat barriers of other tanks. These heat barriers are presently working effectively to control the extent of freezing zone. A problem to be solved in future is to grasp the thermal constants much more exactly with a view to strictly and effectively controlling the thickness of the frozen soil.

Acknowledge

References

1) Japan Gas Association Committee on LNG in-ground storage "Recommended Practice for LNG In-ground Storage." March, 1979

2) S. Goto, "Civil Engineering Prospect for Stockpile and Transport of LNG." J.S.C.E. Vol.65, No.6, 1980

3) Y. Ishimasa, J. Umemura, A. Fujita, C. Rai, "Development and Operational Experiences of LNG In-ground Storage Tank in Japan." Proc. 5th Inst. LNG Conference, Dusseldorf, 1977.

4) C.R. Wylie, Jr. Advanced Engineering Mathematics, 3rd. ed. McGraw-Hill.

Table 1. LNG In-ground tanks of Tokyo Gas

Works	Capacity Kl	I.D.x liquid height M	Quantity	Year of Completion
Negishi	10,000	30 x 14.2	1	1970
	60,000	50 x 30.6	1	1972
	95,000	64 x 29.6	1	1977
	95,000	64 x 29.6	1	1978
	95,000	64 x 29.6	1	1981
	95,000	64 x 29.6	1	* 1982
Sodegaura	60,000	60 x 21.3	2	1974
	60,000	64 x 18.7	5	1976
	60,000	64 x 18.7	2	1977
	62,000	64 x 19.3	1	1979
	58,000	64 x 18.1	1	1979
	130,000	64 x 40.5	1	* 1982
	130,000	64 x 40.5	1	* 1982
	130,000	64 x 40.5	1	* 1983
	130,000	64 x 40.5	1	* 1985

*Under construction

Fig. 3 Design procedure of heat barrier

Fig. 1 Types of in-ground storage tanks
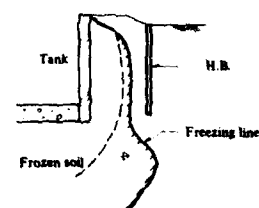
Fig. 4 Freezing line vs. depth of H.B.
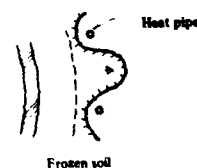
Fig. 5 Freezing line vs. interval of heat pipe

Fig. 2 Schematic drawing of heat barrier

181

Fig. 6 Schematic drawing of storage tank for analysis

Fig. 7 Calculation model

Fig. 8. Partitioned elements diagram (rH = 4 m)
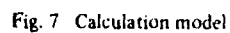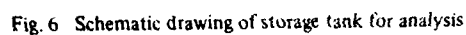
Table 2. Thermal constants

constant material	Before freezing		After freezing		
	k (kcal/mh°C)	Cρ(kcal/m³°C)	k(kcal/mh°C)	Cρ(kcal/m³°C)	L (kcal/m³)
Silt	1.2	860	2.1	500	51,000.0
Mudstone	1.6	770	2.2	520	37,000.0
Concrete	2.0	500	2.0	500	—
Gravel	1.4	530	1.6	440	14,000.0

k Thermal conductivity Cρ. Heat capacity L. Latent heat
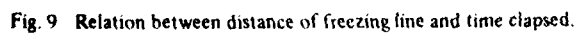
Table 3(a). Case study (axial symmetry model)

Case	Distance rH (m)	Depth zH(m)	Temp. TH(°C)
1.1		33.6	
1.2	4.0	30.6	11.7
1.3		27.6	
1.4		21.6	
1.5		33.6	
1.6	5.0	30.6	23.0
1.7		27.6	
1.8		21.6	

Table 3(b). Case study (three dimensional model)

Case	Distance rH (m)	Interval (m)	Temp. TH (°C)
2.1.A		3	25
2.2.A			40
2.3.A	3	5	30
2.4.A			50
2.5.A		7	40
2.6.A			60
2.1.B		3	15
2.2.B			30
2.3.B	4	5	20
2.4.B			35
2.5.B		7	30
2.6.B			50

Fig. 9 Relation between distance of freezing line and time elapsed.

182

Fig. 10 Relation between depth of H.B. and freezing line
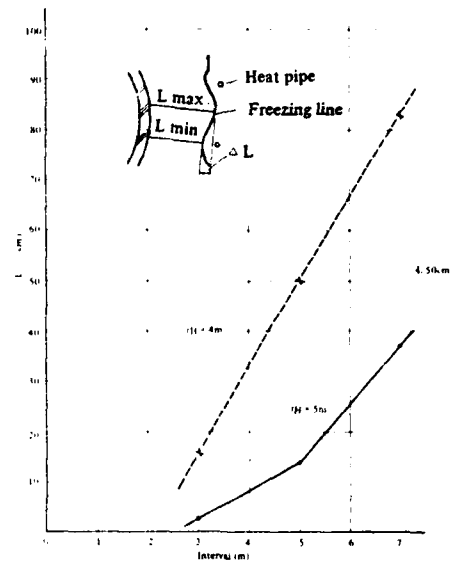
Fig. 12 Relation between interval and $\triangle L$ at L =3m

Table 4. Summary of heat barrier

Tank No.	Capacity (KL)	Works	Year of operation	Distance rH(m)	Depth Z_H (m)	Interval ℓ (m)	Temp. T_H (°C)
Case I	95,000	Negishi	1979	4.0	30.0	4.0	40
Case II	95,000	Negishi	1979	3.0	30.0	4.0	40
Case III	58,000	Sodegaura	1981	5.0	20.0	4.9	30
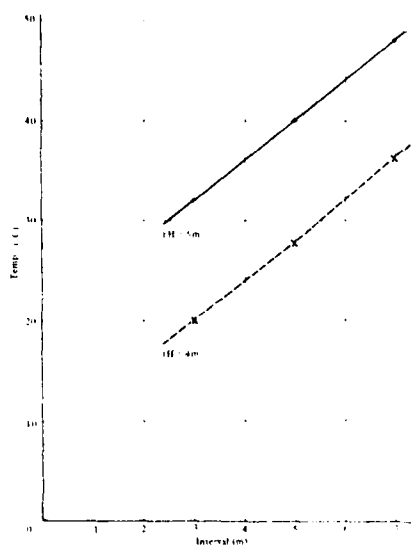
Fig. 11 Relation between interval
and heat temperature at L = 4m
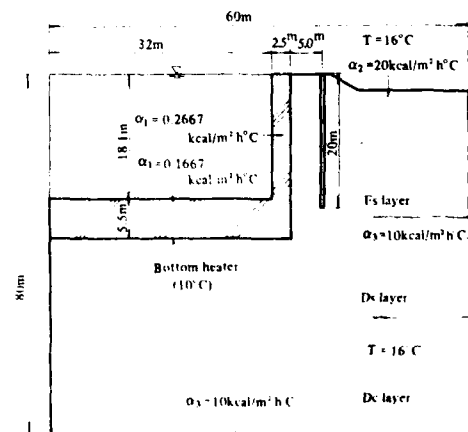
Fig. 13 Calculation model and thermal constants for case III

constant material	Before freezing		After freezing		
Concrete	2.0	500	2.0	500	
Fs layer	1.5	790	2.2	530	39,000
Ds layer	1.8	740	2.3	540	28,000
Dc layer	1.4	810	2.2	530	42,000

183
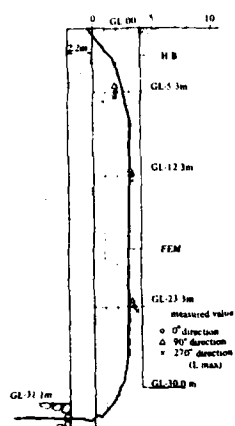
Fig. 14 Distribution of freezing line
(2.5 years after operation of H.B.)
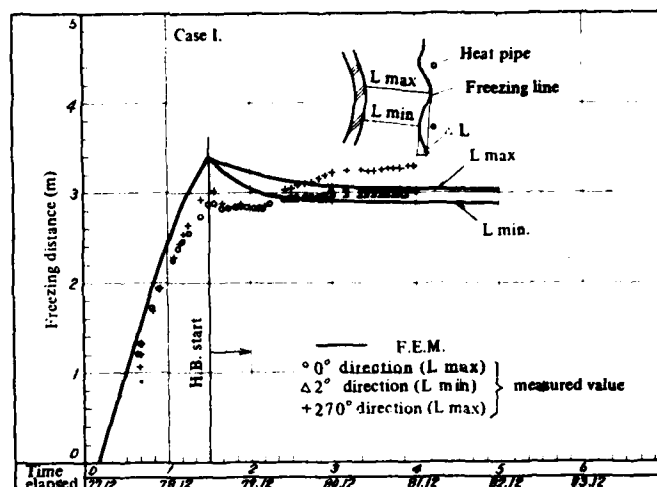
Fig. 15 Progress of freezing line at GL-12.3m
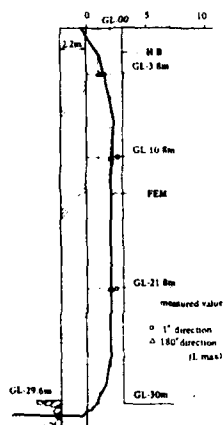
Fig. 16 Distribution of freezing line
(2.0 years after operation of H.B.)
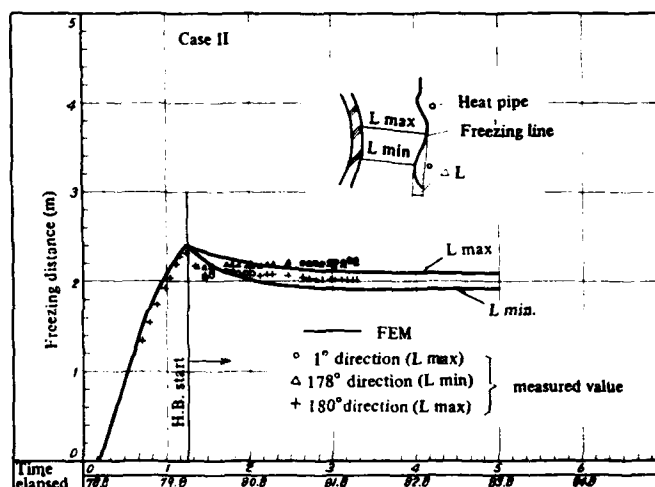
Fig. 17 Progress of freezing line at GL-10.8m
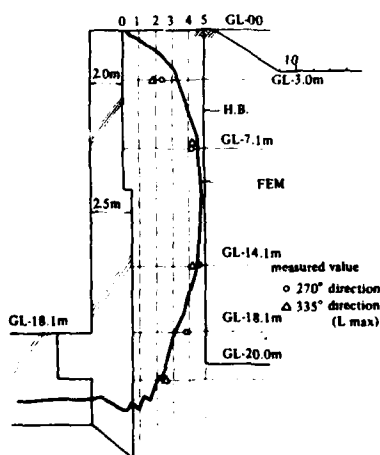
Fig. 18 Distribution of freezing line
(5 months after operation of H.B.)
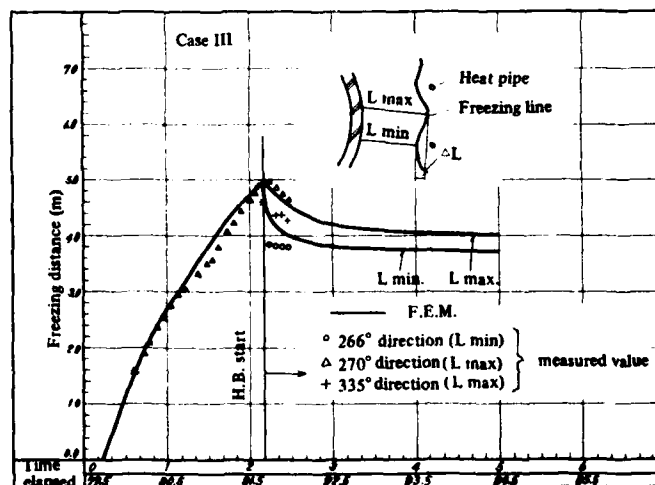
Fig. 19 Progress of freezing line at GL-14.1m

184

EXPERIMENTAL RESULTS ON THE FREEZING OF SATURATED SANDS

Fabio Gori   Fisica Tecnica,
               Fac. Ingegneria,
               Via S. Marta 3,
               Firenze, Italy.
Maura Ughi   Ist. Matematico,
               U. Dini, Firenze,
               Italy.

ABSTRACT

Experimental freezings of two liquids (water and tert-amyl- alcohol) in sands have been carried on in a closed system. A sand with known grain size distribution, mineralogic composition and physical properties has been used. An experimental apparatus reproducing a onedimensional heat transfer phenomenon has been set up. The lower plane has been thermally insulated and the upper one has been kept at constant temperature. A procedure of vibration of the sand has been employed to have a uniform liquid regain distribution at the beginning of the cooling. Temperature has been measured at different distances from the cold source during the cooling. Liquid regain distributions have been measured at the end of the freezing process with the oven drying method. Conductive heat transfer with change of phase has been theoretically investigated. The energy equation has been solved numerically with the finite difference method of Crank. The thermal conductivity of the wet sand has been determined with the relation proposed in the paper of Johansen and Frivik. Experimental temperature and liquid regain results have been discussed and the temperature measurements have been compared with the theoretical results.

INTRODUCTION

Ground freezing presents the very interesting feature of the coupled phenomena of heat and mass transfer. While in a first period the researchers have been mainly interested in the heat transfer, in the last two decades several papers (1-4) appeared dealing with the coupled heat and mass transfer.

Although several questions have been answered to, especially during the two Symposia on Ground Freezing (5-6), it is opinion of the authors that the influence of the physical properties of the water and of the porous medium has not been yet completely investigated.

A research project has been planned to evidentiate the importance of the physical properties of water. Some experiments have already been performed (7) with a cryogenic unity as cooling source. An experimental apparatus in onedimensional geometry has been set up during a set of measurements carried on with a water saturated sand (8).

The aim of the present paper is to obtain experimental temperature and liquid regain profiles during cooling

185

processes carried on with a sand satura-
ted with two different liquids (water
and tert-amyl-alcohol).

EXPERIMENTAL PROCEDURE

The sand mixed with the liquid has
been put in a cylindrical plastic con-
tainer (diameter 105 mm ,lenght 130 mm).
The container has been sealed andvibrated
for four hours in vertical position in
order to obtain a vertical and horizon-
tal uniform liquid distribution. The
lower and lateral surfaces have been
thermally insulated with glass wool.

The thermocouple tips have been
set on the axis of the container at
various heights. The thermocouples have
been inserted by means of steel tubes
(diameter 1 mm) which have been removed
immediately afterwards. This method of
insertion has been used to control
exactly the location of the tips.
Furthermore the uniformity of tempera-
ture on horizontal planes has been veri-
fied.

A metallic plate, inside which
ethyl-alcohol has been circulated, has
been used as the low temperature source.
The ethyl-alcohol has been mantained at
the desired temperature by a thermostat
Haake FK2. The uniformity of the tempe-
rature of the plate surface in contact
with the sand has been verified.

The cold plate has been put over
the container and in contact with the
sand. After the choosen time the cold
plate has been taken off together with
the thermocouples and the liquid regain
has been measured.

The thermocouples used in the expe-
riments (Cromel-Alumel of 0.5 mm diame-
ter) have been calibrated with a plati-
num thermoresistance (100 ohm/0deg.C).
The reference junctions have been man-
tained at constant temperature by a
constant temperature oven. The tempe-
rature measurements have been registe-
red on a Data Logger 2070 HP at diffe-
rent times.

The liquid regain has been measured
by gravimetric method. The sample of wet
sand has been weighted on an analytical
balance (0.1 mg of precision), then
dried in a forced air oven at 105 deg. C
for 12 hours and finally weighted again.

The liquid regain r is defined as

$$r = \frac{W-D}{D} \; 100 \qquad\qquad 1)$$

where W and D are the weights of the wet
and dry samples respectively.

THEORETICAL ANALYSIS

It is considered the onedimensional
thermal conduction neglecting the
influence of the liquid transfer.
The following equations are assumed

$$C_u \frac{\partial T}{\partial t} = \frac{\partial}{\partial x} \left(k_u \frac{\partial T}{\partial x} \right) \qquad 2)$$

in the unfrozen region,

$$C_f \frac{\partial T}{\partial t} = \frac{\partial}{\partial x} \left(k_f \frac{\partial T}{\partial y} \right) \qquad 3)$$

in the frozen one,

$$k_f \left\{\frac{\partial T}{\partial x}\right\}_f - k_u \left\{\frac{\partial T}{\partial x}\right\}_u = \rho_d \; L \; r \; \frac{dX}{dt} \qquad 4)$$

at the interface.

According to the results of
Johansen and Frivik (9), the amount of
unfrozen liquid in the frozen sand is
considered negligible.

The following relations are used

$$C_u = \rho_d \left(c_{ps} + c_{pl} \; r \right) \qquad 5)$$

$$C_f = \rho_d \left(c_{psf} + c_{plf} \; r \right) \qquad 6)$$

where c_{ps} =760 J/kg K, c_{psf} =700 J/kg K
c_{pw} = 4186 J/kg K, c_{pi} = 1967.4
J/kg K, c_{pa} =3150 J/kg K, c_{paf} = c_{pa} ,
and r is taken equal to the average
value of the experimental measurements.

The thermal conductivity of the
sand is determined according to the
following relations , proposed in (9):

$$k = k^0 + (k^1 - k^0) \; f(Sr) \qquad 7)$$

where $k^0 = 0.034 \; n^{-2.1}$
$k^1 = k_n^{(1-n)} \; k_s$
$k_s = k_q^{1/1f_{1-q)}} \; k_r^{(1-q)} \qquad 8)$

$$n= 1-\rho_d/\rho_s$$
$$Sr = r\,\rho_d/(n\,\rho_l)$$

and f(Sr) is defined as

$$f(Sr) = Sr \qquad\qquad 9)$$

in the frozen region.

$$f(Sr) = 0.68\ \log(Sr) + 1 \qquad 10)$$

in the unfrozen region and for the sand used in these experiments. The following values for the thermal conductivities are taken : $k_q=7.7$ W/m K; $k_r=2$ W/m K; $k_w=0.57$ W/m K; $k_i=2.3$ W/m K; $k_a=0.168$ W/m K; $k_{af}=k_a$.

Equations 2)-4) have been integrated numerically with the finite difference method employed in (10)-(12). The boundary conditions are constant temperature on the upper plane and adiabatic condition on the lower one.

The sand used in the present experiments has the properties of table 1.

Table 1 - Properties of the sand.

Grain size distribution

diameter (μm)	% (in weight)
< 100	0.3
100-160	2.2
160-250	9.8
250-400	67.2
400-630	20.1
630-1000	0.4

Mineralogic composition

Quartz	61%
Feldspar	31%
Calcite	<1%
Phyllosilicate et al.	8%

Physical properties

Density of sand	ρ_s=2686 kg/m^3
Non-vibrated dry sand density	ρ_d=1571 kg/m^3
Vibrated dry sand density	ρ_d=1713 kg/m^3

The tert-amyl-alcohol has the following properties: melting point at -8.4 deg. C; boiling point at 102 deg. C;

density equal to 810 kg/m^3; latent heat equal to 52.5 kJ/kg K. Furthermore the volume of the alcohol does not increase during the freezing.

PRESENTATION OF THE RESULTS

The vibration procedure employed has ensured a maximum deviation of 10% of the initial liquid regain from the theoretical value (21.14% for water and 17.12% for alcohol at the saturation). The maximum variation between the initial liquid regain distribution and its average value is 7%.

The experimental results for water are presented in figures 1-2 and for alcohol in figures 3-4. The temperature measurements have been presented dimensionally (deg. C) while the liquid regain has been scaled to the average value (r_m), reported on the same figures.

Figures 1a and 2a present the water regain measured at the end of two experiments performed with different
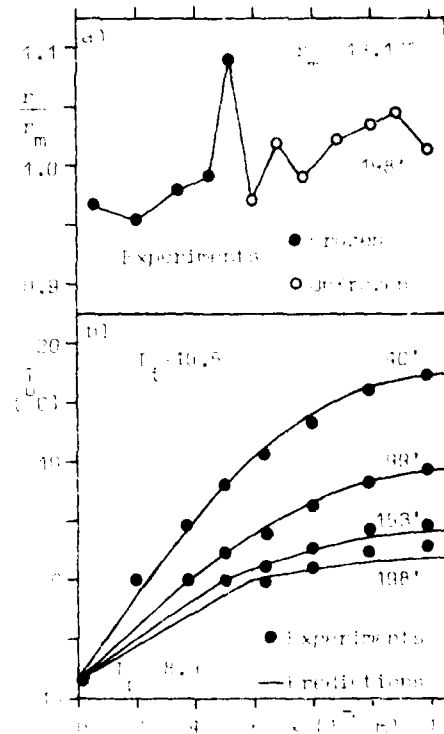
Figure 1 - Results for water sand system.
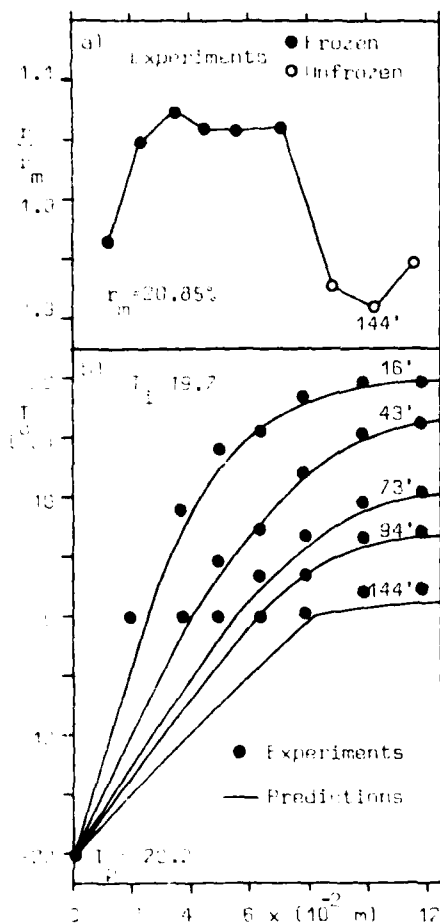
Figure 2 - Results for water-sand system.

Figure 3 - Results for alcohol-sand system.

les are reported in figures 1b,2b,3b,4b.

cold plate temperatures (-8.3 deg. C and -20.2 deg. C respectively). The experimental temperatures measured at different times are reported in figures 1b and 2b.

Figure 3a presents the alcohol regain measured in two experiments performed with the same initial and boundary thermal conditions and with different cooling times. The experimental temperature distributions of figure 3b refer to the longer experiment because those of the shorter one have shown a very good agreement.

Figures 4a and 4b presents the experimental alcohol regain of three experiments and the temperature measurements of the longer one.

The theoretical temperature profi-

DISCUSSION

The experimental water distribution of figure 1a shows a limited change of the water regain; the maximum variation (about 12%) is at the interface between the frozen region and the unfrozen one. In the experiments with a colder plate (figure 2) the water regain increase is of the same order of magnitude (13.5%).

The present experiments confirm the existence of the "cryogenic suction" for the water-sand system but the average water regain increase in the frozen region is small in comparison with the overall average. This conclusion is in agreement with the previous experimental
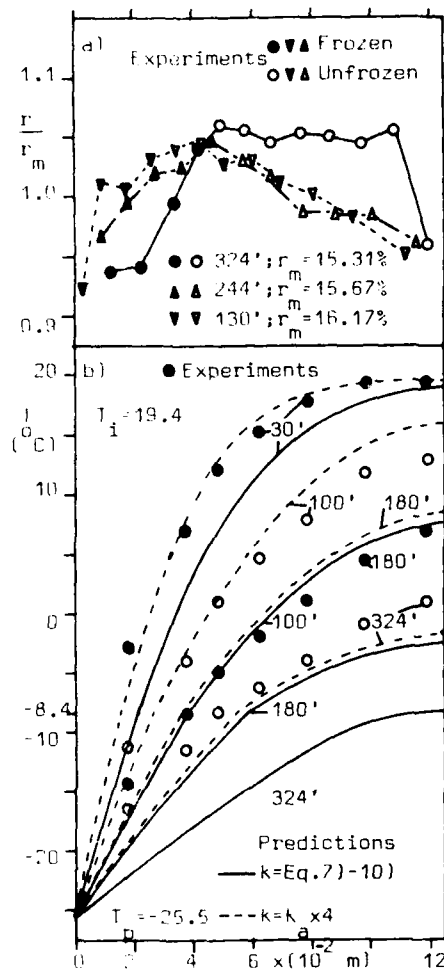
Figure 4 - Results for alcohol-
sand system.

results of the authors (7-8).

The theoretical temperature predi-
ctions of figures 1b and 2b are in good
agreement with the experimental data,
with a slight tendency to be lower.

The experimental distribution of
alcohol regain at the end of the cooling
(figures 3a and 4a) has a different
behaviour than that measured in the
water-sand system. The alcohol regain
in the frozen region has lower values
than in the unfrozen one. This is shown
in figure 3a and it is confirmed by the
results of figure 4a. Such an effect
seems to be more evident in the longer

coolings.

The decrease of alcohol regain in
the frozen region is accompanied by an
increase in the unfrozen one. Anyway the
variation of the average alcohol regain
in the frozen region with respect to the
overall average is in the range of that
measured in (7).

The full line curves presented in
figures 3b and 4b are the temperature
predictions for the alcohol-sand system
calculated with the global thermal con-
ductivity given by equations 7)-10).
Such predictions are not in agreement
with the experimental data which are much
higher, especially at longer times.

The main reason of this disagree-
ment seems to be due to the value assumed
for the global thermal conductivity.
Additional predictions have been presen-
ted in figures 3b and 4b (dashed line
curves) with an "ad hoc" assumption of
the global thermal conductivity.

The existence of the "cryogenic
suction" for the water-sand system and
not for the alcohol-sand system seems to
suggest that the increase of the water
volume at the melting point is one of the
most important causes of this phenomenon,
as already pointed out in (7).
The water volume increase produces a
segregation of the solid particles and a
liquid flow toward the freezing front.
This effect is not a striking one because
of the grain size distribution of the
sand employed.

This physical interpretation seems
to be not able to explain the alcohol
regain decrease in the frozen region in
comparison with the unfrozen one. Further
investigations on non-saturated systems,
on porous media with different grain size
distribution and on the influence of the
freezing front velocity are necessary to
give a complete physical interpretation
of the phenomena involved in ground
freezing. Special attention has to be
given to the problem of the formation of
ice lenses.

CONCLUSIONS

The present experiments confirm

189

that in the freezing of water in this kind of sand a "cryogenic suction" at the interface between the frozen and the unfrozen regions is present.

The temperature measurements during the cooling of the water-sand system are (numerically) predicted very well with the thermal conductivity given by equations 7)-10).

The liquid regain measurements at the end of the cooling of alcohol-sand systems show a different result: "cryogenic suction" is not present.

The numerical predictions for the temperatures, in the case of alcohol-sand system, are in agreement with the experimental data assuming an "ad hoc" value for the global thermal conductivity.

NOMENCLATURE

Symbol	Meaning
C	Heat capacity
c_p	Specific heat
d^p	Diameter of the sand grain
D	Dry sample weight
k	Thermal conductivity
L	Latent heat
n	Porosity
q	Quartz content
r	Liquid regain
Sr	Saturation
t	Time
T	Temperature
W	Wet sample weight
x	Distance from the cold plate
X	Thickness of the frozen region
ρ	Density

Subscripts

a	alcohol
af	frozen alcohol
d	dry sand
f	frozen region
i	ice
l	liquid
lf	frozen liquid
q	quartz
r	rest
s	sand
sf	frozen sand
w	water

REFERENCES

(1) Hoekstra P.,Moisture Movement in Soils under Temperature Gradients with the Cold Side Temperature below Freezing, Water Resour. Res., 2,2,241-250,1966.

(2) Dirksen C. and Miller R.D., Closed-System freezing of Unsaturated Soils, Soil Sci. Soc. Am. Proc., 30,168-173,1966.

(3) Gupta J.P. and Churchill S.W., Heat and Moisture Transfer in Wet Sand During Freezing, 92d An.Conf.ASME, 99-105,Nov.1971.

(4) Jame Y.W. and Norum D.I., Heat and Mass Transfer in Freezing Unsaturated Soil in a Closed System, 2nd Conf. on Soil-Water Problems in Cold Regions.46-62,Sept.1976.

(5) Proceedings 1st International Symposium on Ground Freezing, Elsevier Sci. Publ. Co.,Bochum, 1978.

(6) Proceedings 2nd International Symposium on Ground Freezing, Trondheim University, Trondheim, 1980.

(7) Gori F. and Ughi M.,On some Experiments of Freezing Liquids in Sands, XXXV A.T.I. Congress,I, 133-144,1980.

(8) Gori F., On the Cooling of Sands Saturated with Water, XXXVI A.T.I. Congress, I,1-12,1981.

(9) Johansen Ø. and Frivik P.E., Thermal Properties of Soils and Rock Materials, Proc. 2nd Int. Symp. on Ground Freezing, Trondheim 427-453,1980.

(10) Gori F., Cryosurgical Probe: a Theoretical Prediction of the freezing Front Penetration, 1st

Mediterransan Conf. on Med. and
Bio. Eng.,Sorrento,I,3-1,1977.

(11) Gori F.,Numerical Solutions of
Energy Eq tion in Cryosurgery,
XV Int. Cong. of Ref.,Venice,C1-4,

1979.

(12) Gori F.,On Heat Transfer in Non-
Living Materials around a Cryosurgi-
cal Probe, 2nd Int. Conf. on Num.
Meth. in Ther. Prob.,230-239,1981.

EXPERIENCES AND INVESTIGATIONS USING
GAP FREEZING TO CONTROL GROUND WATER FLOW

Heinz-Bernd Einck, Dipl.-Ing.
Akademischer Rat, Institut of Konstruk-
tiver Ingenieurbau, Ruhr-Universität
Bochum
Albert Weiler, Dipl.-Ing., Head of the
Metro Construction authority, Duisburg

Abstract
In the years from 1977 to 1979, during
construction of the Metro Duisburg,
Federal Republic of Germany, contract sec-
tion 4 with an open excavation was con-
structed by gap freezing.
As there were anyhow high velocities of
ground water stream essential raisings
of velocities in the freezing gaps
appeared by water accumulation.
In order to determine dimensions of the
appertaining equipment and especially
those of the freezing pipes knowledge
about the flowing velocities as exact as
possible was required.
At the begin of the design in 1974 was
decided, first to carry out a measuring
scheme to learn the groundwater flowing
velocity, this was followed by a large
scale (1:1) trial freezing to ascertain
the feasability of the gap-freezing-
method.
When these investigations were scienti-
ficly valued it was established that the
involved was acceptable. The contract
documents were prepared prescribing a
combination of "cover and cut" with gap-
freezing, which meanwhile is called the
"Duisburg method of Metro-construction".

During the construction a large scale
measuring and scientific research pro-
grams were absolved.

ESTABLISHING OF DESIGN PARAMETERS

By aid of comprehensive Finite Element
calculations the situation of ground-
water could be simulated beginning with
investigations on a large scale and
ending with investigations in detail
between two freezing pipes. Besides that
the investigations in detail were also
performed by taking into consideration
the characteristic values of ground
water which are depending on temperature
and the heat flow. The freezing pipes
were considered as cooling sources and
the heat potentials were superposed the
flowing potentials. This made it possible
too, to simulize the configuration of
the frozen parts of soil.

Important results of these investiga-
tions are:

1. The Finite Element investigations
   afford very good values which com-
   parisons by In-situ measurements have
   confirmed.

2. Depending on freezing pipe distances
   and hydraulic gradient it has become
   possible to establish firm multiples
   from ground water end velocity to
   its beginning velocity.

3. Direction of ground water is no lon-
   ger important for the gap freezing
   as inside the gaps it occurs a ver-
   tical rectification to the excavation
   walls.

INTRODUCTION

In the years from 1977 to 1979 the con-
tract sections 4, B5 were constructed by
the application of gap freezing in
Duisburg city, Federal Rupublic of Ger-
many.
The dimensioning of the complete free-
zing plant was based on the results of
large scale testing and in particular

193

the installation of the pipes used for freezing within the diaphragm gaps. Subsequently many calculations were also performed by Maidl and Einck (1977) for determining the expected ground water velocity of flow based on Finite Element programme "GEOSICK."

The results from the above calculations were to be compared afterwards with actual measurements during the freezing phase. This comparison as well as further measurements of temperature distribution and also the freezing behaviour of the soil were the basic factors considered for further investigations with the aim to achieve the possibility of an exact calculation model for gap freezing. Mainly till now experiences are available only for frozen shafts.

Also the calculation method proposed by Victor (1969) did not lead to meaningful results for the Duisburg Construction Method, as this method does not take into account the expanded flow around the frozen parts of soil. However, flow can easily occur around frozen shafts. It can therefore be stated that gap freezing represents a special problem of soil freezing at site.

PRELIMINARY INVESTIGATIONS

First of all investigations of flow behaviour in the vicinity of frozen parts of soil were performed subjected to a given angle of attack of below 45° and a given gradient of 1.35 o/oo. These results mainly for an increase of possible water accumulation could be estimated. Even results in frozen gap area could be obtained by a step-by-step reduction of the investigation area. By this method at the first instance a rough frozen part of soil configuration was given. The results achieved in this way are to be compared with the In-situ measurements. The following figure shows the arrangements for the gaps 128 and 129. Based on the specified procedure for the calculations and measurements for level I the comparisons given here are of im-

portance at the inner side of the building pit as only absolute values of velocities were measured without any directions.

The results during frozen period from 7th April, 1978, to 9th April, 1978, are shown in the following table 1. Better approximation of the values could, however, be obtained if correction factor of dynamic viscosity is also considered and will be explained in detail in this paper.

As the heat flow can also be dealt with the potential theory the complete treatment of the problem of freezing is possible by the superposition of ground

Element 297	Date			
	7.4.78	8.4./11°°	8.4./19°°	9.4./16°°
m / day	9.6	10.0	8.3	2.6
result of calculations	10.7	8.2	8.2	3.2

Table 1. Result of flow measurements and flow calculations.

water flow and heat flow. In order to obtain comparative values for further calculations, besides the already available observation pipes (Fig. 2) in vertical direction, pipes are installed in horizontal direction for the measurement of temperature at six points along the length of the pipe. With such measuring points the possibility to determine extension of frozen soil parts moreover is offered.

Figure 1. Positions of levels.
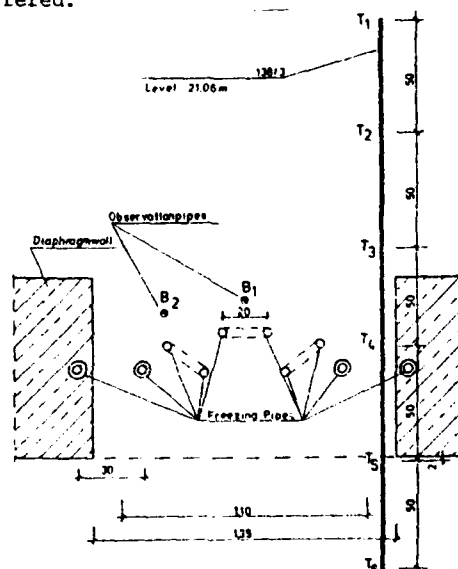
Figure 2. Position of observation pipes.

194

It can be stated in anticipation that the measured temperature values and the heat potential values to be aimed from calculations would prove to be consistent.

INVESTIGATIONS CONCERNING GROUND WATER FLOW

In case of soil freezing at site the ground water flow causes great concern especially where high velocities are prevailing. Therefore, the knowledge of velocities for all following four phases of freezing is of great importance:

1. Cooling the soil and the water down to $0°C$.

2. The initiation and the development of the freezing zone in the soil around the freezing pipes.

3. The development to a wall by the coming into close contact of adjacent freezing zones.

4. Permanent freezing-maintenance of frozen parts of soil.

The decisive velocites of flow are calculated by the following method.

1. Determination of ground-water flow conditions at the beginning of freezing, however, by taking into consideration the already existing structure.

2. Determination of maximum accumulation of water in the completed frozen body.

3. Detail investigations at the important points.

The ground water constants have an significant influence on the heat prevailing conditions depending upon the tem-

peratures. The filter rule of Darcy is applicable in general and is expressed as

$$\frac{Q}{A} = V = k \cdot i$$

Many calculation methods treat the permeability coefficient 'K' as constant for the purpose of simplification. This brings excessive velocity values. However, the coefficient 'K' depends on dynamic characteristics of ground-water such as viscosity and density are expressed as

$$k = K \cdot \frac{g}{\nu} \quad \text{and} \quad \nu = \frac{\eta}{\rho}$$

Where the density ρ as well as the viscosity ν are functions of the temperature. Based on the work by Feldkamp it is possible to express the material constants of water as polynominal functions based on the liquidity temperature Θ (in $°C$) as given in

$$\rho = \sum_{o}^{7} a_k \cdot \Theta_k$$

$$\eta = 10^{-3} \exp \sum_{o}^{4} b_k \cdot \Theta_k$$

This is diagramatically represented in fig. 3 for the kinematic viscosity. It is possible to obtain different permeability coef'icient values 'K' which are considered for further calculation steps.
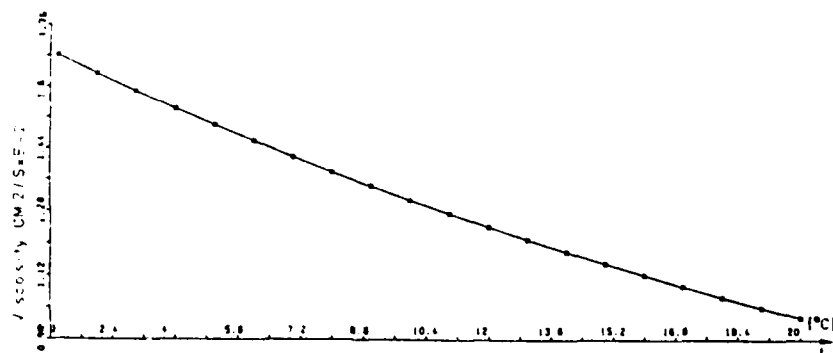
Figure 3. Kinematic viscosity depending on temperature.

HEAT FLOW CONSIDERATIONS

In order to get knowledge about the temperature levels existing and to study then influences the frozen pipes were considered as cooling springs. By superposing the heat flow over the ground water flow, flow dependent Isothermals as potential lines results as shown in fig. 4.

Based on the temperature distribution the local value of 'K' for the rest calculation step is determined. Hence follows as the first result the situation shown in fig. 5.

In the whole gap nearly the same changes of velocity were observed. For the individual elements the difference between the results is in the order of up to 1 % and is therefore neglected being very small. Therefore one can proceed to consider that the gaps "straighten" the ground-water flow parallel to the diaphragm sides. This is very well recognized and also seen in all subsequent calculation steps that the velocity vectors lying as far away as 10 cm from the outer
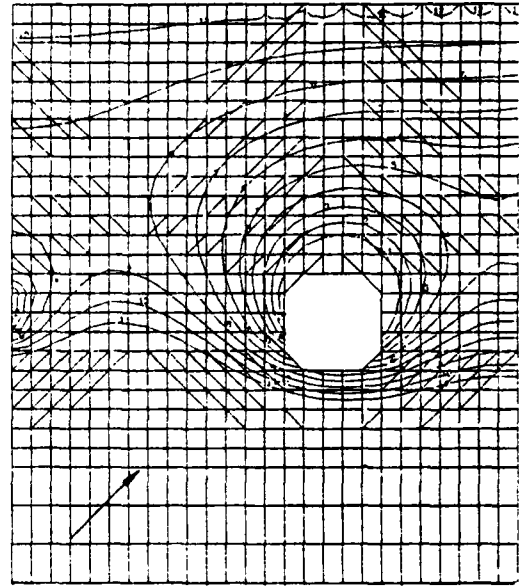
Figure 4. Isothermals as potential lines.
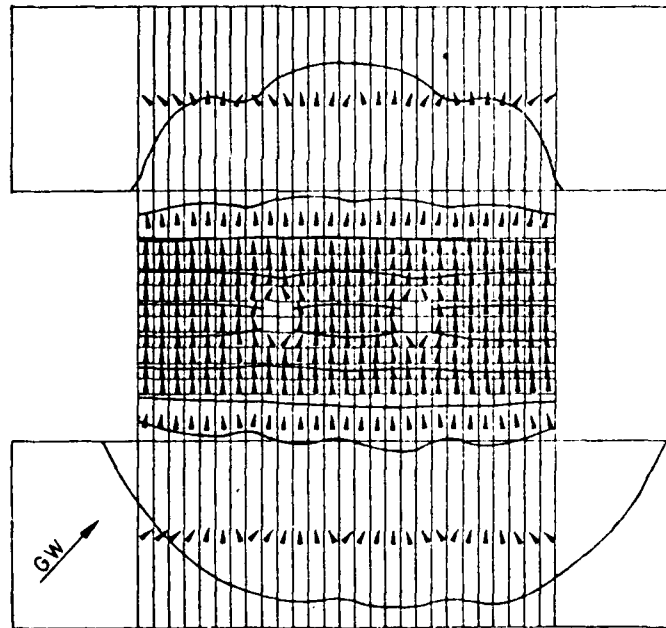
Figure 5. Flow situation in the gap.

edges of diaphragm gaps have the same direction sense. Moreover, Isopotential lines run parallel to the longitudinal axis of the diaphragm gap.

Hence it follows that as long as the pipes used for freezing lie in the gaps, the direction of flow attack will not

influence the flow conditions within the gaps. The freezing progress was simulated step-by-step up to 20 iterations. Very good results with regard to velocities were obtained from the calculations as can be seen in fig. 6.

196
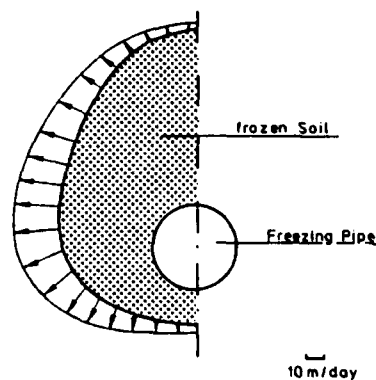
Figure 6.   Velocities around a body.

Figure 7.   Velocities in the cross section.

It is expected that the frozen body will ultimately form an ellipse and that the velocities of flow at LUV and LEE will be smallest and at sides highest as shown in fig. 6. They are plotted as vectors normal to the boundary of the frozen body. It is very interesting to see the distribution of velocity between the frozen parts. Here the maximum velocity at 0° C margin is expected, as it is subjected to the highest fall of potential. In addition to it the k-value is decreased. This results in a comparison of velocity growth. The arrive of maximum velocities for the cross-section *between two frozen parts is represented* in fig. 7.

The decrease of velocity at the edges of the frozen body can be compared to that of a semi-boundary layer behaviour. This layer extends up to a temperature of 2° C in the beginning and up to 4° C with a very advanced freezing process. This circumstance perhaps explains as to why the freezing can be successful even in case of higher velocities of ground-

water. Because of the given grid structure it is not possible to carry out everytime the exact determination of the width of boundary layers. In the tested case it was varying from 4 % to 2 % of the distance between the freezing pipes. This permits the expectations, that when a remaining width of gap of approximately 4 % of the cross-section at the beginning is considered, then the velocity would here already reach a maximum or exceed it as the case may be.

Increased rate of velocity of flow at infinity should be excluded as the flow in the gap corresponds to a situation of half well at the LUV-side and a half inverted well at the LEE-side.

The calculated velocity curve depends on the percentage of contracted area as shown in fig. 8.
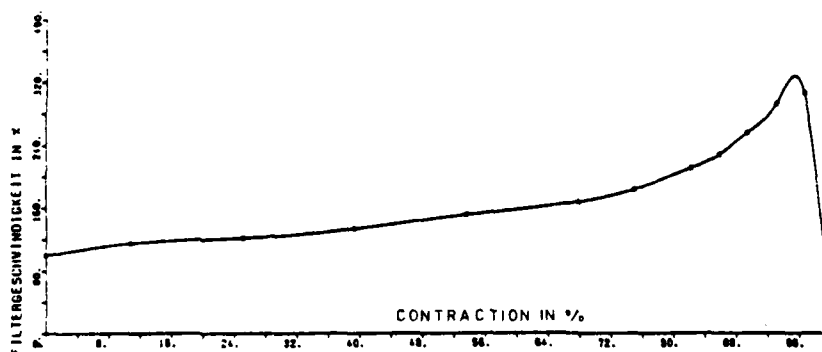
Figure 8.   Filter velocity depending on contraction.

197
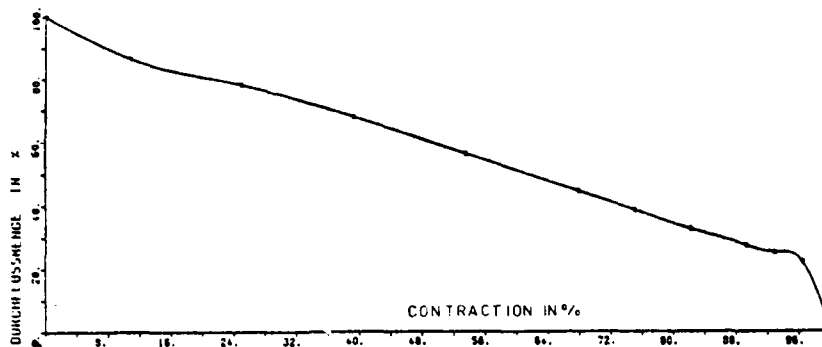
Figure 9. Quantity of flow depending on contraction.

It should be observed that an increase of up to 10 % of the velocities have already resulted from the start of cooling and up to the initiation of icing in the soil. In addition to the above results fig. 9 gives the development of quantity of flow. It is remarkable here to note the fact that with the cooling-off process the quantity of ground-waterflow is reduced considerably. The change in k-value due to temperature changes introduces a semi-contraction of area, although no part of the soil has reached a frozen state. In extreme conditions only 22 % of the beginning quantity of flow can pass through the gap. In other words, flow takes place around the construction. Therefore, the continuity rule otherwise valid in hydrogeology is not valid for the flow through the gap.

$$\Rightarrow Q_1 = v_1 \cdot A_1 \neq v_2 \cdot A_2 = Q_2$$

The most important results are as follows:

1. An increase in maximum velocity of up to 320 % of the beginning velocity (value corresponds to last calculation step 306 %).

2. If the gaps remaining reach a stage of 4 % of the width between the freezing pipes, and if still energy resources are available for further cooling of the ground-water, then because of the expected reduction of the k-value, the closing is guaranteed.

3. During the freezing progress the quantity of flow becomes smaller and smaller. Down to a contraction of area of 90 % the behaviour is found to be linear.

4. A constant 'C' is determined, which depends on the conditions prevailing in the beginning.

$$C = \frac{V_{max}}{V_o}$$

These facts have been confirmed by further calculations with variation of potential drop and the soil permeability K. However, changes in the configuration of the frozen body have taken place. Also based on the third point mentioned above the dimensioning of the freezing measures can be checked. After the evaluation of the maximum velocity on the corresponding quantity of flow the conditions corresponding to the closure could be derived from the extreme conditions in the two components:

(I) Requirement for energy without ground-water flow

(II) Requirement for energy of the ground-water flow

Theoretically, this approach may seem to be slightly less elegant compared with closed form solutions. But in practice once the required charts and tables are prepared, this approach is faster in achieving the desired objectives. For the Duisburg construction method and especially for the construction of the contract section 4 of the Metro in Duisburg city, a procedure as explained above was successfully applied.

198

Father of the idea to develop
a new construction method was
the intention of giving non-
interference with the ecolo-
gic ballance absolute prefe-
rence. Of course is such an
aim for a project of this
magnitude impossible to reach
totaly.

But technical know how
and the courage of the engi-
neers to base their design
on newly established para-
meters combined with the
consequent will to apply
innovations in order to pre-
serve the environment lead to
a successful new construction
method, described herein after
in short.

Construction Method Applied at Contract
"Station König-Heinrich-Platz"

In the contract documents the
design of the site enclosure
prescribed slurry - diaphragm-
walls as sections which were
interrupted by gaps that
during the construction were
made watertight by ground-
freezing. This method, mean-
while known to the construc-

tion world as Duisburg Method
of Metroconstruction, fullfilled
the condition to keep up the
communication of the ground-
water in the following way:

o The diaphragm wall sections (Fig.
  10) of the site enclosure were 5.4
  m long, which on each side were
  interrupted by 1.35-m-long gaps,
  left open.
o These gaps, also called
  windows, were closed by
  groundfreezing. The water-
  tight enclosure enabled
  excavation of the ground
  and construction of the
  underground station in the
  dry. Diaphragm wall sections
  and frost bodies reached
  down into the watertight
  layers of the tertiary clay.
  The frost bodies trans-
  ferred all loads (waterhead,
  earth pressure) by archac-
  tion into the diaphragm
  wall sections.
o After completion of the
  construction and thawing
  of the frozen ground the
  groundwater could stream
  again through the gaps and
  unterneath the tunnel, thus
  reestablishing the original
  situation of groundwater
  communication.
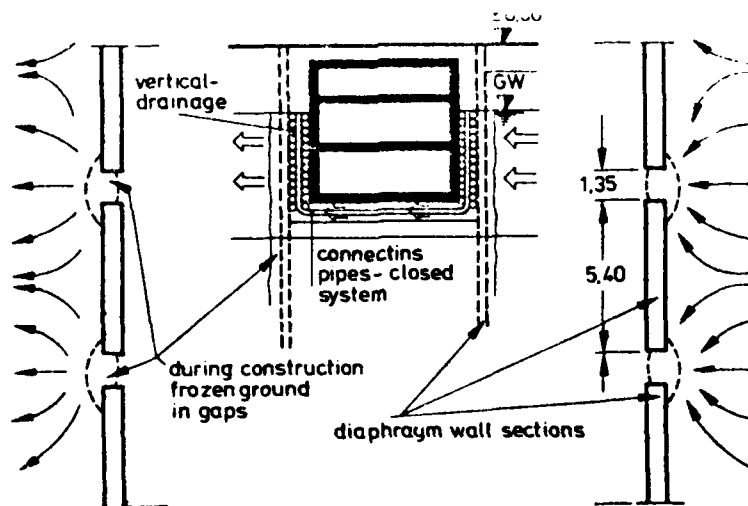
Figure 10: System of the Duisburg method
of Metro construction
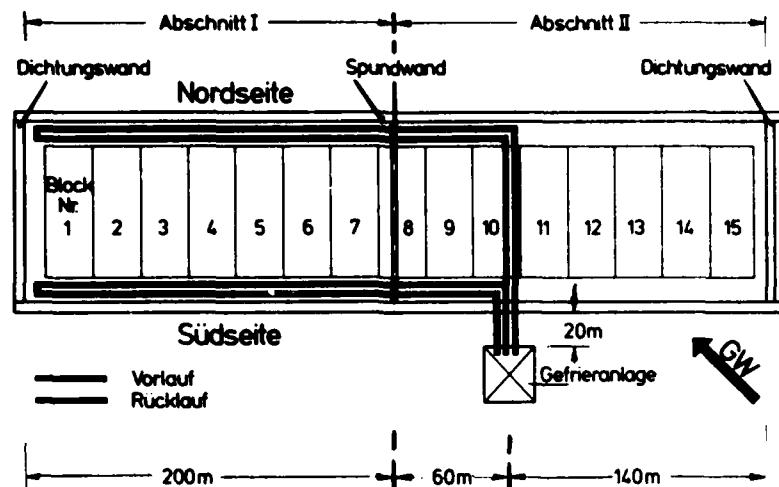
Figure 11: Dividing the contract into
2 sections (plan)

Valuing all results of the
various trials and investi-
gations carried out ahead it
was found that for reasons
of energy providing and cap-
city for the freezing plant
it would be more economically
considering the execution of
construction, to divide the
contract in 2 sections (Fig. 11)
which are to be executed one after
the other.

System of Gap Freezing

The freezing was in every
section carried out in 3
phases.
o Freezing of the gaps in the
  upstream side of the enclo-
  sure walls (south)
o Freezing of the gaps in the
  downstream side of the en-
  closure walls (north)
o Upkeeping the frostbodies
  during the time of excava-
  tion and construction
    For safety reasons in
the first section the free-
zing plant was run on full
output. As a consequence large
ice mountains (Fig. 12) developed
into the working space and were
difficult to remove.
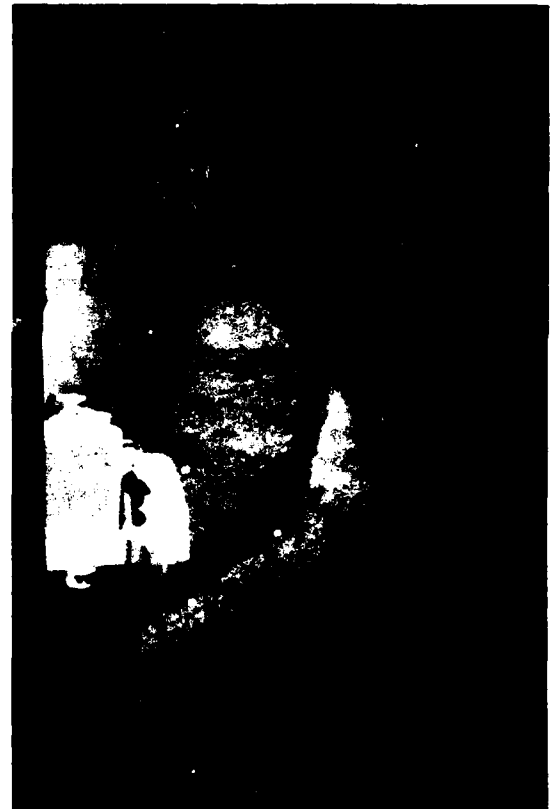
Figure 12: Ice mountains showing
the ground strata

200
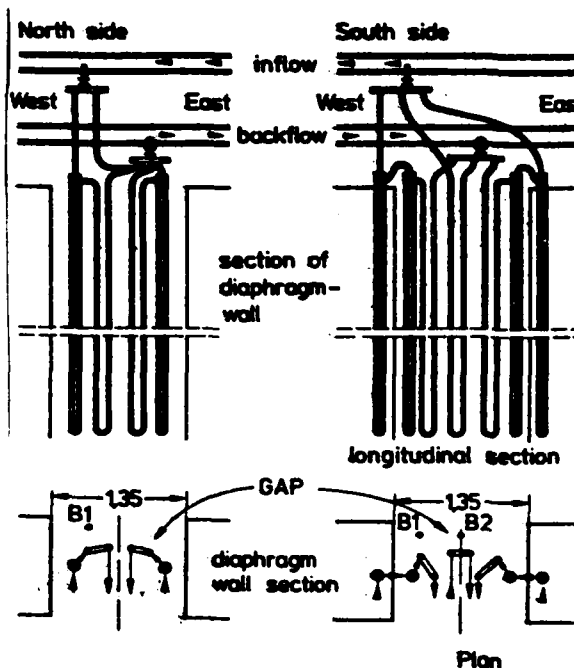
System of freezing pipes and
connection to the freezing plant

Figure 13: Freezing pipe
arrangements
(north + south
side)

The arrangement of the free-
zing pipes (Fig. 13) on north and
south side differed as follows:

o On the upstream side the
freezing cage consisted of
3 U-shaped pipes plus 2
double casing pipes per gap.
Additional were 2 double
casing pipes concreted into
the diaphragm wall sections
on each side of a gap.
o On the downstream side =
lee side of the groundwater
stream one U-shaped pipe
less and no double casing
pipes in the diaphragm wall
sections were installed.

All freezing pipe insta-
llations were assembled as
rigid cage construction which
were inserted into cased pile
bore holes of 110 respective-
ly 90 cm ∅.
This method assured that at
the necessary enormous depth's
of up to 35 m the diversions
were minimalized. When extrac-
ting the casings a 2/8 mm
graded aggregate with 25 %
voidage was back filled. This

vertically exchanged ground
enabled a rapid equalizing of
varying groundwater veloci-
ties and pressure heads in
the different strata levels
as well as guaranteeing homo-
geneous frost bodies having
through out the same heat
conductivity and excluding
the danger of leakages in the
coarse gravel layers and in
the silty patches. Additional
the high voidage resulted in
a strong sensibility
reacting to changes of tempe-
rature during the freezing.
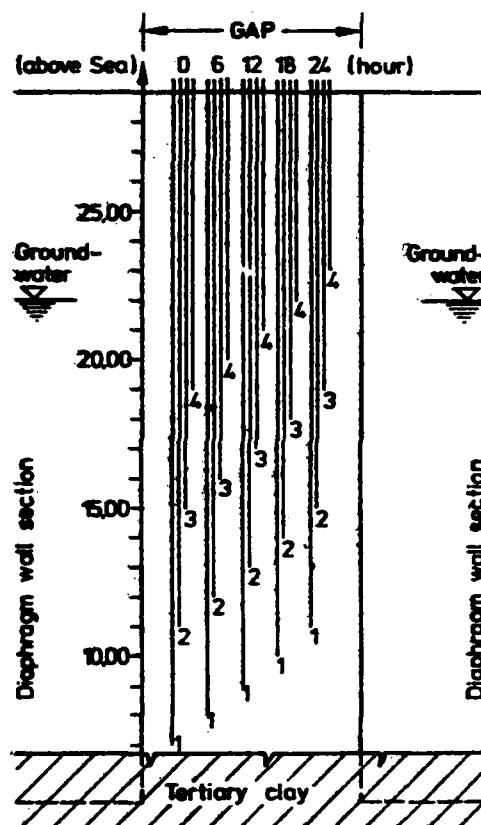
Figure 14: System of thermo
couples for esta-
blishing ground
temperatures over
the whole pipe
length

To be able to establish weak
spots in the frostbodies a
sophisticated temperature meas-
uring scheme (Fig. 14) was devised.

201

Main Features of the Construction Execution

1. Computations using F.E. methods and electromagnetic field plotters showed that a reduction of the groundwater flowing section by 80 % will result in an absolute increase of the groundwater level difference of approximetely 15 cm at tunnel width. Out of the view of environmental protection this value is quite acceptable.

2. The trial freezing showed that the main influence on freezability of a building ground, and the time needed for it, is the ratio (R/r) of freezing pipe centre distance versus freezing pipe diameter (Victor 1969) i. e. the quality of the pipe drilling. The results of the trial freezing led because of the bad ground conditions to the development of a freezing cage, which was inserted in a 110 cm Ø cased bore hole brought down into every gap.

   In order to improve the groundwater flow the cage was surrounded by 2-8 mm aggregate when extracting the casing. The cage features as further innovation, U-shaped freezing-pipes which are considerably cheaper than the conventional double casing type pipes.

3. In addition was on every side of the gap one (conventional) freezing pipe concreted into the diaphragm wall section on the downstream side, this proved very important, since gaps without them were much more difficult to freeze.

4. When calculati the freezing energy needed, it was obvious, that for economic reasons it was necessary to carry out the 400 m long contract in 2 sections. Since in the first stage for safety reasons

the plant was run to long on full output, the excavation of the lowest level proved difficult due to huge ice mountains.

5. The freezing plant consisted of 2 Sabroe aggregates of 2 514 000 K Joule/h output. The total installed electrical input was 1 200 KVA. Freezing media were for the circuits internal: Frigen-gas (CHF_2Cl) external: 30 % Calcium Chloride brine ($Ca\ Cl_2$)

6. The external brine circuit ended in an open tank to have immediate control on any losses, because brine of course will smelt an ice body. On the other hand it is completely harmless and no danger to the groundwater.

7. For the control of the temperature every freezing-pipe cage contained 2 temperature measuringpipes in which over 24 hours every m frostbody was once controlled.

8. For cases of emergency over the whole time of freezing an electric generator was kept on the site for the case of power failure. Additional it was possible to adapt all freezing pipes for freezing with fluid Nitrogene.
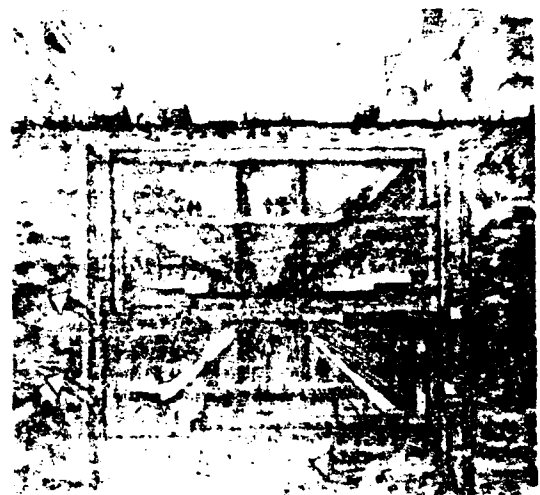
Figure 15: Functioning of the groundwaterflow after completion of the contract

CONCLUSION

The gap freezing has been a technical and economical success and proved to be a method compatible to the environment.

For future application of the method the following points should be considered:

1. The freezing pipe cage should receive a reinforced steel skeleton, because this will further the heat extraction considerably due to its good conductivity and accelerate the freezing process, respectively, allow freezing with higher flowing velocities.
2. Every gap should have on the brine intake line a calibrated valve installed. By an exact setting of the valves a simultaneous closing of all gaps at the same time could be achieved.
3. The temperature measuring should be monitored automaticly, even though the lifting and lowering of the thermocouples itself has to be done manual.
4. The frostbodies should have a thickness for a 72 hour power cut off safety. The plant should be run not to exceed this value.

All points mentioned under 1 to 4 will result in considerable energy saving.

REFERENCES

W. Braun: "The DUISBURG Method solves Ground-Water problems" Construction News, 3/79, London

W. Braun: "Frozen Panels Safeguard German Metro", International Construction 3/79, London

Drost, W., at all: "Isotopenmethoden in der Grundwasserkunde", Journal of Eurisotop 1972, H. 5.

Maidl, B.: "Untersuchung der Grundwasserströmung nach der Methode der Finite-Elemente mit dem Programm "GEOSICK", Ruhr-Universität Bochum 1977

Ständer, W.: "Ansätze zur Berechnung der Frostausbreitung in ruhendem Grundwasser. Inst. für Bodenmechanik der TH Karlsruhe,1967

Victor, H.: "Die Frostausbreitung beim künstlichen Gefrieren von Böden unter dem Einfluß von strömendem Grundwasser. Inst. für Bodenmechanik TH Karlsruhe,69

Weiler, A., Ulrichs, K.R.Nendza, H.:"Untersuchung über eine Bodengefrierung im stark durchströmten Untergrund. Die Bautechnik 53 (1976) H.7, S. 226 - 232".

Weiler, A. Wieczorek, H. Herzog, M.: "Bodengefrierung in Verbindung mit Schlitzwänden. Tiefbau-Berufsgenossenschaft 1978,H.10

Weiler, A.:"Erfahrungen mit der Baugrundvereisung. Die Bautechnik 56 (1979) H.6, S.181-187".

Weiler, A.: "Bodengefrierung beim Bau der Stadtbahn in Duisburg" Hochtief-Nachrichten 1979, H. 3.

Weiler, A.,Vagt, J.: Proceedings for the ECSMFE 1979 in Brighton, Volume 3, S. 299 - 305

Weiler, A., Willert, L., Berichte STUVA-Tagung München, 79

Weiler, A. Maidl, B.:"Erfahrungen mit der Lückenvereisung bei strömendem Grundwasser",Heft 8/79, 21 Jhrg., Tiefbau, Ingenieurbau, Straßenbau

Weiler, A., Müller, R.:"Bau der Stadtbahn in Duisburg, H.1 + 2/80 - Betonnachrichten

Weiler, A., Maidl, B.: "Erfahrungen mit der Lückenvereisung" Vortrag Baugrundtagung Berlin 78

Weiler, A.:"Erfahrungen mit der Baugrundvereisung am Beispiel der Duisburger Bauweise", Vortrag: Kontaktseminar, Ruhr-Universität Bochum, Februar 1978

Weiler, A.:"Neue Bauverfahren im grundwasserdurchströmten Untergrund beim Stadtbahnbau Duisburg" Geologisch-Lagerstättenkundliches Kolloquium RWTH Aachen 6.11.1980

Weiler, A.: "Tunnelbau in vom Grundwasser stark durchströmten Kies- und Sandböden der Rheinterrasse im Niederrheinischen Raum" Vortrag: Lehrstuhl Prof.Dr.Ing. Nendza, Gesamt-Univers.Essen,2/81

Weiler, A.,Vagt, J.: "Proceedings of the ISGF", Trondheim 80, P. 916 - 927

Weiler, A., Vagt,J.:"Tunnels and Tunnelling" 12/81, "Gap freezing solves groundwater problems" P. 31 - 34

Weiler, A.: Vortrag "Tunnelbau im stark durchströmten Untergrund" Düsseldorf "Tunnel 81"

Maidl,B., Einck,H.-B. "Ergänzende Untersuchungen zur Grundwasserströmungssituation Ruhr-Universität Bochum 1977

FREEZING OF SOIL WITH SURFACE CONVECTION

V.J. Lunardini, USACRREL

ABSTRACT

Phase change phenomena arise frequently in applications such as thermal design in permafrost regions, thermal storage of latent heat for solar systems, and the heat treatment of metals. These are problems of conductive heat transfer with solidification phase change. Exact solutions are sought for geometries and boundary conditions which are simple and yet representative of practical systems. Such solutions to this class of problems are limited to a few very special geometries and boundary conditions. One exact solution is that of Neumann for a constant surface temperature after a step change from the initial temperature. This widely used solution does not include convective heat transfer at the ground surface.

For freezing of ground masses the ambient temperature is often controlled rather than the ground surface temperature. An approximate solution for the surface convection ground freezing problem is derived and practical graphs are presented for the depth of freeze, with equations for surface temperature, and surface heat flux versus time.

INTRODUCTION

Problems of freezing and melting occur in permafrost or seasonal frost regions, thermal storage of latent heat, and metallurgy. One is interested in the penetration rate of the phase change interface, the temperature field, and the boundary heat transfer rates. From an engineering viewpoint, exact solutions are sought for geometries and boundary conditions which are representative of significant systems. Unfortunately the mathematical difficulties are such that exact solutions to this class of problems are limited to a few very special cases, Lunardini [10]. However, a number of approximate methods have been developed which can yield solutions acceptable for engineering design. This paper describes one of these approximations: the heat balance integral method.

The integral method has been used with good results for phase change problems; it involves the concept of the temperature penetration depth. Consider the semi-infinite solid shown in Fig. 1. At time t, after the surface temperature has jumped to T_s, the temperature will be disturbed to a depth $X(t) + \delta(t)$. Beyond this depth, the temperature of
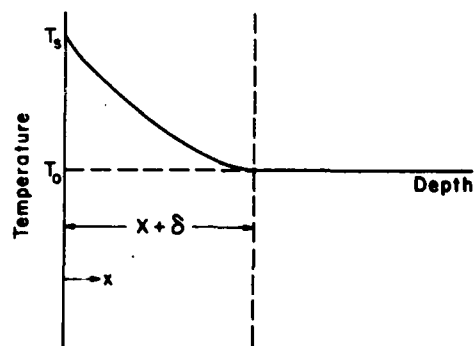
Fig. 1. Temperature penetration depth

205

the solid remains at the initial temperature T_o with no energy transfer. The penetration distance $X + \delta$ is analogous to the boundary layer thickness in fluid mechanics. The solution method is similar to the momentum integral method in that the basic equations are satisfied on average over the volume of thickness $X(t) + \delta(t)$. This avoids solving the partial differential equations at each point.

The conduction equation is

$$\alpha \frac{\partial^2 T}{\partial x^2} = \frac{\partial T}{\partial t} \tag{1}$$

Spatially integrate this equation over the distance $X(t) + \delta(t)$. Thus

$$\int_o^{X+\delta} \alpha \frac{\partial^2 T}{\partial x^2} dx = \int_o^{X+\delta} \frac{\partial T}{\partial t} dx \tag{2}$$

Using Leibniz's rule for a general function Eq (2) becomes the heat balance integral equation

$$\frac{d\xi}{dt} + \alpha \frac{\partial T(0,t)}{\partial x} - T_o \frac{d(X+\delta)}{dt} = 0 \tag{3}$$

where

$$\xi = \int_o^{X+\delta} T(x,t)dx \tag{4}$$

This equation is valid if there is no phase change. For phase change with different properties of the frozen and thawed regions there will be two integral equations as follows

$$\frac{d\xi_1}{dt} - T_f \frac{dX}{dt}$$

$$-\alpha_1 \left[\frac{\partial T_1(X,t)}{\partial x} - \frac{\partial T_1(0,t)}{\partial x} \right] = 0 \tag{5}$$

$$\frac{d\xi_2}{dt} - T_o \frac{d(X+\delta)}{dt} + T_f \frac{dX}{dt}$$

$$+ \alpha_2 \frac{\partial T_2(X,t)}{\partial x} = 0 \tag{6}$$

where

$$\xi_1 = \int_o^X T_1(x,t)dx$$

$$\xi_2 = \int_X^{X+\delta} T_2(x,t)dx$$

The energy balance at the phase change interface is

$$k_1 \frac{\partial T_1(X,t)}{\partial x} - k_2 \frac{\partial T_2(X,t)}{\partial x}$$

$$= -\rho_1 \ell \frac{dX}{dt} \tag{7}$$

The general problem with superheat or subcooling (the initial temperature is above or below the fusion value) will involve two coupled, non-linear differential equations, for the parameters X and δ. The solution will normally be difficult and often requires a starting solution for the singularity at the origin. However, if the initial temperature is T_f, then the problem reduces to only one equation, Eq (5), since the penetration distance $X+\delta$ is now identical to the phase change depth X.

The heat balance integral has been used extensively for single phase problems [1-6] and also for the much more complicated two phase problems [7,8].

SIMPLIFIED METHOD

The integral equations for two phase problems are usually coupled. A variation of the method can be used to find an explicit relation between δ and X. This will uncouple the equations and simplify the solution. If Eqs (5-7) are added together the result will be the overall energy balance.

$$\frac{d}{dt} [\rho_1 c_1 \xi_1 + \rho_2 c_2 \xi_2 + \rho_1 \ell X + (\rho_2 c_2 - \rho_1 c_1) T_f X$$

$$- \rho_2 c_2 T_o (X+\delta)] = - k_1 \frac{\partial T_1(0,t)}{dx} \tag{8}$$

The term $(\rho_2 c_2 - \rho_1 c_1) T_f \, dX/dt$, in Eq (8), is the net sensible flux of enthalpy at the phase change interface due to the sudden jump in the specific heats of the frozen and thawed volumes. This term was omitted in the study by Yuen [9], although his derivations implicitly assumed that $\rho_2 c_2 \equiv \rho_1 c_1$. The retention of this term gives better numerical comparisons to exact solutions.

Eq (7) can be rewritten as two collocation equations, see Lunardini [10].

$$- k_1 \frac{\partial T_1(X,t)}{\partial x} + k_2 \frac{\partial T_2(X,t)}{\partial x} =$$

$$- \rho_1 \ell \alpha_1 \frac{\partial^2 T_1(X,t)}{\partial x^2} \Big/ \frac{\partial T_1(X,t)}{\partial x} \tag{9}$$

$$-k_1 \frac{\partial T_1(X,t)}{\partial x} + k_2 \frac{\partial T_2(X,t)}{\partial x} =$$

$$-\rho_2 \ell \alpha_2 \frac{\partial^2 T_2(X,t)}{\partial x^2} \Big/ \frac{\partial T_2(X,t)}{\partial x} \qquad (10)$$

CONVECTIVE SURFACE HEAT FLUX

Heat flow from the environment, by convection, to a volume which is undergoing phase change is shown in Fig. 2, once thawing has started. This problem is physically more significant than the Neumann Problem since the ambient temperature and convective heat transfer are specified rather than the surface temperature. The surface boundary condition is

$$-k_1 \frac{\partial T_1(0,t)}{\partial x} = h[T_\infty - T_1(0,t)] \qquad (11)$$

For semi-infinite solids the following temperature approximations can be used.

$$T_1 = T_f + a_1(x - X) + a_2(x - X)^2 \qquad (12)$$

$$T_2 = T_f - 2 \frac{(T_f - T_o)}{\delta}(x-X)$$

$$+ \frac{(T_f - T_o)}{\delta^2}(x-X)^2 \qquad (13)$$

Eq (12), the temperature in the region which has changed phase, contains two unknown coefficients. These can be found from the boundary condition at $x = 0$ and Eqs (9, 10), giving

$$\frac{a_2}{a_1} = -\frac{\alpha_{21}}{2\delta} \qquad (14)$$

Ambient
T_∞
h
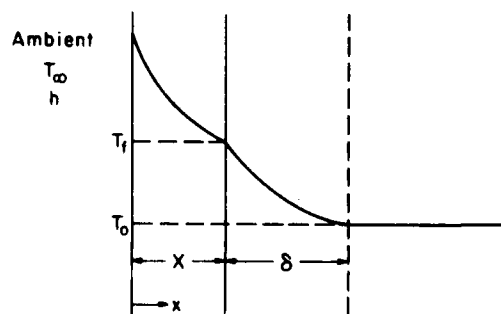
Fig. 2. Surface convection for a
semi-infinite body

$$a_1 = \frac{(T_f - T_\infty)}{X(1 + \frac{\alpha_{21}}{2\delta} X) + \frac{k_1}{h}(1 + \frac{\alpha_{21}}{\delta} X)}$$

Using Eq (13)

$$\phi = \frac{b(\sigma+1)}{2} +$$

$$\sqrt{\frac{b^2(\sigma+1)^2}{4} + \alpha_{21} \sigma (\frac{\sigma}{2} + 1)b} \qquad (15)$$

The energy balance equation, Eq (8), can now be written

$$\frac{dF}{d\tau} = \frac{2(\phi + \alpha_{21} \sigma)}{2\phi(\sigma + 1) + \alpha_{21}(\sigma + 2)} \qquad (16)$$

and

$$F = \frac{S_{Tm} \sigma^2(\phi + \frac{1}{3}\alpha_{21}\sigma)}{2\phi(\sigma + 1) + \alpha_{21}\sigma(\sigma + 2)}$$

$$+ \sigma(1 + c_{21}\theta_m) + \frac{1}{3} c_{21}\theta_m \phi \qquad (17)$$

There is no exact solution for comparison to Eq (16) but it can be shown that when $\theta_m = S_{Tm} = 0$ (single phase problem with latent heat predominating) Eq (16) can be solved as

$$\sigma = -1 + \sqrt{1 + 2\tau} \qquad (18)$$

This is the quasi-steady solution described by Lunardini [10]. The numerical solution to Eq (16), when $\theta_m = 0$, is identical to the heat balance integral solution of Goodman [2]. Lozano and Reemsten [17] derived an exact solution to the single phase problem. For the constant heat flux case it was shown that the exact solution is almost identical to the heat balance integral solution with small Stefan numbers [16]. Unfortunately the exact solution converges very slowly for large values of time and Stefan number and is inefficient for numerical computations. Cho and Sunderland [14] presented an approximate method to the single phase case which also agrees very well with Eq (16). They state that the zero-subcooling case is a good approximation to the subcooling problem, however, this is not true as the subcooling has a significant effect upon the rate of phase change.

The surface temperature is

$$\frac{T_1(0,t) - T_f}{T_\infty - T_f} = \frac{\sigma(2\phi + \alpha_{21}\sigma)}{\sigma(2\phi + \alpha_{21}\sigma) + 2(\phi + \alpha_{21}\sigma)} \quad (19)$$

The non-dimensional surface heat transfer rate is

$$q^* = \frac{(\phi + \alpha_{21}\sigma)}{\sigma(\phi + \frac{1}{2}\alpha_{21}\sigma) + (\phi + \alpha_{21}\sigma)} \quad (20)$$

Eq (16) can be solved by simple, numerical quadrature. Figs. 3-12 are plots of the solution for some values of Stefan number and θ_m, with property ratios given as functions of the volumetric water content for soil systems. The graphs are valid for a-1 soil types since only the frozen to thawed soil properties ratios are needed, Lundardini and Varotta [8]. The heat balance integral method yields solutions which compare quite well with exact solutions and the graphs presented here should be accurate for engineering estimates.
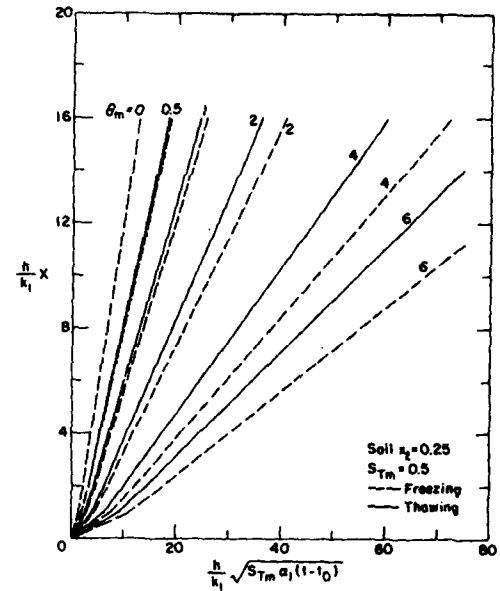
Fig. 4. Surface convection for soil, $x_\ell = .25$, $S_{Tm} = .5$.
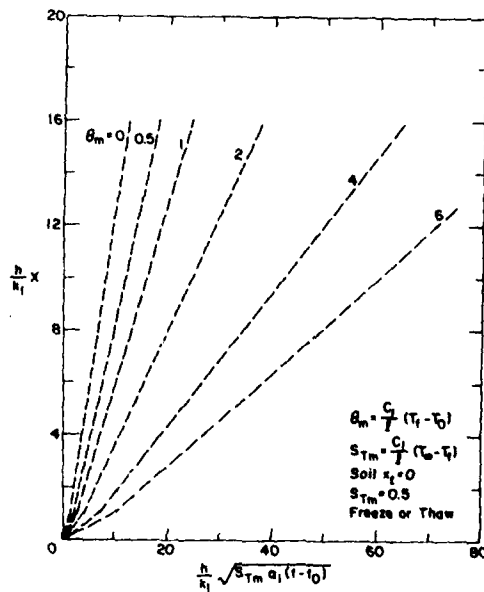
Fig. 3. Surface convection for soil, $s_\ell = 0$, $S_{Tm} = .5$
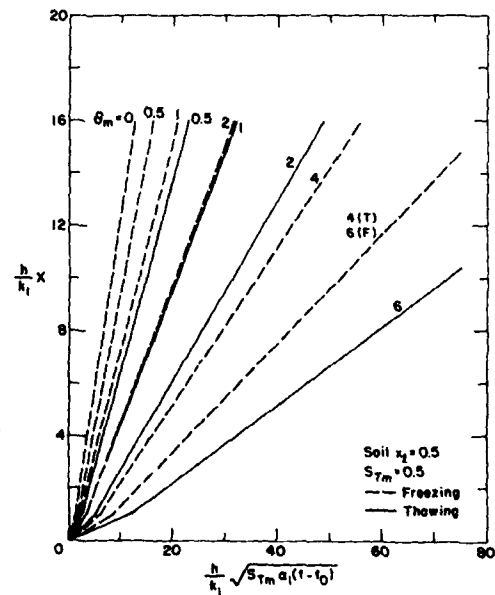
Fig. 5. Surface convection for soil, $x_\ell = .50$, $S_{Tm} = .5$
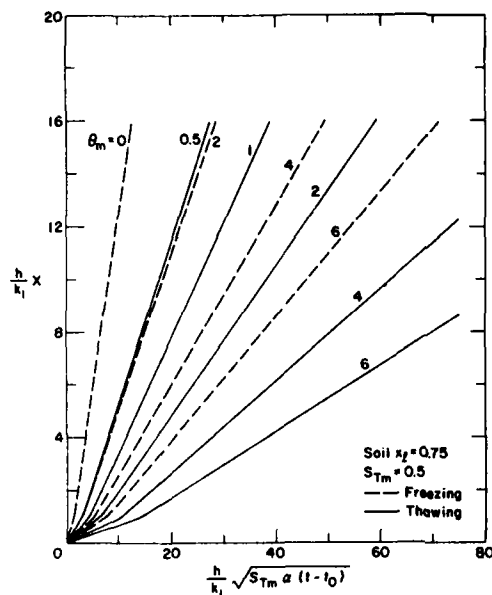
Fig. 6. Surface convection for soil,
x_ℓ = .75, S_{Tm} = .5
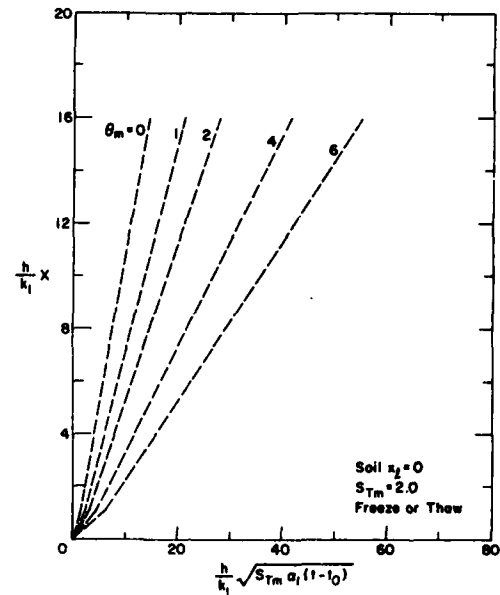
Fig. 8. Surface convection for soil,
x_ℓ = 0, S_{Tm} = 2.0
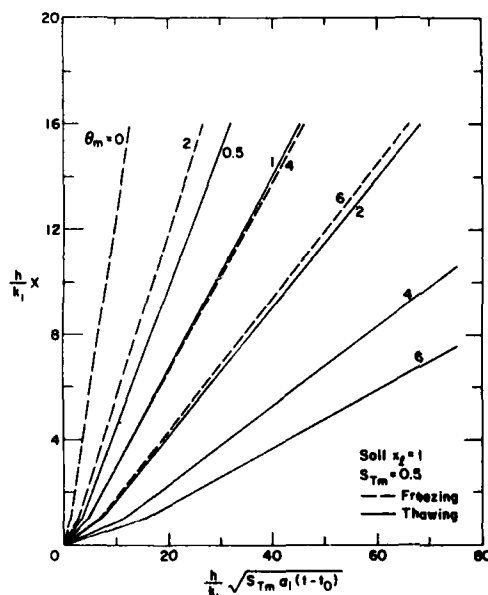
Fig. 7. Surface convection for soil,
x_ℓ = 1.0, S_{Tm} = .5
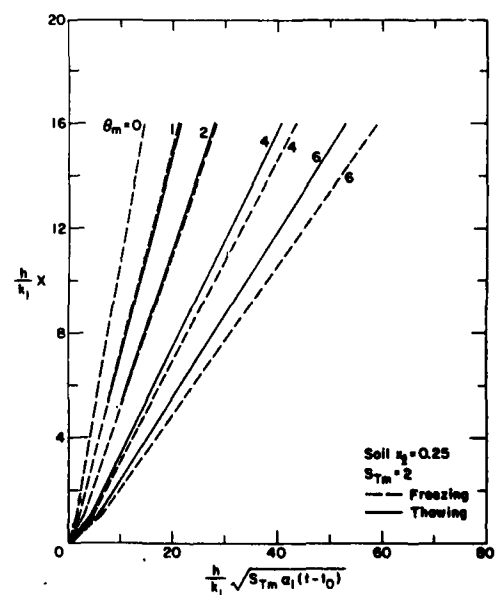
Fig. 9. Surface convection for soil,
x_ℓ = .25, S_{Tm} = 2.0

209
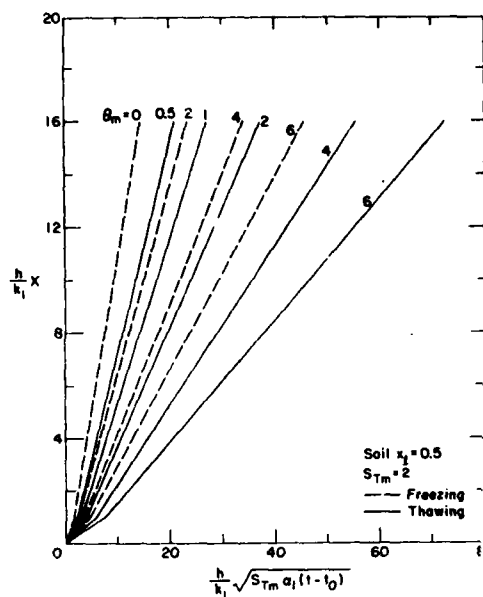
Fig. 10. Surface convection for soil,
x_ℓ = .50, S_{Tm} = 2.0
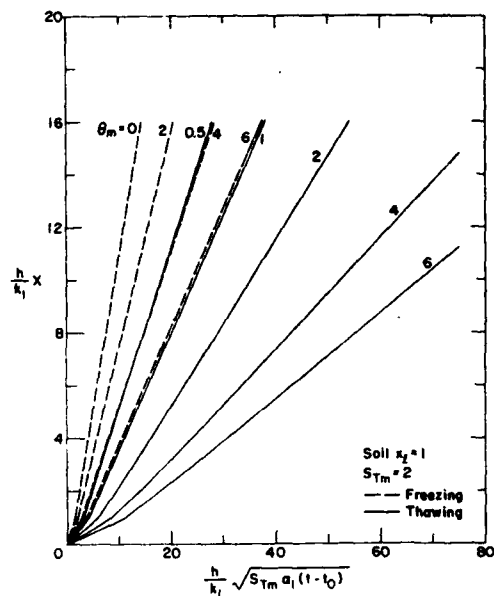
Fig. 12. Surface convection for soil,
x_ℓ = 1.0, S_{Tm} = 2.0
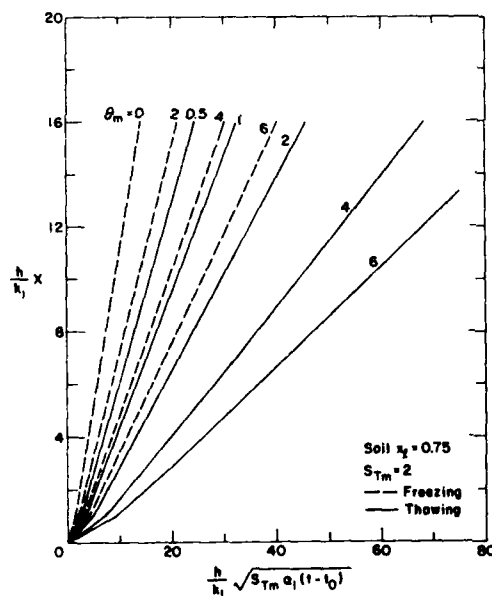
Fig. 11. Surface convection for soil,
x_ℓ = .75, S_{Tm} = 2.0

SURFACE COEFFICIENT OF CONVECTION

The proper choice of the surface coefficient of heat transfer, h, is difficult due to a lack of data. Convective heat transfer in the atmosphere is affected by both mechanical and thermal turbulence and the usual convective heat transfer correlations are of limited value since they are essentially for *neutral stability associated with a logarithmic velocity profile.* Deacon [13] has shown that the velocity profile deviates from the logarithmic form when the atmospheric stability is not neutral. The aerodynamic method, with an analogy between momentum and energy transfer, has been used to obtain relations for the surface coefficient of heat transfer, Lunardini [15, 16]. The velocity and temperature profiles are *assumed to be established horizontally.* The heat transfer coefficient is given by

$$\frac{h\rho_a^{-1}c_p^{-1}}{k_o^2 u_1} = \begin{cases} \left[\dfrac{1-\beta}{\left(\dfrac{z_1}{z_o}\right)^{1-\beta}-1} \right]^2 & \begin{array}{l}\text{stable}\\(\beta = .88)\end{array} \\[3em] \dfrac{1}{\ln^2\left(\dfrac{z_1}{z_o}\right)} & \begin{array}{l}\text{neutral}\\(\beta = 1.0)\end{array} \quad (21) \\[3em] \dfrac{2(1-\beta)^2}{\left[\left(\dfrac{z_1}{z_o}\right)^{1-\beta}-1\right]^2\left[\left(\dfrac{z_1}{z_o}\right)^{1-\beta}+1\right]} & \\[2em] & \begin{array}{l}\text{Unstable}\\(\beta=1.08)\end{array} \end{cases}$$

210

Eq. (21) relates the surface coefficient to the atmospheric stability, surface roughness, and wind speed. Values of the surface roughness are given in Lunardini [10].

EXAMPLE

Calculate the time required to freeze a one meter layer of soil with a convective boundary condition. Consider a fine grained soil with a density of 1670 kg/m^3 and a water content of 15%. The surface is smooth soil with z_0 = 10^{-4} m, wind speed of 4.83 m/s at 1.6 m above the surface, and a moderately unstable atmosphere with β = 1.08. The following properties will be used:

c_1 = 1015.2 J/kg K T_0 = 24.7°C
k_1 = 1.54 W/m K T_∞ = -24.7°C
α_1 = 8.92 x 10^{-7} m^2/s T_f = 0°C
$\rho\ell$ = 5.01 x 10^4 J/kg
h = 30.09 W/m^{2}K (From Eq. 21)

Then θ_m = S_{Tm} = 0.5, and σ = 20.0. Now x_ℓ = 0.25 and from Fig. 4, $\sqrt{\tau}$ = 23.12, thus the time to freeze the layer is t = 35.2 days. With a stable atmosphere h will be about one tenth that of the unstable atmosphere and the time for freeze will increase to 73 days.

Using the Neumann solution, with the surface temperature equal to the ambient temperature, the time required to freeze is 32.6 days. As the ratio of the convective resistance to the conductive resistance, h/k_1, increases the solution approaches that of the Neumann problem.

CONCLUSION

The heat balance integral method can be applied to conduction problems with phase change to obtain good, approximate, solutions. The method is particularly useful for soil systems since the nature of soil systems often precludes obtaining accurate data on the thermal properties.

The main value of the collocation method is that it provides an explicit relationship between the phase change depth and the temperature disturbance depth. This uncouples the system of differential equations for two phase problems and can lead to closed form solutions or to reduced numerical effort. The collocation solution of the Neumann Problem has been shown to be

quite accurate with a worst case accuracy of less than 15%, Lunardini [16]. For most soil systems the accuracy is within 5%.

Quantitative values have been obtained for the previously unsolved case of convection at the surface of an infinite medium. These results generalize the widely used Neumann solution and are applicable to the same physical situations with similar calculation effort.

The results only consider conductive heat transfer and should be considered first approximations if convection occurs.

REFERENCES

1. Goodman, T.R., 1964, "Application of Integral Methods to Transient Non-linear Heat Transfer," 52-122, Advances in Heat Transfer, Vol. 1, T.F. Irvine and J.P. Hartnet., Eds., Academic Press, New York.

2. Goodman, T.R., 1958, "The Heat Balance Integral and Its Application to Problems Involving a Change of Phase," ASME Transactions, 80, 335-342.

3. Goodman, T.R., and J.J. Shea, 1960, "The Melting of Finite Slabs," J. App. Mechanics, Vol. 27, Trans. ASME, 16-24.

4. Poots, G., 1962, "On the Application of Integral Methods to the Solution of Problems Involving the Solidification of Liquids Initially at Fusion Temperature," Int. J. Heat Mass Transfer, Vol. 5, 525-531.

5. Lardner, T.J., and F.V. Pohle, 1961, "Application of the Heat Balance Integral to Problems of Cylindrical Geometry," Trans., ASME Ser. E., Vol. 83, No. 2, 310-312.

6. Bell, G.E., 1978, "A Refinement of the Heat Balance Integral Method Applied to a Melting Problem," Int. J. Heat Mass Transfer, Vol. 21, 1357-1362.

7. Lunardini, V.J., 1980, "Phase Change Around a Circular Pipe," U.S. Army Cold Regions Research and Engineering Laboratory, CRREL Report 80-27, Hanover, N.H.

8. Lunardini, V.J., and R. Varotta, 1981, "Approximate Solution to Neumann Problem for Soils Systems," J. Energy Resources Technology, Vol. 103, No. 1, 76-81.

9. Yuen, W.W., 1980, "Application of the Heat Balance Integral to Melting Problems with Initial Subcooling,"

Int. J. Heat Mass Transfer, Vol. 23, 1157-1160.

10. Lunardini, V.J., 1981, "Heat Transfer in Cold Climates," Van Nostrand Reinhold, New York.

11. Neumann, F., c1860, Lectures given in 1860's, cf. Riemann-Weber, "Die partiellen Differentialgleichungen," Physik (edn. 5, 1912), Vol. 2, 121.

12. Kreith, F., and F.E. Romie, 1955, "A Study of the Thermal Diffusion Equation with Boundary Conditions Corresponding to Solidification or Melting of Materials Initially at the Fusion Temperature," Proceedings of Physical Society, Section B, 68, 277-291.

13. Deacon, E.L., 1949, "Vertical Diffusion in the Lowest Layer of the Atmosphere," Quart. J. Roy. Met. Soc., Vol. 75, 88-103.

14. Cho, S.H., and J.E. Sunderland, 1981, "Approximate Temperature Distribution for Phase Change of a Semi-Infinite Body," J. Heat Transfer, Vol. 103(2), p. 401-403.

15. Lunardini, V.J., 1979, "Sensible Heat Transfer in the Atmosphere," Proceedings of the Seventh Canadian Congress of Applied Mechanics, pp. 769-770.

16. Lunardini, V.J., 1982, "Application of the Heat Balance Integral to Conduction Phase Change Problems," U.S. CRREL Report 216, Hanover, New Hampshire.

17. Lozanc, C.J., and R. Reemsten, 1981, "On a Stefan Problem with an Emerging Free Boundary," Numerical Heat Transfer, Vol. 4, pp. 239-245.

Nomenclature

b	$= 2 k_{21}\theta_m + \alpha_{21} S_{Tm}$
c	– mass specific heat
c_p	– specific heat of atmosphere
c_{21}	$= c_2/c_1$
h	– surface coefficient of convection
k	– thermal conductivity
k_o	$= 0.4$ von Karman constant
k_{21}	$= k_2/k_1$
ℓ	– mass latent heat of fusion
q	– surface heat transfer rate per unit area
q^*	$= q(T_\infty - T_f)/h$
S_{Tm}	$= c_1(T_\infty - T_f)/\ell$, Stefan number
t	– time
t_o	– time at which phase change starts
T	– temperature
u_1	– wind speed at z_1
x	– cartesian coordinate
x_ℓ	– volumetric water content
X	– phase change depth

z_o	– surface roughness
z_1	– reference height of wind velocity
α	– thermal diffusivity
α_{21}	$= \alpha_2/\alpha_1$
β	$=$ atmospheric stability parameter
δ	– temperature penetration depth
θ_m	$= c_1(T_f - T_o)/\ell$
ξ	– integrated temperature
ρ	– density
σ	$= hX/k_1$
τ	$= h^2 (T_\infty - T_f)(t - t_o)/(\rho_1 k_1 \ell)$
ϕ	$= h\delta/k_1$

Subscripts

0	– initial value
$1,2$	– thawed and frozen regions, for thaw case
a	– atmosphere
f	– fusion value
∞	– ambient value

THERMAL MODELING OF FREEZE-THAW DEPTHS IN SOILS

Alfreds R. Jumikis,
Department of Civil and Environ-
  mental Engineering
Rutgers, The State University of
  New Jersey
P.O. Box 909, Piscataway,
New Jersey, 08854   USA

ABSTRACT

Good highway, airfield runway and other structures in cold climate require frost-proof designs although practice frequently falls short of this ideal. It is mainly for these reasons that engineers are now interested in calculations of freeze-thaw depths in soils.

Basically, all contemporary thermal calculations in permafrostology and cryogeotechnical engineering pertaining to freeze-thaw depths in soils are based on the well-known Saalschütz-Stefan formula (1856-1890). This formula, in its turn, is based on the classical Fourier's law (1824) of heat conduction.

nerally, complex thermophysical processes in soil which cannot be effectively studied theoretically, can be imitated by reduced or increased scale models.

This article presents a discussion on thermal modeling of freeze-thaw depth of the Saalschütz-Stefan formula.

The modeling shows that it is correct in model frost freezing tests to work with the same temperatures as they are to be expected in the in-situ prototype.

The time of duration for modeling should not be assumed arbitrarily, but should be derived from the model time scale.

Modeling renders reliable information that helps to evaluate the performance of the prototype, and adds a certainty to design which can never be obtained from mathematics alone. Modeling may warn against errors in prototype design.

In thermal modeling of artificial freezing soils systems there enters into calculations the diameter of the soil freezer pipe. Because usually the soil freezer (and thawing) pipe has an annular cross-section having an annular space between the inside and outside pipes, the so-called equivalent diameter should be figured out and used for the diameter in modeling of soil thermal systems where appropriate. The computation of the equivalent diameter is shown in this paper.

INTRODUCTION

As a result of cryogeotechnical activities in thermal soil mechanics, soil freezing and thawing problems are now being paid increased attention. Thermophysically, soil freezing and thawing are complex heat transfer processes. Mathematically, the thermal processes can be represented by Fourier's partial differential equation coupled with a set of initial and complex boundary conditions. Usually, integration of such Fourier equation in a general form for soil freezing or thawing is mathematically very involved and difficult. This is so because soil is not exactly a homogeneous, isotropic solid, but is a porous heterogeneous material, and that it is quite difficult to comprehend mathematically all thermophysical processes and associated factors that occur in a freezing or thawing soil system. Even if the solution to the heat conduction problem were known, the mathematics of its numerical evaluation is frequently bogged down

213

with burdensom impediments. This explains why, during the course of time, various assumptions for the approximation of a solution to a soil freezing-thawing problem were introduced, assumptions which oversimplify the actual thermal problem considerably.

THERMAL MODELING BY SIMILARITY

Soil freezing and thawing systems can also be studied by method of thermal modeling by similarity on either reduced or enlarged scale. The thermal modeling is an approach in which no simplifying assumptions need to be made.

In this article, the following basic thermal modeling scales are used (subscripts p and m mean prototype and model, respectively):

1) geometric or linear scale:
$L_p/L_m = \lambda$, where L is a linear dimension

2) time scale:
$$t_p/t_m = \tau,$$
where t = time

3) velocity scale:
$v_p/v_m = (L_p/t_p)(t_m/L_m) = \lambda/\tau;$
when $t_p = t_m$, then $\tau = 1$,
and $v_p/v_m = \lambda$

4) temperature scale:
$T_p/T_m = \Theta$
where T = temperature

METHOD OF ATTACK IN THERMAL MODELING

Because the Saalschütz-Stefan formula (1856;1890) is a special solution to the Fourier's general partial differential equation (1)

$$\frac{\partial T}{\partial t} = \alpha \cdot \frac{\partial^2 T}{\partial x^2} \qquad (1)$$

for one dimensional heat conduction in orthogonal coordinates (Refs. 3 and 7), the frost problem in soil may be modeled based on the Fourier's heat conduction equation (1) as set forth.

1. Mathematical Statement of Problem

a) $\frac{\partial T}{\partial t} = \alpha \cdot \frac{\partial^2 T}{\partial x^2}$

b) at $x = 0$, $T = T_s$

c) at $x = \xi$, $T = T_f = 0^oC$

d) continuity condition for heat flow (rate of freezing depth) through the frozen soil:

$$\frac{dx}{dt} = \frac{1}{Q_L} (K_f \cdot \frac{\partial T}{\partial x}) \qquad (2)$$

Equations (1) and (2) are good for the model as well as for its prototype. Here

T = variable temperature, ^oC

t = time

α = coefficient of thermal diffusivity, m^2/h

x = depth coordinate, m,

T_s = surface (microclimate) temperature, ^oC

ξ = frost penetration (= thickness of frozen soil), m

T_f = freezing temperature

Q_L = volumetric latent heat of fusion, $kcal/m^3$

$$Q_L = L \cdot w \cdot \gamma_{dry} = (80) \cdot w \cdot \gamma_{dry}$$

L = mass latent heat of fusion = 80 kcal/kg

w = moisture content of soil by dry weight,

γ_{dry} = dry unit weight of soil mineral particles, or skeleton, kg/m^3

$\frac{\partial T}{\partial x}$ = temperature gradient, $^oC/m$

$\frac{\partial^2 T}{\partial x^2}$ = change in temperature gradient, $^oC/m^2$

K_f = coefficient of thermal conductivity of frozen soil, $kcal/(m \cdot h \cdot ^oC)$

2. Basic Modeling Scales

$$\frac{L_p}{L_m} = \lambda; \quad \frac{K_{fp}}{K_{fm}} = \kappa; \quad \frac{T_p}{T_m} = \Theta; \quad \frac{t_p}{t_m} = \tau$$

Assume $Q_{L_p} = Q_{L_m}$. Then $\frac{Q_{L_p}}{Q_{L_m}} = 1.0$

3. Modeling

Now, by using the appropriate basic modeling scales λ, θ and τ, write Fourier's differential equation (1) for the prototype:

$$\frac{\partial T}{\partial t} \cdot \frac{\Theta}{\tau} = (\alpha_m) \cdot \left(\frac{\alpha_p}{\alpha_m}\right) \cdot \frac{\partial^2 T}{\partial x^2} \cdot \frac{\Theta}{\lambda^2} \quad (3)$$

This equation states that both processes, in the prototype and in its model, are thermally similar when

$$\frac{\Theta}{\tau} = \left(\frac{\alpha_p}{\alpha_m}\right) \cdot \frac{\Theta}{\lambda^2} \qquad (4)$$

From this equation, the modeling law is

$$\tau = \left(\frac{\alpha_m}{\alpha_p}\right) \cdot \lambda^2 \qquad (5)$$

Eq. (5) can be rewritten as

$$\frac{L_p^2}{(\alpha_p)(t_p)} = \frac{L_m^2}{(\alpha_m)(t_m)} = F_o, \qquad (6)$$

where F_o is the Fourier's coefficient (dimensionless, representing the well-known Fourier's thermal modeling law.)

If $\alpha_p = \alpha_m$, then Eq. (5) can be specialized as $\tau = \lambda^2$, $\qquad$ (7) i.e., the freezing time of the soil in the prototype is λ^2-times that of the soil freezing time in the model, i.e., $t_p = t_m \cdot \lambda^2$.

Notice from Eqs. (4), (5), and (7) that the temperature modeling scale θ vanished from the thermal similarity condition. Hence, modeling shows that it is correct in model freezing tests to experiment with the same temperatures as they are to be expected in the in-situ prototype.

Notice also from Eqs. (5), (6) and (7) that the time of duration for thermal modeling should not be assumed arbitrarily, but that it should be derived from the modeling time scale.

By means of Eqs. (5) and (6), the frost penetration depth ξ can be modeled:

$$\tau = \frac{t_p}{t_m} = \left(\frac{\alpha_m}{\alpha_p}\right) \cdot \lambda^2 = \left(\frac{\alpha_m}{\alpha_p}\right) \cdot \frac{L_p^2}{L_m^2} = \frac{\xi_p^2}{\xi_m^2} \qquad (8)$$

and

$$\xi_p = \xi_m \sqrt{\left(\frac{\alpha_p}{\alpha_m}\right)} \cdot \sqrt{\tau} \qquad (9)$$

If $\alpha_p = \alpha_m$, then

$$\xi_p = \xi_m \cdot \sqrt{\tau} \qquad (10)$$

i.e., the frost penetration depth ξ_p in the prototype soil is $\sqrt{\tau}$-times that in the model.

4. Modeling of Freeze-Thaw Depth by Means of Saalschütz-Stefan formula.

The freeze-thaw depth ξ in soil may be modeled by using the Saalschutz-Stefan (1856-1890) equation

$$\xi = \sqrt{\frac{2K_f \cdot |(T_f - T_s)| \cdot t}{Q_L}} = const. \sqrt{t} \qquad (11)$$

As mentioned before, the Saalschütz-Stefan formula (Eq.11) is a special solution to the Fourier's general partial differential equation, Eq.(1), for one-dimensional heat conduction in orthogonal coordinates.

If $K_{fp} = K_{fm}$; $Q_{L_p} = Q_{L_m}$; and if

one experiments with the same tempera-

tures as they occur in the nature (=prototype), then modeling of Eq.(11) results in

$$\xi \cdot \lambda = (const). \sqrt{t} \cdot \sqrt{\tau}, \qquad (12)$$

and

$$\tau = \lambda^2 \qquad (7)$$

which is the same result as obtained from modeling the Fourier's partial differential equation (see Eq.7). By means of Eq. (7), the frost penetration depth ξ_p can be modeled.

A NOTE ON THE EQUIVALENT DIAMETER OF SOIL FREEZER-PIPE USED IN THERMAL MODELING

Relative to pipes with an annular cross-section, Nusselt (1917) found that for pipe sections other than circular, the so-called equivalent diameter d_{eq} should be figured out and used for the diameter in calculations where appropriate.

The equivalent diameter d_{eq} calculates as

$$d_{eq} = \frac{4 \cdot A}{U} \quad [m] \qquad (13)$$

In this equation,
  A= area of the cross-section of the annulus, in m^2, and
  U= that part of the circumference of the outer pipe through which heat between the coolant and soil is exchanged, in m, (Jumikis, 1978, 1980).

For example, in a concentric, annular cross-section whose internal diameter of the outside pipe is D (pertaining to the heat transfer surface pipe-soil), and the outside diameter of the inner (feeder) pipe is d, the equivalent diameter d_{eq} calculates as

$$d_{eq} = \frac{4 \cdot A}{U} = \frac{4\pi(D^2 - d^2)}{4\pi D} = \frac{D^2 - d^2}{D} \quad [m] \qquad (14)$$

SUMMARY AND CONCLUSIONS

1. Basically, all contemporary thermal calculations in permafrostology and cryogeotechnical engineering pertaining to freeze-thaw depths in soils are based on the well-known Saalschütz-Stefan formula (2, 3, 4, 5). This formula, in its turn, is based on the classical Fourier's law of heat conduction (1, 3).

2. Generally, complex thermophysical processes in soil which cannot be effectively studied theoretically, can be imitated by reduced or increased scale models.

215

3. Thermal modeling sho... ...
is correct in model soil freezing tests
to work with the same temperatures as
they are to be expected in the in-situ
prototype.

4. The time of duration for modeling
should be complied with the model time
scale.

5. Thermal modeling is of great
value in exploring new processes; in
improving design and exploitation tech-
niques; in proving or disproving the
correctness of the assumptions made in
the analysis and design of the experi-
ment and prototype in situ, and in
warning against errors in prototype
design. Therefore, thermal modeling
is a useful, practical engineering
design tool.

REFERENCES

1. Fourier, J. B. J., 1824, "Theorie
du movement de la chaleur dans les corps
solides." Paris: Mémoires de
l'Académie Royale des Sciences de
l'Institut de France. Tome IV (for year
1819). Translated from the French by
A. Freeman, 1955, The Analytical Theory
of Heat. New York, N.Y.: Dover Publi-
cations, Inc.

2. Jumikis, A. R., 1966, Thermal Soil
Mechanics. New Brunswick, New Jersey:
Rutgers University Press, pp. 107-109.

3. Jumikis, A. R., 1977, Thermal Geo-
technics. New Brunswick, New Jersey:
Rutgers University Press, pp. 199-204.

4. Jumikis, A. R., 1978, "Some Aspects
of Artificial Thawing of Frozen Soils."
Proceedings of the International
Symposium on Ground Freezing, held
March 8-10, 1978, at the Ruhr Univer-
sity, Bochum, Germany, Vol. 1, pp.183-
192.

5. Jumikis, A. R., 1979, "Thermal
Modeling of Freezing Soil Systems."
Proceedings of the 2nd International
Symposium on Ground Freezing, held June
24-26, 1980, at the Norwegian Institute
of Technology, Trondheim, Norway, pp.
470-483.

6. Nusselt, W., 1917, "Der Warmeüber-
gang im Rohr." Zeitschrift des
Vereins deutscher Ingenieure - Z. VDI,
Vol. 61, 1917, pp. 685-689.

7. Saalschütz, L., 1856, "Über die
Wärmeveränderungen in den höheren
Erdschichten unter dem Einfluss des
nicht-periodischen Temperaturwechsels
an der Oberfläche." Astronomische
Nachrichten, Altona, 1856, Vol. 56.
No. 1321 - 1323, pp.   1 - 44
No. 1331 - 1333, pp. 161 - 206
No. 1338 - 1339, pp. 273 - 298

Stefan, J., 1890, "Über die Theorie
der Eisbildung im Polarmeere,"
Sitzungsberichte der mathematisch-
naturwissenschaftlichen Classe der
Kaiserlichen Academie der Wissenchaften,
Wien, 1890, Vol. 98, Sect. IIa, pp.965-
983.

APPLICATION OF TIME-DOMAIN REFLECTOMETRY
TO DETERMINE THE THICKNESS OF THE
FROZEN ZONE IN SOILS

T.H.W. Baker   Division of Building Research, National Research Council
                 of Canada, Ottawa, Ontario K1A OR6
J.L. Davis   Xadar Corporation, Springfield, Virginia 22151

ABSTRACT

Time-domain reflectometry (TDR) is an electromagnetic pulse technique that has been used to measure the dielectric constant of soils at frequencies between 1 MHz and 1 GHz. The dielectric constant of water is 40 times that of ice making it possible to delineate the frozen/unfrozen interface in soils. Results of laboratory experiments will be presented to show the application of this technique to determine the thickness of the frozen zone in coarse and fine-grained soils. The location of the freezing boundary using TDR will be compared with temperature measurements and interpretations from X-ray photographs.

STUDIES OF PERMAFROST GROWTH AT
AN ARCTIC DRAINED LAKE SITE

A. Judge   Earth Physics Branch, E.M.R., Canada
M. Burgess
A. Taylor
V. Allen

ABSTRACT

Illisarvik Lake on Richards Island, Mackenzie Delta, Canada, was artificially drained in order to investigate the growth of permafrost. Thirty-four boreholes were hydraulically drilled to depths ranging from 15 to 92 m below lake level and were instrumented with temperature cables. Monitoring of ground temperatures beneath the lake and surrounding shore-lines prior to drainage delineated a bow-shaped talik extending up to 32 m below lake bottom. Characteristics of the pre-drainage temperature profiles in the central lake holes were: 1) an upper unfrozen horizon in which temperatures reached a maximum of 2.5°C at roughly 5 m below lake bottom, 2) a permafrost table at depths of 20 to 32 m in the central part of the lake with consistently negative temperature below, 3) negative temperatures below the 5-m maximum temperature, averaging 50 mKm^{-1} in the permafrost section. Two years of post-drainage temperature monitoring revealed 4) that the former talik had completely frozen at near-shore sites (10 m thick of less), whereas 5) only 5 to 6 m of new perma-frost had formed at central sites, and 6) in the unfrozen sections temperatures were close to 0°C. A two-dimensional finite element computer simulation of the formation and growth of Illisarvik suggests a minimum lake age of 900 to 1000 years. Post-drainage conditions in the *first year after drainage were modeled* by studying the microclimatic regime together with the ground thermal regime. Although the predicted profiles agree reasonably well with measured temperatures, the analysis has indicated deficiencies in the observational programme which are now being partially rectified. Several of the instrumented drillholes have been equipped with data-loggers recording every four hours on magnetic tape to study the near-surface thermal regime and to establish precise surface boundary conditions. Automatic time-lapse cameras are being used to observe the pattern of snow cover and the behavior of the residual ponds on the drained lakebed. A geotechnical drill-ing programme to recover core mate-ial is planned for the spring of 1982.

Session III
FROST ACTION
Modeling, mechanism of heaving,
frost susceptibility tests and
heave pressures, and movements
due to frost action

INITIAL STAGE OF THE FORMATION
OF SOIL-LADEN ICE LENSES

Dr. Shunsuke Takagi, U.S. Army Cold
Regions Research and Engineering
Laboratory

ABSTRACT

O'Neill and Miller's equations for
frost heave in the saturated soil/water
system, presented in the 2nd I.S.G.F. at
Trondheim, reduce to heat conduction
equations on introduction of two simpli-
fying assumptions. The reduced equa-
tions are solved by use of the recently
developed analytical method that can
solve the Stefan problem with arbitrary
initial and boundary conditions.

The initial study of the solution
shows that both the lensing front and
the penetration front descend in propor-
tion to $\sqrt{t}$ but the ice lens rises in
proportion to t, at least for some time
after the start of the lensing. The
descent of the lensing front means that
soil particles are picked up during the
ice lens formation of soil-laden (dirty)
ice lenses, while the traditional ice
lenses are soil-free (clear).

Penner observes that the above
temporal relationships last much longer
than the initial stage. Computation of
the solution for a long time is now in
progress. It is hoped that the mathema-
tical basis of Penner's contention will
be disclosed.

INTRODUCTION

O'Neill and Miller [1] proposed a
mechanism of frost heave in saturated
soil/water systems. Their test case
solution, a finite-element simulation of
the evolution of a frost heave, is
plausible and looks like a replica of a
laboratory specimen. Moreover, it is
found that their formulation has the
potential capability of explaining most
of the empirical rules observable in a
saturated soil/water system. This
potential capability seems to have been
generated when Miller [2] added to the
thus-far-built body of the theory a new
element, i.e., the formulation (if
simplified) of the flux of the thermally
induced regelational flow of ice. The
objective of the current paper is to
present an indication of this potential
capability.

O'Neill and Miller's [1] equations
reduce to a type of heat conduction
equation on the introduction of the
following two assumptions: 1) densities
of water and ice are equal, and 2) the
ice content vs freezing temperature
curve [Fig. 1 in ref. 1] is composed of
rectilinear sections. The reduced heat
conduction equations are solved by use
of the recently developed analytical
method [Tao, 3] that can solve the
general type of Stefan problem (the
problem of heat conduction with phase
change) in one dimension with arbitrary
initial and boundary conditions.

Analysis of the problems show that
the frost-heaving soil column has two
internal boundaries, the penetration
front and the lensing front. Let x = 0
be the top of the soil column at time t
= 0. Assume that frost heave starts at
time t = 0 at x = 0. Let x = s(t),
p(t), and -h(t), where x is positive
downward, be the coordinates of, respec-
tively, the lensing front, the penetra-
tion front, and the top of the soil
column that is heaving. According to
the theory of the Stefan problem, they

223

are expressible in the series $\,\Gamma\,$

$$s(t) = s_0 \sqrt{t} + s_1 t + \ldots\ldots$$

$$p(t) = p_0 \sqrt{t} + p_1 t + \ldots\ldots \qquad (1)$$

$$h(t) = h_0 \sqrt{t} + h_1 t + \ldots\ldots$$

The solution of the initial stage shows that

$$h_0 = 0 \qquad (2)$$

but

$$p_0 > s_0 > 0. \qquad (3)$$

The region between the penetration front $p(t)$ and the lensing front $s(t)$ is the frozen fringe (the spreadout freezing zone) which descends with time. If the condition

$$h_1 > 0 \qquad (4)$$

is satisfied, the assumed frost heave can begin. In this analysis the temperature on the top $x = -h(t)$ is the step change applied at time $t = 0$.

The descent of the lensing front implies that soil particles are picked up during the formation of the ice lens. Therefore the ice lens formed by O'Neill and Miller's mechanism is soil-laden (dirty), while the ice lens in the traditional concept is soil-free (clear). The soil-laden ice lens has been experimentally observed many times but is formulated for the first time in this study.

Equations (2), (3), and (4) show that the intrusion of the freezing fronts in the saturated soil/water system is proportional to $\sqrt{t}$ but the heaving is proportional to t, at least soon after the initiation of ice lensing, when the step-change temperature is applied to the top of the soil column. Penner [4,5] observed that these temporal relationships held much longer than the initial stage under this loading condition. The usual experimental assumption, also adopted by him, that the freezing front is simply the 0°C isotherm does not matter to our interpretation of his data. Study of the coefficients in the series in (1) that are higher than those included in (3) and (4) is now in progress. It is hoped that this study will disclose the analytical basis of Penner's contention.

The reason that (2) must come about is that, if $h_0 \neq 0$, the flux $v(t)$ of the water in the unfrozen region, which

is equal to $-dh/dt$ on the equidensity assumption, is infinite at $t = 0$. In addition, the flux $v(t)$ in the unfrozen region is constant with regard to the space coordinate because the water fills the pores that are assumed to be rigid. It is impossible to create a flow satisfying these conditions.

The theory of the Stefan problem shows that the temperature T^{lns} at the lensing front is expressible in a series of $\sqrt{t}$

$$T^{lns} = T_0^{lns} + T_1^{lns} \sqrt{t} + \ldots \qquad (5)$$

It will be seen that T_0^{lns} is formulated by use of the condition $h_0 = 0$.

Mere mathematical processes are not presented in this paper. Therefore, presentation is not made of the derivation of p_0 and s_0, which are the roots of the simultaneous transcendental equations characteristic of a Stefan problem. The derivation of p_0 and s_0 will be included in a future paper dealing with the evolution of soil-laden ice lenses.

O'NEILL AND MILLER'S EQUATIONS

O'Neill and Miller's differential equations apply to the frozen fringe. (Actually they apply to the unfrozen region and the ice lens also. But, if these applications are discussed, a lot of trivial explanations, which are completely avoided in this presentation, would necessarily be added.) They consist of the conservation of mass

$$\frac{\partial}{\partial t}\left(\rho \theta + \rho_i \theta_i\right) + \frac{\partial}{\partial x}\left(\rho v + \rho_i v_i\right) = 0 \qquad (6)$$

and the conservation of energy

$$\sum (\rho c \theta)_n \frac{\partial T}{\partial t} - \frac{\partial}{\partial x}\left(K_h \frac{\partial T}{\partial x}\right)$$

$$- \rho_i L\left(\frac{\partial \theta_i}{\partial t} + v_I \frac{\partial \theta_i}{\partial x}\right) = 0 . \qquad (7)$$

In (6), ρ and ρ_i are the densities of water and ice, θ and θ_i the volumetric contents of water and ice, v and v_i the fluxes of water flow and (thermally induced regelational [Miller, 2]) ice flow. v, v_i, and x are defined to be positive downward. In (7), T is the temperature on the Celsius scale (in conformity with the usage in the extended Clapeyron relation by Miller and Koslow [6]) v_I is the flux of the flow

of ice in the ice lens (defined to be positive downward) that is equal to the rate of the rise of the ice lens, which in our notation is

$$V_I = -\overset{\bullet}{h} \, , \qquad (8)$$

and $\sum(\rho c \theta)_n$ (which is henceforth replaced with R) is

$$R = \rho c \theta + \rho_i c_i \theta_i + \rho_s c_s \theta_s \, , \qquad (9)$$

where c, c_i, and c_s are the specific heats of water, ice, and soil, and ρ_s and θ_s the density and volume content of soil, respectively. K_h and R are assumed to be constant, even though the content of pore ice is variable. ρ_s and θ_s are constant in space and time. The relation

$$\theta + \theta_i + \theta_s = 1 \qquad (10)$$

holds. For a simple treatment, the regelational ice flow [Miller, 2] is assumed to be uniform in the region occupied by the pore ice,

$$v_i = \theta_i V_I \, . \qquad (11)$$

The mass balance at the lensing front shows that the equation

$$\rho_i V_I = \rho_i v_i + \rho v \qquad (12)$$

holds at $x = s(t)$.

Formulation of (6) is readily understandable, but formulation of (7) needs an explanation, which, however, is not given in ref. 1. To derive (7) let h, h_i, and h_s be the specific enthalpies of water, ice, and soil, respectively, given by

$$\begin{aligned} h &= cT + L \\ h_i &= c_i T \\ h_s &= c_s T \, . \end{aligned} \qquad (13)$$

Note that L is on the right-hand side of $(13)_1$. Substitution of the equations in (13) into the total heat content in unit volume

$$H = \rho \theta h + \rho_i \theta_i h_i + \rho_s \theta_s h_s$$

transforms it to

$$H = RT + \rho \theta L \, . \qquad (14)$$

Let q and r be the conductive and convective heat flows, both defined to be positive downward, given by

$$q = -K_h(\partial T / \partial x) \qquad (15)$$

and

$$r = (\rho c v + \rho_i c_i v_i)T + \rho L v. \qquad (16)$$

The conservation of energy is expressed by

$$\frac{\partial H}{\partial t} + \frac{\partial q}{\partial x} + \frac{\partial r}{\partial x} = 0 \, ,$$

which becomes (7) on substitution of (14), (9), (15) and (16), using (6) and (11), and neglecting numerically trivial terms.

SIMPLIFYING ASSUMPTIONS

Two assumptions are introduced: the equidensity assumption,

$$\rho = \rho_i \qquad (17)$$

and the assumption of the sectional linearity of the ice content vs freezing temperature curve.

The equidensity assumption decomposes equation (6) into two equations

$$\begin{aligned} \theta + \theta_i &= \theta_o \\ v + v_i &= V_I(t) \, . \end{aligned} \qquad (18)$$

Reference to (10) shows that θ_o in $(18)_1$ is constant in space and time. Reference to (12) shows that $(18)_2$ is correct, where $V_I(t)$ is a function of t only. Moreover the equidensity assumption reduces the extended form of the Clapeyron equation [(2) in ref. 6] to

$$u - u_i = L\rho T/T_k, \qquad (19)$$

where u and u_i are the pressures of water and ice, respectively, and $T_k = 273$. Finally the equidensity assumption reduces equation (3) in ref. 6 to

$$\psi = BT \, ,$$

Where B is a constant. By this equation, Fig. 1 in ref. 1 becomes simply the ice content (θ_i) vs freezing temperature $(T^\circ C)$ curve.

Taking the simplest case of the sectional linearity, we assume the single ramp formulation (Fig. 1),
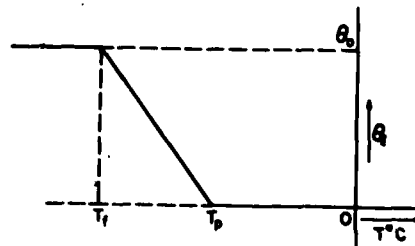
Figure 1. Single-ramp formulation of the ice content (θ_i) vs freezing temperature $(T^\circ C)$ curve.

$$\theta_i = 0 \qquad \text{for} \quad T > T_p$$

$$= \alpha(T_p - T) \qquad \text{for} \quad T_p > T > T_f \qquad (20)$$

$$= \theta_o \qquad \text{for} \quad T_f > T ,$$

where α, T_p, T_f are constants such that

$$\theta_o = \alpha(T_p - T_f) . \qquad (21)$$

T_p is the temperature at the penetration front and T_f is such that at temperatures lower than T_f the pore and film waters are all frozen. Use of $(20)_2$ and (8) reduce (7) to

$$(R + \rho L \alpha)\frac{\partial T}{\partial t} = \rho L \alpha \, \dot{h} \, \frac{\partial T}{\partial x} -$$

$$- \frac{\partial}{\partial x}\left(K_h \frac{\partial T}{\partial x}\right) = 0 . \qquad (22)$$

The flow of liquid water determined in the frozen fringe and the unfrozen region by these equations is along the gradient of temperature. The flow of liquid water against the gradient of temperature that may occur prior to lensing (recognized as the expulsion of liquid water that may occur at the beginning of a freezing experiment) is the effect of the unequal densities and is not included in this paper.

HEAT CONDUCTION EQUATIONS

Suppose that a soil column, composed of a uniform soil, saturated with water, and at constant temperature $T_\infty > 0°C$, extends downward from the surface $x = 0$ to $x = \infty$. At time $t = 0$, the surface temperature at $x = 0$ is suddenly cooled to $T_0 < 0°C$, and is kept at this constant value for $t > 0$. It is assumed that frost heave starts at time $t = 0$ at $x = 0$. For time $t > 0$, the surface rises to $x = -h(t)$, and the lensing front and the penetration front descend to $x = s(t)$ and $p(t)$, respectively (see Fig. 2).

The temperature T_i in the ice lens that is rising at the velocity $-\dot{h}$ is governed by the equation

$$\frac{\partial T_i}{\partial t} - \dot{h} \, \frac{\partial T_i}{\partial x} = \kappa_i \, \frac{\partial^2 T_i}{\partial x^2} , \qquad (23)$$

where κ_i is the thermal conductivity of the ice lens. Transformation of the x coordinate to the y coordinate,
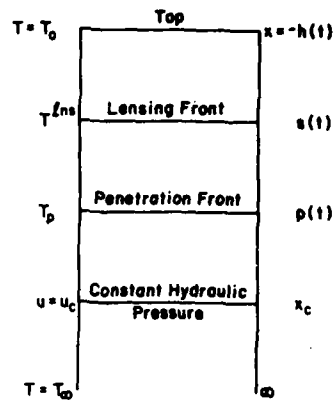
Figure 2. The frost-heaving soil column at time t.

$$y = x + h(t) \qquad (24)$$

whose origin is at the top of the rising ice lens, changes (23) to

$$\frac{\partial T_i}{\partial t} = \kappa_i \, \frac{\partial^2 T_i}{\partial y^2} . \qquad (25)$$

The temperature T_α in the frozen fringe is governed by (22), which becomes

$$\frac{\partial T_\alpha}{\partial t} - \mu \dot{h} \, \frac{\partial T_\alpha}{\partial x} = \kappa_\alpha \, \frac{\partial^2 T_\alpha}{\partial x^2} , \qquad (26)$$

where

$$\mu = \rho L \alpha/(R + \rho L \alpha),$$

$$\kappa_\alpha = K_h/(R + \rho L \alpha) . \qquad (27)$$

Transformation of the x coordinate to the z coordinate,

$$z = x + \mu h(t) \qquad (28)$$

changes (26) to

$$\frac{\partial T_\alpha}{\partial t} = \kappa_\alpha \, \frac{\partial^2 T_\alpha}{\partial z^2} . \qquad (29)$$

The temperature T_u in the unfrozen region is governed by the equation

$$\frac{\partial T_u}{\partial t} = \kappa_u \, \frac{\partial^2 T_\alpha}{\partial x^2} , \qquad (30)$$

where κ_u is the thermal diffusivity of

226

the unfrozen soil saturated with water. Thus, the temperature distributions in the three regions are all reduced to the standard form of the heat conduction equations.

GENERAL SOLUTION OF THE STEFAN PROBLEM

Protnov [7] noticed that the standard form of the heat conduction equation

$$\frac{\partial T}{\partial t} = \kappa \frac{\partial^2 T}{\partial x^2} \qquad (31)$$

yields the general solution

$$T(x,t) = \sum_{n=o}^{\infty} \left(\sqrt{4\kappa t}\right)^n \left\{ A_n G_n \left(\frac{x}{\sqrt{4\kappa t}}\right) + B_n i^n erfc \frac{x}{\sqrt{4\kappa t}} \right\} \qquad (32)$$

(which is written here with Tao's [3] notation), where G_n ( ) is a polynomial and $i^n erfc$( ) a repeated integral of the error function. Takagi [8] indicated the potential applicability of this formula to the frost heave problems, and Tao [3] resolved a difficulty that had still persisted in this approach.

Theoretically, a problem of heat conduction with boundaries moving in the form of (1) is solvable by use of (32). The difficulty that still persisted in this approach is the determination of the coefficients in the series in (1), (5) and (32) by use of the initial and boundary conditions. The determination needs a formula giving the expansion of a function of a function f(g(x)) into a power series of x. Tao [3] found the formula for the expansion in an old book of statistics. The formula is so complicated that it probably was useless before the dawn of the computer age. It is now practicable to substitute x in (32) with a series of (1) and expand it into a series of $\sqrt{t}$ so that the constants in the series in (1), (5) and (32) may be determined by use of the initial and boundary conditions.

In this paper only the n = 0 term in series (32),

$$T(x,t) = A_o + B_o \, erfc \left(x/\sqrt{4\kappa t} \right) , \qquad (33)$$

is used. The constants associated with the n = 0 terms, i.e., s_o, P_o, h_o,

h_1, and $T_o^{\ell ns}$, are determined without use of the formula for expanding f(g(x)), rediscovered by Tao [3]. The limit of the derivative $\partial f(x,t)/\partial x$ of a function f(x,t) on a boundry as time t approaches zero will be computed after multiplying $\sqrt{t}$. This limit will be henceforth called the $\sqrt{t}$ limit. For example, by use of (33), one finds that the $\sqrt{t}$ limit of the temperature gradient at x = s(t) on the side of the frozen fringe is given by

$$\lim_{t \to 0} \sqrt{t} \left. \frac{\partial T_\alpha}{\partial x} \right|_{x=s(t)} = - \frac{1}{\sqrt{\pi \kappa_\alpha}} B_o^* \, * \exp\left[- \left[\frac{(s_o + \mu h_o)^2}{4\kappa_\alpha} \right] \right] . \qquad (34)$$

DETERMINATION OF h_o

In the unfrozen region, which is saturated with water, the flux of pore water v is a function of time only, equal to $-\dot{h}$, i.e.,

$$v(t) = -\dot{h} . \qquad (35)$$

Then, reference to (1)$_3$ shows that h_o must be equal to zero,

$$h_o = 0, \qquad (36)$$

because if $h_o \neq 0$, the flux at t = 0 is infinite throughout the unfrozen region.

CONDITIONS FOR LENSING

The concept of neutral pressure in soil mechanics was extended to the freezing saturated soil/water system by Miller and Koslow [6]. The neutral pressure σ_{ntr} is formulated by

$$\sigma_{ntr} = \chi u + (1-\chi) u_i , \qquad (37)$$

where χ is a stress partition function. O'Neill and Miller [1] use

$$\chi = \left(1 - \theta_i/\theta_o \right)^{2/2} . \qquad (38)$$

The condition for lensing [Miller, 2] is that σ_{ntr} reaches the maximum P at the lensing front,

$$\sigma_{ntr} = P$$

$$\frac{\partial \sigma_{ntr}}{\partial x} = 0 \qquad \text{at } x = s(t), \qquad (39)$$

where P is the total load working on the plane of lensing.

EQUATIONS OF THE FLOW OF UNFROZEN WATER

It will be shown that conditions $(39)_1$ and $(39)_2$ determine the pressure distribution and the pressure gradient of the unfrozen water at the lensing front. For simple treatment, we define

$$Q = 1 - \theta_1/\theta_0 . \qquad (40)$$

Substituting θ_1 from $(20)_2$, we find the functional form of Q in the unfrozen region,

$$Q(x,t) = 1 - (\alpha/\theta_0)\left(T_p - T_\alpha(x,t)\right). \qquad (41)$$

Then χ in (38) is formulated,

$$\chi = Q(x,t)^{3/2} . \qquad (42)$$

Eliminating u_1 in (37) by use of (19), we find the distribution of the hydraulic pressure in the frozen fringe,

$$u(x,t) = \sigma_{ntr} + (L\rho/T_k)\left[1 - Q(x,t)^{3/2}\right] *$$
$$* \; T_\alpha(x,t). \qquad (43)$$

Substituting σ_{ntr} from $(39)_1$, $u(s,0)$, the pressure of liquid water at the lensing front at the time of lens initiation is found,

$$u(s,0) = P + (L\rho/T_k)(1 - Q_0^{3/2})T_0^{\ell ns} \qquad (44)$$

where Q_0 stands for

$$Q_0 = 1 - (\alpha/\theta_0)\left(T_p - T_0^{\ell ns}\right). \qquad (45)$$

The $\sqrt{t}$ limit of the hydraulic gradient at the lensing front is calculated by use of (43) and $(39)_2$

$$\lim_{t \to 0}\sqrt{t}\;\frac{\partial u}{\partial x}\bigg|_{x=s(t)} = \frac{L\rho}{T_k}\;(1 - Q_0^{3/2} -$$

$$- \frac{3\alpha}{2\theta_0}\; Q_0^{1/2}\; T_0^{\ell ns}\,)\lim_{t \to 0}\sqrt{t}\;\frac{\partial T_\alpha}{\partial x}\bigg|_{x=s(t)} . \qquad (46)$$

The flux $v(x,t)$ of the liquid water in the frozen fringe will be formulated by use of $(18)_2$. Substituting (8), (11), and $(20)_2$ into $(18)_2$, and employing the notation T_α in (26), it is given by

$$v(x,t) = - \dot{h}\left[1 - \alpha T_p + \alpha\, T_\alpha(x,t)\right]. \qquad (47)$$

On the other hand, equation (23) in ref. 1 gives the hydraulic conductivity for the unfrozen water flow in the frozen fringe, use of which yields

$$v(x,t) = - k(0)\; Q(x,t)^7 (\partial u/\partial x), \qquad (48)$$

where $k(0)$ is the hydraulic conductivity in the unfrozen region. Equating (47) with (48), the gradient of the unfrozen water in the frozen fringe is formulated,

$$\frac{\partial u}{\partial z} = \frac{1}{k(0)}\; \dot{h}\; Q(x,t)^{-7}\left[1 - \alpha T_p + \right.$$

$$\left. \alpha\, T_\alpha(x,t)\right] \qquad (49)$$

where

$$s(t) \le x \le p(t). \qquad (50)$$

The above equation yields that

$$\lim_{t \to 0}\sqrt{t}\;\frac{\partial u}{\partial x}\bigg|_{x=s(t)} = 0 , \qquad (51)$$

because the left hand side is, by (49), proportional to h_0, which is equal to zero by (36).

FORMULATION OF $T_0^{\ell ns}$

Comparison of (51) with (46) shows that the equation

$$1 - Q_0^{3/2} - (3\alpha/2\theta_0)\; Q_0^{1/2}\; T_0^{\ell ns} = 0$$

must hold at the lensing front. Multiplying by $Q_0^{-1/2}$ and substituting (45) the above equation transforms to

$$1 - (\alpha/\theta_0)\; T_p + (5\alpha/2\theta_0)\; T_0^{\ell ns} = Q_0^{-1/2}.$$

Squaring this equation and multiplying by Q_0 produces the equation for determination of $T_0^{\ell ns}$,

$$\left(1 - \frac{\alpha}{\theta_o} T_p + \frac{5\alpha}{2\theta_o} T_o^{lns}\right)^2 *$$

$$* \left(1 - \frac{\alpha}{\theta_o} T_p + \frac{\alpha}{\theta_o} T_o^{lns}\right) = 1 .$$

Letting

$$\left(\alpha/\theta_o\right) T_o^{lns} = \tau$$

$$1 - \left(\alpha/\theta_o\right) T_p = \lambda , \qquad (52)$$

the equation for T_o^{lns} transforms to the equation for τ,

$$\left[\lambda + (5/2)\tau\right]^2 (\lambda + \tau) = 1.$$

Use of the unknown x, defined by

$$5\tau = \lambda(x-3), \qquad (53)$$

transforms the equation for τ to the cubic equation of x,

$$x^3 - 3x + 2 - 20 \lambda^{-3} = 0 \qquad (54)$$

To survey the range of the roots of (54), the graph of the inverse of (54),

$$\lambda^3 = 20(x-1)^{-2}(x+2)^{-1} \qquad (55)$$

is useful. As shown in Fig. 3, there are three real roots in the range $\lambda^3 > 5$ and one real root in the range $\lambda^3 < 5$. Let ϕ be defined in the domain

$$0 \le \phi \le \pi \qquad (56)$$

by

$$\tan\phi = \left[20(\lambda^3 - 5)\right]^{1/2}/(10 - \lambda^3). \qquad (57)$$

Then, the three real roots are

$$x_1 = 2 \cos(\phi/3) \quad \text{for } 1 \le x_1 \le 2$$

$$x_2 = - \cos(\phi/3) + \sqrt{3} \sin(\phi/3) \qquad (58)$$
$$\text{for } 1 \le x_1 \le 2$$

$$x_3 = - \cos(\phi/3) - \sqrt{3} \sin(\phi/3)$$
$$\text{for } -2 \le x_3 \le -1.$$

The inverse of (57) is

$$\lambda^3 = 5 \sec^2(\phi/2)$$

in the domain (56).

Eliminating τ and α/θ_o from $(52)_1$, $(52)_2$, and $(53)_3$, we find
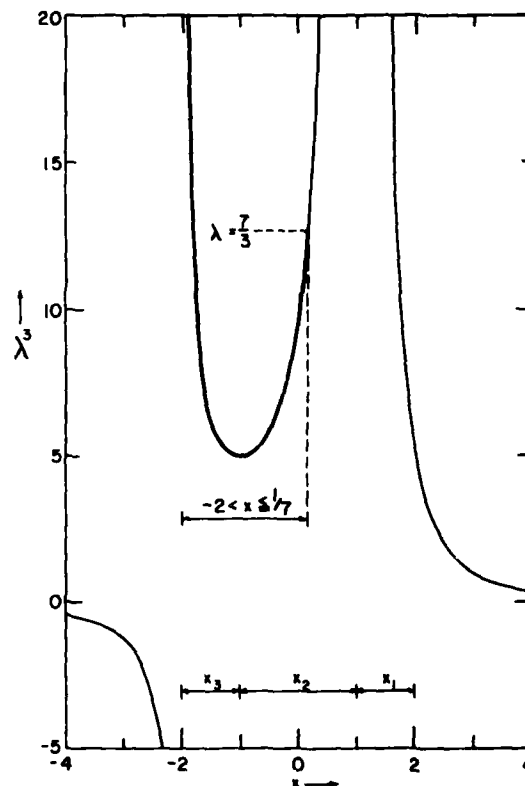
Figure 3. λ^3 as a function of x in (55).

$$T_o^{lns} = (T_p/5) \lambda(3-x)/(\lambda-1). \qquad (59)$$

Thus, we see that T_o^{lns} is determined when T_p and α/θ_o are given. It is obvious from $(52)_2$ that

$$\lambda \ge 1. \qquad (60)$$

Fig. 3 shows that the domain of x that satisfies (60) is

$$-2 < x \le 3. \qquad (61)$$

In addition to (60), the condition

$$T_o^{lns} \le T_p \le 0 \qquad (62)$$

needs be satisfied. Use of (59) in (62) yields the inequality

$$\lambda(3-x)/[5(\lambda-1)] \ge 1,$$

which use of (60) transforms to

$$0 \le \lambda(x + 2) \le 5.$$

229
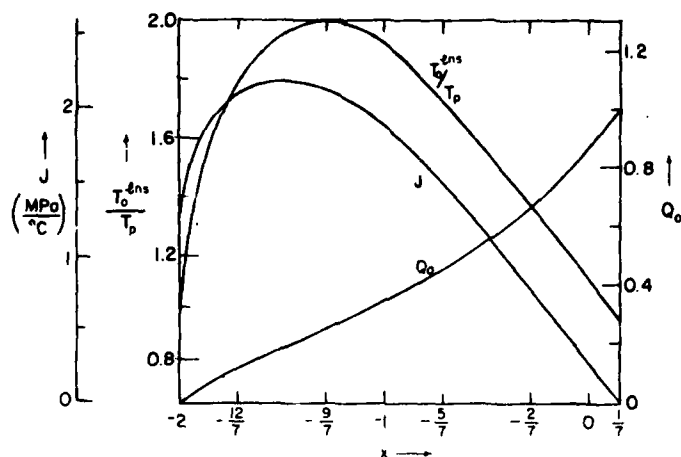
Figure 4. $T_o^{\ell ns}/T_p$, Q_o, and J as a function of x in the domain $-2 \leq x \leq 1/7$.

By forming the cube and substituting λ^3 from (55), the above inequality transforms to

$$4(x+2)^2 \leq 25(x-1)^2. \qquad (63)$$

The range of x that satisfies (61) and (63) is

$$-2 < x \leq 1/7 . \qquad (64)$$

The λ^3 vs x curve in the domain (64) is shown by the heavier line in Fig. 3.

The graph of $T_o^{\ell ns}/T_p$ described by (59) in the domain (64) is shown in Fig. 4. $T_o^{\ell ns}$ reaches the minimum

$$T_o^{\ell ns} = 2 \, T_p \qquad (65)$$

at

$$x = -9/7 .$$

Combining (65) with (62), we find the range of $T_o^{\ell ns}$,

$$2T_p \leq T_o^{\ell ns} \leq T_p . \qquad (66)$$

The expression of Q_o in (45) transforms to

$$Q_o = \lambda(x+2)/5 \qquad (67)$$

by use of $(52)_2$, $(52)_1$ and (53). The graph of Q_o, calculated by (67), is shown in Fig. 4.

FORMULATION OF h_1.

Formulation of the liquid-water flow needs an additional assumption that the pore water pressure be kept constant at some point in the unfrozen region, i.e.,

$$u = u_c \qquad \text{at} \qquad x = x_c \qquad (68)$$

where

$$x_c > p(t) \qquad (69)$$

The pore water pressure $u(p(t),t)$ at the penetration front is found by integrating (49). Letting

$$x = (1-\xi) \, s(t) + \xi p(t), \qquad (70)$$

we find

$$u(p(t),t) = u(s(t),t) +$$

$$+ \left[p(t) - s(t) \right] \int_0^1 \frac{\partial u}{\partial x} (\xi) d\xi .$$

Substituting from $(1)_1$ and $(1)_2$, and letting $t \to 0$, we find that

$$u(p(0), 0) = u(s(0),0), \qquad (71)$$

because the $\sqrt{t}$ limit of the integrand that appears on substitution from $(1)_1$, $(1)_2$, and (49) contains h_o, which is equal to zero due to (36).

The pore water pressure in the unfrozen region is found by integrating the flow equation

230

$$\frac{\partial u}{\partial x} = \frac{1}{k(0)} \overset{\bullet}{h} \, ,$$

where $\overset{\bullet}{h} = h_1$. Thus we find

$$u_c = u(p(0),0) + (h_1/k(0))x_c. \qquad (72)$$

Combining (72), (71), and (44), we find

$$h_1 = [k(0)/x_c]\{u_c - P$$

$$- (L\rho/T_K)(1-Q_o^{3/2}) \; T_o^{\ell ns} \, . \qquad (72)$$

The graph of

$$J = (L\rho/T_K)(1-Q_o^{3/2}) \; T_o^{\ell ns}/T_p \qquad (74)$$

in the domain (64) is shown in Fig. 4, where $L = 3.35176 \times 10^5$ J/kg, $\rho = 10^3$ kg/m^3, and $T_K = 273.16$. If $h_1 > 0$, the assumed frost heave can begin.

CONCLUSION AND SUMMARY

O'Neill and Miller's [1] equations reduce to heat conduction equations by introducing two simplifying assumptions. The reduced equations are analyzed by use of Tao's [3] method that can yield the exact solution of the Stefan problem (the problem of heat conduction with phase change) with arbitrary initial and boundary conditions. The problem studied is the frost heaving that starts immediately after the application of a step-change boundary temperature.

The analysis in the initial short time interval shows that the two internal boundaries, the lensing front and the penetration front, decend in proportion to $\sqrt{t}$, but the top of the ice lens ascends in proportion to t. Penner [5] shows that the above temporal relationships hold much longer than the initial short time interval. Analysis for a long time interval is now in progress.

Penetration front decends a little bit faster than the lensing front. The region between the two fronts is the hrozen fringe.

The reason that the ascension of the top of the ice lens is initially proportional to t is that if it is proportional to $\sqrt{t}$, the flux of pore water in the unfrozen region is infinite at time $t = 0$. The first term h_0 of the

series defining - h(t) must therefore be equal to zero.

The descent of the lensing front means that the ice lens formed by O'Neill and Miller's mechanism is soil-laden. The lens in the classical concept is soil-free.

The first term $T_o^{\ell ns}$ of the series defining of the lensing temperature $T^{\ell ns}(t)$ is determined by the condition that $h_o = 0$. Formulation of $T_o^{\ell ns}$ shows that, for the soil whose partition function χ is given by (38), the factors determining $T_o^{\ell ns}$ are T_p and α/θ_o. $T_o^{\ell ns}$ is in the range (66). These conclusions are valid for the soil whose freezing temperature vs ice content relationship is given by a single-ramp formulation. It is noted that two values of $T_o^{\ell ns}$ arise for a given λ, as may be interpreted by use of Fig. 3.

The second term h_1 of the series expansion of h(t) is formulated, as shown in the derivation of (73), by the conditions of the continuity of the liquid water flow through the unfrozen region, the frozen fringe and into the ice lens. The condition $h_1 > 0$ is necessary for the assumed frost heaving to take place. When the assumed frost heaving takes place, P in (73) represents the frost heave pressure.

The constants in this report are formulated without use of the general solution (32). The rest of the constants must be determined by use of (32) and will be in much more complicated forms. They will be reported in a later paper in which the full use of (32) is made.

ACKNOWLEDGMENTS

NOTATION

c   specific heat

h   height of the ice lens, and enthalpy

$\overset{\bullet}{h}$ dh/dt

K_h	soil thermal conductivity
k	hydraulic conductivity
L	latent heat
P	load on the plane of lensing
p	coordinate of the penetration front
Q	defined by (40)
q	heat flow
R	defined by (9)
r	defined by (16)
s	coordinate of the lensing front
t	time
T	temperature
u	pressure
V_I	flux of the ice flow in the ice lens
v	flux
x	vertical coordinate
α	defined in $(20)_2$
θ	volumetric content
κ	thermal conductivity
λ	defined by $(51)_1$
μ	defined by $(27)_1$
ρ	density
σ_{ntr}	neutral pressure
τ	defined by $(50)_2$

Subscript

i	ice
s	soil
a	frozen fringe
u	unfrozen
o,1	order of the coefficients in a series of $\sqrt{t}$.

REFERENCES

[1] O'Neill, K. and Miller, R.D. (1980) Numerical solutions for rigid-ice model of secondary frost heave. The second International Symposium on Ground Freezing, June 24-26, 1980. Norwegian Institute of Technology. (To be published in a future CRREL Report).

[2] Miller, R.D. (1978) Frost heaving in non-colloidal soils. Proceedings of the 3rd International Conference on Permafrost (Edmonton). National Research Council of Canada, 1: 707.

[3] Tao, L.N. (1978) The Stefan problem with arbitrary initial and boundary conditions. Quarterly of Applied Mathematics 36:223-233.

[4] Penner, E. (1957) Soil moisture tension and ice segregation. Highway Research Board Bull. 168:60-64.

[5] Penner, E. (1977) Fundamental aspects of frost action. Proceedings of the International Symposium on Frost Action in Soils, vol. 2, 17-18. University of Lulea, Sweden.

[6] Miller, R.D. and Koslow, E.E. (1980) Computation of rate of heave versus load under quasi-steady state. Cold Regions Science and Technology 3:243-251.

[7] Portnov, I.C. (1962) Exact solution of freezing problem with arbitrary temperature variation on fixed boundary. Sov. Phys. Dokl. 7(3):186-188.

[8] Takagi, S. (1980) The adsorption force theory of frost heaving. Cold Regions Science and Technology 3:57-81.

CRYOGENIC SUCTION IN SOILS

D. BLANCHARD[*]   M. FRÉMOND[**]

[*]Ecole Nationale des Ponts & Chaussées, 28 rue des St-Pères - 75007 PARIS (France)
[**]Laboratoire Central des Ponts & Chaussées, 58 bld Lefebvre - 75732 PARIS (France)

The cryogenic suction is generally explained by microscopic physics and chemistry. We present a model based on classical notions of the macroscopic theory of continua. These are mainly the deformability of the soil considered as a porous medium and the existence of unfrozen water in the frozen part of the soil.

This model describes only the thermal and hydraulic aspects of the freezing of soils but cannot handle the mechanical aspects such as heaving.

The computations made in one dimension agree with every experimental fact which have been observed in frost susceptible soils.

1. INTRODUCTION

Water movements are important in soil freezing. At the frost line, which separates the frozen and unfrozen parts, a large depression, the cryogenic suction, sucks in a large amount of water which freezes. The thermal and mechanical behavior of soils are widely affected by these mass transfers [1],[2]. By instance, the frost heaving of soils is mainly due to these water movements. It results in a decrease of bearing capacity during the thaw.

The cryogenic suction is generally explained by microscopic physics and chemistry. We give here an explanation based only on classical notions of the macroscopic theory of continua. Our model describes the thermal and hydraulic aspects of soil freezing.

The main points of the model are :

— the existence of unfrozen water in the frozen part of the soil,
— the different densities of ice and water,
— the deformability of the soil. It is caracterized here by different porosities in frozen and unfrozen parts.

2. THE MODEL [7]

We assume that the wet soil is a water saturated porous medium, i.e. there are only three phases : liquid water, solid water and the skeleton of the porous medium. The classical theory of the porous media allows us to define at each point x of the domain Ω, which is occupied by the soil and at each time t, average quantities : temperatures $\theta(x,t)$, head of water $h(x,t)$, ... We assume that the heat exchanges between the different phases are instantaneous so that a single temperature applies to all the phases.

At each time t the porous medium is divided into two parts the unfrozen part $\Omega_1(t)$, the frozen part $\Omega_2(t)$. At the frost line $\Gamma(t)$ between $\Omega_1(t)$ and $\Omega_2(t)$ the temperature $\theta(x,t)$ is zero.

Let us consider at the time t and at a point x of the porous medium Ω a small volume $V(x,t)$. The water, the ice and the skeleton occupy the volumes $V^w(x,t)$, $V^i(x,t)$ and $V^s(x,t)$. The porosity of the porous medium is

$$\varepsilon(x,t) = \frac{V^w(x,t) + V^i(x,t)}{V(x,t)},$$

the water content is :

$$\nu(x,t) = \frac{V^W(x,t)}{V^W(x,t) + V^i(x,t)} .$$

We have indeed $\nu = 1$ in $\Omega_1(t)$ but it is known that there exists unfrozen water in $\Omega_2(t)$, furthermore the water content ν only depends on the temperature θ [3],[14], [5]. Figure 1 shows the caracteristic aspect of the function $\nu(\theta)$.
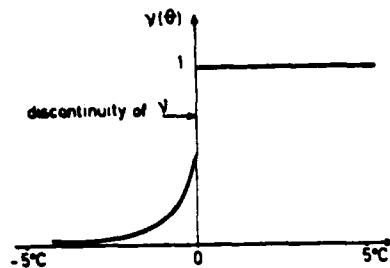
Figure 1. Unfrozen water content as a function of the temperature.

Let us note that the discontinuity of the function $\nu(\theta)$ represents the freezing of a part of the water in the porous medium at the temperature $0°C$.

In order to determine the tempera – ture θ and the head of water h, we write, assuming that we are only considering small perturbations of equilibrium state, the water and ice mass conservation equation and the energy conservation equation [9].

In the energy conservation equation we neglect in $\Omega_1(t)$ and $\Omega_2(t)$ the heat transfered by convection of the skeleton and by diffusion of the water. At the frost line, we consider both conduction and heat transferred by water diffusion since the latent heat of the diffused water is important. It is well known that this is a characteristic aspect of the freezing of wet porous media.

In the water mass conservation equation we keep only the liquid water diffusion which has an order of magnitude bigger than diffusion of ice and convection of skeleton.

With these assumptions, the most simple hypothesis to describe the deformability of the soil is to assume that a constant porosity ε^1 applies to the unfrozen part $\Omega_1(t)$ and a different constant porosity ε^2 applies to the frozen part $\Omega_2(t)$.

We assume :

.Fourier's law : the heat flux vector is $- \lambda \overrightarrow{\text{grad}} \theta$ where λ is the thermal conductivity which can depend on θ.

.the Darcy's law gives the water velocity relative to the soil by $- \frac{m}{\varepsilon \nu} \text{grad} h$ where m is the mobility of the water in the soil.

Let us define the mass by unit volume ρ^i and ρ^W of the ice and water, the specific latent heat of the water ℓ, the volumetric heat capacity of the wet porous medium ρC.

The equations follows :

$\star$in $\Omega_1(t)$:
— water mass conservation equation

$$- \rho^W m \Delta h = 0, \qquad (1)$$

— energy conservation equation

$$\rho C \frac{\partial \theta}{\partial t} - \lambda \Delta \theta = 0, \qquad (2)$$

$\star$in $\Omega_2(t)$:
— water mass conservation equation :

$$- \rho^W m \Delta h = \varepsilon^2 (\rho^i - \rho^W) \frac{\partial \nu}{\partial \theta} \cdot \frac{\partial \theta}{\partial t},$$

— energy conservation equation

$$\rho C \frac{\partial \theta}{\partial t} - \lambda \Delta \theta = - \ell \varepsilon^2 \rho^i \frac{\partial \nu}{\partial \theta} \cdot \frac{\partial \theta}{\partial t}$$

$\star$At the frost line $\Gamma(t)$, where the values on $\Gamma(t)$ of the variables are denoted by 1 or 2 if they are taken on the unfrozen or the frozen side :

$- \theta = 0$,

— water mass conservation equation,

$$m^2 \rho^W (\overrightarrow{\text{grad}}h)^2 \cdot \vec{N} - m^1 \rho^W (\overrightarrow{\text{grad}}h)^1 \cdot \vec{N}$$

$$= - \{\varepsilon^2 \{\rho^W \nu^2 + \rho^i (1-\nu^2)\} - \varepsilon^1 \rho^W\} \vec{W} \cdot \vec{N},$$

($\vec{W}$ is the velocity of the frost line and $\vec{N}$ a normal to Γ unit vector),

— energy conservation equation,

$$\lambda^2 (\overrightarrow{\text{grad}}\theta)^2 - \lambda^1 (\overrightarrow{\text{grad}}\theta)^1 = \ell \varepsilon^2 \rho^i (1-\nu^2) \vec{W} \cdot \vec{N}.$$

The equations are completed by classical initial and boundary conditions : the initial temperature $\theta_0(x)$ is specified and, for instance, the temperature and the head of water are specified on the boundary of the domain Ω.

The inputs of the model are the physical constants ρ^i, ρ^W, ρC, the functions $\nu(\theta)$, $m(\theta)$, $\lambda(\theta)$ and the porosities ε^1 and ε^2. All the parameters can be obtained

surface $x = b$

$$\theta(b,t) = \overline{\theta}_s(t)$$

$$\frac{\partial h}{\partial x}(b,t) = 0$$

frozen zone Ω_2

$$\cdot \; -\rho^w m \frac{\partial^2 h}{\partial x^2} = \varepsilon(\rho^i - \rho^w)\frac{\partial \nu}{\partial \theta}\cdot\frac{\partial \theta}{\partial t}$$

$$\cdot \; \rho C \frac{\partial \theta}{\partial t} - \frac{\lambda^2 \partial^2\theta}{\partial x^2} = -\ell\,\varepsilon\rho^i \frac{\partial\nu}{\partial\theta}\cdot\frac{\partial\theta}{\partial t}$$

frost line $s(t)$
$\left(\vec{W}\cdot\vec{N} = \dfrac{ds}{dt}\right)$

$$\cdot \; \theta = 0$$

$$\cdot \; m^2\rho^w \frac{\partial h^2}{\partial x} - m^1\rho^w \frac{\partial h^1}{\partial x} = -\left\{\varepsilon^2\{\rho^w\nu^2 + \rho^i(1-\nu^2)\} - \varepsilon^1\rho^w\right\}\frac{ds}{dt}$$

$$\cdot \; \frac{\lambda^2\partial\theta^2}{\partial x} - \frac{\lambda^1\partial\theta^1}{\partial x} = \ell\,\varepsilon^2\rho^i(1-\nu^2)\frac{ds}{dt}$$

unfrozen zone Ω_1

$$\cdot \; -\rho^w m \frac{\partial^2 h}{\partial x^2} = 0$$

$$\cdot \; \rho C \frac{\partial\theta}{\partial t} - \frac{\lambda^1\partial^2\theta}{\partial x^2} = 0$$

$x = 0$

$$\theta(0,t) = \overline{\theta}_f(t)$$

$$h(0,t) = \overline{h}(t)$$
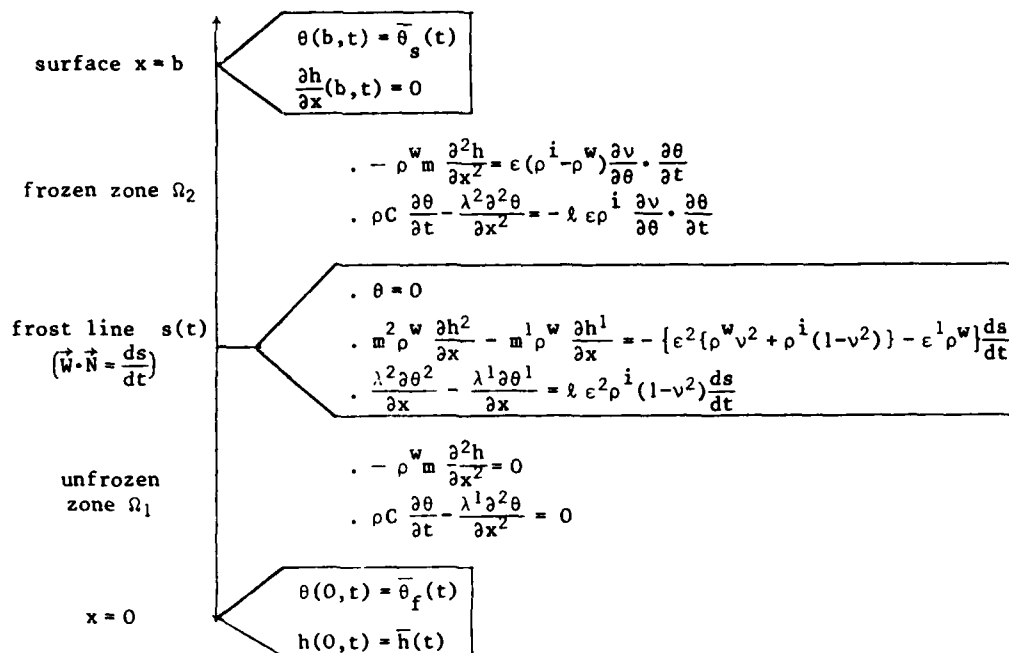
Figure 2. The equations on one dimension.

Datas :

$\rho^w \quad = 1\ 000\ \text{kg/m}^3$

$\rho^i \quad = \quad 900\ \text{kg/m}^3$

$\varepsilon^1 \quad = 0.30$

$\varepsilon^2 \quad = 0.39$

$(\rho C)_1 = 0.27 \times 10^7\ \text{J.m}^{-3}.\text{K}^{-1}$

$(\rho C)_2 = 0.22 \times 10^7\ \text{J.M}^{-3}.\text{K}^{-1}$

$(\lambda)_1 \quad = 1.9\ \text{J.s}^{-1}.\text{m}^{-1}.\text{K}^{-1}$

$(\lambda)_2 \quad = 2.2\ \text{J.s}^{-1}\ \text{m}^{-1}.\text{K}^{-1}$

$\ell \quad = 0.82 \times 10^8\ \text{J.m}^{-3}$

$m_1 \quad = 10^{-11}\ \text{m}^3.\text{s.kg}^{-1}$

$m_2 \quad = 10^{-14}\ \text{m}^3.\text{s kg}^{-1}$

$\overline{h}(t) \quad = 0$

$\overline{\theta}_f(t) \quad = 14°\text{C}$

For $\overline{\theta}_s(t)$ see figure 6.

through experimentation [2], [12].

The outputs are the temperature $\theta(x,t)$ and the head of water $h(x,t)$.

Note. It turns out from an attentive consideration of the skeleton mass conservation equation that the assumptions imply that $\varepsilon^2-\varepsilon^1$ is small with respect to ε^1 and ε^2. That is the case in all practical situations. A complete and detailled description of the equations and mathematical results can be found in [8].

3. RESULTS

We have made calculations in one dimension, for which the equations are represented on Figure 2.

We have the following results :

3.1. During freezing

— A large suction appears almost immediatly at the frost line in a frost susceptible soil. This suction is almost constant in time (Figure 3,4,6). Of course the value of the suction depends on the structure and on the boundary conditions. These facts agree with a well known experimental fact : the cryogenic suction. The value of the suction, already used to estimate the frost heave [4], was up to now estimated by experimentation and practical knowledge.

— if the volume expansion upon freezing is neglected ($\rho^w = \rho^i = 1000$ kg/m^3) the suction increases as it is forecastable.

— if the porosity in the frozen part, ε^2, increases, the suction increases too, because the deformation of the soil increases.

— if ν^2 increases ($\frac{\partial \nu^2}{\partial \theta}$ being constant) or if $\frac{\partial \nu^2}{\partial \theta}$ increases (ν^2 being constant) the suction decreases. From the equations, it turn out that one can consider the frozen part as a water source whose intensity is proportional to $\partial \nu/\partial \theta$ and the frost line as a water sink whose intensity is proportional to

$$\varepsilon^2\{\rho^w \nu^2 + \rho^i(1-\nu^2)\} - \varepsilon^1 \rho^w.$$

— the suction can even vanish for some values of ε^2 and $\nu(\theta)$. Moreover a over pressure can appear at the frost line. Nevertheless this unusual situation has been experimentally observed for non frost susceptible soils, (for instance

sands), [13], [10], [11].
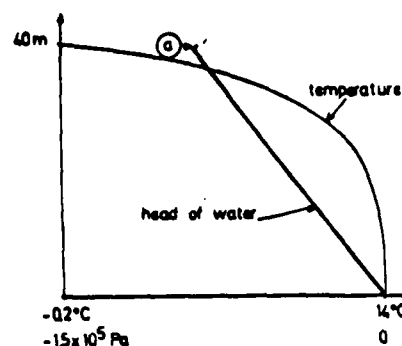
Figure 3. Temperature and head of water in a soil during freezing.
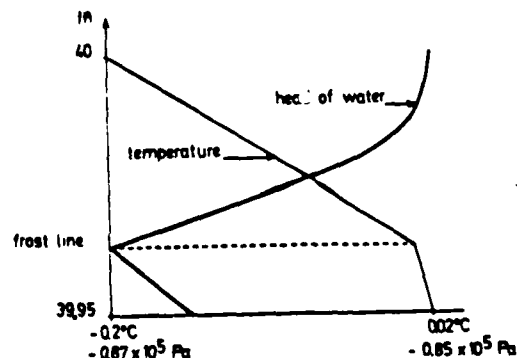
Figure 4. Temperature and head of water near the frost line during freezing (enlargement of part ⓐ of Figure 3).

3.2. During unfreezing

During the unfreezing of the upper surface of the soil the suction decreases rapidly. Moreover the head of water at the frost line is discontinuous (with respect to time t) when the surface temperature becomes again positive (Figure 5 and 6).

These results agree with the experimental aspects of the unfreezing of frost susceptible soils (frost heaving and cryogenic suction disappear [6]).

236
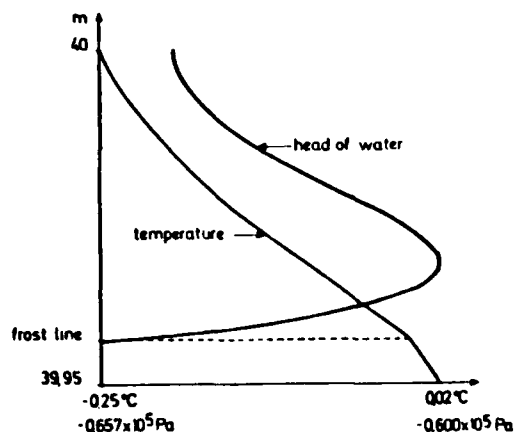
Figure 5. Temperature and head of water near the frost line during unfreezing.
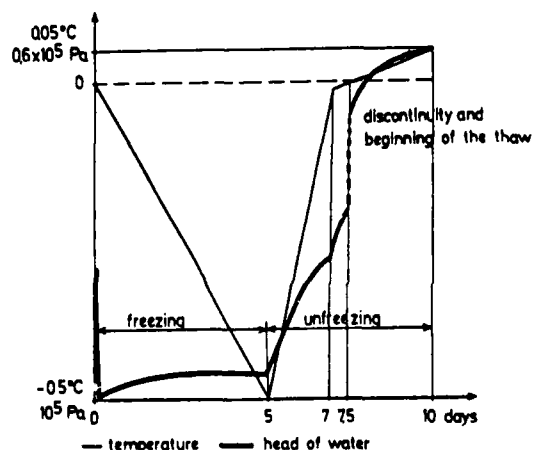
Figure 6. Temperature at the op of the structure $[\theta_s(t)]$ and cryogenic suction at the frost line as functions of the time variable.

4. CONCLUSIONS

Our model is based uniquely on *macroscopic variables* of the classical theory of porous media, *accessible through experiments*. It is sufficient to describe the hydraulic and thermal aspects of soils frcezing. It can predict the value of the suction at the frost line. This suction is due to the existence of liquid water in the frozen zone and to the deformability of the soil. This model does not take into account the mechanical aspects such as frost heave. To do so the velocities of the ice and soil must be taken as additional unknowns.

REFERENCES

[1] L'ACTION DU GEL SUR LES CHAUSSEES, O.C.D.E., 1973.

[2] GEL DES SOLS ET DES CHAUSSEES, ECOLE NATIONALE DES PONTS ET CHAUSSEES, 1977.

[3] J. AGUIRRE-PUENTE ; M. VIGNES ; P. VIAUD, USSR Contribution. Permafrost second international conference, National Academy of Sciences, Washington, 1978, p. 315.

[4] J. AGUIRRE-PUENTE ; M. FREMOND, Applications of methods of functional analysis to problems of mechanics, Springer Verlag, 1976.

[5] D. ANDERSON ; A. TICE, Highw. Res. Rec., 393, 1972, p. 12.

[6] L. CANIARD ; A. DUPAS ; A. PHILIPPE ; J. AGUIRRE-PUENTE ; H. BERTOUILLE, La Station de gel de Caen. Deuxième et troisième expérimentation. Aspects géotechnique et thermique. Rapport interne du Laboratoire Central des Ponts et Chaussées, du Centre de Géomorphologie du CNRS et du Laboratoire d'Aérothermique du CNRS, 1974.

[7] D. BLANCHARD ; M. FREMOND. La succion cryogénique dans la congélation des sols : un modèle macroscopique. Note aux C.R.A.S., Sér. II, 1982.

[8] D. BLANCHARD ; M. FREMOND. Congélation des sols. Modèle macroscopique de la succion cryogénique (to appear).

[9] P. GERMAIN. Cours de Mécanique des Milieux Continus, Masson, 1973.

[10] B. KHASTOU. Etude du gonflement des sols par le gel, thèse, Université de Paris, 1970, p. 19.

[11] J. LIVET. Rapport interne du Laboratoire Régional des Ponts et Chaussées de Nancy, Essais de gonflement au gel, n°42, 1981.

[12] M. SMITH ; D. PATTERSON.- Report do
Dept. of Energy, Mines and Resour-
ces, OTTAWA, 1980, p. 59.

[13] P. WILLI.MS. Private communication.

[14] P. WILLIAMS. Norwegian Geotech.
Inst. Publ. 72, 1967, p. 120.

ASPECTS OF ICE LENS FORMATION

E. Penner, DBR, National Research Council of Canada, Ottawa, Canada K1A OR6

ABSTRACT

It is possible to locate a growing ice lens in a frost heave cell in soil under laboratory conditions by means of a recently devised X-ray technique. If temperature distribution is measured in the sample at the same time, the temperature of the growing face of the ice lens can be determined. The objective of the study was to validate this method under a range of heaving conditions. It was done by determining ice lens temperatures at various overburden pressures and cold side temperatures; then, by adjusting the ice lens temperature for overburden pressure and pore water salt content, the remaining difference from 0°C was expressed in terms of suction. Suction gradients in unfrozen soil under various freezing conditions were subsequently plotted as a function of rate of moisture flow and a proportionality was shown to exist. In addition the calculated permeability coefficient was the expected value for the material, Leda clay. These results lend credence to use of the X-ray – thermal gradient technique for studying thermal behaviour of ice lens growth.

particular soil, Leda clay, using a range of overburden pressures and one-step freezing temperature experiments that form the basis of this paper. Some of the heaving experiments were continued over longer periods to observe ice lens temperature and heave response to changes in cold-side temperature and overburden pressure; representative results are reported.

The main thrust of this paper, however, is to validate the temperatures of ice lens growth measured by the X-ray – thermal gradient technique. This was done by subtracting the freezing point depression attributable to pore water salt content and overburden pressure from the measured ice lens temperatures, and expressing the remaining quantity in terms of suction. With the external water table held at the level of the unfrozen end of the soil specimen (suction = 0) and the estimated suction at the face of the growing ice lens, suction gradients were calculated and plotted against moisture flow rates. The results show that the permeability coefficient value determined from moisture intake during heaving is the value expected for this clay; and that the suction gradient is proportional to the measured flow rate, as it should be. The X-ray – thermal gradient technique for determining ice lens temperatures therefore appears to be a valid method of studying the thermal behaviour of ice lens growth.

Preliminary results were previously presented by Penner and Goodrich (1980) for an X-ray technique designed to determine the position of a growing ice lens in soil specimens frozen in the laboratory. The temperatures at the face of growing ice lenses were determined by means of simultaneous X-rays and temperature measurements in a sample while the heaving process was in progress. Subsequently, more detailed studies were carried out on one

Experimental Materials and Technique

The soil was a marine silty clay from the Ottawa area, with clay size content in the range of 70 to 75% and the remainder in the silt size range. The soil was remoulded and sufficient

water added to bring it near the liquid limit. The test cell (obtained from Northern Engineering Services (NES) Company Limited, Calgary, Alberta) was filled with the fluid mix and consolidated, in stages, to 490 kPa. The sample was then allowed to rebound to the test pressure used during freezing. Two cells, one a copy of the NES cell, were used alternately. A complete description of the cell has been given by Penner and Ueda (1977).

Table 1 gives the pre-freezing sample data. It is to be noted that the rebound upon pressure release is small in Leda clay because the clay size fraction is unusually coarse, consisting largely of rock flour and non-swelling clay minerals. Although a range of overburden pressures was used in the studies, the sample density and moisture content were not noticeably changed. It was possible, therefore, to study the freezing behaviour of this soil at various overburden pressures without there being any effect from overburden pressures on the structure of the sample.

Freezing Procedure

The freezing procedure has become known as the one-step freezing test, dating to early studies by Penner (1957). The frost penetration and the heaving curves are given in Fig. 1.

The cell containing the sample was placed in a constant-temperature chamber held at approximately 4°C ± 0.05. Water-lines were connected and purged with de-aired water to remove air bubbles. After dimensional and thermal stability had been established, crystallization was induced (Penner and Goodrich, 1980) and a constant step-freezing temperature imposed on the cold side.

Glass-encased thermistors were located at the interface between the sample wall and the sample, just behind a thin sheet of Teflon. During all freezing runs the temperature of the sample, heave and water intake were measured at suitable intervals.

The sliding friction of the sample in the cell was measured for both cells; the average of several measurements was found to be 24 kPa. This value also included the friction of the two O-rings, which form a part of the cell design and were in place during friction measurements.

X-ray Technique

At pre-selected times temperature measurements and X-rays of the sample were taken simultaneously through the cell wall. The X-ray beam was positioned at the elevation of the growing ice lens to avoid parallox errors.

The method of determining ice lens temperatures has been described in detail (Penner and Goodrich, 1980), but for completeness it will be described again in brief. An example of X-ray photographs taken at various stages of temperature and pressure is shown in Fig. 2. As the position of the thermistors

Table 1.   Pre-freezing Sample Data

Sample	Cell	Pre-freezing Consolidation P (kPa)	Freezing Pressure (kPa)	*Moisture Content (% dry wt)	Dry Density (kg/m^3)	*Saturation %
A15	1	490	122.6	36.3	1347	94
B16	2	"	"	36.9	1341	95
C17	1	"	"	37.0	1356	97
A13	1	"	318.7	36.4	1375	98
B14	2	"	"	36.0	1370	97
C18	2	"	"	36.4	1367	97
A9	1	"	514.8	36.0	1373	97
B10	2	"	"	-	-	-
C11	1	"	"	35.7	1381	97
D12	2	"	"	35.2	1380	96

*Moisture content and % saturation apply after rebound from consolidation to the pressure used during the freezing process.
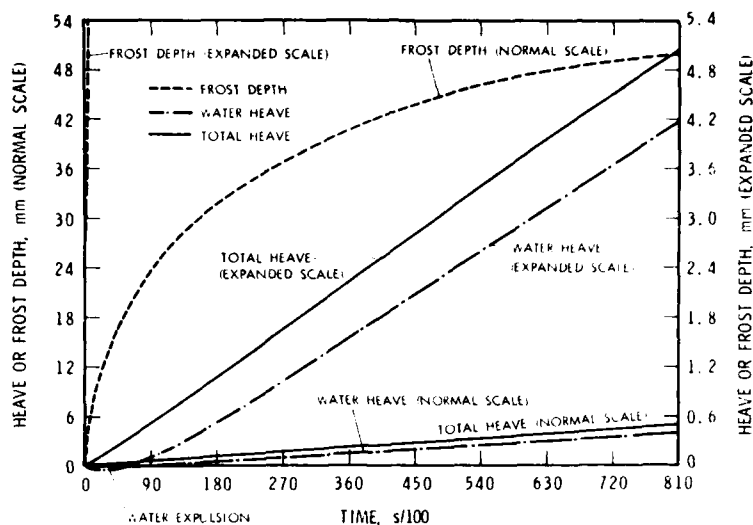
Figure 1. Example of frost penetration, total heave and heave by water intake for the one-step freezing mode with the Leda clay used in this study.
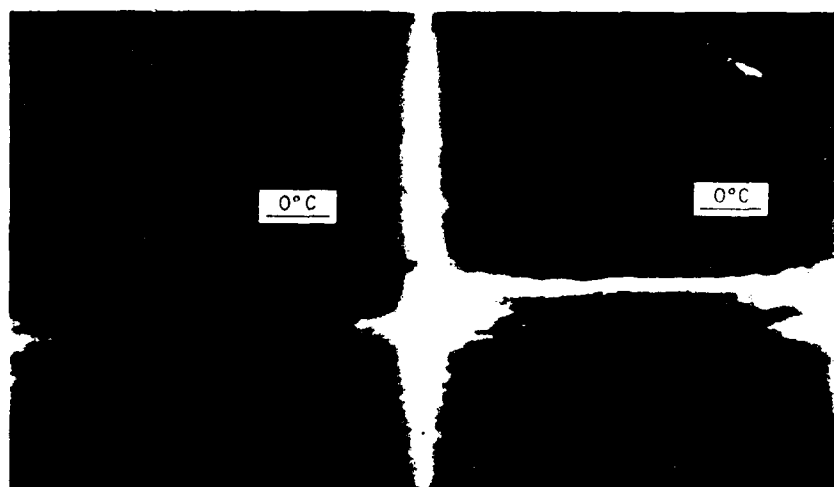
Figure 2. X-rays taken at successive stages of pressure. No. 1 was taken after 87540 s, overburden P = 514.8 kPa, cold-side temperature -3.40°C. Pressure reduced to 72 kPa. No. 2 was taken after a further 85560 s.

may be seen in the X-ray, the temperature gradient can be superimposed and the temperature of the ice lens determined, as shown in Fig. 3.

Results and Discussion

Earlier studies (Penner and Walton, 1979) have shown that for the one-step heaving test the log of the initial total rate of heave is linearly proportional to the overburden pressure/cold-side freezing temperature ratio. The present studies verified this. The results for the particular sample of Leda clay used are given in Fig. 4. The range of pressures is from 123 to 515 kPa and the range of cold-side temperatures approximately -1 to -4°C. The results have a high correlation coefficient of 0.99.

241

NOTE TEMPERATURE AT COLD SIDE
-2.65 TO 172 590 s
-4.10 AFTER 172 590 s

254 670 s

80 760 s

172 590 s

STAGE 3

DISTANCE FROM
0°C 8.99 mm

FACE OF ICE LENS
T -0.668°C

DISTANCE
FROM 0°C
8.52 mm

STAGE 2

STAGE 1

DISTANCE FROM
0°C 11.68 mm

FACE OF
ICE LENS
T -0.508°C

FACE OF ICE LENS
T -0.739°C

THERMISTOR
LOCATIONS

STAGE	1	2	3
COLD SIDE T, °C	-2.65	-2.65	-4.00
OVERBURDEN PRESSURE, kPa	122.6	122.6	122.6
TIME, s	80 760	172 590	254 670

DEPTH, mm

TEMPERATURE, °C

Figure 3. Determination of ice lens
position from X-rays and thermal gradient.

Figure 5 illustrates the position in the sample and the temperature of the ice lens when the overburden pressure is the same but the starting cold-side temperature is different. With a cold-side temperature of -2.49°C the lens temperature at the time of the first X-ray was -0.739°C; when the cold-side temperature was colder (-3.75°C), the ice lens temperature was -0.950°C. A second X-ray was taken of each sample at about the same running time after the first X-ray. Again, the lens temperature was colder when the cold-side temperature was lower. In one of the experiments a third stage was added. Dropping the temperature on the cold side to -4.10°C lowered the ice lens temperature further.

Figure 6 illustrates the temperature and position of the ice lens relative to the 0°C isotherm at about the same cold-side temperature but different overburden pressures. The general pattern was that the higher the overburden pressure the lower the lens temperature after about the same time interval from the start of the test, provided the cold-side temperatures were approximately the same. To be noted also is that the lens temperature difference from 0°C reduces with time. This is illustrated in experiment 1 (Fig. 6) between X-ray 1 and X-ray 2. After X-ray 2 the cold-side temperature was dropped and this, in general, lowered the ice lens temperature. In experiments 2 and 3 the pressure was reduced after X-ray 1, tending to
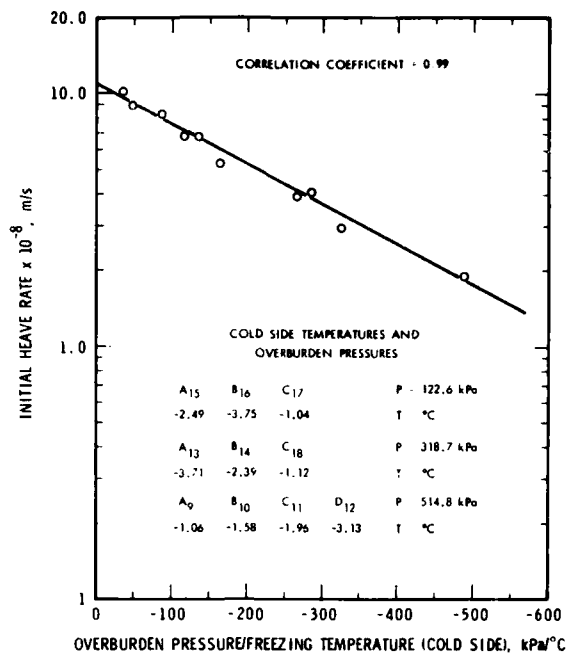
Figure 4. Initial total heave rate vs overburden pressure/cold-side temperature ratio.
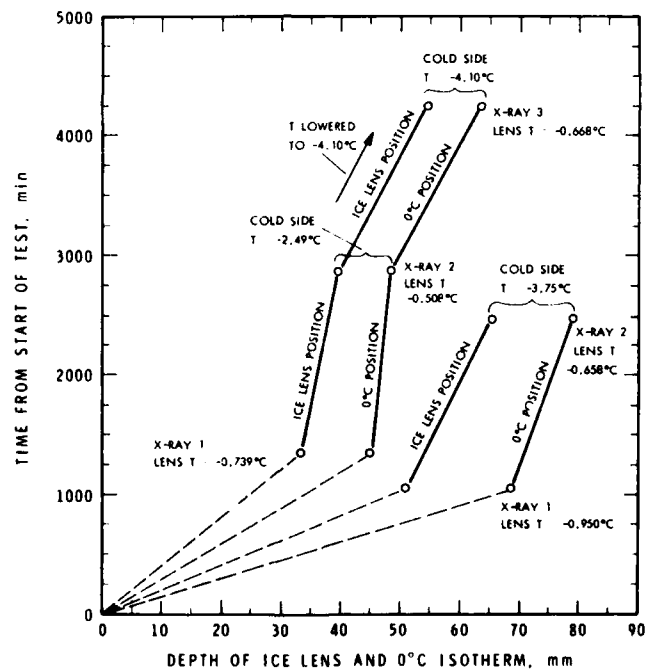
Figure 5. Position and temperature of face of growing ice lens and 0°C isothern vs time at initial overburden pressure of 122.6 kPa.

243
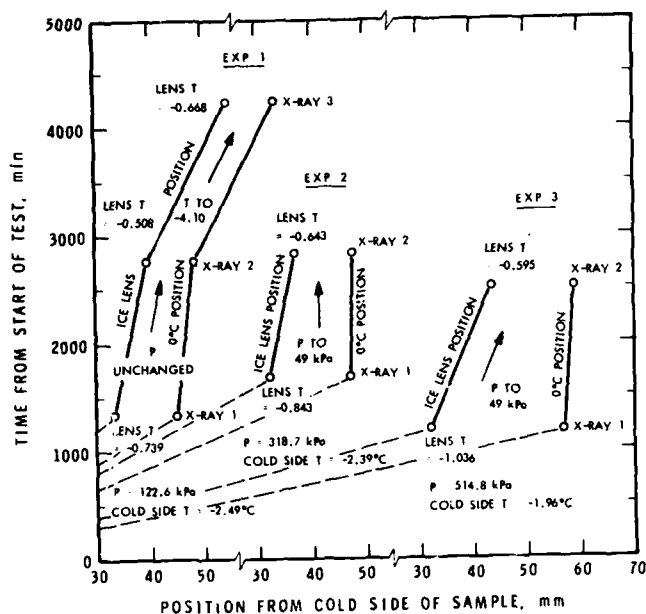
Figure 6. Position and temperature of face of growing ice lens and 0°C isotherm vs time when initial overburden pressures are different.
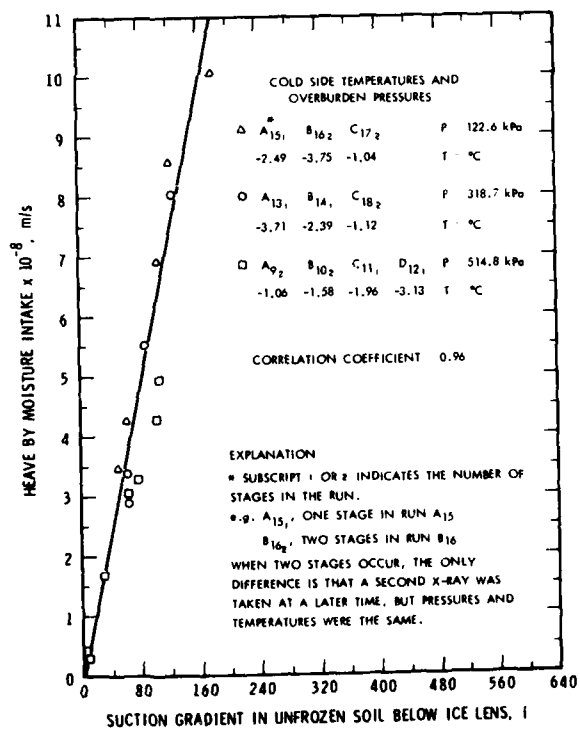
Figure 7. Heave by moisture intake vs suction gradient in unfrozen portion below ice lens.

244

reduce the distance between the lens and 0°C isotherm as well as the temperature depression. Note particularly the large decrease shown by the results of experiment 3.

Finally, the main thrust of the work was to validate the method of determining ice lens temperatures. This was done by estimating suction from lens temperature after allowing for pore water salt content and overburden pressures. With the suction at the base of the unfrozen soil held at zero and the suction estimated at the ice lens, suction gradients were calculated and plotted against moisture flow during heaving (Fig. 7). As may be seen, the flow rate measured during the experiment was linearly proportional to the calculated suction gradient. In addition, the permeability coefficient calculated from Fig. 7 was 6×10^{-10} m/s, a value that compares favourably with other permeability measurements of Leda clay of the same grain size and density (Bozozuk, 1972). This lends credence to the method used for determining the values for ice lens temperature.

Concluding Remarks

The one-step freezing test has shown that calculating ice lens temperatures from the position of the growing ice face, determined from X-rays and thermal gradient, is a valid method of determining ice lens temperature. Trends observed in ice lens temperatures are as might be expected. In general, increasing the overburden pressure lowers the temperature of the lens at the ice front. Lowering the overburden pressure during heaving causes the ice front temperature to increase. Similarly, decreasing the cold-side temperature increases the rate of freezing and lowers the ice-front temperatures.

References

Bozozuk, M. 1972. The Gloucester test fill, Ph.D. Thesis, Purdue University, 184 p.

Penner, E. 1957. Soil moisture tension and ice segregation, Highway Res. Board, Bulletin 168, p. 50-64.

Penner, E., and T. Ueda 1977. The dependence of frost heaving on load application - preliminary results, International Symposium on Frost Action in Soils, University of Luleå, Luleå, Sweden, Proc., Vol. 1, p. 92-101.

Penner E., and T. Walton 1979. Effects of temperature and pressure on frost heaving, Eng. Geol., Vol. 13, p. 29-39.

Penner, E., and L.E. Goodrich 1980. Location of segregated ice in frost susceptible soil, Presented at 2nd International Symposium on Ground Freezing, Norwegian Institute of Technology, Trondheim, Norway.

EFFECT OF SPECIMEN HEIGHT ON FROST HEAVE RATIO IN UNIDIRECTIONAL FREEZING TEST OF SOIL

Tsutomu TAKASHI
Takahiro OHRAI
Hideo YAMAMOTO
Jun OKAMOTO

Research Institute, Seiken Co., Ltd.

2-11-16, Kawarayamachi

Minami-ku, Osaka, Japan

ABSTRACT

Specimen height constitutes one of the most important factors in a laboratory frost heave test. Relations between it and the frost heave ratio have been examined systematically changing such freezing conditions as overburden pressure and frost penetration rate in open-system frost heave tests of Manaita-bridge clay collected in Tokyo, with the following findings:

The frost heave ratio ξ (defined as the ratio of volume increment to initial volume of a specimen) reaches a maximum at a certain value H_0 of the specimen height H. When $H > H_0$, then ξ decreases with increasing H, which can be explained quantitatively by resistance in soil-water movement through the unfrozen part of specimen. Meanwhile, ξ decreases with decreasing H, when $H < H_0$, which can be explained qualitatively by existence of an "in situ water freezing zone" within frozen soil.

For this clay, which is markedly frost-susceptible, H_0 obtained ranges between 2 and 4 cm. In general, H_0 depends on the soil type and freezing condition. In a laboratory frost heave test, H_0 is looked on as the optimum height of a specimen.

1. INTRODUCTION

The soil of a construction site where ground freezing is undertaken is subjected to unidirectional freezing tests in the laboratory so that its frost-susceptibility is obtained beforehand. This study deals with the effect of the specimen height H on the frost heave ratio ξ in such tests.

Takashi et al. (1976) analyzed the effect of resistance in soil-water movement through the unfrozen part within a freezing specimen on ξ, whereby they pointed out that ξ is a function of H.

On the other hand, it has been considered recently that ice segregation occurs within a certain limited zone in frozen soil (Dirksen and Miller, 1966; Hoekstra, 1966; Miller, 1972; Radd and Oertle, 1973; Loch and Kay, 1978; Takashi et al., 1979; Fukuda et al., 1980; Penner and Goodrich, 1980). The authors' view about the position of the zone where ice segregation occurs is shown schematically in Fig.1, where θ_f is the freezing point of bulk water, θ_{init} is the temperature at which ice segregation initiates and θ_{crit} is the critical temperature at which ice segregation comes to an end. The plane $\theta = \theta_f$ is defined as a freezing front. The
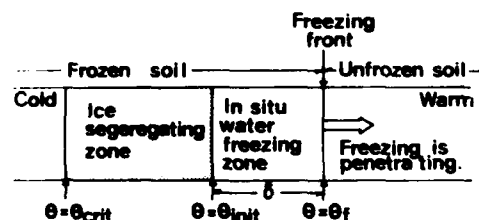
Fig.1 Schematic representation of unidirectionally freezing column of soil

247

zone $\theta_{init} < \theta < \theta_f$ is an "in situ water freezing zone". The zone $\theta_{crit} < \theta < \theta_{init}$ is an "ice segregating zone". This authors' view was described in detail in previous papers (Takashi et al., 1981a and b). According to this viewpoint, the specimen height is to have some influence on the frost heave ratio.

In order to confirm a relation between ξ and H, and to obtain information concerning the optimum H in laboratory tests, a clay is subjected to frost heave tests at various H, systematically changing such freezing conditions as overburden pressure and frost penetration rate.

2. EXPERIMENTAL METHOD

2.1 Preparation of specimens

The soil tested was a diluvial clay (Manaita-bridge clay) collected in Tokyo. It has a markedly high frost-susceptibility. Selected index properties are shown in Table 1.

A specimen was prepared as follows: The soil was air-dried and loosened. Then, it was kneaded over by adding distilled water until the water content attained about 54 %. The load was applied with a piston and a cylinder to the resultant mixture step by step until it amounted to 1.57 MN/m^2. After consolidation of the mixture into a clay block (diameter D=11 cm, height H=8 cm), a specimen (D=10 cm, H=5~6 cm) was trimmed from it.

Six specimens were thus prepared for experimental use in this study.

Table 1 Selected index properties of Manaita-bridge clay #3

Silt 0.074-0.005 mm		33.5 %
Clay < 0.005 mm		66.5 %
Liquid limit	w_L	47.1 %
Plastic limit	w_P	25.4 %
Specific gravity	G_s	2.712
Specific surface area	S_g	136.2 m^2/g

Table 2 Physical properties of specimen

Water content	w	25.7 ± 0.9 %
Wet density	ρ_t	1.99 ± 0.01 g/cm^3
Dry density	ρ_d	1.58 ± 0.02 g/cm^3
Porosity	n	0.416 ± 0.007
Degree of saturation	S_r	97.7 ± 1.4 %
Hydraulic conductivity	k	5 x 10^{-8} cm/s

Their physical properties are shown in Table 2.

2.2 Apparatus and procedure

The apparatus is shown in Fig.2. It allows to conduct a frost heave test under an arbitrary overburden pressure and at an arbitrary constant rate of frost penetration. Concerning water movement, this apparatus is an open-type system in which water is movable easily between the specimen and the water supply tank. The detail of this apparatus was described in previous papers (Takashi et al., 1974; Takashi et al., 1978).

One freezing condition was assigned to each specimen, as shown in Table 3, their being selected systematically around central values: overburden pressure σ_1=247.2 kN/m^2; frost penetration rate U=3.0 mm/h.

After the first run of an experiment as conducted at the initial specimen height (H=5~6 cm), the end of the specimen was cut off for the next run at a reduced height. Thus reducing the height of the specimen for next run,

1 ADJUSTING SCREW	12 SOIL SPECIMEN
2 POLE	13 POROUS PLATE
3 GUIDE	14 COOLING PLATE
4 SPRING	15 POTENTIO METER
5 SLIDE BEARING	16 BOURDON'S GAUGE
6 PROVING RING	17 PRESSURE CONTAINER
7 THERMISTER CONDUIT	18 DIFFERENTIAL TRANSFORMER
8 THERMO ELECTRIC MODULE	19 FLOAT
9 PISTON	20 WATER CUP
10 RING SEAL	21 FLEXIBLE JOINT
11 ACRYLIC RESIN CYLINDER	22 Cu-TUBE
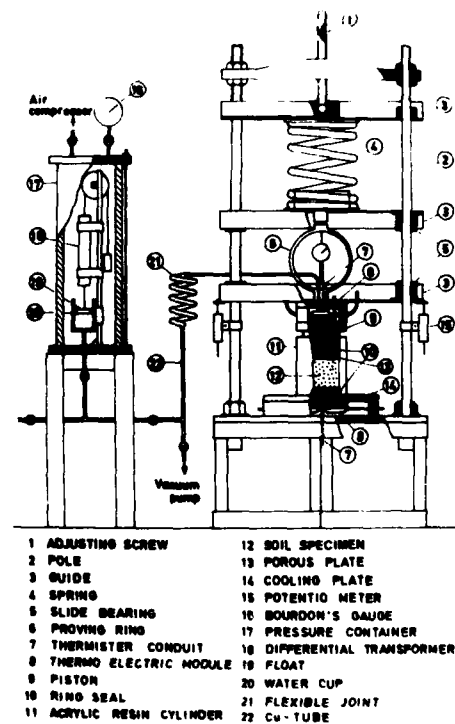
Fig.2 Diagram of apparatus used for frost heave test

the same specimen was used for a number of runs of the experiment. For each run the frost heave test was repeated about 12 times (see Fig.4).

Table 3 Freezing condition assigned to each specimen

		Frost penetration rate U (mm/h)		
		1.6	3.0	5.8
Overburden pressure σ_1 (kN/m²)	70.6	-	Specimen No.1	-
	129.5	-	Specimen No.2	-
	247.2	Specimen No.3	Specimen No.4	Specimen No.5
	482.7	-	Specimen No.6	-

3. RESULTS

Typical curves of frost heaving are shown in Fig.3. It is interesting that frost heaving does not appear in a period of early several hours in each test. This phenomenon implies that ice segregation does not occur within a certain limited zone immediately behind the freezing front.

In each test, freezing was initiated from the lower end of a specimen and penetrated upward to the upper end at a nearly constant rate. When freezing penetrated to the upper end (this corresponded to the "freezing finished" point in Fig.3), the average temperature of specimen was various in response to the cooling rate. In order to unify the amount of unfrozen water remaining in a frozen specimen, the average temperature was made to be -5°C finally.

The frost heave ratio ξ is defined as:

$$\xi = h/H \qquad (1)$$

where h is the total amount of heave and H is the specimen height before freezing.

The water intake or discharge ratio ξ_W is defined as:

$$\xi_W = h_W/H \qquad (2)$$

where h_W is the total amount of water intake or discharge (converted into the water level change in a tank of the same diameter as specimen) during the freezing period. Positive sign of ξ_W means water intake type and negative means water discharge type.

At each specimen height, a test was repeated about 12 times under the same freezing condition. An example of a relation between ξ and the number of repetition of test is shown in Fig.4, in which ξ decreases gradually with increasing the number of repetition up to 8 times and then converges to a constant value. This constant value is defined as the frost heave ratio ξ at this specimen height.

Fig.4 Example of relation between ξ and the number of repetition of test

(a) U: const., σ_1: changed   (b) σ_1: const., U: changed
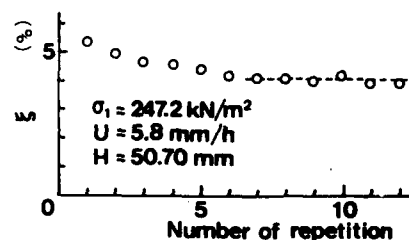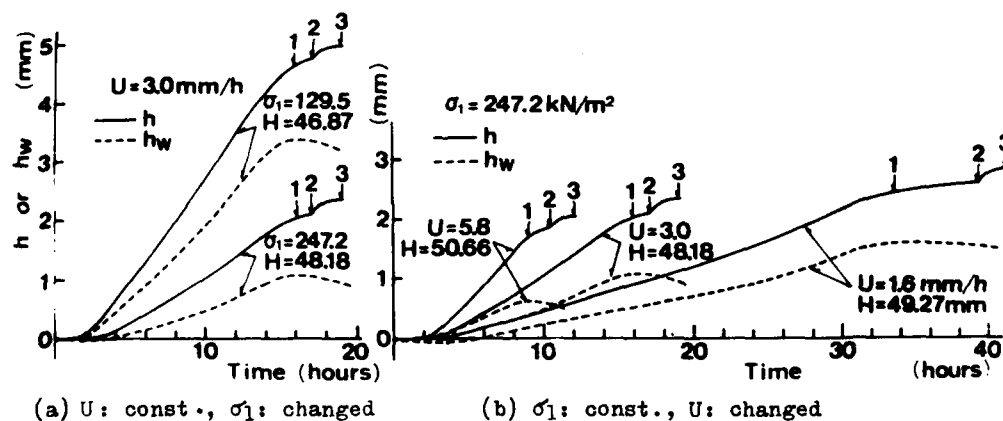
Fig.3 Typical frost heaving curves during freezing
  1. Freezing finished 2. Temperature drop ($\theta_0 = -10^\circ$C) 3. Start of thawing

3.1 Relations between frost heave ratio and specimen height under various freezing conditions

Relations between ξ, ξ_w and H under each freezing condition are shown in Fig.5.

In case of Fig.5(a), where σ_1 is small and frost heaving is relatively large, ξ reaches a maximum at a certain value H_0 of the specimen height H. When $H > H_0$, then ξ decreases gradually with increasing H. Meanwhile, ξ decreases rapidly with decreasing H when $H < H_0$. A similar tendency is also seen to some extent under other freezing conditions.

It is a common feature under all the freezing conditions that ξ_w decreases with decreasing H when $H < H_0$. Especially in cases of Fig.5(c) and (d), the mode of water migration reverses from the water intake type to the water discharge type with decreasing H.

Generally, changes in ξ and ξ_w are similar in tendency, but in cases of Fig.5(b) and (d), ξ does not decrease despite that ξ_w decreases in the region in which H is small. In such cases, the mass balance between frost heaving and water migration is lost. The reason is not known well at present, but may be ascribed to experimental errors, for example, due to a small undulation of the freezing front. Under all the freezing conditions, however, something unusual is obviously taking place to affect the values of ξ or ξ_w when $H < H_0$. This, as will be discussed later, is supposed to be the effect of existence of an in situ water freezing zone within frozen soil.

When $H > H_0$, there are two types of changes in ξ and ξ_w. In the one type ξ and ξ_w decrease with increasing H, while in the other, ξ and ξ_w are constant approximately. The former and the latter take place under the freezing condition in which a large and a small amount of water is taken into, respectively. Therefore, when $H > H_0$, it is supposed that the effect of resistance in soil-water movement through the unfrozen soil appears. This will also be discussed later.

3.2 Relations between frost heave ratio and freezing condition

The following empirical equations were proposed by Takashi et al. (1974, 1978) so that ξ and ξ_w are related
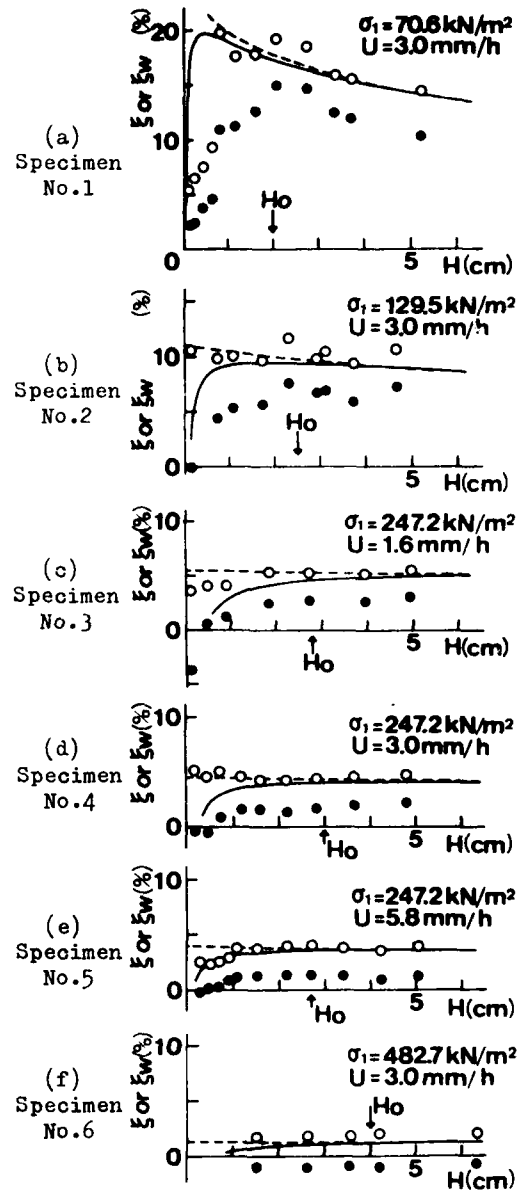
Fig.5 Relations between ξ, ξ_w and H under each freezing condition (open circle: ξ, solid circle: ξ_w)

to σ_1 and U:

$$\xi = \xi_0 + \frac{\sigma_0}{\sigma_1}\left(1+\sqrt{\frac{U_0}{U}}\right) \qquad (3)$$

$$\xi_w = \frac{1}{1+\Gamma}\frac{\sigma_0}{\sigma_1}\left(1+\sqrt{\frac{U_0}{U}}\right) - n_f\frac{\Gamma}{1+\Gamma} \qquad (4)$$

where ξ_0, σ_0, U_0 and n_f are constants concerned with the frost-susceptibility of a soil, and Γ is the volume expan-

250

sion ratio of water when its phase changes to ice (in case of pure water, $\Gamma=0.09$). In equations (3) and (4), however, the effect of specimen height on ξ or ξ_w was not taken into account.

The authors consider that these equations hold basically only in case of a small compound effect of resistance in soil-water movement through unfrozen soil and existence of an in situ water freezing zone. As will be discussed later, the compound effect is minimum at the specimen height H_0. Therefore, analysis using equation (3) and (4) was tried on the experimental data at H_0.

Shown in Table 4 are H_0, $\xi|_{H=H_0}$ and $\xi_w|_{H=H_0}$ under each freezing condition. Relations between $\xi|_{H=H_0}$, $\xi_w|_{H=H_0}$ and $1/\sigma_1$ are shown in Fig.6. Relations between $\xi|_{H=H_0}$, $\xi_w|_{H=H_0}$ and $1/\sqrt{U}$ are shown in Fig.7. According to equations (3) and (4), these relations are to be linear. The results,

Table 4 H_0, $\xi|_{H=H_0}$ and $\xi_w|_{H=H_0}$ under each freezing condition

Specimen No.	Freezing condition σ_1 (kN/m^2)	U (mm/h)	H_0 (cm)	$\xi|_{H=H_0}$ (%)	$\xi_w|_{H=H_0}$ (%)
1	70.6	3.0	2.0	18.3	14.5
2	129.5	3.0	2.5	10.3	6.9
3	247.2	1.6	2.8	5.4	3.2
4	247.2	3.0	3.0	4.5	1.9
5	247.2	5.8	2.7	4.0	1.5
6	482.7	3.0	4.0	2.0	-0.9
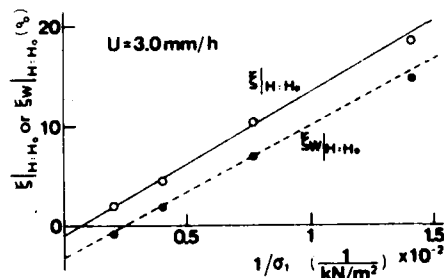
Fig.6 Relations between $\xi|_{H=H_0}$, $\xi_w|_{H=H_0}$ and $1/\sigma_1$
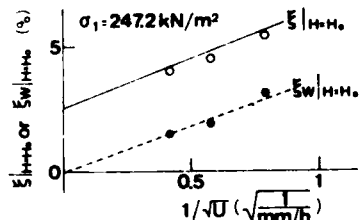
Fig.7 Relations between $\xi|_{H=H_0}$, $\xi_w|_{H=H_0}$ and $1/\sqrt{U}$

shown in Figs.6 and 7, indicate that these equations hold when the specimen height is optimum: $H=H_0$. The values of constants in the equations obtained are shown in Table 5.

Table 5 Values of constants in equations (3) and (4) for disturbed Manaita-bridge clay #3

ξ_0	-0.01
σ_0	8.78 kN/m^2
U_0	1.20 mm/h
n_f	0.389

4. DISCUSSION

4.1 Resistance in soil-water movement through unfrozen soil

The following equations were obtained by Takashi et al. (1976) as a result of an analysis, on the basis of equations (3) and (4), of the effect of resistance in soil-water movement through unfrozen part within a freezing soil specimen on ξ:

$$\xi = \xi_0 + n_f\Gamma + \frac{(1+\Gamma)}{2UH}\left\{D-C\sigma_1-BH\right.$$
$$+\frac{C(2A-B\sigma_1)}{B}\ln\frac{BD+B^2H+C(2A-B\sigma_1)}{2AC}$$
$$\left.-C\sigma_1\ln\frac{D+(2A-B\sigma_1)H/\sigma_1+C\sigma_1}{2C\sigma_1}\right\} \qquad (5)$$

$$\xi_w = \frac{1}{1+\Gamma}(\xi-\xi_0-n_f\Gamma) \qquad (6)$$

where $A = \frac{U}{1+\Gamma}\sigma_0\left(1+\sqrt{\frac{U_0}{U}}\right)$, $B = n_f\frac{\Gamma}{1+\Gamma}U$

$C = k/\rho_w g$, $D = \sqrt{(C\sigma_1-BH)^2+4ACH}$

k is the hydraulic conductivity of unfrozen soil, ρ_w is the density of water, and g is acceleration of gravity. Here, ξ and ξ_w are represented as functions of H, however, the effect of existence of an in situ water freezing zone is not taken into account. When resistance in soil-water movement through unfrozen soil can be neglected: i.e. $k \to \infty$ or $H \to 0$, equation (5) coincides with equation (3).

Calculated values of ξ using equation (5) are shown by broken lines in Fig.5. The value of σ_0 in Table 5 which is determined from Fig.6 should be altered because the effect of H on ξ appears more or less even at $H=H_0$. Therefore at the calculation, the value of σ_0 is redetermined to fit the experimental results. The redetermined

value of σ_0 is 10.12 kN/m^2. The results show that the relation between ξ and H in the region $H > H_0$ can be explained by the effect of resistance in soil-water movement through unfrozen soil.

4.2 Existence of an in situ water freezing zone and an ice segregating zone within frozen soil

The temperature θ_{init} at which ice segregation initiates is deduced from modified Clausius-Clapeyron's equation (Takashi et al., 1981b):

$$\theta_{init} = -\sigma_e/P_{so} \tag{7}$$

where σ_e is the effective stress and P_{so} is the constant ($P_{so}=1.09$ MN/m^2/^{o}C). The temperature θ_{crit} is a constant inherent to soil, representing the critical temperature below which the continuity of veins of unfrozen water within frozen soil disappears and ice segregation cannot occur (Takashi et al., 1981a, b). In the previous study, θ_{crit} of Manaita-bridge clay was estimated lower than -30^oC (Takashi et al., 1981b).

The thickness of an in situ water freezing zone is denoted by δ (Fig.1);

Fig.8 Relation between δ and σ_1 (solid circle: result of supplemental experiment)

Fig.9 Relation between δ and U (solid circle: result of supplemental experiment)

then *frost heaving* cannot occur before the freezing front penetrates up to δ into a specimen. This seems to correspond with the experimental fact that frost heaving does not appear in a period of early several hours in each frost heave test (see Fig.3).

In each test, the temperature of cooling plate is controlled to freeze a specimen at a constant frost penetration rate U as:

$$\theta_c = -a \cdot t \tag{8}$$

where θ_c is the temperature of cooling plate, a is the rate of temperature depression of cooling plate and t is the elapsed time from the initiation of freezing. Then a is proportional to U^2 (Takashi et al., 1975). From this equation the time when $\theta_c = \theta_{init}$ is obtained, and δ is obtained on multiplying it by U:

$$\delta = -U \cdot \theta_{init}/a \tag{9}$$

Then δ is derived from equations (7) and (9) theoretically as:

$$\delta = U \cdot \sigma_e/(a \cdot P_{so}) \tag{10}$$

Thus, δ increases with increasing σ_e or decreasing U, because $a \propto U^2$.

On the other hand, δ was estimated experimentally by multiplying the elapsed time up to the appearance of frost heaving by U. A comparison between δ_{theo} and δ_{exp} is shown in Figs. 8 and 9. Besides, in these figures the results of supplemental experiments are also shown, which were conducted under a wide range of freezing condition using specimen No.6 at H=2.5 cm. Moreover, σ_1 was used in the calculation of δ_{theo} instead of σ_e, which should have been used, because σ_e is not estimable. As shown in Fig.8, δ_{exp} agrees with δ_{theo} under various σ_1. As far as U is concerned, however, a correlation between them is poor (Fig.9).

The configuration of an *in situ* water freezing zone and an ice *segregating* zone within a specimen at the time of finish of freezing is shown in Fig.10 schematically. In case of (a) or (b) in Fig.10, the frost heave ratio ξ (as a whole specimen) changes depending on δ/H. Strict clarification of the dependency of ξ on δ/H calls for a knowledge on the distribution of local frost heaving in the ice segregating zone. However, the knowledge on it is poor at present. Therefore, as a first approximation, it is assumed that
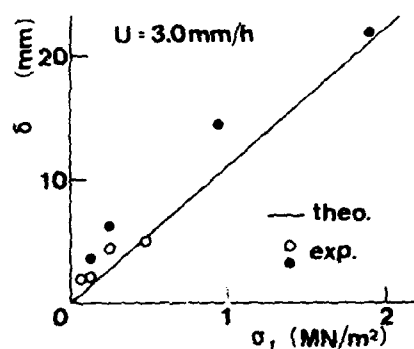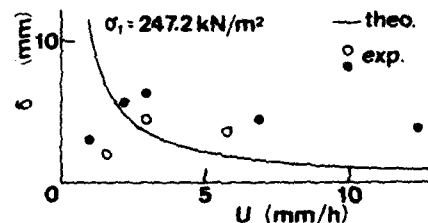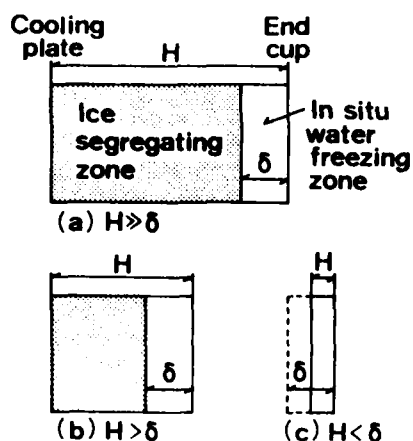
Fig.10 Configuration of in situ water
freezing zone and ice segrega-
ting zone within specimen at
the time of finish of freezing

all the ice lenses are segregated only
at the plane $\theta = \theta_{init}$. Considering that
the hottest ice lens brings about the
screening effect on migration of un-
frozen water and that U in this study
are relatively large, the assumption
is admissible. Then the frost heave
ratio ξ (as a whole specimen) will be
proportional to $1-\delta/H$ as follows:

$$\xi = \xi_0 + (\xi_c - \xi_0)(1-\delta/H) \qquad (H>\delta)$$

$$\text{or} \quad \xi = \xi_0 \qquad (H\leq\delta) \qquad (11)$$

where ξ_c is the frost heave ratio in
case in which the effect of existence
of an in situ water freezing zone is
not taken into account and corresponds
to ξ in equation (5).

Curves calculated by equation (11)
are shown in Fig.5 by solid lines. The
decrease in ξ in the region in which
$H < H_0$ can be explained qualitatively
by existence of an in situ water freez-
ing zone within frozen soil.

4.3 Optimum specimen height in frost
heave test

It is obvious from the above dis-
cussions that the smaller the specimen
height is, the smaller is the effect
of resistance in soil-water movement
through unfrozen soil. Additionally,
a specimen low in height has the fol-
lowing experimental advantages: uni-
directionality of freezing is improved;
friction between a specimen container

and the unfrozen part of a specimen is
reduced; the test period is shortened.

On the other hand, the effect of
existence of an in situ water freezing
zone is determined by the parameter
$1-\delta/H$ and becomes large with de-
creasing H. Therefore, the optimum H
in laboratory frost heave tests is
considered to be near H_0 at which both
resistance in soil-water movement
through unfrozen soil and existence of
an in situ water freezing zone have the
minimum compound effect on ξ. As stat-
ed in 3.2, the experimental results at
the specimen height H_0 obey the empir-
ical equations (3) and (4) approximate-
ly.

In this study, the soil was a
markedly frost-susceptible clay. The
results showed that optimum H of this
clay was within a range between 2 and
4 cm. As frost-susceptibility of an
ordinary clay or silt is lower than the
clay used, the optimum H of it is also
considered to be within the range be-
tween 2 and 4 cm generally. However, in
case that frost-susceptibility of a
soil is higher and frost heave tests
are conducted under such freezing con-
dition as frost heaving occurs easily,
the optimum H will be a little smaller.

4.4 Some problems on practical applica-
tion of results of frost heave test

If the constants in equation (3)
are obtained as results of frost heave
tests at the optimum H, they make it
possible to estimate simply the frost
heave ratio ξ under an arbitrary freez-
ing condition. These constants ξ_0, σ_0
and U_0 are useful as indices concerning
frost-susceptibility of a soil.

However, some problems still re-
main unsolved in applying the results
of frost heave tests to predict the
frost heave amount in the construction
site where ground freezing is under-
taken. For example, in the laboratory
test freezing advances without resist-
ance in water movement from an outer
source to a specimen, whereas large
resistance in water movement exists in
the ground. This difference may be
analyzed to some extent using equation
(5) (Takashi et al., 1976; Takashi et
al., 1977). However, it will be a com-
plicated problem to take into account
the distribution of permeable or im-
permeable layers in the ground.

253

5. CONCLUSIONS

The results are summarized as follows:

(1) The frost heave ratio ξ reaches a maximum at a certain value H_0 of the specimen height H. When $H > H_0$, then ξ decreases with increasing H, which can be explained quantitatively by resistance in soil-water movement through the unfrozen part within a freezing soil specimen. Meanwhile, ξ decreases with decreasing H, when $H < H_0$, which can be explained qualitatively by existence of an in situ water freezing zone within frozen soil.

(2) The optimum H in laboratory frost heave tests is near H_0 at which both resistance in soil-water movement through unfrozen soil and existence of an in situ water freezing zone within frozen soil have the minimum compound effect on ξ. The test results obtained at H_0 obeys approximately empirical equation (3) suggested previously by Takashi et al. (1974; 1978) concerning a relation between ξ and such freezing conditions as overburden pressure and frost penetration rate. Then the constants in the equation are obtained as indices of frost-susceptibility of a soil tested.

REFERENCES

Dirksen, C. and Miller, R.D., 1966. Closed-system freezing of unsaturated soils, Soil Sci. Soc. Am. Proc., 30: 168-173

Fukuda, M., Orhum, A. and Luthin, N., 1980. Experimental studies of coupled heat and moisture transfer in soils during freezing, Cold Regions Sci. and Tech., 3: 223-232

Hoekstra, P., 1966. Moisture movement in soils under temperature gradients with the cold-side temperature below freezing, Water Resources Research Board Special Report, 103: 78-90

Loch, J.P.G. and Kay, B.D., 1978. Water redistribution in partially frozen, saturated silt under several temperature gradient and overburden loads, Soil Sci. Soc. Am. J., 42: 400-406

Miller, R.D., 1972. Freezing and heaving of saturated and unsaturated soils, Highway Res. Record, 393: 1-11

Penner, E. and Goodrich, L.E., 1980. Location of segregated ice in frost susceptible soil, Pro. 2nd Int. Symp. Ground Freezing, 626-639

Radd, F.J. and Oertle, D.H., 1973. Experimental pressure studies of frost heave mechanism and the growth fusion behavior of ice, Permafrost, 2nd Int. Conf., North Am. Contribu., Washington D.C., Nat. Acad. Sci., 377-384

Takashi, T., Masuda, M. and Yamamoto, H., 1974. Experimental study on the influence of freezing speed upon frost heave ratio of soil under constant effective stress, Seppyo, J. Japanese Soc. Snow and Ice, 36, 2: 49-68

Takashi, T. and Masuda, M., 1975. On an exact solution of heat transfer equation in freezing soil with constant freezing speed, accompanying uniform flow of suction water to the freezing front, Seppyo, J. Japanese Soc. Snow and Ice, 37, 1: 13-20

Takashi, T., Masuda, M. and Yamamoto, H., 1976. Influence of permeability of unfrozen soil on frost heave, Seppyo, J. Japanese Soc. Snow and Ice, 38, 1: 1-10

Takashi, T., Ohrai, T. and Yamamoto, H., 1977. Pore water pressure and consolidation in unfrozen soil near the freezing front, Seppyo, J. Japanese Soc. Snow and Ice, 39, 2: 53-64

Takashi, T., Yamamoto, H., Ohrai, T. and Masuda, M., 1978. Effect of penetration rate of freezing and confining stress on the frost heave ratio of soil, Permafrost, 3rd Int. Conf., 1: 737-742

Takashi, T., Ohrai, T., Yamamoto, H. and Okamoto, J., 1979. Upper limit of heaving pressure obtained by observing pore water pressure under partially soil freezing, Seppyo, J. Japanese Soc. Snow and Ice, 41, 4: 277-287

Takashi, T., Ohrai, T., Yamamoto, H. and Okamoto, J., 1981a. Upper limit of heaving pressure derived by pore-water pressure measurements of partially frozen soil, Eng. Geol., 18: 245-257

Takashi, T., Ohrai, T., Yamamoto, H. and Okamoto, J., 1981b. An experimental study on maximum heaving pressure of soil, Seppyo, J. Japanese Soc. Snow and Ice, 43, 4: 207-215

FREEZING RATE AND FROST HEAVE OF SOILS

Liu Hongxu
(Engineer, Heilongjiang Provincial Low Temperature
Construction Science Research Institute)

Abstract

A great number of scholars have
studied the relationship of the
freezing speed and frost-heave of
soils, many of them have conducted
tests on small size specimens in labo-
ratories. Most of their testing re-
sults indicate that a high expansion
rate on freezing is resulted from a
low freezing speed giving enough time
for water migration.

Based on the tests conducted at
original locations at a Frozen Soil
Observation Station, the following
results have been obtained through
analyzing the relationship of the
freezing speed, expansion speed on
freezing, negative temperature gra-
dient, expansion rate, frost-heave
and so on:

When a soil is freezing at a
lower temperature, there exists
greater temperature gradient, higher
freezing speed, higher expansion
speed on freezing, from which higher
expansion rate is resulted.

Water content, type of soil and
temperature are three important fac-
tors generated fro t-heave essential-
ly. If the first two factors are
constant, then various freezing speed
will occur under different negative
temperatures, thus leading to diffe-
rent expanding rate on freezing. In
order to study this problem, not a
few researchers, at home and abroad,
have carried out tests with small
size specimens in laboratory. Based
on the field measurement in situ

carried out in the Longfeng Frozen
Soil Observation Station, Daqing(Long.
125°E, Lat. 46.25°N) and Aihui Frozen
Soil Observation Station (Long. 127°E,
Lat. 50.0°N), both in Heilongjiang
Province, results of study on the
above problem is given in this paper.
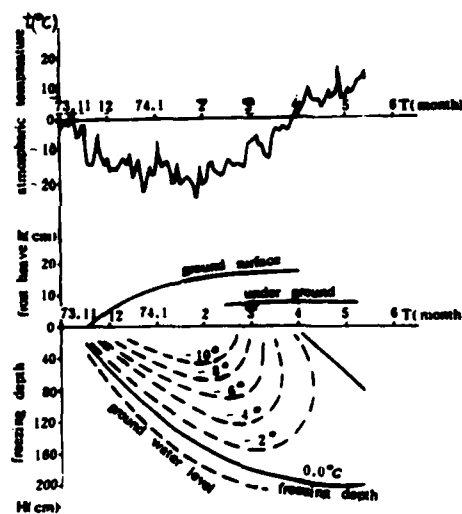
Fig.1 Relationship between t(°c), H(cm)
h(cm), measured at Long-feng
Frozen Soil Observation Station
in 1973-1974

Relations between outdoor tempe-
rature, freezing depth, soil tempera-
ture, water-table, amount of frost-
heave and time in 1973-1974 are shown
in Fig. 1. Amount of frost-heave
generally means the amount of expan-
sion on the ground surface (if not
indicated). When spring comes, ground

255

surface begins thawing, the freezing front surface still goes downward gradually and expansion on freezing does not stop. Owing to settlement in thawing, curve representing amount of heave on surface begins to drop, therefore cannot represent the expansion on freezing of the freezing front, so the expansion curve for the subsoil must be taken in consideration.

The actual annual freezing depth (at which soil temperature is 0°C) is 205 cm. Max. distance between the freezing depth and ground water level is 20 cm., belonging the open system, max. amount of heave is 16.6 cm., average expansion rate on freezing is 3.1%. According to the classification in the Foundation Code for Industrial and Public Buildings (TJ 7-74), the soil can be classified as strong frost susceptible soil.

Fig. 2 shows variation of expansion rate on freezing η (amount of heave per unit freezing depth $\frac{\Delta h}{\Delta H}$ or $\frac{dh}{dH}$, %), freezing speed V (Falling speed of the freezing front, i.e. freezing depth per unit time $\frac{\Delta H}{\Delta T}$ or $\frac{dH}{dT}$, in cm./day), expansion speed v (amount of heave per unit time $\frac{\Delta h}{\Delta T}$ or $\frac{dh}{dT}$, cm./day), gradient of temperature x (negative temperature increment per unit freezing depth, $\frac{\Delta t}{\Delta H}$ or $\frac{dt}{dH}$, in °C/cm.) and amount of heave h (cm.) along the freezing depth H (cm.).

depth. Curves showing the expansion rate on freezing and freezing speed are similar, that means, the greater the freezing speed, the larger the expansion rate.

In the frozen layers in the seasonal frozen soil district, distribution of expansion rate on freezing along depth is not uniform. The rate reaches maximum on the surface and, at last, becomes zero at the bottom of the layer. The portion near the ground surface is called the major frost-heave zone; the lower portion, the secondary frost-heave zone; the lowest portion is the layer which is although frozen but not heaved. Furthermore, at the location where freezing is not developed, no frost-heave will occur. This has been proved by a lot of measurement data. That means expansion on freezing of the upper portion where freezing speed is high is also large, and is small in the lower portion where freezing speed is low. At the base, freezing speed equals zero, expansion also stops. It is shown also that expansion rate on freezing decreases with increase of freezing depth. Although there is fluctuation in temperature gradient, yet obvious variation rule exists, i. e. temperature gradient decreases with increase of freezing depth, or freezing speed decreases with temperature gradient. Relationship between temperature gradient, expansion speed on freezing, expansion rate and freezing speed is shown in Fig. 3.

Fig. 2 Relationship between η, V, v, h, x and H.

from Fig.2, freezing speed decreases with the increase of freezing
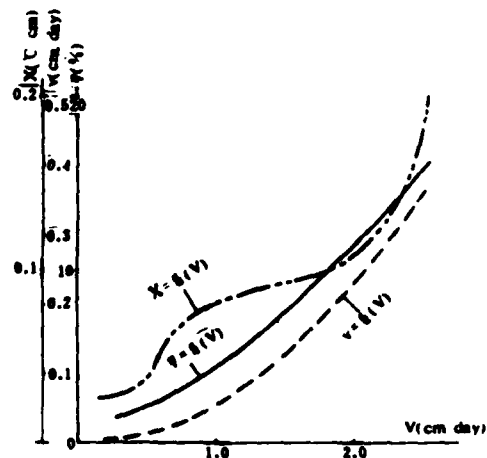
Fig.3 Relationship between x, v, η and V. Particles of cohesive soil are

256

considerable small; the smaller the diameter of the particle, the larger the specific surface and also the surface energy for holding the water film. Compared with other kind of soil, content of unfrozen water in cohesive soil is greater under the same temperature condition. Ice begins to segregate when the temperature of soil attains the freezing temperature $(-0.1 — -1°C)$. In the interval of $0—-3°C$, variation of content of unfrozen water is very great and such interval is called district of liquid phase severely changed; interval of -3 to $-9°C$ is called district of liquid phase moderately changed; interval on which temperature is under $-9°C$ is called district of liquid phase slightly changed. No matter what theory is used to explain the mechanism of water migration, it will be considered from the macroscopic point of view that content of unfrozen water will relatively decrease when amount of water which changes into ice becomes larger. The more the variation of humidity gradient when compared with the initial equilibrium state (i.e. humidity gradient increases), the more the water supplemented from the lower layer. If no phase change occurs in the water of soil and humidity field remains the original quilibrium state, redistribution of water will not carry on, migration of water does not exist also. Humidity gradient here mentioned means the average value of isothermal contours of $0°—-4°C$.

Humidity gradient is the critical factor determining migration of water, not only for frozen soil in winter, but also for evaporation of ground surface in summer. Owing to the increment of humidity gradient induced by evaporation, water in the lower layer will be imbibed to compensate. If change of humidity gradient is not induced by freezing or evaporation but by taking away from a certain layer using other methods (such as by blotting paper), water in the lower layer will also migrate. Phenomenon of water migration is a process in which soil layer losing its humidity equilibrium state will restore its original state as far as possible.

Effects of negative temperature on frost-heave are: firstly, to change water contained in soil into ice, so that volume of soil expands;

secondly, to increase humidity gradient in soil so that water migration is accelerated. Water coming from other layer afterwards freezes at negative temperature, thus expansion on freezing is increased. Amount of frost-heave depends mainly on amount of water migrated from lower layer to the freezing front. Speed of migration depends on magnitude of humidity gradient, in turn, magnitude of humidity gradient depends on magnitude of temperature gradient and, at last, magnitude of temperature gradient depends on outdoor temperature. Increase of humidity gradient is resulted from increase of temperature gradient. Along with increase of temperature gradient, not only humidity gradient increases, but also freezing speed increases. Therefore, in the foundation soil, both increase of humidity gradient and freezing speed are resulted from increase of temperature gradient. If negative temperature is relatively high, or freezing has developed to a certain depth, so temperature at the bottom of the frozen layer is relatively high and temperature gradient is considerable small, less ice will be segregated, humidity gradient will become small and water will migrate slowly causing small expansion rate.
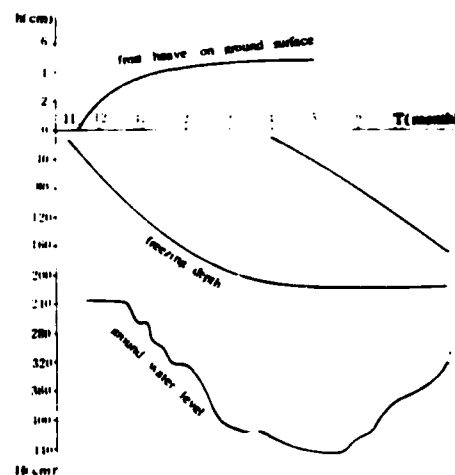
Fig.4 Relationship between H,h,ground water level and time, measured at Aihui Frozen Soil Observation Station.

Fig. 4 shows the measurement

257

results in the Aihui Frozen Soil Observation Station, Heilongjiang Province in 1973-1974. Minimum distance between underground water level and frozen depth is 1.4m, belonging closed system. Frozen depth is 2.20 m, amount of expansion is 4.8cm., average expansion rate on freezing $\eta = 2.2\%$. The soil is classified as weakly frost-heaved soil. Fig.5 shows the relationship between expansion speed on freezing, freezing speed, expansion rate on freezing and frozen depth at the site. Fig. 6 shows relationship of expansion speed on freezing and freezing speed. From Fig.2,3,5 and 6, the relationships obtained in the above two stations are essentially the same.
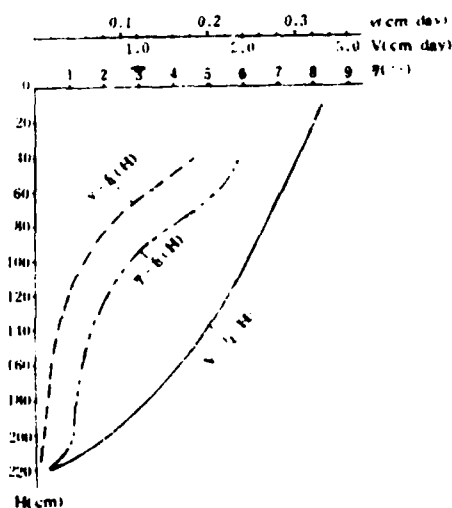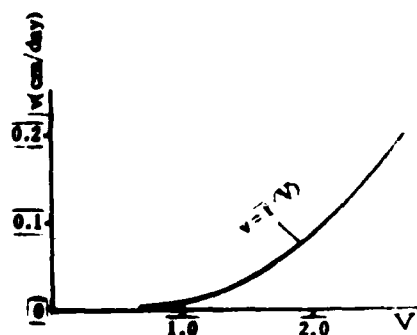
Based on the above analysis, the following points of view are obtained:

1) Effects of negative temperature on frost-heave of soil are:

(i) to change the water in soil into ice, making soil mass expand;

(ii) along with ice segregation, the original humidity field will be damaged, thus forming new humidity gradient and causing migration of water in the lower layer (re-distribution of humidity). In turn, water transferred upward freezes again at negative temperature, accelerating the expansion on freezing.

2) Freezing speed of foundation soil depends mainly on local outdoor temperature in winter. If no special measure is taken, the lower the temperature, the higher the average freezing speed. From Fig. 2 and 5, the annual max. freezing speed in the coldest district in the north part of Northeast, China, is $\leqslant 3$cm/day, which, compared with that used in the frost-heave test in laboratory, is not so high. From the trend of the curve in Fig.3 and 6, there is no precursor for the occurence of the above max. value, that is to say, the present freezing speed has not attained the critical value, at which expansion rate on freezing will be affected.

When freezing speed is below the critical value, the higher the freezing speed, the higher the expansion rate on freezing. Critical freezing speed varies with the type of soil.

When specimens of small size are used in the laboratory frost-heave test, positive temperature still remains at the bottom of the specimen, thus forming higher temperature gradient and lower freezing speed.Therefore, increase of expansion rate on freezing will be resulted. This does not consistent with the actual condition, i.e., there is no heat generated at the bottom of the lower soil layer.

3) Frost-heave test can be carried out in laboratory according actual freezing speed and distribution of expansion rate on freezing along with depth, and then determine the average expansion rate on freezing of foundation soil at site approximately.

Taking Fig.2 as an example which is of an open system, surface soil of 40-40 cm is sampled to make specimens and freezing speed of 2.5 cm./day is selected. If the expansion rate on freezing of $\eta = 16\%$ is obtained, the

Fig.5 Relationship between v, T, η and H.

Fig.6 Relationship between v and T.

258

corresponding average expansion rate
of the foundation soil will be about
8%. If soil , 1.6m beneath the sur-
face, is taken to make specimens, the
soil's own weight should be consi-
dered.

FROST HEAVE CHARACTERISTICS OF SOIL UNDER EXTREMELY LOW FROST PENETRATION RATE

Shigeru Goto : Research Engineer, Research Laboratory of Shimizu Construction Co., Ltd., Japan

Yukishige Takahashi : Chief Civil Engineer, Plant Construction Division, Tokyo Gas Co., Ltd., Japan

ABSTRACT

This paper presents results of the open system laboratory frost heave test which were conducted to examine the frost susceptibility of soil under the stationary condition of nominally zero frost penetration rate. The condition was induced by controlling boundary temperatures to maintain a level of freezing front.

Tests on all specimens have indicated continual heaving even after 2100 hrs, long after the nominally zero frost penetration rate which has been achieved in the earlier stage of the tests.

Furthermore, it is important that the frost heave rate decreases as time elapse. Our analysis shows that the rate of frost heave and, in turn, its amount are influenced mainly by such factors as a degree of overburden pressure, (P), and cold-side temperature (θ_Q). Consequently, it is proposed the following empirical formula for a estimation of the frost heave amount, (h), beyond the termination of the frost penetration.

$$h = \alpha \left[1 - \exp\{\frac{\beta}{P} (\theta_Q - \theta_F)t\}\right]$$

where α and β are the generic constants of soil, θ_F is freezing point of soil and t is elapsed time.

The formula gives on approximate evaluation of frost heave, and shows a significant correlation between the constant α and the medium grain size (D50) of given soil consequently.

1. INTRODUCTION

Studies have widely progressed over the frost susceptibility of soil, partly because it is considered as one of vital factor to design the in-ground LNG storage tank and artificial ground freezing construction method. However, previous research works had been conducted under the constant rate of frost penetration. In other words, few observation have been made under the stationary freezing front of zero frost penetration rate. Such phenomena of zero frost penetration rate can be induced by the heat barrier installed around artificial freezing ground

to thermally protect neighboring structures from expansion of the frost-affect soil.

To examine the frost heave characteristics of soil under the stationary freezing front, the laboratory frost heave test were conducted for long duration of time under nominally zero frost penetration rate which was immediately induced by the controlling boundary temperatures to maintain the level of freezing front within the specimen.

2. PREPARATION OF TEST SPECIMENS

The test specimens used in this laboratory frost heave test were prepared by remolding the sand and silt sampled by the Tokyo Bay. The physical properties of these soils are presented in Table 1. Fig. 1 gives the grain size distribution which has great effect upon the frost susceptibility of soil.

It is well known that the freezing point of soil is depressed if the pore water contains salt. It is also acknowledged by Y o n g and Serag-Eldin[2] that the salt has a direct effect upon the frost susceptibility of soil. In order to eliminate such an undesirable effect, specimens were saturated in pure water.

Pore water pressure is reduced across the unfrozen

Table 1. Physical properties of the soils

			S-1	S-2	C-1	C-2	C-3	C-4
Water content	W	(%)	26.8	9.5	39.8	71.3	75.3	37.4
Specific gravity	Gs		2.780	2.670	2.716	2.719	2.660	2.586
Void ratio	n	(%)	42.7	37.7	53.3	65.8	64.6	50.5
Grading								
Sand (74~2000μm)		(%)	60.0	97.0	27.0	14.0	26.0	40.0
Silt (5~74μm)		(%)	35.5	3.0	53.5	49.0	48.0	46.0
Clav (under 5μm)		(%)	4.5	0	19.5	37.0	26.0	14.0
Liquid limit	Wl	(%)	--		42.2	86.9	56.2	43.1
Plastic limit	Wp	(%)	--	-	23.2	39.6	29.4	21.1

* Notation "S" means Sandy soil and notation "C" means clayey soil.

soil because of the suction effect which occurs at the freezing front. Large deformations due to consolidation of normally consolidated cohesive soil under reduced pore water pressure can in turn affect the measurements[3]. To avert such an effect, each test specimen was preconsolidated by applying a pressure of 412KN/m², which is higher than the overburden pressure of 157KN/m², applied in the experiment.

Each test specimen was a cylindrical type of having a diameter of 60 mm, and approximately 30 mm in height. To supplement the laboratory frost heave test, 90 mm high test specimen was also used.
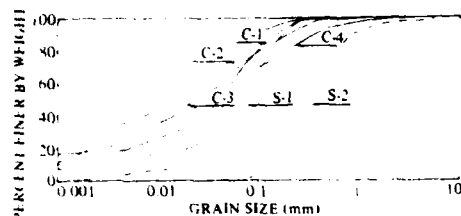
Fig. 1. Grain size distribution curves

3. TEST APPARATUS

Given in Fig. 2 and 3 shows a diagram of the test apparatus which was used for the laboratory frost heave test.

It is widely known that the type of soil, the overburden pressure, and the thermal condition influence the frost heave characteristic of the saturated soil.

The apparatus equipped with loading lever (magnification factor of 40) is capable of adjusting overburden pressure incorporating with the heave effect of specimens by automatically maintaining the lever in its horizontal configuration.

Cooling plates were placed on the top and bottom
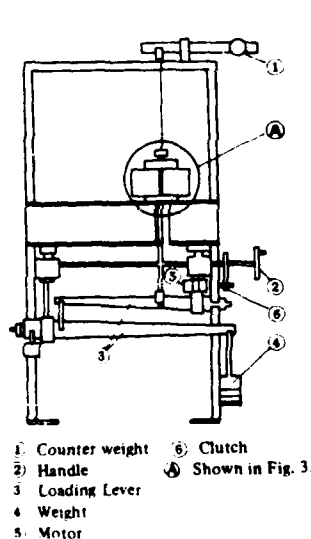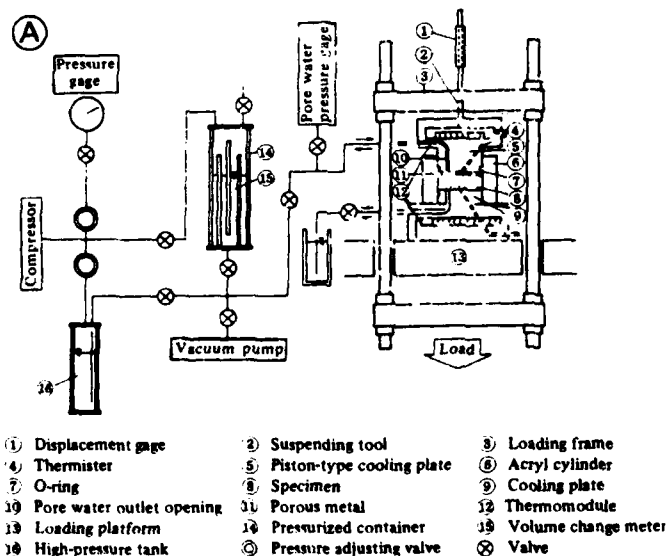
faces of the cylinders. Cylindrical specimens were cooled to a desirable temperature by employing electrically operated unit which gives a immediate response to the needs.

The lower-side cooling unit is mounted with a programable temperature controller, which can vary the cooling temperature along the lapse of time.

The range of working temperature on the upper-side cooling unit is from 263 K to 283 K.

The lower-side cooling unit has the range of working temperature from 251.5K to 273K. Accuracy of temperature control is within ± 0.4K.

A differential transformer type displacement gauge of accuracy within 0.5 %/FS was used to measure the frost heave. Water inflow and outflow were controlled at the upper end of each test specimen. The amount of water flow was measured using an electrostatic volumetric change meter with its accurary of within ± 0.3 %/FS.

4. TEST CONDITIONS AND TESTING PROCEDURES

Boundary temperatures of higher or lower than the freezing point of the soil were maintained for adequate duration of time on top and bottom faces of the cylindrical specimens respectively to achieve the condition of zero frost penetration rate.

The laboratory frost heave test of the open system were conducted to observe the amount of frost heave with respect to parameters such as type of soils, degree of overburden pressures and level of boundary temperatures.

Table 2 shows the different combinations of these parameters for the tests.

Each test specimen underwent the test while packed in an acryl mold. To prevent adverse effect from the intensive friction between the test specimen and the inner wall of this mold, a silicon grease was used on the interface of the mold and the specimen.

In order to protect each specimen from ambient thermal conditions, the exterior face of the mold was in-

1	Counter weight	6	Clutch	①	Displacement gage	②	Suspending tool	⑧	Loading frame
2	Handle	⑩	Shown in Fig. 3	④	Thermister	⑤	Piston-type cooling plate	⑥	Acryl cylinder
3	Loading Lever			⑦	O-ring	⑨	Specimen	⑨	Cooling plate
4	Weight			⑩	Pore water outlet opening	⑪	Porous metal	⑫	Thermomodule
5	Motor			⑬	Loading platform	⑭	Pressurized container	⑮	Volume change meter
				⑯	High-pressure tank	◎	Pressure adjusting valve	⊗	Valve

Fig 2. Test apparatus   Fig. 3. Detail of the cooling system (as 'A' in Fig.-2)

262

Table 2. Combination of test parameter

| | Overburden pressure $P(KN/m^2)$ | Both side temperature (K) | | Specimen height ℓ (cm) |
		Cold-side θ_ℓ	Warm-side θu	
S-1	39	268	278	2
	157			
	235			
	628			
	157	272	274	
		270	276	
		268	278	
		263	283	
S-2	39	271	277	3
			281	
		270	276	
		267		
			279	
	157	271	275	
		270	276	
C-1	157	271	275	
C-2	157	271	275	
C-3	157	263	283	
C-4	157	272	274	
		270	276	
		268	278	

sulated with a foamed urethane and an urethane mat.

For the test conducted on a 90 mm high specimen, soil sample packed in an acryl tube was placed in another acryl tube, and anti-freeze liquid of temperature 272 K was circulated in the annular space for the purpose of insulation.

The laboratory frost heave test was performed on the following sequences.

(1) The test specimen (pre-consolidated under a pressure of 412KN/m² in case of silt) which has been previously saturated with pure water is packed into an acryl mold, and placed between the upper and lower cooling plates.

(2) The test specimen is then loaded with specified overburden pressure until the test specimen completes its settlement.

(3) The whole of the test specimen is next cooled down to the freezing point.

(4) A thermal shock is applied to the lower side of the test specimen so that the test specimen will initiate a core of ice.

(5) The upper-side cooling plate is set to a temperature "θu" (warm-side temperature), and the lower-side cooling plate to a prescribed cold-side temperature "θ_ℓ."

5. TEST RESULTS

Fig. 4 shows the time dependent variation of frost heave amount for soil C-1, C-2, and C-3. Referring to the results of the heat conduction analysis (see the appendix), the frost penetration rate at 50 hours after the start of the test is less than 10^{-10} mm/hr which can be regarded as nominally zero rate for the experimental purposes. The test specimens exhibited continual frost heaving, even after the frost penetration have terminated. This phenom-

ena of continual frost heaving at zero frost penetration rate continued more than 2100 hours. No specimen indicated ceasing of continual frost heaving at the end of each test. Furthermore, it should be noted that there were definite indication of decrease in frost heave rate with respect to time.
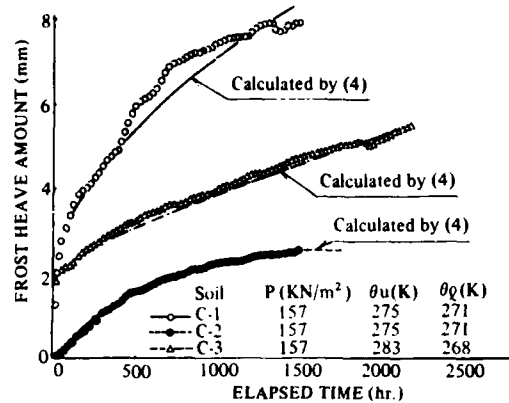
Fig. 4. Time dependent variation of frost heave

Given in Fig. 5 shows the results of the test to examine the effect of overburden pressure upon frost heave. It can be seen that frost heave is significantly affected by the degree of applied overburden pressure and it decreases as the pressure increases.
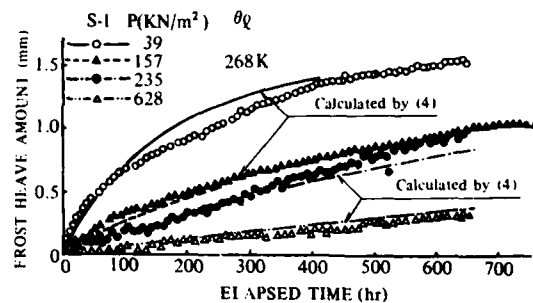
Fig. 5. The effect of overburden pressure on time dependent variation of frost heave

Fig. 6 also shows the results of the test to investigate the effect of the boundary temperatures on the frost heave. Likewise with overburden pressure, boundary temperatures also have the direct influence upon frost heave, the lower the cold-side temperature, the greater the frost heave at each point of measurement.
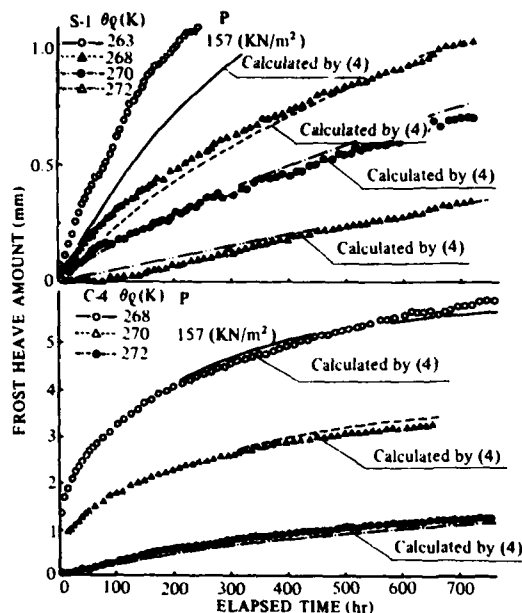
Fig. 6. The effect of cold-side temperature on time depended variation of frost heave

6. DISCUSSIONS

6-1 Derivation of an empirical formula

As described the phenomena of continual frost heaving are observed. The attempt has been made to derive an empirical formula for estimation of frost heave at zero frost penetration rate that incorporates the effect of decreasing frost heave rate with respect to time. Fig.7 shows the reciprocal of frost heave rate as a function of time. The relation between reciprocal of the frost heave rate (dt/dh) and elapsed time (t) is linear on semi-lagarithmic plot sheet. This relation can be written as

$$\log \left(\frac{dt}{dh}\right) = at + b \quad \dots \dots \dots \dots \quad (1)$$

where 'a' and 'b' are constants of positive value. Integration of the factor dt/dh over time leads us to a following expression (2) of frost heave at zero frost penetration rate.

$$h = \alpha \{1 - \exp(-\beta't)\} \quad \dots \dots \dots \dots \quad (2)$$

Fig.8 gives the relation between constant α, β' and prescribed parameters selected for the laboratory frost heave test. α is assumed to be a generic constant of the soil, while β' is assumed as a following expression.

$$\beta' = \frac{\beta}{P} (\theta_F - \theta_\varrho) \quad \dots \dots \dots \dots \dots \quad (3)$$

where θ_F is a freezing point of soil, θ_ϱ is a cold-soide temperature and P is the overburden pressure.
Therefore the frost heave at zero frost penetration rate can be expressed in terms of previously described parameters and constants as follows.

$$h = \alpha \left[1 - \exp\{\frac{\beta}{P} (\theta_\varrho - \theta_F)t\} \right] \quad \dots \quad (4)$$

where α and β are the generic constants of soil and given in Table-3. The results of calculations according to
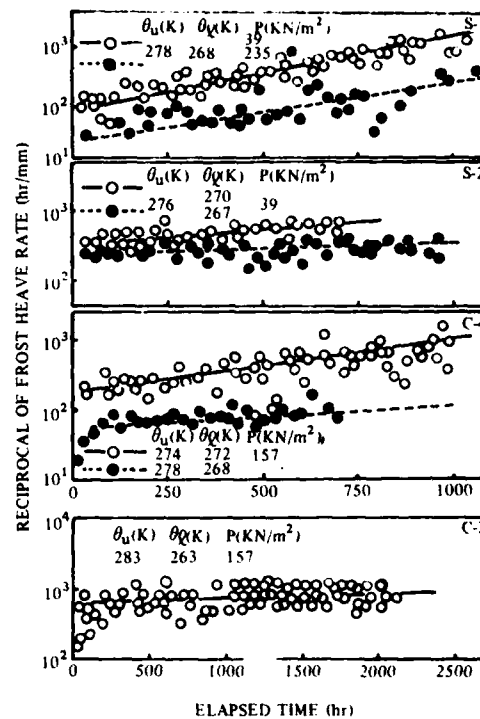
Fig. 7. The relationship between reciprocal of frost heave rate and elapsed time
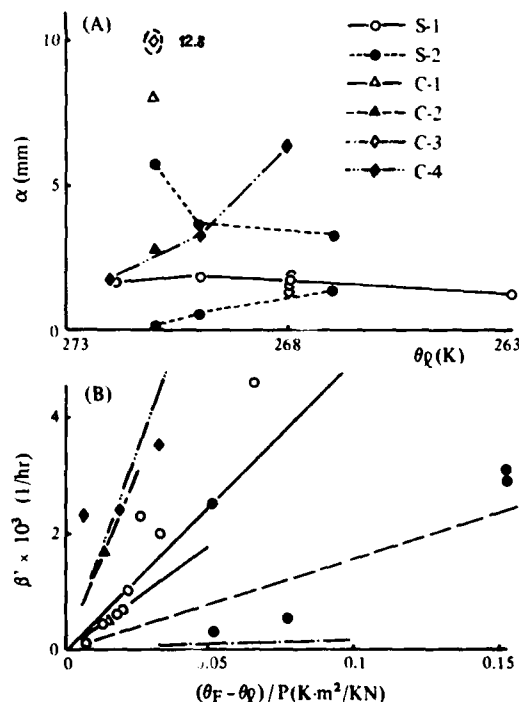
Fig. 8. Relationships between α, β' and θ_ϱ, P

264

the equation (4) with the respective values of α and β are shown in Figs.4 through 6. It can be seen that those results are in good agreement with experimentally observed results.

Expression (4) incorporates well the effects of the overburden pressure, P, and the cold-side temperature, θ_Q, upon frost heave. However, it is of our interest that the effects of P and θ_Q diminish as time passes and the value of frost heave converges to the constant value α.

Table 3. Values of α, β

	S–1	S–2	C–1	C–2	C–3	C–4
α (mm)	1.5	2.2	8.0	2.8	12.8	2.5
β (KN/m²K·hr)	5.2×10^{-2}	1.6×10^{-2}	5.6×10^{-2}	1.3×10^{-1}	2.1×10^{-3}	1.4×10^{-1}

6-2 Confirmation by the heat conduction analysis

To explain the time-varying phenomena of frost heave at zero frost penetration rate from the viewpoint of heat balance, analysis of heat conduction were performed. Fig.9 shows the model used for this heat conducton analysis.

The thermal equilibrium equations on the boundaries of unfrozen soil, freezing fringe (diffused freezing zone), ice lens and frozen soil as follows:

(1) At the freezing front — the interface between unfrozen soil and freezing fringe

$$K_{ff}\frac{\partial\theta_{ff}}{\partial x} - K_{us}\frac{\partial\theta_{us}}{\partial x} = -L\gamma_{us}\frac{d\ell_{us}}{dt} \quad \dots \quad (5)$$

$\theta_{ff} = \theta_{us} = \theta_F$ (freezing point of soil)

(2) At the segregation freezing front, - the interface between freezing fringe and ice lens .

$$K_{i\ell}\frac{\partial\theta_{i\ell}}{\partial x} - K_{ff}\frac{\partial\theta_{ff}}{\partial x} = L\gamma_{i\ell}\frac{d}{dt}h(t) \dots \quad (6)$$

$\theta_{i\ell} = \theta_{ff} = \theta_{sg}$ (segregation freezing temperature)

(3) At the interface between ice lens and frozen soil

$$K_{i\ell}\frac{\partial\theta_{i\ell}}{\partial x} = K_{fs}\frac{\partial\theta_{fs}}{\partial x} \quad \dots\dots\dots\dots \quad (7)$$

$\theta_{i\ell} = \theta_{fs} = \theta_{is}$ (depending on time)

where

K = Thermal conductivity

$\dfrac{d\theta}{dx}$ = Temperature gradient

θ = Temperature

L = Latent heat of fusion of water

γ = Density

$\dfrac{d}{dt}$ = Rate change of a given quantity

h(t) = Amount of frost heave

ℓ = Height of zone

Suffix "uf", "ff", "iℓ", and "fs" denotes "unfrozen soil", "freezing fringe", "ice lens", and "frozen soil" respectively.

The fact that our interest lies on frost heave at zero frost penetration rate and for further simplification of the analysis, the following assumptions are introduced.

(i) The temperature varies linearly in each zone; unfrozen soil, freezing fringe, ice lens , and frozen soil.

(ii) The phase change from water to ice takes place only at the segregation freezing front.

(iii) The heat convectional flow due to water can be ignored.

(iv) The materials in every zones are incompressible.

(v) The thermal constants are independent of temperature.

With these assumptions and the thermal boundary conditions prescribed on top and bottom faces of specimens, we can rewrite the equations (5), (6), (7) as follows.

$$K_{ff}\frac{\theta_F-\theta_{sg}}{\ell_{ff}} - K_{us}\frac{\theta_u-\theta_F}{\ell_{us}} = 0 \quad \dots\dots\dots \quad (8)$$

$$K_{i\ell}\frac{\theta_{sg}-\theta_{is}}{h(t)} - K_{ff}\frac{\theta_F-\theta_{sg}}{\ell_{ff}} = L\gamma_{i\ell}\frac{d}{dt}h(t) \dots (9)$$

$$K_{i\ell}\frac{\theta_{sg}-\theta_{is}}{h(t)} = K_{fs}\frac{\theta_{is}-\theta_Q}{\ell_{fs}} \quad \dots\dots\dots \quad \dots\dots (10)$$

The following equation is obtained considering the assumption (iv).

$$\ell_{us} + \ell_{ff} + \ell_{fs} = \ell \text{ (initial specimen height)}..(11)$$

	Tem-perature	Height	Conduc-tivity	Governing equations	
				Zone	Boundary
Unfrozen soil	θ_{us}	ℓ_{us}	K_{us}	$C_{us}\dfrac{\partial\theta_{us}}{\partial t} = K_{us}\dfrac{\partial^2\theta_{us}}{\partial x^2}$	$\theta_{us} = \theta_u$ $\begin{cases}\theta_{us}=\theta_{ff}=\theta_F\\ K_{ff}\dfrac{\partial\theta_{ff}}{\partial x}-K_{us}\dfrac{\partial\theta_{us}}{\partial x}=-L\gamma\dfrac{d\ell_{us}}{dt}\end{cases}$
Freezing fringe	θ_{ff}	ℓ_{ff}	K_{ff}	$C_{ff}\dfrac{\partial\theta_{ff}}{\partial t} = K_{ff}\dfrac{\partial^2\theta_{ff}}{\partial x^2}$	$\begin{cases}\theta_{ff}=\theta_{i\ell}=\theta_{sg}\\ K_{i\ell}\dfrac{\partial\theta_{i\ell}}{\partial x}-K_{ff}\dfrac{\partial\theta_{ff}}{\partial x}=L\dfrac{d}{dt}h(t)\end{cases}$
Ice lens	$\theta_{i\ell}$	h(t)	$K_{i\ell}$	$C_{i\ell}\dfrac{\partial\theta_{i\ell}}{\partial t} = K_{i\ell}\dfrac{\partial^2\theta_{i\ell}}{\partial x^2}$	$\begin{cases}\theta_{i\ell}=\theta_{fs}=\theta_{is}\\ K_{i\ell}\dfrac{\partial\theta_{i\ell}}{\partial x}=K_{fs}\dfrac{\partial\theta_{fs}}{\partial x}\end{cases}$
Frozen soil	θ_{fs}	ℓ_{fs}	K_{fs}	$C_{fs}\dfrac{\partial\theta_{fs}}{\partial t} = K_{fs}\dfrac{\partial^2\theta_{fs}}{\partial x^2}$	$\theta_{fs} = \theta_Q$

Fig. 9. Analytical model of the specimen

Differential equation of the form (9) can be solved with boundary equations of (8), (10) and (11). The solution is expressed as

$$t = (B+AC)^{\ell_r} A - Ch(t) - (B+AC)\ell n\{A-h(t)\} \quad ...(12)$$

$h(t)$ after the lapse of a sufficient time can be given by equation (13), since $\lim_{t \to \infty} h(t) = A$ holds;

$$h(t) = A \left[1 - \exp\{ \frac{-1}{B+AC} (AC+t)\} \right] \quad ...(13)$$

where,

$$
\begin{cases}
A = \frac{1}{K_{ff}K_{fs}(\theta_F - \theta_{sg})} \{ \ell_{ff}K_i\ell\{K_{fs}(\theta_{sg} - \theta\ell) + K_{ff}(\theta_F - \theta_{sg}) \\
\qquad + K_{us}(\theta_u - \theta_F)\} - \ell K_{ff}K_i\ell(\theta_F - \theta_{sg})\} \\[2mm]
B = \frac{L^\gamma \ell K_i \ell}{K_{ff}K_{fs}(\theta_F - \theta_{sg})} \ell_{ff} \left[\ell - \ell_{ff} \{1 + \frac{K_{us}(\theta_u - \theta_F)}{K_{ff}(\theta_F - \theta_{sg})} \} \right] \\[2mm]
C = \frac{L^\gamma_i \ell \ell_{ff}}{K_{ff}(\theta_F - \theta_{sg})}
\end{cases}
$$

The value for the segregation-freezing temperature was computed by the equations of thermal dynamics derived by Clausius-Clapeyron. The thermal constants of soil were calculated on the basis of their void ratios, the thermal constants of soil particles, ice, and water contained in the specimens.

Fig.10 shows the results of calculating the equations (12) and (13) using the thermal constants and the thermal boundary conditions for the soil "C-4".
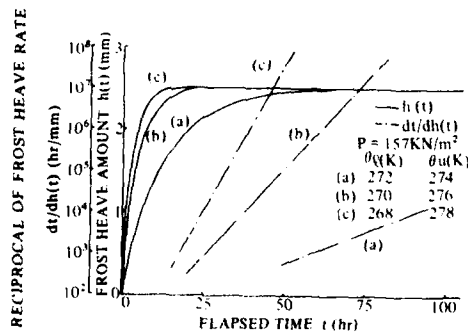
Fig 10 Time dependent variation of h(t) and dt/dh(t) calculated by eq (12), (13)

The time dependent variation of frost heave h(t), can be characterized by the facts that it converges to the constant value as time elapse and that its rate of convergence increases as the temperature $\theta\ell$ decreases. As indicated, the results of heat conduction analysis by the equations (12) and (13) well confirm with the results of calculations performed by the derived empirical equation (4) with respect to the characteristics of the time dependent variation of frost heave, as described, and the effect of the temperature $\theta\ell$ on its behaviour.

However, the following must be noted concerning the analytical results. First, frost heave, h(t), calculated by the analytical method shows faster convergence characteristics than the actual behaviour observed by the experiments. Second, the soil "S-1" was tested under the varying over burden pressure at constant boundary tempera-

tures. The experimental results indicates clearly the pressure dependent characteristics of the frost heave, however the analytical results showed no significant effect of the change in the overburden pressure.

Further studies are taking place to overcome these deficiencies in the analytical method. These deficiencies seem to resulted from the fact that the effect of suction mechanism due to freezing and the effect of hydraulic resistance was not incorporated in the formulation of the heat conduction analysis.

6-3 Height of test specimen and its effect upon frost heave.

Cylindrical specimen of height 90 mm was tested to examine the effect of change in height of specimen upon frost heave. Fig.11 presents the test result of the specimen and also gives the values calculated by the empirical equation (4) with the values of α and β shown in Table 3. It becomes clear that the propensity in frost heaving after the frost penetration rate being nominal zero is similar to that of the 3 cm height test specimens.
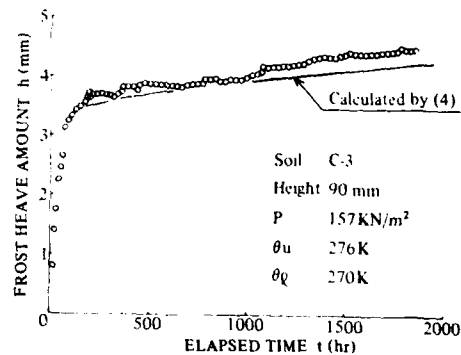
Fig. 11. Time dependent variation of frost heave using with the specimen of height 90 mm

However, corresponding results of calculations by the empirical equation show less agreements with those of the test for the case of 90 mm height specimen (Fig.-4). This indicates that the height of specimen have possible effect on the values of α and β. The height of specimen directly influences on the thermal gradient within the specimen under fixed boundary temperatures, and this change in the thermal gradient, in turn, may well affect the frost heave characteristics.

Further studies as well as experiments have to be carried out to investigate their effect of change in height of specimen upon the phenomena of frost heave in order to apply the proposed method to the design of artifical ground freezing construction method.

6-4 Grain size of soil and its effect upon frost heave characteristic

It is widely known that the grain size of soil has direct influence on its frost susceptibility. Examination was made to clarify the relation between the grain size of soil, in particular that of D50, and each of constants α and β.

The relation between constant "β" and soil grain size "D50" was not established as the result of the laboratory

266

frost heave test. However, significant correlation between "α" and "D50" was observed. The value of α increases as the value D50 decreases (Fig.-12).

It has been recognized that the smaller the grain size of soil, the greater the amount of frost heave. It also appeared that the same tendency as described above held even after the frost penetration rate has become nominally zero.
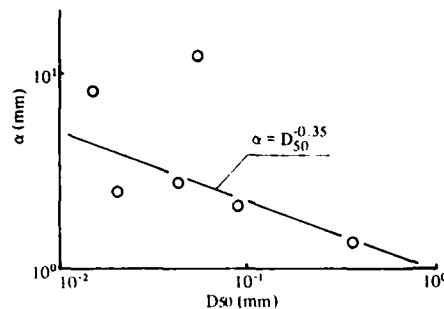
Fig. 12. Relationship between α and D50

7. CONCLUSION

The general characteristics of frost heave observed through the laboratory test conducted on the 3 cm heigh preconsolidated cylindrical soil specimens that have been saturated by pure water confirms the phenomena of continual frost heave even after cease of frost penetration.

The results of experiments and analysis demonstrate the followings frost heave characteristics during zero frost penetration rate.

1) The following empirical equation proposed gives a good approximate, on the amount of frost heave, h.

$$h = \alpha \left[1 - \exp\{\frac{\beta}{P}(\theta_Q - \theta_F)t\} \right]$$

in which θ_Q is a the prescribed value of cold-side temperature, θ_F is a freezing point of soil, P is a overburden pressure, α and β are generic constants of the soil, and t is time.

2) The equation of the form (13) derived from heat conduction analysis resembles the empirical expression of the above form and incorporates sufficiently the time dependent characteristics of frost heave and the effect of θ_Q on this phenomena.

3) It has been observed that there exists a significant correlation between the constant α and the parameter D50, and the value of α is greater for cohesive soil than for sand.

In additon, the effect of change in height of specimen on the frost heave has been observed through the laboratory frost heave test conducted on the 9 cm heigh specimen.

REFERENCE

(1) Ryokai K., Goto, S. and Akagawa, S. 'Frost heave properties of saturated soils under constant overburden pressure.' Reports of the Research Laboratory of Shimizu Construction Co., Ltd., Vol.33, pp.27~36, (1980).

(2) Yong, R.N. and Serag-Eldin, N. 'Salt treatment effects on frost heave performance.' Proc. The 2nd International Symposium on Ground Freezing, pp.680~691, (1980).

(3) Takashi, T., Masuda, M. and Yamamoto, H. 'Effect of hydraulic resistance in unfrozen soil on frost heave.' Seppyo, Vol.36, No.2, pp.1~20. (1976).

(4) Everett, D.H. and Haynes, J.M. 'Capillary properties of some model systems with special reference to frost damage.' RILEM Bull., New ser. No.27, pp.31~38, (1965).

(5) Takashi, T., Yamamoto, H., Ohrai, T. and Masuda, M. 'Effect of penetration rate of freezing and confining stress on frost heave ratio of soil,' Permafrost, 3rd Int. Conf. 1: pp.737~742, (1978).

(6) Konrad, J. and Morgenstern, N.R. 'A mechanistic theory of ice lens formation in fine-grained soil.' Can. Geotech. J. Vol.17, pp.473~486, (1980).

(7) Takagi, S. 'The adsorption force theory of frost heaving.' Cold Regions Science & Technology, Vol.3, No.1, (1980).

(8) Takashi, T., Ohrai, T., Yamamoto, H. and Okamoto, J. 'Upper limit of heaving pressure derived by pore water pressure measurement of partially frozen soil.' Proc. The 2nd International Symposium on Ground freezing, pp.713 ~724, (1980).

APPENDIX: Heat conduction analysis for evaluation of frost penetration rate

The dimension of test specimens used for the laboratory frost heave test were not heigh enough to allow measurements of the frost penetration rate. Therefore, the heat conduction analysis was carried out to estimate the frost penetration rate.

The following assumptions were made.

(i) The effect of water flow into specimen is negligible.

(ii) The thermal constants are independent of temperature.

(iii) Both frozen and unfrozen soils are incompressible.

The governing equations for temperatures of frozen and unfrozen soils are (A1) and (A2) respectively.

$$\frac{\partial \theta_1}{\partial t} = \alpha_f \frac{\partial^2 \theta_1}{\partial x^2} \text{ (frozen soil)} \quad \dots \dots \dots \quad (A1)$$

$$\frac{\partial \theta_2}{\partial t} = \alpha_u \frac{\partial^2 \theta_2}{\partial x^2} \text{ (unfrozen soil)} \quad \dots \dots \dots \quad (A2)$$

where

θ_1 = Temperature of frozen soil

θ_2 = Temperature of unfrozen soil

α_f = Thermal diffusivity of frozen soil
α_u = Thermal diffusivity of unfrozen soil
t = Time

The boundary condition at the freezing front a.e given by equations (A3) and (A4).

$$K_f \frac{\partial\theta_1}{\partial x}\bigg|_{x=X_F} - K_u \frac{\partial\theta_2}{\partial x}\bigg|_{x=X_F} = L\gamma\frac{dX_F}{dt} \quad\dots\dots \quad (A3)$$

$$\theta_1\bigg|_{x=X_F} = \theta_2\bigg|_{x=X_F} = \theta_F \quad\dots\dots\dots\dots\dots \quad (A4)$$

where

K_f = Thermal conductivity of frozen soil
K_u = Thermal conductivity of unfrozen soil
X_F = Location of the freezing front
L = Latent heat of fusion
γ = Density
θ_F = Freezing point of soil

The finite diferential method was applied for heat conduction analysis. Formulations of equations (A1), (A2) and (A3) were carried out by the weight average method.

Values of θ_1 and θ_2 are numerically solved by equations (A1) and (A2) for an assumed value of X_F and this computation was iterated until the value of X_F and equation (A1) and (A2) satisfies the relation expressed in equation (A3). The boundary conditions and the initial conditions applied for the heat conduction analysis are as follows:

$\theta_1 = \theta_\varrho$ (cold-side temperature) at $x = 0$
$\theta_2 = \theta_u$ (warm-side temperature) at $x = \ell$
$X_F = 0$, $\theta = \theta_u$ at $t = 0$
where
ℓ = height of test specimen
Fig. A1 shows the calculation results for the "C-4".

Fig. A1 The result of heat conduction analysis (C-4)

The results of calculation for the frost penetration rate starts to show fluctuations in their values for large values of t and dX_F/dt smaller than 10^{-3} mm/hr. Therefore, the assumption of linear variation of θ_1 and θ_2 with respec: to x was applied to transform the equation (A3) into the equation (A5) which expresses t in terms of X_F as below. This assumption has been verified by the use of finite differential method.

$$t = \frac{L\gamma\{K_f(\theta_F-\theta_\varrho)\}^2}{\{K_f(\theta_F-\theta_\varrho)+K_u(\theta_u-\theta_F)\}^3}\left[\frac{1}{2}X^2 - \frac{K_u(\theta_u-\theta_F)}{K_f(\theta_F-\theta_\varrho)}\right.$$
$$\left. \{X + \ell n\,(1-X)\}\right] \quad\dots\dots\dots\dots \quad (A5)$$

where

$$X = \frac{K_f(\theta_F-\theta_\varrho) + K_u(\theta_u-\theta_F)}{K_f(\theta_F-\theta_\varrho)} \cdot \frac{X_F}{\ell}$$

As the result of this analysis, the value of dX_F/dt under 2K difference in the boundary temperature was determined to be 10^{-10} mm/hr at 50 hrs after the initiation of cooling, which comforms the fact that the frost penetration rate has been nominally zero, after 50 hrs of cooling.
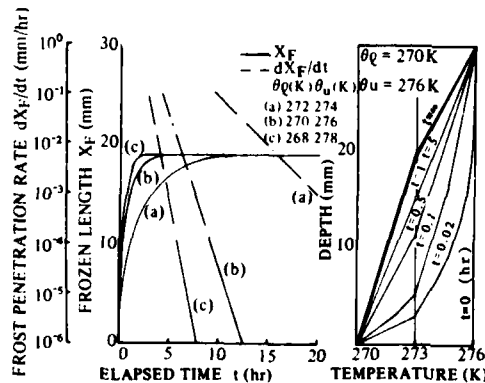
268

FROST HEAVE SUSCEPTIBILITY OF SATURATED
SOIL UNDER CONSTANT RATE OF FREEZING

Kimitoshi Ryokai : Research Engineer Research Laboratory of Shimizu Construction Co., Ltd.
Japan

Mizuhito Iguro : Deputy Manager, Civil Engr. Development Dept.
Shimizu Construction Co., Ltd., Japan

Kiyoshi Yoneyama : Research Engineer, Research Laboratory of Tokyo Gas Co., Ltd..
Japan

ABSTRACT

Introduced hereafter is the results of experiment carried out in Japan to quantitatively obtain the frost heave pressure and displacement of soil subjected to artificial freezing or freezing around in-ground LNG storage tanks. This experiment is conducted to evaluate the frost heave susceptibility of saturated soil under overconsolidation. In other words, this experiment was carried out to obtain the relation of the over-burden pressure and freezing rate to the frost heave ratio by observing the frost heave displacement and freezing time of specimens by freezing the specimens at a constant freezing rate under a constant over-burden pressure, while letting water freely flow in and out of the system.

It has been known that there is the following relation of the frost heave ratio, ξ to over-burden pressure, σ and freezing rate, U of soil tested by procedures described hereafter.

$$\xi = \xi_0 + \sigma_0 (1 + \sqrt{U_0/U})\sigma$$

Where, ξ_0, σ_0 and U_0 are the constants inherent to soil determined by the experiment.

Introduced here are the procedures for frost heave test required to quantitatively obtain the frost heave displacement and pressure of soil. Furthermore, the relation between the frost heave susceptivility and physical properties of soil obtained by this test is reported.

1.   Introduction

The frost heave susceptibility of soil has been evaluated qualitatively on the bases of the physical properties of the soil (grain size, centrifuge moisture equivalent and consistency). It has also been known that the smaller the confined pressure is, the larger the amount of frost heave become. According to these evaluation methods, however, it is impossible to quantitatively obtain the frost heave displacement and pressure. In order to quantitatively obtain the amount of frost heave, it is required to know about the relationship between the confined pressure and freezing rate, and, moreover, the effect of freezing on unfrozen soil as well.

Although the effect of freezing on unfrozen soil in normally consolidated clay has not sufficiently solved yet, the test method for obtaining the frost heave susceptibility of soil under the stress state of over-consolidated zone is proposed by Takashi.[1]

Moreover, this method constitutes a basis for the method of frost heave test in "the Recommended Practice of LNG Inground Storage Tank" of the Japan Gas Association.[2]

The method proposed in the above practice is introduced here and, at the same time, the following facts which have been attained through this experiment concerning the relation between the frost heave susceptibility and physical properties of soil are reported hereunder.

The frost heave susceptibility of soil was found through this experiment to be correlated particularly with the grain size of D50 equivalent to 50% passing on the grain-size accumulation curve, this correlation may be used to approximate the degree of the frost heave displacement and pressure. However, the displacement and pressure are required to be strictly obtained according to the proposed method after all.

2.   Frost heave test at constant rate of freezing

2.1   Boundary temperature condition to maintain the freezing rate at constant

The following temperature conditions are required to keep the freezing at a constant rate. Fig. 1 schematically illustrates test specimen. When the elapsed time is t and the distance from the lower face of specimens is x, the initial conditions are: .

$$x_f = o \qquad at\ t = o \qquad (1)$$

Since the temperatures over the upper and lower faces of specimens are equal to the specified temperatures, θu and θ_ℓ over the upper and lower faces respectively, the follow-

ing equations are given for the boundary conditions:

$$\theta_1 = \theta_\ell \quad \text{at } x = 0 \tag{2}$$

$$\theta_2 = \theta_u \quad \text{at } x = \ell \tag{3}$$

As the temperature in the interface ($x=x_f$) of frozen soil and unfrozen soil is equal to the freezing temperature, θ_f of soil, the following relation holds:

$$\theta_1 = \theta_2 = \theta_f \quad \text{at } x = x_f \tag{4}$$

In addition, in view of the fact that the difference between the heat flux penetrating from the unfrozen soil layer and the heat flux transmitted to the frozen soil layer contributes the progress of freezing front, the following equation is formed:

$$k_1\frac{\partial\theta_1}{\partial x}\Big|_{x=xf} - k_2\frac{\partial\theta_2}{\partial x}\Big|_{x=xf} = L\gamma_1\frac{dx}{dt} \tag{5}$$

Where, θ_1 : Distribution of temperature in frozen soil
θ_2 : Distribution of temperature in unfrozen soil
k_1 : Thermal conductivity of frozen soil
k_2 : Thermal conductivity of unfrozen soil
r_1 : Unit weight of frozen soil
L : Latent heat of freezing of soil
ℓ : Length of specimen

An exact solution is given by Takashi[1], but if it is assumed to be possible to linearly approximate the temperature distributions in the frozen soil layer and unfrozen soil layer in view of the fact that the length of specimens is short, the following equations are formulated:

$$\theta_1 = \frac{\theta_f - \theta_\ell}{x_f} x + \theta_\ell \quad (0 \leqslant x \leqslant x_f) \tag{6}$$

$$\theta_2 = \frac{\theta_u - \theta_f}{\ell - x_f}(x - x_f) + \theta_f \quad (x_f \leqslant x \leqslant \ell) \tag{7}$$

When Equations (6) and (7) are substituted into Equation (5) and it is solved for θ_ℓ by taking into account the relation of Equation (1), the following equation can be obtained:

$$\theta_\ell = \theta_f - \frac{Ut}{k_1}(L\gamma_1 U + k_2\frac{\theta_u - \theta_f}{\ell - Ut}) \tag{8}$$

When the finished time of freezing is t_f ($=\ell/U$) and in case $\theta_u \neq \theta_f$ in Equation (8), it will become difficult to carry out the test since:

$$\lim_{t \to tf} \theta_\ell = \pm\infty \tag{9}$$

Therefore, the temperature over the upper face, θ_u has to be:

$$\theta_u = \theta_f \tag{10}$$

When this condition is substituted into Equation (8), the temperature over the lower face becomes as expressed in the following equation:

$$\theta_\ell = \theta_f - \frac{L\gamma_1 U^2}{k_1} \cdot t \tag{11}$$

In order to carry out the test so that the freezing rate, U will become constant, the temperatures over the upper and lower faces, should be controlled to the temperatures obtained according to Equations (10) and (11).
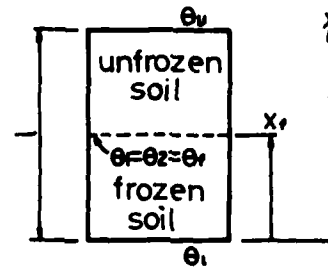
Fig. 1   Model of specimen during frost heave test

2.2   Test apparatus

Fig. 2 illustrates a concept of the frost heave test and Fig. 3, the diagram of the apparatus. This test apparatus with a maximum capacity of 2 tf, is capable of applying a constant pressure to a specimen during test by applying a load to the loading frame (3). As air pressure is applied in the pressurized container (14), it is possible to maintain the pore water pressure in specimen at an arbitrary pressure of up to 10 kgf/cm^2.

Fig. 2   Concept of the frost heave test

(1) Displacement gage   (2) Suspending tool   3 Loading frame
4 Thermister   Piston-type cooling plate 6 Acryl cylinder
7 O ring   8 Specimen   9 Cooling plate
(10) Pore water outlet opening 11 Porous metal   12 Thermomodule
13 Loading platform   14 Pressurized container   15 Volume change meter
16 High pressure tank   Pressure adjusting valve   X Valve
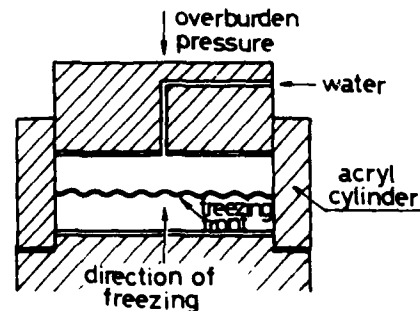
Fig. 3   Frost heave test apparatus

270

Cooling of specimen is carried out electrically by means of thermomodules provided at the upper and lower ends of the specimen. The temperature over upper end of specimen can be controlled to a constant level within a range of $+10° \sim -10°C$, and that of the lower face can be adjusted by programmable control divice at a given time to an desired temperature within the range of $+2.5 \sim -22.5°C$.

The major items of measurements are the amount of frost heave and that of water intake/discharge. The amount of frost heave is measured by a differential transformer type displacement gauge, and the amount of water by an electrostatic volumetric gauge. The results of these measurements are recorded in a digital and analog recorders.

Although the diameter of the cylindrical mold is fixed to 6 cm, and the height up to around 10 cm.

In order to study the dimensional effect of specimens, a large scale apparatus for frost heave test that permits testing of specimens of 30 cm in diameter and $20 \sim 40$ cm in height is also used supplementary.

2.3 Test Method

The procedures for the tests are as follows:

(1) Before starting the test, determine the freezing point of the soil.

2) Form the sample into the specified dimensions. Place filter paper on each side of the specimen and place the specimen into an acryl cylinder.

3) Place the acryl cylinder on the cooling plate and insulate the outer surface of the cylinder.

(4) Saturate the specimen.

5 Mount the apparatus for measuring the amount of frost heave and the amount of water intake/discharge.

6) Consolidate the specimen until the complete settlement is achieved due to pressure of the specified test pressure plus 1 kgf/cm^2.

7) Remove 1 kgf/cm^2 and set the specimen under the specified overburden pressure until displacement stops.

8 Adjust the water level in the apparatus for measuring the water intake/discharge to the level of the top of the specimen.

9 Lower the temperatures over the upper and lower faces of the specimen to the freezing point of the soil.

10 Set the temperature of the lower cooling plate lower than the freezing point of soil, to form ice cores at the lower end of the specimen.

11 After confirming, the formation of ice cores by observing displacement due to frost heave or by measuring amount of water intake/discharge, reset the temperature of the lower cooling plate to the freezing point of soil.

12 Adjust the rate of temperature fall of the lower cooling plate constant to let the frost penetration rate constant.

13 Measure the displacement due to frost heave, and the amount of water intake/discharge at various time.

14 After the freezing front has reached the upper end of specimen, maintain a specified temperature ($-10°C$) and confirm the termination of frost heave.

15 Measure the amount of natural defrosting settlement. Although the number of test specimens required to
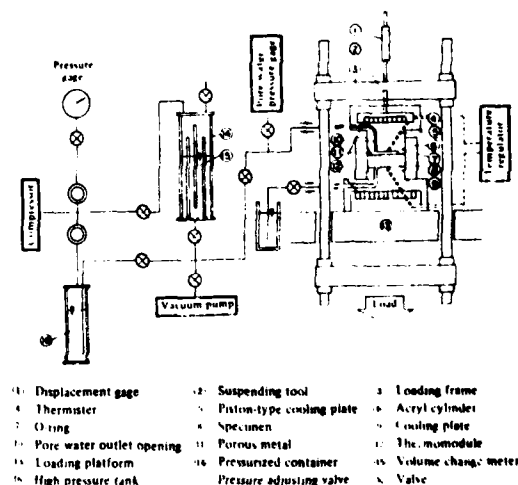
determine the soil-inherent constants varies for different types of soil, it is necessary to carry out tests on a reasonable number of specimens in case of soil with large frost heave susceptibility by changing the overburden pressure, σ and freezing rate, U. One such example is shown in Table 1.

Table 1 Amount of test specimen

	σ_1	σ_2	σ_3	σ_4	σ_5	σ_6
U_1	O	O	O	O	O	O
U_2		O			O	
U_3		O			O	
U_4	O	O	O	O	O	O

where, $\sigma_1 > \sigma_2 > \cdots\cdots > \sigma_6$
$U_1 > U_2 > U_3 > U_4$

2.4 Analytical procedures

Kinoshita[3], Takashi et al.[1] found that the following relation exists between the frost heave ratio, ξ and the overburden pressure, σ. When frost heave test is carried out under a constant overburden pressure and constant rate of freezing while letting water freely flow in or out of the system (Fig.4(a)):

$$\xi = A + B/\sigma \qquad (12)$$

Where A and B are the regression constants.

Moreover, Takashi, et al.[1] expressed the effect of the freezing rate, U on the frost heave susceptibility of soil as follows:

$$\xi = C + D/\sqrt{U} \qquad (13)$$

Where C and D are the regression constants.

In addition, Takashi et al.[1] introduced the following emperical equation which incorporates the effects of both the overburden pressure and the freezing rate by correlating the two effects, as indicated in Fig. 4(b):

$$\xi = \xi_0 + \sigma_0 (1 + \sqrt{U_0/U})/\sigma \qquad (14)$$

Where, ξ_0, σ_0 and U_0 are the constants inherent to soil determined experimentally (hereinafter these constants are referred to as "the constants of frost heave").

Where the ratio of water intake/discharge is to be ξ_w, the following relation is established between the water intake/discharge ratio, ξ_w and the frost heave ratio, ξ. according to the water balance:

$$\xi = \xi_0 + n_f\Gamma + (1 + \Gamma)\xi_w \qquad (15)$$

Where Γ is the volumetric frost heave ratio when pore water freezes, and n_f a constant obtained experimentally.

ξ_0, σ_0, U_0 and n_f in Equations (14) and (15) can be obtained as follows:

First of all, ξ_0 is obtained, as shown in Fig. 4(a), by establishing, for each freezing rate, a straight line that represents the relation between ξ and $1/\sigma$ and averaging the values of intercepts on ξ ordinate.

271

oo is obtained, as shown in Fig. 4(b), by arranging all of the test results in terms of the variables ($\xi - \xi_0$) σ and $1/\sqrt{U}$ and by establishing linear relation and finding the value of intercept on ξ ordinate.

Uo is obtained from the gradient of the above straight line, $\sigma_0\sqrt{U_0}$. As shown in Fig. 4(c), the relation between ξ and ξ_w is represented by a straight line having a gradient of $(1 + \Gamma)$. n_f is obtained from the gradient of the straight line $(1 + \Gamma)$ and the coordinate value ($\xi_0 + n_f\Gamma$) at the intercept of the straight line with the ξ-axis.

3. Relation between frost heave susceptibility and physical properties of soil

3.1 Properties of specimens

The specimens used for the test come into 49 types, and the grain size accumulation curve is as shown in Fig. 5. Among the soil in Fig. 5, the soil which stands by itself and the one which does not stand by itself when it is formed into specimens are classified into clayey soil and sandy soil, respectively, in view of convenience.

Meanwhile, the specimen Dc in the diagram is a specimen used to study the effect of freezing/thawing and the effect of length of specimen on the frost heave susceptibility.

All specimens of sandy soil are disturbed, but those of clayey soil are not except the two. The two specimens of clayey soil and those of the sandy soil were formed into specimens by agitating and saturating after adding pure water, and reconsolidating at Ko condition.

3.2 Test conditions

The preliminary studies were made on the effect of freezing/thawing and the effect of length of specimens exerted on the frost heave susceptibility of soil. In order to study the above effects, a preload of 4.2 kgf/cm² was applied to the specimen, Dc prior to testing. From this specimen, four test pieces of 1, 2, 3 and 7 cm in height were prepared, and freezing and thawing were repeated five times for each specimen.

In order to study the effect of diameter in addition to that of the height of specimens, test was also carried out by using the specimens of diluvial clay of 25 cm in height and 30 cm in diameter.[4]

This test was carried out under the following conditions of overburden pressure and freezing rate. When the overburden pressure is low, it seems that the apparent overburden pressure actually applied to the specimen was higher than the initially applied pressure in the amount of stress attributable to the resistance of movement of pore water. Consequently, the minimum value of the overburden pressure was determined to be 0.5 kgf/cm² in view of the fact that the frost heave ratio obtained according to Equation (14) and the actual measurement were not equal.[5] The maximum value was selected to be 12.8 kgf/cm² taking into account the frost heave pressure presuming the condition of the ground surrounding the in-ground storage tank.

Lower freezing rate resulted in continual formation of ice lense adjacent to the upper boundary of specimen, and freezing was never completed. Thereby the reliability of data was reduced. Therefore, the range of freezing rate
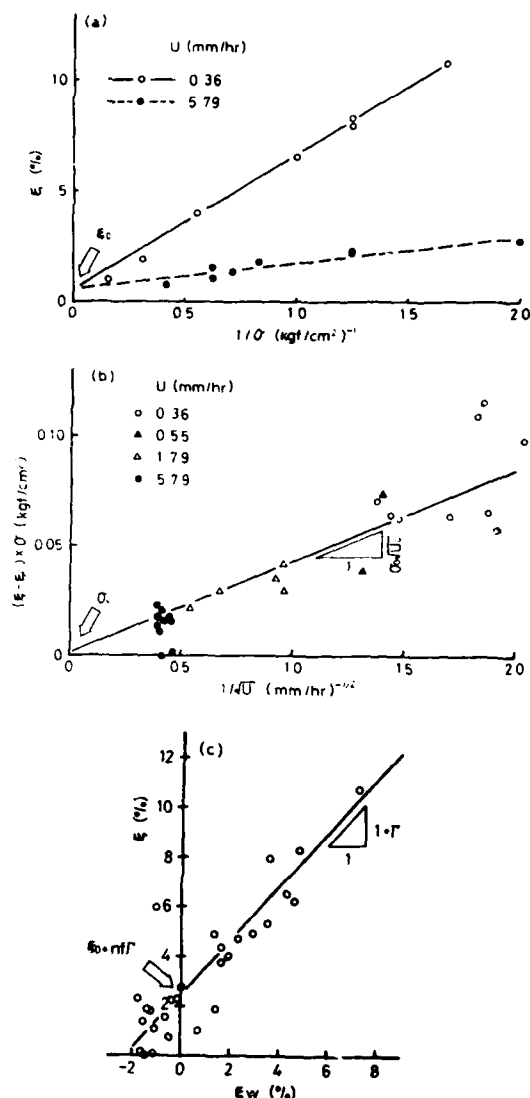

Fig. 4 Results of frost heave test (a) ξ v.s. $1/\sigma$, (b) ($\xi - \xi_0$) $\times$ σ v.s. $1/\sqrt{U}$ (c) ξ v.s. ξ_w
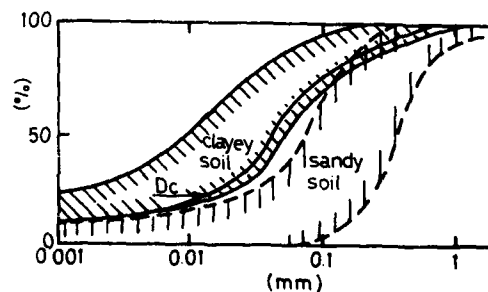

Fig. 5 Grain size accumulation curve

272

was set to be 0.5 ~ 15.0 mm/hr. As a method for preventing a phenomenon of continual formation of ice lense before the complete freezing of specimen, it was found to be effective to place a perforated plate of polyvinyl chloride on the upper part of specimen.

3.3 Results of tests and discussions

(1) Variation in time of the amount of frost heave and water intake/discharge

Fig. 6 shows the variation in time of the temperature of lower cooling plate, amount of frost heave, and that of water intake/discharge during experiment. Frost heave was commenced when the temperature of lower cooling plate was lowered to the temperature at which ice cores are formed. Variation of the amount of frost heave and that of water intake/discharge was nearly linear during the progress of freezing. This indicates the fact that freezing progressed at nearly constant rate on the condition that the cooling surface temperature was controlled according to Equations (10) and (11). The end of freezing can be identified according to the inflection point of the change with time of the amount of frost heave and that of water intake/discharge. The fact that frost heave continued for a certain period of time even after the end of freezing is considered to be caused by the secondary expansion due to temperature drop in frozen soil.

Frost heave did not progress for a certain period of time even after the start of freezing. This is considered to be caused by the fact that what Takagi, et al. called "diffused freezing zone" was not formed completely and the water intake capacity was not sufficiently demonstrated in the zone.

(2) Effect of freezing and thawing

Fig. 7 shows the relation between the frost heave ratio, ξ and the frequency of freezing and thawing, N.

A little variation due to the effect of freezing and thawing on frost heave was observed throughout specimens of different heights for the first cycle of freezings and thawings but no variation was observed from second cycles.

When each test conducted under different condition of freezing rate and overburden pressure was performed on newly replaced specimens, we can expect variation in properties and discrepancies in dimensions of specimens.

Taking into account these factors and assuming that the above extent of difference in the frost heave ratio would be negligible in practical application on the condition that the test load was within the over-consolidated zone, the same specimens were repeatedly used in the test described below.

(3) Effect of the height of specimens

Fig. 8 shows the relation between the frost heave ratio and the height of specimens. The frost heave ratio showed a maximum value when the height of specimen was around 2 cm.

In case the specimen was frozen while absorbing water, the pore water pressure on the freezing front dropped as freezing progressed, and the effective stress increased by as much as the pressure drop

The fact that the effective stress increased means that the overburden pressure increased. Therefore, the frost heave ratio became smaller.

Since freezing progressed while discharging water, the positive value of water pressure was induced on the freezing front which results in decrease in the effective stress on the front, hence it was expected that the frost heave ratio was to become larger as the height of specimen became higher as shown in the solid line in the diagram. However, when the height of specimen became larger
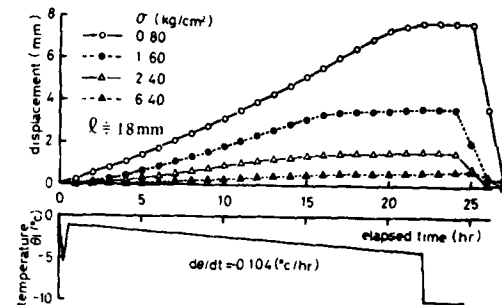
Fig. 6   Variation in time of the temperature of lower cooling plate and amount of frost heave.
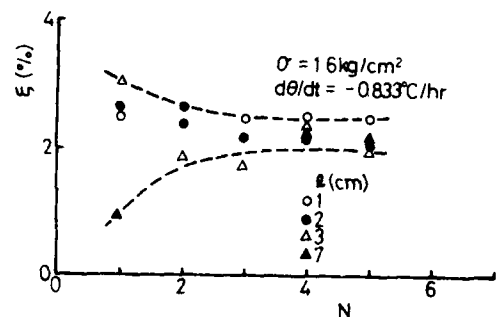
Fig. 7   Relation between frost heave ratio, ξ and frequency, N of freezing and thawing.
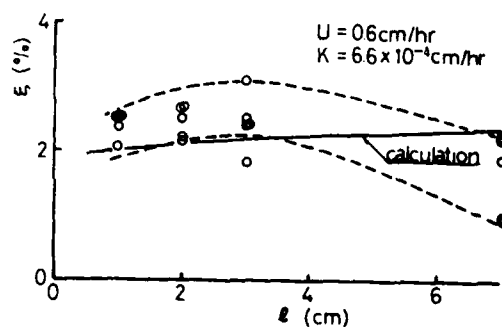
Fig. 8   Relation between frost heave ratio, ξ and height of specimens, l.

273

than 2 cm, the frost heave ratio became larger. This phenomena can be explained by the fact that, for the height being as large as 7 cm in contrast to the diameter of 6 cm, the overburden pressure was increased due to induced friction on the interface of the specimen and the acryl cylinder in spite of the provision of silicon grease to reduce the friction.

On the other hand, in case the height of specimen was smaller than 2 cm, the smaller the height, the smaller did the frost heave ratio become. In addition to the above reason, this was caused due to the fact that there existed a limited zone i.e. so called "diffused freezing zone" rather than the total surface area for adsorption of water. Any frost heave did not take place until such zone was developed.

Moreover, comparative study was made on the frost heave susceptibility of mud stone using small specimen of 6 cm in diameter and 2 cm in height and large specimen of 30 cm in diameter and 25 cm in height (Fig.9). In case of the large specimen under $\sigma = 3.9$ kgf/cm^2 the measurements are not reliable because of a large quantity of ice lense formed adjacent to the upper boundary of specimen. In case of the specimen under $c = 0.9$ kgf/cm^2, however, the ice lense was formed regularly, and there appeared the value smaller than that obtained according to the empirical formula derived for the small specimens. This is due to the fact that the smaller frost heave ratio was induced since the apparent overburden pressure increased due to the resistance of water movement as previously described. When the frost heave ratio is corrected according to the equation[5] incorporating such resist-

ance to the water movement, the frost heave ratio of 37.6 % calculated for small specimen corresponds very well to that of 35.1 % of the large specimen.

Judging from the above observations, the diameter of 6 cm and the height of 2 cm were adopted as the standard dimensions of specimens, since testing by increased height of specimen resulted in unnecessarily longer period of test required and increase in the resistance on the surface around the specimen.

(4) Relation between constats of frost heave and physical properties of soil

It has experimentally been known that the frost heave susceptibility of soil can be evaluated according to simply the size of soil grains obtained through analysis of the grain size. Generally, the soil with a

Fig. 9 Comparison of frost heave ratio between large specimen (30 cm in diameter and 25 cm in height) and small specimen (6 cm in diameter and 2 cm in height).
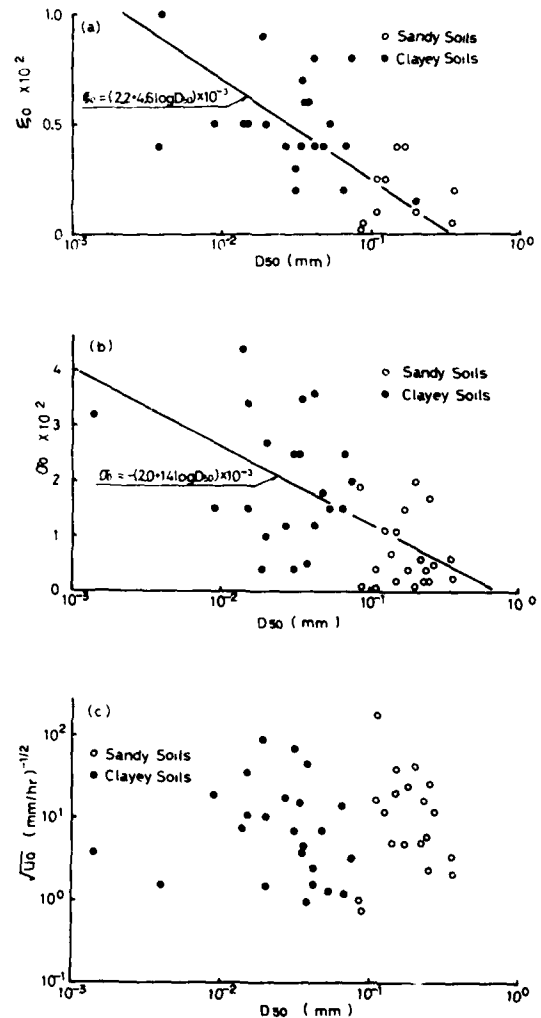
Fig. 10 Relation between D50 and the coefficients of frost heave (ξo, oo, Uo).

274

grain size of 0.1 mm or greater is not susceptible to frost heave, but the smaller does the grain size become, the greater the frost heave susceptibility, and the susceptibility reaches the maximum value when the size becomes 2 to 5 μm. However, should the size become far smaller, it is said that the permeability is reduced thereby resulting in difficulty to supply water and the frost heave susceptibility becomes smaller on the contrary.

Having the method for analysis established as in the equation (14), studies were made here on the effects of the grain size, content of clay, specific surface area and consistency on the coefficient of frost heave.

1) Effect of grain size and content of clay

When the grain size of D50 corresponding to 50 % passing on the grain size accumulation curve becomes smaller logarithmically, the coefficients of frost heave (ξo, σo, Uo) tends to become larger. However, the correlation between $\sqrt{Uo}$ and D50 is insufficient. Consequently, in view of the fact that Uo can be obtained according to the slope and intercept of the graph on the relation between ($\xi - \xi$o), σ and $1/\sqrt{U}$, study was made on the correlation between $\sigma_o\sqrt{U_o}$ and D50 to achieve less variance (Fig. 11). As a result, the more excellent correlation has been obtained.

Moreover, σo $\sqrt{Uo}$ tends to increase as the content of clay, Vc or the content of (clay + silt), Vcs increases. The extent of the correlation appears more significantly in case of Vc than Vcs (Fig. 12).

The respective coefficients tends to increase, should the value of the specific surface area become larger.

2) Effect of consistency

σo $\sqrt{Uo}$ became larger as the plasticity index, Ip and the liquid limit, W_L became larger. However, any correlation with the plastic limit, Wp was not observed (Fig. 13). The former tendency is caused due to the fact that the higher the values of W_L and Ip, the higher the content of fine particles. The latter tendency is considered to be caused due to the fact that Wp does not change as much as W_L although Wp increases, though not linearly, along with the increase in the specific area of clay.

Since the coefficient of frost heave has been shown to be correlated with the grain size of D50 as the above, it has become relevant that these relations can be used to macroscopically obtain the displacement and pressure of frost heave. In order to obtain exact values of the displacement and pressure, it is necessary to conduct the proposed frost heave test at a constant freezing rate.
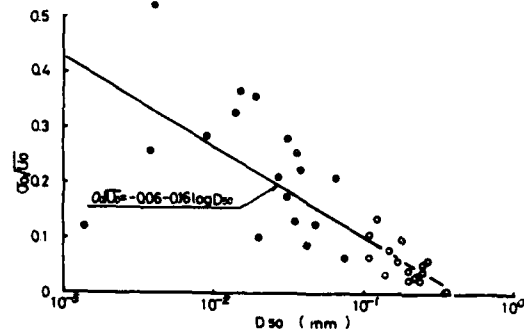
Fig. 11 Relation between D50 and σo $\sqrt{Uo}$.
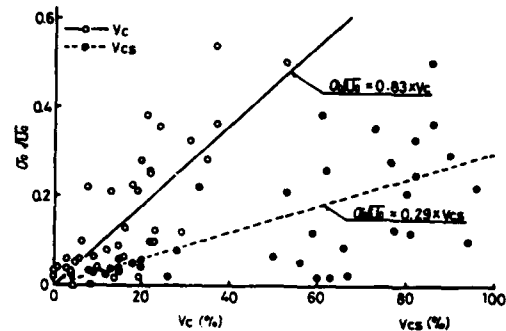
Fig. 12 Relation between content of clay, Vc or clay + silt. Vcs and D50.
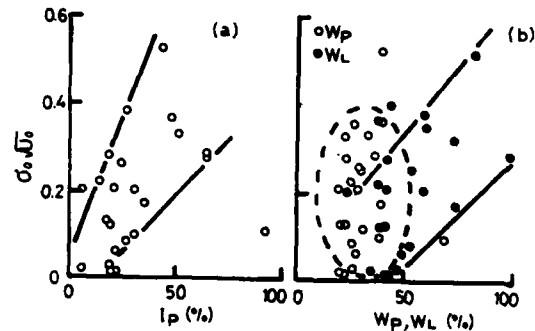
Fig. 13 Relation between consistency and σo$\sqrt{Uo}$

275

4. Conclusion

As a result of determining the frost heave suscepti-
bility of saturated soil in the over-consolidated zone
through testing specimens under constant freezing rate and
under constant overburden pressure, while letting water
freely flow in and out of the system, the following facts
have been made clear:

(1) In order to quantitatively obtain the displacement
and pessure of frost heave of soil, the proposed frost
heave test has been proved to be effective and the
empirical form of equation (14) was shown to be
relevant in describing the frost heave ratio in terms of
overburden pressure and freezing rate.

(2) ξ_0, σ_0, U_0 and $\sigma_0 \sqrt{U_0}$ that indicate the frost heave
susceptibility of soil are correlated to the grain size of
of D_{50} equivalent to 50% passing on the grain size
accumulation curve, contents of clay and silt, and
consistency. Since these constants are particularly
correlated to D_{50}, this relation can be used to ob-
tain the displacement and pressure macroscopically

(3) In case soil is frozen while intaking water, the frost
heave ratio becomes larger as the length of specimen
increases, but the ratio becomes smaller when the
length is increased to a certain level on the contrary.

(4) The freezing and thawing history does not exert
significant effect on the frost heave susceptibility of
soil.

5. Postscript

It can be concluded that the test proprosed herein is
very effective as a method for obtaining the frost heave
susceptibility of soil in the overconsolidated zone. In the
future, it is necessary to investigate the frost heave sus-
ceptibility of soil taking into account the displacement of
unfrozen soil within the specimen of normally consolidated
clay, where the effect due to freezing appear significantly.

References:

1) T. Takashi, T. Orai, H. Yamamoto (1977), Freezing
Expansion of Soils in Frozen Ground Working
Method, Soil and Foundation, Vo. 25.

2) Japan Gas Association (1979), Recommended
Practice for LNG Inground Storage, Tests on Soil
Freezing.

3) S. Kinoshita (1972), Frost Heave Test, Low
Temperature Science, Physics Division.

4) S. Goto, K. Ryokai (1980), Frost Action of the Soil
surrounding a LNG Inground Storage Tank, 2nd
Intern Symp. on Ground Freezing.

5) T. Takashi, M. Masuda, H. Yamamoto (1976),
Influence of Permeability of Unfrozen Soil on Frost
Heave, Snow and Ice, Vol. 38, No. 4.

FROST SUSCEPTIBILITY TESTING OF
A COMPACTED GLACIAL TILL

P. Garand, Project Engineer, Geos,Inc., Montréal, Canada
B. Ladanyi, Professor, Dept. of Civil Engineering,
  Ecole Polytechnique, Montréal, Canada

ABSTRACT

On the basis of a cold room study involving a compacted glacial till, the authors propose an experimental method for determining the frost susceptibility of compacted earth materials by measuring the maximum drop of hydraulic potential generated at the warm side of the supercooled fringe during segregational freezing. This potential drop was found to be relatively independent of the soil skeleton microstructure and of the degree of saturation during compaction, but increased with the thermal gradient. The maximum rate of frost heaving also increased with increasing thermal gradient but decreased with an increasing saturation during compaction.

The results of frost heaving tests have been compared with two mathematical models for representation of frost heave test results. When the frost front still penetrates into the soil and the thermal field has not yet stabilized, the heave can be approximated by a linear relationship between the heave and the square root of time. However, when the frost front stabilizes, the heave can be very closely approximated by a hyperbolic relationship, which enables a simple determination to be made of the asymptotic value of frost heave after very long periods of time.

INTRODUCTION

It is now generally accepted that in frozen soils the occurence of a layer of unfrozen adsorbed water on the soil matrix enables water movement to take place. The work of Burt and Williams (1976), Loch and Kay (1978) and Horiguchi and Miller (1980) are explicit to this effect.

Segregational frost heave was previously seen as a phenomenon occurring at the interface of a discrete ice lens and the soil matrix. It is now viewed as the interaction between a drop in hydraulic potential generated by a porous medium subjected to spatial variations of physical, thermodynamic and chemical properties, and the thermal and mechanical constraints governing these variations.

The potential difference between different areas of a saturated porous medium is recognized as the driving force of fluid movement. This has been formulated by Jumikis (1966) in describing primary and secondary potentials as being externally applied and internally induced potentials. In a saturated porous medium the hydraulic potential at a point in a pore can be expressed as the sum of different primary and secondary potentials. These primary and secondary potentials may be non exhaustively defined as the gravity potential, the capillary potential, the thermodynamic and also, as studied by Loch (1978), the osmotic potential.

The recognition of the existence of the frozen fringe between the ice lens and the unfrozen zone led researchers to reassess what is now called the primary frost heave theory and to develop the bases of what is called the secondary frost heave theory (Loch and Miller (1975), Miller (1980),

277

Hopke (1980)). These models give an insight into the role of the stress partition between phases as a regulator of lens initiation in rhythmic ice banding. The Konrad and Morgenstern (1980, 1981) model in turn puts the emphasis on the permeability of the frozen fringe as the main regulator in lens initiation and growth. On these premises it can be seen that, while the development of a drop in hydraulic potential acting as an initiator takes place, fluid motion subjected to mechanical restraints and varying permeability acts as a regulator.

Since the formulation of phenomenological models of segregation freezing is still in evolution, the work reported hereafter was intended as a descriptive study of frost heave behavior. A specific kind of frost heaving test is described enabling the definition of a parameter taking into account the evolution of the thermal field during the test. This parameter, called the maximum drop of hydraulic potential, seems to be a good alternative indicator of the frost susceptibility of a compacted soil. In addition, proposals are made concerning the mathematical modelling of the heave test results and their extrapolation to longer time periods.

TEMPERATURE FIELD

Frost heave testing of soil samples is usually done by controlling the temperature field by means of thermal constraints at the extremities of the sample. A discussion made by Miller (1980) about quasi-steady states and true stationary states of one-dimensional heat flow in a sample will permit an interpretation of a specific type of frost heave test.

Consider a sample subjected to an initial isothermal temperature field slightly above the freezing point of pure water. Then suddenly a difference of temperature is applied at the extremities of the sample. One end of the sample is subjected to what will be called the cold side temperature ($T_2 < 0°C$) and the other end to the warm side temperature ($T_1 > 0°C$), as shown in Figure 1. The frost front penetrates the sample from the cold side towards the warm side. At the beginning the thermal gradient near the cold side and the warm side will be important, the frost front penetration will be rapid and the frozen fringe will be of small thickness. As time passes the isothermal conditions of the middle of the sample will disappear and the thermal
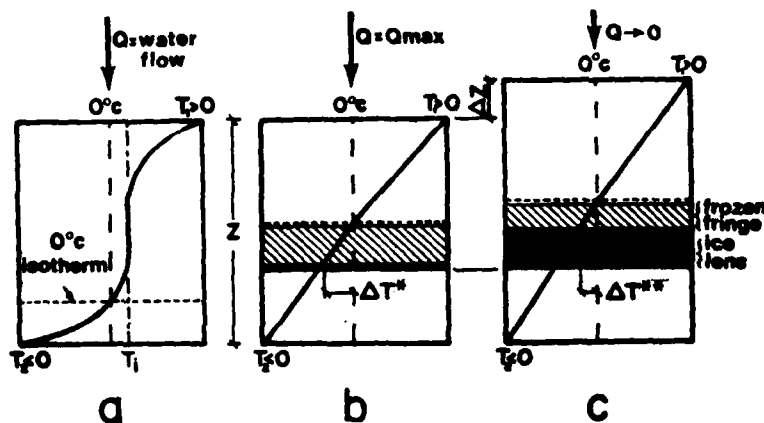
Figure 1. Thermal regime during the tests.

a - Rapid penetration of frost front.

b - Slowing of frost front and initiation of ice lens, thickness of frozen fringe at its optimum for maximum drop of hydraulic potential.

c - Trend towards true stationary heat flow, warming of the colder side of the frozen fringe ($\Delta T^{**} < \Delta T^*$) due to the length increase of the sample (ΔT).

278

gradient will tend to become linear in the frozen and unfrozen zones of the sample. There will be a moment during which the frozen fringe will be subjected to such a thermal gradient that the initiation of an ice lens can take place. This means that at this particular moment the thickness of the frozen fringe is at an optimum value and that the temperature distribution along its length permits the maximum quantity of unfrozen water to subsist and therefore the maximum permeability to exist. After this moment, the water migration tends to increase the heat flow toward the ice lens and to increase its thickness. The length of the sample therefore increases and the mean thermal gradient decreases. Warming of the cold side of the frozen fringe takes place and the rate of heave consequently diminishes. This phenomenon continues until true stationary state, as described by Miller (1980), is reached involving zero rate of heave. This behavior has been observed by the authors in a series of tests described hereafter.

GRANULAR MICROSTRUCTURE OF COMPACTED SOILS

It is now well known that the microstructure of compacted soils is influenced by the water content during compaction and the importance of the compaction energy. The smaller these two factors are, the more flocculated is usually the soil microstructure. As the water content and the compaction energy get greater, a trend towards a dispersed microstructure takes place, along with an increase in the degree of saturation of the soil during compaction. The microstructure of the soil influences the vertical permeability. The more the particles are oriented, the more the anisotropy of permeability is apparent.

The type of compaction energy also has an effect on soil microstructure. Dynamic compaction has more influence on the particle orientation than static compaction. The use of the punching effect of a small surface loading for the purpose of compaction helps the creation of a dispersed microstructure by the shearing effect it creates. This structural anisotropy of the soil may have an influence on measured frost heave.

EXPERIMENTAL APPARATUS AND METHODOLOGY

An isolated lucite testing cell, similar to the one used by Penner and Ueda (1977) and developed by Northern Engineering Services, was used. Referring to Figure 2, the cell consists of a cylindrical chamber in which a soil sample (G) can be compacted. A piston (C) can move inside the chamber in order to apply vertical pressure on the sample. A plastic membrane (U) joining the piston to the inside shell of the cell enables the piston to move without losing the water from the sample. A dead load on the piston rod (K) permits stress application on the sample. Upper (D) and lower (H) heat exchangers are located in the piston and the base plate (I) on which the isolated walls of the cell rest. The heat exchangers are each fed (L,N,O,Q) with ethylene glycol antifreeze mixtures at controlled temperatures from two circulating baths. The joint tightness between the upper (B) and lower (F) walls of the cell and the upper (A) and lower (formed by I and H) confining plates is

Figure 2. Testing cell as modified by the authors.

279

insured by plastic rings (R) and by the screw tightening of five rods (J). Water diffusion discs are located on the top (E) and bottom (S) of the sample. A water intake at the bottom of the sample (P) permits its saturation. During the test the sample freezes from bottom to top, so that the unfrozen zone can be displaced by heave with a small resistance from the chamber wall, covered with a teflon membrane. Thermistors (T) are set into the lower (F) wall to monitor the temperature.

The preparation of the test involves static compaction by means of a plate shaped as a sector of a ring and fixed on the rod of a pneumatic press. Compacted in layers one inch thick, the soil is then saturated by applying partial vacuum at the top of the sample by a tube (M), and water pressure at the bottom by a water intake pipe (P). When water flow stabilizes, a permeability test is run on the sample. During these operations, the piston is blocked in place. The cell is then placed in a cold room at +1°C and left until isothermal conditions are attained in the sample. During this curing of the sample, the feeding container and the cell are pressurized under a 15 kPa pressure. The dead load is applied so that the sample is subjected to a vertical effective stress of 5 kPa.

The test begins by connecting the circulating baths to the heat exchangers in order that constant cold and warm side temperatures can be applied at the bottom and top of the sample. As the freezing front progresses, water intake is monitored by weighing the container feeding the sample with water by means of a water intake (M) in the cell.

Simultaneously, the heave of the sample is measured by means of a micrometer (V) and the temperature distribution in the sample by means of thermistors.

PHYSICAL PROPERTIES OF SAMPLES AND TEST CONDITIONS

The soil tested is a glacial till composed by weight of nearly 64% of sand, 26% of silt and 3% of clay. The remainder (gravel) was discarded by retaining for testing the fraction passing #4 U.S. standard sieve. The final proportions by weight of grain size components are approximately 70% sand, 27% silt and 3% clay. The plastic and liquid limits of the passing #200 sieve are 9% and 15% respectively.

The standard Proctor compaction test yields an optimum water content of 7.6% for a dry mass density of 2080 kg/m³.

The physical state in which the samples were subjected to the tests and the thermal conditions during the six tests done are presented in Table 1. The water content (w%), dry mass density (ρd), degree of saturation (Sr) are given during compaction (suffix 1) and after the saturation (suffix 2), and permeability measurement (k) are given. The warm (T_1) and cold (T_2) end temperatures of the sample, the mean thermal gradient of the sample (∇T), the unfrozen zone thickness (Z_1), the ratio of the frozen zone thickness to the sample thickness (Z_2/Z), are also given in Table 1. The initial total thickness (Z) of all the samples was 10 cm.

Table 1. Physical conditions of the samples and thermal conditions of tests.

Test number	During compaction			At the start of the tests (after saturation)				Thermal conditions during tests				
	w_1	ρd_1 kg/m³	Sr_1	w_2	ρd_2 kg/m³	Sr_2	k m/s	T_1 °C/cm	T_1 °C	T_2 °C	Z_1 cm	Z_2/Z
1	7.8%	2080	70%	9.5%	2080	95%	1.1×10^{-6}	1.68	5.2	-5.5	5.0	.51
2	8.1%	2090	82%	9.0%	2080	86%	4.5×10^{-7}	2.12	8.4	-12.2	3.9	.62
3	5.1%	2090	53%	8.6%	2080	81%	2.6×10^{-6}	1.97	9.1	-10.9	4.5	.56
4	5.1%	2090	53%	8.6%	2090	82%	4.4×10^{-6}	.97	4.3	-5.0	4.6	.55
5	7.8%	2080	48%	9.5%	2080	81%	1.1×10^{-5}	.98	4.8	-5.2	4.8	.53
6	7.1%	2090	72%	9.0%	2090	84%	1.7×10^{-6}	1.15	5.4	-6.3	4.6	.55

280

TEST RESULTS

The heave measured by a micrometer (Hm) follows closely that evaluated by the following expression:

$$He = \frac{Q}{A} \times C \qquad (1)$$

where (Q) is the quantity of intake water distributed over the cross section area of the sample (A) and corrected for the water to ice phase change dilatation of 9% ($C \approx 1.09$). This distribution over the total cross area is justified by the fact that, in all cases, only one discrete pure ice lens with planar faces was observed over the total cross section of the sample. The rate of heave ($\overset{o}{H}$) is then computed by:

$$\overset{o}{H}_n = \frac{(He)_{n+1} - (He)_n}{t_{n+1} - t_n} \qquad (2)$$

where $(He)_{n+1}$ and $(He)_n$ are the cumulative heaves at times t_{n+1} and t_n respectively. This mean value of $\overset{o}{H}_n$ applies during a period of $t_{n+1} - t_n$ and will be representative of the real value of time $\overline{t}_n$ where:

$$\overline{t}_n = \frac{t_{n+1} + t_n}{2} \qquad (3)$$

A typical test result is presented in Figure 3, where the position of the $0°C$ isotherm, Hm, He and $\overset{o}{H}n$ are plotted as functions of time. It can be seen that an expulsion of water takes place at the beginning of the test due to the rapid penetration of the frost front. Then, as the frost front penetration slows down, water flows into the sample to feed the ice lens until a maximum rate of heave is reached. After this point, the rate of heave diminishes until heave is nearly stopped as the *final thermal regime tends to* approach true steady state. For each test, the maximum rate of heave ($\overset{o}{H}max$) is noted down and serves to compute the maximum drop of hydraulic potential ($\Delta\phi max$) at the warm end of the frozen fringe by using the relationship:

$$\Delta\phi max = \overset{o}{H}max \frac{Z_1}{k} \qquad (4)$$

where $\overset{o}{H}max$ is the maximum rate of heave, Z_1 is the thickness of the unfrozen zone and k is the previously
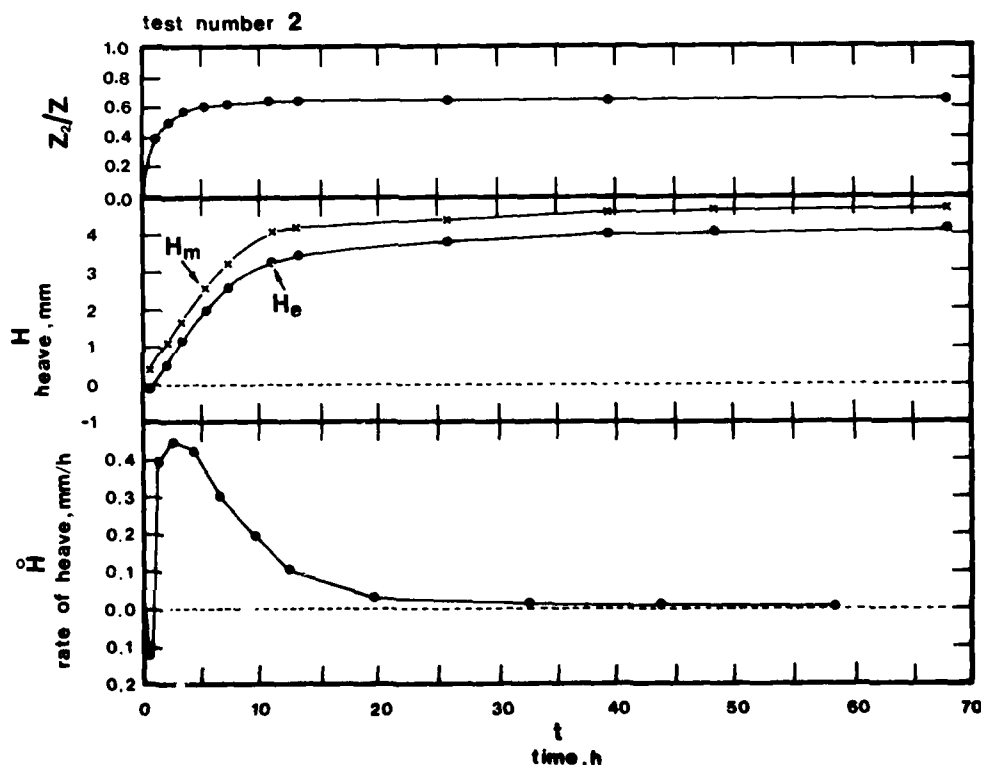

Figure 3. Typical results of frost heave test.

281

measured permeability of the unfrozen sample. Results of these computations are presented in Table 2.

The maximum rate of heave ($\overset{\circ}{H}$max), at relatively constant degree of saturation during compaction (Sr_1), was found to increase with the mean thermal gradient in the sample (∇T) as shown in Figure 4.

On the other hand, Figure 5 shows that, at relatively constant ∇T, Hmax diminishes when Sr_1 increases. This behavior can be explained by the dependency of the hydraulic conductivity (k) on the degree of saturation during compaction. It can be seen from Table 1 that k decreases when Sr_1 increases. The soil microstructure, offering more resistance to fluid flow as Sr increases, tends to slow down the rate of heave of the sample.

The maximum drop of hydraulic potential ($\Delta\Phi$max) is found to increase with the degree of saturation during compaction (S_{r1}). But, as can be seen in Fig. 6, this increase follows different rates depending on the thermal gradient ∇T. For an increase of S_{r1} from 53% to 83%, the increase of $\Delta\Phi$max is 81 cm of water when $\nabla T \simeq 2^\circ C/cm$ (tests 2 and 3), but when $\nabla T \simeq 1^\circ C?cm$, this increase is nearly four times smaller, as can be seen by the results of tests 1, 4, 5 and 6 (Fig. 6). This strong dependence on ∇T is shown more clearly when max is plotted against ∇T for the same tests, as in Fig. 7, where the effect of S_{r1} nearly disappears. This relative independence of $\Delta\Phi$max on the soil saturation suggests that $\Delta\Phi$max can be chosen as an acceptable descriptive parameter of the soil grains capability to generate segregational heaving independently of the matrix microstructure or type of compaction.

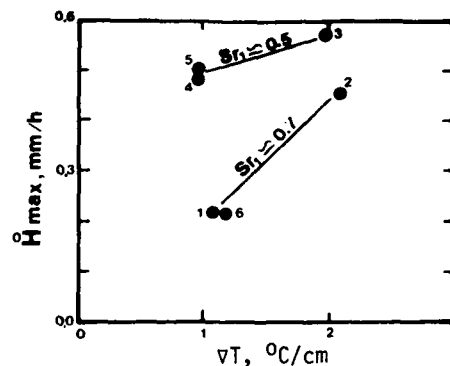Figure 4. Hmax as a function of ∇T.
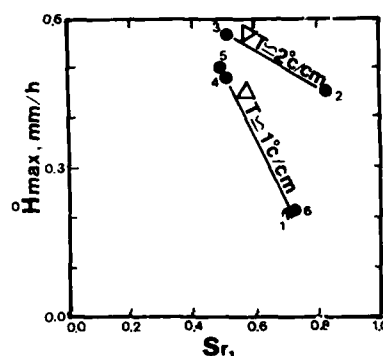
Figure 5. Hmax as a function of Sr_1.

Table 2. Maximum rate of heave and drop of hydraulic potential.

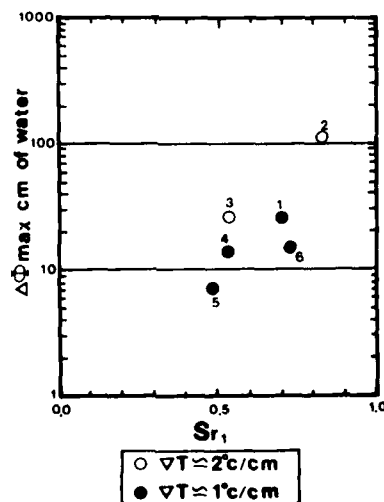|	$\overset{\circ}{H}$max mm/h	$\Delta\Phi$ cm
	.	.
	.	.
	.	27.3
	.	.
	.	.
	.	.

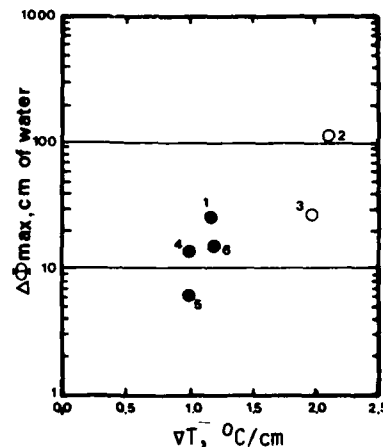Figure 6. $\Delta\Phi$max as a function of Sr_1.

Figure 7. $\Delta\Phi$max as a function of ∇T.

282

CHRONOLOGICAL EVOLUTION OF FROST HEAVE DURING THE TESTS

The transient heat flow taking place at the beginning of the test suggests that the evolution of heave may follow a power law similar to that used by Caniard (1977). He has found a linear correlation between cumulative heave and the square root of the frost index in a test in which thermal conditions were similar to the ones prevailing at the beginning of our testing procedure. Frost heave results were therefore plotted as function of the square root of time since constant temperatures at the ends of the sample were used. Figure 8 shows a good linear correlation between cumulative heave and square root of time in the first 10 to 15 hours of the tests. As the thermal regime tends to become stationary, heave diminishes and this linear correlation is no longer valid.
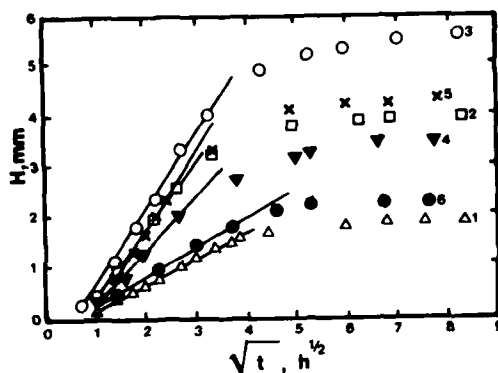

Figure 9. Hyperbolic model.

$$H = \frac{t}{(dt/dH)_0 + (1/H_{ass})}$$

The use of this model for representing the test results is shown in Figure 10. The fit of experimental data to the theoretical transformed hyperbola is quite acceptable after a time period following the one covered by the straight line portion of the previous model. The computed asymptotical values of the heave (H_{ass}) after a very long period of time are presented in Table 3. One finds they are slightly superior to the measured values of cumulative heave (H_{max}) at the end of the tests.

Figure 8. H as a function of $\sqrt{t}$.

Since heave seems to tend towards an asymptotic value when true stationary state is reached, an hyperbolic model similar to Kondner's hyperbolic stress-strain relationship (see Wong and Duncan 1974) was adapted by the authors in order to estimate the value of cumulative heave after an infinite time. The model is presented in Figure 9 in its two forms. Figure 9-a represents the hyperbolic curve in its real form as a function of heave (H) and time (t). Figure 9-b represents the same curve as a linear relation in a transformed system defined by t/H and t.

Figure 10. t/H as a function of t.

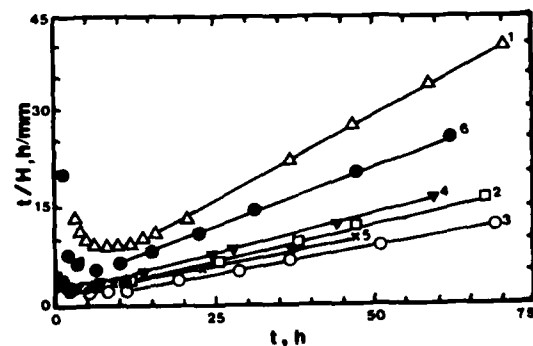Table 3. Asymptotic and maximum value of measured cumulative heaves.

Test	1	2	3	4	5	6
Hmax, mm	1.91	4.06	5.67	3.62	4.56	2.43
Hass, mm	1.95	4.50	5.95	4.00	5.60	2.50

283

CONCLUSION

The proposed interpretation of the heave test, which considers the evolution of the thermal field, enables the computation of the maximum drop of hydraulic potential, a parameter derived from the maximum rate of heave and hydraulic conductivity of the sample. The fact that this parameter is nearly independent of the soil microstructure but is very sensitive to the thermal gradient makes it a good indicator of the potential of the grains to generate cryogenic succion whatever their orientation might be.

In addition, it was shown that the time dependence of heave linearizes in a heave vs square root of time plot, when the frozen fringe is still in evolution and near its optimum thickness. Afterwards, as thermal conditions tend towards a stationary state, the hyperbolic model enables a reasonable extrapolation of the test results for long time intervals to be made, which has an importance in connection with the heave prediction of buried chilled gas pipelines.

Since this study covered only one type of soil, it would be of interest to extend it to a variety of other frost susceptible soils.

ACKNOWLEDGEMENTS

REFERENCES

BURT, T.P. and WILLIAMS, P.J.(1976)"Hydraulic Conductivity in Frozen Soils". Earth Surface Processes, Vol. 1, pp. 349-360.

CANIARD,L.(1977) "Frost Susceptibility of Soils. Experimental Method for Classification of Soils According to their Degree of Frost Susceptibility". Soil Freezing and Highway Construction Seminar-Course,Carleton University - Ecole Nationale des Ponts et Chaussées.

HOPKE, S.W.(1980) "A Model for Frost Heave Including Overburden". Cold Reg. Sci. and Tech., Vol.3, pp. 111-127.

HORIGUCHI,K. and MILLER,R.D.(1980). "Experimental Studies with Frozen Soil in an Ice Sandwich Permeameter". Cold Regions Science and Technology,Vol.3, pp. 177-183.

JUMIKIS, A.R.(1966) Thermal Soil Mechanics, Rutgers University Press, New Jersey.

KONRAD,J.M. and MORGENSTERN,N.R.(1980) "A Mechanistic Theory of Ice Lens Formation in Fine-Grained Soils". Can. Geotech.J., Vol.17, pp. 473-486.

KONRAD,J.M. and MORGENSTERN,N.R.(1981) "The Segregation Potential of a Freezing Soil" Can. Geotech. J., Vol.18, pp. 482-491.

LOCH, J.P.G. and MILLER, R.D.(1975) "Tests of the Concept of Secondary Frost Heaving". Soil Sci. Soc. of America, Proc., No.39, pp. 1036-1041.

LOCH,J.P.G.(1978) "Thermodynamic Equilibrium Between Ice and Water in Porous Media". Soil Science, Vol. 126, pp. 77-80.

LOCH,J.P.G. and KAY,D.(1978) "Water Redistribution in Partially Frozen, Saturated Silt Under Temperature Gradients and Overburden Loads". Soil Sci. Soc. of America J., Vol. 42, pp. 400-406.

MILLER, R.D.(1980) "Computation of Rate of Heave Versus Load Under Quasi-Steady State". Cold Regions Sci. and Tech., Vol. 3, pp. 243-251.

PENNER,E. and UEDA,T.(1977) "The Dependence of Frost Heaving on Load Application". Proc. Int. Symp. on Frost Action in Soils, Lulea, Sweden, pp. 92-101.

WONG,K.S. and DUNCAN,J.M.(1974) "Hyperbolic Stress-Strain Parameters for Nonlinear Finite Element Analyses of Stresses and Movements in Soil Masses".Berkeley, California, Res. Report No. TE-74-3.

HEAVING PRESSURES AND FROST SUSCEPTIBILITY

E.Y. McCabe, Research Student, Dept. of Civil Eng.,
University of Aston, United Kingdom.
R.J. Kettle, Senior Lecturer, Dept. of Civil Eng.,
University of Aston, United Kingdom.

When frost susceptible soils freeze and the heave is restricted, heaving pressures are generated which will threaten pipelines or structural units embedded in the soil. Thus, it is important to accurately eva'uate the maximum heaving pressures for individual soils.

Heaving pressures measured under laboratory conditions are presented. Cylindrical specimens, of either 120mm or 145mm diameter, were subjected to freezing from the top surface in an open system. Heave was restricted by a stiff reaction frame and the heaving pressures were monitored continuously. During freezing the specimen was supported in a multi-ring cell which eliminated friction between the sample and the mould and prevented adfreeze at this interface. The heaving pressures were significantly greater than those recorded in earlier studies without the multi-ring supports.

The initial tests were performed on a highly frost susceptible mixture of sand and ground chalk and included a study of the influence of specimen size and thermal parameters on heaving pressure. The frost susceptibility of this matrix was modified by additions of between 10 and 50 percent of selected coarse particles, sub-divided into two groups of 3.35-20mm and 20-37.5mm.

It is clear that the heaving pressures increase with freezing time but at an ever decreasing rate. The introduction of coarse particles to the frost susceptible matrix clearly reduced both the maximum heaving pressure and the required freezing period. Linear relationships were obtained between heaving pressure and aggregate content, the individual relationships being dependent on aggregate type. Heaving pressures were also linearly related to frost heave but, again, the type of coarse aggregate was important.

It has been clearly demonstrated that freezing behaviour of granular mixtures depends not only on the fine fraction but also on the amount and type of coarse particles in the mixture.

INTRODUCTION

In the United Kingdom the frost susceptibility of materials used in highway construction is assessed by subjecting laboratory-prepared samples to the Transport and Road Research Laboratory (TRRL) frost heave test (1) (2). One of the major disadvantages of the test is time element involved, a 24 hour conditioning period being required prior to the 250 hour freezing test. Recent revisions (3) have been proposed to the test procedure and, although the freezing period has been shortened, the longer conditioning period will still produce a total test period of approximately two weeks between sample receipt and final assessment of frost susceptibility. Thus, there is considerable merit in producing alternative test methods that can produce more rapid assessments of frost susceptibility.

It has been suggested (4) (5) (6) that one such alternative approach may be the measurement of the heaving pressures

produced when a freezing soil is restrained. Initial investigations of heaving pressure, at least on a carefully controlled basis, were undertaken by the U.S. Army Corps of Engineers at CRREL (7). In an earlier investigation (8) measurements were made of the heaving pressures using similar equipment to that developed at CRREL (9). These proved to be very useful for predicting the onset of heaving in cement stabilised materials (10). In that work it was also possible to develop limited relationships between frost heave and heaving pressure. However, at the time, it had not been realised how important the cold plate temperature was in controlling the heaving pressures (11).

In the current investigation (12) of frost action in granular soils, a renewed interest has been stimulated in the accurate measurement of heaving pressure. This has stemmed from three, related considerations:-

(a) Influence of such pressures on structural designs involving low temperatures, e.g. storage facilities for LNG, cold stores, ice rinks, etc.
(b) Examination of the use of heaving pressures as an alternative/adjunct to frost heave for assessing frost susceptibility.
(c) An additional parameter to be considered in assessing frost activity in soils.

In addition, this investigation would provide an opportunity to examine the influence of thermal factors in the development of heaving pressures. This paper, therefore, details a test method for measuring heaving pressure and presents the results obtained with the equipment.

MATERIALS

The basic matrix consisted of a highly frost susceptible mixture of sand and ground chalk(mixing ratio 4:1). Three types of coarse particles were selected - Blast furnace Slag, Rowley Basalt and Caldon Low Limestone. These coarse particles were subdivided into two groups : 3.35-20 mm and 20-37.5 mm. Each aggregate was presieved and blended so that each group had the same particle size distribution. The influence of the coarse aggregate on freezing behaviour was studied by the introduction into the matrix of up to 50% of the selected coarse particles. Figure 1 shows the particle size distribution for the matrix itself

togegher with those for mixtures containing 10,30 and 50 percent of the 3.35-20mm aggregate (12)
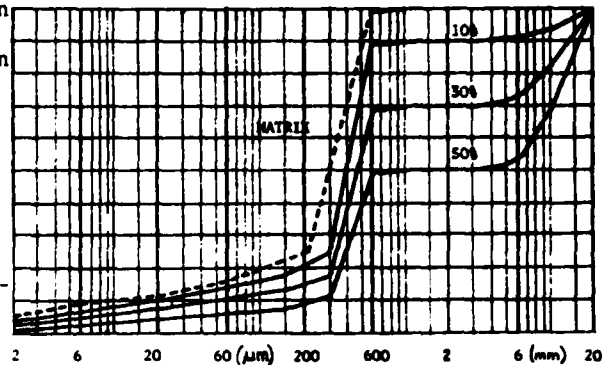
FIGURE 1. PARTICLE SIZE DISTRIBUTION

APPARATUS AND TEST PROCEDURE

The apparatus was based on that used in earlier studies (7) (8) but was modified (12) (13) to reduce frictional restraint and adfreeze between the specimen and the mould. The general arrangement is shown in Figure 2.

1) Load Cell   2) Aluminium frame
3) TED/Cryostat   4) Steel Mould
5) Rubber membrane 6) Perspex Rings
7) Sample   8) Porous Stone
       9) Steel Base Plate

FIG. 2. FINAL FORM OF EQUIPMENT

286

The specimen was supported by a multi-system consisting of four 25 mm rings and one 15 mm ring to give a specimen height of 115 mm. The rings were made from perspex tubing and two sets were produced - 120 mm and 145 mm internal diameter. Each set of rings could be accommodated in a suitable steel mould to achieve 1 mm clearance between the rings and the mould. Specimen preparation followed the same basic procedure for both specimen sizes.
The rings were secured together with adhesive tape to prevent displacement during compaction and were inserted into the mould which was already bolted to the steel plate. A ring cla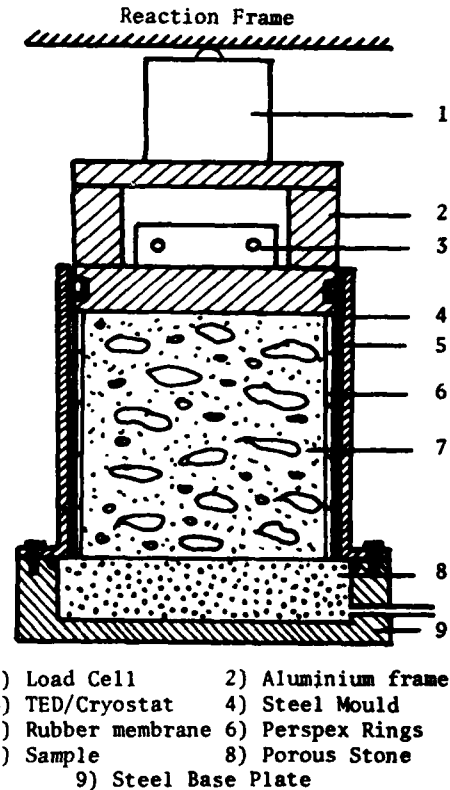mp was fixed to the upper edge of the mould to prevent relative movement of the rings during compaction. The specimen was compacted following the Proctor test (14) procedure with a 2.5 kg hammer. However, due to the differences in diameter, it was necessary to use more blows per layer to achieve the required level of compaction. The specimens were produced to the maximum dry density and optimum moisture content as determined in the B.S. standard (14) compaction test (Proctor).
After compaction the steel test-plate was unbolted, the mould lifted clear and the adhesive tape removed from the rings. The specimen was trimmed with a straight edge and positioned on top of the recessed base-plate which contained a porous stone. The rings were greased and a rubber membrane was slid over them. A further coat of silicon grease was applied to the membrane to eliminate any possible friction between rubber membrane and the wall of the mould. The steel mould was replaced over rings and was bolted to the base plate. An aluminium supporting frame, with thermoelectric device (TED) and load cell, was placed on top of the specimen and the whole assembly transferred into a cold cabinet where it was located inside a reaction frame. A water supply was connected to the base plate and the specimen was left to condition for 24 hours at a temperature of + 4.0°C. At the end of the conditioning period the load cell was rigidly secured against the reaction frame. The load cell, TED, water cooler and trace recorder were switched on and test continued until maximum heaving pressure achieved.

It is believed (13) that, by introducing the multi-ring ring system combined with a rubber membrane, the effects of adfreeze and friction were eliminated. At the end of the test the specimen could be removed by inverting of the mould, allowing it to slide out under its own weight. The recorded heaving pressures were 200% greater than the pressures measured using the initial equipment (12).

Later in the programme the TED was replaced by a cryostat. A closed unit was placed on top of the aluminium supporting plate, instead of the TED, and chilled liquid was circulated through this unit to freeze the specimen. This system proved to be more reliable and allowed several tests to be run simultaneously under the same temperature conditions. Providing that the temperature on the top of the specimen was the same, it was found that the recorded heaving pressures with the TED or the cryostat were not significantly different.

It has been demonstrated (15)that the greatest heaving pressures are generated under the stiffest constraints, such as load cells. The load cell does not permit surface heave (15) and so records not only heaving pressures due to ice lensing, but also those due to the freezing and expansion of the in-situ, pore water as the zero isotherm penetrates through the soil. In the TRRL frost heave test (1) (2) (12), the total heave includes both the volumetric expansion of the pore water as well as the heave due to the formation of ice lenses. It was, therefore, decided to measure the heaving pressures under conditions of severe restraint with a load cell.

DEFINITION OF MAXIMUM HEAVING PRESSURE

From the capilliary theory of frost heaving it can be shown that heaving pressure is inversely related to pore size (16) (17) and it has been suggested (17) (18) that the maximum pressure will particularly depend on the smaller pores. However, in freezing tests it will be essential to consider both this primary heaving and secondary heaving (19) (20) with ice lenses growing behind the freezing front. This produces heaving pressures considerably greater than those predicted by the capilliary theory (19). It has been reported (11) (21) that these pressures are dependent on both the temperature of the cold plate and the soil type. The measurement of such pressures can involve freezing periods in excess of 100 days since the terminal value is approached

at an ever decreasing rate (11). Therefore, in order to limit the present test programme, it was decided to adopt an arbitrary definition for the maximum heaving pressure.

In earlier work (8) the maximum heaving pressure was arbitarily defined as that pressure recorded when the rate of increase was less than $0.001MN/m^2/hr$ ($1KN/m^2/hr$). This criterion has the advantage of limiting the testing time especially when the soil is being tested for classification purposes, although it is not an absolute parameter.

To justify this assumption, a test was undertaken on the fine grained matrix of sand and snowcal for a period of 500 hours. Between 100 and 150 hours the rate of increase in heaving pressure was less than $0.3KN/m^2/hr$. After 200 hours freezing, the rate increase further diminished and between 250 and 500 hours no increase was recorded. As the experimental programme was concerned with granular materials and as the time to reach limiting heaving pressures was relatively short (150 hours or less) it was decided to measure heaving pressure until the increase is less than $0.1KN/m^2/hr$. The heaving pressure corresponding to this value is reported as the maximum heaving pressure.

INFLUENCE OF THERMAL PARAMETERS

One of the objects of the study (12) was the formulation of a standard procedure for measuring heaving pressure. It was, therefore, essential to study the effects of the boundary conditions on heaving pressure. To assess the viability of using heaving pressure for predicting frost susceptbility, the measured pressures can be compared with heave data from the TRRL frost heave test, this being the standard test in the U.K.

The initial boundary conditions in the heaving pressure test were designed to produce a temperature gradient through the specimen similar to that reported (1) (12) for frost heave specimens. Thus, the temperature at the top of specimen was $-4.5^{\circ}C$, whilst the water bath at $+4.0^{\circ}C$ produced $+3.5^{\circ}C$ at the base of the specimen. Prior to the detailed programme, it was necessary to assess the effects of changes in the boundary temperatures on the pressure.

a) Temperature of Cold Plate
This study was performed on specimens prepared from the highly frost

susceptible matrix. Thermocouples were inserted through the centre of each ring so that the temperature gradient through the specimen could be determined. The porous stone in the base plate was replaced by a perforated brass plate with filter paper placed on the upper face. By connecting the two pipes in the base plate to a thermostatically controlled, circulating bath, it was possible to control the water temperature to close limits. In this test, the water bath was operating at $+4^{\circ}C$.

After 24 hours conditioning at $+4.0^{\circ}C$, the specimens were frozen from the top with the top temperature subjected to step changes when the heaving pressure reached its arbitarily defined maximum at a given temperature. The temperature of the cold plate was reduced by a specified amount and again held steady until a new maximum pressure was obtained. The initial temperature of the cold plate was $-2.0^{\circ}C$. The relationship between heaving pressure and the temperature of the cold plate is shown in Figure 3 and the corresponding temperature gradients are given in Figure 4.

As the temperature of the cold plate is reduced, the heaving pressure increases linearly between $-2.0^{\circ}C$ and $-4.5^{\circ}C$ - above $-1.5^{\circ}C$ initial nucleation was not achieved. At temperatures below $-4.5^{\circ}C$, the relationship deviates from the initial line and the pressure increases at a diminishing rate. Similar behaviour has been reported by Takashi (11). It was not possible to continue the tests at temperatures below $-9.0^{\circ}C$ as the cryostat could not constantly maintain such low temperatures. As the top temperature decreases, the zero isotherm penetrates through the specimen as can be seen from the distributions in Figure 4. Although the circulating water was maintained at $+4.0^{\circ}C$, the penetrating zero isotherm also decreased the temperature at the bottom of the specimen so producing a temperature gradient through the brass plate.

It has been suggested (22) (23) that the rate of frost heaving is dependent on the amount of heat removed from the freezing front and so another test series was undertaken to examine this behaviour.

b) Temperature Gradient
It was decided to maintain the freezing front (zero isotherm) at a constant location but to vary the
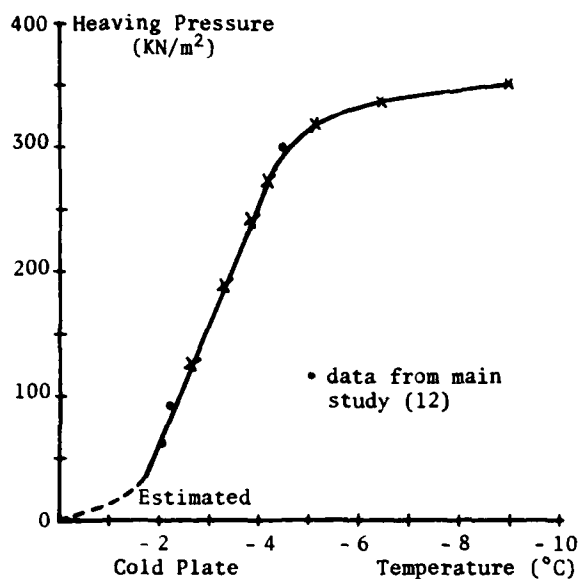
FIGURE 3 HEAVING PRESSURE
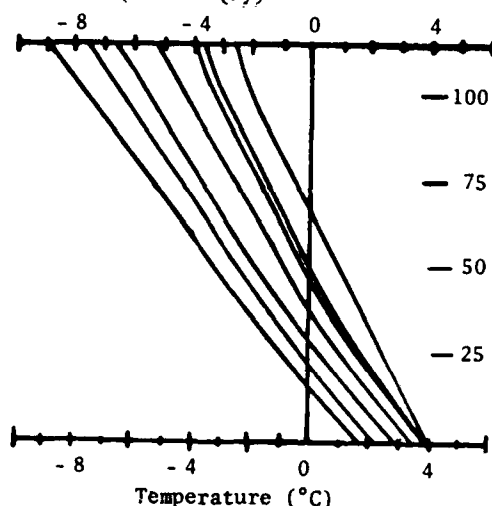AGAINST COLD PLATE TEMPERATURE
(SERIES (a))

FIGURE 5 HEAVING PRESSURE
AGAINST COLD PLATE TEMPERATURE
(SERIES (b))

FIGURE 4 TEMPERATURE
GRADIENT (SERIES (a))

FIGURE 6 TEMPERATURE
GRADIENT (SERIES (b))

temperature gradient in the frozen zone. Thus, as the temperature of the cold plate was reduced it was necessary to increase the temperature of the circulating water to maintain a stationary zero isotherm. This location was that achieved in the normal test conditions - top temperature, - 4.5°C, bottom + 3.5°C. The relationship between heaving pressure and cold plate temperature is shown in Figure 5 and the corresponding temperature gradients are given in Figure 6.

It should be noted that although the bottom temperature remained sensibly constant at 3.5 to 4.0°C, this was only achieved by progressively raising the temperature of the circulating water from + 4.0°C to + 7.0°C as the cold plate temperature was reduced from - 5.0 to - 9.0°C.

A comparison of Figure 3 with Figure 5 indicates good agreement between the results of the two tests in the range 0 to - 4.5°C. At lower temperatures the heaving pressure continues to increase,

289

albeit at a decreasing rate, in both tests. However, at these lower temperatures, the heaving pressure increases more rapidly with the stationary freezing front than with the penetrating freezing front.

In both tests the freezing rates, or cold plate temperatures, were the same but larger temperature gradients were obtained with the stationary freezing front. This is attributed to the higher temperatures at the bottom of the specimen which indicate an increase in the rate of heat extraction. It, therefore, appears that an increase in the rate of heat removed from the freezing front produces an increase in the heaving pressure. For both experiments the deviation of the heaving pressure relationship from the initial linear relation was at approximately - 4.5°C for the test material. With such a cold plate temperature, the temperature gradient and location of the freezing front are similar to those of the frost heave specimen (1). Absolute compatability is not possible due to differences in the height of the two specimens e.g. 115 mm and 150 mm. To minimise differences in procedure between the heaving pressure and the frost heave tests, it was decided to test the heaving pressure specimens under these conditions i.e. cold-plate at - 4.5°C and circulating water bath at + 4.0°C. This, it was hoped, would permit subsequent comparisons between the results of the two tests.

SPECIMEN SIZE

To study the effect of large particles, 20-37.5 mm, on heaving pressure it was proposed that a larger specimen of 145mm diameter should be used, this being similar to that used in modified frost heave tests (3) (24). It has been reported (3) (24) that the specimen size can influence the heave recorded in the frost heave test. It was, therefore, decided to undertake a series of tests to examine whether such differences could be observed in heaving pressure tests.

With the cryostat it was possible (12) to test two specimens simultaneously so that direct comparison could be made between the results obtained with different sized specimens under the same boundary conditions. It was clear that the size of the specimen did not have any significant effect on the measured heave values and this has been discussed in detail elsewhere (12).

EXPERIMENTAL RESULTS

Mixtures containing 3.35-20 mm particles were, therefore, tested in 120 mm specimens whilst those with 20-37.5 mm particles were tested in 145 mm specimens. Both groups were tested under the same conditions. Before commencing this study it was decided to check the repeatability of the test. Five tests were carried out on nominally similar specimens of the matrix material and analysis of these results gave a coefficient of variations of less than 3%. It was, therefore, decided that tests on two nominally similar specimens would give an acceptable measure of heaving pressure for the test programme. It should also be noted that this variation is significantly lower than that reported (3) (8) for frost heave tests and, so, encourages consideration of the test as an alternative method for assessing frost susceptibility. The duration of each test depended on the time the specimen took to reach the observed maximum value and typical plots of heaving pressure against time are shown in Figure 7. The results of the heaving pressure tests are summarised in Table 1, together with the appropriate heave values.

DISCUSSION

a) Aggregate content. The relationships between heaving pressure and the percentage of aggregate are shown in Figures 8 and 9 for the two aggregate groups, 3.35 - 20 mm and 20 - 37.5 mm. As aggregate content increases, the heaving pressure is reduced. In general, the relationships between heaving pressure and aggregate content are linear for all the materials tested. However, the individual relationships are very dependent on aggregate type, this being apparent with both aggregate size groupings. The importance of aggregate type becomes more marked as the content increases.

For given freezing conditions, the extent of frost action in granular mixtures is related to pore size (16) with heaving pressure being inversely related to pore size, providing that water is freely available at the freezing front. The pore structure is influenced by grain size and, since coarser materials will contain considerably fewer fines per unit volume (also per unit cross-section in a given plane) of material, they will exhibit reduced frost activity. Large particles
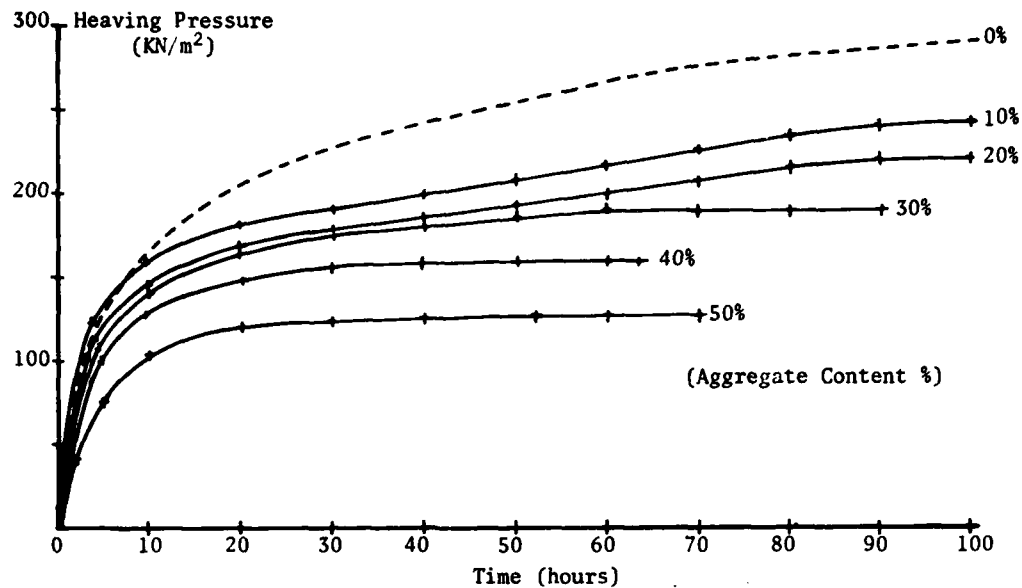
FIGURE 7. HEAVING PRESSURE AGAINST FREEZING TIME.
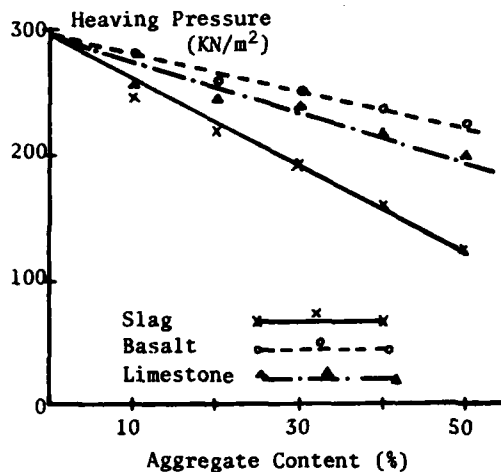
FIGURE 8. HEAVING PRESSURE AGAINST
AGGREGATE CONTENT (3.35.20mm) PARTICLES
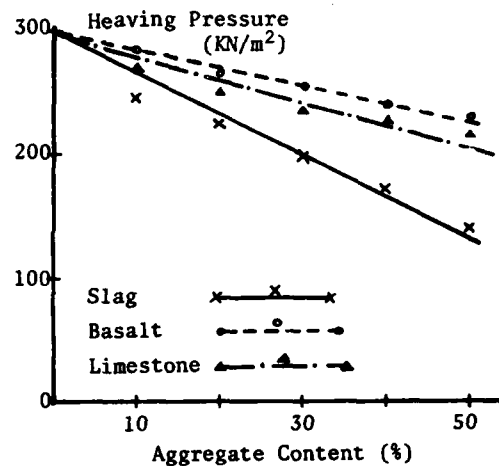
FIGURE 9. HEAVING PRESSURE AGAINST
AGGREGATE CONTENT (20-37.5mm) PARTICLES.

will also lie across the freezing plane
with a portion of the particle above and
a portion below and so will offer
frictional and displacement resistance
to the heave forces located in the plane
of freezing(25).

    With porous coarse particles, ice
lensing could occur within the particles
and this would contribute to the develop-
ment of heaving pressure. The exact
effect would depend on the relationship
between pore structure within the
particle and that of the surrounding
matrix. Such behaviour has been reported
with some porous aggregates (8). The
three aggregates used in this study had

low absorption values (12) and so ice
lensing within the particles is unlikely
to have been a significant factor in
these tests. However, the differences
in effect between the three aggregates
may be due to differences in their
internal pore structure (12). Similarly
the three aggregates would have differ-
ing effects on the thermal properties of
the material, particularly in the region
immediately adjacent to each particle,
and so this would also account for
different trends reported for the three
aggregates.

b) Particle size. From the results in

291

Table 1 it appears that both aggregate groups, 3.35 - 20 mm and 20 - 37.5 mm, have similar effects on heaving pressure. As the aggregate content increases it appears that the 3.35 - 20 mm particles may be more effective in reducing heaving pressure than the 20 - 37.5 mm particles. This is most apparent with the Slag and the Limestone mixtures although the individual differences are not significant.

At a given aggregate content, both groups would occupy the same volume in the specimen but the 3.35 - 20 mm fraction will possess a larger, particle surface area. Thus, compared with the 20 - 37.5 mm particles, these particles would occupy a greater proportion of any freezing plane, and so would be expected to be more effective in reducing forces associated with frost action, in this case, the heaving pressure. In addition, the increased surface area of the 3.35 - 20 mm particles would increase the frictional and displacement resistance to the heaving forces at the freezing front.

c) Frost Heave. The frost heave values for all the materials were obtained by subjecting them to the standard TRRL frost heave test (2) (12) and the results are included in Table 1. The relationships between heaving pressure and frost heave for the 3.35 - 20 mm particles are shown in Figure 10. A similar trend has also been recorded (12) with the 20 - 37.5 mm particles.

For all the materials tested, the heaving pressure is linearly related to frost heave. However, both frost heave and heaving pressure would appear to depend on aggregate type and separate relationships are obtained for each aggregate. At any given aggregate content, it should be noted that both the amount and nature of the fine fraction of any particular mixture are the same. Thus, the observed differences in freezing behaviour can be attributed to the type of coarse aggregate, these differences becoming more apparent as the aggregate content increases. It would, therefore, appear that frost susceptbility criteria based solely on the amount of fine material are inappropriate for such mixed material where both the amount and type of coarse aggregate are signigicant factors.

It seems that the measurement of heaving pressure could be an additional aid for assessing the frost susceptibility of soils and granular mixtures. Such
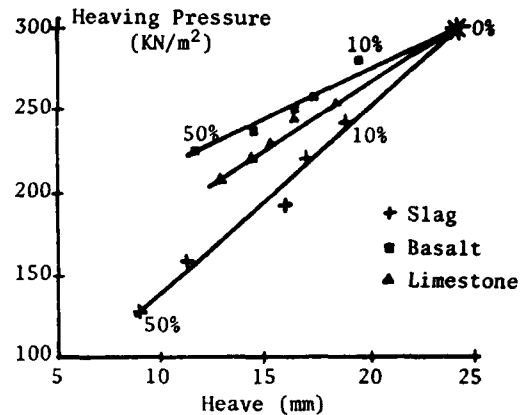
FIGURE 10. HEAVING PRESSURE AGAINST HEAVE (3.35-20mm) PARTICLES.

information is liekly to be of particular use where a structure will provide a restraint to ice formation. Such an approach will require a future correlation between laboratory data and field observations. However, it is possible to define limiting pressures for frost susceptibility based on a comparison with the existing heave criterion. For the present work, the results in Figure 10 indicate that materials which developed heaving pressures of less than 150 KN/m^2 were non-frost susceptible when subjected to the frost heave test.

CONCLUSIONS

From the experimental data discussed in previous sections, it is possible to present the following major conclusions:-
(1) The multi-ring freezing cell and lubricated rubber membrane forms a reliable system for measuring heaving pressures on a routine basis and produced results with a coefficient of variation of less than 3%.
(2) The temperature of the cold plate has a significant influence on the heaving pressure, with the pressures being inversely related to temperature. This relationship is influenced by the location of the feezing front in the specimen and so it is vital to define and control the boundary conditions when measuring heaving pressure.
(3) In mixed materials the magnitude of the heaving pressure is inversely related to coarse aggregate content. Similar behaviour was observed with both 3.35 - 20 mm particles and 20 - 37.5 mm particles.
(4) The freezing behaviour of such mixed materials is also significantly

292

influenced by the type of coarse aggregate.

(5) Frost susceptibility criteria based only on the fine fraction would appear to be inappropriate for these mixed materials.

(6) For the materials tested, heaving pressure and frost heave appear to be linearly related and so the development of frost susceptibility criteria based on heaving pressures should be considered.

(7) From the available **data**, it would appear that materials which develop heaving pressures of less than $150/KN/m^2$ are not frost susceptible when subjected to the frost heave test.

References

(1) CRONEY, D and JACOBS, J.C. The frost susceptibility of soils and road materials. Road Research Lab, Crowthorne, Report LR90. 1967.

(2) TRANSPORT AND ROAD RESEARCH LABORATORY. The LR90 Frost Heave Test - interim specification for use with granular materials. Report SR318 1977.

(3) SHERWOOD, P.T. Research at TRRL on the frost-susceptibility of roadmaking materials. Proc. of Symposium on Unbound Aggregates in Roads, Univ. of Nottingham, 7/8 April. Vol II Discussion pp 151-160. 1981.

(4) OBERMEIER, S.F. Frost heave susceptibility research. Proc Symposium on Frost Action in Roads (OECD) Oslo. Vol 1 pp 251-266. 1973.

(5) MARTIN, R.T. and WISSA, A.E.Z. Frost Susceptibility of Massachusetts Soils - Evaluation of rapid frost susceptibility tests. M.I.T. Soils Publication 320.1973.

(6) SAETERSDAL, R. Heaving conditions by freezing of soils. Proc. Second Int. Symposium on Ground Freezing. NTH, Trondheim 24-26 June, pp 824-836 1980.

(7) HOEKSTRA, P., CHAMBERLAIN E. and FRATE, T. Frost heaving pressure. Highway Research Record 101, pp 28-38 1965.

(8) KETTLE, R.J. Freezing behaviour of colliery shale. Ph.D thesis University of Surrey 1973.

(9) KETTLE, R.J. and WILLIAMS, R.I.T. Frost heave and heaving pressure measurements in colliery shales. Can. Geotech. Jour. Vol. 13,No.2 pp 127-138. 1976.

(10) KETTLE, R.J. and WILLIAMS, R.I.T. Frost action in cement stabilised colliery shale. Transportation Research Record 641, pp 41-48. 1977.

(11) TAKASHI, T., OHRAI, T., JAMAMOTO, H. and OKAMOTO, J. Upper limit of heaving pressure derived by pore water pressure measurements of partially frozen soils Proc. Second Int. Symposium on Ground

Freezing. NTM Trondheim 24-26 June pp 713-724. 1980.

(12) McCABE, E.Y. Freezing behaviour of granular materials. Ph.D thesis (to be submitted) University of Aston in Birmingham 1982.

(13) KETTLE, R.J. and McCABE, E.Y. Heaving pressures as a means of assessing frost susceptibility. Proc. of International Seminar on Frost Heave Testing, held at University of Nottingham, 9 April pp. 5-1981.

(14) BRITISH STANDARDS INSTITUTION. Methods of testing soils for civil engineering purposes. BS1377:1975.

(15) OSLER, J.C. Some considerations of heave and heaving pressures in frozen soil. Paper presented to VIth World Highway Conference, Montreal, Quebec 7th October 1970.

(16) EVERETT, D.H. and HAYNES, J.M. Capillary properties of some model pore systems with special reference to frost damage. Bulletin RILEM Vol 27 pp 31-36 1965.

(17) PENNER, E. Heaving pressures in soils during uni-directional freezing. Can. Geotech. Journal Vol 4 pp 398-408 1967.

(18) PENNER, E. Frost heaving pressures in particulate materials. Proc. Symposium on Frost Action in Roads (OED), Oslo. Vol. I pp.379-385. 1973.

(19) MILLER, R.D. Freezing and heaving, of saturated and unsaturated soils.Highway Research Record 393 pp 1-11. 1972.

(20) MILLER, R.D. Frost heaving in non-colloidal soils. Proc. Third International Conf. on Permafrost, Edmonton, Alberta pp 707-713. 1978.

(21) RADD, F.J. and OERTLE, DH. Experimental pressure studies of frost heave mechanisms and growth fusion behaviour of ice. Second International Conf. on Permafrost, Yakutisk, USSR. North American Contribution pp 377-384. 1973.

(22) HORIGUCHI, K. Effects of the rate of heat removal on the rate of frost heaving. Proc. of First International Symposium on Ground Freezing. Ruhr Univ, Bochum, FRG. pp 25-30 1978.

(23) LOCH, J.P.G. Influence of heat extraction rate on ice segregation rate of soils. Frost i Jord. No.20 pp 19-30 1979.

(24) JONES, R.H. Development and applications of frost susceptibility testing. Proc. Second Intern. Conference on Ground Freezing. NTH, Trondheim pp 748-759 1980.

(25) KAPLAR, C.W. Phenomenon and mechanism of frost heaving. Highway

TABLE 1. HEAVING PRESSURE AND HEAVE RESULTS

TYPE OF AGGREGATE	AGGREGATE CONTENT (%)	HEAVING PRESSURE (KN/m^2)		FROST HEAVE (mm)	
		3.35 - 20 mm PARTICLES	20 - 37.5 mm PARTICLES	3.35 - 20 mm PARTICLES	20 - 37.5 mm PARTICLES
BLASTFURNACE SLAG	0	300	301	24.36	26.67
	10	242	246	18.9	22.5
	20	220	224	17.0	20.2
	30	192	198	16.0	18.1
	40	160	172	11.2	12.8
	50	127	140	9.0	10.7
ROWLEY BASALT	10	280	282	19.5	23.4
	20	258	264	17.3	20.7
	30	250	255	16.4	18.6
	40	238	240	14.4	15.5
	50	225	230	11.6	12.6
CALDON LOW LIMESTONE	10	254	265	18.4	23.2
	20	246	250	16.4	21.2
	30	230	236	15.2	19.8
	40	218	228	14.3	18.0
	50	200	215	13.6	15.8

GROUND MOVEMENTS ASSOCIATED
WITH ARTIFICIAL FREEZING

R.H. JONES   University of Nottingham, U.K.

ABSTRACT

The possibility of ground movements
(frost heave or settlement after thawing)
is of concern to clients who are
considering using artificial ground
freezing (AGF) as the temporary support
for tunnels and shafts in close
proximity to other structures.
Two groups of AGF case histories,
are considered, namely
(a) Major shafts sunk in Britain between
1947 and 1976,
(b) Tunnels reported at ISGF 78 and 80.
Published and unpublished data has
been synthesised to provide a state of
the art review of:-
(1) movements, particularly heave,
which have been associated with AGF;
(2) methods used to predict heave;
(3) techniques for limiting movements.
The shafts form two sub-groups within
which common features permit useful
comparisons. Conditions in the tunnels
were more diverse. However, with proper
attention to techniques on site, move-
ments associated with tunnelling using
AGF are generally acceptable and compare
favourably with other alternative
methods of construction. It is
concluded that a check list for case
histories and some form of reference
testing for frost heave would facilitate
future studies.

INTRODUCTION

When AGF is being considered as a
possible temporary support system the
client will often question the
contractor about the magnitude of frost
heave and subsequent settlement to be
expected. These aspects are particu-
larly important when tunnelling at
shallow depth under built-up areas or
when the permanent headgear is to be
installed to facilitate mine shaft
sinking.
Movement results from a complex
interaction of many factors so that the
contractor's estimate tends to be made
on the basis of previous experience and
engineering judgement perhaps backed by
relatively simple semi-empirical calcu-
lations. If significant movements
appear likely, special precautions may
be taken to minimise them. Meanwhile,
research workers are endeavouring to
obtain a greater understanding of the
processes involved and to develop better
predictive techniques.
Good case histories are vital to
all involved in AGF: they supplement the
contractor's personal experience, they
may allay the fears of the client by
showing that similar jobs have been
completed without unacceptable movements
and finally they provide field data
needed by research workers to develop
and validate new predictive techniques.
It is unrealistic to review the
whole of the literature produced since
the first application of AGF over 100
years ago. Instead, a cross section
has been reviewed consisting of:-
(1) Major shafts sunk in Britain in the
period 1947-1976.
(2) Tunnels reported at the previous
International Symposia at Bochum
(1978) and Trondheim (1980).
These two groups are sufficiently

large to provide a reasonably represen-
tative cross section. Information on
the tunnels has been supplemented by
other publications and personal enquiry.
Additional data was obtained from the
records of Foraky Limited who were the
contractors for all the British shafts.
Since 1977, 10 further shafts and two
drifts have been sunk with AGF during
the development of the Selby coalfield.
Records of the movements at these sites
are expected to be published shortly.

The case histories are summarised
in Tables. Whilst reducing the data
from many sources to a common format
inevitably involves simplification,
interpolation and interpretation, care
has been taken to present as accurate an
account as possible.

The emphasis of this paper is on
frost heave but it is recognised fully
that movements and weakening of the
ground associated with thawing are also
of major concern. It is hoped to
consider these aspects in more detail in
a future study.

CASE HISTORIES

Shafts

Within the period reviewed, 10 mine
shafts were sunk for the National Coal
Board (NCB) and six on the Ely Ouse –
Essex water supply scheme for the Essex
and the Great Ouse River Authorities at
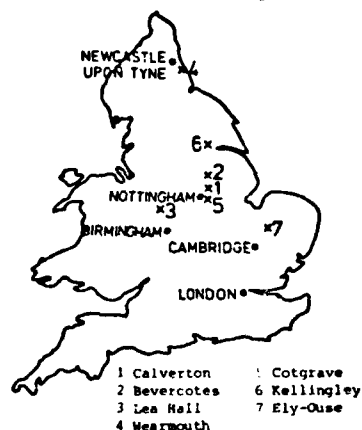the locations shown in Fig. 1.

Fig. 1 Location of Shafts

The ground was frozen from the surface
by circulating chilled brine through
vertical freeze tubes, (two shafts which
were frozen from an intermediate level
have not been considered). Ground

temperatures in observation holes,
temperatures and flow rates of the brine
and the rate of water expulsion from the
central pressure relief hole were moni-
tored routinely. No other sub-surface
instrumentation was installed. Salient
features of the works are given in
Table 1. The times are approximate
since brine circulation did not
necessarily start through all tubes
simultaneously and ice wall closure has
to be estimated conservatively.

The Ely Ouse shafts were located
along a 19 km (12 mile) length of
aqueduct tunnel. The job was described
in detail by Collins et al 1972. The
shafts passed through the Lower and
Middle Chalk and penetrated about 3 m
into the underlying Gault Clay.
Between the Chalk and the Gault is the
Cambridge Greensand which is usually
thinner than 300 mm and consists of
sandy and chalky marl with phosphate
nodules (coprolites) (Chatwin 1961).
At some sites the Chalk was overlain by
superficial deposits of peats, silts,
sands and gravel.

The average dry density of the
Chalk was 1.73 Mg/m^3 and its moisture
content 20%. In this area the chalk
varies between bands of tough, blocky
white rock and softer greyish marls.
Chalk is usually a very frost suscep-
tible material (Croney et al 1967).

The Gault is a very stiff, often
calcareous fissured silty clay. Whilst
the liquid limit often exceeds 70,
values down to 35 are not unknown. The
range of plastic limits (PL) is about
18 to 28 and the natural water content
is often at or below the PL. The dry
density is usually between 1.5 and
1.75 Mg/m^3.

Regular level readings indicated
frost heaves of between 24 and 144 mm.
This was of little consequence and
resulted in a very few fractures of
freeze tubes.

An interesting feature is that the
frost heave at the Blackdyke shaft,
where the chalk outcrops, continued
after refrigeration had ceased (Fig. 2).
A similar phenomenon has been observed
in laboratory experiments (De Beer et al
1980). However, at Blackdyke, brine
freezing ceased on December 5th. Thus
atmospheric temperatures which may well
have been below 0°C, could have been
responsible for this additional heave.
The similarity of the peaks in the
heave-time curves for the outer points
at 80 and 105 days supports this
hypothesis.

296

REF	LOCATION & DATE	Depth to Water table/m	Depth below surface/m	Strata	Finished internal dia/m	Depth frozen/m	Freezing circle pitch dia/m	Freeze tube spacing/m	Freeze tube dia/mm	Initial brine temp °C	To closure/days	Total freezing/days	HEAVE/mm	NOTES
1	CALVERTON No 2 (Notts, England) 1947-9	19	0-105 Bunter Set 105-196 Permian Marls & Limestones >196 Coal Measures		6.3	125	10.0	1.22	76 to 150	-20	60	265	0	No detailed observations but movement insignificant
2	BEVERCOTES No 1 (Notts, England) 1952-56 No 2		0-3 Drift 3-6 K.Waterstones 6-15 Green beds 15-204 Bunter Set 204-360 Permian >360 Coal Measures		7.3 7.3	248 252	13.4 -do-	1.23 -do-	125 -do-	-20 -do-	183 203	478 423	152 ? 200	Heave began after 70 days
3	LEA HALL No 1 No 2	2	0-20 Alluvium 20-69 Keuper Set 69-185 Bunter Set		7.3	218 222	12.2 -do-	1.13 -do-	125 -do-	-19 -do-	116 137	534	NR	Below 143 m Bunter is known at Littleworth Set
4	WEARMOUTH (Tyne & Wear England) 1953-1955		21 Boulder Clay 21-95 Permian Marls & Lst Coal Measures		7.3	108	12.2	1.13	125	-20	116		NR	NR = no record
5	COTGRAVE No 1 (Notts, England) 1955-1957 No 2		0-128 Keuper-Marl 128-162 K.Waterstones 162-247 Bunter Set 247-259 Permian Marl Lst & Breccia >259 Coal Measures		7.3 7.3	268 268	13.4 13.4	1.24 1.24	125 125	-20 -20	153 154	410 554	429 380	Many fractured tubes No. 2 sunk first
6	KELLINGLEY No 1 (W. Yorks, England) 1958-60 No 2	5.5	0-13 Bunter Set 13-149 Permian Marls & Limestones >149 m Coal Measures		7.3 7.3	195 195	14.0 -do-	1.22 -do-	125 125	-18	189 201	662 671	100 106	Excavation dia = 9.75 m Some heave associated with grout injection
7	ELY-OUSE (Cambs, England) 1968-69	Near Surface												
	(a) BLACKDYKE		0-22 Chalk >22 Gault		4.5	24.4	7.0	0.92	114	-22	37	105	85	
	(b) LITTLE OUSE		0-12 Superficial 12-23 Chalk >23 Gault		4.5	25.6	7.0	0.96	125 & 76	-27	31	105	49	Superficial - peats silts, sands & gravels
	(c) LAKENHEATH		0-15 Superficial 15-28 Chalk >28.0 Gault		4.5	31.7	7.0	0.92	114		37	75	24	
	(d) LARK		0-12 Superficial 12-42 Chalk >42 Gault		4.5	45.1	7.3	0.96	114	-33.7	36	83	53	
	(e) WORLINGTON		0-58 Chalk >58 Gault		4.5	60.4	7.3	0.96	114	-29.7	29	140	144	55 mm settlement subsequently
	(f) KENNETT		0-13 Superficial 13-71 Chalk >71 Gault		7.31	74.3	10.9	0.96	125	-22	53	200	43	

PUBLISHED SOURCES OF DATA

1. Hill 1957, Wadsworth 1958. 2. Wadsworth 1958, Smith et al 1973. 3. Wood 1956. 4. Wood 1958   5. Redfern & Pinder 1964, Wood 1957. 6. Maishman 1959, Firth & Gill 1963. 7. Collins & Deacon 1972.

These sources were checked and supplemented where possible with Foraky Limited Records.

N.B. The table excludes shafts at Hawthorn Co. Durham & Boulby, Cleveland which were not frozen to the ground surface.
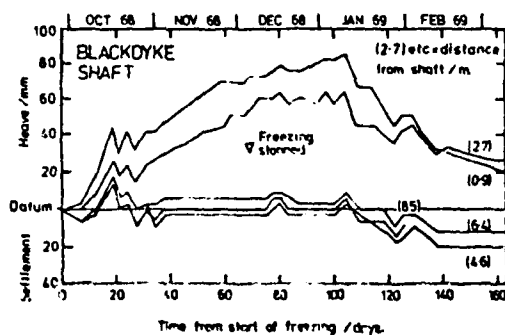
Fig. 2 Heave at Blackdyke Shaft

The new mine shafts were sunk through the Permo-Triassic rocks which lie unconformably over Coal Measures. Twin shafts at the same colliery, are unlikely to be more than 100 m apart. The sequence of the strata is:-
Keuper Marl. Comprising red brown mudstones and silty mudstones interspersed with a number of sandstones or siltstones (skerry bands), gypsum and anhydrite. The red marl is composed of silt sized aggregations of clay minerals and its geotechnical properties are dependent on its state of weathering as shown in Table 2 (Chandler et al. 1973).

Table 2 Keuper Marl Properties

	Unweathered	Weathered
Liquid Limit, LL	25–35*	35–60
Plastic Limit, PL	17–25*	17–33
Plasticity Index, PI	13–15*	17–25
Natural Water Content %	5–15	15–35
Bulk density, Mgm⁻³	2.43–2.24	2.17–1.84

*May be non-plastic

For roadworks in the U.K., cohesive soils with a PI greater than 20 are regarded as non-frost susceptible (Croney et al 1967).
Keuper Waterstones are interbedded thin marly brown sandstones and soft sandy marls and variegated shales.
Green beds were formerly considered a subdivision of the Waterstones but may be treated as a separate division particularly in North Notts. They comprise green/grey silty mudstones and siltstones with some red/brown bands.
Bunter Sandstone. When fully developed the sequence consists of an Upper and Lower Mottled Sandstone separated by the Bunter Pebble Beds. However, the Upper stratum is absent in Notts and Yorkshire. The sandstone is soft and fine grained, red with yellow and white mottling. The

Pebble Beds are coarser yellow sandstones and contain pebbles up to about 350 mm size. The Bunter series is a major aquifer and an important component in the water supply of the region.
Upper Permian Marl is similar in lithology to the Middle Permian Marl (see below).
Upper Magnesian Limestone consists of platy grey limestones which are absent in Notts.
Middle Permian Marl is a red mudstone with bands of grey sandstone, gypsum and anhydrite. It unites with the Upper Marl in the absence of Upper Magnesian Limestone. The Marl is usually an effective aquiclude.
Lower Magnesian Limestone is a yellow dolomitic limestone. The Magnesian Limestones are important aquifers for water supply in the North of England.
Lower Permian Marl consists of grey argillaceous marly mudstones (Marl Slate).
Basal Permian Sands and Breccia consist of grey sand conglomerate and breccia. Being both water bearing and weakly cemented they can behave as running sands and present a serious obstacle to shaft sinking.

It should be noted that the Bunter sandstones and the Magnesian Limestones may be fissured.

In the early projects, it is unlikely that any routine measurements of heave were made. However, Maishman (1975) considered that heaves of up to 75 mm were insignificant. Since greater movement would have prompted observations and records, the unrecorded heaves are thus likely to have been less than 75 mm.

The most interesting shaft is undoubtedly Cotgrave where heaves of over 400 mm were observed. Many of the freeze tubes fractured. The heave was attributed to frost action in the Keuper Marl, probably mainly in the top 50 m or so. Certainly one break in a freeze tube was recorded at 11.4 m.

The initial moisture content of the Marl appears to have been in the range 9 to 17%. Assuming that the plastic limits were in the same range, this material would be considered to be frost susceptible in the context of road construction. In the shaft freezing, water was readily available from skerry bands and in particular from the 1.8 m thick Cotgrave Place Skerry which occurred at a depth of 33 m. It is hoped to undertake some frost heave tests on undisturbed samples of a

298

similar marl and to study this case history further in the light of those results.

Tunnels

The case histories are summarized in Table 2. Four tunnels reported at Bochum but for which no record of heave was given have been excluded. Similarly the Helsinki tunnel (Vuorela et al 1980) is omitted but it is understood that Luke and Norie of the Consulting Engineers (Mott, Hay and Anderson) will be presenting heave results at the Tunnelling '82 Conference.

The ground conditions at the tunnels are much more diverse than at the shaft sites, making comparison difficult. Furthermore, extraneous factors such as dewatering occur more frequently. The best of the case histories is Milchbuck for which detailed results of the extensive testing and instrumentation have been published in a number of papers (Table 3).

Description of the frozen ground

Kiriyama et al (1980) and Akiyama et al (1980) were amongst the authors at ISGF80 who reported observing ice lenses in artificially frozen ground. Schuster (1980) observed rhythmic ice banding in saturated silty clays and clayey silts although there is frequently no surface heave due to consolidation of adjacent material. Gravels, sands and even quite silty soils do not show ice segregation. Ice lenses were found in both the chalk and clay on the Ely-Ouse schemes (Collins et al 1972).

DATA REQUIRED FROM CASE HISTORIES

The headings of Tables 1 and 3 list many of the major details which must be known if a case history is to be used to build up a general picture of the heave to be expected from AGF. Important items which are not tabulated either because of lack of space or because they were not available in a sufficient number of cases, include excavation diameter, details of lining and of plant. A number of other very important facts would best be presented graphically. These include time based plots of heat extraction, coolant temperatures, heave, sinking and lining progress. When the studies are extended to thaw behaviour, grouting details must be considered and it must be clear from the records whether observations have been continued until all movement has ceased.

For tunnels, a longitudinal section showing the variation of the soil profile and ground water level in relation to the construction and the measuring points is essential for detailed study. For all cases, the geotechnical properties of the soil, in particular grading, plasticity, density, moisture content, engineering description and classification of the soil should be quoted. Given this information, the thermal properties, frost susceptibility and permeability of the soil can be estimated although direct measurements are preferable. Results of in-situ permeability and pressuremeter tests would be advantageous.

Two neglected areas are the description of frozen ground exposed during the excavation and details of sub-surface movements. Whilst funding is an obvious problem, there is little doubt that the lack of inclinometers, extensometers, pressure cells, piezometers etc., and the results which could be obtained from them, is a serious hindrance to the interpretation of the observed surface movements on many jobs.

It is hoped that this paper might stimulate discussion and perhaps lead to the development of a check list which could be used in the preparation of future case histories. This might encourage all the parties, such as the specialist freezing contractor, general contractor, consulting engineer, client, testing specialist etc., to contribute data. Many of the best case records are those where data has been published by representatives of several organisations. Finally, the value of full case histories in which no movements occurred should not be underestimated.

FROST HEAVE TESTING

Tests in which volume changes are recorded when a sample of soil is frozen under controlled conditions in the laboratory are basic to several predictive methods. It is an advantage if both freezing and thawing behaviour can be observed and it is essential to have the facility to test undisturbed samples. Tests primarily related to the problem of frost heave of roads have been reviewed recently (Jones 1980, Chamberlain 1981).

Table 2 Details of Recent Tunnels Constructed With The

Aid of Artificial Ground Freezing

REF	TYPE LOCATION	GROUND CONDITIONS			FREEZING									TIME		MOVEMENT/mm[4]		INSTRUMENTATION[5]	NOTES
		Depth to water table/m	STRATA	Properties quoted	Finished dimensions Ht x width or dia/m	Length/m	Cover/m	Coolant[2]	Tube direction[3]	Freezing circle pitch dia/m	Freeze tube spacing/m	Freeze tube dia/mm	Initial brine temperature °C	To closure days	Total freezing/days	ACTUAL	PREDICTED		
1	Sewer CHARRAT Switzerland	2–2.5	Alternating layers of silt, sand & gravel		1.5 dia	14	3.5	LN₂	H	2.4	0.6			3		0			Fluctuating ground water level
2	Shield jointing TOKYO Japan	12	0–2.5 Loam 2–6 Clay 6–7 Sand 7–9 Silt 9–12.5 Sand >12.5 Fine sand	SPT	3.14 dia	7	25	Br	IH			89	–30	45	> 160	0	0		Freeze tubes @ 15° to horizontal
3	Sewer WASHINGTON DC USA	1.5	Clayey Sand, Sand & Silt	Gr w SPT γ	3.8 dia	33.5	2.7	Br	H	4.8	0.9	90	–15	31	56	+125	+50 to 130		Closure probably earlier
4	Metro ESSEN W. Germany	2.7 to 7	Fill Silt		7 x 9	120	5.7 to 9.5	Br	I			89	–20	21		0 –60			
5	Road Milchbuck 1 ZURICH 2 Switzerland		Moraine (Gravel-sand-silt)	Gr w P γ	12.1 x 14.2 Note 7	100 35	6 to 8	Br	IH		1 to 1.25	140	–40	9	101 60	+105 –45 +40 –60	60	E I	GW lowered first. Heave less than 10 mm on later stages. 2–4 mm under buildings
6	Removing piles JAPAN		Silt	P⁶	5.2	20	13	Br	H	7.2		101	–27	18	110	6			Precautions taken otherwise 90 mm heave expected
7	Metro Kudanshita Section TOKYO Japan	Tidal River above Tunnel	Fine sand Silt Sand & Gravel		5.3 x 11 Twin box	47.2	5	Br	H			102	–21	210	710	310		I	Ground water flow 1–6 m/day Froze bottom of river Trial freezing undertaken
8	Rail OSLO Norway	5	Fill Sandy gravel Limestone	w Gr	Twin single trk.			Br	H	–	1.0 to 1.2		–30 ?			+25 –20 to –40			Frozen arch 5 m thick

NOTES 1. Parameters quoted Gr = grading, P = frost heave, w = water content, γ = unit weight.
        2. Br = Brine, LN₂ = Liquid Nitrogen.
        3. Tube direction H = horizontal IH = inclined, near horizontal I = inclined.
        4. Movements + = heave – = final settlement.
        5. Instruments – Temperature & level points standard. E = extensometer, I = inclinometer.
        6. Test done but no results quoted.   7. Outside of lining.

SOURCES 1. Stoss & Valk 1979.   5. Bebi & Mettier 1980, Aerni & Mettier 1980, Huder 1979.
        2. Takashi et al 1979.   6. Kiriyama et al 1980.
        3. Jones et al 1978.   7. Miyoshi et al 1979.
        4. Valk 1980.   8. Josang 1980 + Private communication.

The heat flow in AGF is initially very high but drops rapidly as the frozen zone extends. Up to closure, the heat flow is determined by the ratio of the diameter of the frozen zone to that of the freeze tube. For a typical installation the heat flow drops from about 200 W/m² to 30 W/m² as this ratio rises from 4 to about 12.5 at closure. The heat flow across the freezing front continues to decrease as the ice wall thickens and may be less than 10 W/m² at the end of the freezing period. This is not dissimilar to the heat extraction rates considered in road problems.

For AGF applications, it is desirable to study the behaviour of soils under significant confining pressures. The tests summarised in Table 4 all have this facility. The Zurich apparatus was developed specifically for testing in connection with the Milchbuck tunnel. The Japanese and Canadian facilities were developed to assist studies in respect of LNG storage and chilled gas pipelines respectively. Although the results have been presented somewhat differently, all the tests confirm that heave decreases as the pressure increases.

A prototype multi-ring cell for testing 100 mm diameter x 150 mm high specimens under vertical pressures of up to 700 kPa, recently constructed at Nottingham (Jones 1981), is now being evaluated.

It seems that the lack of any generally accepted routine test for frost heave related to AGF may be a major obstacle to generalising the experience gained from case histories. Despite the many difficulties involved in reference testing, perhaps the industry should give serious consideration to this aspect.

METHODS USED TO PREDICT HEAVE

A realistic analytical (mechanistic) approach to the prediction of heave from AGF requires a very complex model. Factors to be considered include:-
(1) Changes in pore-water pressure and both vertical and lateral effective stresses as freezing proceeds. The hydraulic gradient may be towards or away from the freezing front.
(2) Compression and/or consolidation of unfrozen ground.
(3) Volume changes in already frozen ground due to contraction which may lead to shrinkage cracks at low temperatures. On the other hand at low stress levels

and warmer temperatures, heaving of already frozen ground may occur.
(4) The major movement will take place in the direction of minimum restraint which may not be coincident with the direction of heat flow.
(5) If there is a circle of freeze tubes the stress conditions within the ring after closure are considerably different from those on and beyond the outer freezing front.

The modelling of the AGF frost heaving process is, therefore, much more complex than the corresponding problem for roads or pipelines. Although there are several well known mathematical models of the frost heaving process, their application even to fairly simple field conditions is fraught with difficulty. Nevertheless, attempts to develop analytical techniques have increased greatly our understanding of the magnitudes of the various processes involved in frost heaving and further benefit is expected from continuing studies.

Against this background it is perhaps not surprising that in the few case histories in which a predicted heave was quoted, the estimate was made by semi-empirical means.

Jones et al 1978, 1979 used the method described by Schuster (1972) to quantify the heave. In this method the in-situ stresses are compared with the combined effective intergranular pressure and potential frost heave expansion pressure determined by laboratory tests. Good agreement between the predicted and observed heave was reported.

Table 4   Details of Frost Heave Tests

	ETH. ZURICH[1]	JAPANESE[2]	CANADIAN[3]
COLD TEMP/°C - control - location	-10 Air Constant Top	FP[4] to -10 Surface Varies, CRP[5] Bottom	Surface Constant (Staged) Bottom
WARM TEMP/°C - control	+15	FP[4] Heat exchanger	+1.9 to +2.4 Chamber
LOAD SYSTEM Vert press/kPa CYLINDER	Spring ≤ 300 Rings	Frame ≤ 1100 Acryl	Air piston ≤ 700 Teflon
SPECIMEN Ht/mm Dia/mm		20 60	102 102
MEASUREMENTS	Total heave	Total heave (as heave ratio). Water flow	Heave rate Water flow

NOTES 1. Bebi et al, 1979, Huder 1979. 2. Japan Gas Association 1979. 3. Penner et al 1977. 4. Freezing point. 5. Const. rate of penetration (0.47 to 7.6 mm/hr).

301

Laboratory tests on a representative Milchbuck sample, indicated that a volume expansion of about 2½% could be expected on site. The maximum heave observed (in the first section) was roughly 50% more than the predicted heave. When allowances are made for the volume of frozen soil being greater than envisaged and also for the extreme variability of this material, this agreement between prediction and reality is reasonable.

No forecasts of heave appear to have been made for the shafts. Subsequently, Sanger et al (1979) showed that a very simple method could forecast the actual heave usually within a factor of 2. It was assumed that the clay expanded by 9%, that half this expansion was manifested as vertical movement and that the permeability of the chalk was high enough to permit drainage. However, ice lenses of up to 3 mm were observed in the chalk (Collins et al 1972) possibly due to impeded drainage after closure. Only 1½ mm thick lenses were observed in the clay. It therefore appears that the agreement of predicted and observed values may have been fortuitous.

PRECAUTIONS TO PREVENT EXCLINE MOVEMENTS

When ground conditions indi that heave may be a problem, the r. : of damage is usually minimised by takun precautions both with the installin and its operation. Loss of groun during the drilling of horizontal helms can be prevented by the use of suit. stuffing boxes (Harris et al 1982). Frost heave damage to the installation can be minimised by ensuring that joints in the freeze tubes are secure. The outside of the tubes can be greased to facilitate relative movement between the tubes and the frost heaving ground.

Heave can be reduced by restricting the growth of the ice wall once the minimum thickness for structural stability has been achieved. Intermittent freezing during the maintenance stage is helpful (Bebi et al 1979, Valk 1980, Jones et al 1978, 1979) and has the added advantage of reducing the overall cost. At Milchbuck, faster excavation requiring shorter freezing periods was undoubtedly a factor in reducing the heave between the first and subsequent stages (Table 1). Elsewhere, the growth of the frozen zone has been restricted

by insulating part of the tube (Kiriyama et al 1980) or allowing the coolant to circulate only through the lower portion (Wind 1979). The growth of the frozen zone may be restricted by the use of heating pipes (Miyoshi et al 1978).

Other methods which have been used to minimise frost heaving are:
.dewatering (Bebi et al 1980, Kiriyama et al 1980),
.to raise the viscosity of the pore water by using an additive (Kiriyama et al 1980, Miyoshi et al 1978),
.to prevent confined freezing (Kiriyama et al 1980) although clearly this is not practical if a ring of freeze tubes must be employed.

Finally, the frost heave can be absorbed at least partially by drilling relief holes to permit volume expansion (Brending 1980, Kiriyama et al 1980).

Freezing is frequently accompanied by ice lensing and overconsolidation of the adjacent soil. Settlements on the aggravated by the effects of excavatio are likely to exceed the frost heave ι nay be controlled to some extent by a careful programme of grouting.

A recent state of the art paper (Attewell 1977) summarises settlements from 30 tunnels constructed by a variety of methods. The settlements range from 3 to 280 mm with an average of '. ' Even assuming that the settlements after thaw may exceed the heave ι. 20% (Jones et al 1979) the movements associated with AGF compare favourably with those experienced with other methods.

CONCLUSIONS

The conclusions which have emerged from the foregoing study are:-
(1) Consideration should be given to agreeing some guidelines for case histories.
(2) There are significant advantages when a case history is reported by a number of the specialists involved.
(3) Some form of reference testing for frost heave would be useful.
(4) The British shafts form two groups within each of which there are sufficient common features to make useful comparisons. More detailed studies are envisaged.
(5) There was a much greater diversity amongst the conditions experienced in the group of tunnelling case histories making comparison and prediction much more difficult. However, with careful attention to procedures on site, the

302

movements experienced with AGF compare favourably with those reported for other techniques.
(6) Other case histories, for example those from Selby coalfield should be considered and the review process extended to include further consideration of thawing effects.

ACKNOWLEDGEMENTS

REFERENCES

AERNI, K. & METTIER, K. (1980) 'Ground freezing for the construction of the three lane Milchbuck Road Tunnel in Zurich, Switzerland', ISGF80, Preprints p. 889-895. Discussion Proc. p. 115-120.

AKIYAMA, T. & IGURO, M. (1980) 'A model test tank using artificial ground freezing method', ISGF80 Proc. p. 141.

ATTEWELL, P.B. (1977) 'Ground movements caused by tunnelling in soft ground', State of the Art Report. Conf. on Large Ground Movements and Structures. Dept. of Civil Eng. and Building Technology UWIST, Cardiff, p. 812-948.

BEBI, P.C. & METTIER, K.R. (1979) 'Ground freezing for the construction of the three lane Milchbuck Road Tunnel Zurich, Switzerland', Tunnelling '79, p. 245-255.

BOSCH, H.J. (1979) 'Construction of a sewer in artificially frozen ground', Eng. Geol. 13, p. 547-550.

BRENDENG, E. (1980) 'Early experience with ground freezing in Norway' ISGF80, Preprints p. 896-906.

CHAMBERLAIN, E.J. (1981) 'Comparative evaluation of frost susceptibility tests', Trans Res Rec. 809, p. 42-52.

CHANDLER, R.J. & DAVIS, A.G. (1973) 'Further work on the engineering properties of Keuper Marl', CIRIA Report No. 47, London.

CHATWIN, C.P. (1961) 'East Anglia and adjoining areas', Brit. Reg. Geol., HMSO London.

COLLINS, S.P. & DEACON, W.G. (1972) 'Shaft sinking by ground freezing: Ely-Ouse Essex scheme', Proc. ICE Supp. Paper 7506S, p. 129-156.

CRONEY, D. & JACOBS, J.C. (1967) 'The frost susceptibility of soils and road materials', Trans Rd Res Lab Rep. LR90, Crowthorne.

DE BEER, E., BUTTIENS, E. & MAERTENS, J. (1980) 'Research of the behaviour of non-cohesive soils when treated by artificial freezing', ISGF80 Preprints p. 338-353.

FIRTH, G.W. & GILL, J.J. (1963) 'The sinking of the Kellingley shafts', Trans Inst Min Eng 123 (Dec), p. 147-166.

HARRIS, J.S. & NORIE, E.H. (1982) 'Construction of two short tunnels by artificial ground freezing', ISGF82 Proc

HILL, A. (1951) 'Calverton Colliery', Trans Inst Min Eng 110, p. 77-97.

HUDER, J. (1979) 'Geotechnical analysis' Information Bull. 112, IGB ETH Zurich, p. 31-42 (In German).

JAPAN GAS ASSOCIATION (1979) Recommended practice for LNG storage.

JOSANG, T. (1980) 'Ground freezing techniques used for tunnelling in Oslo City Centre', ISGF80, Preprints p. 969-979.

JONES, J.S. & BROWN, R.E. (1978) 'Soft ground tunnelling by ground freezing: a case history', Trans Res Rec 684, p. 28-36.

JONES, J.S. & BROWN, R.E. (1979) 'Design of tunnel support systems using ground freezing', Eng. Geol. 13, p. 375-395.

JONES, R.H. (1980) 'Developments and applications of frost susceptibility testing', ISGF80 Preprints p. 748-759.

JONES, R.H. (1981) 'The prediction of frost heave', Proc. Seminar Univ. of Nottingham p. 1-6.

KIRIYAMA, S., ISHIKAWA, Y. & KUSHIDA, Y. (1980) 'Artificial ground freezing in shield work', ISGF80 Preprints p. 940-951. Disc Proc p. 131.

MAISHMAN, D. (1959) 'Shaft sinking using the freezing process', Iron and Coal Trades Review 30, Oct. 1959.

MAISHMAN, D. (1975) 'Ground Freezing', Ch. 9 of Methods of treating unstable ground (Ed. F.G. Bell) p. 159-171. Newnes-Butterworth, London.

MIYOSHI, M., TSUKAMOTO, T. & KIRIYAMA, S. (1979) 'Large scale freezing work for subway construction in Japan', Eng. Geol. 13, p. 397-428.

PENNER, E. & UEDA, T. (1977) 'The dependence of frost heaving on load application - preliminary results', Int. Symp. Frost Action in Soils, Lulea, Sweden, Vol. 1, p. 92-101.

REDFERN, A. & PINDER, B.S. (1964) 'Shaft lining and grouting problems associated with Cotgrave and Bevercotes

Shafts', Co..._.y Guard 209, (Dec)
p. 817-826.

SANGER, F.J. & SAYLES, F.H. (1979)
'Thermal and rheological computations
for artificially frozen ground construc-
tion', Eng. Geol. 13, p. 311-337.

SHUSTER, J. . (1972) 'Controlled
freezing for tempora., ground su_. .'
1st North Am. Rapid Ex-. & Tunnelling
Conf. Chicago.

SCHUSTER, J.A. (198., '_.,.. . .
quality assurance for construction
ground freezing'. Disc. ISGF80 Pr..
p. 109-114.

SMITH, E.G., RHYS, G.H. & GOOSEN., R.F
(1973) 'The geology of the county
around East Retford, Worksop and
Gainsborcugh', HMSO.

STOSS, K. & VALK, J. (1979) 'Uses and
limitations of ground freezing with
liquid nitrogen', Eng. Geol. 13,
p. 485-494.

TAKASHI, T., KIRIYAMA, S. & SATO, ..
(1979) 'Jointing of two tunnel .... ..
using artificial underground f ....'
Eng. Geol. 13, p. ....9.

VALK, J. (1980) 'The successfull
application of an unusual ground
freezing method to secure tunnel
excavation', ISGF80 Proc. p. ....

VUORELA, M. & ERONEN, T. (1980.
'Driving of Metro Tunnels with the aid
of artificial ground freezing at
Helsinki', ISGF80 Freprints p. 907-915.

WADSWORTH, A. (1958) 'Recent shaft
sinking developments in the Midlands',
Trans Inst Mining Eng. 117 (April)
p. 397-416.

WIND, H. (1979) 'The soil freezing
method for large tunnel constructions',
Eng. Geol. 13, p. 417-423.

WOOD, A.F. (1956) 'Sinking at Lea Hall
Colliery', Colliery Guard 192 (March).
p. 336-340.

WOOD, A.F. (1957) 'Cotgrave Colliery
Sinking', Colliery Guard 194 (January),
p. 97-105.

WOOD, A.F. (1961) 'Rapid sinking at
British Colliery', Mining Mag. 105 (Oct)
p. 213-219.

N.B. Proceedings of ISGF78 (Bochum) were
reprinted in Eng. Geol. Vol. 13, 1979.
Proceedings of ISGF80 (Trondheim) were
published in two volumes (Preprints and
Proceedings). Selected papers appear in
Eng. Geol. Vol. 18, 1981.

FROST ACTION OF FREEZING GROUND
SURROUNDING UNDERGROUND STORAGE
OF A COLD LIQUID

Seiiti   KOSITA and Masami FUKUDA
    Institute of Low Temperature Science, Hokkaido University, Sapporo, Japan
Takeshi ISHIZAKI
    Research Institute of Tokyo Gas Co. Ltd , Tokyo, Japan
Hideo YAMAMOTO
    Research Institute of Seiken Co. Ltd., Oosaka, Japan

Abstract

A small tank in the shape of a cylinder 80 cm in diameter and 50 cm in depth was placed in a basin, filled with a silty soil, of the frost test field in Tomakomai, Hokkaido, Japan, with its top at the same level as the ground surface in the basin. The double wall (two steel sheets 10 cm apart) constituted the exterior of the side and bottom. As a cold liquid at temperature of -23°C was poured inside the gap of the double wall and circulated, the soil around the tank began to freeze sideways and downwards from the tank. Studies made are as follows: (1) the progress of the freezing front was measured and preestimated; (2) frost heaving characters of the tank and the ground surface around it were observed; (3) soil-water migration was calculated by measureing moisture tensions at several points within the soil; (4) soil pressure acting on the tank was measured.

Introduction

Underground storage tanks of LNG (-162°C) and LPG (-42°C) as large as 6-13 x 10⁴ kiloliters in capacity have been recently constructed in great numbers in Japan. Ground surrounding a tank has been freezing, extending to a wide area (10-20 m). A large heaving force acts sometimes upon the outer wall of the tank; also a large stress is developed inside the freezing ground. Therefore, it calls for an investigation into the freezing behavior of the soil around a large underground storage tank containing such cold liquids in advance for designing its construction. In this connection, this study was devoted to looking into these phenomena in detail using a small tank of 80 cm in diameter and 50 cm in depth, which was placed in a basin of the frost test field in Tomakomai, Hokkaido, Japan. The basin (5 x 5 m wide and 2 m deep) had been filled with a frost susceptible soil, that is, a silty soil named Tomakomai silt[1]. The top of the tank was made at the same level as the ground surface in the basin. A cold liquid at temperature of -23°C was poured inside the gap between two steel sheets, 10 cm apart, which constituted the double wall of the side and bottom of the tank. As it was circulated in the entire gap, the soil began to freeze sidewards from the side-wall of the tank and downwards from the bottom of the tank. Measurements were made of temperature and moisture tension inside the soil, heave amount on the soil surface, frost penetration depth and soil pressure acting on the tank. The progress of the freezing front was preestimated by using the FEM method, whereupon their results were compared with the results obtained by actual measurements. After the cooling of the tank was discontinued, core borings were made to collect frozen soil samples. Their layer structures were observed and water contents were measured.

Instrumentation

The tank used was a steel cylinder of 80 cm in outer diameter and 50 cm in depth. The exterior of the side and bottom was the double-wall type, and the gap between two walls was 10 cm. The tank was placed in the center of a basin

305

(5 x 5 m wide and 2 m deep) which
had been filled with Tomakomai silt.
The top of the tank was made at the
same level as the ground surface as
shown in Fig. 1. The soil filled in
the basin, which was almost homo-
geneous, had the wet density of
1.64 g/cm^3 and the water content of
54 % at the initial stage before cooling
the tank. Meanwhile, it had the
thermal conductivity of 0.706 Kcal/mh°C
when unfrozen and 1.354 when frozen;
the specific heat capacity of 473
Kcal/m^{3}h°C when unfrozen and 298
when frozen.

A cold liquid of ethylenglycol was
prepared by a refrigerator, which was
set at a distance of 5 m from the basin,
and to the gap of the double wall of
the tank through vinyl pipes, which
were covered with the thermal insulator.
The temperature of the liquid was kept
at -23°C during the test. Cooling was
conducted for 8 days. The mean air
temperature was 13°C, and the tempera-
ture of the soil which was not influenced
by the cooling of the tank was also 13°C
during the test. The water table in the
basin was set at a depth of 1.4 m below
the soil surface, or at a depth of 90 cm
below the bottom of the tank.

Thermocouples were set inside the
soil around the tank at the levels of 20
and 40 cm in depth along a vertical plane.
At both levels 6 thermocouples were set
at intervals of 25 cm as shown in Fig. 2.
Dial gauges were set on the top of the
tank and at several points on the ground
surface to measure the heave amount.
Frost penetration meters of the Yahagi-
type[2] were set at several points around
the tank to measure the frost penetration
depth. Pressure gauges were set on the
outer wall of the tank at the levels of
20 and 40 cm below the top of the tank
along one vertical line and also along the
the opposite vertical line at the levels of
20 and 40 cm. The pressure increase
due to soil freezing was measured.
Porous cups were set at the level of 30
cm as shown in Fig. 3. They were
connected to pressure transducers
through vinyl tubes and the moisture
tension was measured at each point as
the height of the water head.

Results and discussions
(1) Measurements and preestimations for
   the progress of the freezing front
   The progress curves of the freezing
front obtained by temperature measure-
ments (solid line) and frost penetration
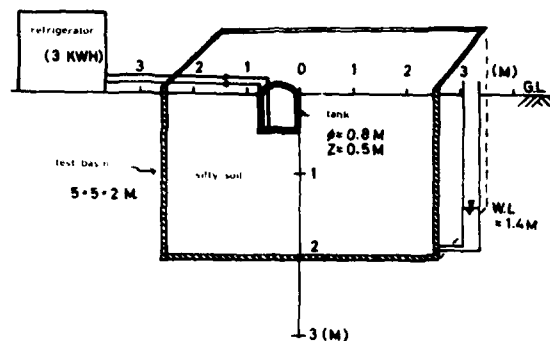meters (circle) are shown in Fig. 4 for

Fig. 1 Location of a test basin, a tank
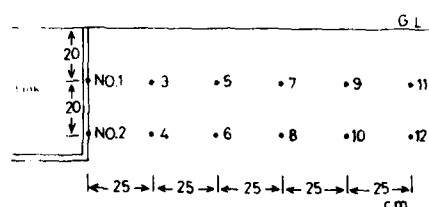and a refrigerator

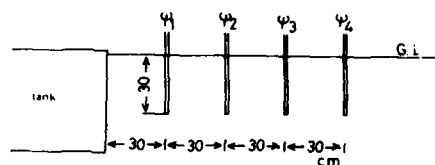Fig. 2 Location of thermocouples
(Nos. 1-12)

Fig. 3 Location of porous cups to
measure moisture tension ($\psi_1 - \psi_4$)

.the downward direction from the bottom
of the tank and for the sideward direc-
tion at the levels of 40 and 20 cm below
the ground surface. They reached the
depths of 44, 31 and 26 cm respectively
at the last stage of cooling.

Preestimations were made by the
FEM method on the following assumptions
: (1) nonstationary and axial symmetry,
(2) node number 183 and element number
36, (3) at the initial stage operations
were made at intervals of 6 minutes, (4)
the initial soil temperature 13°C, the air
temperature 13°C.

The progress of the freezing front
around the tank obtained by the FEM
method is shown in Fig. 5, where at the
last stage (stationary) the front reaches
the depth of 69 cm from the bottom of
the tank. The front reaches the depth
of 30 cm after 8 days from the beginning

306

of the cooling at the level of 20 cm deep below the ground surface; this value fits very well with the value obtained by the measurement, 31 cm.

(2) Heaving amount and water content profile of the frozen soil

The heaving processes of the tank and the ground surface at several points around the tank (25, 50 and 80 cm from the periphery of the tank) are shown in Figs. 6 and 7. All the curves show almost constant heaving rates. At the final stage of the test the heave amount reached the maximum values 5.5, 7.2, 4.9 and 2.0 cm respectively for the tank, distances of 25, 50 and 80 cm from the tank. Although the frozen area reached furthest at the distance of 30 cm from the tank, heaving on the ground surface appeared on the area which was 100 cm distant from the tank.

After the discontinuation of the cooling of the tank core borings were conducted to collect frozen soil samples *along the vertical lines 5 and 18 cm* distant from the tank. They were subjected to measurements at every 5 cm interval. The water content profiles obtained are shown in Fig. 8. The water content increases with increasing depth, and amounts to a maximum value of 150 % at the level of 70 cm below the ground surface, which is the bottom of the *frozen layer, while at the lower level* (80 cm below the ground surface) the water content of the unfrozen soil is only 52 %. This was to due to the existence of distinctive ice lenses in the frozen layer.

(3) Water migration in the freezing soil around the tank

Because the water level was 40 cm below the bottom of the tank, the soil surrounding the tank was at an unsaturated condition. When the cooling of the tank began, the soil water migrated towards the freezing front from the unfrozen part. Therefore, the soil water migration was occurring inside the unsaturated unfrozen soil. In order to find out a change in soil water content during the freezing moisture tensions were measured at the points of 30, 60, 90, 120 cm distant from the tank on the level of 30 cm in depth below the ground surface along one vertical plane. The results are shown in Fig. 9, where ψ_1, ψ_2, ψ_3 and ψ_4 mean the moisture tension at distances of 30, 60, 90 and 120 cm from the tank respectively. The curve of ψ_1 shows a distinctive increase. The curve of ψ_2 shows a slight increase.
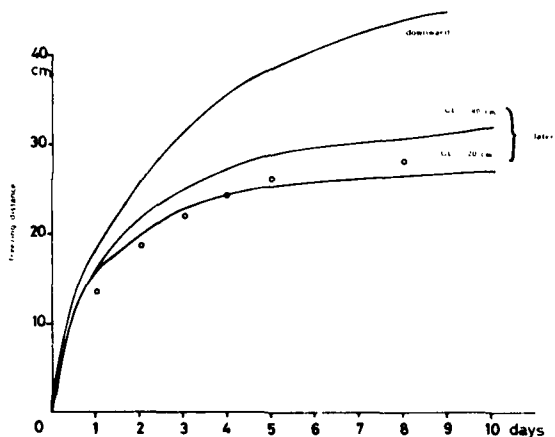

Fig. 4   Change in freezing distance in downward and sideward directions (circles: obtained by the frost penetrometer)
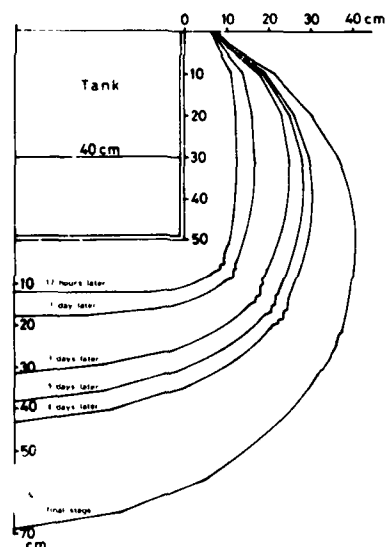

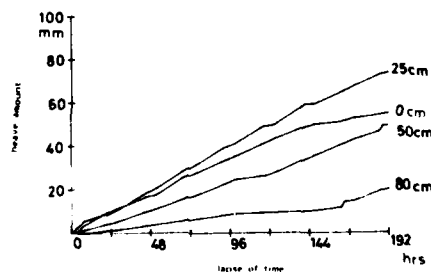Fig. 5   The progress of the freezing front around the tank

Fig. 6   Change in heave amount at the top of the tank (0 cm) and on the ground surface at distances of 25, 50 and 80 cm from the tank

However, the curves of ψ_3 and ψ_4 show some fluctuations around constant value. This means that there was no water migration at points further than 90 cm in distance.

The moisture migration through the *unsaturated* soil occurs according to the gradient of moisture tension by the following equation:

$$Q = K (\psi) \, d\psi/dx \qquad (1)$$

where Q is the water flow and $K(\psi)$ is the hydraulic conductivity which it depends on moisture tension. For the Tomakomai silt $K(\psi)$ was already obtained as the function of moisture tension[3]:

$$-\log_{10} K(\psi) = A + B\psi \qquad (2).$$

The difference, ψ, is shown in Fig. 10. From equation (1) and (2) the value of Q is calculated and changes in moisture flow during the test is shwon in Fig. 11. The value of Q spreads in a range from 0.08 - 0.11 g/day·cm^2 and the total quantity of water migrated towards the freezing front is about 1 g/cm^2, which shows a good fit with the result obtained from the water content increase of the soil after freezing.

(4) Increase in soil pressure acting on the tank

Pressure gauges were set on the wall of the tank at the levels of 20 (N_1) and 40 cm (N_2) in depth below the top of the tank along one vertical line and also at the levels of 20 (S_1) and 40 cm (S_2) in depth below the top of the tank along the opposite vertical line. Changes in pressure are plotted with the lapse of time in Fig. 12. The curves of N_2 and S_2 show an abrupt increase for the first 24 hours and then keep almost constant values, 0.25-0.28 Mpa and 0.15-0.18 Mpa, respectively. However, the curves of N_1 and S_1 show no distinctive increase. In several hours after the beginning of the cooling of the tank, a large number of cracks appeared on the ground surface along the periphery of the tank at each 20-30 cn. interval. They were spreading radically, widening, and stretching downwards according to the progress of the freezing front. At the last stage of the test the cracks were 50-100 cm long, 0.5-1 cm wide and 10-30 cm deep. These cracks caused the release of the stress accumulating inside the freezing soil. Therefore, the soil pressure at the shallow level showed no increase. The values of the soil pressure will be again examined at the next test[4].
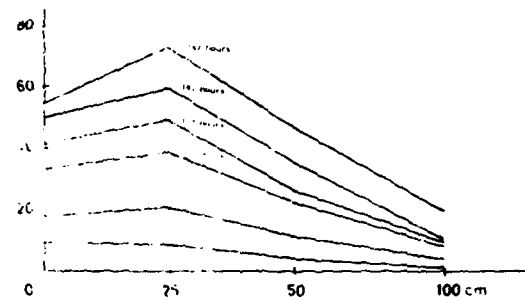

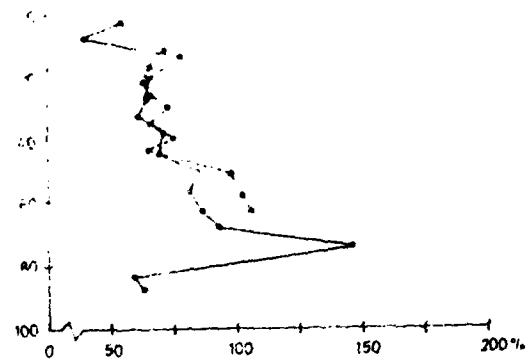Fig. 7 Change in heave amount on the ground surface

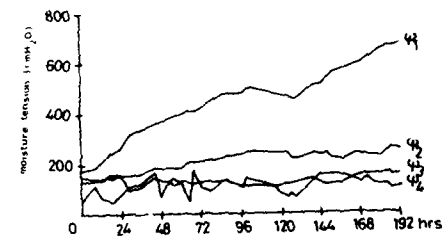Fig. 8 Water content profile of cores taken along the vertical lines 5 and 18 cm from the tank

Fig. 9 Change in moisture tension at distances of 30, 60, 90, 120 cm from the tank (ψ_1, ψ_2, ψ_3, ψ_4 respectively)
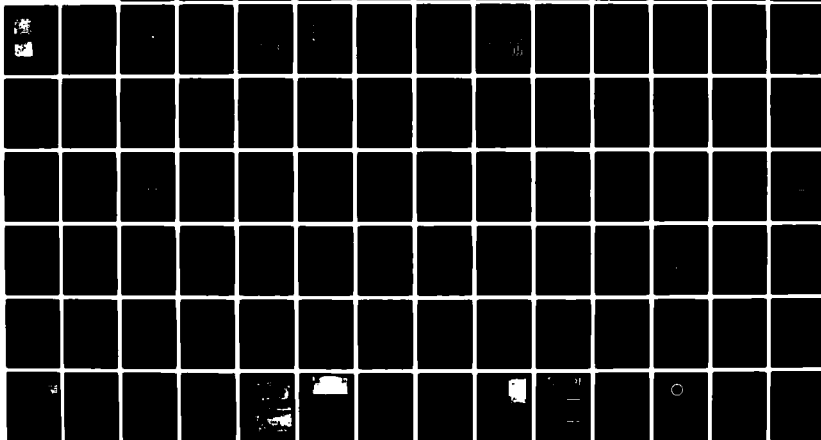
References
1) S. Kinosita 1979 Effects of initial
   soil-water conditions on frost heaving
   characteristics. Engineering Geology,
   13, 41-52.
2) H. Yahagi 1980 Development of a
   new type frost penetration meter.
   Reports of Basic Studies on Frost
   Action (S. Kinosita ed.), 51-58.
3) M. Fukuda 1979 Measurement of
   hydraulic conductivity of unsaturated
   Tomakomai silt. Low Temperature
   Science, 38, 193-195.
4) M. Fukuda et al 1982 It will be
   reported at the annual meeting of the
   Japanese Society of Soil Mechanics
   and Foundation Engineering.

Fig. 10 Change in gradient of moisture
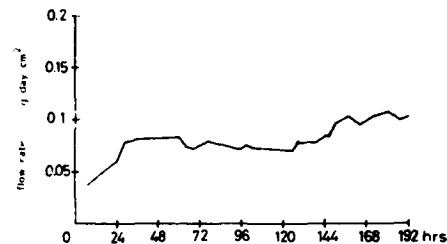tension between distances of 30 and 60
cm from the tank

Fig. 11 Change in flow rate between
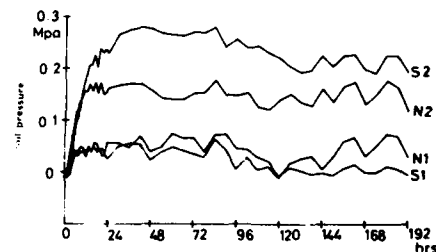points 30 and 60 cm distant from
the tank

Fig. 12 Change in soil pressure
acting on the wall of the tank at
depths of 20 cm (N_1, S_1) and
40 cm (N_2, S_2)

DEVELOPMENT OF A METHODOLOGY FOR PREDICTING GROUND SURFACE SETTLEMENT ABOVE TUNNELS IN SOFT GROUND SUPPORTED BY GROUND FREEZING

John S. Jones, Jr.   Law Engineering Testing Company,
Harald W. Van Aller   Washington, D.C.

ABSTRACT

The use of ground freezing techniques for tunnel support is becoming increasingly important. Utilizing the finite element methods, a technique has been developed to predict surface settlements for various configurations of tunnel depth, diameter and frozen zone shape and size. Two basic soils types have been used for the study: sands and clays. The sandy soils are modeled with parameters representing Manchester fine sand and are assumed to have no volume change due to the freeze-thaw process. The clays are modeled with various combinations of plasticity indices and overconsolidation ratios. The unfrozen stress-strain properties of the clay soils are generated from linear regression analyses using correlations with cam-clay theory. The properties of the frozen soils were obtained from various testing results reported in the literature on clays. The degree of thaw-settlement is modeled by utilizing correlations of the water content plastic limit ratio to the volume decrease (thaw consolidation) that occurs during the freezing process. A 9% pore volume ex-pansion is assumed for saturated clays during the freezing process. This expansion causes a significant change in the state of stress in the ground surrounding the location of the tunnel.

Analytical models have been developed to evaluate the full response of tunnels supported by ground freezing. These models consider the effects of 1) the initial freezing operations on the surrounding unfrozen soil (clays), 2) the creep behavior of the frozen soil following cavity excavation (sands and clay), and 3) the stresses imposed on the final liner after the frozen soil thaws. Surface deflection is presented as a function of various parameters, including tunnel depth, diameter, freezing temperature, frozen soil thickness, depth to water table, and soil type and characteristics.

Several tunneling projects, utilizing ground freezing for support, have been instrumented to obtain surface deflections and temperature gradients. These projects have been used to verify the analytical models.

**Session IV
ENGINEERING DESIGN
AND CASE HISTORIES**
Shafts and open excavations,
shaft linings and low-temperature
concrete, tunnels, pipelines,
and foundations and slopes

GROUND FREEZING FAILURES—CAUSES AND PREVENTION

John A. Shuster   President, Geofreeze Corporation

ABSTRACT

Frozen earth structures rarely, if ever, collapse in the classic sense of a structural failure; however, on occasion they do fail to perform as planned, resulting in significant delays and cost over-runs.

Selected examples of failures of ground freezing systems for shafts, tunnels, deep excavations, and structural underpinning on an international basis are presented, together with remedial measures taken. The various elements of each example are discussed and general conclusions drawn to assist engineers and contractors employing ground freezing techniques in the future to avoid the pitfalls of the past.

RECENT DEVELOPMENTS IN GROUND FREEZING PRACTICES AND FUTURE PERSPECTIVES

F. Gallavresi   Construzioni Steciali S.P.A., Italy
G. Rodio
C. Presa

ABSTRACT

The paper analyzes the various fields of application of the different soil freezing systems (liquid nitrogen, brine and mixed methods) from the technical and economic viewpoints, especially as regards their competitiveness vis-à-vis the alternative conventional soil improvement methods, both in current practice and in future market perspectives. Furthermore the paper reviews the treatments, relevant to tunnels and large-diameter shafts, carried out in Italy, in particular difficult ground conditions, during the last two years (1979-1981). These recent case histories are analyzed and illustrated with the aid of a large photographic documentation.

GROUND FREEZING APPLICATIONS IN UNDERGROUND MINING CONSTRUCTION

Bernd Braun   - Special Projects Manager - Deilmann-Haniel GmbH
William R. Nash - Chief Mining Engineer   - Frontier-Kemper Constructors

ABSTRACT

The paper outlines applications of ground freezing work in underground mine construction in the United States.

INTRODUCTION

Where site conditions require temporary support, the application of ground freezing to mine shaft construction has successfully minimized the risk (or contingency costs) of this aspect of mine development.

Recent improvements in the sciences of frozen ground engineering and refrigeration technology have opened up new applications for ground freezing due to advantageous economics.

The risks and cost uncertainty inherent in the application of alternative methods such as dewatering, grouting, slurry walls, caissons or combinations of these can be substantial, even with thorough geotechnical investigations and conservative design.

Some of the the main advantages of the ground freezing method are:

. Less sensitive to advance geologic prediction.
. Provides several temporary functions, such as support of an excavation, groundwater control (as the freeze wall is impervious) and structural underpinning.
. Adaptable to practically any size, shape or depth.
. Excavation can be kept unobstructed as no bracing or sheathing is usually required.
. No disturbance of the groundwater table or the groundwater quality.

MINE SHAFTS

Mine shaft utilization can be any of the following:
. Man & Material Access
. Ventilation
. Production
. Emergency Escape

Water can pose many problems to mine shaft construction in the penetration of water-saturated sediments in the shaft collar overlying the bedrock and in the penetration of aquifers of high water volume, high pressure or both. The water entering a shaft will not only hinder the sinking process but, if lining quality is to be assured, water must be diverted during concrete placement to prevent segregation of the cement and the aggregates.

GROUND FREEZING FOR MINE SHAFT CONSTRUCTION

The use of ground freezing in construction is not new. The first application of ground freezing for mine shaft construction was in 1883 during sinking of a shaft for the Archibald mine in Schneidlingen, Germany. On the North American continent, freezing was used in 1888 to

319

sink a shaft for Chapin Mining Company in Iron Mountain, Michigan. In potash mining, the first use of freezing was in 1886 when it was applied by the Jessenitz Company in Mecklenburg, Germany. To date the maximum frozen depth in Canada has been 2,245' (684m). (Please see Table I.)

Ground freezing's application is the most broad of alternative construction methods. (Please see Figure 1.)

The ground at a mine shaft location is most often frozen via the circulation of a refrigerated brine solution pumped through pipe casings installed circumferentially around the shaft outer diameter. The determination of the depth of the freeze pipes is dependent upon the elevation of an impervious strata or rock-type beneath the water bearing section. It is below this frozen zone and in the impervious rock that the shaft seal is constructed.

Freeze wall growth in the ground is measured in temperature monitoring holes installed in the ground and equipped with temperature sensors at critical locations. Furthermore, temperatures, brine flow, and pressures are observed within the brine circuit system. Frequently, ultrasonic techniques are used to verify integrity and extent of a freeze wall.
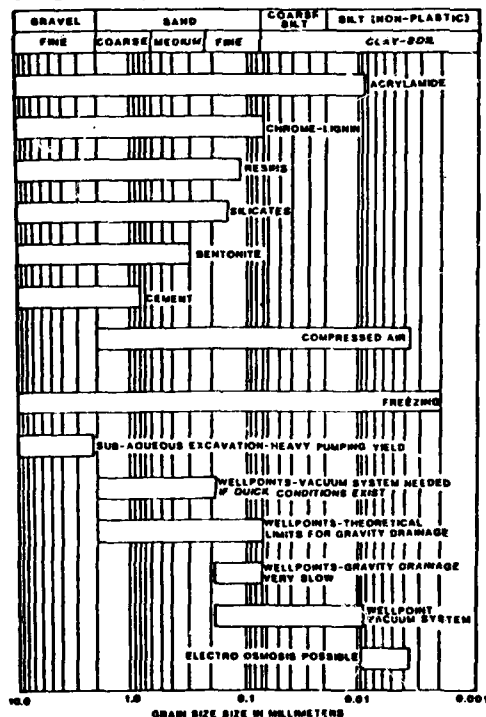

Figure 1   From Am Cyanamid

MINE SHAFT GEOTECHNICAL INVESTIGATION

The investigation of a prospective shaft location should encompass the following items:

1. Preliminary Study

    A. Literature Search (Water, Oil, & Gas Well Logs)
    B. Case Histories - Nearby Construction of Shafts

2. Pilot Hole Drilling & Testing (Soil & Rock)

    A. Soil Borings & Log
        (1) Blow Counts
    B. Rock Core Log
    C. Geophysical Well Logging
        (1) Neutron
        (2) Density
        (3) Self-Potential
        (4) Resistivity
    D. Hydrologic Tests

3. Laboratory Testing

    A. Soil Index Properties
        (1) Grain Size
        (2) Moisture Content
        (3) Saturation
        (4) Atterberg Limits
        (5) Porosity
        (6) Density
    B. Permeability (Soil and Rock)
    C. Unconfined Compressive Strength (Soil and Rock)
    D. Poisson's Ratio

4. Groundwater

    A. Regional Conditions - Flow, Etc.
    B. Chemical Analysis

The preliminary study should be as thorough as possible. It is an inexpensive source of valuable data. (Data that must be correlated to the particular site.)

The drilling program represents the opportunity to obtain soil, rock, and water information from a single hole.

The drilling log of the hole records lost circulation, water inflow, etc.

The rock cores and the drilling log, coupled with the geophysical logging data provide the necessary information to determine the intervals to be tested for hydrologic data (drill stem and injection tests).

320

TABLE I (ALL DIMENSIONS IN METERS) MINE	LOCATION	NORTH AMERICAN MINE SHAFT GROUND FREEZING YEAR STARTED	SHAFT DIMENSIONS	SHAFT DEPTH	FREEZE DEPTH
Chapin Mining Co.	Iron Mt., MI	1888	4m x 5m		30
PCA	Carlsbad, NM	1952	4.6 ∅	233	107
PCA	Sask., Can.	1955	4.9 ∅	1,051	914
Myles Salt Co.	Louisiana		4.9 ∅	228	761
International Minerals	Canada	1957	5.5 ∅	1,030	0-70 363-437
Duval	Carlsbad,NM	1963	4.26 & 3.65∅	305&279	128
International Minerals	Canada	1963	5.64 ∅	1,021	468
Allan Potash Mines	Canada	1964	4.9 ∅	1,089	625
Allan Potash Mines	Canada	1964	4.9 ∅	1,089	625
Alwinsal Potash of Can.	Canada	1964	5.5 ∅	1.004	527
Noranda Mines Ltd.	Canada	1965	4.9 ∅	1,052	591
Noranda Mines Ltd.	Canada	1965	4.9 ∅	1,052	591
Cominco Ltd.	Canada	1965	4.9 & 5.64∅	1,089	684
PCA	Sask.,Can.	1967	5.5 ∅	1,068	548
PCS	Canada	1967	4.9 ∅	1,021	461.
PCS	Canada	1967	4.9 ∅	1,000	469
Cargill	Louisiana	1969	4.9 ∅	378	70
Cargill	Louisiana	1973	4.9 ∅	478	76
PCS	Canada	1974	4.26 ∅	1,004	527
Amax Coal Co.	Illinois	1974	6.09 ∅	228	38
Diamond Crystal	Louisiana	1975	2.44 ∅	470	70
Island Creek Coal Co.	Kentucky	1975	6.09 ∅	122	54
Morton Salt Co.	Louisiana	1977	5.5 ∅	381	64
Peabody Coal Co.	Illinois	1978	6.09 ∅	122	53
Selco Mining Corp.	Quebec,Can.	1979	3.65 ∅	61	61
White County Coal Corp.	Illinois	1979	6.7x9.8, 6∅	335	41
Domtar	Goderich,Ont.	1980	6.09 ∅	518	61
Les Mine Salin	Mad.Is.,Can.	1980	6.70 ∅	122	43
Turris Coal Co.	Illinois	1981	5.5,6.09,&7.3∅	87	64
Asarco Exploration	Timmons,Ont.	1981	3.65 ∅	174	43

FREEZE DESIGN

The freeze design phase consists of six distinct steps which must be completed for every project:
. Assemble Design Criteria - Material properties for the soil, rock, water-applied loads and structural surcharge, if any, at the site.

. Determine Technical Feasibility of Freezing - Based on design criteria, site and project constraints, and known characteristics of the freezing method and the environment to be frozen.

. Complete Structural Analysis - Of the frozen earth mass to determine the geometry required for overall stability and related internal stresses and the effect of time on the stress-strain relationship.

. Thermal Analysis - To determine refrigeration method to be employed, as well as amount and duration of refrigeration necessary to form and maintain the desired frozen earth mass.

. Select Specific Construction Approach and equipment to install the required freezing system.

. Estimate the cost of the work as designed.

Each of the design steps mentioned above could be the subject of an extensive technical paper. Though a thorough treatment of these steps is beyond the scope of this paper, some comments are appropriate.

During preliminary freeze design, it is sufficient to use simplified calculations for structural design based on ideal elastic material concepts. For thermal calculations, approximations as proposed by Sanger (Ref. 8), Kamenskii (Ref. 9), Jumikis (Ref. 1), or Vialov (Ref. 10) are adequate. The preliminary design must include specification of special additional data or testing which might be needed for the final design, such as:
. Undisturbed samples to characterize strength and/or deformation behavior of the frozen soil.

. Undisturbed samples to test frost heave and thaw consolidation behavior of the soil.

. Hydrologic data, for example, from the installation of piezometers.

The state of the art freeze design methods for mine shafts under difficult ground conditions uses finite element analyses for structural as well as thermal computations. The final freeze design should include the following items:

A. Objectives of design
B. Freeze wall structural design
C. Freeze wall thermal design
D. Layout of refrigeration piping system
E. Optimization of refrigeration plant capacity and plant installation
F. Instrumentation for monitoring freezing process
G. Pressure relief pipe in shaft
H. Specification for prefreezing period till freeze wall has required thickness
I. Specification for maintenance freezing
J. Constructibility review and approval of excavation methods in the frozen zone

Quality assurance during actual execution of the work includes:

A. Monitoring of freezing process during prefreezing
B. Monitoring of water levels in pressure relief hole and piezometers
C. Monitoring of freezing process during maintenance freezing
D. Monitoring of ground movements
E. Monitoring of thawing process
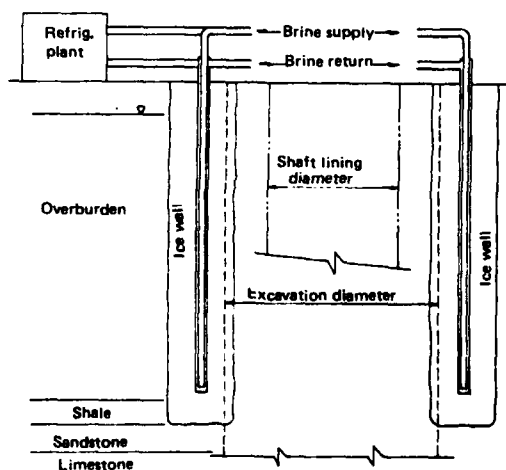
Typical Mine Shaft Collar Freeze
Figure 2

322

SHAFT LININGS

In most cases the ultimate desire of the owner of a completed shaft is for that shaft to be dry. The watertightness of any shaft will depend on the shaft lining system to be used, such as:
. Cast-in-place concrete
. Slipformed concrete
. Steel
. Composite concrete and steel
. Composite concrete plus steel plus bitumen for absolute watertightness and flexibility.

The decision as to which lining should be implemented depends upon the purpose or utilization of the shaft, its geologic conditions, the expected subsidences due to mining activities, and/or the relative costs of constructing the shaft versus the cost or practicality of operating the shaft with continuous water inflows.

TYPICAL FROZEN SHAFT WORK ACTIVITIES

The typical activities at a frozen mine shaft construction project include:
. Site investigation and selection (usually by owner)
. Mobilization
. Freeze collar construction
. Refrigeration and temperature monitoring hole drilling including installation of pipes
. Directional survey of all pipes installed
. Surface piping system for freezing and monitoring
. Refrigeration plant installation
. Prefreezing to build required freeze wall
. Shaft plant installation
. Maintenance freezing during sinking and lining
. Collar excavation and lining
. Shaft excavation and lining
. Station excavation and lining
. Sump construction
. Permanent Facilities Installation (Headframe, shaft equipment, fan, emergency man hoist)

CASE HISTORIES

Coal Mine Shaft Project No. 1

The construction of two 20' (6.1m) diameter air shafts was performed for a coal company in the Illinois Basin. The geological cross section of the proposed shaft sites consisted roughly of the following:

0' to 20'	Compacted Fill	(0 to (6m)
20' to 23'	Silt	(6m to 7m)
23' to 85'	Sand & Gravel	(7m to 25.9m)
85' & below	Shale	(25.9m) to bottom

The water table was located at approximately 25' (7.6m) below ground surface. The owner chose to use an open concrete caisson of 24' (7.3m) internal diameter with 3'-0 (.9m) thick walls which was designed to penetrate the saturated overburden intended to seat and seal itself in the shale.

Groundwater inflow into the caisson at the shale contact proved excessive and the use of an "ice wall" to prohibit further inflow was implemented.

The construction of an ice wall was successful in preventing the water inflow from the saturated overburden. This particular freezing application was as a water cutoff, not as a structural wall.

The water table was 25' (7.6m) below the surface. The caisson shoe had been seated at approximately 85' (25.9m) below the surface.

The design of the freeze was such as not to allow the ice wall to reach the existing caisson wall, thus not exerting any detrimental pressures on the concrete cylinder.

Ground Freezing Shaft Data

. Theoretical outside radius of ice wall   24'-0 (7.3m)

. Theoretical inner radius of ice wall 19'-0 (5.3m)

. Freeze hole location radius 22'-0 (6.7m)

. Number of freeze holes – 35

. Freeze hole depth 125'-0 (38m) (40' into the shale)

. Caisson diameter (I.D.) 24'-0 (7.3m)

. Wall thickness – 3'-0 (.9m)

. Temperature hole radius location 16'-0 (4.9m)

Freeze pipes were installed using rotary drilling techniques. Difficult ground conditions, cobbles and the disturbance of the ground by the caisson caused many drilling problems.

Average ground temperature was maintained at 15°F (-10°C) using a calcium chloride brine circulation medium.

The two freeze plants had 70 tons of refrigeration capacity each.

Both shafts were excavated through the frozen contact zone below the caissons using drilling and blasting.

Upon the completion of the caisson underpinning, the main shaft collar foundation was excavated and the reinforced concrete bearing set was placed. Atop this foundation concrete, a slipform was installed and the final lining was placed monolithically to the collar of the shaft.

The use of the slipformed concrete lining eliminates construction joints through the interval of the saturated overburden. This slipformed concrete lining was designed for hydrostatic loading and was terminated in an impervious shale at the bearing set. The completed shafts are dry.

Mine Shaft Collar - Project No. 1
Note freeze pipe manifolding in foreground; in background brine return tank.

Case History Coal Mine Project No. 2

A coal mine ventilation shaft located in the flood plain of the Ohio River was constructed using ground freezing through the saturated overburden.

The 20' (61m) finished diameter shaft was to be 400' (122m) deep to the coal seam with the excavation and lining of a 20' (6.1m) deep sump.

The water table was located 18'-0 (5.5m) below ground surface.

The geological cross section of the shaft location was comprised of the following lithology:

0'- 7'	Silty Clay	(0- 2.1m)
7'- 18'	Silty Sand	(1.2- 5.5m)
18'- 23'	Brown Sand	(5.5- 7.0m)
23'- 27'	Gray Sand	(7.0- 8.3m)
27'- 32'	Clay	(8.3- 9.8m)
32'- 44'	Clayey Silt	(9.8-13.4m)
44'- 45'	Sand	(13.4-13.7m)
34'- 58'	Silty Clay	(13.7-17.7m)
58'- 63'	Clay	(17.7-19.2m)
63'- 67'	Clay with Sand	(19.2-20.4m)
67'- 97'	Coarse Sand	(20.4-29.6m)
97'-117'	Coarse Sand	(29.6-35.7m)
117'-146'	Medium Sand	(35.7-44.5m)
146'-152'	Coarse Gravel	(44.5-46.3m)
152'-159'	Shale	(46.3-48.5m)

A concrete collar was placed 40' (12.20m) square. Sixteen-inch diamete (.4m) sonotubes were used as concrete blockouts for the freeze pipes and temperature holes.

Two 110-ton capacity refrigeratic plants were used for Stages I and II freezing with one plant used to maintain the freeze.

Ground Freezing Shaft Data

Finished shaft	20'-0 ∅	(6.1m)
Freeze circle	36'-0 ∅	(11 m)
Depth of freeze	175'	(53.3m)
Liner plate depth	155'	(47.2m)
Freeze pipe casing	5"∅ Sch40	(127 m)
No. of freeze pipe	36	
Liner plate diameter	26'	(7.9m)
Temp.probe circle	44'-0 ∅	(13.4m)
Temp. probe holes	3 @ 120°	

Conventional excavation methods (a crane, 630 Eimco and liner plates) were used through the frozen unconsolidated overburden. A bearing set was excavated in a competent limestone formation approximately 30' (9.2m) below the rock contact. A reinforced concrete foundation was placed and then a 3'-0 thick, (.90m) reinforced, monolithic, slipformed concrete lining was installed.

After the slipform demobilization, a conventional shaft sinking headframe and associated plant (concrete forms, drill jumbo, muckers, etc.) was mobilized and both the intermediate shaft and shaft station were excavated and concrete lined.

The total project duration was nine months. No groundwater inflows have occurred in the top 175' of this shaft.

CASE HISTORY JEFFERSON ISLAND SALT MINE, LOUISIANA

A drilled ventilation shaft with a steel lining through an unstable water-bearing overburden had to be abandoned and backfilled due to lateral ground displacements, up to 2" (51mm) per year, a phenomenon quite common in the Gulf Coast area, and maximum settlements of 10" (254cm) per year. Overstress and buckling of the steel liner, which in turn led to cracks and considerable fresh water inflows, represented a deadly threat to the salt mine.

Deilmann-Haniel, a shaft-sinking contractor from Germany, and the Terra-freeze Corporation, now a division of Frontier-Kemper Constructors, were awarded the contract to design and build a new vent shaft 8' (2.44m) I.D. Based on their combined experience in ground freezing and the design and construction of watertight, flexible shaft linings.

The design called for (1) a temporary support and groundwater control system to safely sink the shaft through the overburden, and (2) a shaft lining system flexible enough to tolerate the expected ground movements without affecting its watertightness.

The soil consisted of fill, soft plastic clays and sands to a depth of approximately 175' (53m) to the salt contact. As the shaft location was at the flank of the dome, the top 50' (15.2m) of the salt was fissured. The water table was approximately 20' (6.1m) below the surface.

Ground freezing was chosen to provide temporary ground support and water control. Liner plates (12 gage) were used as the preliminary lining. Between the preliminary and final lining, a 1.5' (.46m) annulus was filled with an asphalt made of a special bitumen with finely crushed limestone added as filler to achieve a density of 81 PCF (1,297kgm3). This asphalt (with the physical properties of a viscous fluid) separates the final lining from the surrounding strata allowing relative movements between the two. The final lining is anchored in a 9' (2.74m) high reinforced concrete foundation ring at approximately 244' (74.4m) depth which will transfer the loads of the water-tight lining into the strata. The final lining consists of a structurally rein-forced concrete cylinder, comprised of prefabricated concrete rings 8" (20cm) thick and 40" (102cm) high, and a con-tinuous steel liner (3/8" (10mm) thick)

for watertightness.

The first 4' of the annulus immedi-ately above the foundation ring was backfilled with concrete to achieve a permanent attachment of the final lining to the foundation. Atop this backfill concrete a seal was constructed.

On a 25' (7.6m) diameter circle, 28 holes were drilled to 245' (75m) depth and 3" (76mm) I.D. refrigeration pipes were installed. Due to the difficult soil conditions, a 5" (127mm) casing had to be set to the salt contact using a top drive rotary drill rig equipped with a Tigre Tierra casing hammer and careful mud control.

The refrigeration pipes were grouted into the salt using saltcrete. Both inclinometer and gyro surveys were used to check the alignment of the holes. Three ground temperature-monitoring pipes and one pressure relief pipe in the center of the shaft were installed.

Two low-temperature refrigeration plants with screw compressors and a capacity of 110 TR each at -13°F (-25°C) temperature produced the required refrigeration during the prefreezing period. One plant was sufficient to maintain the freeze wall after estab-lishing the structurally-required wall.

Low brine temperatures averaging -36°F (-38°C) had to be used to estab-lish a freeze wall of adequate strength, as saturated sodium chloride with a freezing point of -6°F (-21°C) was present at the salt contact.

The use of low temperatures in salt will cause contraction cracks which can extend below the refrigeration pipes and through the shaft area to be excavated. These contraction cracks could lead to inflows in the shafts and, potentially, if they connect to fresh water can cause loss of the shaft if not properly sealed.

This particular problem was first recognized some 15 years ago when Deilmann-Haniel performed the construc-tion of a potash shaft in Lower-Saxony. In the interim, R & D work has been performed in this field by Deilmann-Haniel. Using FEM and FDM analyses it can be shown that these contraction cracks occur regardless of how freezing is applied. These cracks can be pre-dicted with an FEM analysis if the properties of the salt are known. Procedures and materials (a special nonshrink grout that sets at low temperatures) have been developed to seal these cracks prior to excavation.

Both the sinking and lining through the overburden and the sealing of the salt contraction cracks were successfully completed on this project without incident. This was the first time such a flexible, watertight lining had been installed in the United States.
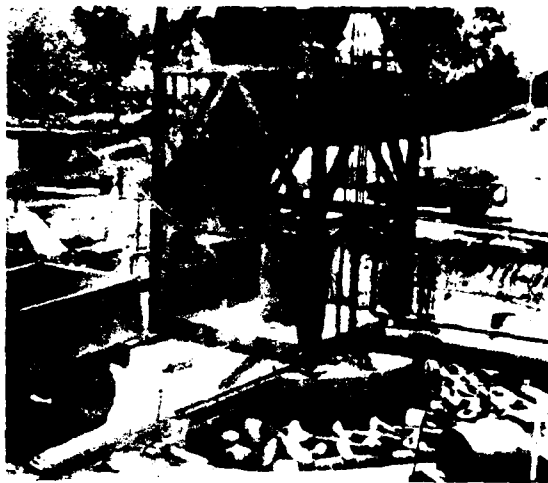
Shaft Collar at Jefferson Island
Note: – Freeze piping & manifolding.
– Headframe & dump
– Muck bucket
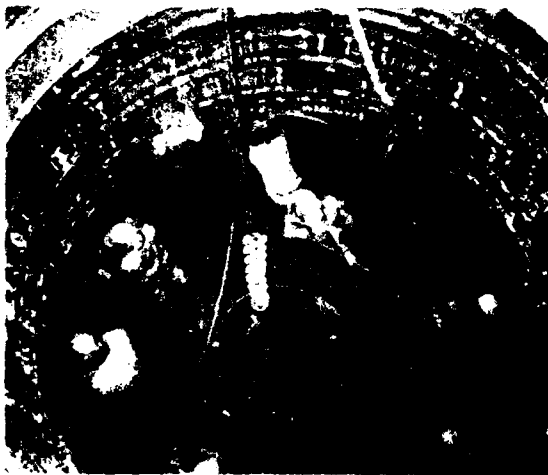
Shaft Excavation at Jefferson Island
Note: – Excavation above water table.
– Liner plate installation.

REFERENCES

1. Jumikis, A. R., "Thermal Soil Mechanics," Rutgers University Press, State University, New Brunswick, New Jersey.

2. Tsytovich, N. A., "The Mechanics of Frozen Ground," Scripta Book Company, Washington, DC.

3. Shuster, J. A., "Controlled Freezing for Temporary Ground Support," 1st North American Rapid Excavation & Tunneling Conference, Chicago, Illinois, June, 1972.

4. Shuster, J. A. & Bernd Braun, "Some Notes on Concreting Against Frozen Earth," Terrafreeze Corporation, Lorton, Virginia.

5. Kersten, M. S., "The Thermal Properties of Soils," Bulletin 28, Engineering Experiment Station, University of Minnesota, Minneapolis, Minn., 1949.

6. Vialov, S. S., "Rheological Properties and Bearing Capacity of Frozen Soils," (Russian), Translation 74, CRREL, 1959.

7. Scott, S. A., "Shaft-Sinking Through Blairmore Sands and Paleozoic Water-Bearing Limestones," Canadian Mining and Metallurgical Bulletin, Feb., 1963.

8. Sanger, F. J., "Ground Freezing in Construction," Journal of the A.S.C.E., Vol. 94, No. SMI, 1968.

9. Kamenskii, R. M., "Thermal Engineering Calculation of the Frozen Soil Watertight Cutoff of Dams, Taking into Account the Mutual Influence of the Columns," (Russian), Gidrotekhnicheskoi Stroitel'stvo, No. 4, April 1971, pp. 38-42.

10. Vialov, S. S., "The Strength and Creep of Frozen Soils and Calculations for Ice-Soil Retaining Structures," (Russian), Translation 76, CRREL, 1962.

CONTROL OF FREEZING PROCESS
ON EXAMPLE OF DEEP SHAFTS SUNKEN
FOR POLISH COPPER MINES

Kot F. Unrug, Professor of Mining Engineering, University of Kentucky, Lexington, KY

ABSTRACT

Copper deposit in Polish lower silesia district is covered by thick, up to 430m, Tertiary and Quantemary overburden consisting of waterbearing sands, gravels and also coherent strata with different consistency as clays, weak shales and lignites. Calculated water inflow to the shaft is about 40 m^3/min with the head up to 4.0 MPa of the bottom of the tertiary strata.

Several problems encountered during sinking of the first shafts resulted in considerable improvement of designing and control of the applied freezing method. Within the frozen complex some most trouble creating strata have been specified and extensive testing program was carried out to record their mechanical and thermal characteristics. The freezing pipe design also has been changed, to prevent ruptures and brine escapes into the rock mass, as well as was established the optimum radius of the circle and distance of freezing holes. It has been found that the current control of the propagation of frozen mantle and its thickness is essential for safe sinking.

Mechanical boring of the shaft bottom was developed as a first such successful attempt ever done. This was combined with the lining erection technology, resulting in minimum exposure of the unsupported shaft section in terms of time duration and its length.

Ultrasonic monitoring of the actual state of freezing of rocks appeared to be a most important tool to prevent

risk in the sinking process.

HDYROLOGICAL CONDITIONS

Development of the lower silesia copper deposit started in 1960 and four large complex mines have been constructed, with 20 shafts, all sunken with freezing ground technique within the water bearing overburden. The generalized geological column is as follows.

-Quaternary: 40 to 100 metres with two water-bearing levels;

-Tertiary: mainly clays, silts, sands and gravels, brown coal series, of total thickness 250-400 metres with two water-bearing levels separated by clays;

-Triassic: composed of aquiferous sandstones with thickness of 90-250 metres;

-Permian: clay shales 0-35 metres thick, anhydrites 80-100 metres thick, shales 0-0.6 metres thick, Rotliegendes, consisting of water bearing sandstones. Fig. 1

The mineralization zone (halcosine, chalcopirite bornite and others, with metal content 1.2-5%) occurs in limestone and dolomitic Permian, underlaying it pitch shales and Rotliegendes sandstone rocks. The deposit is bedshaped. with an incline of 3°-6° due south and has alternating thickness 3-5m.

There are five water horizones: quaternary, tertiary, Bunter sandstone, gehstain and Rotliegendes. The first two are playing most important role in the shaft sinking operation. Rocks within these formations have low geotechnical parameters what combined with the hydrostatic pressure of water
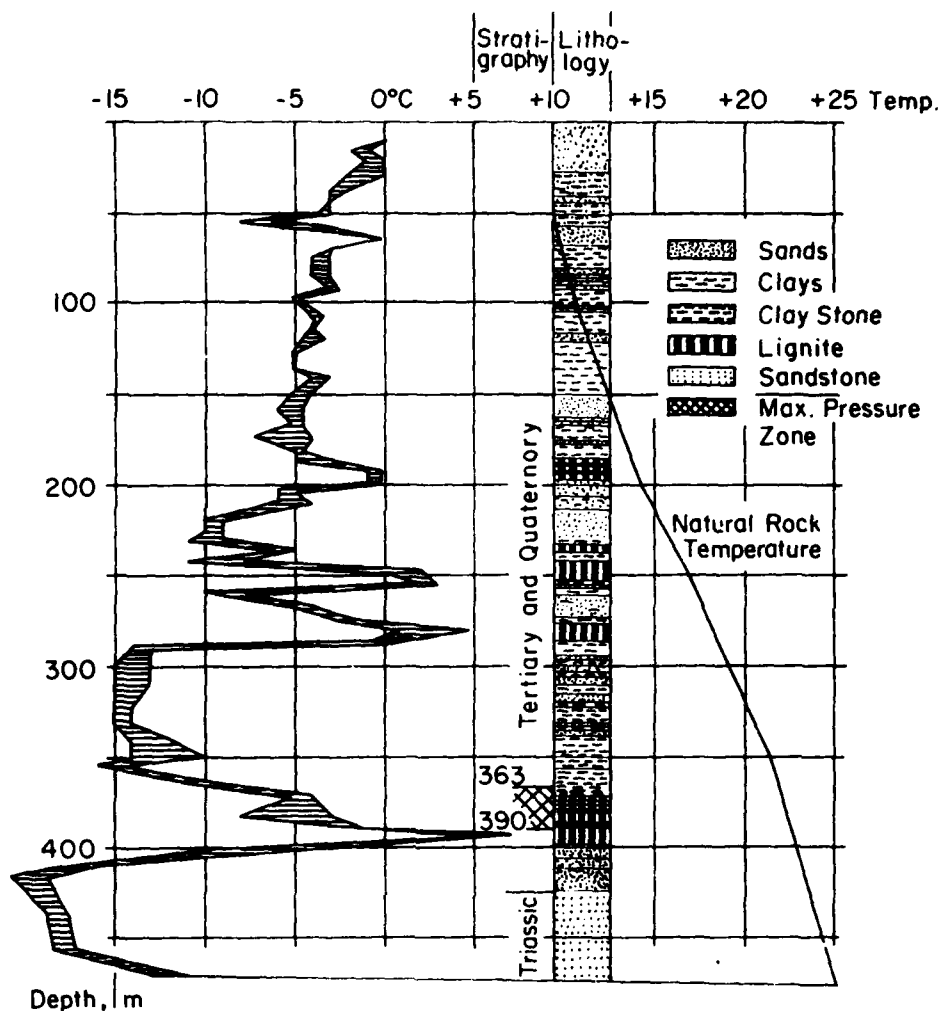
Fig. 1 - Range of temperatures during shaft sinking with corresponding geological
column and natural temperature distribution

creates an adverse condition for shaft sinking. All water levels stabilize close to the surface what proves that in spite of some insulating nonpermeable layers, exists communication among the water horizons through the faults system. The filtration coefficients are high, so the calculated water inflow to the shaft (38-40m^3/min with the pressure 2.5-4.0 MPa) overruns the limit for normal sinking methods.

The percentage distribution of water bearing strata within the frozen part of the geological column varies between 31.6 and 36.8%. Coherent strata are represented by 45.7 to 51.2%, lignites 5.7-8.1% and the rest 6.1-16% create Bunter sandstone strata.

Lignites have thickness alternating from 0.1 to more than 10m.

The physical properties of rocks are low, especially the angle of internal friction, resulting in high lateral pressure reaching 7 MPa when calculated for shafts 7.5m diameter in light.

PROPERTIES OF FROZEN ROCKS

The extensive testing program of frozen rock has been carried out to es-

328

blish their physical properties. In
spite of substantial diversity of results
for various types of rocks some techno-
logically valid division has been made.

Gourp "S" - "safe" which comprises
different sands with high water content,
and 0.05-2.0mm grain size.

Group "D" - "dangerous"; where can
be counted clays, silts and argils.
Within this group some especially dan-
gerous rocks have been specified due to
the exceptionally low compressive
strength and unpredictable properties.
In these rocks for instance compressive
strength is:

in temperature-5°C; 1 to 1.8 MPa
in temperautre-15°C; 3.0 to 5.7 MPa
These rocks do not have elastic proper-
ties, and creep phenomena were observed
in early stages of loading. To obtain
samples of rocks with intact structure,
5x5x5cm and 7x7x7cm cubes were cut from
the shaft bottom during the sinking
operation. In thermoses they were
transported to the laboratory where the
temperature was lowered to the desirable
level for testing.

A considerable decrease in strength
has been observed of the samples of
sands being thawed and frozen again.
Their strength is in average only 60%
of those frozen only ones. Clay be-
haviour is much worse because cyclic
freezing destroys completely its struc-
ture.

RHEOLOGICAL PROPERTIES

Compressive strength traditionally
used as a main designing consideration
appeared to be nonconclusive in light
of newer investigations, which indicated
relationship between the strength and
time of loading. During shaft sinking,
after rock is exposed stresses increase
gradually in a longer time resulting in
much lower ultimate strengtn values when
compared to the ordinary compression
test. Figs. 2 and 3 are showing these
relationships from Russian investiga-
tions [4]. As it is observed from the
diagram the long term strength is 1.5
to 2.0 times less than the short term
compressive strength. Referring to tnat
for the time of exposure of unsupported
shaft wall 12 hours, a diminishing fac-
tor 1.5 should be used where only com-
pressive strength tests are available,
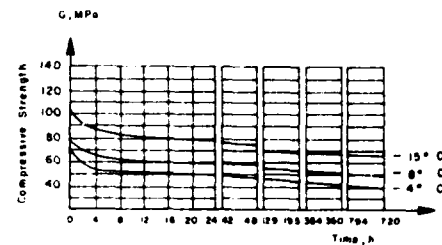and factor 2 for longer exposure time.

Fig. 2 - Relationship between compressive
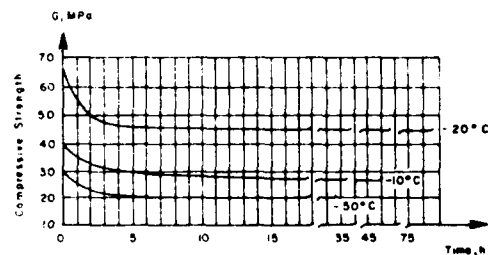strength of sands, freezing tem-
perature and duration of load.

Fig. 3 - Relationship between compressive
strength of clays from freezing
temperature and duration of load.

THERMAL PROPERTIES

The natural rock temperature which
depends on depth and geothermal grade
(Fig. 1) is lowered by freezing in a
different rate according to the thermo-
physical properties of particular strata.
So the pace of freezing process of dif-
ferent rocks starting from fastest ones
can be listed as follows: sandstones,
wet coarse sands, wet fine sands, moist
sands, sandy clays, clay., clays with or-
ganic matter, lignites with clay, lig-
nites. It has been observed that even
relatively low temperature does not
mean that all free water has been fro-
zen. Figs. 4 and 5 show how thermal
properties influence development of fro-
zen rock mantle. For instance in clays
in -30°C about 30-50% of free water stays
unfrozen. It depends on the size of
pores (percentage of capilar water).

Thermal conductivity expressed by
the unit Kcal/m^{o}Ch for water in +20°C is
0.514, for ice in 0°C is 2.0. For sands
depending on moisture content and tem-
perature varies between 2.03 t0 2.92,
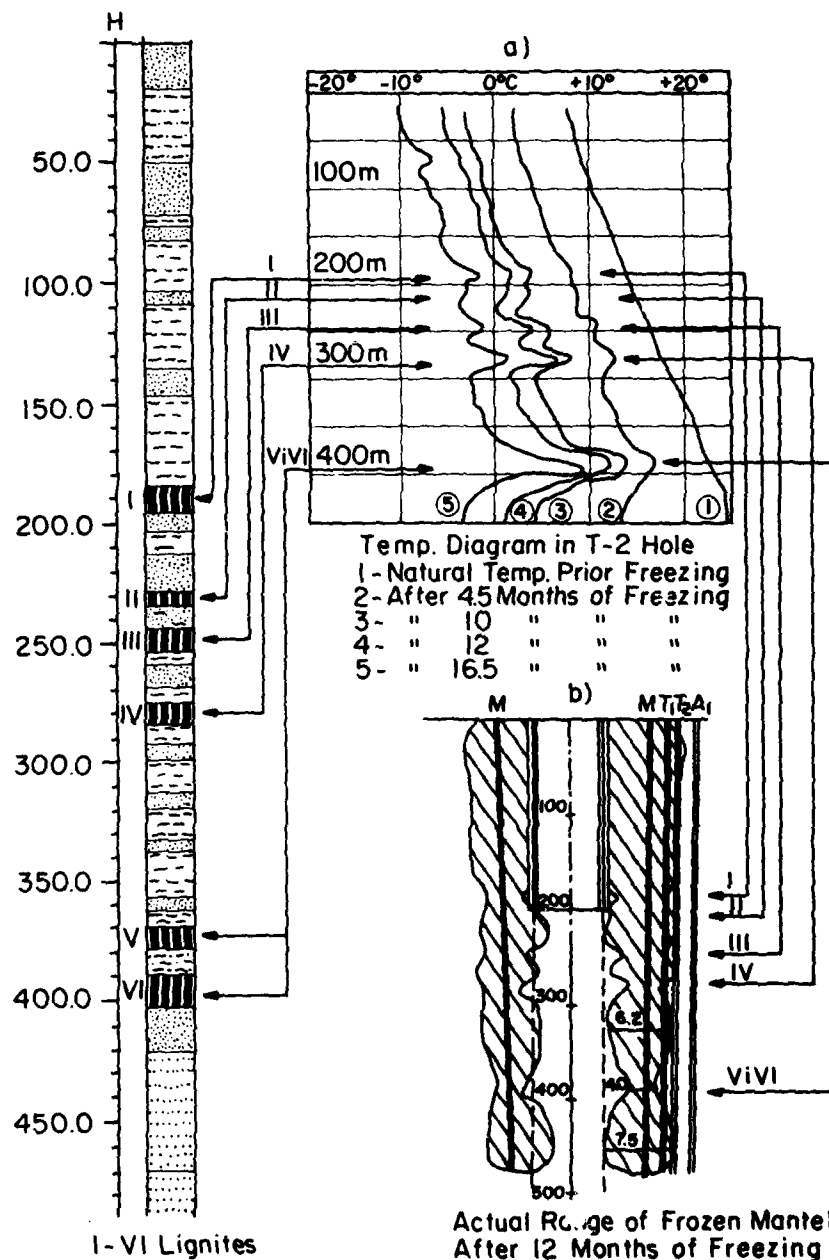while for clays 0.3 to 1.6.

329

Fig. 4 - Temperature distribution depending on rock type (a) and frozen mantle thickness as function of temperature (b).

VOLUMES CHANGES OF ROCKS WHEN FROZEN

Another laboratory study has shown a phenomenon of volumetric changes of frozen rocks with temperature. As it was expected these changes are dependent on water content in pores. In a case of sands the excessive water during freezing
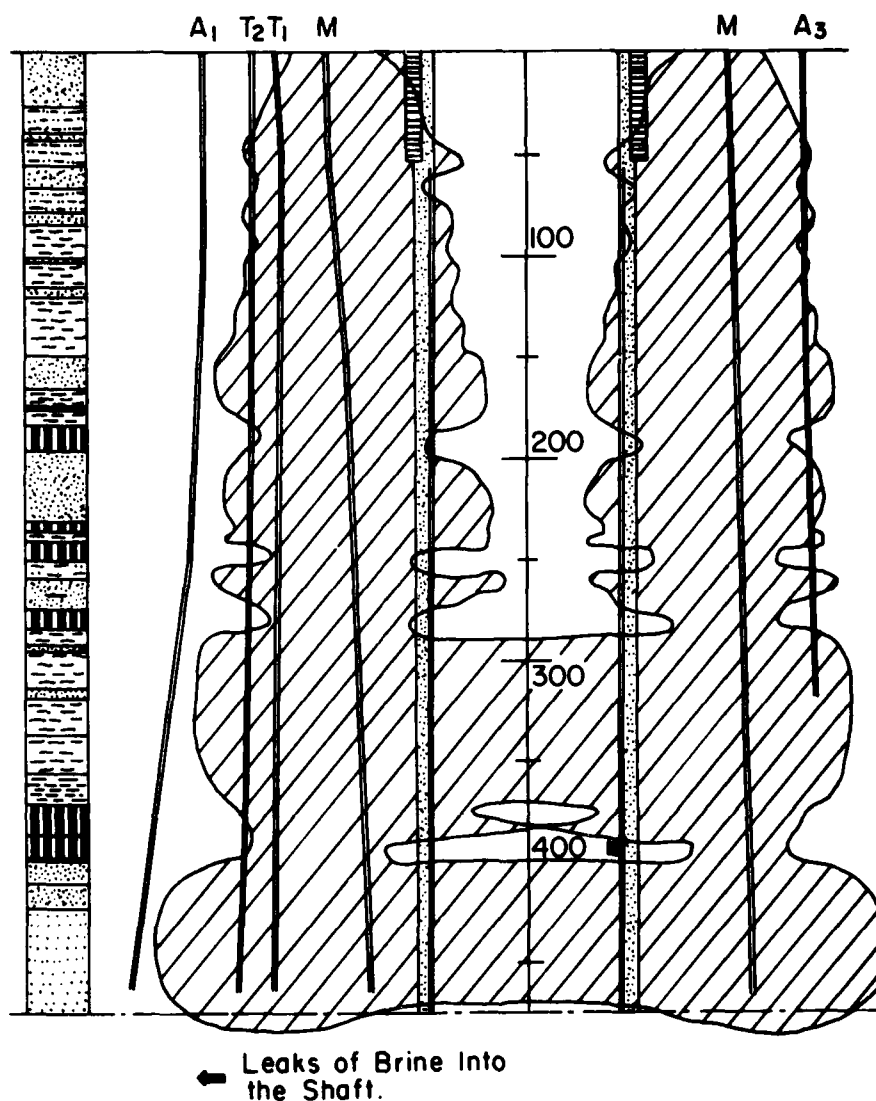
330

Fig. 5 - Frozen mantle thickness diagram as it was measured by ultrasonic survey when reached by sinking.

is pushed out by the front of advancing frost. In clays where filtration coefficient is low it is not possible and as a result, clays have larger volume increase than sands.

During ground freezing before the sinking starts, and after the frost mantle is closed even in sands free water can not find way to go unless the dewatering hole is provided in center of the shaft. An increase of volume is a cause of large stresses which are released when shaft excavation is made. Observed are then radial displacements of shaft walls, and sometimes shaft bottom upheaves.

Changes of volume can also explain a phenomenon of high pressure appearing when first time frost appears on the permanent lining after its installation.

331

When concrete is placed behind the
tubings (cast iron)(Fig. 8) it produces
heat due to the exothermical nature of
cement hydratation. This thaws the im-
mediate contract of frozen rocks causing
volume decrease of warmed up material.
Pressure acting on the outer perimeter
of the shaft mantel imposes its creep
toward the excavation in this case, and
produces confinement of the lining.
When frost second time advances through
the previously thawed material increase
of volume causes high stresses, because
of rigidity of shaft lining. In several
cases cracks in the lining were observed
in time corresponding to the above de-
scribed process.

FREEZING PROCESS

The freezing stations for the shafts
sunken recently with 7.5m in inner dia-
meter were implemented with 2 stages
ammonia compressors allowing to obtain
temperature even below $-40^{\circ}C$. This
gives an important additional capacity
in case of some problems encountered
during the sinking. The condensation
temperature was $+35^{\circ}C$, reducing con-
siderably water consumption when com-
pared with previously applied aggre-
gates. The other technical parameters
were as follows: freezing depth - 470m,
steel freezing pipes diameter/thickness
140/8mm, inner poliethylene pipes
75/4.3mm, freezing station capacity for
2 shaft site $3x10^{6}$Kcal. Brine flow
12-13m^{3}/min, with volume $320m^{3}$, power
installed (for 2 shafts) 3500kW, water
consumption $0.8m^{3}$/min. Mean brine tem-
perature $30^{\circ}C$ with flow rate 0.5-0.6m/sec
(in annular space), Reynolds number 2500.
Applied system - one section
freezing; time of active freezing 110-
233 days. Difference in temperature be-
tween intake and return brine $3^{\circ}C$. Di-
ameter of the freezing holes circle -
16m. Distance between freezing holes
1.25m (Fig. 6).

VERTICALITY OF FREEZING HOLES

Deviation from the plumline in-
creases with depth of drilling. The
positive correlation has been found be-
tween the deviation of holes and problems
encountered during the sinking. To
assure verticality of the freezing holes
is worth to sacrify some time during the
drilling. Once the survey of deviations
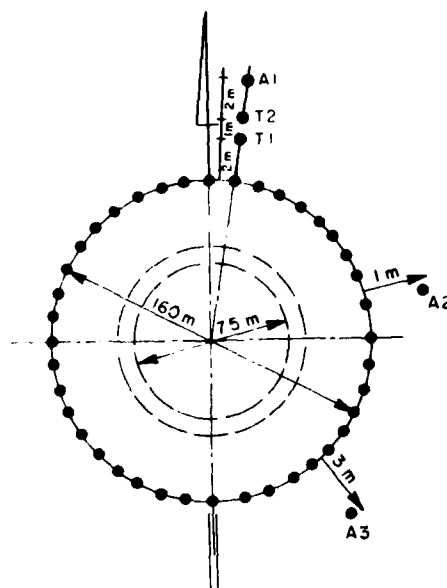has been done, the dangerous sections
can be determined when compared with

Fig. 6 - Freezing holes cirlce and loca-
tion of control holes

geological column and location of dif-
ficult to freeze rocks. These areas of
potential problems have to be closely
watched to assure safe sinking.

CONTROL OF THE ROCK MASS FREEZING PROCESS

The theory of freezing process is
well developed including analog and nu-
meric modelling. The main difficulty
exists however when gathering of input
data is concerned, and because of that
a field control system remains as an ul-
timate way of generating information as-
suring safety of the operation.
Measurements of temperature provide
part of information however under high
confining pressure consolidation of rock
not necessarily starts at $0^{\circ}C$.
Thermal hole locations is shown in
Figs. 6 and 7.
The second control method is based
upon the difference in velocity of elas-
tic wave travelling through the frozen
and non-frozen rock. Two sounds,emitter
and receiver are lowered in the
neighbor holes in a way assuring their
position on this same depth. An impulse
from emitter to receiver goes through
the rock between pipes and the time of
penetration is recorded, allowing to cal-
culate velocity.
The system "AMA" being used for ul-
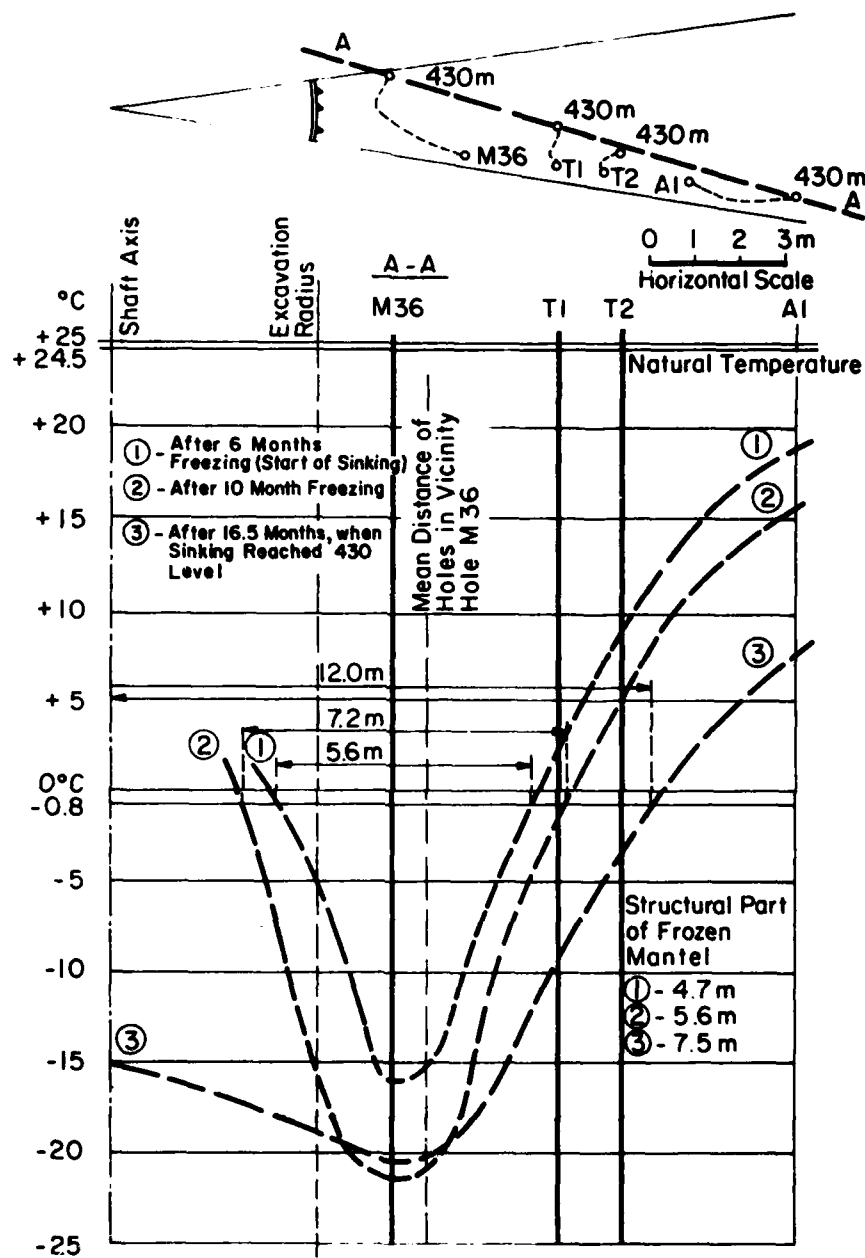tasonic measurements has the following

332

Fig. 7 - Distribution of temperature within frozen mantle on 430m level (sandstone) depending on freezing duration.

features: Frequency range 500-20000Hz the range of measurement in non-frozen ground is 1-3m, in frozen ground 3-6m. Emitter power in impulse 20KW range with the measurement time of wave passing, 6-10µsek. Fitness of measurements (time of passing acustic wave) 5%, fitness of measurement of relative damping of acustic wave is 20%; temperature range of work +35 to -35°C. Examples of wave velocities in:

    water - 1450m/sek
    ice - 4300m/sek
    rocks - 16°C sand ~ 800m/sek
          - 17°C sand ~ 2000m/sek

Ultrasonic control was used parallely to the measurements of temperature in thermal holes. Through the study of geological column, physical properties of rocks and survey (every 50m) of freezing hole deviations, the most critical zones were found where ultrasonic examination was done independently to routine measurements.

The obtained results allowed to check whether frozen mantle was closed or not. To do the measurements the inner PE (poliethylene) tubings had to be removed (wined on spools) from the pair of holes to be tested. Than the sounds could be sunk into the holes. Measurement between the holes with deviations in opposite direction is usually a logical choice. However this can differ substantially on particular levels and therefore requires an individual judgement in each case.

FREEZING PIPE BURSTING

Freezing pipe bursting is the most dangerous event when sinking operation is concerned. An escaping brine thaws frozen rocks and when the "hole" in frozen mantle will develop, there is no more protection against water and flow rocks when present in the vicinity.

Such a perforation of the frozen mantle it is the common cause of the accidents resulting in flooding of the
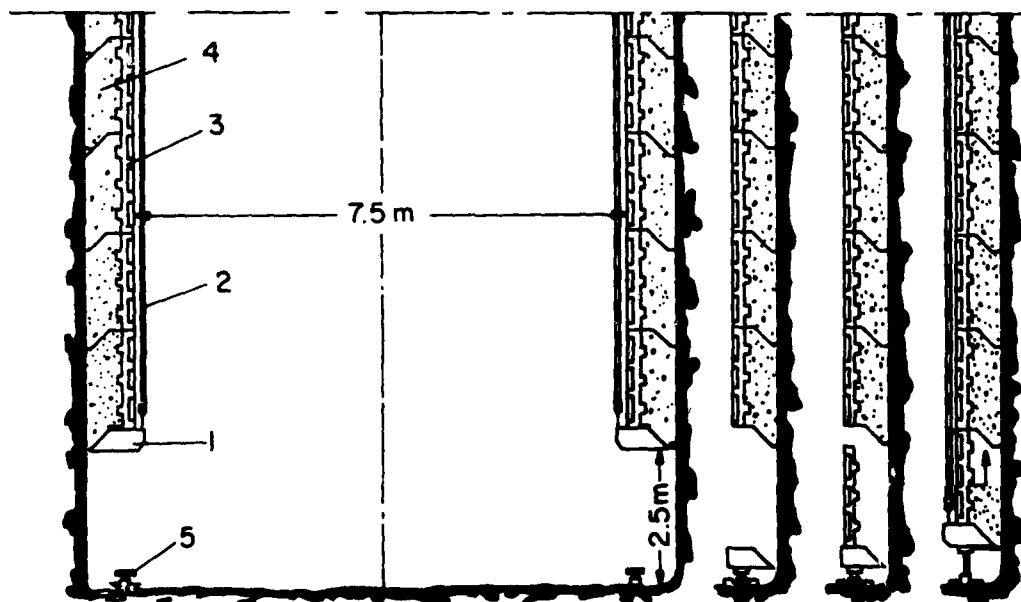

Fig. 8 - Underhanging system of tubing lining installation. I, II, III, IV - consecutive phases of construction. 1. Installation ring, 2. Cables supporting assemble ring, 3. tubbings, 4. concrete (back filling), 5. hydraulic jacks supporting assemble rings.

shaft. In literature are known several case studies of such disasters, which are difficult to handle and always very costly and time consuming.

In early shafts which were sunk without necessary experience in the region some serious problems occurred including flooding of one shaft. The rupture of the freezing hole was the cause of it. In certain shafts pipe bursting was nearly involving half of all pipes. The control of volume being in circulation was assured by a float installed in the return brine tank, signalizing when brine level starts to drop. The visual inspection of return pipes allows to determine what hole is leaking and this one was cut off. The so-called rescue casing, smaller in diameter was then put into the hole what proved to be an effective way to deal with the problem, however the thermal conditions of heat transfer deteriorated substantially in such a hole.

After research being done to identify the causes of pipe fracturing, following explanation has been found. Due to the uneven rate of freezing in different rock types, e.g., sands freeze much faster than clays, freezing pipe is caught in certain levels. Then after some period of time clays freeze with increase of volume and therefore a tensions force acts on the pipe.

It should be noticed that pipe bursting was monitored, during an active freezing period long before a shaft head approached the corresponding level.

To cope with this problem, steel used for pipes has been changed for the one with increased deformability. The connectors have been redesigned to maintain even outside diameter of the whole pipeline - (before connectors were sticking out). An outside bituminous coating of pipes also was considered to utilize the creeping within the bituminous layer, allowing on relative movement betwene the pipe and frozen rock.

There were identified also some other reasons of bursting being related to the hole deviations (too close to the shaft) and bending of the pipe, when shaft wall deformed toward the opening. The underhanging system of tubing lining installation (Fig. 8) has eliminated to large extent deformation of shaft wall, because unsupported shaft wall is at the most 2.5m in height.

CONCLUSION

For successfuly shaft sinking with application of the freezing method to great depth the following recommendations can be done:

- to maintain verticality of freezing holes, even when it will considerably increase drilling time.
- freezing pipes should have high strength with large allowable deformation, and tight couplings.
- wide application of control method is desirable as e.g. - ultrasonic one, enabling monitoring of actual size of frozen mantel, and its strength.
- testing of physical properties of frozen rocks with creep characteristics.
- realistic calculations of frozen mantel thickness based upon well defined properties of rocks.
- selection of freezing station parameters adequately to the optimum freezing regime.
- introduction of new cooling agents, with less viscosity and density, to decrease pumping costs. Such a medium should not defreeze rocks when pipe burst occurs.

REFERENCES

1. T. Glazor, J. Plesniak, T. Kopec: "Shaft Freezing to the great depths" - Conference on New Technology of Shaft Sinking - Czestochowa, Poland 1974.
2. Hilbig, P., Kratzach, H.: Die messtechnische Uberwachnung eines obsatzweise geofrozen Schachtes, W. Germany, Opladen 1971.
3. Kteczek 2. State of stress and strain in frozen rocks around the shaft as a function of time, Gornictwo Z.37, Academy of Mining & Metallurgy, K akow, Poland 1971.
4. Tiutiunnik, P.M., Stability of shaft walls sunk with freezing method, Szachtnojc Straitelstwo 1964/1, USSR.
5. Ostrowski, W.J.S., Design Considerations for modern shaft linings, CJM Bulletin 1972, Canada.

EMPLOYMENT OF ROCK FREEZING TECHNIQUES
FOR SINKING DEEP MINE SHAFTS

Losj,I.F.,Dipl.Eng.,Shaktspetsstroy,Moscow,USSR
Florov,I.N.,Dipl.Eng.,Shaktspetsstroy,Moscow,USSR.
Lownin,Yu.A.,Cand.Sc.(Eng.),Shaktspetsstroy,Moscow,USSR.
Varenishev,V.M.,Cand.Sc.(Eng.)Shaktspetsstroy,Moscow,USSR.

In the USSR two mine shafts were constructed with the application of deep (620m.)rock freezing technique.The whole of the rock mass were frozen from the surface to the final depth since within this depth range the rocks were flooded and some of them -unstable.

The rocks were clays,sands,limestones and chalk deposits.The ground water head came to 5.3 MPa at the final depth.According to the design at the construction of the mine shafts of 7.5m. in diameter the deep rock freezing was carried out through 66 freeze columns staggered along two concentric circumferences of 14.5m. and 19m. in diameter respectfully. Formation of a frozen rock cofferdam was carried through in two descending stages:the upper stage (to the depth of 270m.) was frozen by the freeze columns of the inner row and the lower stage-by all the freeze columns in the both rows.

The freeze columns were made of steel pipes with outer diameter of 146 mm. and wall thickness of 11mm.Inside these steel casings thre were mounted steel freezepipes of 60mm. in diamet.. descended to the final shaft depth and steel freeze-pipes of 104mm. in diameter used within the upper stage depth limits.All the pipes were arranged concentrically. Under operation of the upper stage freeze columns the brine flow was supplied into boreholes through the annular interpipe space between the inner wall of the casing of 146 mm. in diameter and the outer wall of the freezepipe of 104mm. in diameter,while its return upflow passed through the annular interpipe space between the inner and the outer walls of the freezepipes of 104mm. and 60mm. in diameter respectfully. For freezing the lower stage rock mass the brine flow was supplied into boreholes through the freeze-pipes of 60mm. in diameter and back to the surface it wasrturned within the upper stage bounds through the annular interpipe space between the outer and the inner

337

walls of the freezing pipes of 60mm. and 104mm. in diameter respectfully. In this case the annular interpipe space between the outer and the inner walls of the freezepipe and the casing of 104mm. and 146mm. in diameter respectfully was cleared out of the brine with the aid of the compressed air supply.

At every mine shaft the rock mass freezing was ensured by a freezing plant with refrigerating output of 2.000.000 kcal/hr. For the upper stage rock mass freezing the brine temperature was -20°C and for the lower stage rock mass freezing it was -35°÷40°C.

The freeze holes were bored with average 1.4m. deflection from the vertical position and their greatest spacing was not more than 2.7m. An automatic temperature measuring system was designed and used for controlling both the freezing system operation and the process of the frozen rock cofferdam formation.

Data of the systematic temperature control at the mine shafts enabled to get much information about the freezing system behaviour in service and the process of the frozen rock cofferdam formation.

Specific features of the deep rock freezing regime were characterised by a sharp increase in time necessary for the refrigerating equipment to run up to stable temperature regimes of operation and an unexpectedly high temperature losses throughout the freeze columns' depth.

At the upper stage rock mass freezing with the compressors running in the regime of single-stage compression of the refrigerant the period of time required to attain the limiting high vaporization temperature of -25°C was 80-90 days for the mine shaft No. I and 60-70 days for the mine shaft No.2. At the lower stage rock mass freezing the period of time required to attain steady refrigerant temperatures of below-30°C was 90 days for the mine shaft No.I and 180 days for the the mine shaft No.2. At the upper stage rock mass freezing for the time when the compressors run in the regime of single-stage compression the refrige-

rant temperature drop at the inlet and the outlet of the freeze columns of the inner row decreased from 5-7°C to 2.0-2.5°C and after the changeover to the low-temperature freezing it increased again up to 6-7°C.

In the process of rock mass freezing to the shaft full depth the refrigerant temperature drop at the inlet and the outlet of the freeze columns of the outer row changed insignificantly (from 3.5 to 1.7°C).

At the lower stage rock mass freezing the refrigerant heating in the freezepipes of 60mm. in diameter came to 15-20°C at the beginning of the freezing process and then it gradually dropped to 10-12°C by the 180-th day.

In the initial period of the rock mass freezing the refrigerant temperature difference at the outlet of the freeze column and at the upper stage final depth came to 18-19°C and only by the end of the freezing process it dropped to 4-5°C.

Besides there were established significant deviations of the freeze columns' individual operating regimes from the average which increased in proportion to the depth growth.

Non-uniformity in the temperature regimes of some freeze columns in service was + 10°C at the initial period and only by the 150-th day after the beginning of freezing it became stable at the value of + 5°C that constitutes 20% of the refrigerant mean temperature.

According to observations effected at the mine shafts with the aid of thermometric columns the beginning of formation of the frozen rock cofferdam at the bottom of the upper stage rock mass due to great temperature losses throughout the depth was recorded only on the 15-th-30-th day after the freezing system run-up.

Data of temperature measurements enabled to calculate a process of the frozen rock cofferdam formation and to define freezing rates for different rocks.

Predictions of the frozen rock cofferdam state were taken as a basis for schedulling shaft sinking works.

As shown above, disadvantage of

338

the freeze column design employed
is in a considerable heat exchan-
ge between the brine flows moving
in opposite directions.

Both the refrigerant heating while
it flows down in the freeze pipe
and its cooling when it flows up
are unfavourable .If the first
factor extends the freezing time,
the second factor reduces the ref-
rigerating output of the freezing
plant.The said disadvantages did
not cause significant obstacles in
formation of the frozen rock cof-
ferdam of designed dimentions,
though it took much more time.
At the depth of 500-600m. the thi-
ckness of the frozen rock coffer-
dam was 5.5-8.5m. and it depended
on both the heat-conductivity of
different rocks and the direction
of the borehole deflection from
the vertical position.

Certain difficulties were caused
by pipe breakages in the freeze
columns.

The freeze columns' breakages we-
re detected in the areas of inter-
bedding of rocks having different
physical.mechanical and thermal
properties both in thawed and fro-
zen state.Moreover,breakages in
the freeze columns occured in the
interbed contact zones of stiff
rocks(frozen sand,sand-stone,li-
mestone)with heaving rocks(marl,
clay,loam,clay shale and etc.).

The freeze columns breakages at
small,mean and great depths occur-
ed before starting shaft sinking
works and especially in the pro-
cess of shaft sinking give eviden-
ce to the existence of a comlica-
ted stressed-strained condition
for the freeze columns which grows
up throughout the time beginning
from the setting of freeze pipes
into boreholes and till the acco-
mplishment of shaft sinking.

As it was recorded at various pro-
jects,breakages of the freeze co-
lumn pipes,before shaft sinking
were observed,as a rule,during
the period of cyclic changes in
the temperature and hydraulic be-
naviour of the freeze columns in
operation,i.e. at the sharp inc-
rease of the brine temperature in
the freeze columns from -30°C to
-I0°C,then at its intensive drop
to -30+35°C and at reiteration of
the similar temperature changes
of the brine,the freeze pipe me-

tal and the heaving rocks adjacent
to the freeze column.The contact
areas between heaving clays and
stiff rocks in frozen state were
of the greatest danger for the fre-
eze column pipes as the thermal
deformations of clay heaving at
the initial pressure of 4-5 MPa
within the temperature range from
0°C to -20°C constituted I.I-I.5
per cent and the heaving pressure
increased up to I6-2I MPa.It was
established that after stabiliza-
tion of the freezen clay tempera-
ture within the range from -I2°C
to -20°C and the heaving pressure
within the range from I6 to 2I MPa
the elastic strains of heaving ex-
pansion for these clays constitu-
ted from 0.8 to I.I per cent in
case of conditionally- instanta-
neous unloading.Since the moistu-
re content of heaving clays in
their precontact areas with water
saturated sands and stiff rocks
was much higher than in the midd-
le of the stratum,the ultimate
strains of elastic unloading were
arranged for the contact areas.The
said type of the frozen rock mass
deformations was mostly dangerous
for the freeze column pipes,espe-
cially in case of blasting rock
excavation technique as within the
short periods of time the freeze
columns' deflections might beco-
me ultimate.

In accordance with the up-to-date
conceptions of mechanics of solid
medium at the shaft wall uncove-
ring there are taken place a sho-
rt-lived elastic unloading of the
frozen rock mass and a development
throughout the time of non-elastic
creep strains both in front of the
shaft face and along the radius
from the snaft centre to deep in-
to the rock mass.Around the unco-
vered part of the shaft there is
developed a zone of non-elastic
strains. In course of time the
boundary of this zone is shifted
deep into the rock mass in front
of the shaft face and along the
radius in the direction of the fre-
eze columns.Radius of the non-
elastic strain zone development is
depended on a rock excavation te-
chnique,size and duration of the
shaft wall exposure,stratum thick-
ness and strength characteristics
of rocks penetrated,shaft sinking
diameter,shaft shore response.

339

Data of in-situ measurements of the shaft uncovered walls and face displacements proved by the character of their development throughout the time the validity of these general principles of mining pressure effects. According to in-situ measurements during the first 5-6 hours after explosion the shaft wall displacement rate in sandstone at the place of its contact with clays (mark-359.9m.) and in clays (marks 363,5m-383,0m 383.0m.) was of 1.7-2.7mm/hr respectfully and during the following 5-7 hours it was about 0.5-1-5mm/hour. For the first hours of observations the shaft wall radial displacements totalled 20-30mm. and for the following more extended period of time they were only of 5-18mm. After the shaft wall shoring the frozen rock deformations were not discontinued but depending upon a stope height and a shore response they continued to develop throughout the time. In case of small stopes (1.5-2.0m. in neight) and a strong shore response (multilayer shore) deformations of the frozen rocks became stable during the first 5 days after the shaft wall shoring. When the stope height in the frozen clays was increased up to 5-6m. deformations of the shaft wall shore and the rocks came to their ultimate values 20-30 days later after shoring.

In this connection at the great stope heights especially in the precontact areas of clays and stiff rocks the freeze columns that turned out to be within the region of the frozen rocks' intensive deformations, as a rule, broke down. As it took place, in the first turn there were broken down those freeze columns in the inner row that have been set nearer to the exposed shaft wall. The freeze columns in the outer row were kept respectfully safe with the exception of 2-3 pieces per every mine shaft.

At mine shaft sinking the blasting technique was employed for the rock excavation and for the shaft shoring there were used cast-iron tubings being installed following the stoping in the direction from the top to downwards.

In the process of the mine shaft sinking within the depth range of 363-371m. there was observed an intensive clay heaving at the shaft rock walls attended with the opening of vertically-oriented cracks as well as the shaft face rock heaving accompanied by the formation of cracks that broke up the shaft face rock into blocks of 15x15x30 cm. in size. At this depth range after the fitting of cast - iron tubings and the concreting of a space between the tubing backside and the shaft rock wall the shore ring No.301 dislocated aside so that the holes for joint bolts in the horizontal flanges of the next shore ring tubings had to be displaced to make it concentric. Dislocation of the shore ring No.301 was as great as 45mm.

The intensive clay heaving was also observed within the depth range of 374.0-400.0m.

In construction of the vertical flexibility node that served as a compensator in subsequent rock dewatering(the depth range of 475.5-481.4m) the horizontal butt joints at the 3 shore rings fitted just above the node were gapped with the opening of 1-12mm.

The cause of this difficulty lies in the joint effect of the intensive rock deformations and some technological factors. The node was constructed in the area of thick clay stratum.

For its construction the shaft sinking diameter was increased by 1m. per 3 meters of the shaft height. The intensive radial displacements of clay occured even during the node construction that made it necessary to erect an outer tubing shore ring additional to other shielding constructions. This caused the vertical displacement of clays in downward direction towards the shaft wall rock exposure under the vertical flexibility node. While displacing downwards the clays caused tensile stresses in the tubing shore ring column in a local area above the vertical flexibility node. The difficulties occured made it necessary to conduct special observations of the shaft wall rock deformations and to correct both the sinking technique and the shoring technology in dangerous areas.

At present the abovementioned difficulties are being analysed and

studies.
Preliminary conclusiouns made by
the practicing engineers who had
participated in the shafts' sin-
king works are as follows:
I.Validity of calculation of the
frozen rock cofferdam thickness
by the method suggested by prof.
S.S.Vyalov was proved by practice.
2.The pipes providing the refri-
gerant supply to the freeze colu-
mns must have maximum thermo-
insulating properties and the fre-
eze pipes inside the freeze colum-
ns-maximum deformation capacity.
3.Exposure of the shaft rock wall
must be of a minimum in time and
height.
4.At the depths of more than 300
meters the freeze boreholes must
be not least than 3 meters away
from the shaft rock wall.

TEMPERATURE, STRESS AND STRAIN MEASUREMENTS DURING AND AFTER CONSTRUCTION OF CONCRETE LININGS IN FROZEN SANDSTONE

P.F.R. Altounyan   Dept. of Mining Engineering, Univ. of Newcastle upon Tyne
M.J. Bell   Shaft Sinking Branch, National Coal Board
I.W. Farmer   Dept. of Mining Engineering, Univ. of Newcastle upon Tyne
C.J. Happer   Selby Project, National Coal Board

ABSTRACT

Vibrating wire strain and temperature gauges and total stress cells and piezometers were installed in a 7.3m internal diameter concrete shaft lining at a depth of 232m in frozen saturated Bunter Sandstone. Observations of temperature changes during concrete hydration and stress changes during thawing of the icewall, led to the following main conclusions:

a) Rises in temperature during hydration of the cement in the concrete lining raised rock temperatures to a level where they would not affect hydration of the concrete at the rock-concrete interface.

b) Following thawing of the icewall, hydrostatic and total lining stresses were identical.

1. INTRODUCTION

When concrete shaft walls are cast against frozen strata during shaft construction, lining thicknesses are increased by 150mm (Auld, 1979; Weehuizen, 1959) to allow for incomplete hydration of the concrete in contact with the icewall. There is, however, no experimental evidence to justify the assumption that the temperature of the concrete adjacent to the icewall will be reduced during the initial stages of hydration to temperatures of around 4°C, where hydration is inhibited.

During sinking of shafts through frozen Bunter Sandstone in the Selby Coalfield, an opportunity arose to measure temperature in shaft linings and adjacent sidewalls at Whitemoor Mine. Instrumentation was designed and installed with the objective of measuring temperature variation in a nominal 600mm thick lining and at distances up to 1m into the frozen ground. In addition total stresses, strains and piezometric pressures were measured in the lining and at the lining/rock interface after placing of the lining and following the subsequent thaw.

2. STRATA AND SHAFT DETAILS

Whitemoor Mine shafts have a planned depth of 920m. The first 20m of shaft is through glacial drift overlying 260m of Bunter Sandstone. The remaining succession comprises Permian marls and limestones to 500m. These lie unconformably on the Middle Coal Measures. The surface level is 7m A.O.D. and the ground water level is approximately 10m below ground level. The Bunter Sandstone has high permeability and porosity. Packer permeability inflow borehole tests at an adjacent shaft site give permeability coefficients of:

Depth(m)	Permeability coefft. (m/s)	Estimated inflow to 10m shaft (1/m)
42.34- 52.03	5.01×10^{-6}	175
130.79-143.53	1.80×10^{-6}	205
200.94-210.63	2.10×10^{-6}	340

The average horizontal permeability coefficient of borehole specimens was 8.14×10^{-6} m/s and the average porosity

of borehole specimens was 34.4%. Other geotechnical average data from dry laboratory specimens were:

Uniaxial compressive strength 9.8 MN/m²
Uniaxial deformation modulus 5.5 GN/m²
Cohesion 2.8 MN/m²
Coefficient of internal friction 0.50
Dry unit weight 1.84 KN/m³
Specific gravity 2.67

Some tests were also carried out on frozen core specimens giving modified geotechnical data:

Uniaxial compressive strength 36.2 MN/m²
Uniaxial deformation modulus 7.5 GN/m²

During drilling of exploration boreholes there was low core recovery in the Bunter Sandstone, confirming the general picture of a weak high porosity sandstone in which the major part of the water flow was through the porespace. Selection of groundwater freezing to control water inflows and ensure side-wall strength at low depth was made at an early stage in the project. Detailed design of freezing is given by Wild and Forest (1981).

The shafts at Whitemoor Mine were 7.3m (24ft) internal diameter with nominal concrete design thickness of 0.6m, throughout the frozen zone. The specified concrete was 45 MN/m² sulphate resisting concrete to class 4 Building Research Establishment (U.K.) Digest 174.

3. INSTRUMENTATION

The basis of the instrumentation has been described by Altounyan (1982). It comprised vibrating wire temperature gauges, vibrating wire strain gauges and piezometers and stress cells with vibrating wire transducer outputs. These were multiplexed at source and monitored from the surface through a single shaft cable.

The general arrangement of the instrumentation layout at a depth of 232m is illustrated in Figure 1. At the level selected, overbreak had increased the lining thickness to an average of 950mm. Temperature gauges were installed at 90° intervals in the frozen rock and concrete. Boreholes were drilled 1.2m into the frozen rock and four temperature gauges mounted longitudinally in a p.v.c. tube were inserted so that the centre of the outer gauge was 50mm from the shaft sidewall. The other gauges were 320mm, 770mm and 1170mm

from the sidewall. The hole was initially filled with grease to ensure optimum conductivity. Three temperature gauges were installed directly into the concrete, mounted on a rebar attached to the shuttering and hanging rods. The gauges were positioned (see Table under Figure 1) centrally and as close as practicable to the surface, backwall and axis of the lining. Strain gauges were located at 60° intervals. These were cast in pre-cured concrete briquettes and located on the shuttering and backwall to measure inner and outer lining hoop strains. Mercury filled pressure cells were located at three of these locations at the rock-lining interface to measure total radial stresses. Piezometers were located in 500mm boreholes back-filled with bentonite pellets at the same locations to measure piezometric pressures.

4. RESULTS

The results can be grouped in three categories: the change in temperature during cement hydration in the setting concrete; the change in temperature of the saturated/frozen sandstone during natural and forced thawing after cessation of the freeze, and the increase in ground water pressure and associated lining stresses and strains during the thawing of the icewall.

Continuous temperature observations were taken for 37 days after casting of the lining. The thaw was started 13 days after casting of the lining.

Figure 2 shows typical temperature measurements in the lining and icewall from one array (gauges 8-13) of temperature gauges. These are reproduced as an isometric projection in Figure 3. The following points may be noted:

a) A maximum temperature of 50.0°C at gauge 13 near the centre of the lining and of 49.8°C at gauge 12, 290mm from the rock concrete inter-face, occurred 29 hours after pouring of the concrete. A peak temperature of 38.4°C at gauge 14 occurred 29 hours after pouring of the concrete.

b) The effect of the exothermic reaction due to hydration is to increase temperatures in the icewall to above freezing point. At gauge 11, 50mm into the rock an initial temperature of -1.1°C, initially relatively high, due to the presence of warm air in the excavation, was raised to 0°C after 12 hours and reached a peak
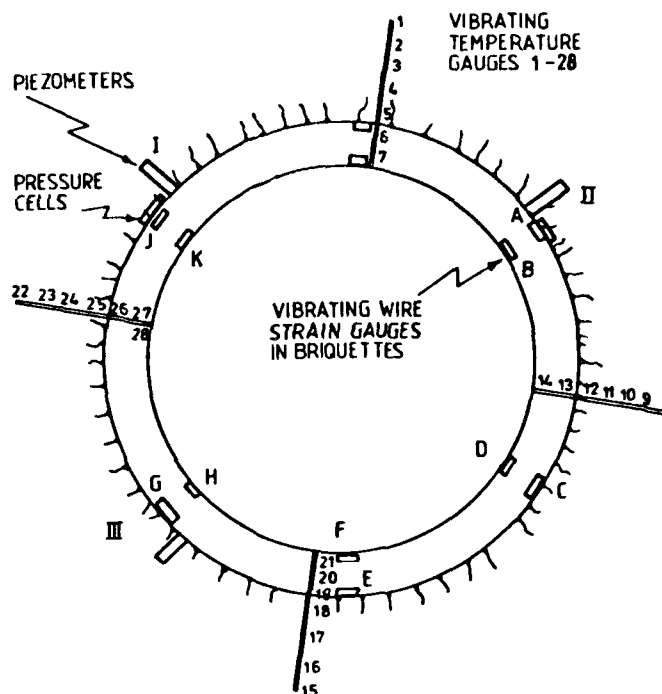
344

Figure 1. General layout of instrumentation around Whitemoor Mine No. 2 shaft at 232m in frozen Bunter Sandstone.

Position of temperature gauges

Gge No	Dist mm	Gge No	Dist mm	Gge No	Dist mm	Gge No	Dist mm	Gge No	Dist mm	Gge No	Dist mm	Gge No	Dist mm
7	115	6	340	5	555	4	790	3	1060	2	1510	1	1910
14	115	13	490	12	755	11	1095	10	1365	9	1815	8	2215
21	115	20	145	19	615	18	875	17	1145	16	1595	15	1995
28	110	27	465	26	770	25	925	24	1195	23	1645	22	2045

* Gauge Nos 4, 11, 18, 25 installed in the frozen ground 50mm from rock surface. Lining thicknesses, including overbreak, were 740mm at array 1-7; 1045m at 8-14; 825 at 15-21 and 875 at 22-28. Nominal shaft diameters were: inside 7320mm; outside 9090mm. Average freeze tube spacing was 687mm in a 1400mm diameter ring. Freeze tube steady state temperature was -30°C.
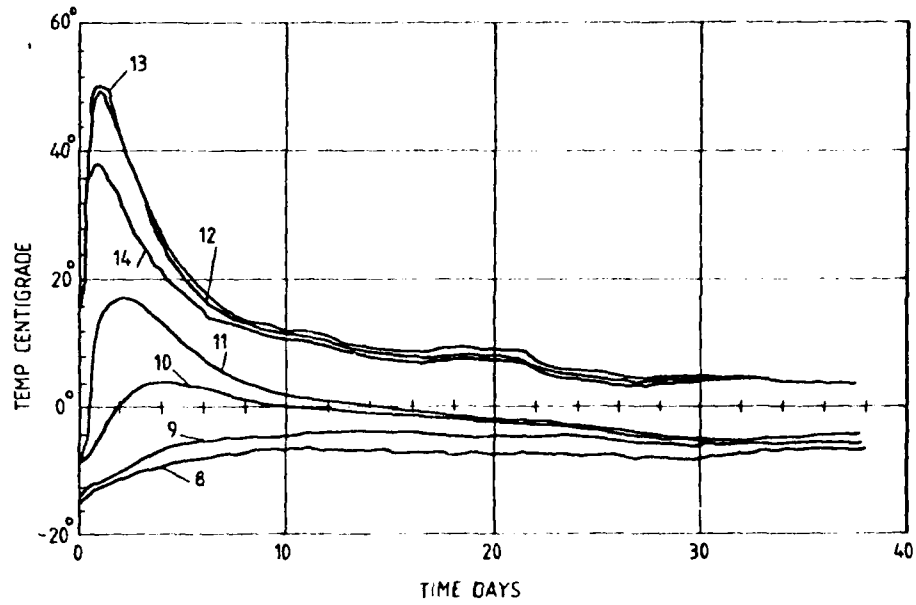
Figure 2. Change in temperature with time after pouring of concrete at gauges in array 8-14. Note position of gauges - 11, 50mm into icewall; 10, 320mm into icewall; 9, 720mm into incewall and 8, 1170mm into icewall. The concrete was 1045mm thick and gauge 12 was 290mm from the icewall; gauge 13 was 550mm from th_ icewall and 495mm from the shaft surface, and gauge 14, 115mm from the shaft surface.
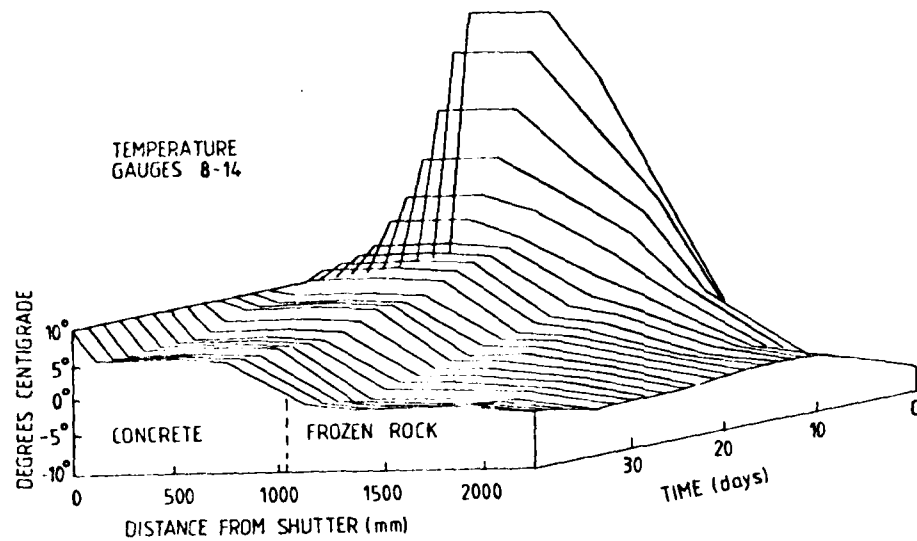

Figure 3. An isometric projection of the temperature profile with time through the shaft wall at array 8-14.

346

of 16.9°C after 54 hours. Gauge 10, 320mm into the rock recorded an initial temperature of -8.8°C, reached 0°C after 46 hours and a peak of 4.1°C after 98 hours.

c) Gauges 9 and 8, respectively 770mm and 1170mm into the rock recorded initial temperatures of -12.4°C and -14.2°C and although temperature rose significantly, it did not reach freezing point.

d) Gauge 11 did not monitor refreeze until 13 days after initial pouring of the concrete. None of the gauges in the concrete had recorded a temperature lower than 4°C when detailed observations ceased after 37 days.

Figure 4 plots change in temperature with time at the shaft wall/icewall interface, following cessation of freezing. Forced freezing started at -15°C and rose in stages to 0°C. The first major breach of the icewall occurred after 209 days (Table 1) and lining stresses - initially having a minor geostatic effective stress component - gradually rose to hydrostatic stress levels.

previous observations by Altounyan and Farmer (1981) of the very low strata disturbance caused by groundwater freezing.

ii) The lining strains can be shown to exactly relate to the hydrostatic stresses in accordance with Lame's theorem, and a computed deformation modulus of 33.6 GN/m² compares with the design modulus range for 45 MN/m² concrete of 27-38 GN/m².

CONCLUSIONS

a) The effect of the exothermic reaction during freezing was to increase temperatures in the icewall to above freezing. Gauges 50mm into the icewall did not monitor freezing point until 13-14 days after pouring of concrete. It may be concluded that the presence of the ice wall did not inhibit hydration of the concrete at the rock-lining interface.

b) Following thawing, total and hydrostatic stresses on the lining at the rock-lining interface were identical, indicating zero geostatic component of radial lining stress, and minimum

Table 1. Total stress and hydrostatic pressure readings.

Time after concrete pour(days)	Total stress-pressure cells (MN/m²)			Hydrostatic pressure-piezometers (MPa)		
	I	II	III	I	II	III
15	0.37	0.40	0.33	0	0	0
200	0.40	0.42	0.36	0.03	0.05	0.04
209	0.67	0.66	0.63	0.50	0.53	0.56
217	0.68	0.69	0.65	0.48	0.38	0.49
300	2.20	2.11	2.17	2.22	2.20	2.21

From data on total stress and hydrostatic pressures obtained from pressure cells and piezometers in Table 1, the following points may be noted:

i) There is a close correlation between piezometric and total stresses. The average piezometric stress for three gauges after 300 days was 2.21 MN/m². This compares with a theoretical piezometric pressure of 2.18 MN/m² if the ground water level is assumed 10m below ground surface. The average total stress is 2.16 MN/m², indicating zero contribution to lining stresses from the back-wall rock - even though this was a relatively weak rock. This confirms

disturbance of strata by groundwater freezing.

ACKNOWLEDGEMENTS

REFERENCES

ALTOUNYAN P.F.R. (1982) Measurement of stresses, strains and temperatures in concrete shaft linings. Proc

Symp. Strata Mechanics, Newcastle
upon Tyne, April 1982.

ALTOUNYAN P.F.R. and FARMER I.W. (1981)
    Tunnel lining pressures during
    groundwater freezing and thawing.
    Proc. 5th Rapid Exc. Tunn. Conf.,
    San Francisco, 784-800.

AULD F.A. (1979) Design of concrete shaft
    linings. Proc. Inst. Civ. Engrs.
    Pt. 2 Res. & Theory, 67, 817-832.

WEEHUIZEN J.M. (1959) New shafts of the
    Dutch State Mines. Proc. Symp.
    Shaft Sinking & Tunnelling. London
    Inst. Min. Eng.

WILD W.M. & FORREST W. (1981) Application
    of the freezing process to ten shafts
    and two drifts at the Selby project.
    Mining Engineer, 140, 895-904.
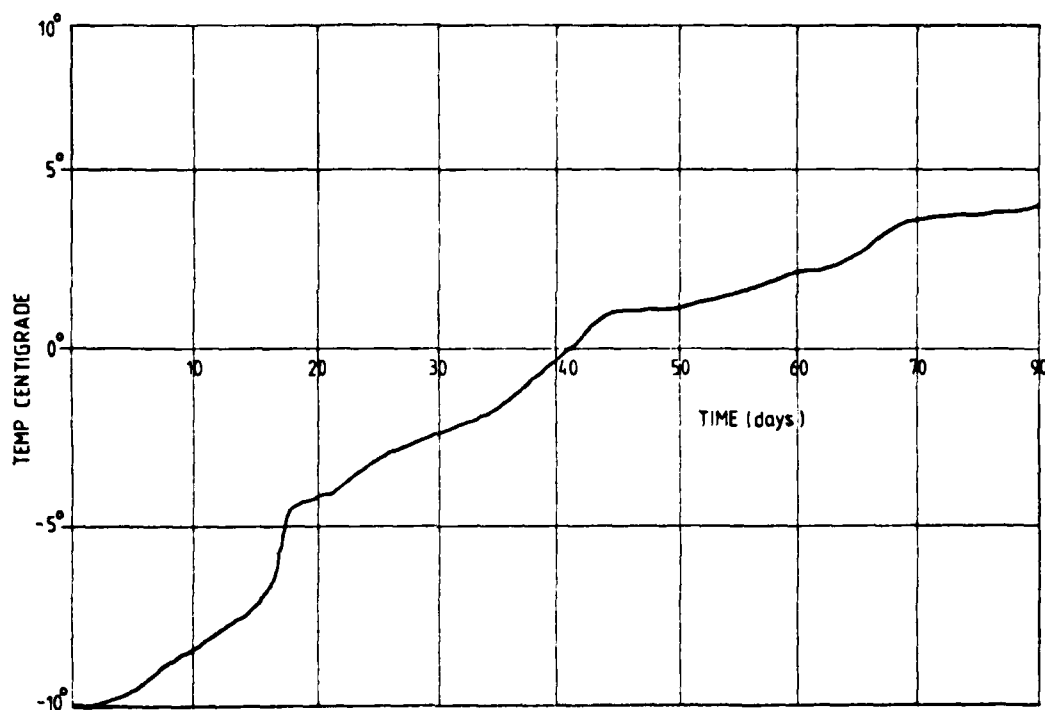
Figure 4.   Change in temperature with time at the shaftwall-rock interface during
thawing of the icewall. (Zero time is equivalent to 40 days on Figure 1)

348

INTERACTION OF FROZEN SOILS WITH WELLS AND PIPELINES

M.M. Dubina   Institute of
Physical and Technical Pro-
blems of the North, the USSR
Academy of Sciences, Yakutsk

A BSTRACT

When designing reliable st-
ructures of the wells bored in
permafrost, it is necessary to
make use of some calculation me-
thods to estimate the mechani-
cal effects of thermal interac-
tion between these structures
and surrounding frozen soil. In
this paper irreversible strain
manifestation in permafrost near
uncased well during ground de-
frostation and thawing produced
by the heat release within the
hole is considered. Correspon-
ding mechanical problem solu-
tion is used to estimate the ge-
ometrical parameters of wellbore
wall forming during this process.
Then relations for calculation
of the freeze-back pressures
both at freezing of the water
bear masses outside of a string
set and at its congelation wi-
thin the interstring space are
suggested. The calculation mo-
dels are established according
to the methods of the theory of
plasticity and those of visco-
elasticity. As a result, some
calculation formulae of rock
stability parameters and those
of casing string loading for the
case of permafrost thawing aro-
und the wellbore and at its
freeze-back have been obtained.

INTRODUCTION

Heat release within the
well during its drilling in per-
mafrost results in defrostation
and thawing of the latter. The
strength of defrosted and thawed
rock is less than that of frozen
one. Clearly, with the extension
of defrosted and thawed zone
near the well the rock pressure
influence is growing and leads
to a loss of soil stability in
the walls of uncased wellbore and
to emergence of some supplementa-
ry loads affecting the string set
when the well is cased. This
rock stability loss in the well-
bore walls contributes to the
cavern formation which represents
sources of further complicati-
ons during casing and exploita-
tion of the wellbore. As an
example of such a complication,
we can take the cased string
squashing due to the freeze-back
pressure. As known [1], such a
pressure may form both at water
bear mass freezing within the
caverns when the well structure
is loaded from the outside (ex-
ternal freezing), and at its
freezing in the intercolumn
space (internal or interstring
freezing).

The problem of stress re-
distribution at rock defrosta-
tion along the hole, as well as
that of its freeze-back, are
considered there for the axially
symmetric plane strain case. The
particularity of these problems

consists of the presence of moving boundaries characterizing a discontinuity of the physical-mechanical medium properties of its density and of mechanical state equation parameters or a change of state equation type. This feature is explained by the existence of frozen, thawed and freezing material zones near the wellbore.

Let us take the axis line of the wellbore as the symmetry axis z tied to a rock bulk coordinate system with a radial component r and a tangential one φ. In accordance with the axial symmetry and plane strain condition, the displacement vector has only one component u which is not equal to zero in the radial direction. The strain tensor components in the radial $\mathcal{E}_r$ and tangential $\mathcal{E}_\varphi$ directions are tied with the stress tensor components $\mathfrak{G}_r$, $\mathfrak{G}_\varphi$ and $\mathfrak{G}_z$ by Henky's relations implying the volumetric deformation at the phase change with a linear coefficient α which, in the general case, is a function of the radius r [2]. The stress and strain tensor components of these relations satisfy the equilibrium and compatibility equations, the mechanical state equation and the Cauchy relations connecting together strain and displacement.

The state equation mentioned is used here in three forms. Firstly, in the form of linear relationship between stresses and strains (Hooke's law) for the elastic stage of deformation. Secondly, the plasticity state of the medium is described by the Coulomb-Mohr equation [3]:

$$\mathfrak{G}_{max} = \mathfrak{G}_{min} N_i^t + 2 c_i N_i ,\qquad (1)$$

where $\mathfrak{G}_{max} = max\{\mathfrak{G}_r, \mathfrak{G}_\varphi, \mathfrak{G}_z\}$, $\mathfrak{G}_{min} = min\{\mathfrak{G}_r, \mathfrak{G}_\varphi, \mathfrak{G}_z\}$; $N_i = tg(\gamma_i/2 + \pi/4)$; γ_i is the rock internal friction angle; c_i is the rock cohesion; $i := m$ is the thawed or inferior strength zone; $i := b$ is the zone that became frozen due to the process considered, $i := f$ is the unmelted permafrost zone. This zone notation is valid throughout the material exposed. Thirdly, the rheological effects of rock deformation will be considered from the point of

view of the linear theory of viscoelasticity by means of the state equation

$$\mathfrak{G}_{\varphi\varphi} = 2 G_i [\mathcal{E}_{\varphi\varphi} - \int_{t_*(r)}^{t} R_i(t, \tau) \mathcal{E}_{\varphi\varphi}(\tau) d\tau], \qquad (2)$$

where $\mathfrak{G}_{\varphi\varphi}$ and $\mathcal{E}_{\varphi\varphi}$ are, respectively, stress and strain tensor components; $R_i(t, \tau)$ is the relaxation core; t is the process time; $t_*(r)$ is the phase change moment at the medium point with the coordinate r; and $G_i = E_i / [2(1 + \nu_i)]$, where G_i, E_i, ν_i are, respectively, the shear modulus, the Young's modulus and the Poisson's ratio. The index i in (1), (2) and further denotes a medium deformation zone.

In the problems investigated the radial component of stress tensor $\mathfrak{G}_r$ and that of displacement vector u are assumed as continuous on the all discontinuity boundaries of state equations and their parameters. At the elastic-plastic deformation interface we satisfy the continuity conditions of such a transition according to [2].

WELLBORE WALLS STABILITY

The permafrost defrostation and thawing process results in the formation around the wellbore with the radius a of the inferior rock strength zone of the radius $S(t)$. Physical-mechanical parameters of the latter $r < S$ differ from those of the unmelted permafrost that occupies the region $r > s$. The rock pressure and hydrostatic pressure action, respectively, $\gamma_r h$ and $\gamma_w h$, provokes the stress concentration growth with the increase of the well depth h. At the depth h_a, the rocks of the inferior strength are subjected to the irreversible deformation accordingly with the condition (1). With the depth growth and at the constant radius value of inferior rock strength zone ($S = const$), the radius of rock plastic deformation zone, R_p increases from the value of $R_p = a$ for $h = h_a$ up to $R_p = S$ for $h = h_m > h_a$ and at the depth $h_w > h_m$ it is the unmelted permafrost that

350

starts to deform irreversibly ($R_p > S$ for $h > h_{sf}$). The rocks that have attained the irreversible deformation state offer the inferior stability and, under unfavorable conditions, can cave in the uncased well. Then, in some approximation, h_a can be interpreted as a depth of possible cavern formation and R_p as their radius R_k. This approach to the cavern formation differs from some author's suggestions where R_k is assumed to be equal to the radius of thawed zone.

The total of the above-mentioned relations and conditions on the region boundaries brings to an equation system which, for the case $a \leqslant R_p \leqslant S$, can be reduced to the equation for R_p taken as a function of h

$$\delta_f h \frac{2C_m N_m}{N_m^2-1} - \left(\frac{2C_m N_m}{N_m^2-1} - \delta_w h\right)\left(\frac{R_p}{a}\right)^{\frac{1}{N_m^2}-1}\left[1+\frac{1-N_m^2}{2N_m^2}\left(1-\frac{C_f}{S^2}\left(1-\frac{E_f}{E_m}\right)\right)\right] \quad (3)$$

and to the formula for determination of the wellbore wall displacement

$$u_a = \frac{3R_p^3(1-N_m^2)}{4E_m N_m^2 a^2}\left(\frac{2C_m N_m}{N_m^2-1} - \delta_f h\right), \quad (4)$$

where δ_f and δ_w are, respectively, the specific weights of frozen soil and fluid within the wellbore.

For the case when $R_p \geqslant S$ the solution of the original system leads to the following formulae for calculating R_p and u_a :

$$\frac{2N_f^2}{N_f^2+1}\left(\frac{2C_f N_f}{N_f^2-1} - \delta_f\right)\left(\frac{R_p}{S}\right)^{\frac{1}{N_f^2}-1} = \frac{2C_f N_f}{N_f^2-1} - \frac{2C_m N_m}{N_m^2-1} +$$
$$+\left(\frac{2C_m N_m}{N_m^2-1} - \delta_w h\right)\left(\frac{S}{a}\right)^{\frac{1}{N_m^2}-1}, \quad (5)$$

$$u_a = \frac{3R_p^3(1-N_f^2)}{4E_f a^2 N_f^2}\left[\frac{2C_f N_f}{N_f^2-1} - \frac{2C_m N_m}{N_m^2-1} +\right.$$
$$+\left.\left(\frac{2C_m N_m}{N_m^2-1} - \delta_w h\right)\left(\frac{S}{a}\right)^{\frac{1}{N_m^2}-1}\right]\left(\frac{a}{S}\right)^{\frac{1}{N_m^2}-1}. \quad (6)$$

Expressions for h_a, h_{sm} and h_{sf} can be easily found from (3) and (5), assuming that $R_p = a$ and $R_p = S$. The given here relations are published in [4]. The calculations show the increase of the radius R_p with the growth of h having the plot convexity directed to the well axis and the augmentation of h_a, h_{sm}, h_{sf} with the rock strength.

EXTERNAL FREEZE-BACK

Elastic-plastic model

Mathematical models of the freeze-back have been examined in [1, 5,6,9,10]. Those publications however did not deal with the analysis of the possible existence of external pressure maximum, P_m which is independent of the initial radius of freeze-back boundary S_o. The existence of the quantity P_m follows from the given in [6-8] diagrams of the experiment carried out in the real wellbore conditions. In [10], for assessment of the external freeze back contribution to the total load affecting the casing strings from the frozen rocks, an elastic-plastic process model is taken, not allowing for the rock pressure contribution. In accordance with [10], the value of pressure P at the frozen rock plastic deformation for $N_l = 1$, $\lambda_m = 0$ and $d = const$, can be determined by the formula

$$P = q_f\left\{1 + \ln\left[\frac{E_f d}{q_f}\left(1-\frac{S^2}{S_o^2}\right)\right]\right\}, \quad (7)$$

where λ_n is the effective coefficient of set string elastic compliance, q_f is the frozen rock shear yield stress, the formula (7) being valid for $R_p > S_o$ that is possible when $P > q_f$. From the problem solution the pressure is equal to q_f when R_p reaches the boundary S_o. According to the evidence available in the literature on the question, the quantity q_f is not sufficient to squash the casing strings, so that prior to creation of the squash threatening load level the frozen rocks are subjected to plastic deformation and the freeze-back pressures can be calculated from the formula (7).

For calculating P_m from (7) we have at $S_o \gg S$

$$P_m = q_f\left(1 + \ln\frac{E_f d}{q_f}\right), \quad (8)$$

where there are no geometric parameters of the problem, but P_m to be a parameter of the medium mechanical reaction on the external freeze-back process. As to the values of mechanical parameters of the problem, taken as

given in [6-8], the difference between the values of P_m calculated from (8) and those measured by the mentioned paper authors is about 20% with the trend of the calculated values excess over the measured ones. Also note that the maximum pressure calculation with the help of (8) should be made for q_f and E_f taken at the corresponding frozen rock temperature T_f . Pressure values obtained on the basis of the model suggested are less than those determined from the ice melting phase diagram known as the Bridgeman's dependence in the limits of $0°C > T_f > -22°C$ [11].

Viscoelastic model

If using the rock state equations that do not include the parameter of time, then, the maximum pressure P_m represents the asymptote for the case of the unconfined growth of the initial freezing zone radius. When allowing for the rheological effects of rock deformation, the external freeze-back pressures can have the extremums not only on the freezing time interval boundaries, but within them. This can be shown analytically [12] .

Using the state equation (2) and the described solution procedure for determining the external freeze-back pressures at $\lambda_n = 0$, $\alpha = const$ and those of liquid-like thawed zone, we find the formula

$$P=3\alpha\left\{\left(1-\frac{S^2}{S_o^2}\right)(G_f-G_R)-\int_o^t\left(1-\frac{S^2(\tau)}{S_o^2}\right)\left[G_fR_f(t\cdot\tau)-G_RR_R(t\tau)\right]d\tau\right\}(9)$$

Considering an example of viscoelastic model of the medium in the form of the "Maxwell body", then, from the condition of existence of the pressure extremum $dP/dt = 0$ at the maximum pressure formation time moment t_m , we find the equation

$$\frac{E_f\tau_{Rf}}{E_f\tau_{Rf}}\left(\frac{S_o}{\tau_{Rf}}+U\right)e^{-\frac{t_m}{\tau_{Rf}}}-\left(\frac{S_o}{\tau_{Rf}}+U\right)e^{-\frac{t_m}{\tau_{Rf}}}=U\left(\frac{E_f\tau_{Rf}}{E_f\tau_{Rf}}-1\right),(10)$$

where τ_{Ri} is the relaxation time; U is the constant freezing boundary propagation rate for the linear relationship $S(t) = S_o - Ut$, the reliabi-

lity of which for this problem being shown in [8].

From (10), for $\tau_{Rs} = \tau_{Rf} = \tau_R$ it follows that

$$S_o = S(t_m) + U\tau_R ln\left(1+\frac{S_o}{U\tau_R}\right) . \qquad (11)$$

This formula proves the existence of the maximum P_m in that particular case of the relaxation time equality in the unmelted frozen zone and in the refrozen one. In the general case, the pressure maximum may not occur within the freezing time interval. This depends upon a definite relation of geometric elastic and rheological region deformation parameters and upon the process time defined from the solution of a corresponding heat-transfer problem. The methods of heat-transfer problem solution are available in [9, 13].

INTERSTRING FREEZE-BACK

The computer is the most convenient tool for calculating a multistring well structure in the case of the possible water bear mass freezing in any interstring space. Here we take the simpliest case of the calculation formula for the interstring pressures P in the two-string well structure loaded by the pressure P^- acting from the inside of the internal string, by the hydrostatic interstring pressure P_H and by the external pressure P^+ which may contain the external freeze-back pressures considered in the previous item. According to [14], for the hydrostatic stress distribution, the interstring pressures can be defined as

$$P=P_H+\left[3\alpha\left(1-\frac{S^2}{a_{ci}^2}\right)+\frac{2\lambda_{cz}P^+}{a_{cz}}\left(1+\frac{a_{ci}\lambda_{oi}P^-}{a_{cz}\lambda_{cz}P^+}\right)\right]/\left\{\frac{2\lambda_{cz}}{a_{cz}}\left(1+\frac{a_{ci}\lambda_{ci}}{a_{cz}\lambda_{cz}}\right)+\frac{S^2}{a_{cz}^2K_f}\left[\left(1-\frac{a_{cz}^2}{S^2}\right)\frac{K_f}{K_m}+\frac{a_{cz}^2}{S^2}-1\right]\right\},(12)$$

where $\lambda_{cj} = a_{cj}^2/(E_{cj}\delta_{cj})$; $a_{cj}, \delta_{cj}, E_{cj}$ are, respectively, the radius, thickness and the elasticity modulus of the strings; $j = 1$ is the internal string, $j = 2$ is the external string; K_m and K_f are, respectively, the volumetric elasticity modulus of thawed and frozen phases of the freezing water bear mass. The calculati-

ons show that in contrast to the external freeze-back pressures the internal ones are able to attain the equilibrium pressure values defined from the ice melting phase diagram. This is due to the greater rigidity of freezing mass confining strings in contrast to the rock mechanical properties. So, the interstring freezing is more dangerous than the outerstring one.

PRACTICAL APPLICATION OF THE THEORY

The suggested results together with corresponding drilling and exploitation of wellbores interval heat-transfer problems solutions [9,13] , make it possible to predict parameters of cavern formation in the frozen rocks and string squashing by the freeze-back pressures. Besides, this approach permits to calculate some precautions against squashing. Regarding in (7) P as equal to the external squashing pressure for the case of full freezing (S coincides with the outer radius of the external string), it is possible to find the corresponding value of S_0 from which, with the help of the solutions of problems concerning cavern formation and thawing caused by drilling, it is not difficult to determine the change limits of the controllable drilling parameters. If the controllable drilling is impossible, then, from (7) and the solution of heat-transfer problem we can find a permissible idle time, when heat release into surrounding frozen rocks is absent. The formulae (8)-(11) can be used when designing the well structure able to withstand the maximum freeze-back pressures, noting that the physical-mechanical rock parameters entering these formulae are regional characteristics for any particular wellbore. The expression (12) together with the heat-and-mass transfer problem solution can be used both for the calculation of the permissible idle time and for the determination of the permissible characteristics of freezing water bear mass and of structural well features.

REFERENCES

1. Griaznov G.S. Particularities of the well deep drilling in permafrost regions. Moscow, "Nedra", 1969, 168p.

2. Kachanov L.M. Foundations of the plasticity theory. Moscow, "Nauka", 1969, 420p.

3. Harr M.E. Principles of the theoretical mechanics of soils. Publ. house on Building, 1971, 320p.

4. Dubina M.M. Limit equilibrium of the thawing well walls in permafrost. -In: Transfer processes in the deformable disperse media. Yakutsk, 1980, pp.89-95.

5. Shalavin A.M., Andrienko L.V. External efforts affecting the casing string during well exploitation in permafrost conditions (external pressure). "Izvestia vuzov. Neft' i gaz", 1978, No 4, pp.17-20.

6. Goodman M.A. and Wood D.B. A mechanical model for permafrost freeze-back pressure behaviour. SPEJ, vol.15, No 4, Aug.1975, pp.287-301.

7. Perkins T.K., Rochan J.A. and Knowles C.R. Studies of pressure generated upon refreezing of thawed permafrost around wellbore. -JPT, Oct. 1974, pp. 1159-1161. Trans. AIME, 257.

8. Goodman M.A. and Wood D.B. Permafrost freeze-back pressure behaviour. -JPT Forum, JPT, Aug., 1975, pp.949-950.

9. Dubina M.M., Krasovitsky B.A., Lozovsky A.S., Popov F.S. Thermal and mechanical interaction between engineering structures and permafrost. Novosibirsk, "Nauka", 1977, 149p.

10. Dubina M.M. Elastic-plastic deformations induced by the refreezing of thawed rock bulk around the wellbore. -In: Continuum mechanics methods. Yakutsk, 1977, pp.80-87.

11. Tsytovich N.A. The mechanics of frozen soils, Moscow, "Vysshaya shkola", 1973, 446p.

12. Dubina M.M. Plane viscoelastic problem concerning the axially symmetric refreezing. -In: Transfer processes in the deformable disperse media. Yakutsk, 1980, pp.84-88.

13. Bondarev E.A., Krasovitsky B.A. Temperature condition of oil and gas wells. Novosibirsk, "Nauka", 1974, 87p.

14. Dubina M.M. Estimates as to the danger of natural temperature field disturbance around the cylindrical structures in permafrost. -In: Heat protection of engineering structures and communications in the Far North. Yakutsk, 1980, pp.110-125.

STUDY OF THE FREEZING PRESSURE ACTING ON A SHAFT LINING

Chou Wanxi, Associate Pro-
            fessor, Huainan
            Mining College,
            PRC

The carboniferous layer in
Panji coal mining district is
almost completely covered by water-
bearing overburdens of varying
thickness. The total thickness of
soil overburdens is more than
200 m.

For the sinking of shafts
through this overburden the freez-
ing method is employed. The rein-
forced concrete lining has been
applied in Panji shafts.

It is found that freezing
pressure augments with the increase
of depth of the soil, the distri-
bution of which being uneven. The
freezing pressure resulting from
the deformation of the freezing
wall is likely to give rise to
the breaking of the reinforced
concrete lining.

The freezing pressure is
measured in several shafts. The
behaviour of the freezing pressure
is described and calculation me-
thod is proposed for stress

analysis of the shaft lining under
non-uniform freezing pressure.

Freezing Pressure in General

A freezing wall, cylindrical in shape, is artificially formed by freezing and frozen soil prior to the shaft sinking operation. Sinking process may be carried out safely within the wall without danger of influx of underground water. The freezing wall resists both water pressure and ground pressure applied by the water-bearing soil outside, ensures a temporary stabilization of the shaft site during the sinking operation and prevents the freezing tubes from being horizontally displaced too much from their initial positions.

The freezing pressure is the pressure of the freezing wall acting upon the shaft. How does this freezing pressure come about? About the cause of the freezing pressure there raged for many years a great controversy. However, it has generally been accepted that a relatively practical approach to this question would seem to be:

1. Prior to the formation of the freezing wall, the soil has already been under some kind of stress, the initial stress. After the freezing wall has been formed, an additional stress, the temperature stress, results under the action of the temperature field.

From this it follows that the stress on every point is an overlap of these two stresses. In other words, prior to the excavation of the shaft, the freezing wall has accumulated a great amount of energy; and, as soon as sinking operation begins, this energy tends to release, thereby resulting in a pressure acting on the shaft -- the freezing pressure.

Considering that the initial stress is related to both the depth and the physico-mechanical behaviour of the soil layers, and that the temperature stress is related to temperature, it is inferred that the freezing pressure is not only a function of temperature but also a function of both the depth and the physico-mechanical behaviours of the soil. Accordingly, the actual freezing pressure varies with the depth of the soil.

Let P_f stand for the freezing pressure, P_s for the initial stress of the soil, and P_t for the temperature stress, we have

$$P_s = \gamma H K \qquad \cdots (1)$$

where γ represents the average volume of the overlying soil; H the depth of the soil; and K the horizontal thrust coefficient of the soil.

$$P_t = \mu t_o \qquad \cdots (2)$$

where t_o represents the average temperature of the frozen soil; and μ the temperature stress coefficient which means an increment of the frozen soil stress for every $1^\circ C$ increase of the average temperature of the soil. According to our definition, therefore, we obtain

$$P_f = P_s + P_t \qquad \cdots (3)$$

or

$$P_f = \gamma H K + \mu t_o \qquad \cdots (4)$$

For sandy loam, we may put K= 0.4--0.6; for sand layer, K=0.4--0.6; for sandy clay, K=0.4--0.5; for sandy gravel, K=0.4--0.6. The temperature stress coefficient may be determined in this way: for sandy loam, μ=0.2--0.4; for sand layer, μ=0.1--0.2; for sandy clay, μ=0.4--0.5; for clay layer, μ=0.4--0.6; for sandy gravel, μ=0.

Not only can the formulae listed above be used to explain the ground pressure found during the shaft sinking operation by the freezing process, but they can also be used to estimate the freezing pressure which will be of value for shafts to be designed and sunk by the freezing process.

The freezing wall may be viewed as an elastoplastic mass which is in a plastic state under the action of the ground pressure and the water pressure from the outside, and whose deformation, under the stress of the frozen soil, develops as time goes by. This has been sufficiently proved by physicomechanical tests made on the behaviours of the frozen soil. Figure 1 shows the creep curves of the frozen soil. Obvious creep deformation can be seen before lining operation; and, after lining has been completed, this kind of deformation is retarded, thereby a freezing pressure acting on the lining occurs. This explanation for the freezing pressure is
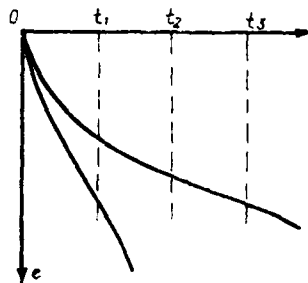
Figure 1 Rheological curves
for frozen soils

Figure 2. Freezing ground failure,
about a shaft

convincingly practical.

It would be lopsided to regard the freezing pressure merely as a frost-heaving force. Nor would it be all-sided to think of the frost-heaving force resulting from re-freezing (i.e., freezing again after thawing) as primary and decisive.

A Preliminary Analysis on the Anomaly in Freezing Pressure

Normally, freezing pressure has been found to behave like this: beginning with a sharp rise, followed by a stable stage, and ending with or without fall as temperature increases. Sometimes, however, during the transition from a sharp rise to the stable stage, as well as in the stable stage, there has been observed an abrupt rise followed by a fall in readings shown on some or all of the pressure gauges embedded at a certain observation level. This 'jump' has been directly related to change in soil state, upon which we speculate as follows:

1. The frozen soil about the shaft site wall, under the action of freezing wall's weight, the water and ground pressure from the outside, and the temperature stress, tends to transit to a plastic state. Spiral-shaped fissures form between the shaft lining and the freezing circle when these fissures cross each other and form cone-shaped slides as shown in Figure 2, a 'jump' in freezing pressure in a certain locality will result. After

these cone-shaped slides have been out of balance, the energy within the frozen soil is capable of self-adjusting back to its original value, that is, the freezing pressure will return to its stable stage, as shown in the pressure curve 3-1 in Figure 3.

2. A 'jump' in the freezing pressure has also been observed on longitudinal view at a certain observation level, which can also be explained as a 'jump' in the freezing pressure. In this case, however, the fissure in the frozen soil are inclined, forming a ring of conic cross-section round the shaft lining as shown in Figure 4. If, as is often the case, the ring moves inwards, a 'jump' in the freezing pressure will result on all the pressure gauges at a certain observation level, as can be seen from the abrupt rise and fall in the three pressure curves shown in Figure 5.

The Effect of Stress-Relieving Slots

During the sinking of Southern Air Shaft by the freezing process, as many as twelve stress relieving slots were excavated in order to
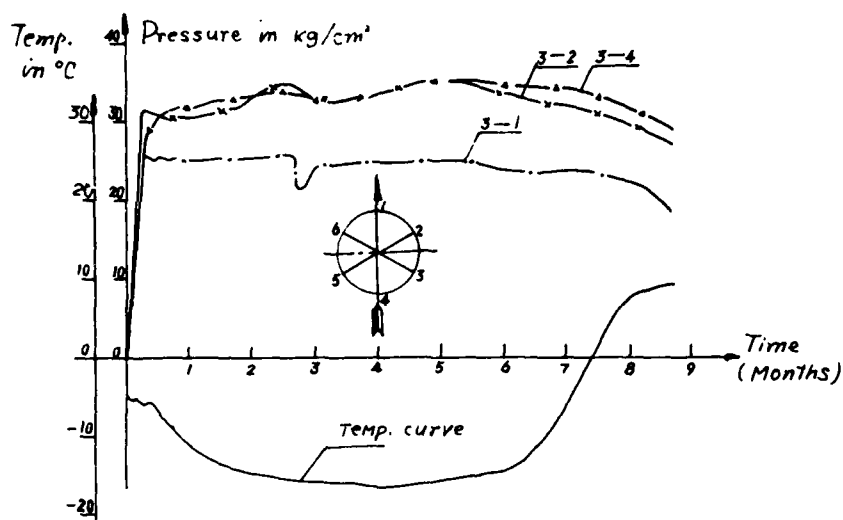
Figur 3. Radial Soil Pressure and Soil Temperature at the 185 M Depth in Southern Air Shaft
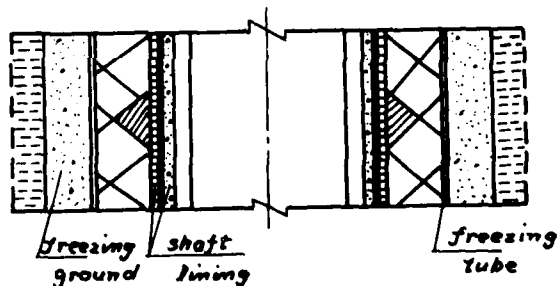

Figure 4 Freezing ground failure

decrease the freezing pressure of the calcareous clay layers. The sectional area of the slots is 200x300 mm². In order to determine whether these slots can play a role in stress relieving, load cells were embedded at a distance of 30 centimetres from the slots. Results of freezing pressure mea-surements showed that the freezing pressure of the consolidated clay layer at the 130 m observation level round the Southern Air Shaft was not lower than that of the similar layer round the East Air Shaft which is 882 m away but where no pressure-relieving slots have been excavated. It is there-

358
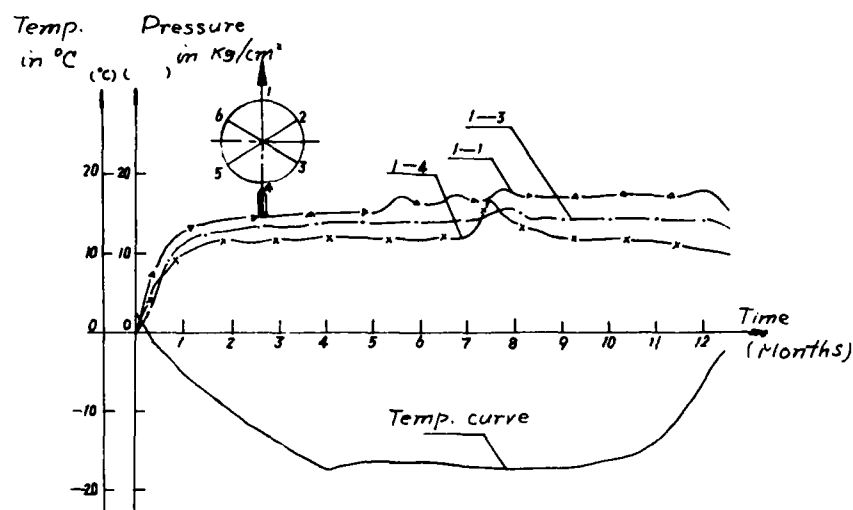
Figure 5. Relation between Freezing Pressure and Ground
Temperature at a Depth of 105 M, Southern
Air Shaft.

fore doubtful whether such pressure-relieving slots will work.

The Function of Temporary Masonry Lining

Field measurements have shown that the temperature of the temporary masonry lining is much lower that that of the concrete lining. For the former the temperature recorded in the initial stage after embedding the load cell ranges from −4.2°C to +6.8°C. Whereas for the latter the temperature recorded an average of +40°C. Weighing one case against the other, it has been found that the masonry lining is advantageous in that it can protect the concrete lining from freezing. However, because of the limited strength of the masonry brickwork it is necessary to pour the concrete in time beside the layers where the freezing pressure is relatively great so as to protect the brickwork from being broken or squeezed out. On the other hand, owing to its

brickwork structure, the masonry lining will transmit the stresses it has to bear, very rapidly, to the outer concrete lining.

Take for an example, on the seventh day after the Southern Air Shaft had been sunk through the consolidated clay layer 170 m below the surface, the freezing pressure recorded was as high as 17–29.6 kg/cm^2; correspondingly, the stresses upon the reinforcing bars within the outer reinforced concrete lining were 525–1,045 kg/cm^2. By contrast, at the Eastern Air Shaft which had been built without any temporary masonry lining, the stresses upon the reinforcing bars within the outer reinforced concrete lining were extensively found to be as high as 1,000–1,600 kg/cm^2, other things being equal. This testifies to the fact that the masonry lining plays some role in reducing the internal stress of the outer reinforced concrete lining.

Notwithstanding, there arises another problem that the increase

359

Table 1. Results of in situ measurement at Eastern Air Shaft

Observation level's NO.	Depth of soil (M)	Soil type	P_{max} (kg/cm²)	P_{min} (kg/cm²)	$\omega = (P_{max}-P_{min})/P_{min}$	Months after lining operation
1	40	sand	1.5	0.4	2.75	10
2	70	sand	9.8	6.1	0.5	17
3	110	sand loam	20.7	16	0.29	8
4	137	clay	24.2	17.4	0.36	3
5	170	sand loam	28.8	22.1	0.3	2
6	220	sand	/	/	/	/
7	278	gravel	32.0	19.7	0.6	6

in the strength of concrete with the passage of time is still lagging behind the rapid rise of the freezing pressure. In order to reduce the internal stress of the outer reinforced concrete lining, it is necessary to lengthen properly the time interval between masonry lining operation and concrete lining operation. To be more specific, if the outer reinforced concrete lining work begins at such a time when the freezing pressure have reached their peak values and thus remain stable, that is, after two or three cycles of the masonry lining have been completed (according to our present speed of shaft sinking operations), then the internal stress of the outer reinforced concrete lining will be minimized eventually.

Non-Uniform Freezing Pressure

Nonhomogeneity of soil, inclination of freezing tubes and non-uniform thickness of freezing wall result in non-uniform freezing pressure and non-uniform stresses upon the reinforcing bars of the reinforced concrete lining and non-uniform temperature around the shaft site wall.

Figure 6 shows the relation between the freezing pressure and soil temperature and also shows the non-uniform distribution of the outer load. Figure 7 shows the curves of the reinforcing bars' stress at the same observation level.

Let P_{max} stand for the maximum freezing pressure at one observation level; P_{min} for the minimum freezing pressure at the same level, for the non-uniformity ratio of external pressure; and $\omega = (P_{max}-P_{min})/P_{min}$. Table 1 shows certain results of in situ measurement and non-uniformity ratio of freezing pressure at the Eastern Air Shaft.

It is found that non-uniformity ratio varies with the type of soil. Freezing pressure at sand or gravel layers is more non-uniform than that at clay and sand loam layers.

Stress Analysis of Shaft Lining under the Action of Non-uniform External Ground Pressure

The distribution of non-uniform ground pressure around a shaft is most frequently specified in the form as shown in Figure 8. Ground pressure is broken down into two components: a uniform pressure
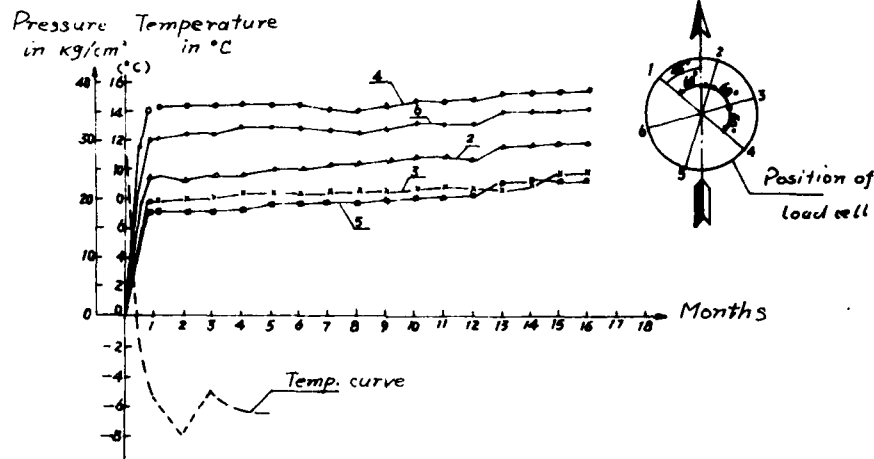
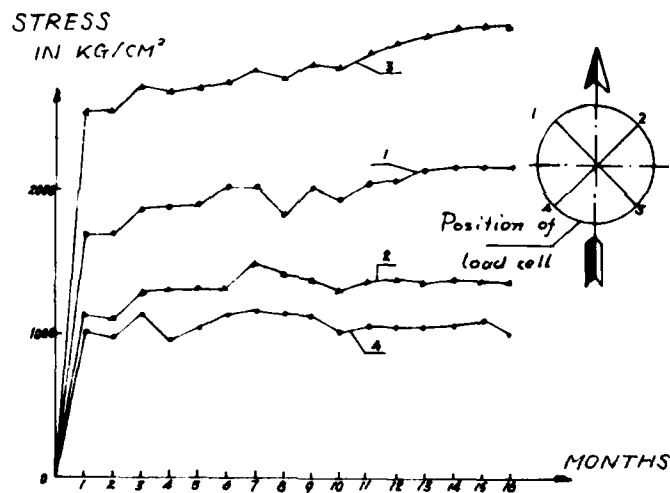Figure 6. Relation between soil pressure and soil temperature

Figure 7. Curves of reinforcing bars's stresses

over the whole lining and a non-uniform component which varies from zero to a maximum in each quadrant.

The ground pressure P at any point on the lining can be determined as follows:

$$P = P_o + \frac{P_1}{2} (1 + \cos 2\theta) \quad \cdots \cdots (3)$$

where:

P = external pressure acting at any point on the lining
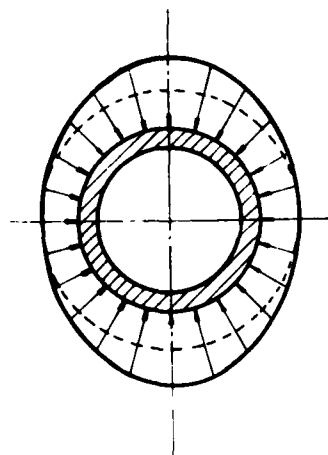
P_o = uniform external pressure component

361

Figure 8 Unequal load on shaft lining

a   denotes internal radius of
    the lining
b   denotes external radius of
    the lining

References

(1) N.A. Tsytovich The Mechan-
ics of Frozen Ground, McGrow-Hill
Book Company
(2) Chou Wanxi Report on in
Situ Measurement of Ground Pressure
at the Southern Air Shaft of No.2
Panji Colliery, Proceeding of
Huainan Mining College, No.1, 1981
(3) Chou. et al. Engineering
Handbook of Mining Construction,
Chinese Coal Mining Book Company, 1980

P_1 = non-uniform external pres-
    sure component
= angle measured from major
  pressure axes

The stresses at any point on
the circular lining is determined
by formulae based on elastic theory.

$$\sigma_r = \frac{P_1}{2}\frac{b^2}{b^2-a^2}\left[1-a^2r^{-2}+\frac{1}{(b^2-a^2)^2}\left\{b^4+b^2a^2+2a^4\right.\right.$$
$$-2a^2(2b^4+b^2a^2+a^4)r^{-2}$$
$$\left.\left.+b^2a^4(3b^2+a^2)r^{-4}\right\}\cos2\theta\right]$$
$$+P_0\frac{b^2}{b^2-a^2}(1-a^2r^{-2})$$

$$\sigma_\theta = \frac{P_1}{2}\frac{b^2}{b^2-a^2}\left[1+a^2r^{-2}+\frac{1}{(b^2-a^2)^2}\left\{2(\ ^2+3a^2)r^2\right.\right.$$
$$-(b^4+b^2a^2+2a^4)-b^2a^4(3b^2+a^2)r^{-4}\left.\left.\right\}\cos2\theta\right.$$
$$+P_0\frac{b^2}{b^2-a^2}(1+a^2r^{-2})$$

$$\tau_{r\theta} = \frac{P_1}{2}\frac{b^2}{(b^2-a^2)^3}\left\{(b^2+3a^2)r^2-(b^4+b^2a^2+2a^4)\right.$$
$$-a^2(2b^4+b^2a^2+a^4)r^{-2}+b^2a^4(3b^2+a^2)r^{-4}\sin2\theta\left.\right\}$$

Let = P_1/P_0, where denotes
non-uniformity ratio of ground
pressure distribution, and let
r=a, r=b, the tangential stresses
can be calculated as follows:

$$\sigma_\theta\Big|_{r=a} = P_1\left\{\frac{b^2}{b^2-a^2}-\frac{2b^2(b^2+a^2)}{(b^2-a^2)^2}\cos2\theta+\frac{1}{\omega}\frac{2b^2}{b^2-a^2}\right\}$$

$$\sigma_\theta\Big|_{r=b} = P_1\left\{\frac{b^2+a^2}{2(b^2-a^2)}+\frac{b^4+6a^2b^2+a^4}{2(b^2-a^2)^2}\cos2\theta+\frac{1}{\omega}\frac{b^2+a^2}{b^2-a^2}\right\}$$

where:
    P_1 denotes non-uniform exter-
       nal pressure
    = P_1/P_0 denotes non-uniformity
         ratio of external pre-
         ssure

362

A STUDY OF SINKING DEEP SHAFTS USING ARTIFICIAL FREEZING, DESIGN OF SHAFT LININGS AND METHOD OF PREVENTING SEEPAGE

Qiu Shiwu, Mining Engineer, Department of Scientific Research,
        The Two-Huai Coal Base Construction GHQ, Huainan, PRC
Wang Tiemeng, Associate Chief Engineer, Metallurgical and Building
        Research Institute, Beijing, PRC

The Two-Huai Mining Districts are covered with Quarternary overburdens, 200-770 m in thickness, composed of silt sand, fine-grained sand, moderately coarse sand, sandy clay and effervescing clay, all highly water-bearing.

Artificial freezing method is employed for shaft sinking. Steel reinforced concrete double linings are applied. Owing to the complicated hydro-geological conditions, fractures are found, chiefly caused by the frost heaving force and the ground pressure, resulting thereby in water seepage.

A new type of water-tight plastic shaft lining is developed and adopted, which proves effective up to a maximum depth of 318 m.

The freezing process under thick overburdens are studied, causes of cracking and seepage analyzed and the new type of water-tight shaft lining and its water prevention mechanism described.

1. Introduction

The Quaternary of the Two-Huai coal field, 200-770 m in thickness, highly water-bearing, complicated in soil conditions, involves thereby difficult problems in choosing a suitable structure form of shaft lining for shaft sinking by freezing method. The main difficulty lies in that fractures in circular shape are found in the concrete lining during sinking accompanied with serious water seepage after thawing, any follow-up procedures of which would be expensive, let alone the postponement of the production cycle.

Steel plate lining or plastic lining is employed in certain countries, the degree of water-tightness depending apparently on the effect of sealing. While the steel plate lining is satisfactory, the technology and cost involved are rather complicated and exorbitant. The plastic lining is of advantage as far as cost is concerned, but proves unsatisfactory because water-tightness is not ensured under water head with high pressure.

A type of sliding, water preventive polyethylene lining is developed and is given to test in the Two-Huai mining district with satisfactory results. The structure of this type of lining is based on the new water-sealing theory or the lining fracture controlling 'sliding layer theory.' The main idea is to enhance the water seepage preventive power of the inner concrete lining itself.

2. The Lining Fracture Controlling 'Sliding Layer Theory'

Investigations and in situ observations show that the fracture found in the concrete lining during sinking by freezing method results largely from a special kind of 'deformation load'--deformation due to contraction caused by temperature.

The structure of the frozen lining is a complex structure composed of the frozen soil (rock included), the outer lining and the inner lining. Factors such as temperature, humidity, excavation, etc., generally tend to bring about deformation of this complex structure as a result of expansion and contraction. The deformation between the linings caused by mutual restraint result in restraint stress such as freezing pressure, swelling

pressure, excavation deformation pressure, temperature contracting stress, etc.

2-1 Temperature state of double shaft lining

The double shaft lining is characterized by the variation of temperature during construction stage. The outer lining is first completed and is in a state of low temperature (-6° to -10°C). Then, after a relatively long period of say 2 to 3 months, casting of the inner lining is started. The temperature reaches 40 to 50°C in 20 to 30 hours under heat of hydration after casting, and at the same time the temperature of the outer lining, under heat conduction, also tends to rise to about 0°C. The concrete is thus in a plastified state with no stress produced. This stage is regarded as the initial state of the inner and outer linings.

The temperature of the inner lining starts decreasing gradually, whereas that of the outer lining starts increasing gradually, causing therefore an increment of modulus of elasticity, which results in restraint stress through deformation difference. The steady temperature during the eventual thawing is supposedly to be approximately 10°C, in which case the temperature fall difference (40°-10°C) of the inner lining would be 30°C, while the temperature rise (0°-10°C) of the outer lining would be 10°C. Thus the inner lining is subject to an axial pull and the outer lining to an axial compress due to the mutual restraint. The restraint pulling deformation exerted on the inner lining exceeds the latter's pull limit, bringing about thereby the circular-shaped fracture of regular pattern.

2-2 Establishing of Temperature Stress Ordinal Differential Equations

The contracting deformation of the inner lining being subject to the restraint of the outer lining, a shearing stress is therefore found in between the linings and displacement occurs in the mean time.

Assuming that the shearing stress is proportional to the displacement, we have

$$\tau = -C_x u \qquad (1.)$$

where τ = shearing stress at a particular point on the contracting surface of the inner and outer linings

u = horizontal displacement at a particular point on the contacting surface of the inner and outer linings

C_x = ratio factor, the shearing force which brings about the unit displacement.

In accordance with the equilibrium equation $\sum_x = 0$ we obtain

$$N + dN - N + Q = 0 \qquad (2)$$
$$d\sigma_x H + \tau d_x = 0$$
$$\frac{d\sigma_x}{dx} - \frac{\tau}{H} = 0 \qquad (3)$$

For horizontal displacement

$$u = u_o + \alpha T x \qquad (4)$$

Assuming

$$\sqrt{\frac{C_x}{HE}} = \beta \qquad (5)$$
$$\frac{d^2 u}{dx^2} - \beta^2 u = 0 \qquad (6)$$

the general solution of the above differential equation would be:

$$u = A \operatorname{ch}\beta x + B \operatorname{sh}\beta x \qquad (7)$$

Boundary conditions of definite integral constants:
(central displacement = 0, stress at two ends = 0)

$$x = 0, \quad u = 0, \quad \operatorname{sh} 0 = 0, \quad A = 0$$
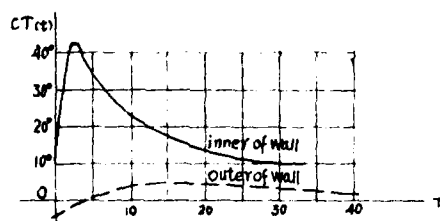$$x = \frac{L}{2} \quad \sigma_x = 0$$

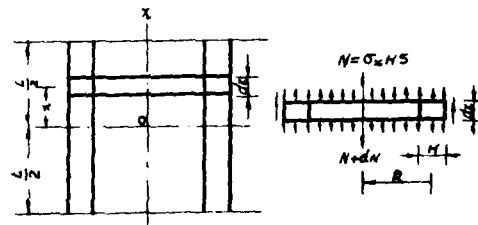§ig. 1: Temperature variation Curves of inner and outer lining.

fig. 2: Calculation Diagram of Stress.

364

$$E \frac{du}{dx} = E\left(\frac{du}{dx} - \alpha T\right) \qquad (8)$$

$$\beta = \frac{\alpha T}{\beta ch\beta \frac{L}{2}} \qquad (9)$$

Thus we have the formula for displacement u:

(displacement at ends u, maximum horizontal stress, shearing stress)

$$u = \frac{\alpha T}{\beta ch\beta \frac{L}{2}} - sh\beta x \qquad (10)$$

$$\sigma_x = E\left(\frac{du}{dx} - \alpha T\right) = -E\alpha T\left(1 - \frac{ch\beta x}{ch\beta \frac{L}{2}}\right) \qquad (11)$$

$$\tau = -C_x u = -\frac{C_x \alpha T}{\beta ch\beta \frac{L}{2}} sh\beta x \qquad (12)$$

$$x = 0, \quad \sigma_x = \sigma_{max} = -E\alpha T\left(1 - \frac{1}{ch\beta \frac{L}{2}}\right) \qquad (13)$$

Fracture is found at the central part where stress is maximum, causing it therefore to break into two sections, if it should go beyond the tensile strength; in addition, for each section there will be stress distribution of its own. The maximum stress is still retained at the central part but to a lesser degree, because the length has been reduced by 50%. However, each of these two sections would in turn break into two subsections, should the stress exceed its tensile strength, and would continue breaking until the stress at the central part becomes less than the tensile strength. This is what we called 'mechanism of again-and-again-breaking from the central part.'

And when this horizontal stress reaches the ultimate tensile strength, the pulling deformation of the concrete reaches correspondingly its ultimate:

$$\sigma_{xmax} = R, \quad \varepsilon = \varepsilon_p, \quad R = E\varepsilon_p \qquad (14)$$

under which circumstances L is calculated as the maximum space of the expansion cracks:

$$[L_{max}] = 2\sqrt{\frac{EH}{C_x}} \, arcch \frac{\alpha T}{\alpha T + \varepsilon_p} \qquad (15)$$

For the fraction appearing in Equation 12, the ultimate stress deformation is negative (compress deformation) if T is positive (rise of temperature); and is positive (tensile deformation) if T is negative (fall of temperature or contraction). The signs of the two terms in the denominator are always different to each other. Equation 12 may be expressed in terms of absolute value for clear and convenience sake:

$$[L_{max}] = 2\sqrt{\frac{EH}{C_x}} \, arcch \frac{|\alpha T|}{|\alpha T| - \varepsilon_p} \qquad (16)$$

The above equation is established at a time when the maximum stress just reaches the tensile strength and there appears no breaking. If, however, the maximum stress exceeds slightly the tensile strength, breaking will occur, the minimum space being

$$[L_{min}] = \frac{1}{2}[L_{max}]$$

The following formula for the average space of the cracks is thus obtained:

$$[L] = 1.5\sqrt{\frac{EH}{C_x}} \, arcch \frac{|\alpha T|}{|\alpha T| - \varepsilon_p} \qquad (17)$$

In calculating the maximum temperature stress and taking into consideration the variation of modulus of elasticity (E(t)) and that of the relaxation factor (H(t)), the temperature fall is divided into several stages ΔT, the final stress should then be:

$$\sigma_{xmax} = \sum_{n=1}^{n} \frac{E(t)\alpha\Delta T}{1 - \mu}\left(1 - \frac{1}{ch\beta \frac{L}{2}}\right) H(t) \qquad (18)$$

The displacement of one end of the cracked section is determined by the above formula:

$$u = \frac{\alpha T}{\beta} \cdot \frac{sh\beta x}{ch\beta x} = \frac{\alpha T}{\beta} \cdot Th\beta \frac{L}{2}$$
$$= \frac{\alpha T}{\sqrt{\frac{C_x}{HE}}} Th\sqrt{\frac{C_x}{HE}} \cdot \frac{L}{2} \qquad (19)$$

The width of the crack W is the sum of the displacement at the two ends:

$$W = 2u \qquad (20)$$

3. Application of Water Preventive Shaft Lining in the Two-Huai Mining Districts

The characteristics of the newly designed water preventive shaft lining based on the 'sliding layer theory' are as follows:

a) Polyethylene sheet in 2-1 layers of 1.0-1.5 mm thickness is incorporated in between the inner and outer linings as the sliding layer of the inner lining.

b) Lime rocks or precast concrete blocks (400 mm thick) are employed for the outer lining and grouting of cement sludge is effected in order to resist any radial displacement of the frozen wall.

c) On building up the outer lining, cracks resulting from squeezing as well as strip-offs are found in individual wall sections, which causes an unevenness on

365

frozen soil / the outer of the wall. / Plain layer. / the lamellar of the polyethyene. / the inner of the wall.
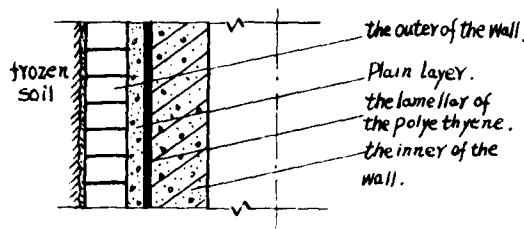
Fig. 3: Structure Diagram of water preventive Shaft lining.

the inner wall of the outer lining. Casting of concrete 250 mm in thickness is carried out on the inner wall of the outer lining with a view to obtaining a smooth and flat base for the incorporation of the polyethylene layer.

d) In the beginning, two polyethylene layers are laid with the outer layer nailed to the outer lining, using polyethylene polymer as an adhesive agent. Later, however, only one layer is nailed (with no adhesive or welding).

e) Structure of reinforced concrete is adopted for the inner lining.

f) Special but simple measures are taken to prevent any possible existence of water force passage as a result of certain unforeseen causes.

This new type of shaft lining is economically advantageous, cost per metre of which being half as much as that of the 'AV type water preventive shaft lining.' Another new type of sliding layer, which costa only one-tenth as

much as that of the polyethylene sheet type, is being developed at the Two-Huai mining district. Research work is also being carried out on concrete and its additives with such properties as high strength, water seepage resistance and low contraction rate.

References

1. Qiu Shiwu: Water-sealing effect and mechanism of the plastic water preventive shaft lining with sliding layer. Proceedings of the Third National Symposium on Artificial Freezing and Shaft Sinking, 1981.
2. Wang Tiemeng: Temperature stress and fractures of double layer concrete shaft lining. Proceedings of the Symposium on Shaft Lining, 1980.
3. Effect of Restraint, Volume Change and Reinforcement on Cracking of Massive Concrete. Report of A.C.I. Committee 207, 1973.

Table 1. Water-sealing effect of ten shafts where the new type watersealing linings are employed.

Name of shafts	Number of polyethylene sliding layers	Joint by	Depth laid (m)	Watersealing effect
Haizi main shaft	1	adhesive	93–279.6	no cracks or leakage found
Haizi auxillary shaft	1	adhesive	122–278.7	ditto
Haizi central air shaft	1	adhesive	123.3–279.3	ditto
Haizi west air shaft	1	adhesive	123.9–295.9	ditto
Panji No. 2 auxillary shaft	2	outer layer by nail inner by adhesive	81–216	ditto
Panji No. 2 west air shaft	2	ditto	97–318	ditto
Panji No. 2 south air shaft	2	ditto	7–314	ditto
Panji No. 3 main shaft	2	ditto	95.2–230.7	ditto
Panji No. 3 auxillary shaft	2	ditto	50–261	ditto
Panji central air shaft	1	without adhesive	17.7–196.6	ditto

FIELD STUDY OF INSTRUMENTED GULLIES AND MANHOLES IN FROST-SUSCEPTIBLE SOILS

Sven Knutsson   University of
Luleå

In Scandinavia, a lot of manholes and gullies, designed for the drainage of rain water, get damaged during winter due to frost action mainly because of the heave of frost susceptible backfill. The concrete rings are pulled apart and the joints between the rings are opened. When thawing starts, water and soil flows into the gullies through the opened joints and the inflowing material prevents the rings to return to their original positions. When thawing has taken place, the gullies still remain in an uplifted position, with the covers above the pavement. They are then out of function and are easily damaged in the course of ordinary road maintenance. The repair cost is considerable.

In order to study the behaviour of manholes and gullies with and without a newly invented rubber sleeve mounted over the joints, a field test was performed during the winter 1980/81 in Luleå, Sweden. It concerned 11 gullies, 3 of which were constructed in a conventional way and 8 with rubber sleeves. They were all located in highly frost susceptible soils and were exposed to frost heave.

The paper describes the instrumentation installed as well as the results obtained. The growth of the frost bulb around the gullies, as well as movements in these and in the surrounding soil are reported. The results of the full scale tests have shown that the new rubber sleeve almost completely prevents damage of the gullies. The study has yielded a better understanding of frost heaving in and around such constructions.

INTRODUCTION

Gullies and manholes made of concrete rings are often damaged due to frost action, when the surrounding backfill consists of frost-susceptible soil. During frost heave, the concrete rings are pulled apart and the joints between the rings get opened. When thawing takes place, soil flows into the gully through the opened joints, Fig. 1. This results in:

- loss of material outside the gullies, giving rise to large settlements
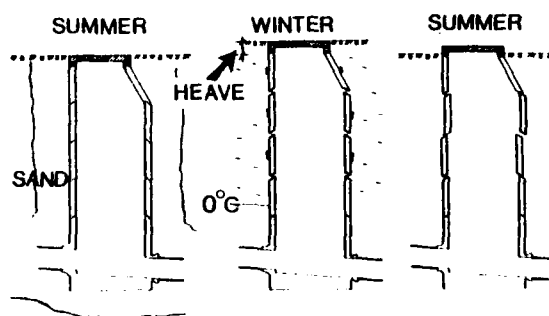- inability for the lifted rings to go back to their initial position, resulting in a permanent heave.

Fig. 1. Manhole placed in frost suscep-
tible soil .

The problem can usually not be solved by surrounding the construction with non frost-susceptible sand. However,

367

Figure 2 removed at author's request.

the problem can be largely eliminated by use of rubber sleeves.[1] The sleeves are placed over each joint and thus it gives the different parts of the gully movability during the frost heave. During thaw the sleeves prevent soil to flow into the gully and consequently the rings can go back to their original position.

To study the efficiency of this rubber sleeve, a full-scale field test concerning 11 gullies was conducted in the winter of 1980/81. 8 of them had the new rubber sleeve while 3 were built in the conventional way.

[1] The sleeve was invented by Mr. Thord Engström, Luleå, Sweden.

FREEZING INDEX

The successive growth of the freezing index in Luleå during the winter 1980/81 is shown in Figure 3.

It can be seen that freezing started in mid-October, which is about two weeks earlier than normal. In the beginning of November freezing became more intense and the rate of increase of the freezing index is fairly constant until the end of January 1981, when the growth almost ceases. This period was extremely warm with above-zero temperatures for two days. The maximum daily mean air temperature during this week was as high as +6.6°C.

368
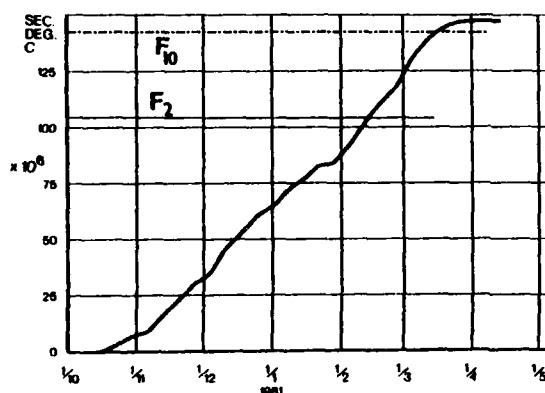
Fig. 3. The successive growth of the freezing index in Luleå, 1980/81. F_2 represents the median value and F_{10} the frost index which is exceeded one year out of ten, in the statistical sense.

INSTRUMENTATION AND SOIL CONDITIONS

Each gully was instrumented to yield information of:

- the movements of the concrete rings during the freezing and thawing periods
- the vertical movements in the surrounding frost-susceptible soil
- the temperature situation in the soil surrounding the gully.

Most of the gullies studied consisted of three concrete rings, 1 m in height and 0.4 m in diameter. During construction, 3 bench marks were installed in each of the three concrete rings in order to detect tilting during heave and thaw. In addition to this a bench mark was mounted on the iron top cover of each gully.

In order to study vertical displacements in the surrounding frost-susceptible backfill, three bench marks were installed at different depths (0.1, 0.6 and 1.1 m) below the ground surface, Fig. 4. Each bench mark consisted of a base plate (0.20 m x 0.20 m) connected to a vertical rod which was surrounded by a casing. The space between the rod and the casing was filled with grease to guarantee the mobility of the rod during the winter.
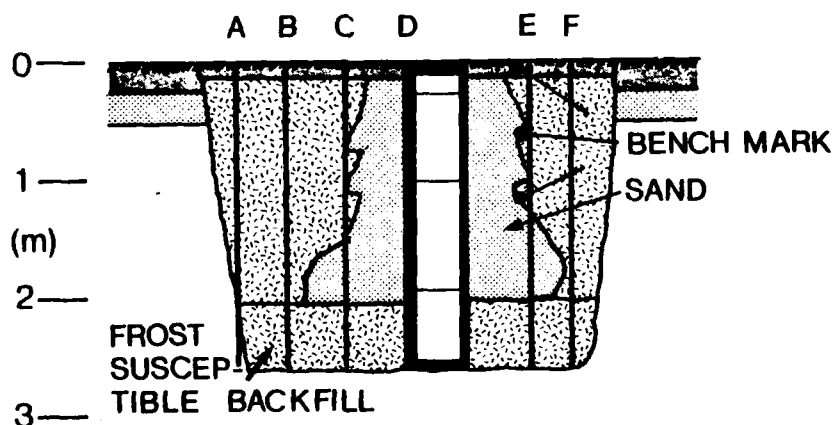

Fig. 4. Instrumentation of a gully.

369

The soil temperatures were measured by means of thermocouples. These were placed vertically at a distance of 0.33 m in 6 sections, Fig. 4. In this way the temperature distribution, both vertically and radially, was obtained at each time the temperatures were read.

Temperature and displacement were observed at a time interval of about 12 days during wintertime and of about 7 days during spring.

Fig. 5 shows the grain size distribution curves for the frost-susceptible soil as well as the corresponding curve for the sand backfill adjacent to the gully. During construction, this sand was compacted to an average degree of compaction of 89%.
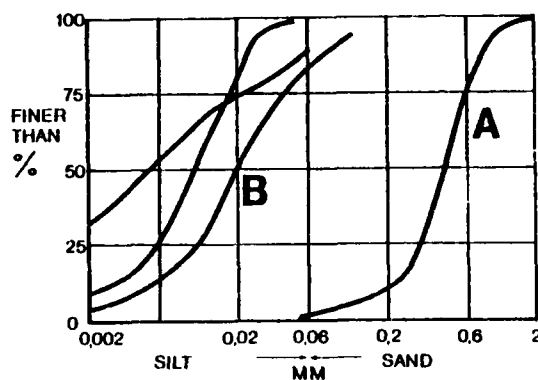
Fig. 5.   Grain size distribution curves. Curve A represents the sand surrounding the gully. B represents the frost-susceptible soils used in the study.

RESULTS AND DISCUSSION

The instrumented gullies behave similarly during winter heave and thaw settlement. Differences are explained by different soil and groundwater conditions as well as minor differences in design and construction. The main outcome of the field study will be reported here.

Temperatures and frost depth

The frost penetration has been derived from the temperature readings. It is interpreted as the 0°C-isotherm here. For the gully shown in Fig. 4 the frost penetration changes with time as shown in Fig. 6.

It is obvious from this figure, that the frost penetration is considerably larger in sections C and D, close to the gully, than in sections A and B. This is most obvious in December and January, when the frost penetration in section D is 2,15 times larger than in section A. This difference is explained by ventilation effects in the ducts, resulting in an inflow of cold air in some gullies and outflow of warm air from others. Consequently, a reduced frost penetration is observed close to some of the gullies. As soon as the perforated top is covered with snow and ice, the ventilation ceases and this is noted as a reduced frost penetration in section D. Maximum frost penetration was observed in the end of March. In sections A and B the observed penetration depth agrees reasonably well with the expected depth calculated by use of the conventional theory for one-dimensional freezing from the ground surface. However, in the sand (sections C and D) it is overestimated since the influence of radial heat inflow from the surroundings is neglected.

When thaw started in the beginning of April, the frost penetration in section D was reduced very quickly. In the other sections it was reduced more slowly, which illustrates the influence of radial heat flow from the gully. This heat flow is mainly caused by melting water, which flows along the inside of the gully. The radial thaw is very sensitive to changes in the air temperatures. The last 10 days of April were cold, air temperature was well below the freezing point, and this immediately increased the frost penetration depth. In the beginning of May, when the thawing index amounted to $3.7 \cdot 10^6$ degree seconds C, the immediate vicinity of the gully was thawed, while the fine-grained backfill was still frozen. In this material thaw was not completed until mid June, which is in accordance with the theory of one-dimensional thaw.

Frost heave

Fig. 7 shows the heave in the frost-susceptible backfill at three different depths. The frost heave due to the expansion of the pore water is marked as well. The difference between the total heave and this heave is caused by ice lensing.
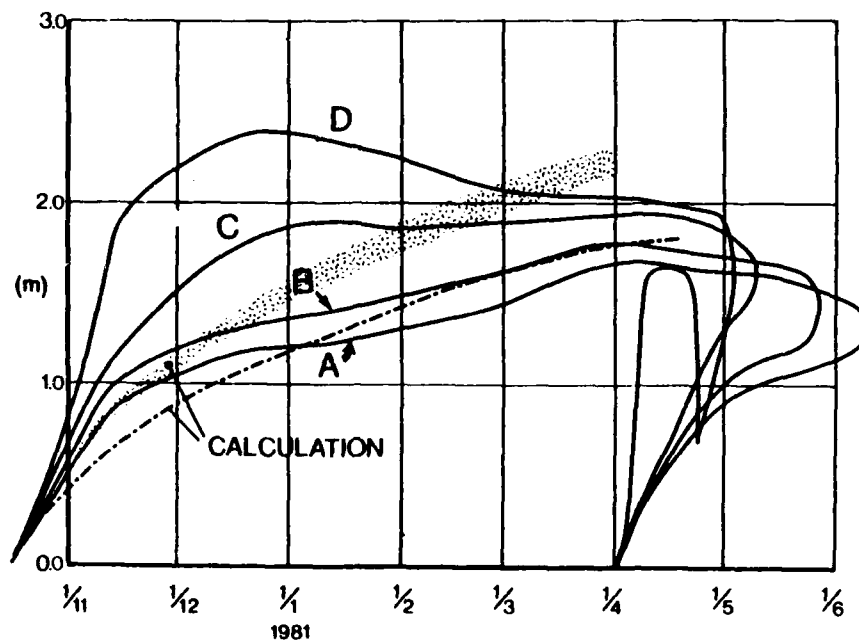
370

Fig. 6. Frost penetration as a function of time for four sections at different radial distances (r) from the gully.

A   r = 1.38 m   C   r = 0.45 m
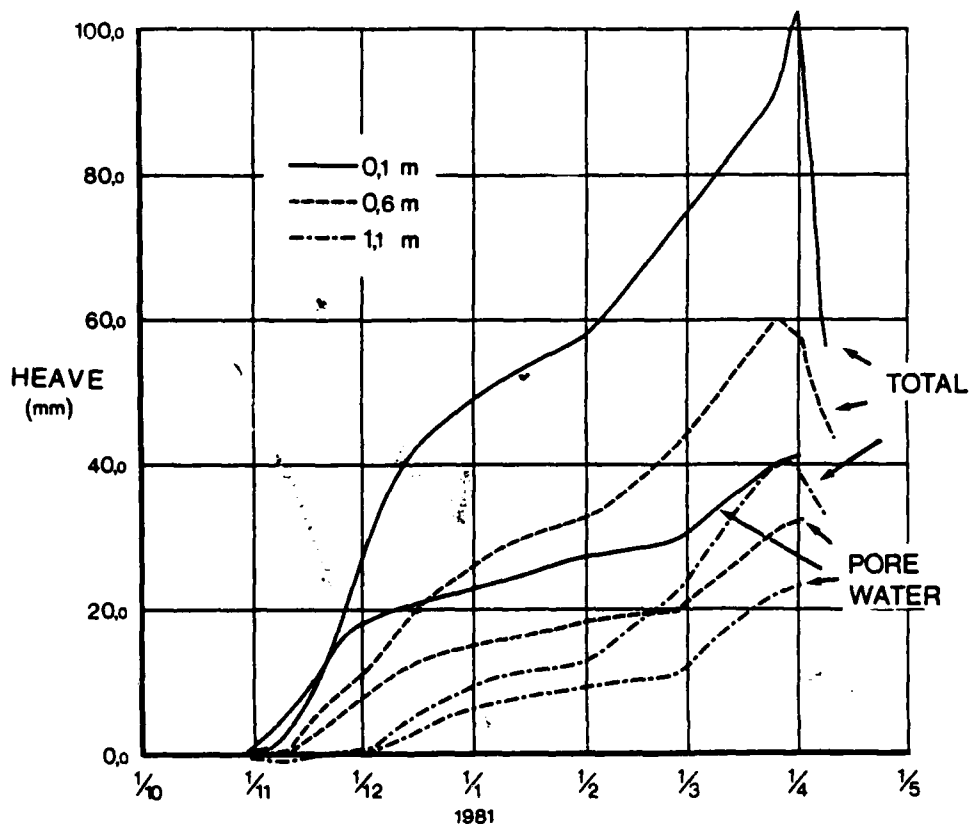B   r = 0.95 m   D   r = 0.05 m

Fig. 7. Total heave and heave due to freezing of the in-situ pore water.

371

In Fig. 8 the relative expansions of each of the two layers (0.1-0.6 m and 0.6-1.1 m) are shown as a function of time. From this figure it is obvious that the largest expansion due to ice lensing took place in the upper layer. This supports the idea of ice-lensing within already frozen soil (Miller, Williams, Penner). Since the ice-lensing in the shallow layer is larger than in deeper situated and therefore warmer layers, the total stress as well as the temperature on the cold side seems to influence the growth of the ice lenses (cf. Penner 1977, 1978).

below the lower level of respective concrete ring. It should be noted, that the heaving of the concrete rings in the gully started later and was not as large as the heave in the surrounding soil. The lower ring (1.95-2.65 m below the ground surface) was unaffected of the frost heaving, even though the frost penetration depth was as deep as 2.4 m. This means, that the friction between the unfrozen soil and this ring was high enough to prevent heave.
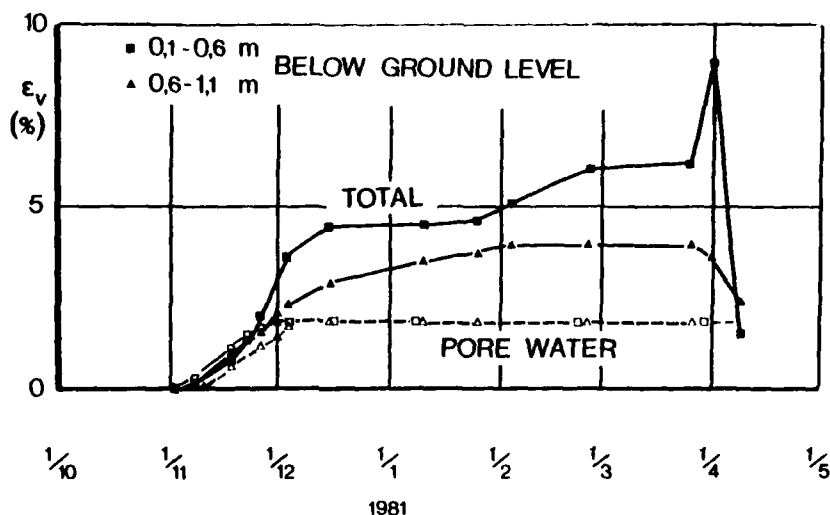

Fig. 8.   Volume expansion in the two layers 0.1-0.6 m and 0.6-1.1 m. The broken line shows the expansion due to freezing of the in-situ pore water.

The increasing rate of ice lensing in the upper layer in February is explained by the extremely warm period in the end of January which was followed by a cold period. During the warm period, a lot of snow melted causing excess water, which could percolate into the freezing soil. When the air temperatures turned negative again, this water was frozen and consequently the rate of ice lensing increased.

Fig. 9 shows the movements of the different parts of a gully provided with rubber sleeves. It can be seen that the top cover (0-0.4 m) as well as the two upper rings (0.4-1.05 m and 1.05-1.95 m) began to heave at about the same time, i.e. the end of November. At this time the frost depth was already 2.1 m in section D (Fig. 6) and consequently well

The tests have showed that a layer of non frost-susceptible soil (sand) around a construction placed in highly frost susceptible soil does not prevent heaving of the construction unless the water content is so low or the temperatures in the frozen sand are so high that the frozen sand can be sheared off when the surrounding soil heaves. This is normally not the case and therefore the heaving in the surrounding soil is transmitted through the frozen sand to the gully.

Since the amount of heave in the frost-susceptible soil is different at different depths, the frozen sand column will usually be teared off. The openings which are thus formed will be filled with water which turns into ice which produce "ice lenses" in the coarse
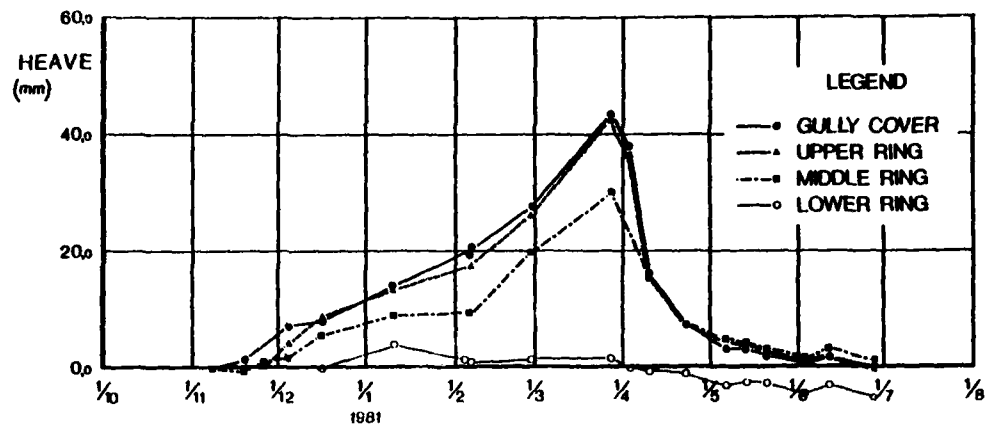
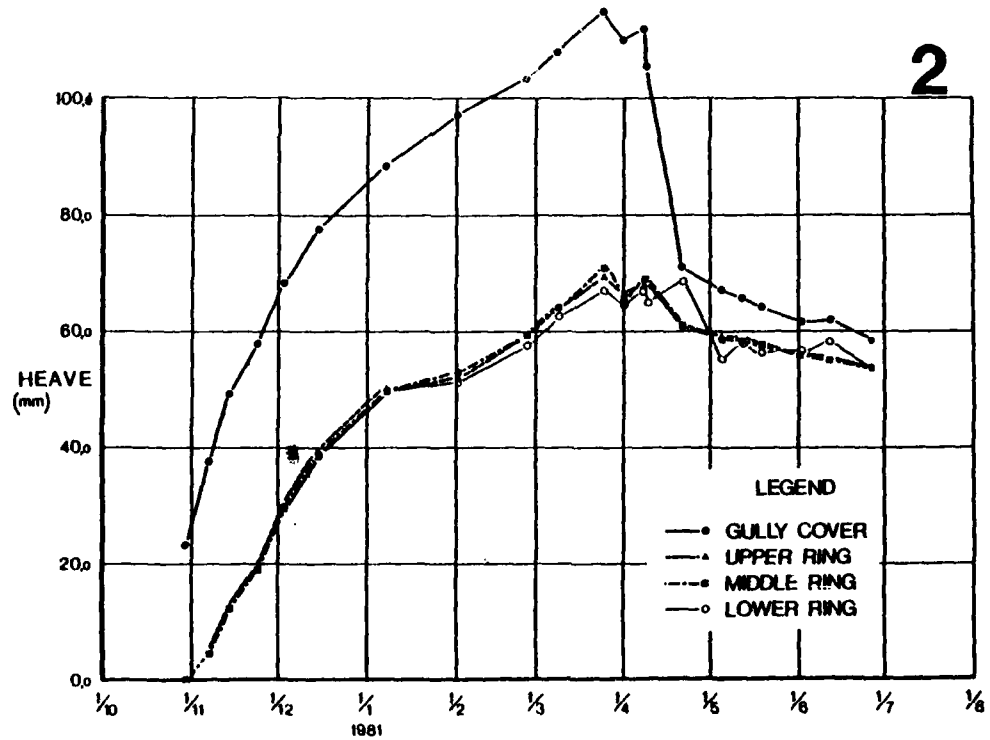Fig. 9. Heave and thaw due to frost action in a gully with the new rubber sleeve.

Fig. 10. Heave due to frost action in a conventionally constructed gully.

373

backfill as well. When thawing starts,
the thawing front progresses both from
the surface and radially from the gully.
When the frozen sand thaws, its excess
content of ice produces a high pore
water pressure which reduces the effective
stresses and thereby also the friction
between the thawed sand and the concrete
ring in the gully. This low friction
explains the rapid settlement of the up-
lifted parts of the gully already a few
days after the start of thaw, Fig. 9.
Within 5 weeks after the onset of thaw,
all parts of the gully have returned to
their original position. Fig. 10 shows
the corresponding heave of a gully con-
structed in a conventional way. This
gully remains uplifted about 60 mm when
thaw is finished. After one or two addi-
tional freezing cycles this gully has to
be repaired.

REFERENCES

Miller, R.D., 1977 Lens initiation
in secondary heaving. Proc. Int. Symp.
Frost Action in Soils, University of
Luleå, 2:68-74.
Penner, E. and Veda, T., 1977. The
dependence of frost heaving and load
application. Proc. Int. Symp. Frost
Action in Soils, University of Luleå,
1:92-101.
Penner, E. and Walton, T., 1978.
Effects of temperature and pressure and
frost heaving. Proc. Int. Symp. on Ground
Freezing, University of Bochum, 2:65-72.
Williams, P.J., 1977. Thermodynamic
conditions for ice accumulation in
freezing soil. Proc. Int. Symp. Frost
Action in Soils, University of Luleå,
1:42-53.

STRENGTH DEVELOPMENT OF CONCRETE PLACED
IN FROZEN SOIL AND THE THERMAL EFFECTS

Yang Yuji
(Engineer, Heilongjiang Provincial Low Temperature
Construction Science Research Institute)

Abstract

When concrete is placed in frozen soil, it will be at negative temperatures in a short time, hydration stops, and strength develops slowly, and reaches 50% of its design strength only.

This paper describes a complex admixture ($NaNo_2$ - Na_2So_4) which can make concrete placed in frozen soil to reach its design strength. A lot of testing data, which were adopted in some projects, are given in the paper.

In addition, this paper describes the thermal effect of hydration heat of cement on frozen soil surrounding the concrete placed. The thermal effect in frozen soil (range of thermal effect, thawing depth and freezing-interval) was measured for concrete with heated aggregates and unheated aggregates. Recommendations for use of such admixture are given in the paper.

The first problem encountered in concreting in frozen soil is to maintain the hydration process of cement at negative temperature, so that the design strength of concrete will be obtained. Hydration rate of cement depends on temperature essentially. At low temperature, hydration rate of cement will retard, or gradually stop when temperature becomes negative. When concreting is performed in frozen soil, temperature inside concrete decreases rapidly and balances with the surrounding temperature due to the effect of the frozen soil. Strength gain of concrete only relies on the initial temperature and the limited hydration heat of cement itself. Once the temperature inside concrete decreases under $0°C$, no strength can be gained. It is found in practice that the final strength of concrete placed in frozen soil is only up to 50% of the design strength.

Along with the development of construction in China, and in order to satisfy the requirement of construction in the frozen district and the construction of vertical shaft, we have to carry out concreting in frozen soil and the concrete placed must be guaranteed to have sufficient strength in a given period to subject external loads. At the same time, it is required that the structure of frozen soil should not be destroyed by concreting; so that construction can be carried on normally. In order to fulfil this purpose, we adopt the technique of "negative temperature concreting" based on test results.

HARDENING MECHANISM OF CEMENT WITH COMPLEX ADMIXTURE $NaNo_2$ - Na_2So_4

1. Anti-freezing mechanism

Anti-freezing effect is obtained by adding some electrolytes in the mixing water to reduce the saturated vapor pressure and the freezing point of the solution. Temperature at which ice is segregated from the solution (freezing point) is proportional to the concentration of the solution. Electrolytes frequently

used are as follows (Tab. 1)

Tab.1   Electrolytes frequently used as admixtures

Freezing point	Concentration% (No. of gr. of unhydrated material in 100gr of water)									Temperature at which solid phase is segregated from solution	
	2	4	6	8	10	15	20	25	30	$g/100g\,H_2O$	°C
NaCl	-1.2	-2.4	-3.5	-4.8	-6.0	-9.3	-12.7	-16.0	-21.1	30.1	-21.2
CaCl$_2$	-0.9	-1.9	-2.8	-3.9	-5.0	-8.5	-12.6	-17.5	-23.9	42.7	-55.6
K$_2$Co$_3$	-0.6	-1.3	-2.0	-2.5	-3.2	-5.0	-7.3	- 9.8	-11.6	56.5	-36.5
NaNo$_2$	-0.9	-1.8	-2.7	-3.6	-4.5	-6.0	-6.9	- 7.8	-8.9	61.3	-19.6

It is shown from Tab.1 that the effect of chlorides to reduce freezing point is most obvious. But owing to the corrosive action of chlorides to reinforcement, great care must be taken for the use of such admixtures in reinforced concrete structures. Based on the construction condition in China and a lot of test results, NaNo$_2$ is chosen as an anti-freezing agent to reduce the freezing point of the mixing water, so that liquid phase in hardening concrete will be proved.

2. Accelerating mechanism

Existence of liquid phase in concrete only keeps concrete not to be frozen at a certain range of negative temperature. But, if strength gain is required, accelerators, such as Na$_2$So$_4$, should also be added to accelerate the hardening of cement.

Adding in the mixing water when concreting, Na$_2$So$_4$ reacts with C$_3$A in the cement clinker minerals and Ca(OH)$_2$ in the hydrated product, forming calcium sulphate and C$_3$AS. At the same time, Na$_2$So$_4$ can increase the solubility of CaO, accelerate the hydration of C$_3$S, and in turn, its product NaOH can also increase the solubility of CaSO$_4$ - 2H$_2$O and C$_3$A, forming C$_3$AS, thus making the hydration reaction of cement clinker minerals continue and complete.

Products of calcium sulphate and C$_3$AS in the reaction occurs in the beginning of the establishment of cement-water system. At that time, the system is in a colloidal and plastic state and the structure of which has the property of trigger deformability and no internal stress will exist. Even though there is internal stress, it will be very small, and does not

do harm to the structure of concrete, in contrast, it will improve the density of concrete.

TEST RESULTS

By adding both anti-freezer and accelerator, strength gain of concrete will be obtained in the negative temperature condition. Appropriate quantity of complex admixture added will decrease the freezing point of concrete to -8°C. Tests were performed in the temperature of -9°—-11°C.

Materials used in tests:
Cement - 500# ordinary Portland cement.
Coarse aggregate - gravel, 0.5-3cm.
Fine aggregate - medium sand.
Design strength of concrete (mark)- 400kg/cm^2, 200kg/cm^2.
Development of concrete strength is shown in Tab. 2.

It is shown from the Tab.2 that, if appropriate quantity of admixture is added, concrete strength continues to develop in the temperature of -9°—-11°C. If concrete specimens are buried in frozen soil of -10°C, strength gain will be better owing to the constant surrounding temperature and interruption of water evaporation in concrete.

In order to satisfy the need of underground construction, tests had been carried out for concrete with large slump. The same above effect is obtained (Tab.3).

APPLICATION IN THE PRACTICAL CONSTRUCTION

In order to testify the effect of winter concreting mentioned above in the practice, we selected a perennially frozen district for field test, the temperature of the ground in the

376

district was -1°C and -5°C. In the -5°C frozen soil, concreting was performed for two piles of different diameters. One of the piles was 80cm. in diameter and 1m. in length. Concrete was placed down to 1-2m beneath ground surface. Temperature in ground was -2—-4°C. Concrete was mixed with heated aggregates and unheated aggregates respectively. Initial temperature of the former was 16 — 31°C and that of the latter was -1 —+2°C. The other pile was 26cm. in diameter, 5.5 m. in length; temperature of ground was about -5°C; concrete was mixed with heated aggregates.

Owing to the difference of ground temperature, different amounts of anti-freezer ($NaNo_2$) were added. Concrete mix proportions and amount of admixture were as follows (Amount of admixture added was represented as percentage of water weight for $NaNo_2$, and of cement weight for other admixtures):

Concrete mix: 0.5:1:2.1:3.25 for the large pile
0.6:1:2.4:3.8 for the small pile

Amount of admixtures: $NaNo_2$ 4% + Na_2SO_4 3% + $C_6H_{15}O_3N$ 0.03% for -3°C (larger pile)

$NaNo_2$ 3% + Na_2SO_4 3% + $C_6H_{15}O_3N$ 0.03% for -6°C (smaller pile)

Description of construction:
(1) For the larger pile, Frozen soil was excavated by labor. At the time of excavation, 10cm. of soil under ground surface had frozen, beneath the depth of 10cm. was the unfrozen layer, further beneath was layer, ice content of which was above 60%. Total excavation depth was 2m. under ground surface. Concreting was done only up to 1m. of depth. After compacting, concrete placed was covered with straws for isolation and filled with frozen soil up to ground surface.
(2) For the small pile, excavation was performed by drilling machine. Diameter and depth of the hole drilled were checked afterward, and then concrete mix was placed. In order to guarantee the quality of pile, impact was applied at the same time during drilling, then vibro-compacting was achieved. The measurement data in the practice are given in Tab. 4.

RANGE OF THE THERMAL EFFECT AND STRENGTH TEST OF CONCRETE PLACED IN FROZEN SOIL

In order to compare the effect of initial temperature of concrete on the temperature of the surrounding frozen soil and to observe the development of hydration heat, concrete was mixed with heated aggregates and unheated aggregates respectively. The above effect is shown in Fig.1,2,3 for concrete mix with unheated aggregates, and in Fig. 4,5,6, for concrete mix with heated aggregates.
(1) For pile of 80cm. diameter, no matter what kind of concrete mix used, max. temperature can reach within 2 days (1— 2°C), radius of molten soil reaches 20cm. (Fig.2 and Fig.5). About 7 days after, iso-thermal contours of 0°C appears at the edge of the pile (Fig. 3,6). After placing, range of effect of hydration heat in concrete on the surrounding frozen soil can be 1m. approximately. Time at which the temperature in the core of the pile decreases to 0°C is about 13 days for concrete with unheated aggregates and 17 days for concrete with heated aggregates.
(2) For pile of 26cm. diameter, the effect of outdoor temperature is very small owing to adopt drilling machine for excavation. Although diameter of the pile is rather small, yet thermal effect is more abvious because heated aggregates were used in mixing. Temperature in concrete decreases rapidly to negative owing to the temperature of the underneath layer is too low, so its effect on the surrounding foil is also small. Faraway about 20cm. from the wall of the bore, temperature of soil is 0°C, and that at the wall is 0.5°C (Fig.7). After 46 hr., temperature at the bore wall becomes 0°C (Fig.8). 5 days later, temperatures in the interior of concrete decrease under 0°C basically, and on the 7th day, approaches that of frozen soil gradually (Fig.9). Range of effect of concrete temperature on surrounding frozen soil is about 1m., but the depth of molten soil is not obvious.
(3) Test of concrete strength. Strength test specimens were made in wooden moulds and at the same time with the testing pile. After moulding, specimens were buried in a curing pit in situ, over which frozen soil was filled up to the ground surface. Temperature in the pit was about -3°C at the beginning, but gradually decreased along with outdoor temperature. Strength of specimens at different ages is shown in Tab.5.

377

It is seen from tests that, because initial temperature of the concrete mix is higher than that of frozen soil and heat releases from the hydration process of cement, temperature in the interior of concrete increases to $7.4°C$, 7 hr. after placing, although concrete is mixed with unheated aggregate, especially in the case of the large pile. Later on, although temperature of concrete decreases continually, yet there is an interval of 7 days in which temperature of concrete remains above $0°C$. This fact is very advantageous for the strength gain in the pile. It is shown from Tab.5 that, owing to the stable ground temperature and slow transmission of heat in the pile, strength of core specimens taken from the large and the small piles reaches or exceeds the design strength (200 kg/cm^2) in 7 months under appropriate amount of admixture, but strength of test cubes (10 cm^3.) at the 7-month age is lower than that of core specimen because they have smaller vol. and quicker transmission of heat. Furthermore, outdoor temeprature gradually decreases daily, temperature of the surrounding soil has fallen below the expected temperature ($-5°C$).

COMMENTS ON THE APPLICATION OF "NEGATIVE TEMPERATURE" CONCRETE IN FROZEN SOIL

(1) From concrete placed in the frozen soil, it is shown that temperature in concrete keeps above $0°C$ for a considerable long period owing to the initial positive temperature of the mix and the hydration heat and it is beneficial for the strength gain. But, if the initial temperature of concrete mix is too high, and the structural member to be concreted is too massive, the hydration heat generated in concrete is also high, so it will cause the temperature of the surrounding frozen soil increase rapidly and melt. Thus, it is not beneficial for the construction performed continuously on the frozen soil. Therefore, initial temperature of the mix should be about $0°C$ and the mix should have a certain workability. If this can be done, heating of aggregates may be avoided and the adverse consequence produced by the higher hydration heat can be overcome; thawing depth of frozen soil can be reduced and no damage to the structure of frozen soil will occur.

(2) For the case of the small pile, hydration heat can hardly maintain because of its small diameter. Though this is not beneficial to the strength development of concrete, yet it is beneficial to the surrounding frozen soil. So, if the lowest temperature of frozen soil during construction is considered, at the same time appropriate quantity of anti-freezer($NaNO_2$) is added in the concrete mix, strength development of concrete can be proved.

(3) The reason why concrete with anti-freezer placed in frozen soil gains strength in negative temperature is that anti-freezer lowers the freezing point of concrete mix. Therefore, in the selection of amount of anti-freezer, it is important to consider the actual lowest temperature of frozen soil and variation of outdoor temperature during period of construction. If outdoor temperature and temperature of frozen soil is lower than the design temperature, anti-freezing or isolation measures should be taken or quantity of $NaNo_2$ added in concrete mix should be increased in order to avoid freezing.

378

Tab.2 Development of concrete strength in -10°C

No.	Mark of concrete Mix	Cement Content kg/m³	Admixture and its quantity % (1)			Curing Condition °C
			$NaNO_2$	Na_2SO_4	$C_6H_{15}O_3N$	
1	400 / 0.45:1:1.295:3.18	425	—	—	—	20
2	"	"	13.3	3	0.03	- 10
3	"	"	"	"	"	- 10 (buried in soil)
4	200 / 0.6:1:2.2:4.72	286	—	—	—	20
5	"	"	13.3	3	0.03	- 10

No.	Compressive Strength (2)							
	R_3	R_7	R_{14}	R_{28}	R_3mon	$R_3mon+1mon$	R_1yr	R_2yr
1	137/100	215.7/100	271/100	306/100	328.3/100	349.3/100	411/100	440/100
2				205.3/67.1	237.1/72.2	238/68.1		
3				225.3/73.6	257.1/78.3	266/76.2		396.7/90.2
4	77/100	131/100	164/100	194.3/100	236/100		243/100	355/100
5	13.8/17.2	55.3/42.2	122.7/74.8	163/86.5	183.3/77.7	•	239/96	278.3/81.2

Note: 1. Quantity of admixture: % of wt. of mixing water for $NaNO_2$
% of wt. of cement for other admixtures
2. Numerators are the actual strength; Denominators are percentages of concrete strength with no admixture.

Tab.3 Development of concrete strength with large slump in negative temperature

No.	Mix.	Amount of cement kg/m³	Admixture and its quantity (1) %			Curing Condition °C	Slump cm.
			$NaNO_2$	Na_2SO_4	$C_6H_{15}O_3N$		
1	0.55:1:1.2:2.8	440	—	—	—	15	17
2	0.49:1:1.2:2.8	"	2	1.6	0.03	- 1	18
3	0.48:1:1.2:2.8	"	"	"	w+NNO(1%)	- 1	20
4	0.5:1:1.2:2.8	440	—	—	—	15	19
5	0.46:1:1.2:2.8	"	8.7	3	0.03	- 5	21
6	0.44:1:1.2:2.8	"	9.1	3	w+NNO(1%)	- 5	19
7	0475:1:1.34:2.02	500	—	—	—	8	10
8	0.46:1:134:2.02	"	2.2	2	0.03	- 1	13
9	0.45:1:174:2.40	"	"	"	+NNO6.5%	- 1	11

No.	Compressive strength kg/cm²						
	R_3	R_7	R_{14}	R_{28}	R_3mon	R_2yr	R_4yr
1	72	146	238	333			
2	38	102	226	196		309	394
3	66	162	218	264			433
4	61	137	183	260			
5	32	34	137	211		405	435
6	22	77	144	209		422	427
7		R5 115		255			
8		132		240	284		
9		135.		295	313		

Note: (1) % of wt. of mixing water for $NaNO_2$ and % of wt. of cement for other admixtures.
(2) NNO water reducing agent.

Tab.4 Measurement data during pile concreting

Type of piles	Outdoor temperature during construction C°	Temperature of material & solution of admixture				Initial tem. of concrete mix °C	Slump cm	Vol. wt. Kg/m³	Remark
		Cement	Sand	Aggregate	Solution				
Φ26cm. L=5.5M	− 7	−13°	−13°	50°−70°	26°	6−20	10−14	2360	hot mixing
Φ80cm. L=1.0M	−10	−13°	2°	2°	25°	−1− 2	17−20	2310	cold mixing
Φ80cm. L=1.0M	− 3	−12°	−12°	40°−80°	20°	16−31	16−20	2310	hot mixing

Note: temperature of the bottom of the cave: −5°C for Φ26cm pile;
                                    −4.8——5.4°C for Φ80cm pile;
                                    −4——5°C for Φ80cm pile.

Tab.5 Strength of the piles and test cubes

No.	Item	Mark of conc. / Mix	Amount of cement kg/m³	Slump cm.	Admixture & its quantity (1)			Comp. Strength kg/cm² (2)		
					NaNO₂	Na₂SO₄	C₆H₁₀O₃N	R₇	R₂₈	R₇mon
00		200 / 0.6:1:2.4:3.8	300	5	—	—	—	— / 38.1	— / 60.2	— / 93
26	Φ26	200 / 0.6:1:2.4:3.8	300	10	8.3	3	0.03	— / 81.8	141.6 / 155.6	207 / 162
80	Φ30	200 / 0.5:1:2.1:3.25	350	17	4	3	0.03	— / 102.9	132.5 / 157.5	225.5 / 136

Note: (1) Quantities of admixture: % of wt. of mixing water for NaNO₂;
                                    % of wt. of cement for other admixtures.
      (2) Denominators are strength of 10×10×10cm specimens buried in frozen
          soil;
          Numerators are strength of core specimens taken from piles.
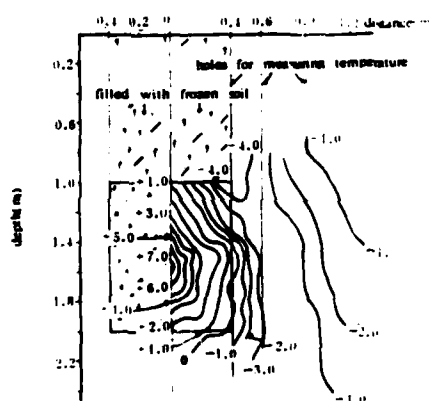
Fig.1 Thermal effect of cold mixing
      on frozen soil (7hrs after
      mixing for Φ80-1 pile).
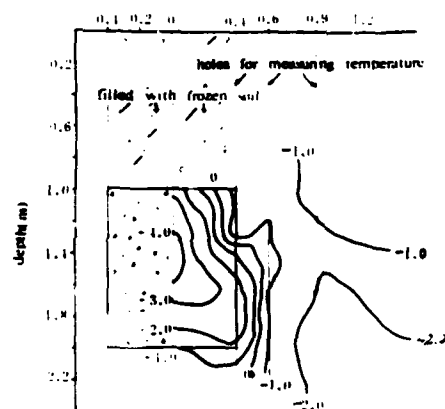
Fig.2 Thermal effect of cold mixing
      on frozen soil (47hrs after
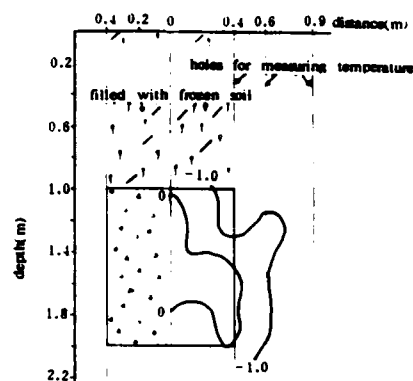   concreting for Φ80-1 pile).

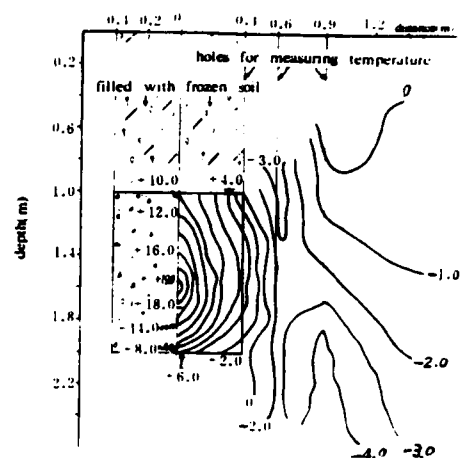Fig.3 Thermal effect of cold mixing on frozen soil (7days after concreting for φ80-1 pile).

Fig.4 Thermal effect of mixing with heated aggregates on frozen soil (7hrs after concreting for φ80-2 pile).
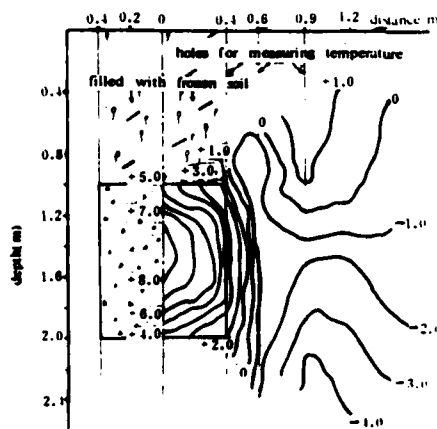

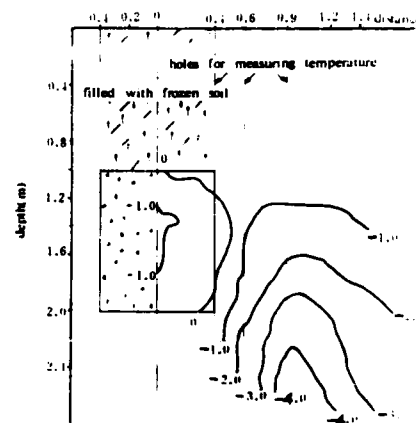Fig.5 Thermal effect of mixing with heated aggregates on frozen soil (41.5hrs after concreting for φ80-2 pile).

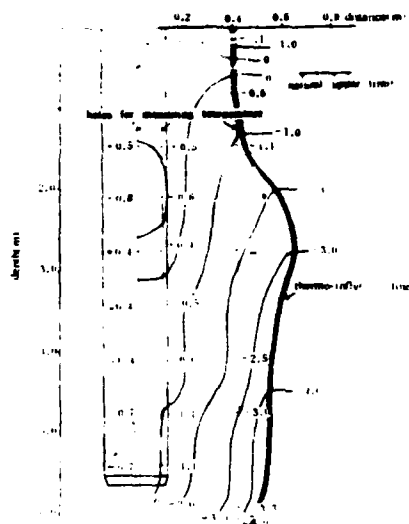Fig.6 Thermal effect of mixing with heated aggregates on frozen soil (7 days after concreting for φ80-2 pile).

381

Fig.7 Thermal effect of concrete pile
on frozen soil(7hrs after con-
creting for ϕ26 pile).
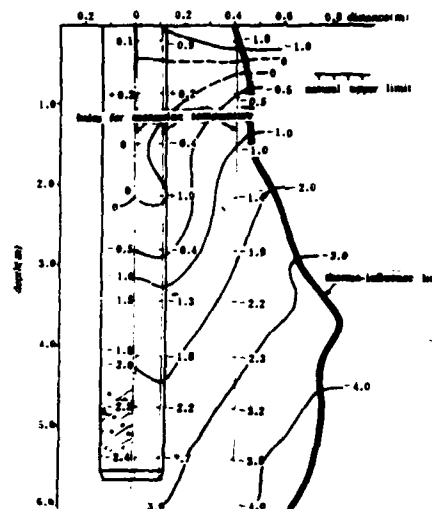
Fig.8 Thermal effect of concrete pile
on frozen soil (46hrs after
concreting for ϕ26 pile).
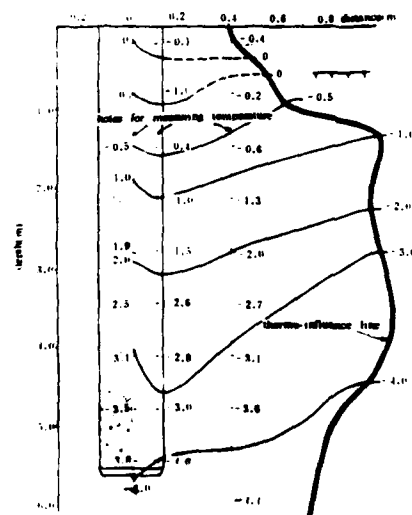
Fig.9 Thermal effect of concrete pile
on frozen soil (7 days after
concreting for ϕ26 pile).

382

CONSTRUCTION OF TWO SHORT TUNNELS USING ARTIFICIAL GROUND FREEZING

John S. Harris   Foraky Limited,   Contractors   England
E. Hugh Norie   Mott, Hay & Anderson, Consultants   England

ABSTRACT

As part of a pipeline upgrading scheme, a short length of new tunnel was required between two existing shafts each lying close to a water course - a river estuary and a sea-going canal.

Horizontal freeze tubes were drilled into place toward each old shaft from a new larger diameter shaft sunk at the mid point. Following refrigeration by an ammonia-brine system the tunnels were advanced by hand excavation and lined with bolted concrete segments.

The freeze tube drilling toward the canal shaft encountered a consistent timber obstruction just short of their intended length. As this could not be penetrated with the drilling method in use some vertical freeze tubes were installed to seal the end of the horizontal ice-cylinder.

This allowed tunnelling to start while further short horizontal freeze-tubes were installed from the old shaft until they too reached the obstruction. By refrigerating this section with liquid nitrogen a lengthy delay was avoided.

The method of drilling and placing horizontal freeze-tubes below the ground water table in alluvial soils, with a minimum of ground disturbance and loss is described.

Records of movements are given.

INTRODUCTION

Two major aqueducts supplying water to the Merseyside region of England are carried in tunnel beneath the Manchester Ship Canal and the River Mersey at a point where the two waterways are less than 50 metres apart, separated by a strip of land known as No-Man's Land. The First Crossing of the canal and river, completed in the 1890's, comprises a tunnel under the canal and a separate tunnel under the river. Water was carried through the tunnels in pipelines; these were brought to the surface at No-Man's Land via shafts, and carried across it at surface level. A second crossing of the canal and river was built in the present century.

By the mid 1970's, the three rivetted wrought steel pipelines of the First Crossing were reaching the end of their safe life. At this time, the Second Crossing was just able to carry the total demand of both crossings, allowing the First Crossing to be taken temporarily out of commission. This made it feasible to consider replacing all of the First Crossing pipelines at the same time. Following detailed studies, the decision was made to take advantage of this situation to replace the First Crossing pipelines with a single, large diameter pressure lining. A pressure lining was designed, just smaller than the internal diameter of the existing tunnels, to be grouted in to form an integral structure with them.

This will give a very large increase in capacity to the crossing as well as providing a system with minimal future maintenance.

An integral part of the pressure lining scheme was the connection of the two existing tunnels of the First Crossing with a new low-level tunnel across No-Man's Land. This would allow the pressure lining to be made continuous throughout the crossing, resulting in minimum head losses and maximum capacity.

Ground conditions at No-Man's Land comprise lenticular alluvial deposits, including very soft to soft clays, soft clayey silts and peat, to a depth varying between 12 and 15 metres. These deposits overlie loose to medium dense sands and gravels. The gravels are underlain by stiff boulder clay, followed by weathered sand stone. The new tunnel, with an axis level approx. 14 metres below ground level, would lie partly in the alluvial deposits and partly in the sands and gravels. The water table is on average about 3 metres below ground level, and is governed in the main by water level in the canal, although there is some influence from tidal variations in the river. At low tide, the head difference between the canal and the river is approx. 4 metres.

CHOICE OF CONSTRUCTION METHOD

The ground conditions at No-Man's Land posed various difficulties for tunnelling. The most critical factors affecting the eventual choice of construction method were firstly the need to maintain safe working conditions at all times, and secondly the ensure the integrity of the canal bank. Any significant ground disturbances could have resulted, in particular in the loose sands, in a dangerous increase in hydraulic gradient at critical locations through No-Man's Land, with the risk of a consequential failure by piping between the canal and the river.

Initial consideration was given to constructing the connecting tunnel by cut-and-cover, but this alternative was rejected, firstly on grounds of costs, influenced particularly by the very high ground pressures immediately above the sands, and secondly, because the risk of hydraulic interconnection between the canal and river was significantly higher than would have been the case with bored tunnelling. Various bored tunnel alternatives were examined. These included compressed air tunnelling, the use of injection techniques and the use of ground freezing. For the short length of tunnel involved, the use of a tunnel shield would have been un-
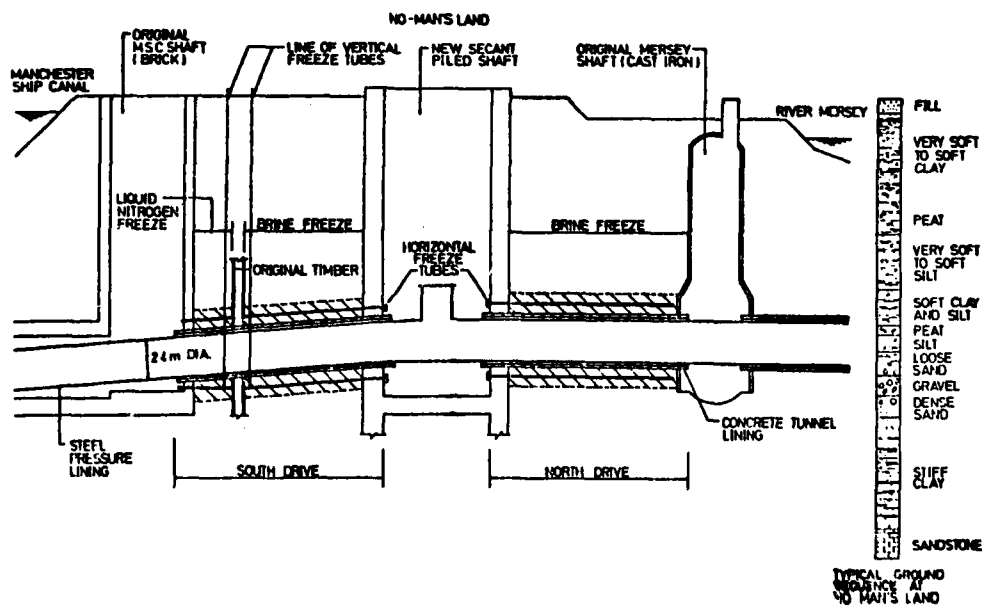

Figure 1. Longitudinal section through tunneling work

384

economic, and the methods examined were intended to avoid the need for a shield.

For the clays, silts and peat in the upper part of the tunnel, ground injection using any of the available systems would at best have been partially effective, and was not considered to be reliable for either ground or ground-water control. Compressed air working was rejected because of the risk that a major loss of air could occur in the vicinity of the existing shafts, where there was a strong likelihood of voids existing at the original temporary works. Because of obstructions at and below ground level, the extent of these works could not be assessed in advance, and no records of their construction existed.

The only method considered practicable for ground control during tunnelling was the use of ground freezing, with specific precautions being adopted to minimise the attendant risks due to ground disturbance during the freezing and thawing cycle. Minimization of disturbance led to the decision to carry out ground freezing horizontally from tunnel level rather than vertically from the surface in order to reduce the extent of the freeze, and hence ice lens formation, in the materials overlying the tunnel. Ice lenses could grow to a significant size in these materials, if frozen vertically, leading to the formation of voids as the ice thawed and a reduction in the hydraulic resistance of the ground.

An ice wall around the tunnel was designed as a cylinder. This was required to have a minimum thickness of 1.2 m to carry ground and groundwater loadings.

The existing shafts to the Manchester Ship Canal and River Mersey tunnels were too small to allow the installation of the steel pressure lining sections in economic lengths. A new shaft was therefore proposed, midway between the existing shafts, of a sufficient diameter to accomodate the pressure lining sections and to allow standard drilling equipment to be used during the installation of freeze tubes. The new tunnel was therefore planned to be driven in two sections, one north and one south, from the new shaft. Each tunnel section was about 12 metres long, giving a reason-able length for drilling for the installation of freeze tubes. A greater length of drilling could have created difficulties with drill stem deflection in the gravels of the tunnels.

It was recognised that the success of the work would depend on careful control of the ground surrounding the tunnel during thawing. Multiple stage backgrouting of the tunnel lining was called for during the thaw to ensure that the ground remained tight and that sufficient support was given to the tunnel lining, in particular at shoulder level, in the softer materials. As a further precaution, cut-off wing-walls were constructed from the central shaft perpendicular to the line of the tunnels to increase the length of water path between canal and river. The wall of the shaft itself was taken down to a cut-off in the boulder clay, and the wingwalls were taken down to this stratum as well. This additional precaution was found to be necessary, following decommissioning of the First Crossing and the removal of the original pipes from the Manchester Ship Canal shafts, when probe drilling through the shaft lining revealed the existence of extensive voids both between the shaft and the original temporary works timbering, and towards the underside of the canal.

Despite the very poor ground conditions and the high ground and water loadings at tunnel level, it was decided to use a segmental tunnel lining of precast concrete rather than cast iron or steel. The lining did not need to be fully watertight since the internal steel pressure lining would obviate this requirement. It was also considered that the mult. ple stage back-grouting, in conjunction with detailed monitoring of lining deflections, could be used to minimize lining distortion and thus keep bending moments within the limits for a concrete lining.

THE FREEZING SYSTEM

To satisfy the specified minimum ice-wall thickness of 1.2 m the 20 freezetubes were placed on a nominal 5.0 m diameter circle for the 3.4 m diameter excavation. A true circle was not possible for drilling to avoid joints between the secant-piles
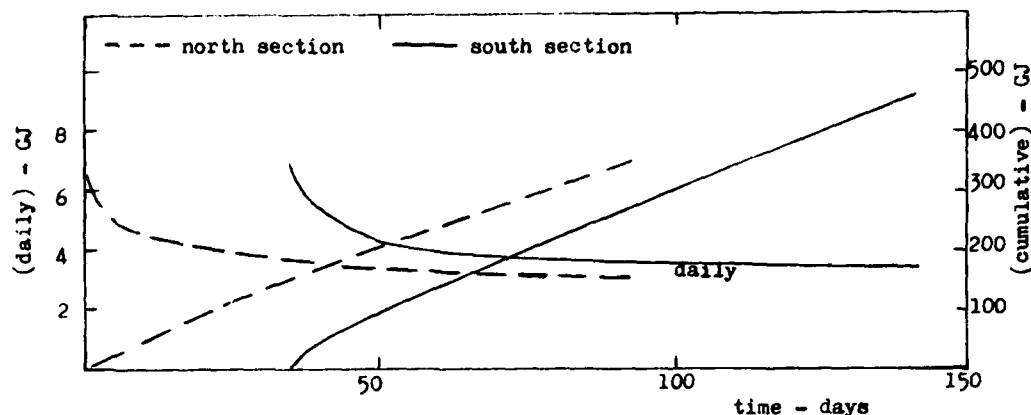
Figure 2. Heat extraction.

used by the Main Contractor to form the wall of the temporary working shaft; instead an octagonal pattern was employed.

Twin conventional two-stage ammonia compressors, each rated to extract 84 kW at -30°C evaporation temperature were selected. Either could achieve the frozen state for one tunnel in 3 weeks, while acting as reserve for the other in the event of a breakdown. Calcium chloride brine was used as secondary refrigerant, with heat dissipation to the canal water.

The intended phased programme of freezing and tunnel construction was affected by two influences (see also "timber obstruction").

The target for the north tunnel was a cast-iron shaft to which the freezetubes were drilled. Refrigerant circulation was effective to within 0.2m of the shaft, and this was sufficiently close for the ice-bond/ seal to form within the programme time. Monitoring of thermocouples installed in observation holes, centre-hole drainage observations at the working shaft, and frost growth inside the cast-iron shaft being in order, excavation commenced on schedule.

However, when the cast-iron was pierced at approximately tunnel centre, water at +2°C issued. The only anomaly that could be identified was that at invert level the ice-wall was below sump water level in the cast-iron shaft. The water level was being controlled within convenient limits by intermitt-

ant sump pumping. By intensifying the refrigerative effort to the lower freeze tubes, and segregating the water movement in the sump away from the face being refrigerated, full closure was rapidly achieved and the tunnel completed without further incident.

INSTALLATION OF FREEZE TUBES

The diameter of the working shaft was governed by the clearance needed, through its ring beams, to lower and manhandle the 6 m long, 2.8 m diameter steel sleeves that would form the final lining in the existing and new tunnels, and to provide a 6 m working length for freezetube drilling. A clearance of 8.5 m diameter satisfied these requirements.

Drilling was undertaken through a stuffing-box mounted on short flanged pipes pre-set into the secant piles.

A valved cutting-head was fitted directly to each freezetube so that a whole unit would function as casing, drill-rod and freezetube. The non-return valve allowed drilling flush to pass into the ground only which, combined with the stuffing-box assembly, effectively prevented ground loss. Once drilled to full penetration, a plug was placed behind the cutting head to seal the valved tip against brine-loss into the ground. A (water) pressure test was applied to each assembly before completing the freezetube furnishing and charging with brine.
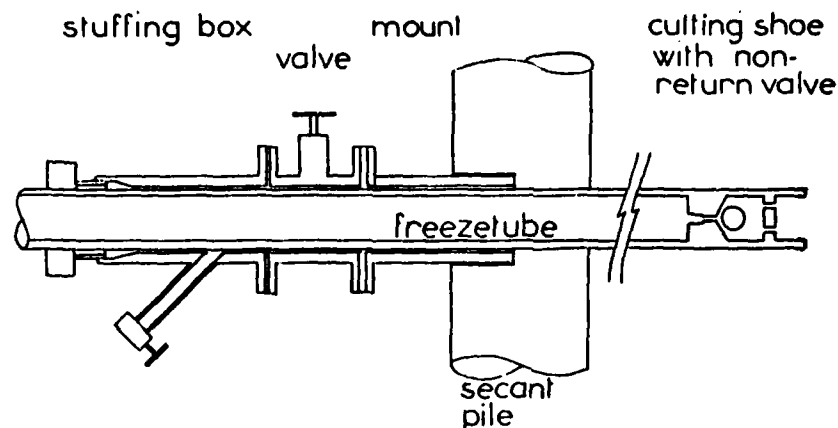
386

Figure 3. Drilling arrangement.

TIMBER OBSTRUCTION

While preparations for freezing the north tunnel section were in progres, further probing behind the (south) brick shaft, adjacent to the canal, disclosed an apparent barrier of timbers right across the line of the south tunnel. It was felt, and eventually confirmed, that they were the remains of the soldiers and walings that formed a temporary works cofferdam for the original canal tunnel construction.

The planned south section freezing system was therefore shortened to just reach the timber barrier, supplemented by three vertical freezetubes to ensure closure across the end of the cylinder, thus allowing tunnelling to proceed while a supplementary system for the remaining 1½-2m was prepared.

In order to limit any delays (and attendant costs) in completing the south section the short portion was frozen with liquid nitrogen. A splayed pattern of 32 freezetubes was installed from within the brick shaft (its diameter equalled that of the tunnel that would enter it); additionally, to provide intensive refrigeration at the timber barrier whose thickness and condition was unknown, six vertical freezetubes were installed along its estimated location.

When excavated, the timbers were found to be 0.6 m x 0.35 m in section and perfectly preserved.

A total of 66 Mg of liquid nitrogen was consumed over 5 days in establishing the frozen state, and a further 308 Mg over 34 days in maintaining the ice-body while the tunnel was completed. A similar quantity was consumed over 55 days refrigerating the timbers via the vertical freezetubes.

SITE MEASUREMENTS

Owing to the very constricted site layout above the tunnel, it was not possible to take measurements for heave at the surface. The measurement of movements was confined to the tunnel sections themselves; this was combined with the observation of any overstress in the original shafts.

The north tunnel construction, carried out first, showed small movements upwards as the freeze was discontinued. The maximum vertical movements upwards, approx 9mm, occurred 4 weeks after discontinuation of the freeze. This movement subsequently reversed, and over the following 5 weeks the tunnel moved downwards by about 3mm, probably due to vertical ground loadings being re-established on the lining as the frozen arch of ground above the tunnel lost its strength. The final movement recorded was 6mm upwards.

The south section rose about 2mm following discontinuation of the freeze, and subsequently moved downwards by 4mm,
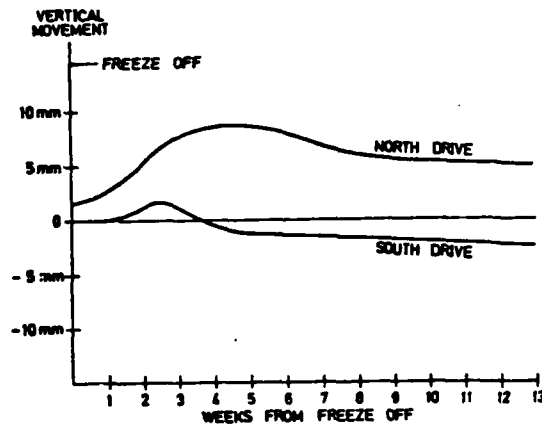
387

Figure 4.

giving a final movement downwards of about 2mm.

The above movements were very small; any differences between north and south sections were probably accounted for by minor variations in ground conditions. The tunnels showed no significant loss of circularity, and it may be concluded that the backgrouting carried out during the thaw was successful in keeping movements within small limits. No signs of overstress were observed in the original shafts or in the tunnel lining.

Measurements were discontinued in the north section after 5 months and in the south section after 3 months, when the pressure lining was installed.

CONCLUSIONS

1. The work was executed safely and, within the limits of external influences, expeditiously; the result fully justified using artificial ground freezing.

2. For minimal ground loss during horizontal drilling below the water table the combination of stuffing-box and non-return valve in the cutting head is particularly suitable.

3. Small external heat influences, such as are generated by moving water, can be dealt with and overcome.

4. Liquid nitrogen refrigerant is very valuable for dealing quickly with unforeseen situations.

5. Ground movements associated with a sub-level horizontal frozen cylinder in mixed strata were nominal.

A CASE HISTORY OF A TUNNEL
CONSTRUCTED BY GROUND FREEZING

Hugh S. Lacy, Associate, Mueser, Rutledge, Johnston & DeSimone, New York, N.Y.
John S. Jones, Jr., Chief Engineer, Law Engineering Testing Co. Washington, D.C.
Brien Gidlow, Vice President, O'Brien & Gere Engineers, Inc., Syracuse, New York

ABSTRACT

Artificial ground freezing was used for structural support and groundwater control for a 37 m long, 3.2 m diameter tunnel located about 2 m beneath high speed railroad lines in Syracuse, New York. A double row of freeze pipes spaced approximately 0.9 m on-center was used around the periphery of the tunnel above the spring line, while only a single row of freeze pipes was required below the spring line. Excavation of the frozen soil within the tunnel was accomplished with a small road header tunnel boring machine. Subsurface conditions consisted of cinders above the spring line of the tunnel with loose silty fine sand below. The moisture content of the cinders had to be increased using a bentonite slurry prior to soil freezing. Various types of instrumentation were used to monitor performance of the freezing system, including heave-settlement points; temperature measurements; slope inclinometers and frost indicators. The results of in situ testing of frozen soil, laboratory testing of frozen soils, computer analysis to predict stress-deformation-time characteristics under static and cyclic loading, the instrumentation program including a comparison of estimated and measured performance are discussed.

SITE CONDITIONS

When construction of a 3.2 m diameter, 37 m long tunnel has to pass 2 m below the base of railroad tracks, it was found that freezing a horizontal cylinder of ground below the tracks prior to tunneling was the most cost-effective solution. This site is located along the southeastern side of Onondaga Lake in Syracuse, New York. The tunnel passes beneath the mainline tracks between Albany and Buffalo with no alternative routes should it be made impassable during tunneling operations. With a requirement to maintain train speeds of 55 mph for 80 to 90 trains per day, it was important to use a tunneling method that would provide a high degree of safety.

Subsurface Conditions

The site is underlain by deep compressible soils extending approximately 67 m below the ground surface with fine sand overlain by cinders at the tunnel level.

The upper 3 m of soil is fill consisting of layers of loose black cinders and dark gray coarse to fine sand with varying amounts of gravel, silt and obstructions. Below the fill is about 7.6 m of loose gray silty fine sand to sandy silt with a trace of shells and some organic silty clay layers. In situ permeability tests indicated the permeability of the silty sand to be about 2×10^{-4} cm/sec.

The groundwater is 1.5 to 2 m above the tunnel invert with the normal level of the adjacent lake 0.9 m above tunnel invert. As a result of the great depth of compressible deposits, changes in the level of the groundwater table at the tunnel site would result in large settlement.

ALTERNATIVE CONSTRUCTION METHODS

Several alternative means of supporting the tracks during tunneling were investigated. Construction of a pile supported trestle was not feasible due to the limited track access caused by the high volume of train traffic. Site and track curvature constraints prevented relocation of the trackage. Multiple rail track reinforcement provided insufficient support for the span created by this large diameter pipe. Lowering of the groundwater table prior to tunneling was not considered feasible due to anticipated large track settlement. Chemical stabilization of the soil was considered a marginal solution and a field test program demonstrated that the soils at the level of the tunnel could not be consistently stabilized with chemicals. A field test program was also conducted to evaluate the effectiveness of freezing of the soil.

TESTING PROGRAM

A testing program was necessary to demonstrate that reliable support could be provided by freezing the relatively thin cover of cinders randomly mixed with sand. The test program particularly addressed variability in strength and elastic modulus, strain deformations under constant and cyclic loading as experienced by trains passing over the tunnel. Deformation of the frozen tunnel relative to adjacent unfrozen ground was also evaluated.

Field Testing

The field test program consisted of six freeze pipes placed in predrilled holes at a spacing of 0.9 m. Pipes with thermocouples were inserted midway between exterior and interior pipes and 0.6 m outside the freeze pipes. Calcium chloride brine was circulated and temperatures dropped from +7.5°C to -0.2°C in ten days. Pressuremeter tests performed in 7.6 cm diameter holes drilled in the frozen ground between the freeze pipes determined the strength and elastic modulus of the frozen soils. The modulus of elasticity of the frozen soils was determined from radial compression at relatively low values of strain. One such test was made on unfrozen cinders for comparison purposes. The location of this field test is shown on Figure 1. The results of these tests, shown in

Table 1, indicate low and variable strength and moduli for the cinders. During the freeze test period the ground surface heaved less than 2.5 cm.
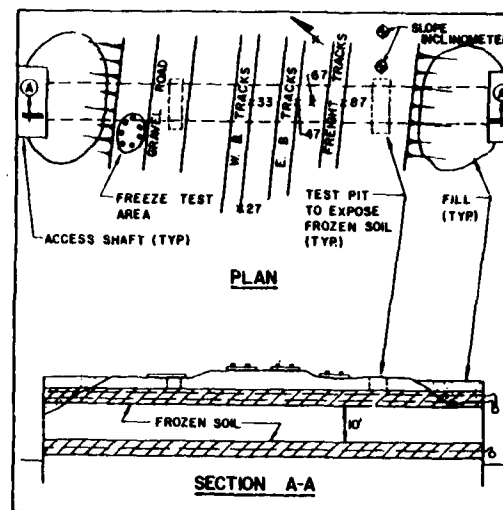

Figure 1. Tunnel Section

Laboratory Testing

As attempts were unsuccessful in obtaining undisturbed frozen samples of soils during the field test, 5 and 7.6 cm diameter undisturbed samples of unfrozen soils were recovered from eight shallow borings, transported to the laboratory and frozen while still intact in the sample tube to a temperature of -20°C. The samples were then extruded from the tubes for visual examination and further testing. One of the purposes of further testing was to evaluate the uncertain strength of the cinders, which tended to fall apart when attempts were made to core the frozen cinders during the field tests. Three unconsolidated-undrained triaxial tests were performed on each of the two soil types at specimen temperatures of -7°C and -1°C to determine the ultimate short-term strength of frozen soil. Some of the test results are included in Table 1. As expected, it was found that the strength was highly dependent on natural moisture content as well as temperature of the specimen. Strength tests on the silty fine sand samples fell within the general range of published information, while the strength of the frozen cinders was significantly below published data. The strength of the frozen cinder fill at this site is strongly dependent upon the amount of free water in its voids. Three samples tested at

390

-1°C had strengths of 3.9 to 8.1 tsf at moisture contents of 25 to 39 percent. Two samples tested at -7°C had strengths of 16.1 and 22 tsf with moisture contents of 28 and 29 percent, respectively. Specific gravity and absorption tests on cinder samples yielded specific gravities ranging between 2.05 and 2.10 with respective absorptions of 22 and 15 percent, suggesting that samples with moisture contents in the low 20 percent range essentially had almost no free pore water. This explains the low strengths of the drier samples. The strength of the silty sand increased from 14 to 64 tsf as the soil temperature dropped from -1° to -7°C.

Strain rate tests were performed by applying a constant stress varying between 50 and 90 percent of the ultimate short-term compressive strength and measuring the time to reach failure under the imposed stress. These tests consisted of five cinder samples at -7°C and one sample at -1°C. These tests show a substantial increase in strength with a relatively small increase in moisture content. The results of these tests are shown on Figure 2 as the reciprocal of the constant applied load vs duration of load before creep failure occurs. The design maximum applied stress of 8.7 tsf is below the level at which creep failure would occur for the estimated time periods that a train would be positioned directly over the tunnel.

first one-half minute, held constant for 1.75 minutes, then cycled at about 4-1/2 minute intervals for 100 cycles. The results of these tests are summarized in Table 1 indicating a reduction in the equivalent elastic modulus after 100 cycles to about one-third of the first cycle values. This value is similar to

TABLE 1
SUMMARY OF SOIL PROPERTIES

	Cinders		Silty Fine Sand	
	q_f(tsf)	E(tsf)	q_f(tsf)	E(tsf)
Frozen Soil:				
Laboratory Tests				
a. Quick Test	22 (31)	1500	70.5	2750
b. Cycle Test	11			
1 cycle		1450 (30)		2750
		1466 (29)		2750
50 cycles		550 (30)		1158
		550 (29)		1100
100 cycles		449 (29)		1000
c. Creep Test	17.6 (31)	462 (failure at 266 hrs)		
Field Tests	38	5633	120	9979
	--	9391		(~12°C)
	35	4502		
	39.5	18229		
	13.2	1543		
	--	3299		
	58	10336		
Values Used for Analysis				
	22	450 (low)	65	1000 (low)
		3500 (high)		6000 (high)
Unfrozen Soil:				
Laboratory Tests				
a. Quick Test	1.1 to	45 to	1.2 to	
	2.0	70	2.8	100
Field Test	11.8	120		73.5
	31.0			
Values Used for Analysis				
	80 (low)		100 (low)	
	240 (high)		500 (high)	

NOTES:
1. Assumed Poisson's ratio = 0.35
2. q_f = compressive strength
3. E = modulus of elasticity
4. Frozen soil tested at 7°C except where noted
5. The number in parenthesis is the moisture content for the cinder samples
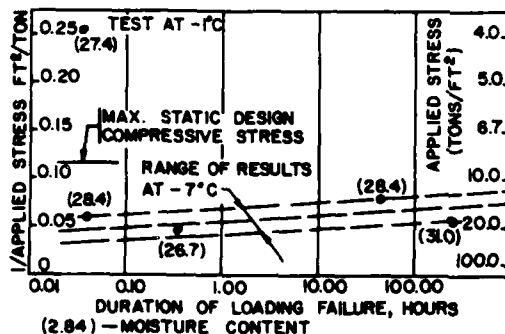6. Low moisture content test results are not included in this table

Figure 2. Test on Frozen Cinders

Cyclic triaxial loading tests were performed to determine the strength and deformation behavior of the frozen soil under dynamic loading conditions similar to that resulting from passing trains during tunnel excavation. A cyclic loading to approximately 50 percent of the short-term ultimate compressive strength of the cinder fill with moisture content at 30 percent was applied during the

the equivalent creep modulus value for cinders with moisture contents of about 30 percent. It was concluded that despite the heterogeneous nature of the in situ material, parameters of the frozen soil, such as strength and modulus of elasticity could be established for this material with reasonable confidence.

Measurement of Track Deflections

Track deflections were measured under normal operating conditions prior to tunneling to provide control data for comparison to measurements made during construction. These deflection measurements also provide an indirect means of

checking the results of stress-strain analyses for the tunnel. Two methods were used to measure the rail and tie deflections due to subgrade compression; direct reading using a surveyors level and a photographic method. The surveyors level was set up 15 m away from the track at a location permitting direct reading of scaled metal strips secured to ties and a steel bar driven into the subgrade between two ties. Visual observations were made prior to and while trains were passing. A high-speed camera with a telephoto lens was set up 9 m from the track with a surveyors rod mounted as a reference benchmark ten feet from the rail. Photographs were taken prior to and while train engines were passing indicating the top of rail deflection. Maximum rail and tie deflections were approximately 0.6 cm. Average rail deflection was 0.51 cm, while average tie deflection was 0.34 cm. The 0.17 cm difference in average deflection between the rails and ties suggests that the tracks are well-maintained, as the vertical play between tracks and ties can be over 2 cm for poorly maintained tracks. Measurement of the deflection of the steel bar driven 0.76 m below the ballast surface indicated deflections of .15 to .45 cm of subgrade compression as engines passed.

ANALYSIS OF PERFORMANCE UNDER TRAIN LOADING

The stress analyses for this tunnel were described in the First International Symposium on Ground Freezing by Jones and Brown (Ref. 2). Since that time additional studies have been performed to incorporate the effects of the freezing process in the analyses. Volumetric expansion of the soil during freezing causes significant movements and stress changes in the unfrozen soil regime. Finite element modeling of this phenomenon indicated ground surface heaving of up to 4 cm could be expected during the freezing period. Essentially no movement was calculated during the excavation period due to the very shallow overburden. Due to the types of soil present, approximately 3 cm of thaw consolidation, as discussed by Chamberlain (Ref. 3), was anticipated.

DESIGN REQUIREMENTS

Based on the analysis of maximum permissible stresses under train loading,

it was determined that the minimum frozen wall thickness should be approximately 0.9 m and that a minimum of a 1.2 m thickness should be provided across the crown of the tunnel to assure continuity of the frozen ring in the heterogeneous cinder fill. A minimum of 26 freeze pipes were required as shown on Figure 3. For thermal considerations, the ratio of the freeze pipe spacing to pipe diameter was required to be less than 13 throughout the tunnel length. Additional pipes were required to be installed in areas where this requirement was not met. The contractor was limited to installation methods that would minimize the loss of ground beneath the tracks, but permit penetration of obstructions where encountered. Temperatures of the frozen ground midway between freeze pipes had to be −10°C or below. It was also required that the moisture content of the cinder fill above the groundwater table be raised. As various tests had indicated part of the cinder fill to be highly permeable, it was required that an annulus of dilute viscous drilling fluid be placed around each of the freeze pipes during installation to increase the available free pore moisture and provide effective freezing of the upper cinder fill. Maximum injection pressures of this drilling fluid were limited.
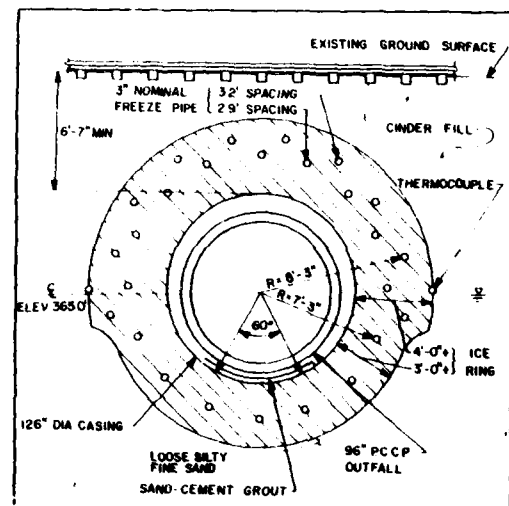

Figure 3. Planned Cross-Section of Tunnel

Liner Plate and Grouting

Following mining of the tunnel, placement of liner plate followed by packing pea gravel and grouting with

392

cement was specified. The use of liner plate support permitted more time for installation of the conduit pipe, and allowed early removal of the freeze unit and pipes, reducing energy costs.

Sheeted Access Shafts

In order to limit groundwater lowering adjacent to the tracks, continuous steel sheet piling was driven around each access shaft extending 15.2 m deep into the underlying clay. All pumping was limited to within these cofferdams. Observation wells were used to demonstrate the groundwater level was not being lowered beneath the track. Ground freezing was not considered for the access shafts as it would have to be maintained during the entire construction period and was not cost effective.

Monitoring of Ground Freezing

Extra horizontal pipes were required for the purpose of monitoring freezing of soil at four locations around the horizontal tunnel cylinder. Thermocouples were placed at five intervals along each of the pipes. Normal monitoring of the coolant was also specified. Frost indicators, consisting of one-inch diameter plastic pipe were installed in the ground. A clear plastic pipe filled with water mixed with methylene blue was suspended in this pipe. As the water froze, the blue colored liquid became white. Removal of these insert tubes indicates the level of adjacent frozen ground. Two test pits were required across the tunnel alignment adjacent to the tracks after the ground was frozen to examine visually the extent and the quality of the frozen soil. This provided a direct means of determining the moisture content of the frozen cinders and permitted drilling of holes through the frozen ground between freeze pipes to verify that the minimum thickness of the frozen cylinder was provided. Prior to commencing freezing, control elevations were to be established on the rails and on steel pins driven between the tracks at intervals to distances 7.6 m each way from the tunnel centerline along the tracks.

CONSTRUCTION PERFORMANCE

Certain aspects of the construction are described in another paper presented at this conference (Ref. 1).

Casing Installation

The Contractor elected to install 20 cm diameter schedule 40 steel freeze pipe casings in which the refrigerant piping would be later installed. The use of this casing provided an increased section modulus to allow better control and greater capacity to resist buckling during installation of the horizontal freeze pipes. The Contractor also proposed to use a continuous rotary flight auger to remove material from within the casing. The auger consisted of flights contained inside the casing with an articulated front section which could be adjusted up or down to maintain proper casing alignment. A hydraulic sensor on the casing head was connected to a panel in the access shaft to monitor vertical alignment. The articulated head could then be adjusted accordingly through a control rod mechanism on the boring machine.

The first casing was started at the bottom of the tunnel face on May 15, 1980. After proceeding less than 20 m, an obstruction was encountered. After several unsuccessful attempts to advance the casing, a television camera, used to inspect the inside of sewer pipes, was inserted into the casing. The camera showed rounded stones 8 cm to 20 cm in diameter at the face of the casing. These stones were too large to be returned by the auger through the casing. Attempts to break the stones by impact were not successful.

The next casing was started at approximately the 8 o'clock position on the tunnel face and was successfully completed the same day. In general, the remaining casings (21) above the 8 o'clock and 4 o'clock points were successfully installed at a rate of one per day. During these installations, two of the casing pipes had wandered out of horizontal alignment and were later substituted for the required monitoring holes in which thermocouples were placed for ground temperature monitoring.

The remaining five casings below 8 o'clock and 4 o'clock were more difficult to install. The first casing was abandoned and was replaced by two additional casings 0.2 m higher and 3.5 m north and south of the original casing. A temperature monitoring casing on the north side of the tunnel was relocated to a potential "weak spot" on the south side of the tunnel to be used as a freeze pipe should this need be indicated by the temperature monitoring data. In all, four (4) additional casing pipes were added in order

to obtain proper spacing to insure an adequate frozen ring. A cross-section of the final pipe locations is shown on Figure 4.
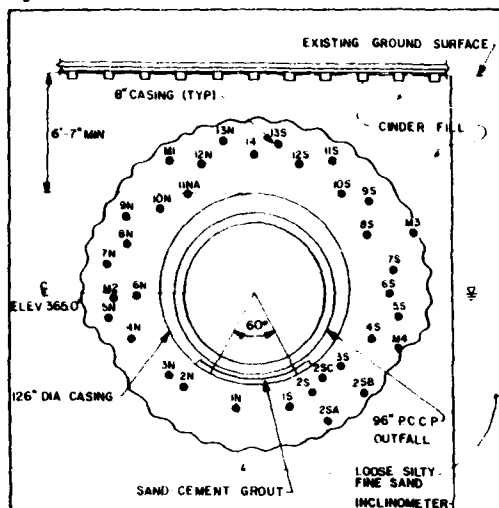

Figure 4. Actual Freeze Pipe Location

Increasing Cinder Water Content

Once the installation of the casings and freeze pipes was completed, water was sprayed on the ground surface. Water was also added through slotted holes in the casing pipes through a gravity head feed box. By monitoring the groundwater levels with the observation wells and piezometers, it was determined that groundwater levels had not been raised enough to assure a 30 percent water content in the cinders.

To further increase the water content in the cinders, bentonite slurry was pumped through the slotted casings into the surrounding cinders. The slurry was gradually thickened until it no longer flowed into the soil under the limited head. The slurry also filled the annular space and provided thermal conductivity between the casing and the freeze pipes. The use of slurry also facilitated removal of the freeze pipes after completion of the freezing since the slurry could be thawed by addition of warmer fluids in the freeze pipes. Approximately 13,000 gallons of bentonite slurry was used. It was estimated the slurry would allow the freezing of a 1.2 m wall thickness in the cinders.

Monitoring of Freezing

Figure 5 shows the variation in temperature vs the distance from the

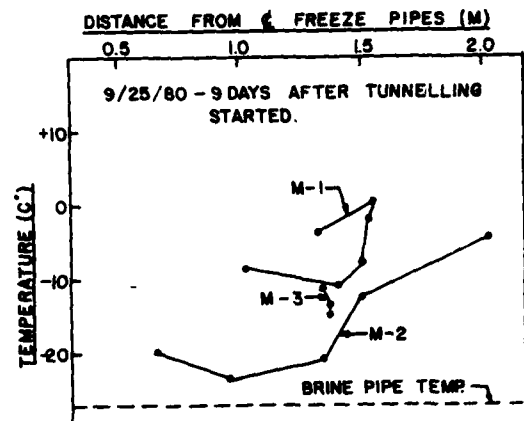average centerline of the frozen ring.

Figure 5. Temperature vs Distance from Freeze Pipe

Some of the variation in frozen ground temperature can be attributed to variations in distance of these monitor points from two nearby freeze pipes. Figure 6 shows the variation in soil temperature with time for two typical monitor points, as well as the variation in brine temperature. As expected, the point closest to the freeze pipes responded rapidly as the second freeze unit was added and the brine temperature dropped. Further from the freeze pipe, the temperature dropped more slowly; and as the second unit was discontinued, the soil temperature remained relatively constant, rather than rising with the brine temperature.
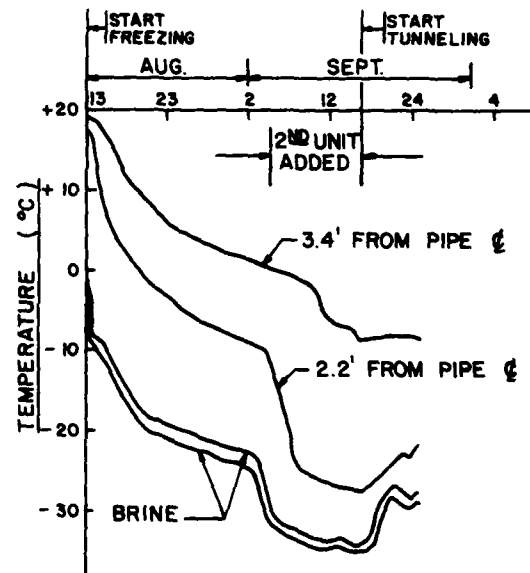

Figure 6. Soil Temperature vs Time

394

Prior to excavation of the test pits, temperature profiles were measured in the frost indicator holes adjacent to one of the test pit locations. This procedure consisted of removal of the frost indicator tubing, followed by filling the receiver pipe with salt brine, allowing temperatures to stabilize, and lowering a thermocouple and recording the temperature variation with depth. This procedure proved to be a useful tool when correlating this information with other temperature information and the test pit results and aided in assuring consistency across the roof of the tunnel.

On September 12, 1980 test pits were dug to verify the extent of frozen area. A backhoe penetrated 0.6 m of unfrozen ballast and sand plus 0.2 m of partially frozen cinders before encountering refusal. A jackhammer was used to penetrate the frozen ring to determine its thickness. After approximately 0.8 m of penetration the bit on the jackhammer froze in place and could not be removed. A second hole was dug along the centerline of the tunnel and a hole was chiseled in the frozen earth and water was added. Little water was lost from the hole indicating little porosity. The jackhammer indicated a 1 m frozen zone with no weak zones encountered. This physical observation and probing agreed well with information developed from the thermocouples and frost indicators. Samples of the frozen ground had moisture contents above 30 percent.

Tunnel Excavation and Support

On September 16, 1980 tunnel excavation began on the east face. Excavation was started using a crew with jackhammers. For the first 2 m, progress was made using this method since most of the material being removed was not frozen. By September 22, 1980 excavation progress had ceased due to extreme difficulty in mining the frozen material. The frozen soil at this point was relatively fine-grained and had the consistency of soft rock.

The excavation subcontractor walked off the job shortly thereafter and the general contractor immediately started searching for alternative excavation methods. A pneumatic hammer mounted on a backhoe was tried with little success. A continuous rock mining machine was brought in and excavating progress increased to more than 2 m per day. At this rate the excavation could keep ahead of the liner plate and grouting installation

The rate of excavation was controlled by the placement of the liner plate, rather than by the mining machine. The placement of the liner plates was such that no more than 1.6 m of exposed tunnel was allowed at any point. At that point additional liner plates were installed, packed with pea gravel and grouted using gypsum-based grout to produce quick setup under the cold conditions. Grouting voids were found by tapping the plate for hollow spots and confirmed by cutting the plates at selected locations. Regrouting was then required and again was inspected.

During the tunneling several obstacles were encountered including an abandoned 40 cm diameter water main, railroad ties and miscellaneous debris.

Displacement Measurements

Figure 7 shows the variation in track level after adjustments are made for reballasting of the track. Remote
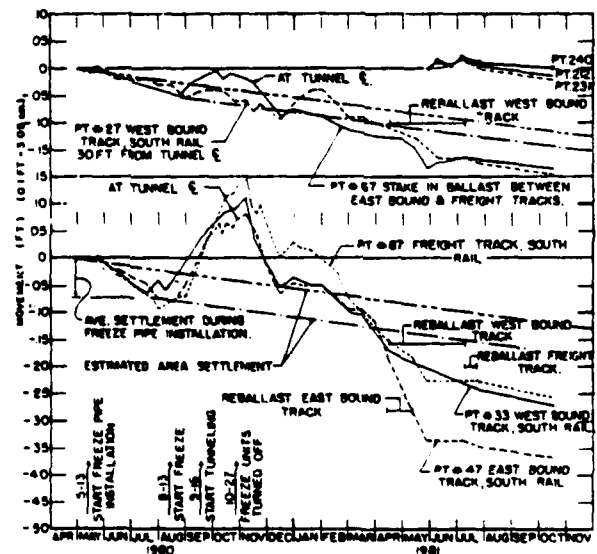
Figure 7. Variation of Track Level

readings indicate that the general area is settling at the rate of about 2.3 cm per year. Following settlement during freeze pipe installation that averaged 1.5 cm, the tracks experienced up to 6 cm heave during the period of artificial freezing. No discernable settlement occurred during tunneling. After the freeze unit was turned off, the tracks settled three to four cm, followed by what appears to be a slight natural frost heave from cold air temperatures during the winter months. Differential settlement at the tunnel continued until late

May. Settlement since that time has been parallel to the rate of area settlement. Settlement point No. 27 which is 9 m from the tunnel centerline, is shown for comparison purposes. At this location, there was no significant heave during the artificial freezing period, but a pronounced frost heave during the following winter months. Settlement after the construction period is 1.5 cm greater than area settlement, indicating a variation in normal area settlement or additional settlement caused by minor groundwater lowering for adjacent shaft excavation. Net settlement after compensating for settlement during freeze pipe installation that is greater than area settlements, as represented by Point No. 27, ranges from 0.7 cm to 4.3 cm. It is concluded that the net settlement was 12 to 72 percent of total heave due to soil freezing.

The slope indicators showed a lateral displacement of approximately 1.3 cm outward during the freezing period.

COMPARISON WITH PREDICTED PERFORMANCE

Displacement measurements provide the primary comparison between predicted and measured performance. The finite element analyses that incorporated the frost heave and thaw consolidation phenomena fairly accurately predicted the associated ground movements during the entire freezing process. The predicted heave of 4 cm was approximately 70 percent of the maximum heave anticipated. No settlement was anticipated during construction and was confirmed by the analyses. The predicted ground surface subsidence from thaw consolidation was almost identical to the measured displacement at Point 33 and approximately 50 percent of the measured displacement at Point 47.

The variations in observed surface movements from those predicted are believed to be caused by variations in the thickness of the bentonite grouted zones along the track, as well as variations in the rate of frost lensing.

ACKNOWLEDGEMENTS

REFERENCES

(1) Maishman, D. and Powers, J. P., "Ground Freezing for Tunnels - Three Case Histories", The Third International Symposium on Ground Freezing, June 22 - 24, 1982.

(2) Jones, J. S. and Brown, R. E., "Temporary Tunnel Support by Artificial Ground Freezing," The First International Symposium on Ground Freezing, Bochum, Germany, 1978.

(3) Chamberlain, E.J., "Overconsolidation Effects of Ground Freezing," The Second International Symposium on Ground Freezing," Trondheim, Norway, 1980.

396

GROUND FREEZING IN TUNNELS
Three Unusual Applications

Derek Maishman
J. Patrick Powers
         Vice Presidents,
         FreezeWALL Inc.,
         U.S.A.

INTRODUCTION

The three case histories described herein illustrate the broad versatility of the ground freezing method in solving tunneling problems. It is possible to construct various types of underground structures of frozen earth, to cutoff water and to support loads. These case histories illustrate a horizontal cylinder, an arch, and a bulkhead, all of frozen earth. Other shapes are possible, their variety limited only by the ingenuity of the designer.

Successful application of ground freezing requires a thorough understanding of the technology involved, including the flow of heat through the soil and its other thermal properties, the increase in soil strength resulting from reduced temperatures, and the equipment and processes used to achieve the desired effect.

Ground freezing is also affected by the degree of saturation of the soil, and the movement of ground water in the soil. The site specific water conditions must be evaluated to assure a successful application of the method. Particularly with clays, laboratory tests are advisable in samples of the soil to be frozen, to establish temperature and strength parameters for purposes of design.

Adequate instrumentation is required to insure that the desired soil strength, and the intended shape and dimensions of the frozen structure have been achieved.

Finally, successful ground freezing demands satisfactory solutions to practical construction problems. Some of these problems are similar to those in other geotechnical installations, some are unique to freezing. The case histories will illustrate a variety of such problems: the difficulties they presented, and the solutions that were found.

An additional paper is being presented at this Conference on one of the case histories. Lacy et al [1] gives technical data on the Syracuse project. This paper will emphasize the general nature of the construction problems, and the practical solutions achieved.

CASE HISTORY 1:

DAMAGED SEWER TUNNEL, DETROIT, MICHIGAN

This example illustrates the use of ground freezing under both emergency conditions and extended operation, to form a unique underground structure.

A 12 foot 9 inch (3.9 m) diameter interceptor sewer tunnel in Detroit during a routine inspection in January of 1980 was found to be in imminent danger of collapse. Apparently a leak had developed in the secondary concrete lining, and ground water leaking into the sewer had carried fine sand, creating a cavity under the sewer. Upstream of the break the tunnel had settled an estimated four feet. The settled section exhibited severe stress cracking. (Fig. 1 is a photograph taken after the sewage had been diverted.)

The sewer served an estimated quarter of a million people.

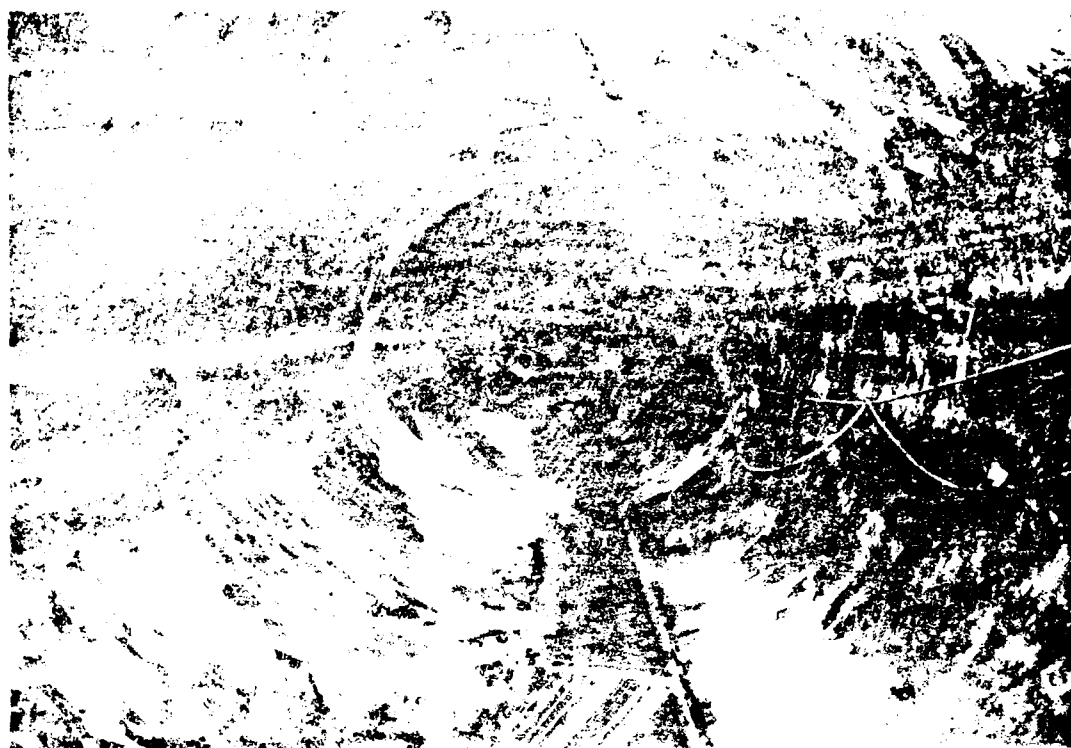The Detroit Water & Sewerage De-

Fig. 1

partment instituted several simultaneous steps in an effort to prevent a catastrophe. Emergency pump stations were set up to pump the raw sewage into surface streams if necessary. Work was begun placing large diameter steel pipes through the distressed area, to maintain some flow in the event of collapse. Construction of bypass was initiated, although this would take some months to complete. (Fig. 2a)

Meanwhile efforts were made to prevent further deterioration. Settlement pins indicated continued settlement in measurable amounts almost daily. Test drilling alongside the tunnel encountered a major void. An attempt was made to fill the void by gravity grouting with cement. The settlement appeared to accelerate, and the effort was suspended.

Concurrent with the above operations, the possibility of a ground freezing solution was investigated. Analyses indicated that a series of arches of frozen earth, founded on undisturbed soil on either side of the tunnel, (Figures 2b, 2c), would carry the overburden load. If the arches could be formed quickly enough, the tunnel lining would settle a little more, and with the overburden load removed, might be able to support its own weight.

Because of the urgency, the liquid nitrogen (L N$_2$) process was selected to form the arches as rapidly as possible. But if the effort succeeded, the ground support would have to be maintained for some months. Maintenance cost with L N$_2$ would be prohibitive. A brine refrigeration plant to maintain the freeze was mobilized concurrently with the L N$_2$ equipment. Thus from its inception, the 15 Mile Road project was a unique combination of L N$_2$ and refrigerated brine.

The freeze pipes and connecting piping had to be compatible with either process. At L N$_2$ temperatures (-320°F, -195°C) steel piping can shatter on impact. The polyethylene and rubber pipes common to brine systems would be as fragile as eggshells when exposed to L N$_2$.

The size of L N$_2$ freeze pipes and connecting piping is small, in comparison with that of brine systems. But the density of freeze pipes is greater, for efficient use of the process.

The changeover from L N$_2$ to brine presented potential problems. Normal circulating temperature of refrigerated brine is about -15°F (-26°C). The freezing point of brine concentrations normally used is -31°F (-35°C). If the

398

FIG. 2A

FIG. 2B

CROSS SECTION
TYPICAL NITROGEN FROZEN RIB

FIG. 2C
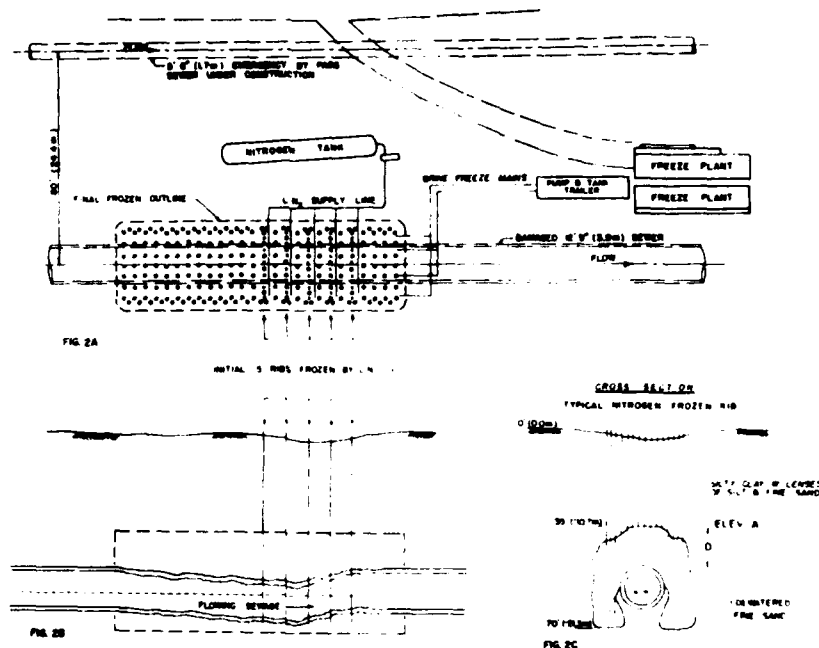
brine were introduced too quickly after
the L N$_2$ was shut off, it might solidify,
fail to circulate, and damage the freeze
pipes and connecting piping. If it was
introduced too late, the strength of
the previously formed frozen arches
might deteriorate.

A further complication was pre-
sented by the geometry of the frozen
structure. Note in Figure 2c that the
dimension D has an optimum value suffi-
cient to support the overburden pres-
sure. Heat energy pumped from the soil
above elevation A would be of negligible
benefit. Yet the cost of pumping the
energy would be significant. In the
case of the emergency L N$_2$ freeze, the
nitrogen consumption would be very
high. And for the brine freeze, addi-
tional plant capacity would be required,
and excess power consumption over the
extended maintenance period would be a
substantial cost.

A major problem was presented by
the drilling of the freeze holes. A
large number of holes had to be drilled,
and quickly. The tolerance on verti-
cality would be very close, to provide
spacing at depth, close to design. The
holes would be drilled into badly dis-
turbed ground. A mistep, for example
if heavy drill steel dropped suddenly
into a void, could trigger the collapse
of the tunnel.

An application requiring liquid
nitrogen in such large quantity (a total
of 700 tons (636,000 kg)) is unusual.
Finding the special equipment to trans-
port the L N$_2$ from its source, and store
it at the site, would be a problem.

399

Most of these problems were antici-
pated; some developed as the work pro-
gressed. The final design and execution
had these elements:

A system of five individual frozen
arches, each 3' 3" (1.0 m) thick, and
spaced 8 feet (2.44 m) on centers, were
created by the L N₂ process over the most
distressed part of the tunnel. It was
hoped that these would support the over-
burden pressure, the natural arching
strength of the soil spanning the gaps
between the frozen arches.

Spacing of the freeze pipes for the
L N₂ arches was 2 feet (0.61 m) half the
normal spacing of brine pipes in this
type of application. Every second pipe
was 4 inches (0.1 m) in diameter, so
that it could be subsequently converted
to brine. Intermediate pipes were
2 inches (0.05 m) in diameter. The
smaller diameter pipes were designed to
accommodate the evaporating liquid nitro-
gen, and the larger ones cold nitrogen
gas.

All freeze pipes were steel. For
the L N₂, rigid connecting piping was
steel; flexible connections were
braided bronze hose. To avoid unneces-
sary heat loading, the freeze pipes were
insulated above elevation A, (Fig. 2c).
Two types of insulation were used. Ini-
tially, foamed polyurethane was sprayed
on site inside temporary molds set
around the freeze pipes on the surface
to produce a nominal 2 inch (.05 m)
thickness; however, this was replaced
as soon as possible by custom built
insulated pipe consisting of a similar
thickness of insulation extruded between
the freeze pipe and a tough outer P.V.C.
sheath.

The insulation presented some
difficulties during installation of the
freeze pipes in the drilled holes. How-
ever, subsequent monitoring indicated
that the effort was effective in drama-
tically reducing the amount of heat
pumped from the soil above elevation A.

The L N₂ supplier provided an insu-
lated tank of 21,000 U.S. gallons
(80 m³) capacity for site storage. A
fleet of special vacuum insulated trucks
was assembled from as far away as Texas,
to transport the L N₂ from the source in
Albion, Michigan.

Drilling of holes for the freeze
pipes proved to be a sifnificant pro-
blem. Work began with rotary soil
boring rigs, using bentonite drilling
fluid. The method proved slow, parti-
cularly with the careful procedures

necessary to avoid damage to the tunnel.
Loss of drilling fluid into the voids
was troublesome. There was concern
over the verticality of the holes.

A better solution proved to be a
specially adapted pile rig, with a
continuous flight auger mounted in leads
and powered by a hydraulic tophead
drive. This rig was capable of pro-
ducing up to 15 holes per 10 hour shift.
It operated on mats, so that leveling
was convenient to assure verticality,
and to spread the potential surcharge
load on the tunnel as much as possible.

Through the coordinated effort of
a great many determined people, the
work advanced rapidly. Consideration
was first given to ground freezing on
February 1st. The decision to proceed
was made on February 2nd. Twelve days
later, on February 14th, liquid nitro-
gen was flowing into the freeze pipes.
On February 18th, the monitoring thermo-
couples showed the arches were approach-
ing completion. The morning settlement
readings on February 20th, sixteen days
after work began on site, indicated
movement of the tunnel was arrested,
for the moment.

But if the distressed tunnel had
become quiet, little else on the pro-
ject slowed down. Work on the bypass
pump station and pipeline was moving
along. The emergency pump stations
were nearing completion, although now
it was hoped they would never have to
be used, and the environmental damage
could be avoided. Within the tunnel,
work continued on the steel pipes
through the distressed area.

Drilling of freeze pipes continued.
As shown in Figure 2a the plan was to
fill in between the L N₂ arches to pro-
vide more reliable support. It was
also decided to extend the solid arch
beyond the limits of the critically
damaged zone. This was intended to pre-
vent further deterioration, and to pre-
pare for repair after the sewage was
bypassed.

It was possible to monitor condi-
tions between the L N₂ ribs using inter-
mediate brine pipes not yet in service.
Figure 3 shows that nine days after
start of L N₂ flow, the midway tempera-
ture between the arches was below 32°F
(0°C) indicating the gap between the
ribs had closed.

The changeover from L N₂ to brine
went according to plan. (Fig. 4) Two
units each of 83 tons refrigeration
capacity (at -20°C brine delivery)
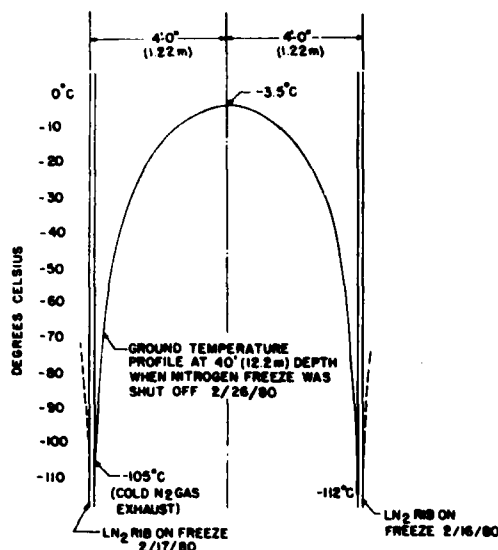
FIG. 3 JOINING OF ADJACENT RIBS
AFTER NINE DAYS FREEZING WITH
LIQUID NITROGEN

were installed. At the start both units
were put on line as soon as possible to
accelerate the formation of the brine
freeze. After formation, one unit oper-
ated intermittently and the other re-
mained in place as standby.

In April the bypass was completed,
and the tunnel bulkheaded and dewatered.
By this time much of the concrete in the
distressed area had collapsed, forming
a pile of rubble in the invert. The
frozen arch and its buttresses formed
the only support over what had become
a cavern, roughly 18 feet (5.5 m) high,
and 42 feet (12.8 m) long. (Fig. 5)

A decision was made to reconstruct
the existing tunnel, rather than to
drive a new tunnel on a different align-
ment. The reconstruction option repre-
sented a significant saving. It would
not have been available without the
frozen arch.

The reconstruction was accom-
plished without exposing personnel in
the cavern. First, rubble and muck were
cleaned from the invert with a grapple,
and the invert was overexcavated. Next,
the invert was replaced by a mass con-
crete pour.

It was now the end of July and
three factors combined to cause diffi-
culty with the freeze system. First,
the summer ambient conditions imposed an
increased discharge temperature on the
freeze plants. A heat pump like a water

pump loses capacity with higher energy
change. Second, the high ambients
increased the losses through the insu-
lation of the surface piping.

The above two conditions were
satisfactorily within the safety factors
designed into the refrigeration system.
Brine temperatures, and ground tempera-
tures within the arch, could be main-
tained at necessary levels.

However, a third condition within
the tunnel itself presented a very
difficult problem. Ventilation was
necessary to provide safe and workable
conditions for the repair crews working
in the tunnel. With surface air
temperatures running above 90°F (32°C)
during the day, the fans were imposing
a very significant heat load on the
underside of the arch. Construction
operations, particularly the heat of
hydration of the concrete, added addi-
tional load. The arch began to erode
from underneath. Tiny pats of clay
would thaw, fall away like intermittent
rain drops, and expose the material
above it to the heat load. The deter-
ioration was slow, but progressive.
The tips of some of the freeze pipes
began to appear.

The work was accelerated, in an
attempt to finish before the arch
weakened to the danger point. Conven-
tional steel ribs with wood lagging were
advanced into the cavern, keeping per-
sonnel at all times under the protection
of the completed structure.

It was realized that if the under-
side of the arch could be thermally
insulated the deterioration would stop.
But the insulation would have to support
the droplets of thawed clay for some
period of time until the temperature
was lowered and the deterioration
stopped. Sprayed insulation was con-
sidered impractical. If it did stick
to the sweating surface, the weight of
thawing clay droplets would almost
surely push it loose before the tempera-
ture had dropped sufficiently.

One method to insulate the roof of
the cavern was attempted. Although it
was not successful, it is reported here
to add to the professional understanding
of these matters.

At one Conference treating with the
problem, someone suggested that toy
balloons floated up to the arch might
accomplish the purpose. The conferees
eyed each other warily around the table,
in the manner of men unsure if they are
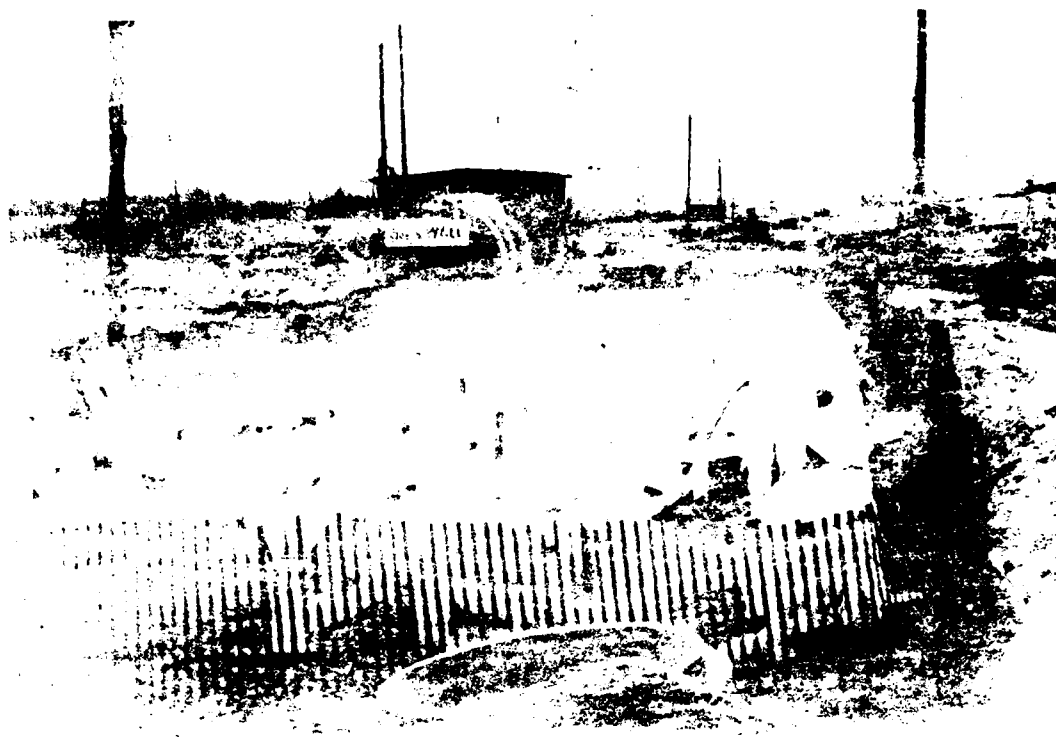being chivvied. But the idea made
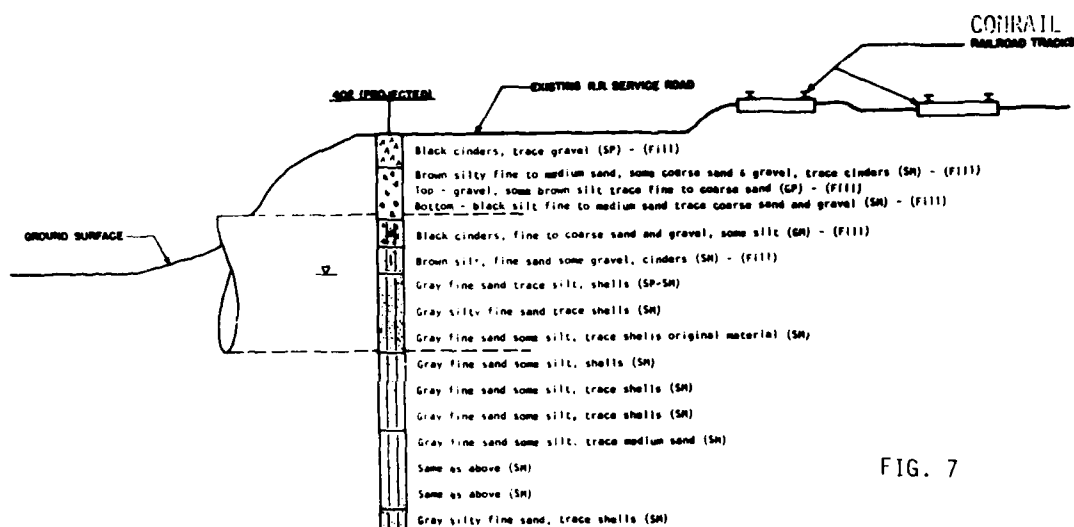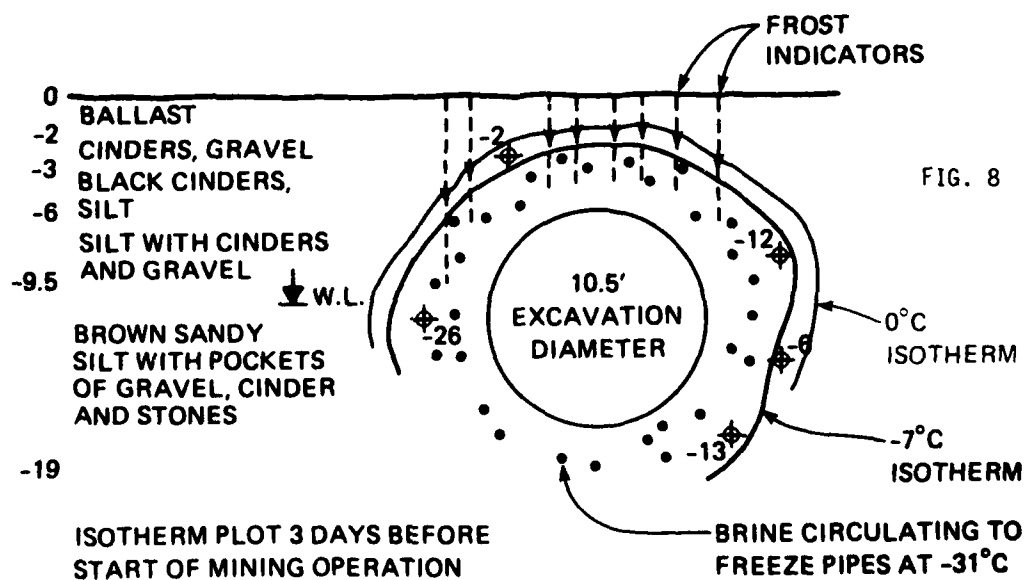
401

FIG. 4

FIG. 5

402

Black cinders, trace gravel (SP) - (Fill)

Brown silty fine to medium sand, some coarse sand & gravel, trace cinders (SM) - (Fill)
Top - gravel, some brown silt trace fine to coarse sand (GP) - (Fill)
Bottom - black silt fine to medium sand trace coarse sand and gravel (SM) - (Fill)

Black cinders, fine to coarse sand and gravel, some silt (GM) - (Fill)

Brown silt, fine sand some gravel, cinders (SM) - (Fill)

Gray fine sand trace silt, shells (SP-SM)

Gray silty fine sand trace shells (SM)

Gray fine sand some silt, trace shells original material (SM)

Gray fine sand some silt, shells (SM)

Gray fine sand some silt, trace shells (SM)

Gray fine sand some silt, trace shells (SM)

Gray fine sand some silt, trace medium sand (SM)

Same as above (SM)

Same as above (SM)

Gray silty fine sand, trace shells (SM)

FIG. 7

FIG. 8

ISOTHERM PLOT 3 DAYS BEFORE
START OF MINING OPERATION

403

sense. The balloons could rearrange themselves to release clay droplets, until the temperature dropped and the freeze was reestablished. Since the cost was negligible and no harm could ensue, it was decided to try. The tunnel superintendent made one proviso. He insisted that the attempt he made on the graveyard shift, when a minimum number of his people would be underground. Tunnel workers, he said, are a special breed. He did not want them to think their managers on the surface had become unsound.

A toy manufacturer was located, and a supply of balloons and a helium bottle rushed to the site. The balloons floated up into the desired position as planned. Hopes rose with them. Unfortunately, before the brightly colored blanket could be fully established, the first balloons were beginning to drift down. The lowered temperatures had cooled the helium. The balloons contracted and lost buoyancy. They drifted slowly down, became caught in the ventilation draft, and were swept away.

On the basis of this experience, the use of helium filled balloons for insulating arches of frozen earth is not recommended.

The tunnel crews continued their work with proven, less exotic methods. The monitoring instruments indicated there was more than ample strength remaining in the arch. But the constant patter of clay droplets gave everyone a sense of urgency.

In early August the lining of ribs and lagging was completed across the cavern, and concrete was pumped into the space around and above the lagging. Except for final cleanup, the rescue was complete.

A series of arches of frozen earth, formed in a matter of days by the rapid L N₂ method, had saved a tunnel in imminent danger of collapse. A more extended operation with a continuous arch formed by the more economical refrigerated brine process, continued to preserve the tunnel, and provided conditions under which repair could be accomplished.

Figure 6 shows the observations made of a settlement pin on the centerline of the tunnel, together with monitoring of ground temperatures during and after termination of the brine freeze.

Directing site operations for the Detroit Water and Sewerage Department was Mr. James Heath. Walbridge Aldinger

Company was construction manager, coordinating the complex series of operations. John Rakolta, Jr. was Project Manager and Mr. Alvin Daum, Superintendent. Work within the tunnel was performed by Michigan Sewer Company under the direction of Mario di Ponio. Neyer, Tiseo and Hindo were geotechnical consultants, Mr. Jerry Neyer being partner in charge. L N₂ and the specialized tanks and trucks were provided on schedule by Airco Industrial Gases.

STRENGTH VS. SATURATION
FROZEN SOIL SAMPLES

① FINE GRAINED SILTY SOIL (SANGER, 1964)

② FINE SAND, -12°C, 1.33×10⁻⁴ mm⁻¹ (BAKER, 1972)

③ PEABODY SANDY GRAVEL, -1.1 TO -17°C, 1380 PSI/MIN. (KAPLAR, 1971)

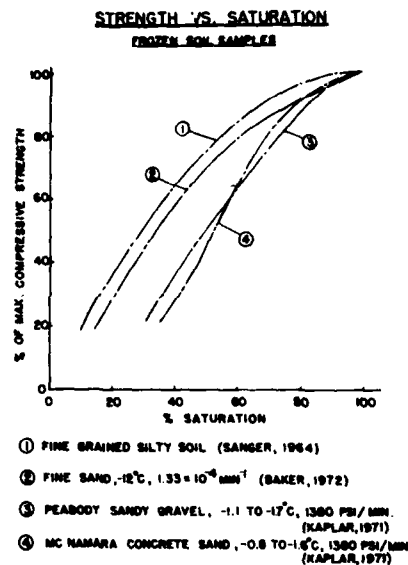④ MC NAMARA CONCRETE SAND, -0.6 TO -1.6°C, 1380 PSI/MIN (KAPLAR, 1971)

Fig. 9

CASE HISTORY 2:

ONONDAGA SEWAGE TREATMENT PLANT SYRACUSE, N.Y.

The outfall from Onondaga Sewage Treatment Plant in Syracuse, N.Y. required a crossing underneath the main line of Conrail. Unlike the emergency situation in the previous Case History 1, there was ample time to consider the various options at Syracuse, which was fortunate, given the complexity of the problem, and the number of agencies whose interests had to be considered.

The design grade of the 10' 6" (3.2 m) tunnel enclosed outfall was at shallow depth, and it would under usual circumstances have been built by cut-and-cover methods, using a conventional shoofly. But this was Conrail's main line, with an average of 85 trains

404

passing daily, including heavily loaded freights, as well as the high speed passenger services of Amtrak. Conrail considered the line its 'aorta'. Even short interruptions would seriously disrupt service between New York and Chicago.

Tunneling was the necessary choice. But with only 7 feet (2.1 m) between the arch of the tunnel and the base of the rail, a high degree of risk was involved. Even with skilled crews and careful procedures, failure of a tunnel face is always a possibility. Beneath Conrail's aorta, such a failure could become a catastrophe.

The ground, in tunnel terms, was 'bad'. A generalized profile is shown in Figure 7. Clay, sand and silt, with fill to various depths. The fill ranged from sand to cinders to railroad ballast. Despite the care during the geotechnical investigations, it was apparent in such variable ground that the tunneling conditions would not be fully appreciated until the tunnel was driven.

Planning began well in advance, and was extensive and thorough. Lacy et al [1] point out that the ground freezing option was considered early on. With the face protected by a horizontal cylinder of frozen earth, with primary lining brought up close behind the face, the operation seemed feasible and safe. The ground freezing test installation was performed, to confirm the suitability of the method at this site, and to provide data for final design.

When the construction phase began, three practical problems had to be faced. First, the need to jack horizontal freeze pipes 126 feet (38.4 m) through variable soil, maintaining the accuracy of freeze pipe spacing that was essential to a reliable freeze. If the pipes wandered too far from their intended location, the strength of the frozen cylinder would be in question. If the pipes wandered into the way of the tunnel, they could present an obstacle to progress. And if the freeze pipes were damaged while tunneling, the integrity of the frozen cylinder might be in jeopardy.

The second problem occurred because the upper part of the frozen cylinder was above the normal ground water table. Effective freezing of granular soils is a function of the degree of saturation. The diagram, Figure 9, shows typical relationships of frozen strength and

percentage saturation for some natural soils from various sources, compiled by the National Research Council of Canada. At Syracuse, the material above the water table was basically a cinder fill and special tests were necessary to characterize the frozen properties at various levels of water saturation, as described by Lacy et al [1]

The third problem involved the actual mining, and grew out of the inherent geometry of a horizontal cylinder of frozen earth. The ideal situation would be to maintain the frozen cylinder, and mine soft or lightly frozen ground within its protection. But the freeze pipes must pump whatever heat load comes radially from the outside. In the process, they will also pump heat outward from the center of the cylinder. It is not practical to prevent the tunnel face, with time, from freezing solid. Mining would be in frozen earth.

The three problems were addressed as follows:

1. From thermal and hydraulic considerations, the freeze pipes needed to have an approximate diameter of three to four inches (76 to 102 mm). But such slender pipes would have little moment of inertia to resist deflection, and would wander off alignment. It was decided to jack 8 inch (203 mm) diameter, heavy wall steel sleeves, and install the freeze pipes within them. The sleeves were advanced by hydraulic pressure, while an auger close to the cutting edge moved material back through the sleeve to the jacking pit. Quantity of material was carefully monitored. The method was effective except where rocks and other unexpected obstacles were encountered. In such cases deflection, and, in one case, refusal occurred The equipment had some degree of steering capacity. Periodically surveys were carried out, and attempts were made to bring the sleeve back to the desired alignment. Final proof of the effort was available when the sleeve emerged into the receiving pit. Overall performance was reasonable. It was found necessary to install 30 sleeves, versus the 26 theoretically necessary if the alignment of each sleeve had been true. Recalculations made during the installation were used to determine where extra sleeves were required.

2. The problem of unsaturated soil above the water table had been anticipated. Injection of fluid to achieve saturation was to be accomplished in two ways. The sleeves above the water table were perforated, so that fluid could be injected through them. And arrangements were made for inundating the ground surface between the tracks. Creating a mound in the ground water table is not difficult; maintaining the mound until it has been frozen is another matter. In soils as permeable as some of the sand and cinder fills on this project, the mound dissipated rapidly when injection stopped.

The solution decided upon was to inject bentonite slurry through the perforated sleeves. Due to its viscosity, the fluid would develop the mound more slowly but dissipation of the mound would also be slow. Further, arrangements were made to chill the injected slurry with the refrigeration plant at hand. Lower temperatures increased the viscosity of the pre-hydrated slurry. And it created a situation where the transition from saturated soil within the ground water mound, to frozen soil, was continuous and the chilled slurry accelerated the formation of the freeze. The techniques succeeded, in that a frozen cylinder of the necessary strength was developed.

3. The problem of excavating frozen soil in the tunnel heading had been anticipated. However, the tunnel subcontractor had underestimated the strength of the frozen earth. The clay spades and jackhammers he had provided for proved incapable of mining the material efficiently and on schedule.

A Dosco roadheader (Fig. 10) of the type developed for mining soft rock was brought to the site. Its cutter head ripped the frozen earth with good efficiency, and the schedule was restored. The tunnel was completed without interruption to railroad service. Some track movement occurred, heaving up to 2.5 inches (.06 m) during freezing and settlement of about 1.5 inches (.04 mm) afterwards. This was within safe tolerances.

Designer of the project (see Lacy et al [1]) was o"Brien and Gere, with Brian Gidlow, principal in charge. Geotechnical engineers were Mueser, Rutledge, Johnston & Desimone. Hugh Lacy was project manager. General contractor was M. A. Bongiovanni, Inc. The

sleeve pipes were jacked by Street Bros. of Syracuse, N. Y.

CASE HISTORY 3:

TUNNEL, DETROIT SEWAGE TREATMENT PLANT

In this application, ground freezing was used to protect against a contingency which fortunately never occurred.

The City of Detroit Sewage Treatment Plant along the River Rouge is founded on 80-90 feet (25-27.5 m) of soft clay. Foundation design is complex, and construction excavation presents extraordinary problems. Excavation for large concrete tanks, for example, must be done in segments; the design of the structure must be suited with care to loading during construction, as well as final loads. Tunneling for new additions to the plant piping is usually done by advancing a closed face shield, with small ports through which the muck is extruded onto the conveyor. The ease with which the soft clay flows is extraordinary. If the gated ports are too wide, excess muck flows into the tunnel and ground settlement quickly occurs, threatening existing structures. If the ports are not open enough, the underexcavation can cause heave at the surface even with forty feet (12 m) of cover. It

FIGURE 11

407
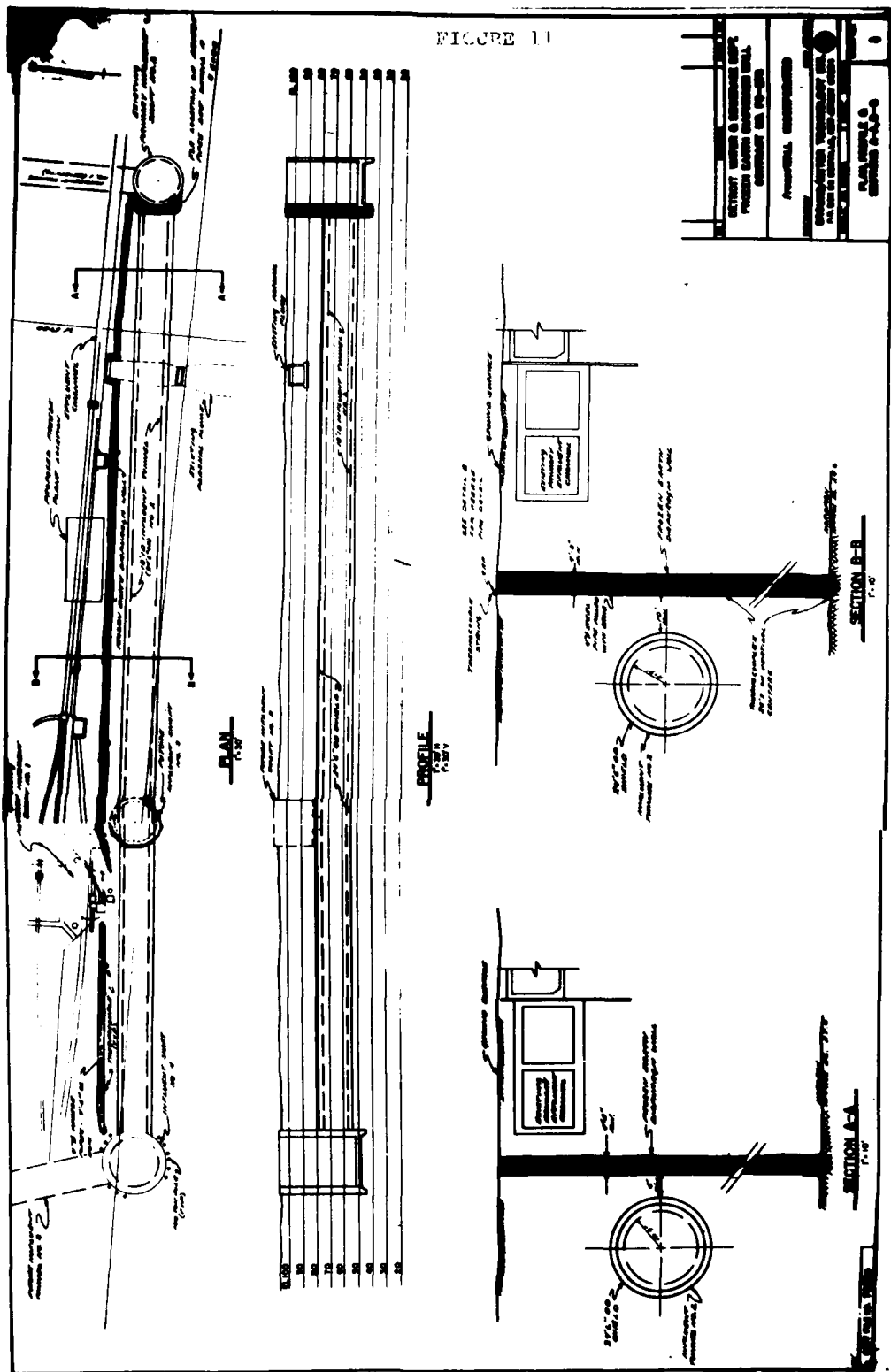
was reported that during the drive of an 18 foot (5.5 m) tunnel some years before the project discussed herein, one of the ports in the shield was inadvertently left cracked open on Friday night. Some hundreds of cubic yards (m^3) of soil seeped through the small opening into the stationary shield, causing settlement of up to 10 feet (3 m) over the weekend.

The 1980 additions to the plant required driving of a 24 foot 6 inch (7.74 m) tunnel approximately 700 feet long. As shown in Figure 10 the tunnel was close to and well below the existing primary effluent channel. There was concern that if loss of ground occurred the channel might be damaged, seriously disrupting operation of the entire plant.

A bulkhead of frozen earth was designed, with sufficient short term strength to support the foundation material under and beside the channel in case loss of ground occurred into the tunnel. Frozen earth is subject to creep; long term loading must be much less than short term loading if excessive deformation is to be avoided. In this case however, any loss of ground could be repaired quickly with backfill, and the load across the bulkhead re-balanced. This concept permitted a more economic design of the freeze.

All the freeze pipes and connecting headers were installed in advance of pushing off with the tunnel. However, to reduce the amount of refrigeration capacity required the system was utilized in a leapfrog fashion, activating pipes in advance and turning them off after the shield had safely passed. With careful coordination of the tunneling schedules and the time required for freeze formation, monitoring instruments showed that the frozen bulkhead was always up to design strength as the shield went by.

Freeze pipes 83' (25.3 m) in depth were established in one line on 4.5 ft. (1.37 m) centers. The average period required to form a specified section of frozen bulkhead was seven weeks and plant was provided to actively maintain a fully formed frozen bulkhead at least 75' (23 m) ahead of and 50' (15 m) behind a tunnel face moving at a projected 50-60 feet (15 m - 18 m) per week. In practice, modifications to the face equipment by the tunneling contractor caused some interruption to progress and it was possible to maintain a longer

length of bulkhead "on-freeze". It was interesting to observe, about 4 months after the freeze plants had been demobilized, that adjacent excavations for another structure (Influent Shaft No. 3 shown in Figure 11), revealed a continuous frozen membrane still in place.

Ground freezing was also used to protect the intricate termination of the tunnel. The 24.5' (7.74 m) O.D. tunnel was to end at an existing circular concrete junction chamber, 35 feet (10.7 m) in outside diameter. The shield profile was essentially vertical. The intersection of the tunnel, a horizontal cylinder, with the vertical junction chamber would leave a gap of unsupported earth at the spring line of 3.9 feet (1.2 m). The natural ground would be treacherous enough to control when the closed face of the shield was gutted. Beyond that it was reported that the existing structure had been built with considerable difficulty, and the ground was expected to be disturbed. Steel sheeting was still in place.

Horizontal freeze pipes from within the junction chamber were impractical because the structure was in use carrying warm fluids. Downtime permitted was the minimum necessary to cut through and make the connection.

Figure 12 shows the array of vertical freeze pipes. A high density was needed, to handle the heat load from the warm fluids inside the chamber, and to reduce the time of freeze formation. Precise scheduling was critical. If the freeze was formed too early, the closed face shield would be unable to advance to make contact with the existing structure. If the freeze was late, there would be a schedule delay in completing the tunnel.

In any event, the tunnel crews were able to make the drive without significant loss of ground. The frozen bulkhead became in effect an insurance policy. The termination freeze successfully accomplished its purpose.

Hubbell Roth and Clark were designers for the City of Detroit. Walbridge, Aldinger Company was the general contractor. Tunnel contractor was Greenfield Construction Company, with Larry Gilbert in charge.

FIG. 12

TUNNEL TERMINATION FREEZE
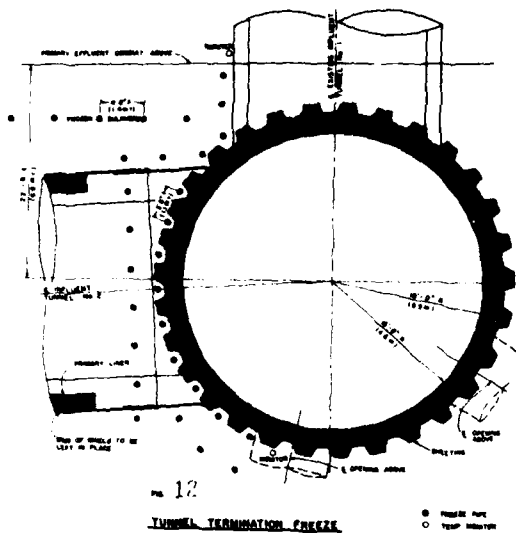
REFERENCE:

1. LACY, H.S., JONES, J.S., and
   GIDLOW, B. N. (1982), Tunnel
   constructed through cinders by
   ground freezing. Third Inter-
   national Symposium on Ground
   Freezing, Hanover, N. H.

CONTOUR GROUND FREEZING
FOR TUNNELING

Trupak N.G.,Dr.Sc.,Prof.Moscow Institute of Mines.
Macksimovich D.G. ,Chief.Eng.
Mitrakov V.I.,Cand.Sc.,TsINIIS,Moscow,USSR.

The method of artificial freezing is considered to be universal special technique for tunnelling through water bearing soils.

The method has bee.. successfully used in the USSR for the construction of Metro lines in tough tunnelling conditions.

However when driving shallow tunnels in alluvial deposits containing ground water, the method proved to take a great deal of time and to be very expensive.

Ground water table lowering under such conditions ap- ...red to be ineffective due to t .. low coefficient of filtration ($K_f = 1.1 \cdot 10^{-4} - 2.3 \cdot 10^{-4}$ m/s) and interstratification of water bearing and water proof soils.

Compressed air method (caisson method) for tunnelling has certain disadvantages too. It requires high employment level and unfavourably affects tunneller's health,causing physical stress.

The mentioned factors have necessitated the development of new more progressive methods of tunnelling through unstable water bearing soils.

Contour ground freezing along and across tunnel route and subsequent ground water table lowering within closed contour may be regarded as one of such methods.

The method has been used for the first time for one of Moscow metro lines.

Tunnel was driven through clay formation, moraine loamy clays, water-saturated sands and sandy loams.

Vertical freezing wells of 1.1m spacing formed two rows of frozen ground walls of 1.5m thickness parallel to 300m long tunnel section. Freezing wells were driven through tight soil up to 2-3m.

Unit consisting of 8 compressors of AY-4CO type was installed for freezing operations. Freezing temperature in operating regime ammounted to -20° (-22°)C.

The whole tunnel section was divided into 10 compartments of 20-40m length by means of transverse rows of frozen ground walls.

The process of freezing was controlled according to temperature measurements in thermometric bores, water table measurements in observation bores and trial pumping of water from compartments.

Water bearing soil in compartments was drained by means of wells equipped with deep borehole pumps.

Coefficient of filtration of water-bearing soils being low ($K_f = 1.1 \cdot 10^4 - 2.3 \cdot 10^{-4}$m/s), normal water table lowering would take a great deal of time.Besides,undrained soil of 2-3m height would ovelay waterproof strata making tunnelling difficult. Water volume within one compartment am-

411

mounted to 0.6-1.8 thous.m^3.

To increase the efficiency of water lowering wells compressed air was pumped into soils being drained.

The rate of filtration and accordingly discharge of water lowering well were monitored by pressure alteration of compressed air.

Drainage was carried out in accordance with the following three schemes:

1. Compressed air not being released.

Drainage being conducted according to this scheme, saturation of compartment with compressed air and pressure increase up to required level were developing at a low rate to achieve more complete water displacement by compressed air. This scheme was used for soils characterized by rather low coefficients of filtration and located at the top of the compartment. Finally, when residual water level was becoming negligible and there appeared a danger of pump interruption due to compressed air in the latter, the second scheme should be introduced.

2. Compressed air being released.

This scheme was designed for intensification of water influx to water-pumping well and provision of smooth pump running. It was reached by pressure difference between air supplying and water pumping wells as a result of controlled release of compressed air from the latter.

3. Without water pumping i.e. by gravity feed.

This scheme was used for comparatively shallow tunnels and sufficient bearing capacity of top natural or artificial waterproof strata (taking into account overlaying soils).

A number of wells were driven within every compartment after checking the tightness of the latter. The wells were as follows: water lowering, air supplying and observational.

The length and construction of water lowering wells were different depending on hydrogeological conditions.

The wells after drilling and casing were equipped with immersible pumps.

Air supplying wells also differed by their construction and purpose. Thus, air supplying wells of P_1 type were designed for compressed air supply for the whole length of compartment to be drained; while wells of type P_2 and P_3 - for compressed air supply for lower or top water bearing stratum, that's why they were fitted with filter column of the length corresponding to the thickness of drained layer.

To make drainage of the soil more efficient immersible pumps were installed below the top of water confining stratum while air supplying wells were drilled up to this stratum. In compartments where water bearing soils were divided by waterproof layers, well drilling was envisaged in every layer. The number of wells for every compartment was determined relative to volume of water to be pumped, compartment size and hydrogeological conditions.

Air supply was provided by stationary compressor unit. Air supply scheme took into account separate air supply for every well the possibility of compressed air pressure check, mains line interruption and air release during drainage and after it.

Peak admissable pressure of compressed air was taken relative to bearing capacity of waterproof stratum and overlaying soil. Admissable pressure being estimated, the possibility of frozen ground walls continuity disturbance was taken into account. Compressed air temperature should not have exceeded +25°C to prevent its influence on frozen ground walls.

Various regimes of compartment soil drainage have been tested:
-gravity feed through water lowering wells, compressed air being delivered into compartment and the pressure being gradually increased up to the peak admissable value (1 regime);
-water pumping and simultaneous delivery of compressed air

412

the pressure being lower compared
to the first regime (2 regime);
    -two stage drainage.
    The first stage involved wa-
ter pumping and excluded air de-
livery until well capacity decre-
ased to 1.5-1.0m³/hour.
    The second stage involved si-
multaneous water pumping and com-
pressed air delivery after well
collar had been sealed(3 regime).
    After testing the third regi-
me was taken as the main operating
regime.
    Immersible pumps ЭЦВ6-10-50
were used for water pumping.The
period of soil drainage in one
compartment was on average 7 days.
    Ground water table measure-
ment during drainage was performed
by means of level gauge УЭ -50.
    Its performance is based on
the principle of closure of cir-
cuit between the gauge placed in
the well and ground.
    Gauge contact with water in
the well was sensed by milliam-
meter mounted into its body.
    As experience has shown the
use of compressed air for incre-
ase of water lowering wells capa-
city may be considered to be ef-
ficient in the case of occurence
of top and upper airproof soils
(fig.1).
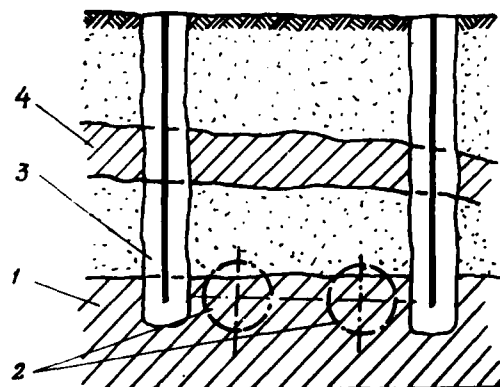
Fig.1 Scheme of contour gro-
und freezing in the presence of
natural waterproof layer
    1-lower waterproof layer
    2-running tunnels
    3-wall of frozen ground
    4-top natural waterproof
      layer

The top natural airproof lay-
er being absent, artificial stra-
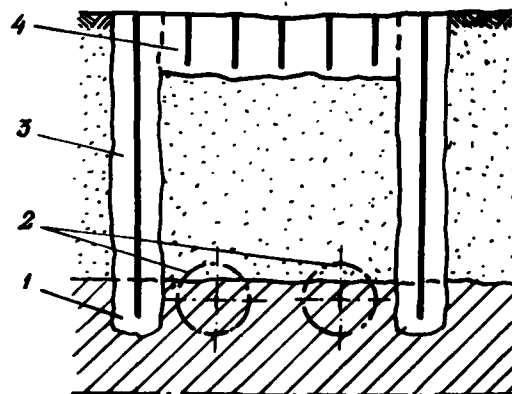tum of frozen soil was formed
(fig.2)

Fig.2 Scheme of contour gro-
und freezing in the presence of
artificial upper waterproof layer.
    1-lower waterproof layer
    2-running tunnels
    3-wall of frozen ground
    4-top waterproof layer of
      frozen ground
In such cases shallow free-
zing wells were drilled from the
ground surface within compartment
area at a depth of 2m below gro-
und water table.
    When excavating,the protec-
ting frozen soil contour of com-
partment was in a regime of pas-
sive freezing.
    Total number of wells located
in 300m long section was as fol-
lows: freezing wells-2021; water
lowering wells-30;observation
wells -40.
    Ordinary shields were used
for tunneling after drainage of
the compartment.All tunnelling
operations were successful.
                Conclusion
    A newly developed method of
soil drainage aids to overcome dif
ficulties encountered when tunnel-
ling in tough geological conditions.
    The method has made possible
construction of tunnel section by
ordinary shield excluding compres-
sed air.Due to the method soils ha-
ve been drained to natural mois-
ture state.
    Compartments isolation has

413

became possible in the lack of waterproof layer thanks to upper layers freesing.

Excess pressure developed in compartments allows water lowering to be carried out in soils having low coefficient of filtration.

ARTIFICIAL GROUND FREEZING IN SHIELD WORK

Tsutomu Takashi
Shiroh Kiriyama
Osamu Akimoto

Tokyo Branch, Seiken Co., Ltd.
2-5, 2-chome, Kudanminami
Chiyoda-ku, Tokyo, Japan

ABSTRACT

The number of shield works has been increasing in Japan. For these several years, various work conditions have made the shield diameter larger, deepened the work place in the ground, and complicated the shield works such as driving of sharp curve, jointing of two shields, and so on. This paper reports two examples of freezing works.

1--- Twin shield tunnels of upper and lower line for two rows of trunk water supply of 2.4 meters inside diameter were constructed at the residential district of Tokyo.

Two shields, 3.55m outside diameter, had already been constructed at jointing point of which the depths of cover were 9.5m (upper) and 25.5m (lower) respectively, then, slurry shields machines arrived at each constructed shield, at an angle of 60°.

Freezing method was applied for supporting the jointing of shield tunnels. The ground consisted of loam and water-saturated diluvial layers called Musashino Terrace Gravel Layer and Tokyo Gravel Layer.
(Freezing work period: Aug. 18, 1979 - Aug. 20, 1980)

2--- A pneumatic shield, 12.84m outside diameter, for railway tunnel, started from the shaft into the diluvial sand layer and silty sand layer at a depth of 19.5m in the central area of Tokyo.

Freezing was used for initial driving of this shield.
(Freezing work period: Sept. 5, 1980 - May 15, 1981)

INTRODUCTION

Accompanying the increasing and complicated shield works, the shield method in conjunction with freezing of soil has been rapidly increasing in popularity in recent civil engineering practice of Japan. This paper reports two cases of them.

Freezing method used for jointing of two shields were reported by Takashi, Kiriyama and Kato (1978)[1], where the ground were frozen by freeze pipes drilled outward from the tunnel or drilled from ground surface. Authors executed a few works of these kinds of freezing after that.

In example 1, authors report about a new type of jointing, that is, twin shields of upper and lower line where at first the lower shield machine arrived and was jointed, the same was done for the upper shield. Authors then describe a devised drilling method to pierce both the upper and lower shields in detail.

Freezing used for starting of a huge shield was reported by Kiriyama, Ishikawa and Kushida (1980)[2], too. Though more than twenty freeze works have been carried out already at the departure shaft, in all of them, the ground of shield driving section was frozen.

In example 2, authors report about an initial shield driving in which a roof type frozen sand wall was formed by utilizing diluvial clayey layer and about the measured amount of frost heaving.

EXAMPLE 1. JOINTING WORK OF EACH TWIN
SHIELD TUNNELS OF UPPER LINE
AND LOWER LINE

This construction was a part of the laying of water mains by the Water-Works Bureau, Tokyo Metropolitan Government.

Working area was the Yamanote diluvial plateau, Tokyo. Ground was composed of Musashino Terrace Gravel Layer and Tokyo Gravel Layer. When twin shields of upper line and lower line were jointed to the other twin constructed tunnels, freezing was adopted, as both a structual support system and an impermeable barrier.

Other methods were rejected because of the following reasons;

-- Dewatering
To lower the water table of water-saturated gravel layer is difficult.

-- Grouting
To form sufficient watertight and retaining wall is not feasible.

-- Compressed Air
Welding work in the conditions of highly compressed air is dangerous.

GENERAL OUTLINE OF WORK

Twin tunnels of upper line and lower line were already constructed at the depths of 9.5m (upper line) and 25.5m (lower line) under the intersection respectively. Lower slurry shield (diameter 3.55m) arrived at the jointing site at the angle of 60°, and was jointed to the lower constructed shield tunnel, then upper shield arrived at the jointing site and was jointed to the upper constructed shield tunnel (Fig. 1).

Limited freeze pipes with insulation (ϕ114.3mm) were installed vertically around the constructed twin shield tunnels from the ground surface. Especially, in order to freeze the ceiling and floor ground of the tunnel, eleven freeze pipes (l=31.7m) were installed by drilling of the freeze holes run-through both upper and lower constructed shields. Attached-freeze pipes were installed on the inside of five rings of segments to unify the frozen soil and segments. Around the slurry shield, frozen wall was formed before the arrival of the shields. Freezing period was 75 days around the constructed tunnel and 45 days around the arrival shield. After formation of frozen
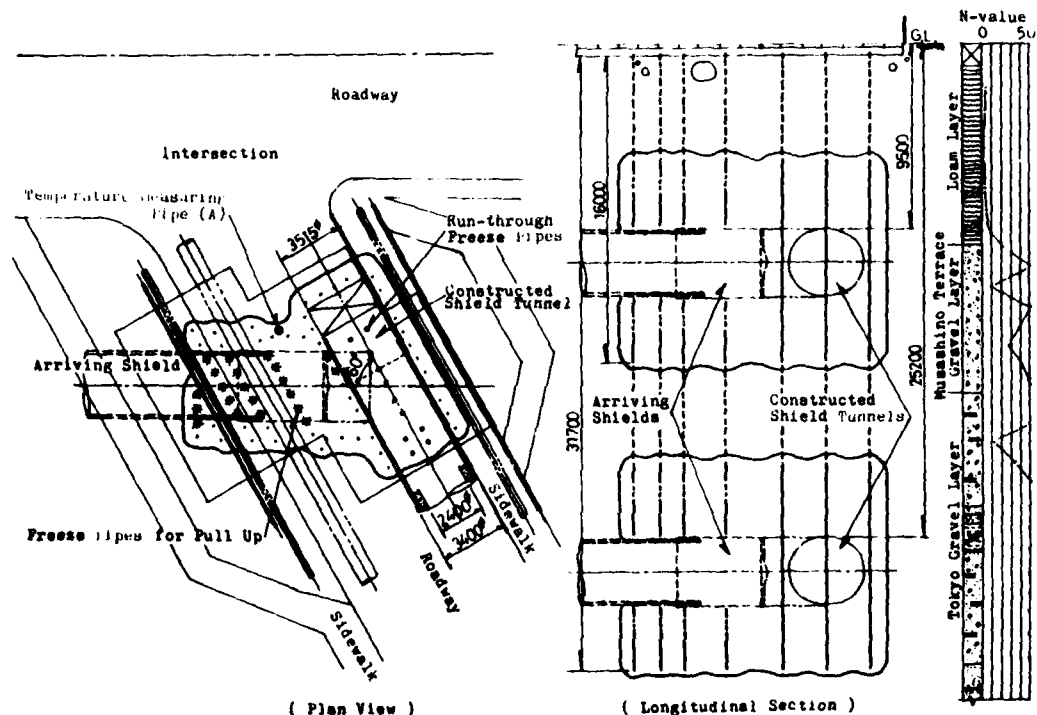

(Plan View)   (Longitudinal Section)

Fig. 1   Arrangement of Freeze Pipes

416

soil wall, freeze pipes embedded along the route of arrival shields were pulled up by means of the "thawing and pull up" method, as reported by Kiriyama, Ishikawa and Kushida(1980)[2]. After lower shield arrived, attached-freeze pipes were installed on the inside of five rings of steel segments, as well as the constructed tunnel. Then, skin plate of the constructed shield was cut out, frozen soil was excavated by pneumatic breaker, and cutter plate of the slurry shield was removed. Then the arrival shield was driven by jacks again, and tunnel lining was constructed by welding each skin plate. After lower freeze work was completed, the upper one was made by using the same freeze pipes which were pulled up to 16.0m beneath the ground surface.

INSTALLATION OF RUN-THROUGH FREEZE PIPES

Drilling of run-through freeze pipes was made as follows (Fig. 2):

1- Drilled to upper shield crown with a casing (ϕ355.6mm) and a pipe (ϕ318.5 mm) inserted in it.
2- Checked the opening position with a pipe (ϕ267.4mm) and attached a packer (ϕ318.5mm) inside the shield.
3- Cut out skin plate with the pipe (ϕ267.4mm) and inserted the pipe (ϕ267.4mm) to the upper-shield floor and welded.
4- *Cut out skin plate of the upper-shield floor with a metal-crown (ϕ241.8mm) in the pipe (ϕ267.4mm) as a guide, and drilled to lower-shield crown with tricone drilling bits (ϕ229.0mm).*
5- Inserted a pipe (ϕ190.7mm) and grouted the space between the pipe (ϕ267.4mm).
6- Checked the opening position with a pipe (ϕ165.2mm) and attached a packer (ϕ216.3mm) inside the shield.
7- Cut out skin plate of lower-shield crown with the pipe (ϕ165.2mm) and inserted the pipe (ϕ165.2mm) to the lower-shield floor and welded.
8- Cut out skin plate of lower-shield floor with a metal crown (ϕ139.8mm) in the pipe (ϕ165.2mm) as a guide, and drilled to fixed depth with tricone drilling bits (ϕ127.0mm).
9- Installed freeze pipes (ϕ114.3mm) by welding joints and filled void around the pipes and made measurement of pipe deviation.

FREEZE PIPES AND FREEZING PLANT

Type of freeze pipes (ϕ114.3mm) was "limited freeze pipe with insulation" as reported by Kiriyama, Ishikawa and Kushida (1980)[2].

To freeze the ground around lower-tunnel, length of freeze pipes was 31.7m of which freezing length was 10.7m and insulated length was 21.0m.

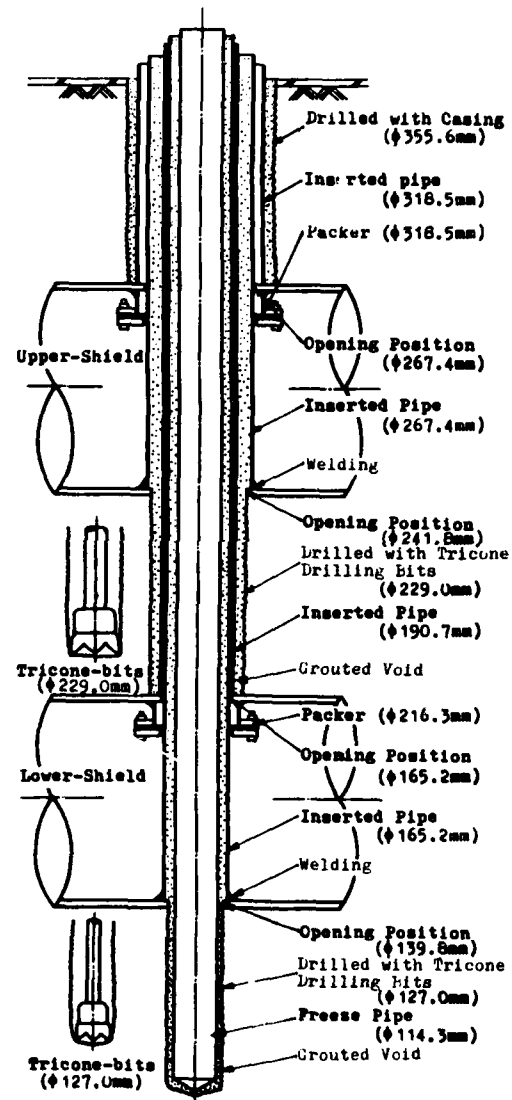The total of freeze pipes was 80.

Fig. 2 Installation of Run-through Freeze Pipe

417

The freezing unit consisted of two 75KW refrigerators (62900Kcal/h at C.T.= +40°C, E.T.=-27°C) and one 37KW refrigerator (41800Kcal/h at C.T.=+40°C, E.T.= -27°C).

Ground temperature and brine temperature during freezing are shown in Figure 3.

PULLING UP FREEZE PIPES

Freeze pipes embedded along the route of arrival shield had to be pulled up to the level of just over shield crown by means of the "thawing and pull up" method[2].

21 freeze pipes and 3 temperature measuring pipes were pulled up before arrival of lower and upper shield.

REGENERATION OF FREEZE PIPES

After the lower freezing work, lower freeze pipes were pulled up and regenerated to freeze the ground around the upper tunnel. The length of these regenerated freeze pipes became 16.0m with freezing length of 10.7m and insulated length of 5.3m (pulled-up freeze pipes numbered 80).

EXAMPLE 2. STARTING OF LARGE DIAMETER SHIELD

This construction was the driving of a large pneumatic shield tunnel (diameter 12.84m) on the second Ueno Tunnel Construction District in Tohoku Shinkansen Line (from Tokyo to Morioka) of the Japanese National Railways. The shield was driven in the diluvial layer.

The Upper Tokyo Sand Layer and the Upper Tokyo Silty Layer existed over the depth of the center of the shield. Under them, there existed the Lower Tokyo Silty Layer and the Lower Tokyo Sand Layer. The Upper Sand Layer between the Silty Layer, filled up with artesian ground water. To construct the departure shaft of continuous diaphragm wall under the road and to secure the space of slurry disposal plant, the primary-excavation shaft of 9.4m depth was made.

Under these conditions, besides freezing, some auxiliary methods for initial driving of shield with the soil cover under shield-diameter were examined.

The were rejected for the following reasons:
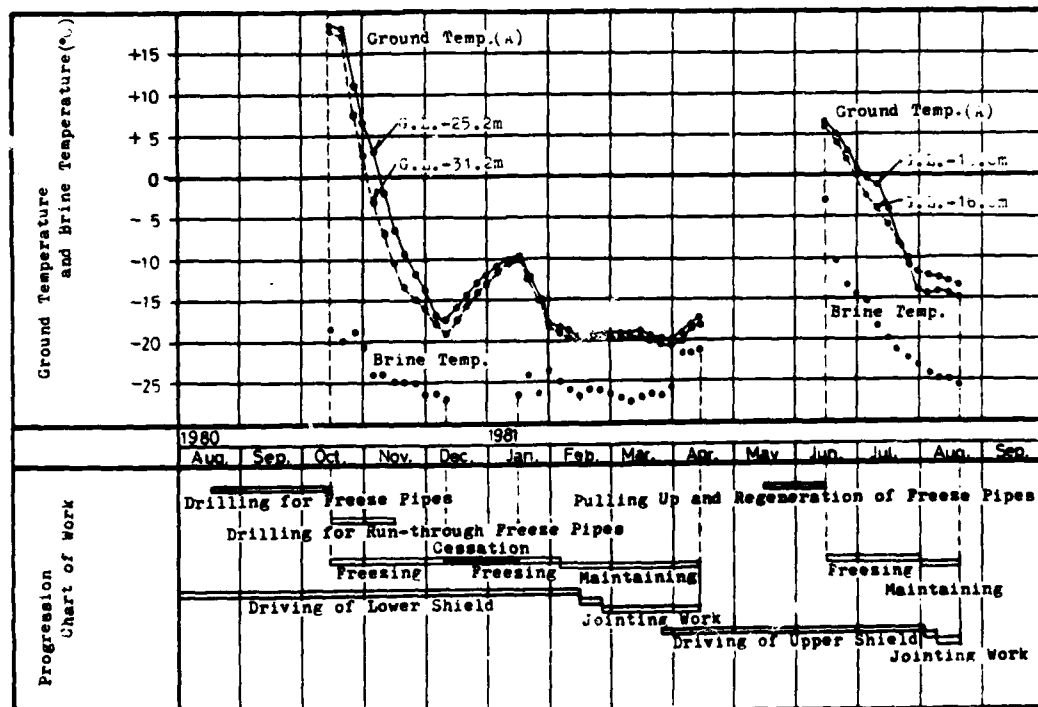
-- Compressed air method at the shaft

Fig. 3 Ground Temperature, Brine Temperature and
Progression Chart of Work Executed

418

The compressed air method is expensive because the shaft needed a sufficient space to start the world's biggest shield and operational efficiency is extremely bad.
-- Grouting

This is unreliable in strength and water-tightness without aid of compressed air.

Therefore, freezing was adopted to make initial driving without aid of compressed air and to install the pneumatic equipment in the tunnel.

OUTLINE OF WORK

The influence of frost heaving was examined before freezing work. This was because there existed frost-susceptible silty soil below the center of shield and a 10 floors building with 2 floors underground on the right side in front of the freezing zone. To reduce amount of frost heave, the ground around the tunnel, except under it, was frozen, then roof type frozen wall was formed, because authors checked that the strength of silty soil below the center of the shield was sufficient and that the pore water did not lie in the sand below the shield.

Length of freezing area was determined to be 17.5m to install pneumatic equipments which needed 15.5m and not to freeze the pile foundation of the above mentioned building. As to roof type frozen soil, thickness of both sides of the tunnel was 4m and ceiling was 4.5m (Figure 4).

Freeze pipes were installed from primary-excavated shaft in order not to use the road.

Reducing the influence of frost heave to the building, authors would have installed displacement-absorption holes as occasion demanded.

ARRANGEMENT OF FREEZE PIPES

In front of the shaft----16 limited freeze pipes (ϕ101.6mm, l=14m) with the spacing of 0.8m were installed at the distance of 0.3m from continuous dia-
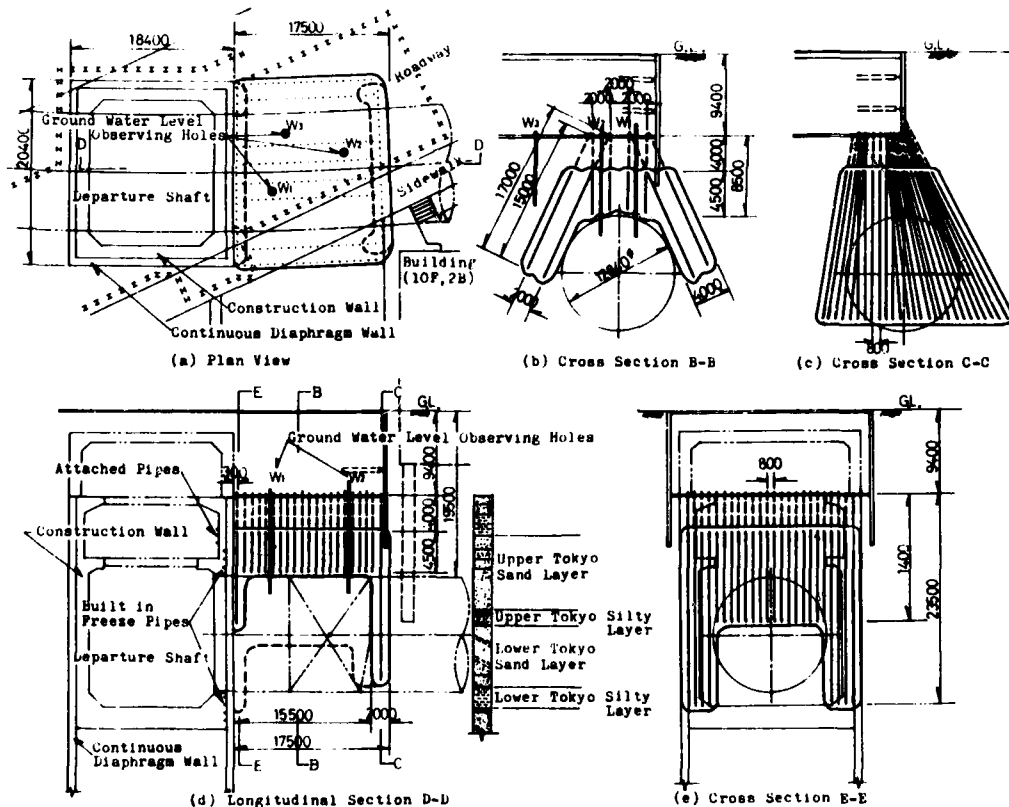

(a) Plan View (b) Cross Section B-B (c) Cross Section C-C

(d) Longitudinal Section D-D (e) Cross Section E-E

Fig. 4 Arrangement of Freeze Pipes

419

phragm wall. On both sides of them, 4 limited freeze pipes (ϕ101.6mm, l=23m) were installed respectively (Fig. 4-E).

In roof of the above shield ---- On both sides of roof, inclined limited freeze pipes (ϕ 101.6mm, l=17.5m and 15.5m) were installed at an angle of 25°, and in the part of ceiling of the roof, vertical limited freeze pipes (ϕ101.6mm, l=8.5m) were installed with the spacing of line of freeze pipes 2m. The spacing of freeze pipe was 0.8m in the shield driven direction. Total freeze pipes were 178 (Fig. 4-B).

In front of the shield---- Owing to the working area, 27 limited freeze pipes were installed in fan shape with the spacing of 0.8m at the bottom of the pipes (Fig. 4-C).

In and on construction wall----When construction wall of the shaft was built, built-in freeze pipes (ϕ101.6mm, l=18m×8 l=4.2m×34) were installed in it with the spacing of 0.8m to strengthen adfreezing between the wall and frozen soil. Upper 3 pipes (50mm×100mm sq.) were attached on the construction wall.

PREDICTION OF AMOUNT OF FROST HEAVING AND ITS COUNTERMEASURE

1-Prediction of Amount of Frost Heaving

Undisturbed silty soil (SM) and fine sand (SF) were obtained and frost heave ratio was examined in an open system in the laboratory. As a result of examination, silty soil showed high frost susceptibility, as shown in Figure 5. Authors calculated the amount of frost heaving at the ground surface and floor of the primary excavation shaft (Fig. 6).

Calculation was based on "Calculating method of frost heaving (three dimensions)" by Tobe and Akimoto (1979)[4].

Amount of frost heave at the depth of pile foundation was predicted to be about 14mm.

2-Countermeasure of Frost Heaving

1) Control of formation of excess frozen wall by controlling of brine supply.

2) Dewatering of the unfrozen upper Tokyo Sand Layer by a vacuum pump.

3) Installation of "displacement-absorption hole", near the building, as reported by Enokido and Yamada (1978)[3].

3-Measurement of Frost Heaving

The level of the ground surface, the floor of the primary excavation shaft and the building have been measured at 135 days after freezing initiation. (Fig. 6).
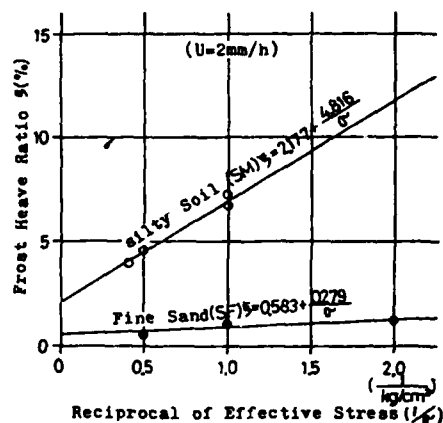

Fig. 5 Frost Heave Ratio of Soil (U=2mm/h)

4-Results

At the ground surface (B) and the building (C), amount of frost heaving was less than that of the prediction as shown in Fig. 6.

There, most of the frost heaving came out to the primary excavated shaft because of smallness of over burden pressure.

Total displacement of building was 9mm. As grouting for stabilization of unfrozen zone raised about 5-6mm (Figure 7), therefore, only 3-4mm of displacement was raised by freezing.

Hence, two displacement-absorption holes were installed experimentally instead of installation of 20 holes as a countermeasure of displacement of the building and their workability was checked.
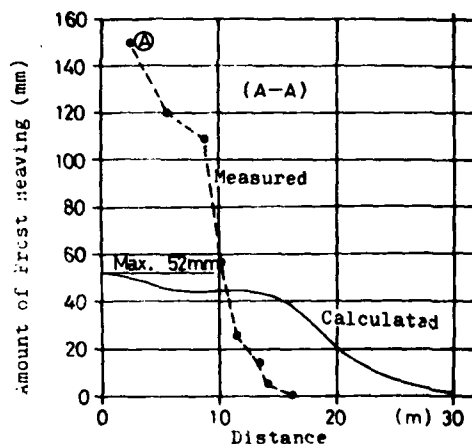
Contrary to these phenomena, piles of primary excavation shaft were raised so much that the measures were taken to support the piles by jacks which were able to adjust finely.

Maximum displacement of pile was 110mm.

## GROUND WATER LEVEL OBSERVING HOLE AND CONFIRMATION OF IMPERVIOUS LAYER

Roof type frozen wall was rooted into the middle of silty layer as an impervious one. To confirm this imperviousness and closure of roof type frozen wall, 3 ground water level observing holes were installed as shown in Fig. 4.

By measurement of change of ground water table (Fig. 8), authors confirmed imperviousness of silty layer and closure of frozen wall as follows:

420

1) Before closure of frozen wall, the rise of water level due to grouting was observed.
2) A few days before and after closure of frozen wall, grouting was stopped but the rise of water level was observed by freezing.
3) The change in water level, when grouting was resumed after closure of frozen soil, was different than that in 1).

Amount of Frost Heaving at Floor of Primary Excavation Shaft vs. Distance
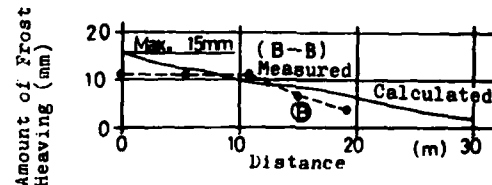
Amount of Frost Heaving at Ground Surface vs. Distance
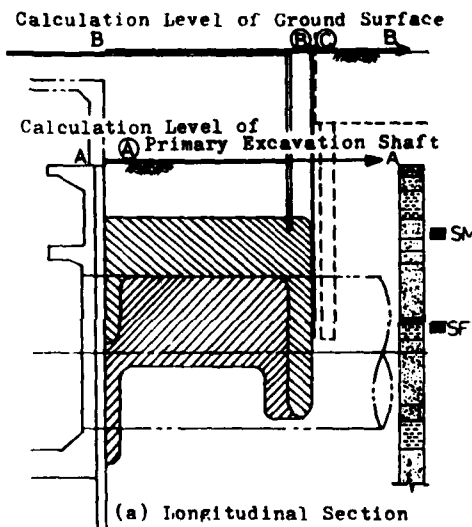
(a) Longitudinal Section
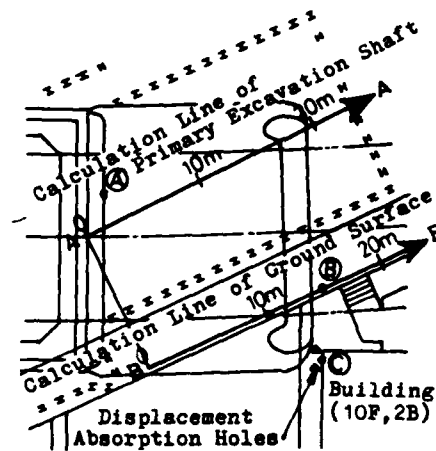
(b) Plan View

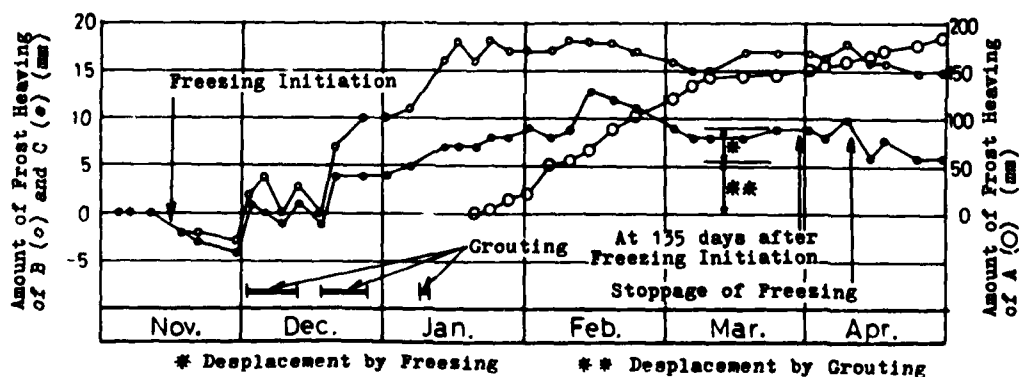Fig. 6   Measurement and Calculation of Amount of Frost Heaving (at 135 days after freezing initiation)

* Desplacement by Freezing   ** Desplacement by Grouting
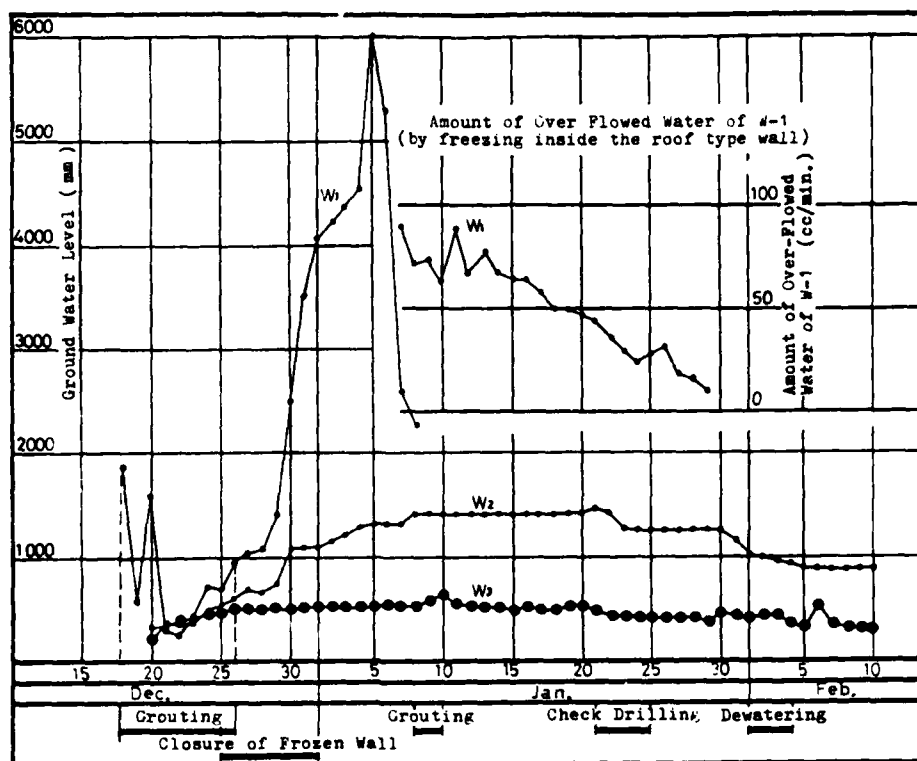
Fig. 7   Amount of Frost Heaving vs. Time

421

Fig. 8 Measurement of Ground Water Level

CONCLUSION

In the jointing work of each twin shield tunnels of upper- and lower-line, authors made the installation of freeze pipes by run-through drilling method.

This method made it possible to freeze the ground under the shield without using drilling machine in the tunnel.

In the starting work of extraordinary large diameter shield, the less volume of frozen diluvial silty soil by roof type had no effect on frost heaving to the neighboring buildings.

Starting of shield was completed safely and economically.

As the installation method of displacement-absorption holes was established, authors would confirm their efficiency and made one of feasible measures to reduce the influence of frost heaving to the neighboring structures, in future.

REFERENCE

1) Takashi, T. Kiriyama, S. and Kato, T.; "Jointing of two tunnel shields using artificial underground freezing", ISGF '78 session III. pp, 339-348, 1978.

2) Kiriyama, S. Iahikawa, Y. and Kushida, Y. "Artificial ground freezing in shield work", ISGF'80 session D. pp. 940-951, 1980.

3) Enokido, M. and Yamada, M.; "Influence reduction of frost expansion in unfrozen soil zone around artificial frozen soil", Japan Society of Civil Engineers, pp. 79-92, April, 1978.

4) Tobe, N. and Akimoto, O.; "Calculating method of frost heaving (three dimension)", 34th Symposium of Japan Society of Civil Engineers, session III, pp. 243-244, Oct. 1979.

CONSTRUCTION OF A TUNNEL UNDER A MAJOR RAIL WAY WITH THE AID OF TEMPORARY BRIDGES AND V-SHAPED ICEWALLS

Ilkka Vähäaho, Geotechnical Department of Helsinki City, Finland

Teuvo Eronen, Lemminkäinen Oy, Helsinki, Finland

ABSTRACT

As an alternative for the implementation of a pedestrian tunnel, planned to be built in 1983 in the northern suburbs of Helsinki a new support system was developed relying on temporary bridges and V-shaped icewalls. The tunnel is to be driven under a four-track electrified permanent way in busy use. The uninterrupted passage of trains during underpinning work was a design restriction.

In the freezing alternative, use will be made of temporary bridges 21.5 metres long, from the Finnish State Railways, which can be set up in a matter of hours. In the course of installing the temporary bridges, it is possible to excavate 2 metres deep ditches under them, adjacent to the bridge crosswise to the tracks, to facilitate the insertion of casings for freeze pipes. It is intended to drill the casings in a way that the drillings from opposite sides will intersect each other underneath the centre line of the tunnel. The walls and floor of the tunnel excavation will be strengthened with a V-shaped "ice trough" formed by the freezing process. The completely dry conditions underfoor will be an added advantage.

The 1.35 metre dimension chosen for the icewall is in order to ensure sufficient stability against slope failure and bending failure in the walling. Advance tests were carried out for the dimension parametres and to allow for the extent of thawing settlement

1. GENERAL

It is planned to build a light traffic tunnel 41.5 m long 5.2 m wide and 4.3 m high under a busy four-track electrified permanent way in the northern suburbs of Helsinki. The permanent way is composed of sand, gravel and boulders and rests on a sloping bed of soft clay varying from 3-6 m in thickness. The lower face of the clay is at a depth of 6.5-8 m below the railway and the clay has a water content between 40-85% dry weight and a shear strength of 11-24 kN/m^2. The bedrock is up to 17 m below ground level in places and the tunnel floor is 6 m below the tracks (Fig. 1.).

2. CONSTRUCTION ALTERNATIVES

The uninterrupted passage of trains during underpinning work was a design restriction. The following construction alternatives were examined:
- driving the tunnel by hydraulic force
- operating with the protection of a sheet wall
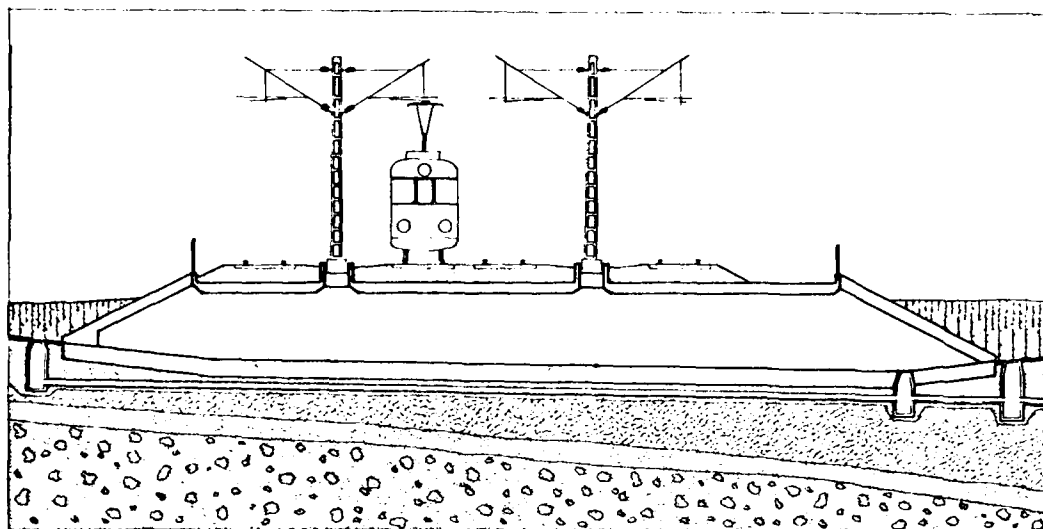- freezing

Fig. 1. Longitudinal section of the finished tunnel

Driving the tunnel under the tracks by means of hydraulic force was rejected on economic grounds due to the extremely compact and almost impenetrable permanent way. The alternative of using sheet wall piling to support the excavation was also examined. Construction of the piling would have to take place during the night when the reduced rail traffic would allow the interruption of electric power supplying the tracks. The sheet wall would later serve as the inner face of the tunnel. The slowness and expense of sheet pile driving as well as the uneven settlement of the permanent way due to its mixed composition caused work on this alternative to be abandoned.

Fig. 2. Typical load-strain curve of frozen clay

3. FREEZING

3.1 Preliminary tests

3.11 Compression tests

At the initial stage, 15 undisturbed sample borings, of which 14 were clay and one silt, were frozen to a temperature of -10^0C. The rate of loading was 100-200 kN/m^2/min. A typical load-strain curve is shown in fig. 2..The tests were carried out using borings 50 mm in diameter and 100 mm in length with a point load (CBR test)
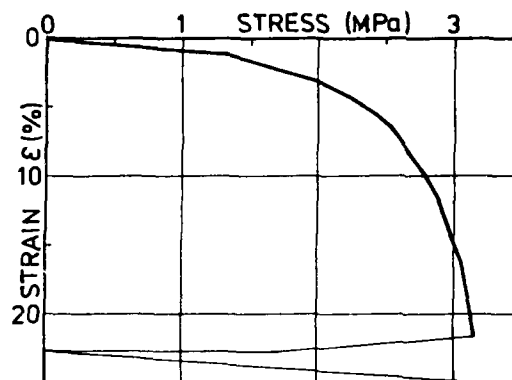
3.12 Shear tests

Additional undisturbed sample borings of the same size as in the compression tests were used in this case. The unfrozen borings were compressed to a degree equivalent to existing loading conditions and when frozen to a temperature of -10^0C were then subjected to a shear test. Normal compression tests were also carried out on these samples with the aim of establishing whether the shear strength may be determined on the basis of compression tests. The rate of loading was 200 kN/m^2/min.

424

in both cases. Frost heaving was also measured from the samples. Five shear tests and six comparative compression tests were carried out.

It was established in the course of these tests that there was a ratio of 2 between the compression strength of frozen clay under a 10% strain and the shear strength measured from borings. A frost heave average of 5% was recorded.

3.13 Compression tests on frozen and thawed samples

Ödometer tests were carried out to establish the behaviour of frozen and thawed soil. The samples were first compressed to a degree corresponding to conditions before construction began. The samples were then frozen to -10^0C so as to correspond to conditions when the freezing process has already occurred but before construction begins. The actual conditions were then simulated a stage further by a tension mock-up corresponding to conditions after construction but before thawing began. The samples were then allowed to thaw and further loading was carried out to establish what would occur after thawing.

The above test pattern was modified so as to discover the behaviour under strain of clay that had been frozen and thawed two and three times. Fig. 3. shows an ödometer test carried out on clay that has been frozen and thawed three times. The same fig. 3. also shows for comparison a normal ödometer test on an unfrozen boring sample from the same depth.

Worth noting is the almost 30% strain figure that was consequent on stage one of freezing and thawing. After stage two of the process, settlement was less than 7% and after stage three less than 5%.
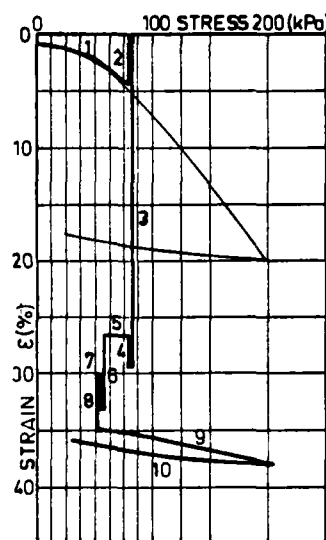

Fig. 3. Typical ödometer test on a sample frozen and thawed three times and compared with a normal ödometer test sample.
- 1 preloading
- 5 partially unloading
- 10 unloading
- 2,4 and 7 freezing at -10^0C
- 3,6 and 8 thawing

3.14 Calculations

An average 10% strain for the frozen clay gives a compression figure of 2.884 MPa. Correspondingly, the momentary shear strength averaged 1.428 MPa. If the shear strength is estimated on the basis that it will withstand a load for 100 hours, the figure will be 700 kN/m^2 or approximately 53 times greater that the shear strength of the clay before freezing. Bending strength is estimated at 1.0 MN/m^2.

The frost heave of the clay is 5.3% on average. There is an average thawing settlement of 22.3% after stage one of freezing and thawing, 6.9% after stage two and 6.2% after stage three.
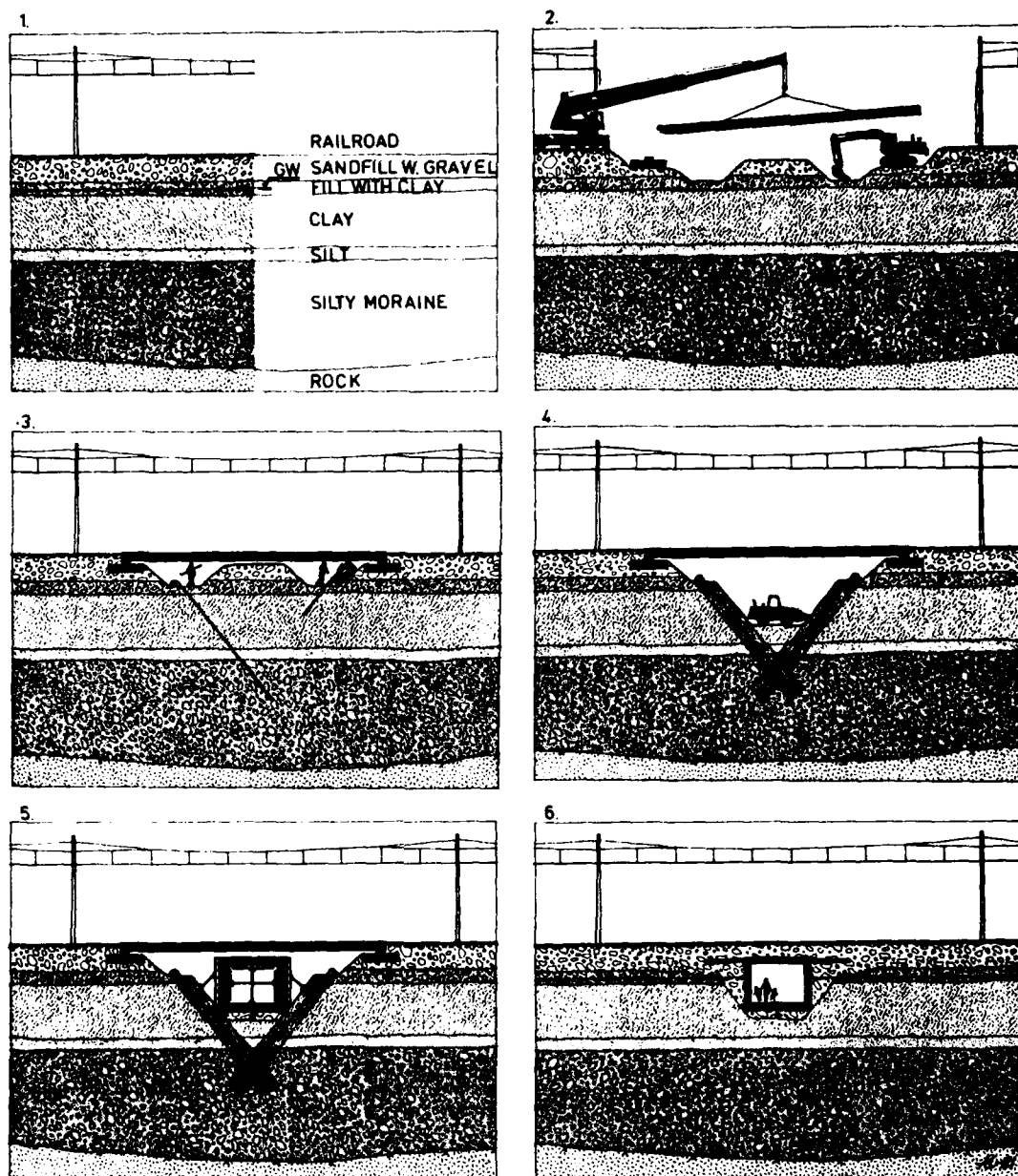
Fig. 4. Phases of tunnel construction:

    4.1 Situation at start

    4.2 Placing of temporary bridges and excavation of trenches

    4.3 Drilling the casings for freeze pipes and freezing

    4.4 Excavation between the icewalls

    4.5 Construction of the concrete tunnel

    4.6 Finished tunnel after removal of temporary bridges

3.2 Dimensioning

An icewall thickness of 1.35 m is sufficient to resist slope failure and bending failure. A margin of 200 mm is left for possible frost heaving between the temporary bridge and the permanent way. To prevent large-scale frost heaving in the region of 500 mm, the excavation and construction work is to occur between stage one thawing and stage two freezing as the heaving may then be kept within a margin of 150 mm.

3.3 V-shaped icewall

The uninterrupted passage of trains during work on the tunnel is a design restriction. The use of temporary bridges is necessary since the tunnel roof is separated from the tracks by a layer of earth in the region of 1 metre thick.

The most economical alternative for supporting the tunnel excavation appears to be that of freezing by means of freeze pipes driven diagonally downwards from above. The freeze pipes are placed so as to form a V-shaped icewalled excavation at right angles to the tracks under which the tunnel can then be laid.

The V-shape has the following advantages over horizontal or vertical freezing:
- the frozen vault is constructionally advantageous
- use can be made of short freeze pipes resulting in greater accuracy and lower drilling costs

The V-shape has the disadvantage in practice of requiring longer temporary bridges due to the way the diagonal freeze pipes lessen the working width.

3.4 Phases of tunnel construction (Fig. 4.)

Construction of the tunnel begins with the placing of temporary bridges spanning 21 m. The placing of these takes only a few hours and can be carried out at night without interrupting rail traffic. Together with the placing of the temporary bridges, trenches about 2 m in depth are excavated under them in order to drill holes for the freeze pipes (Fig. 4.2).

Due to the restricted drilling height under the bridges, the holes are drilled using 1 m long tubes which are welded together to form a casing. The holes are drilled so that they intersect holes drilled from the opposite trench on a line through the tunnel centre at a depth of approximately 9.5 m (Fig. 4.3).

The icewalls form a constructional vault below the tracks so that the tunnel may be built in dry conditions while trains run overhead along temporary bridges springing from beyond the excavation (Figs. 4.4, 4.5).

On completion of the tunnel, the freezing equipment is removed, filling takes place and the temporary bridges are taken away. The tracks have to be inspected while thawing of the icewalls takes place and any variations due to thawing corrected (Fig. 4.6).

4. SUMMARY

The choice of temporary bridges and a V-shaped icewall is for the following reasons:
- rail traffic has to continue uninterruptedly during work on the tunnel
- the tunnel roof is to be not more than 1 metre below the tracks while the tunnel floor is to be laid in clay with a water content
- the V-shape permits smaller volumes to be frozen and offers a constructionally advantageous form

Second stage freezing is suggested in order to reduce thawing settlement. After first stage freezing, the thawing process is carried out and then the actual freezing process takes place after which the tunnel construction starts. This procedure is based on the results of freezing tests

427

which indicate that the biggest
thawing settlement follows the
first stage freezing.

NEW FREEZE PIPE SYSTEMS FOR NITROGEN FREEZING

Rebhan, Dieter   Linde AG
Industrial Gases
Division,
West Germany

Abstract

A number of field and laboratory experiments have been carried out using new kinds of freezing pipe systems.
These systems particularly enable freezing to be performed in stages. They further enable liquid gas consumption to be minimized. One system is particularly suitable for shaft freezing while another lends itself to tunnelling.

Introduction

Soil freezing using liquid nitrogen as the refrigerant has been employed in Western Europe since about 1970. Intensive further development has been pursued in recent years. Confronted with a wide range of in some cases difficult problems, engineers sought new solutions and also improved freeze pipe variants. The further developed technology has been subjected to laboratory trials and in a number of cases also to field testing. The impartial listener may at first regard the subject of "freezing pipe system" to be of secondary importance. A closer look, however, reveals its significance: the choice of the optimum system decides not only the technical but also the economic success of nitrogen freezing.

Aims in Developing Freezing Pipes

The nitrogen freezing method is characterised by:

- low investment costs
- extremely high and flexible freezing capacity
- costs for nitrogen as the refrigerant.

To ensure that this superior technology is economically employed it is therefore necessary

- to minimize the maintenance times by proper planning of the civil works schedule and qualified, rapid execution of the civil works in the protection of the freeze zone;

- to aim at the smallest possible freeze zone volume. This is achieved by optimum design of the freeze zone geometry taking into consideration the function of the freeze zone;

- to constantly monitor freezing with regard to the actual freeze zone boundaries, freezing time and optimum control of the nitrogen supply during the period the freeze zone is maintained and, not least,

- to ideally select and adapt the freeze pipe system.

A high standard has been reached in respect of the equipment above ground for nitrogen freezing. For this reason it is particularly significant to develop freeze pipe systems in addition to careful planning and execution to further improve the economics of the process while simultaneously achieving technological advances.
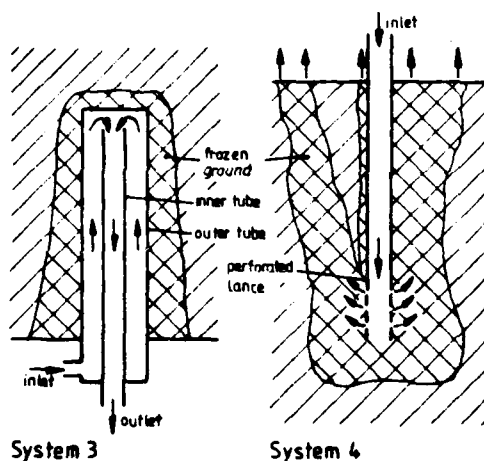
New Freeze Pipe Systems

The conventional nitrogen freeze pipe was basically adopted from brine freezing and, like the latter method, operates with concentric twin pipes (Fig. 1).
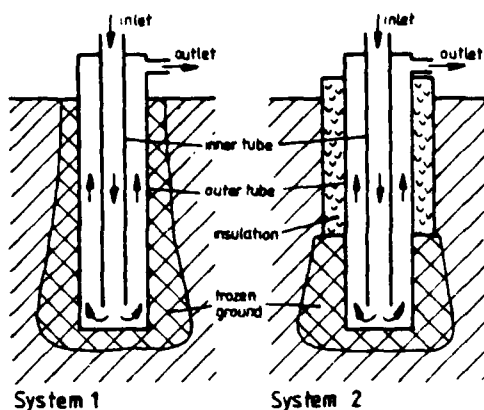
System 1   System 2

System 3   System 4

Figure 1

Conventional Freeze Pipe Systems

System 1

Freeze pipe consisting of concentrically arranged downcomer and riser. Up to three pipes connected in series may be depending on the application.

Advantage   : simple
Disadvantage : recooling effect

System 2

Insulated outer pipe for freezing zones along the freeze pipe in which it is not allowed to freeze.

Advantage   : specific freezing
Disadvantage : recooling effect, high costs for drilling an insulation

System 3

Structure as System 1, not inner pipe but outer pipe charging (annular space charging)

Advantage   : can be used with rising freeze pipe (soil higher than head)
Disadvantage : recooling effect: inner pipe degassing

System 4

Freeze pipe consisting of perforated lance. Liquid nitrogen is injected directly into soil.

Advantage   : optimum utilization of refrigeration
Disadvantage : can only be used in porous soils; irregular freeze zone

In view of the high refrigeration capacity of nitrogen and the high costs for large-diameter freeze pipes and boreholes, the diameters have been reduced to 2". Upipes have been rarely used to date. The principle reason for this appears to be the higher costs for drilling and fabrication.
The normal case is for the liquid nitrogen to enter the freeze pipe at the upper end of the concentric double pipe. To assist understanding of what is said in the following sections, this part of the freeze pipe can be termed the head and the part of the freeze pipe at the opposite end the bottom.
The liquid nitrogen flows through the downcomer, entering the annular space between outer and inner pipe at the bottom, flows through this space to the head absorbing heat from the soil to then escape into the atmosphere in the form of a vapour. This method is known as inner pipe charging.
It is known that several freeze pipes can be operated in series to achieve enhanced efficiency. The possibility of degassing the inner pipe, also known as annular space charging, has been often practiced. This paper does not deal with these

and other conventional methods.

Investigations have shown that a consid-
erable heat exchange takes place between
the warmer gas flowing out and the liquid
gas flowing in. This effect is evident
both with inner pipe charging and to a
greater extent with outer pipe charging.
This heat exchange may lead to the waste
gas temperatures at the head and the
temperature conditions along the freeze
pipe being incorrectly assessed - with
disastrous results. Cases have existed
in practice when employing annular char-
ging and with an unfavourable ratio of
inner to outer pipe diameter of temper-
atures below -130°C being measured at the
head in the waste gas - normally reason
for cutting back the nitrogen supply -
although the soil temperature had not yet
reached 0°C. Such errors in judgement
could have fatal consequences since the
freeze zone in the head area is well
formed while it is still inadequate in
the soil area. Moreover, recooling of the
refrigerant flowing out at a specified
waste gas temperature at the head means a
reduction in the freezing capacity and a
time delay which in turn means an addi-
tional flow of heat to the system. In
other words, the freeze pipe cycle is
carrying heat which is not the purpose
of the method.
The search for a remedy resulted in im-
provements through employing inner pipe
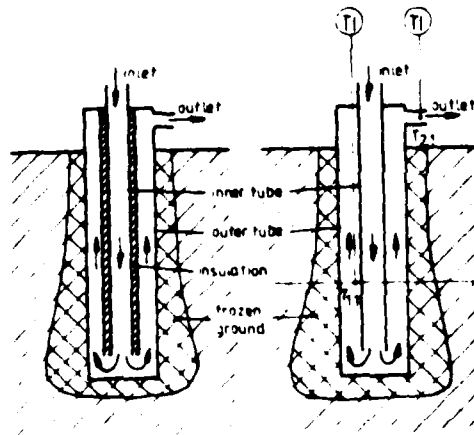insulation (Fig. 2).

Inner Tube Insulation and Reference Measurement

The inner tube is provided with a high-
quality insulation which largely prevents
recooling of the refrigerant flowing out.
By means of temperature measurement $(T_{1,1})$
it is possible to specify an efficiency
level at a random location - and thus a
local minimum wall thickness. Based on
reference temperature measurements at the
head $(T_{2,1}$ etc.) the same temperature con-
ditions can be transferred to other freeze
pipes $(T_{2,2}$ etc.) without elements $(T_{1,2}$
etc.) requiring to be fitted to the latter
freeze pipes.

Harmonizing the dimensions of the inner
and outer pipe is of considerable signi-
ficance particularly when using annular
space charging. However, only by insula-
ting the inner pipe is it possible to de-
cisively influence the recooling effect.
Measurements reveal that it is still
possible to use 2" outer pipes despite in-
sulating the inner pipe. A further addi-
tional improvement is provided by plastic
inner pipes since the latter have an in-
sulating effect in contrast to metal pipes.
Only a small number of plastics have
adequate cold resistance however and are,
due to their suitability, expensive.
Past practice was to insulate the outer
pipe along those stretches of a freeze
pipe where it was either not necessary or
not possible to freeze the soil. This is
still required in some cases even today
where it is not permitted to the freeze soil.
In those cases in which for instance an
ice seal is to be created at a certain
depth and it is immaterial whether the
soil above is frozen or not and the prime
consideration is to save on energy there
is a more economical method available to-
day than insulating the outer pipe.
The inner pipe is insulated as described
above and a temperature control system em-
ployed which does not scan the freeze head
for the actual temperature measurements
but rather measures the waste gas temper-
atures in the freeze pipe at the point
where the planned freeze zone ends. By em-
ploying reference measurements, additional
savings can be achieved in the costs for
measurement work since it is then only ne-
cessary to carry out measurements in part
of the freeze pipes in the area of the
proposed freeze zone. The reference
measurement is taken at the head in the
waste gas and the nitrogen supply con-
trolled on the basis of the original or

Figure 2

431

reference measurement. This method enables not only the drilling costs to be cut and savings to be made in the insulation but also reduces the energy consumption and enables the temperatures in the freeze zone to be better assessed.

The smaller freeze zone which forms in the waste gas area is not generally a disturbing factor. One restriction which should be noted is that this method can only be practically employed with inner pipe charging and not with outer pipe charging.

A further new method is employed for instance in freezing tunnel roofs. The normal procedure in such cases is to work from a head chamber. The problem which usually arises here is that it is necessary to operate with rising freeze pipes. In this case the soil is higher than the head of the pipe. If a conventional inner pipe is now charged, it is very difficult or even impossible to monitor and assess the waste gas temperatures because the liquid nitrogen, influenced by the "Leidenfrost phenomena", bubbles down and rapidly runs back from the bottom to the head largely unevaporated without having absorbed adequate heat. As is known, this effect can be prevented by feeding in via the annular space and degassing through the inner pipe. If this was done, however, problems were sometimes encountered regarding the recooling of the waste gas mentioned above and insufficient degassing through the inner pipe particularly with long freeze pipes and when starting up when there is a large development of gas. A further obstacle proved to be the fact that the feed pressures in the tunnel have to be kept as low as possible for safety reasons to prevent any risk being created for the tunnel workmen if there should be an unforeseen fracture in the feed or distributor line. An improvement can be achieved here using a so-called cascade lance (Fig. 3).
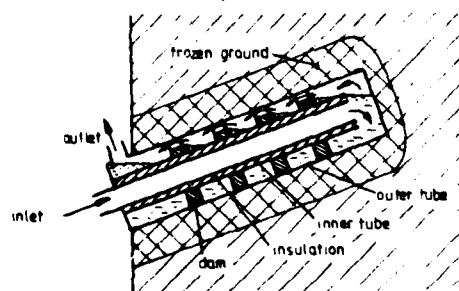
Cascade Lance

Particularly suitable for rising freeze pipes and inner pipe charging. Barriers of flexible material form "dams" which delay the return flow of the liquid nitrogen.

The ideal design is achieved if the thinnest possible inner pipe is selected and insulated. For economic reasons it is recommended to use a modular system which enables the expensive lances to be reused. Elastic discs are fitted to the insulated inner pipe which act as overflow weirs for the liquid nitrogen and at the same time facilitate degassing. These barriers are spaced in line with the slope of the freeze pipe, spacing normally being approx. 1 m. This variation enables the inner pipe to be charged without the liquid nitrogen flowing out. The result is very uniform cooling of the soil and utilization of the nitrogen along the freeze pipe.
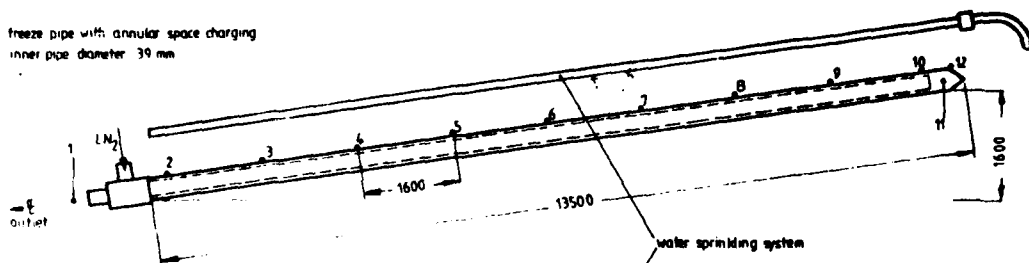
A further positive side effect compared to the conventional annular space charging commonly employed is achieved from the fact that the weak point of freezing which is in the area of the maximum waste gas temperature can be assessed visually at the working face. By way of contrast, the minimum formation of frost with conventional annular space charging is at the bottom of the freeze pipe, exactly at that point where it is most difficult to assess.

The test measurements performed have their own clear message in this respect (Fig.4). A further development of freeze pipe resulted from economic considerations. It is known that the maintenance time of a freeze zone has a decisive influence on the economics of nitrogen freezing. Technical and cost benefits are achieved when sinking shafts or driving large-cross section tunnels to drill and case longer sections, to provide fewer chambers and to keep the installation required for freezing out of the working area as much as possible. The consequence of this, however, is that the construction and maintenance times for the freeze zone increase.
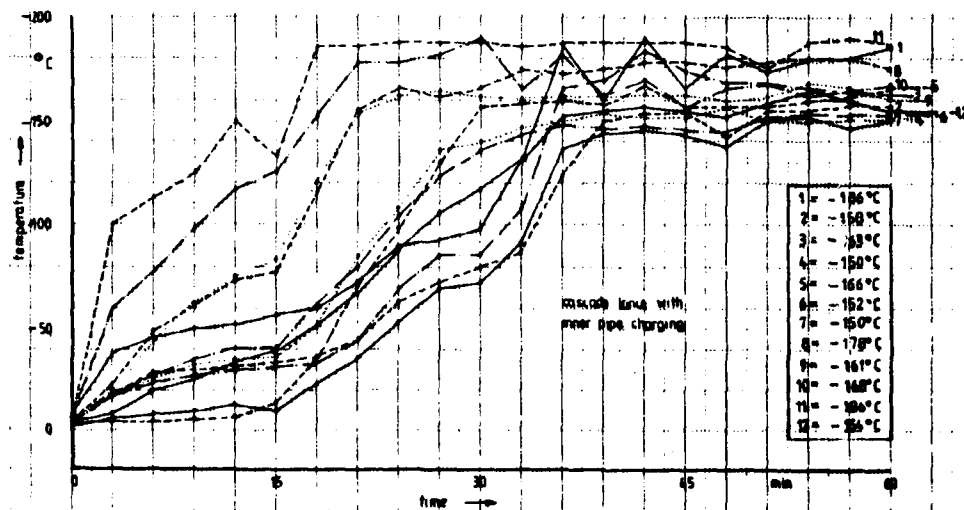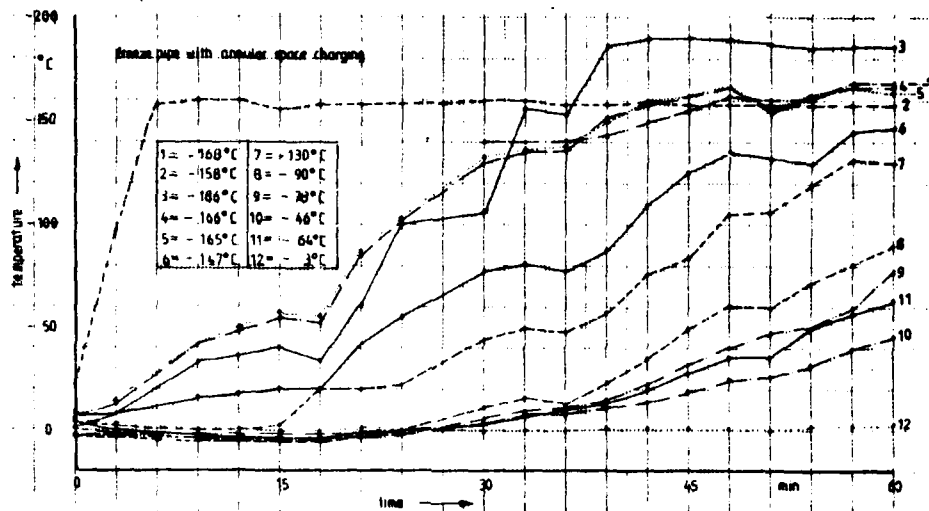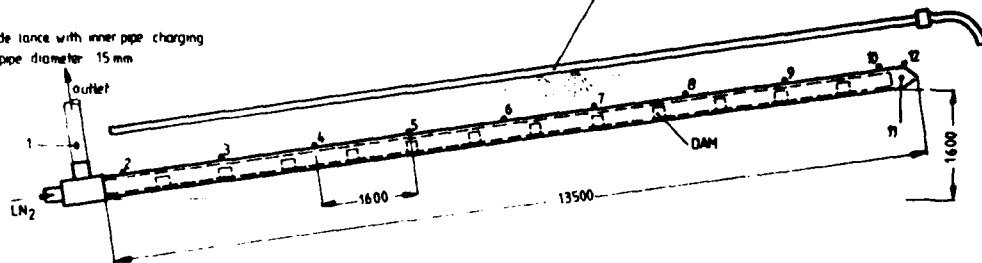
Figure 4
Temperature measurements at a cascade lance compared directly with measurements obtained with conventional annular space charging with a different inner pipe diameter. An obvious factor here is the more uniform cooling in the case of the cascade lance.

Figure 3

432

freeze pipe with annular space charging
inner pipe diameter 39 mm

LN₂

outlet

1600

13500

water sprinkling system

cascade lance with inner pipe charging
inner pipe diameter 15 mm

outlet

LN₂

1600

13500

1600

DAM

1600

freeze pipe with annular space charging

temperature

1 = -168°C	7 = +130°C
2 = -158°C	8 = -90°C
3 = -186°C	9 = -70°C
4 = -106°C	10 = -46°C
5 = -165°C	11 = -64°C
6 = -147°C	12 = -3°C

time   min

cascade lance with inner pipe charging

temperature

1 = -186°C
2 = -168°C
3 = -83°C
4 = -150°C
5 = -166°C
6 = -152°C
7 = -150°C
8 = -178°C
9 = -161°C
10 = -146°C
11 = -104°C
12 = -186°C

time   min

433

This is where the laboratory-tested moveable freeze pipe comes into play (Fig.5).
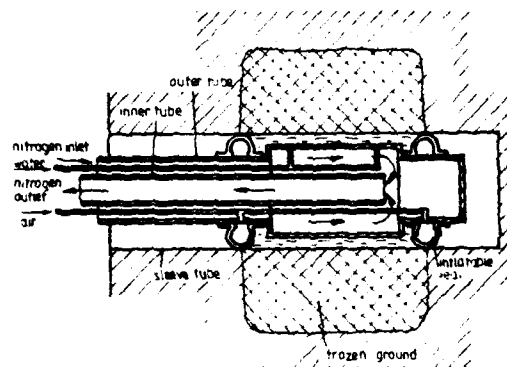

Figure 5

Moveable Freeze Pipe

To minimize maintenance times the moveable freeze pipe is positioned in line with the progress of driving.

The sleeve is formed by the drill pipes or an inserted outer pipe. A moveable freeze pipe is positioned in this sleeve at the point to be frozen. The moveable pipe is then re-positioned in the sleeve as required, in line with the progress of the work, and then charged with nitrogen.
Water or another fluid trapped in the gap-like annular chamber and frozen at the start of the operation provides a contact between the moveable pipe and the sleeve. Inflatable seals prevent the contact fluid from running out and the gap is thawed at the end of the freezing operation by using, for instance, hot water, enabling the moveable pipe to be re-positioned. Appropriate supply lines are placed in the respective sleeve.
At first glance the system appears to be rather involved. However, it is undoubtedly economic due to the savings in nitrogen consumption possible. It is obvious that the moveable pipes require to be carefully handled. A prerequisite for using this, as well as the following method, is that it is at all possible to freeze sections for geological reasons. Consequently, a method which enables groundwater levels to be dammed by sealing layers is of interest in shaft construction. In such cases it is worthwhile considering

freezing in stages in line with the progress of work and thus to save energy for maintaining the freeze zone. For instance, boreholes are made down to the final depth and freeze pipes inserted sealed off in line with the level of the sealing layers (Fig. 6).
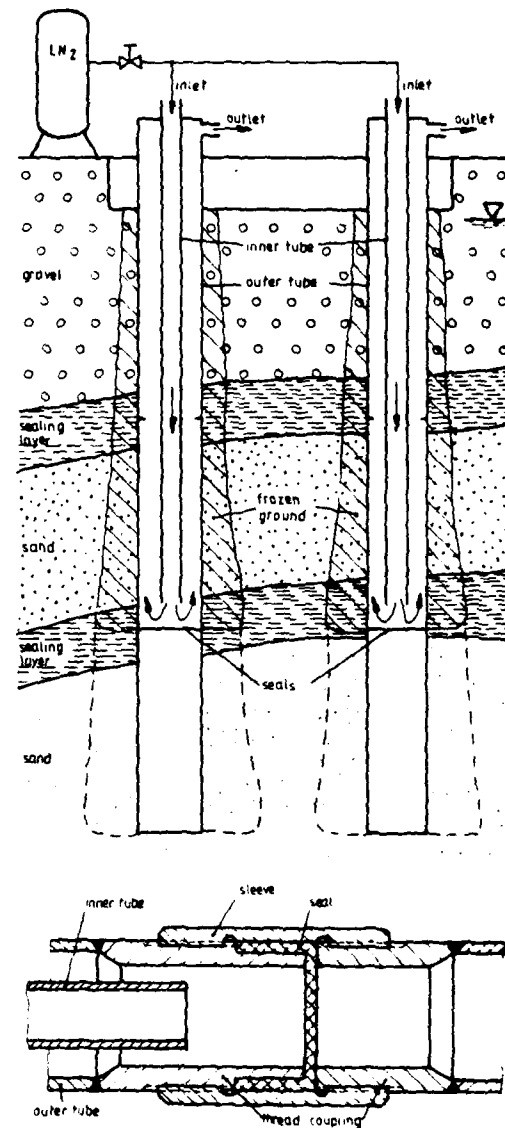

Figure 6

Freeze lance with seals as might be used in shaft construction for instance. Enables step-by-step freezing adapted to the progress of shaft sinking work.

Trials have been conducted with seals in the form of plastic caps which can easily be cut, punched or burnt through. This enables further sections to be opened and frozen in stages in advance of excavation. If this is followed by support work, it is recommended to aim for maximum economy by means of inner pipe insulation and reference temperature control.

In conclusion, brief reference is made to a novel tunnel driving method operating with the help of and protected by a freeze zone.

The problems associated with the handling and operational safety of shield driving and compessed air particularly in tunnel structures near the surface in unstable, water-bearing and greatly alternating soils are known. Searching for suitable alternatives gave rise to the idea of developing a device consisting essentially of a freeze pipe and an excavation device (Fig. 7).
Step-by-step freezing running ahead of excavation enables even lengthy sections to be economically frozen and thus sealed and secured. Since the advancing freeze zone ensures that the freeze pipe is always adequately embedded, it can, if

appropriately designed, act as a tie rod or abutment for the excavation tools. Advantageous working is possible if a starting and finishing shaft are used since freezing can be charged and controlled for instance from the finishing shaft while the starting shaft is being excavated unimpeded. If the drill pipe is designed appropriately it can be used as an outer freeze pipe. The drill pipe sections can be removed and re-used after being exposed. Use of several freeze pipes is conceivable for larger tunnel cross sections. Problems are only likely to be encountered in positioning the boreholes as accurately as possible.

It should be mentioned at this point that the tunnel driving system last mentioned is at present only in the planning stage and we are not yet talking about a laboratory- or field-tested method. The aim in presenting this method and in referring to the improved freeze pipes mentioned above is to provide new impulses for soil freezing with nitrogen and to illustrate recent developments.
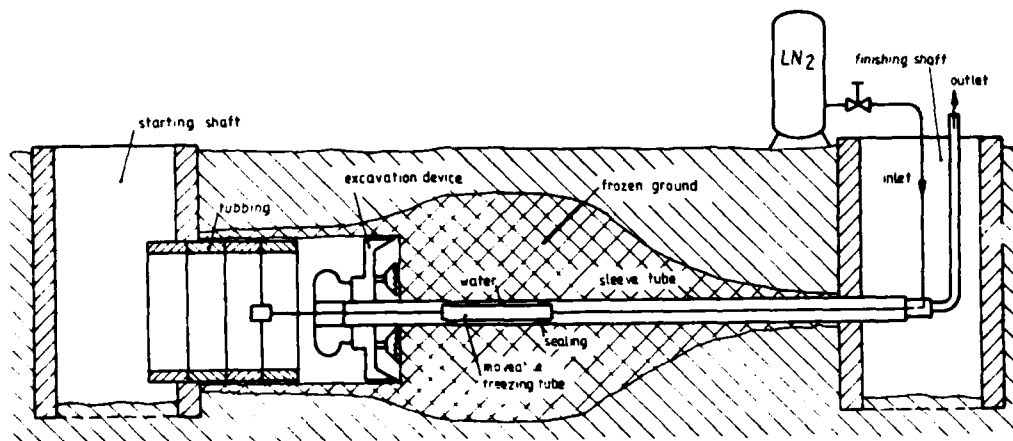

Figure 7

Novel tunnel freezing method in principle

Use of the moveable freeze pipe and drill pipe designed as sleeve and anchor for driving or excavation equipment.

STUDIES OF SOIL FREEZING AROUND A BURIED PIPELINE IN A CONTROLLED ENVIRONMENT

P.J. Williams   Geotechnical Science Laboratories,
M.W. Smith   Carleton University,
M.M. Burgess   Ottawa, Canada
J. Aguirre-Puente

ABSTRACT

Proposals for construction of refrigerated natural gas pipelines have earlier lead to concern about the danger of pipe disturbance due to frost heave and related stresses. There is an immediate need for scientific knowledge concerning the thermodynamic processes associated with soil freezing under the conditions associated with buried pipes. This paper describes a full-scale experiment in which the thermal regime, frost heave and related effects associated with a cooled pipe are being studied. The facility, in Caen, France, is 18x18 m and has previously been used for testing road sections in relation to frost action.

PIPELINE STABILIZATION PROJECT
AT ATIGUN PASS

H.P. Thomas, Sr. Project Engineer   Woodward-Clyde Consultants   Anchorage, AK, USA
E.R. Johnson, Mgr. Civil Engineering Alyeska Pipeline Service Co. Anchorage, AK, USA
J.M. Stanley, Sr. Civil Engineer   Alyeska Pipeline Service Co. Anchorage, AK, USA
J.A. Shuster, President   Geofreeze Corporation   Lorton, VA, USA
S.W. Pearson   Engineering Consultant   Little Rock, AR, USA

ABSTRACT

Atigun Pass is located in the Brooks Range, 268 km south of Prudhoe Bay, Alaska. At 1450 m above sea level, it is the highest point on the Trans-Alaska Oil Pipeline. In 1979, two years after start-up, Alyeska Pipeline Service Company discovered that a 120-m segment of insulated buried pipe on the south side of the Pass was experiencing settlement as a result of thawing of ice-rich permafrost. They found that the unanticipated thawing was caused by groundwater flow. During the summer of 1980, Alyeska undertook an intensive effort to control this groundwater and stabilize this section of the pipeline.

Primary elements of the project were surface drainage, grouting and ground freezing. Challenging aspects included: (1) the remote arctic location with its severe climate, short construction season and formidable logistics, and (2) pioneering application of grouting and ground freezing in a permafrost area. Purpose of the grouting was to reduce ground-water velocities sufficiently to enable subsequent refreezing of the thawed zone under the pipeline. The ground freezing was done using a 350-kW (100-ton) portable mechanical refrigeration plant which circulated chilled brine through 268 vertical freeze pipes. To maintain the frozen zone after mechanical freezing was complete, 143 free-standing heat pipes (identical to those used in the thermal VSM which support elevated sections of the pipeline) were installed.

Ground temperatures and pipe settlements in the area have been closely monitored through the 1981 season. Results of this monitoring indicate that the ground has remained frozen beneath the pipe and additional pipe settlements have been negligible.
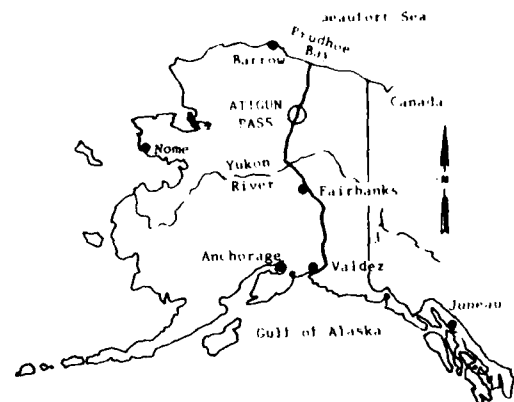
Figure 1. Route of the Trans-Alaska Pipeline

INTRODUCTION

The Trans-Alaska warm oil pipeline extends from Prudhoe Bay on the North Slope to Valdez on the south coast of Alaska (see Fig. 1). The line was generally elevated above the ground surface in areas of unstable permafrost. However, at Atigun Pass, because of avalanche hazards, two segments of the pipeline were buried in a special box of insulation designed to retard

439

heat flow from the pipeline to known thaw-unstable supporting materials. Design of this box was based on conductive heat flow.

In 1979, two years after startup of the pipeline, Alyeska Pipeline Service Company discovered that a 120-m segment of the insulated buried pipe on the south side of the Pass was experiencing settlement. An investigation was immediately undertaken to determine the cause of this settlement and plan for remedial measures to be taken. This paper describes essential features of a pioneering project to stabilize this section of the Trans-Alaska Pipeline.

SITE DESCRIPTION

Surface Conditions

Atigun Pass is located in the Alaskan Brooks Range, 268 km south of Prudhoe Bay. At 1450 m above sea level, it is the highest point on the Trans-Alaska Pipeline. Remote from distribution centers, the area is characterized by rugged terrain and severe climatic conditions. On the south side of the pass, the pipeline follows a steep narrow valley alongside a stream which drains two steeply-sloping cirque basins totalling about 115 ha. The valley sides are typically avalanche-prone talus slopes. The ground surface is typically rubbly and devoid of vegetation. Winters in the area are long, cold and dark, and summers are short and cool. Summer runoff results from snowmelt and rainfall. Breakup starts in early June and freeze-up occurs by mid-September. Freezing index ($^{\circ}$C) for the area is about 4000 degree-days.

Subsurface Conditions

Subsurface conditions at the site are summarized in Fig. 2. Two primary geologic strata are present: (1) a variable thickness of undifferentiated glacial, colluvial, and fluvial material, and (2) underlying bedrock. The unconsolidated deposits are a mixture of talus, avalanche debris, glacial deposits and stream-washed materials (varying proportions of boulders, cobbles, gravel, sand and silt). The bedrock is interbedded quartzite, conglomeratic quartzite and shale which is typically highly sheared. The depth to bedrock increases to the south. Prior to pipeline construction and startup in 1977, the subsurface was completely frozen and considerable visible ice was present in the colluvium, thereby rendering this material non-thaw-stable. For this reason, south of Sta. 8825, the buried pipe was encased in a special box of insulation designed to retard heat flow from the pipeline to the underlying
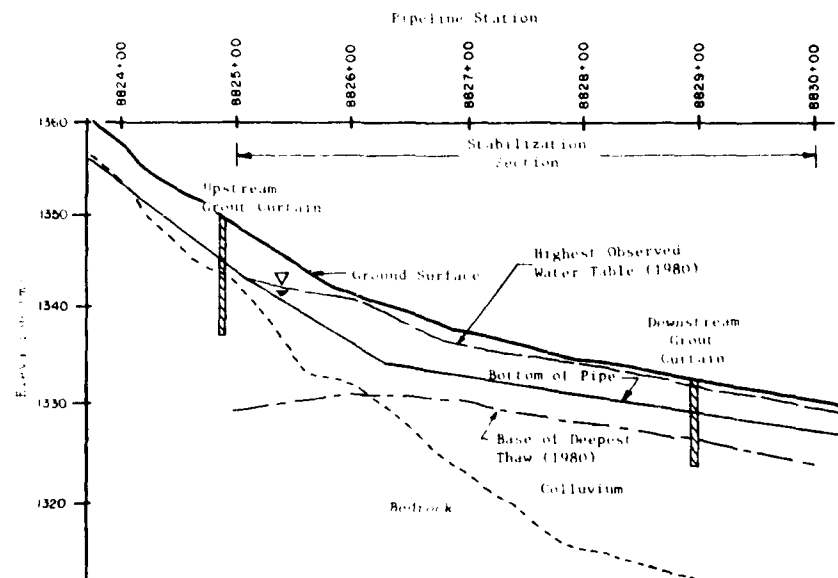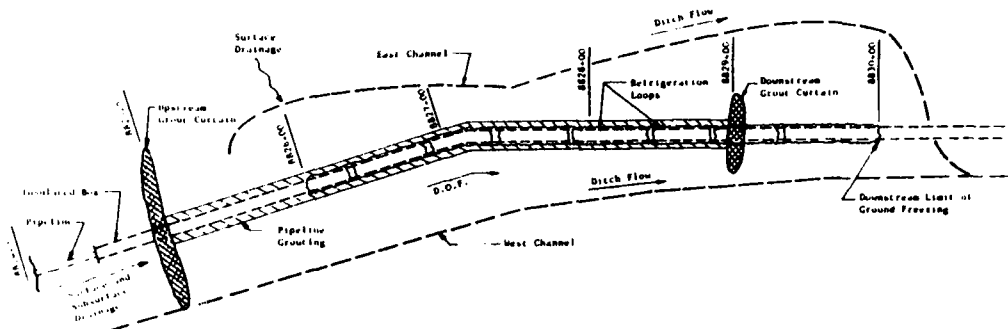

Figure 2. Geologic Section Along Pipeline

permafrost.

From the sloping water table evident in Fig. 2, it is apparent that there was groundwater flow through the site from north to south. This flow occurred in both the thawed colluvium and the thawed bedrock and was a powerful agent of thawing. Measurements made at the site during summer 1980 indicated localized groundwater flow velocities as high as 100 m/day.

Flowing Groundwater

Control of the flowing groundwater was one of the key elements of the stabilization project. Figure 3 shows the conceptual plan developed. As the major source of runoff and recharge was north of the stabilization area, it was planned to construct an impervious grout curtain at Sta. 8825 to bring flowing groundwater to the surface at

Figure 3. Conceptual Design of Stabilization

Figure 4. Permafrost Thaw and Pipe Settlement Comparison

STABILIZATION DESIGN

By 1980, pipe settlement in the area had reached 45 cm. It appeared that the cause of this settlement was thawing of the ice-rich colluvium and that this thawing had been accelerated by groundwater warmed up by flowing along the uninsulated buried pipe north of Sta. 8825. Objective of the the stabilization design was to halt further pipe settlement.

that point. From there, it would be channelized into a system of drainage ditches as shown. A second grout curtain was to be constructed at Sta. 8830.

Permafrost Thaw and Pipe Settlement

Instrumentation installed during Summer 1980 enabled close monitoring of thawing and pipe settlement. Where thermistor strings were placed close to pipe-settlement-monitoring rods, close correlations between thawing and pipe settlement such as that shown in Fig. 4 were observed.

Remedial Measures

To prevent further pipe settlement and create a frozen buffer zone against further thawing of unstable permafrost, it was planned to artificially freeze back the ground beneath the pipe through a series of vertical freeze pipes schematically depicted in Fig. 5. As thawing had reached bedrock north of Sta. 8826, the freezeback was planned to be done between Stations 8826 and 8830. The zone to be frozen was about 6 m wide and extended down permafrost (6 to 9 m deep).

For successful ground freezing, it was considered necessary to reduce groundwater flow velocities along

pipeline to below 2 m/day. To do this, it was planned to fill voids in the thawed colluvium by injecting bentonite-cement slurry grout along the pipeline. The downstream curtain was to help contain the slurry.
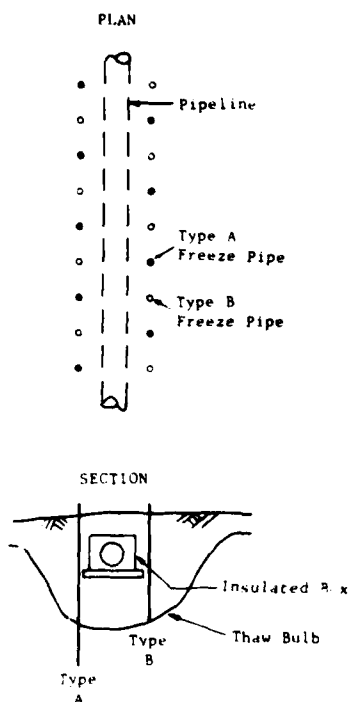
PLAN

SECTION

Figure 5.   Ground Freezing Plan

CONSTRUCTION

Grouting and Surface Drainage

Between mid-June and the end of September, 1980, some 450 m^3 of cement-silicate and 370 m^3 of cement-bentonite grout were injected into vertical boreholes along the pipeline between Stations 8825 and 8830. The cement-silicate grout was used for the grout curtains and the cement-bentonite grout was used between the curtains. Initial grouting was done at the location of the upstream grout curtain at Sta. 8825. It was soon discovered that the thaw bulb at that location was wider and deeper than had been anticipated. For this reason, the upstream curtain was abandoned after completing only one of the planned three rows of grout holes. Efforts were intensified to complete a groundwater cutoff at the location of the downstream curtain, Sta. 8829.

The thaw bulb was found to define the limits of grout penetration - as well as the groundwater aquifer. Effectiveness of the grouting was measured by pumping tests, dye tracer tests, and by observations made in groundwater monitoring wells. At the downstream curtain, a final water table differential of 3.4 m across the curtain was the best evidence of the curtain's effectiveness. Upstream of the curtain, groundwater flow velocities were reduced from about 40 down to about 6 m/day. During ground freezing, flow velocities were probably less that this because of lack of recharge in late summer.

Two flash floods which occurred in June 1980 emphasized the importance of proper drainage at the site. At the time of these storms, the existing natural drainage channels were inadequate to carry the surface runoff. Starting on September 8, 6000 m^3 of soil and rock were excavated from the west and east drainage channels. A flow crossover was provided at Sta. 8830 by two 1.2-m-diam corrugated metal pipe culverts.

Active Ground Freezing

During September and October 1980, 1.4x10^5 kWh of heat were extracted from the ground by a large portable refrigeration plant which circulated chilled brine through 268 vertical freeze pipes.
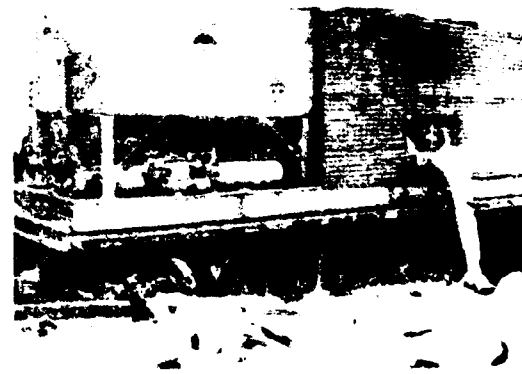

Figure 6.   100-ton Mobile Refrigeration Plant

Equipment. The refrigeration plant used was a large portable unit specially developed for ground freezing (see Fig. 6). As shown in Fig. 7, the plant had two different cooling loops with a rated capacity of 350 kW. The first stage was the ammonia stage which

442

chilled the brine. Heat was removed from the ammonia by water circulation and air fans. The second stage used circulated chilled calcium chloride brine to cool the ground. Heat absorption by the plant was obtained by monitoring supply and return temperatures for the plant and each freeze pipe group. In addition, brine flow rates were measured directly by flow tests at the brine tank and indirectly through pump curves for the brine pump.

The ground freezing section extended from Sta. 8826 to 8830 and included 268 vertical refrigeration holes providing a total of 2200 m of refrigeration pipe below ground. The system was divided into 24 groups and was set up
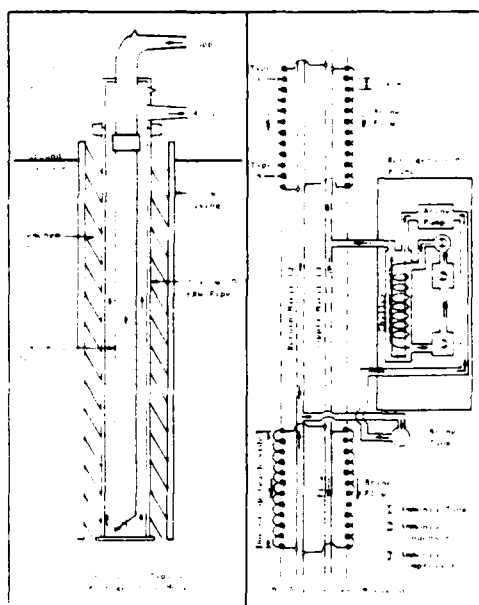

Figure 7. Active Ground Freezing System

in a series-parallel circuit. Figure 7 also shows a typical refrigeration hole and control head. The refrigeration pipes were spaced at 1 m centers on both sides of the pipeline offset approximately 1.6 m from pipe centerline. The refrigeration holes alternated between Types A and B. Type A holes were designed both for mechanical refrigeration and to receive a heat pipe (described later) after ground freezing was complete by penetrating the frozen ground about 3 m. The shallower Type B holes were used for mechanical refrigeration only. South of Sta. 8827, the A and B holes were nominally 9 m and 6 m deep, respectively.

North of Sta. 8827 where the thaw was deeper, both types of holes were nominally 12 m deep. Many of the refrigeration holes were also used for grout injection during the grouting program.

Figure 8 shows a view of the ground freezing setup and Fig. 9 shows an overall site view.

Figure 8. View of Ground Freezing Setup

Figure 9. Site View

Operation. The production ground freezing began on September 4. The sequence of freeze pipe group activation is presented in Fig. 10. Activation started at the downstream end and proceeded northward. Average chiller output temperatures were -22 to -29°C. Shutdown criteria were (1) a maximum ground temperature of -7°C between refrigeration pipes, and (2) frozen ground 1.5 m from the line of refrigeration pipes. These criteria were checked at five thermistor string cluster locations. Freezeback times are shown in Table 1. Shutdown criteria were met at all of the clusters prior to shutdown. At the end of refrigeration, the plant had operated 38 days and was estimated to have extracted approximately 1.4×10^5 kWh of heat from the ground. Shortest

TABLE 1

FREEZEBACK TIME FOR ACTIVE GROUND FREEZING

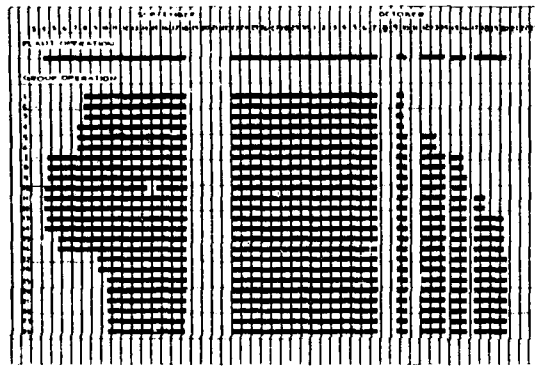| Nominal Pipeline Station	Closest Refrigeration Pipe Groups	Total Length of Refrigeration Pipes (m)	Days of Operation Required To Satisfy Shutdown Criteria	Thaw Bulb Depth at Start of Freezing (m)	Freezing Rate (m/day)
8826+00	23	114			
	24	97	31	8 – 10	.27 – .30
8826+50	21	105			
	22	96	19	3 – 4	.18 – .21
8827+50	15	91			
	16	91	25	6 – 7	.27
8828+50	9	91			
	10	91	24	6 – 7	.27 – .30
8829+50	3	91			
	4	91	15 – 16	5 – 6	.37 – .43
	5	91			
	6	92			

Figure 10. Refrigeration Plant and Group Operation

freezing time required was south of the downstream grout curtain where the thaw bulb was narrow and groundwater flow was minimal. The longest freezing time was at the north end where the thaw bulb was most extensive. The total cumulative heat extraction was about twice the amount calculated to cool and freeze an idealized volume of soil around the pipe that is 6 m wide, 7.5 m deep and 120 m long. This suggests that as much as half of the heat extracted came from flowing groundwater.

The freezing went well in spite of the adverse site conditions. Air temperatures as low as $-16°C$ did cause certain operational problems with the plant including freezing of cooling water supply hoses and freezing of the cooling tower. Air locking in the uphill (northern) refrigeration pipe groups was also a problem; it appears that this could have been avoided by

setting the brine supply tank at a higher elevation. Also, the refrigeration capacity of the system was limited by the capacity of the generator which was used.
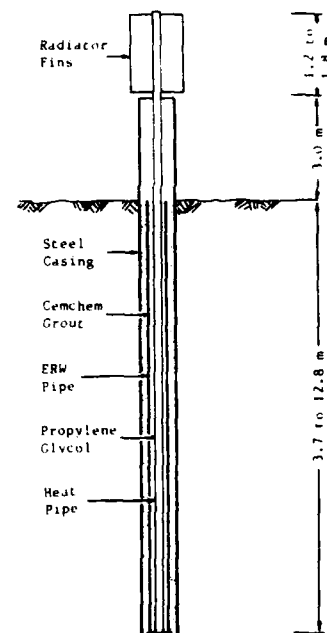

Figure 11. Typical Free-Standing Heat Pipe

Passive Ground Freezing

To maintain the frozen zone, free-standing heat pipes (see Fig. 11) were installed in all the Type A refrigeration holes. Closed steel tubes

444

containing anhydrous ammonia and topped
by a radiator, these were the same heat
pipes used by Alyeska in the thermal
vertical support members (VSM's) which
support the elevated pipeline.

Rated heat extraction capacity of
the Alyeska heat pipe is 60 W/m of
embedment. A total of 143 heat pipes
having a total embedded length of 1323
m were installed at the site by October
30, 1980. The heat pipes project 3 m
above the ground surface to prevent the
radiators from becoming buried by local
drifting snow. Figure 12 shows a view
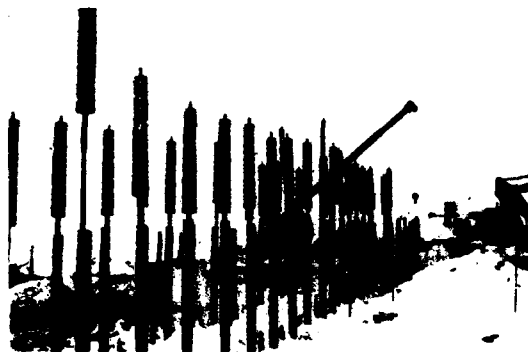of the completed installation.

Figure 12. Completed Installation of
Heat Pipes

PERFORMANCE

Ground Temperatures

The thermal performance of the
remedial methods used to stabilize the
pipe was inferred from thaw depths
determined through analyses of local
soil temperature measurements. The
potential consequences of additional
pipe settlement dictated that the
subsurface thermal regime be well de-
fined. Consequently, 65 thermistor
strings were installed in the repair
area during 1980 and eleven additional
strings were added for more detailed
information in 1981. Ground tempera-
tures were monitored on a weekly basis
during the summer months and on a
monthly basis during the remainder of
the year.

The ground temperature data
indicated that the active refrigeration
was effective in establishing a zone of
frozen soil beneath and alongside the
insulated box. This frozen zone ex-
tended vertically from the ground sur-
face to the original permafrost and lat-

erally approximately 6 m to either side
of pipe centerline.

The free-standing heat pipes
installed at the conclusion of active
refrigeration subsequently functioned
throughout the winter to provide
additional freezing capacity thereby
enlarging the lateral extent of the fro-
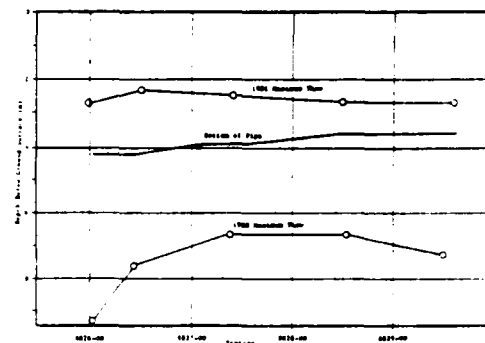zen soil mass.

Figure 13. Thaw Depths Observed at
Thermistor Cluster Locations

Soil temperatures observed during
the summer of 1981 showed ground
thermal performance exceeding expecta-
tions (see Fig. 13). The maximum depth
of thaw in 1981 was only 2.5 to 3 m
compared with 7 to 9 m in 1980. The
base of the thawed zone remained well
above the bottom of the pipe and mostly
remained at or above the top of the
insulated box. There was no evidence of
thaw beneath the pipe nor was there
evidence of water flow within or
the box as was the case before the
repair activities began. Since the heat
pipes began functioning as air tempera-
tures dropped during September 1981,
the soil above the pipe was essentially
refrozen to ground surface again the
end of September.

Pipe Movement

Settlement monitoring rods
installed on the pipeline in the
stabilization area starting in 1979. By
Summer 1981, 16 rods had been installed
at a maximum 15 m spacing. During
summer months, rod elevations were
checked by a weekly level survey.

Figure 14 shows some typical data
for one of the rods. During 1980 (prior
to the ground freezing), all rods
showed a similar trend following the
groundwater flow cycle: initial
settlement in June, continuation

445

through July and August, and leveling
off in September. Pipe settlements
observed in 1980 ranged up to 13 cm and
rates approached 8 cm/mo. As can be
seen in the figure, pipe settlements
during 1981 were negligible. This
provides persuasive evidence that the
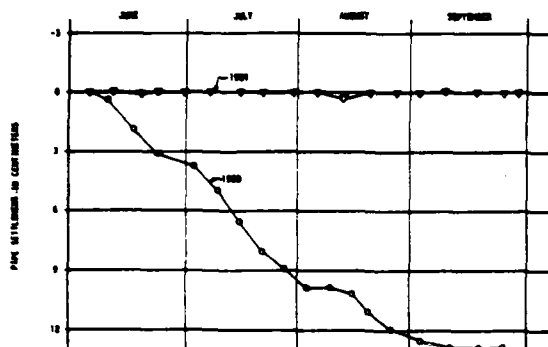1980 pipe stabilization efforts were
successful.

Figure 14. Pipe Settlement vs. Time at
Sta. 8828

ACKNOWLEDGEMENTS

ARTIFICIAL FREEZING OF SOILS IN
A BASE OF HEAD-FRAMES

Vyalov,S.S.,Dr.Sc.,Prof.,Research Institute of Bases and
    Underground Structures,Moscow,USSR.
Sadovsky,A.V.,Cand.Sc.,Research Institute of Bases and
    Underground Structures,Moscow,USSR.
Meliksetov,S.S.,Cand.Sc.,DonGiproOrgshaktStroy,Donetsk,USSR.

Building of head-frames and sinking of mine shafts in coal mines in unstable and water-saturated soils has been realised in many cases by artificial freezing. Usually all construction works and mining operations are carried out in the following succession: freezing of soils,erection of temporary head-frame,sinking of shaft, installation of casing.Then soil isthawed,temporary head-frame is dismounted and permanent head-frames erected.

DonGiproOrgShaktStroy and NIIOSP (Research Institutes) have developed a construction method where soil freezing and erection of permanent head-frame are done in parallel.Such order of operations cuts down the cost and time of construction due to the fact that temporary head-frame becomes unnecessary.

Soil tests conducted by NIIOSP in the shaft base at the Donetsk coal-field made it possible to put into the practice the abovenoted construction method.

Soils conditions at the site were presented up to the depth of 25m. by loams and clays;then down to 65m. silty saturated sands laid, capable to collapse.This situation necessitated to sink shaft using freezing technique (Fig.I). Tests showed that clayey soils of the upper layer were frost susceptible soils.Therefore to control deformation of bases induced by frost heaving of clay soils,it was recommended to carry out partial freezing,i.e. at the depth lower than 25m.,with the upper layer being not frozen.

With this the said upper layer played a role of a distributing slab,thus reducing head-frame base deformation caused by heaving of frozen sands and the settlement due to their thawing.Moreover,to eliminate the effects of head-frame tilt a possibility was provided of shifting hoist-machine 200mm. from the central axis.

Soil freezing operations started in the mine shaft base on June,20, 1977.Temperature regime control of soil-ice-casing started on October, 25,1978,i.e. three weeks after the period of active freezing,and continued till November,23,1979,when the thawing of ice-soil-casing was completed.Copper-constantan thermo-couples were used to measure temperature.Thermometers were placed at five depths:-25m.,-35m., -40m.,-50m. and -55m. At each depth 12 thermometers were positioned along two orthogonal directions spaced at 1.5m.,2.5m.,3.5m. from the shaft wall.To install the thermometers in the walls and in the soil-ice-casing horizontal holes were bored,where boring casings with thermometers were placed. As there was some risk to damage freezing columns when holes were bored the length of said holes and,consequently,the zone,where
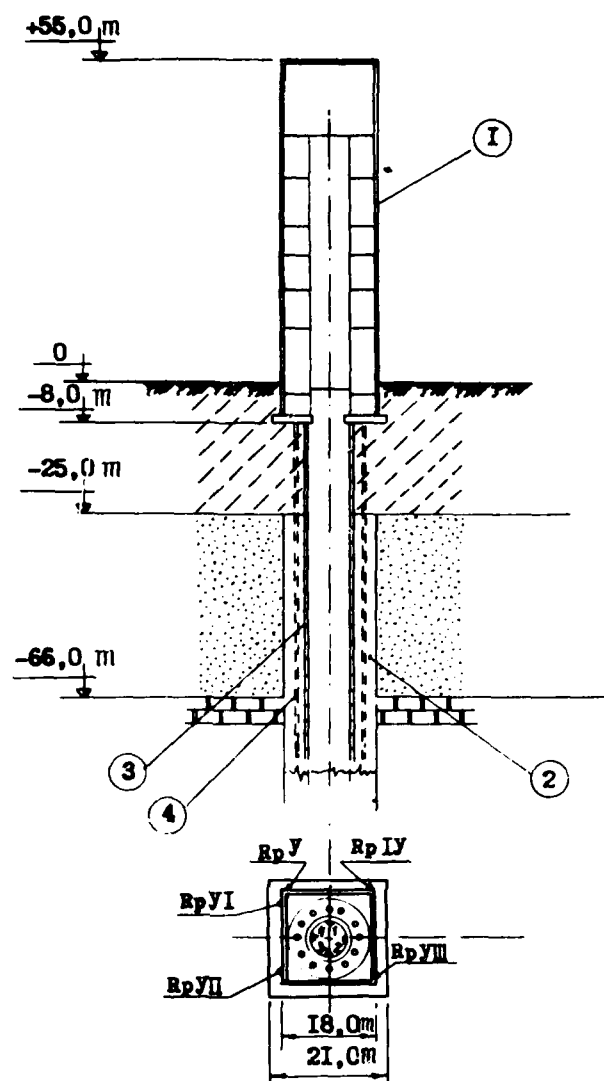
447

Fig.I. Diagram of the head-frame base: I-head-frame; 2-soil-ice-casing; 3-shaft lining; 4- freezing column.

temperature was measured,was limited by a depth of 3.5m. from the shaft wall.With this,the point removest from the wall,where temperature of soil was measured was located at 0.5m. from freezing column axis.

Below measured temperatures around the shaft at the most important moments are given.Such moments were: October 24,1978 (end of active freezing); May 25,1979(thawing of the soil-ice-casing began as it was registered by thermometers) August,18,1979 (the moment of practically complete thawing of frozen soil).

Temperature epures show (Fig.2-4) the nonuniformity of temperature distribution with the depth of soil-ice-casing and in plan.It is characteristic that temperature dropped down with the changing of depth,and the lowest temperatures were observed at the depth of 55m. Such distribution of temperature is quite naturally;it is explained by convective heat exchange between rock soil and the air circulating in the shaft.It is more difficult to explain nonuniformity of temperature distribution in horizontal plane.The temperature difference was here 3-4°C.
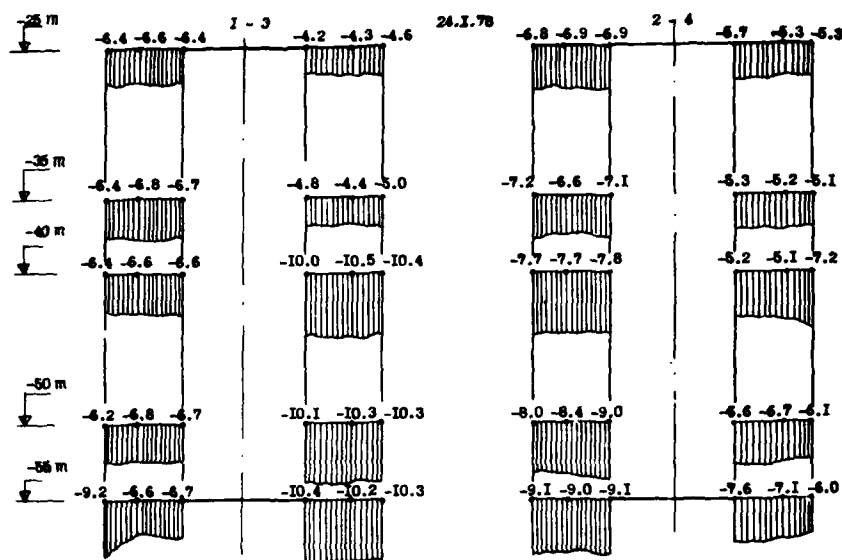
448

Fig.2. Measured temperatures around the shaft at the end of active freezing (October,24,1978).
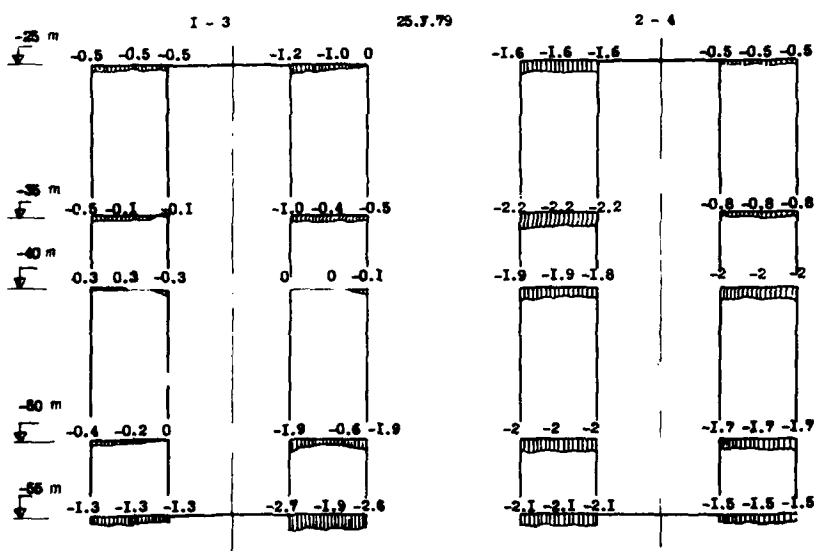
Fig.3. Measured temperatures at the beginning of thawing (May,25,1979).

Such nonuniformity of temperature is the most dangerous at the moments of it transfer through zero point, because it can be the reason of nonuniform settlement and head frame tilt.

In spite of the revealed nonuniformity of temperature distribu-tion the considerable nonuniformity of settlement has not been observed; and this fact can be explained firstly by weak heaving of sands and their comparatively not high deformation while thawing, and secondly by the distributing function of the upper 25 me-

449

ter layer of the nonfrozen clay so-il. Observations of head-frame deformations in the shaft were controlled by means of levelling special marks installed on the outside of the head-frame wall.

The results of observations, given in Fig.5, made it possible to represent how the head-frame deformations proceeded in the process of soil freezing in it base and the following thawing.
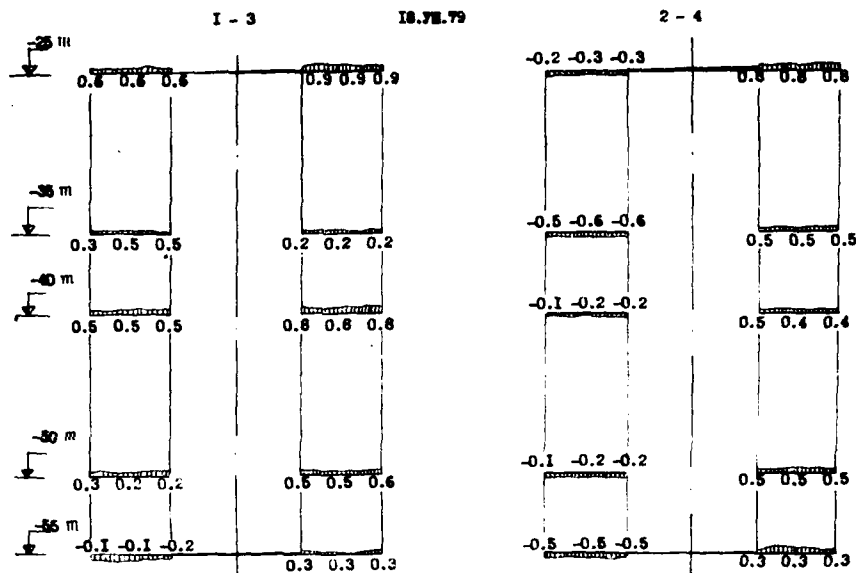

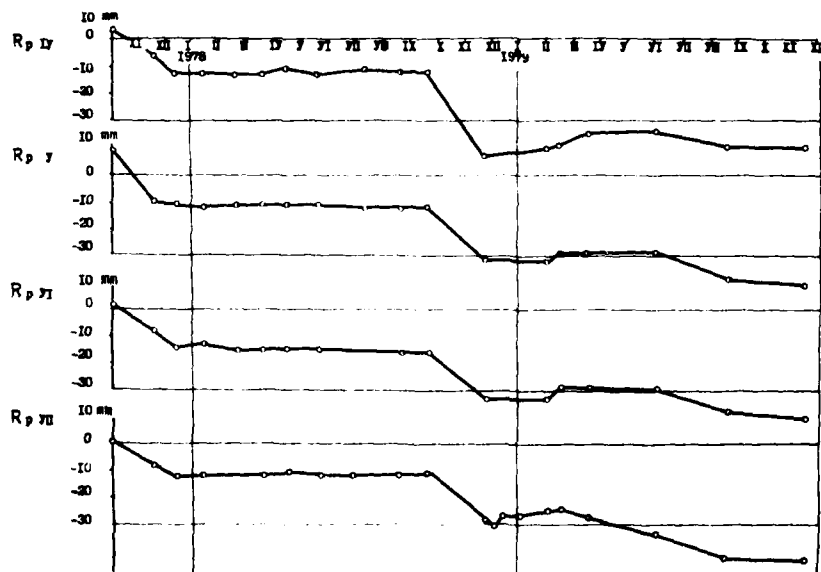Fig.4. Measured temperatures at the end of thawing (August,18, 1979).

Fig.5. Vertical deformations of the head-frame.

To our opinion it is possible to pick out some characteristic phases of head-frame deformation:
- lifting(microlifting)
- primary settlement
- stable position
- settlement due to thawing
- stable position.

Each of the abovenoted phases is conditioned by the processes which take place in the soil around the shaft with their freezing and thawing,and by the effect of head-frame weight,acting as a load on the soils of base.

Microlifting of head-frame can be explained by heaving of sands during their freezing.Lifting was negligible and has the maximum value - 10 mm.(from the observations of one of the points). Lifting of head-frame then was equilibrated by primary settlement induced by the consolidation of clay soils under the action of the weight of the head-frame being erected.In the average this settlement was 12-15 mm.(from the observations of all points).Then the phase of head-frame stable position came with the soil-ice-casing formed completely.After active freezing of soils their gradual thawing began due to the heat coming through the shaft and from the surrounding rock massif.During this phase the maximum settlement was observed.For instance, the relative part of settlement due to thawing was 32 mm.(from the observations of the point RIY) but the total maximum settlement was 44 mm. Then the attenuation of deformations was observed and head-frame took its stable position. Here some discrepancy should be noted that appeared from the comparison of temperature and deformation data of head-frame.So,from the data of leveling the maximum settlement of head-frame took place from the middle of September up to December,1978; and temperature data showed the frozen state of soil in a base of head-frame. The following conditions can be the reason of such discrepancy. The thickness of soil-ice-casing wall according to preliminary calculations was about 7 m. As it was noted above,in order to avoid the possible damage of freezing columns,the holes with the ter-

mometers installed,were deepened to the depth of 3.5m. into the soils,adjacent the shaft walls.So, the temperature of soil-ice-casing was controlled only on the inside, from the axis of freezing columns to the shaft wall.

Taking into account the water content of sands it can be supposed that after the period of active freezing (I.09.78) thawing of soil-ice-casing began on the outside, whereas the inside was cooled by winter air.And this fact entailed the settlements during the period from the middle of September till December,1978.

Non-uniform deformations of base were the most dangerous for the stability of head-frame.The preliminary calculations showed that the tilt of head-frame foundation due to the settlement of base while it thawing can be 0.003. And 0.005 was taken as the design value accounting unforeseen factors. The control of head-frame deformations showed that the **actual** tilts,caused by non-uniform settlement of base,were much less than the design ones.The maximum tilt-0.0007 was stated during the period of the maximum settlement with the height of head-frame 40m.Such tilt could give rise to deviation of 3sm. from the vertical upper point of head-frame. However with the further thawing the gradual diminishing of tilt up to 0.00033 took place.

So,the srttlement of head-frame due to soil-ice-casing thawing was practically uniform. Analysis of control data of soils in a base and head-frame stability permitted to make conclusion that it is suitable and techically possible to use the proposed construction technology,incorporating the parallel operations of artificial freezing of soils and mine shaft sinking and erection of permanent head-frame at the same time. The use of partial freezing made it possible to avoid the considerable deformations of structure due to frost heaving and the subsequent settlement of clay soils in the upper layers of base. Cryogen and postcryogen deformations of irrigated sands did not appear to be a hazard to the stability of head-frame shaft.

451

The data received indicate the possibility of promotion the proposed construction technology in other coal mines,disposed in the identical geological conditions.

KUPARUK RIVER MODULE BRIDGE FOUNDATION STABILIZATION: CASE HISTORY

A. Christopherson   Peratrovich and Nottingham, Inc., U.S.A.

ABSTRACT

The Kuparuk River Bridge on the North Slope of Alaska is designed for 2300-ton oil field modules which may be the heaviest design loads ever for a bridge structure. It is also unique in another way--the entire bridge is founded on permafrost. Within four months of bridge completion, several modules of varying weights were transported, the largest being 1700 tons. To adequately support these large loads and provide long-term foundation pier stability, a ground freezing program was undertaken to refreeze natural and construction thaw zones below the seasonal river active layer and to decrease the temperature of existing frozen ground within the influence of the freezing front.

This paper describes the design methods and construction procedures used, the monitored ground temperatures during and after construction, and the foundation performance during module moves. By establishing a thermistor string monitoring program, the freezing effects considered in the initial thermal design were determined. Instrumentation performance and problems are reviewed, and results of passive refrigeration (heat pipe) operation designed to maintain frozen soil is evaluated.

THE EFFECT OF FREEZE-THAW CYCLES
ON THE STRUCTURE AND THE STABILITY
OF SOIL SLOPES

L. E. Vallejo, Assistant Professor, Department of Civil Engineering,
Michigan State University, East Lansing, MI 48824.

ABSTRACT

Saturated soils such as cohesive glacial tills, lake and marine clays when subjected to low freezing rates develop a particulate structure, that is stiff lumps of soil surrounded by a reticulate ice network. If these soils form part of a slope, upon thawing a mixture of soil lumps and water slide down it. A recently introduced method of stability analysis, the particulate approach, which takes into consideration the granular structure of thawing slopes involves four soil parameters in its analysis. They are: 1) the soil lumps volume concentration ratio, C, 2) the angle of internal friction between the lumps, ϕ', 3) the bulk unit weight of the lumps, γ_s, and 4) the unit weight of the fluid medium, γ_w. From field and and laboratory studies designed to determine the effect of freeze-thaw cycles on the structure of cohesive soils, it was found that the first two parameters decreased progressively in value with the number of freeze-thaw cycles. The third remained relatively constant, as did the fourth. In view of the particulate approach of stability analysis, a decrease in value of the first two parameters will represent a decrease in the stability of thawing slopes. Therefore, freeze-thaw cycles will make the stability of thawing slopes a time-dependent process.

INTRODUCTION

It has been reported by Mackay (1974), McRoberts and Nixon (1975), Van Vliet and Langohr (1981), Brown et al (1981), and Vallejo and Edil (1981) that when saturated fine-grained glacial tills, lake and marine clays are subjected to low rates of freezing they develop a reticulate ice structure characterized by soil blocks of different sizes and shapes surrounded by a continuous ice network (Fig. 1). The ice

■ ice   □ soil
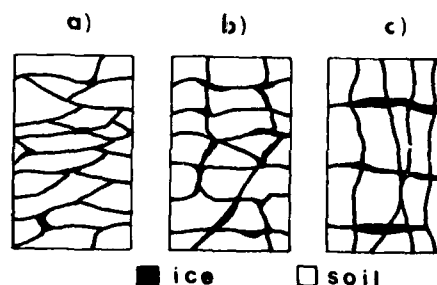
Fig. 1   Schematic Representation of Soil-Ice Structure at Shallow Depths in Silty and Glacial Clays Under Slow Freezing Rates: a) foliated or platy, b) lenticular or platy, c) angular blocky (after Van Vliet and Langohr, 1981).

veins forming the reticulate ice structure have thicknesses of up to 5 mm (Brown et al, 1981) and are normally alligned parallel and vertical to the ground surface. The vertical veins usually form when ice fills shrinkage

cracks in the soil (Williams, 1967; Anderson et al, 1978). The reticulate ice grows using the water contained in the soil blocks it surrounds causing their consolidation in the process (Mackay, 1974). This consolidation by ice compression makes the soil blocks very stiff. The presence of these stiff soil blocks in the active layer of permafrost areas has been reported by McRoberts and Morgenstern (1973).

Upon thawing, soils with a reticulate ice structure will become a mixture of stiff blocks of soil and water. If this mixture forms part of a natural slope, and if a critical depth of thaw is reached in the slope, the blocks of soil and water will slide (Vallejo, 1980; Vallejo and Edil, 1981). After failure, the water resulting from ice melting will mix with part of the original soil blocks, and the moving mass will be converted into a matrix of liquid-like soil slurry (mud) in which dispersed blocks of soil are present. Therefore, when making a stability analysis of thawing slopes, two different stability analyses need to be made. The first one involves the stability of the slope at the moment of thawing. During this stage, the slope at shallow depths is formed by a predominantly solid phase (stiff soil blocks) within which a minor fluid phase (water) is located (Fig. 2). The second one involves the

Fig. 3 Geometry of a Solifluction or Mud Flow (after Vallejo, 1981)

The theory for the stability analysis of thawing slopes during their two failure stages has been developed by Vallejo (1980, 1981).

Stability Analysis During Thawing

At the moment of thawing a previously frozen slope with a reticulate ice structure can be represented by Fig. 2. The stability of this system of soil blocks plus water has been analyzed by Vallejo (1980) as follows.

The stress, τ, produced by gravity on the mixture of soil lumps and water on the plane of failure can be represented as

$$\tau = \gamma_{mix} \, d \, \sin \beta$$

$$= [\gamma_f \, (1 - C) + C \, \gamma_s] \, d \, \sin \beta$$

$$= [\gamma_f + (\gamma_s - \gamma_f) \, C \,] \, d \, \sin \beta \qquad [1]$$

where d is the thickness of the sliding mass, C is the ratio of the volume occupied by the soil blocks and the volume of the whole mass, γ_s is the bulk unit weight of the soil blocks, γ_f is the unit weight of the fluid medium (equal to that of water at
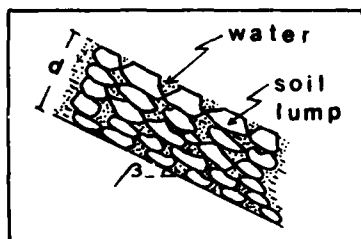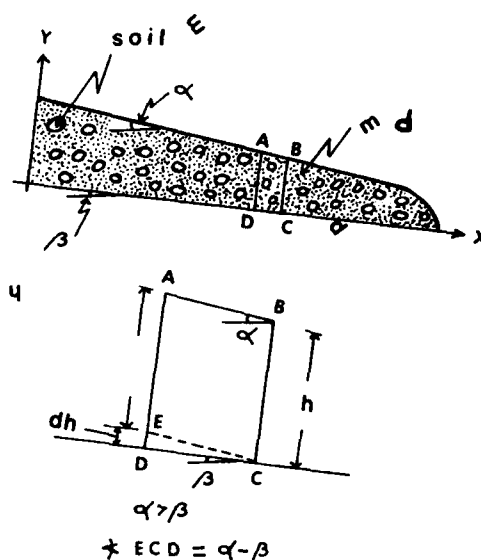

Fig. 2 Particulate Structure During Thawing (after Vallejo, 1980).

stability of the failed soil mass. During this stage, the moving mass is formed by a predominantly semi-fluid phase (mud) and a minor dispersed solid phase (small blocks of soil). The failed mass, according to McRoberts and Morgenstern (1974, see their Fig. 3) and Chandler et al (1976, see their Fig. 13), forms solifluction lobes or tongues, the free surfaces of which have larger inclinations than the bed

on which they move, as shown by Fig. 3 .

456

the moment of thawing), and β is the inclination of the plane of failure.

The shear resistance, s , to failure is given by the following expression

$$s = (\gamma_s - \gamma_f) \, C \, d \, \cos \beta \, \tan \phi' \qquad [2]$$

where ϕ' is the effective angle of internal friction between the soil blocks.

At limit equilibrium conditions, by combining Eqs. [1] and [2], the critical slope inclination at which movement will just take place can be obtained from

$$\tan \beta = \tan \phi' \, [\frac{(\gamma_s - \gamma_f) \, C}{\gamma_f + (\gamma_s - \gamma_f) \, C}]$$

[3]

Equation [3] takes into consideration the particulate structure of the sliding soil mass and explains well instabilities on low-angled thawing slopes (see Table 2 of Vallejo, 1980) independently of excess pore water pressures on the plane of failure. Methods of stability analysis presented by Chandler (1970) and McRoberts and Morgenstern (1974) assume the failing soil mass of Fig. 2 as rigid-homogeneous-continuous and need excess pore water pressures to explain instabilities on low-angled thawing slopes.

Stability Analysis of Solifluction Lobes

After failure of the thawing slopes occurs, the resulting moving mass forms mud-lobes or mud-tongues in which stiff blocks of soil are dispersed and barely float (McRoberts and Morgenstern, 1974). The free surface of the lobes have greater inclination than the bed on which they move (McRoberts and Morgenstern, 1974; Chandler, et al, 1976). The stability of the mud-lobes which usually move at low velocities (2 mm/day to 4 m/day) has been conducted by Vallejo (1981) using Fig. 3. According to Vallejo (1981), when considering the forces on section ABCD of the mud-lobe, and at limit equilibrium conditions, the following equation applies

$$\gamma_{mix} \, h \, \tan \, (\alpha - \beta) + \gamma_{mix} \, h \, \sin \beta = c_u$$

[4]

where, h is the average thickness of the lobe, α is the inclination of the lobe's free surface, c_u is the undrained shear strength of the mud, and the rest of the terms as defined before.

If the bed of the mud-lobe has a low inclination ($\beta \approx 0$), Eq. [4] becomes

$$\gamma_{mix} \, h \, \tan \, \alpha = c_u \qquad [5]$$

An analysis of Eq. [5] shows that the stress causing the movement of solifluction or mud-lobes on beds of very low inclinations is a function of their free surface inclination, the average mud-lobe's thickness, and the mud's unit weight.

THE EFFECT OF FREEZE-THAW CYCLES ON THE STRUCTURE AND THE STABILITY OF SOIL SLOPES

An analysis of Eq. [3] shows that the critical slope inclination, β , at which failure will be initiated in a frozen slope that upon thawing develops a granular or particulate structure depends upon the values obtained during thawing by the soil parameters such as the effective angle of internal friction between the soil blocks, ϕ', the soil blocks volume concentration ratio, C , and the bulk unit weight of the soil blocks, γ_s . The unit weight of the fluid medium, γ_f , at the moment of thawing can be considered constant and equal to that of water, γ_w .

It is shown next, using the field and laboratory investigations conducted by Krumbach (1960) and Wood (1976) on the effect of freeze-thaw cycles on the structure of cohesive soils, that the value of the parameters ϕ', C and γ_s change with the number of freeze-thaw cycles. These changes will make the stability of thawing slopes a time-dependent process.

To facilitate the study of how much effect the number of freeze-thaw cycles has on the value of ϕ', C and γ_s forming part of Eq. [3], the ratio between brackets in Eq. [3] is replaced by

$$m = [\frac{(\gamma_s - \gamma_f) \, C}{\gamma_f + (\gamma_s - \gamma_f) \, C}] \qquad [6]$$

Also, the following two relationships, easily obtained from Eqs. [1] and [6] will be used

$$C = \frac{\gamma_{mix} - \gamma_f}{\gamma_s - \gamma_f} \qquad [7]$$

and

$$m = \frac{\gamma_{mix} - \gamma_f}{\gamma_{mix}} \qquad [8]$$

Krumbach's Field Studies

Krumbach (1960) conducted field studies to determine the changes in bulk density that occurred when saturated fine grained glacial tills were progressively subjected to decreasing freezing temperatures. The glacial soils formed part of locations on Kent and Clinton Counties in the State of Michigan. Krumbach made field measurements up to a depth of 38 cm of the changes that took place in soil bulk unit weight before during and after one freezing period. He found that as the freezing temperatures decreased with time, the bulk unit weight of the frozen soils (γ_{mix}) also continuosly decreased with time. Using the soil data obtained by Krumbach (1960), the values for the parameters m and C given by Eqs. [6], [8] and [7] were calculated for the dates before, during and after a complete freezing period was in effect in the field. This was done in order to have an understanding of what was the effect of one freezing perion on the structure of the soil. The results are shown in Table 1.

Table 1. Values of Parameters m and C Before and After One Freezing Period for Soils from Clinton County, Michigan (data from Krumbach, 1960)

Date and Depth	Temp. °C	γ_{mix} kN/m³	γ_f kN/m³	γ_s* kN/m³	m**	C***
Depth: 4 cm						
10 Nov. – 1959 (Day before freezing period started)	9	17.05	9.8	17.05	0.43	1
8 March – 1960	-10	8.53****	–	–	–	–
29 March–1960 (End of freezing period– First day of thawing)	11	12.05	9.8	17.05	0.19	0.31
30 March – 1960	12	–	–	–	–	–
31 March – 1960	2.5	15.09	9.8	17.05	0.35	0.73
Depth: 18 cm						
10 Nov. – 1959	9	18.13	9.8	18.13	0.46	1
15 March – 1960	-7.5	9.03****	–	–	–	–
29 March – 1960	11	11.37	9.8	18.13	0.14	0.19
30 March – 1960	12	–	–	–	–	–
31 March – 1960	2.5	15.48	9.8	18.13	0.37	0.68

* γ_s was assumed to remain the same as γ_{mix} before freezing started.

** Calculated using Eq. [8] and $\gamma_f = \gamma_w = 9.8$ kN/m³

*** Calculated using Eq. [7]

**** Lowest γ_{mix} recorded during freezing period. The low value of γ_{mix} was due to voids or pores present in the frozen soil.

An analysis of the results of Table 1 shows that the values of m and C at the end of the freezing period are smaller than those calculated before the freezing period started. Therefore, it can be concluded by means of the above results and Eq. [3] , that if the soil of Clinton County, Michigan formed part of a natural slope, the critical inclination that this slope can sustain without failing during thawing conditions, will be smaller than the one it can sustain before the freezing perion started. Therefore, one freezing period caused the structure of frozen glacial soils to change detrimentally with respect to their stability.

Laboratory Studies Conducted by Wood

Wood (1976) conducted laboratory studies designed to determine the effect that the number of freeeze-thaw cycles had on the structure of Leda Clay from the St. Lawrence Valley in upper New York State. The Leda Clay used by Wood in his freeze-thaw experiments was found to contain fissures and joints that divided the clay into small three dimensional intact blocks. When saturated samples of this type of clay were subjected to freezing temperatures, ice formed

first in the fissures and joints. As the time of freezing increased the ice in the fissures grew using the water trapped in the pores of the intact blocks. During this process of ice growth the blocks become consolidated and stiff.

Wood also found that as the number of freeze-thaw cycles increased the original intact blocks of Leda Clay decreased progressively in size, the reason being that as the ice grew during the freezing periods, the resulting compressive forces not only consolidated the clay blocks but broke them into smaller pieces.

Using the mercury porosimetry technique, Wood (1976) measured the changes in internal porosity experienced by the individual intact blocks of Leda Clay during 16 cycles of freezing and thawing. Table 2 shows his porosity measurement results as well as changes in the bulk unit weight, γ_s , of the intact blocks of clay and values for the parameter m . In Table 2 two porosities are given for the same total volume of intact blocks of clay plus ice filling the fissures and joints. One is the porosity, n_s , related to the pore space in the individual intact blocks of clay; the other one, n_i , is the porosity related to the fissures and

Table 2. Changes in Soil Parameters as a Function of the Number of Freeze-Thaw Cycles (data from Wood, 1976)

n_s ***	n_i ***	γ_s kN/m^3	C *	m **	Number of Freeze-Thaw Cyles
0.546	$\simeq$ 0	–	1	–	0
0.513	0.033	17.91	0.967	0.444	1
0.505	0.041	18.07	0.959	0.447	2
0.498	0.048	18.16	0.952	0.448	4
0.475	0.071	18.55	0.929	0.453	8
0.460	0.086	18.85	0.914	0.457	16

* C calculated using Eq. [9] $C = 1 - n_i$

** Calculated using Eq. [6] with $\gamma_f = \gamma_w = 9.8$ kN/m^3

*** In Table 2 , n_s , is the porosity related to the pore space of the intact blocks of clay. n_i is the porosity related to the fissures and joints space.

joints space which are filled by ice that surrounds the intact blocks of clay. Also, using n_i it can easily demonstrated that

$$C = 1 - n_i \qquad [9]$$

where C is the volume concentration ratio of intact blocks of clay.

An analysis of the results of Table 2 shows that as the number of freeze-thaw cycles increases, the volume concentration ratio of the intact blocks of clay, C , decreases. The bulk unit weight of the clay blocks slightly increased and the parameter, m , stayed relatively the same. Next it will be shown that the angle of internal friction between the blocks of clay, ϕ' , is directly related to the soil block's concentration ratio, C .

Relationship Between ϕ' and C

It is well known from laboratory triaxial compression tests on granular materials conducted by Bishop and Eldin (1953), Bjerrum et al (1961), and Kirkpatrick (1965) that the effective angle of internal friction, ϕ' , of these materials is directly related to the porosity, n , of the granular samples during testing (Fig. 4). Since the grain volume concentration ratio, C , is related to the porosity (C is equal to one minus the porosity), ϕ' can also be related to C. This has been done in Fig. 4 obtained from Bjerrum et al (1961) which shows the dependance of ϕ' and n for the case of sands sheared in triaxial compression. An analysis of this Figure shows that the smaller is the value of C, the smaller is the value of ϕ'.

Since it has already been demonstrated (see Tables 1 and 2) that the effect of the processes of freezing and thawing and their repetitiveness when applied to cohesive soils that develop a granular structure during freezing (Fig. 1) is to produce a decrease in their block concentration ratio, C , it is also expected, therefore, that their angle of internal friction, ϕ' , will also decrease. If these soils with a granular structure form part of a natural slope, it can be concluded that the cummulative effect of freeze-thaw cycles on the active layer of the slope will be to decrease its stability. This later implication can be easily deduced
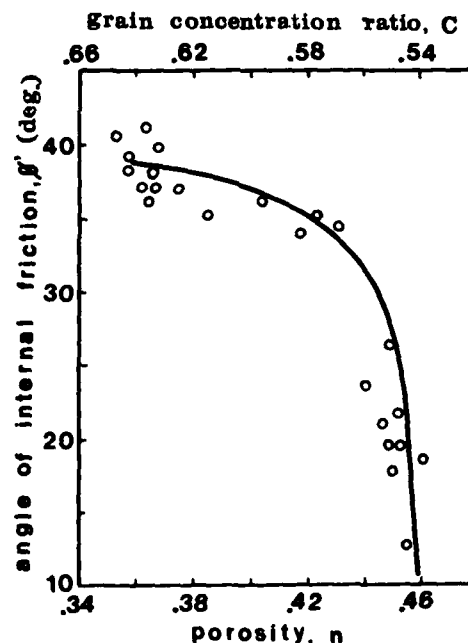

Fig. 4 Relationships Between ϕ' , n and C for Sands Sheared in Triaxial Compression (after Bjerrum et al, 1961)

from an analysis of Equation [3].

CONCLUSIONS

On the basis of the study presented, the following observations can be made.

Saturated cohesive soils that develop a particulate structure when frozen (soil lumps surrounded by ice), tend to decrease in volume concentration of soil lumps as the number of freeze-thaw cycles increase. This decrease in soil lump concentration brings a decrease, during thawing, of the angle of internal friction between the lumps. If these type of soils form part of a slope, freezing and thawing will eventually cause the failure of the thawing slope, resulting from the accumulative detrimental effect of freeze-thaw on the frictional shearing resistance of the slope forming materials.

460

REFERENCES

Anderson, D. M., R. Pusch, and E. Penner (1978). Physical and thermal properties of frozen ground. In: Geotechnical engineering for cold regions. Edited by O. B. Andersland and D. M. Anderson. McGraw-Hill Book Co., New York, pp. 37-102.

Bishop, A. W., and A. K. G. Eldin (1953). The effect of stress history on the relation between φ and porosity in sand. Proceedings of the Third Int. Conf. on Soil Mechanics and Found. Eng., Zurich, Switzerland, Vol. 1, pp. 100-105.

Bjerrum, L., S. Kringstad, and O. Kummeneje (1961). The shear strength of fine sand. Proceedings of the Fifth Int. Conf. on Soil Mechanics and Found. Eng., Paris, France, Vol. 1, pp. 29-37.

Brown, R. J. E., G. H. Johnston, J. R. Mackay, N. R. Morgenstern, and W. W. Shilts (1981). Permafrost distribution and terrain characteristics. In: Permafrost engineering design and construction, Edited by G. H. Johnston. John Wiley and Sons, New York, Chapter 2, pp. 31-72.

Chandler, R. J. (1970). Solifluction on low-angled slopes in Northamptonshire. Quarterly Journal of Eng. Geology, Vol. 3, pp. 65-69.

Chandler, R. J., G. A. Kellaway, A. W. Skempton, and R. J. Wyatt (1976). Valley slope sections in Jurassic strata near Bath, Somerset. Proceedings of the Royal Society of London, Series A, Vol. 283, pp. 527-556.

Kirkpatrick, W. M. (1965). Effects of grain size and grading on the shearing behaviour of granular materials. Proceedings of the Sixth Int. Conf. on Soil Mechanics and Found. Eng., Montreal, Canada, Vol. 1, pp. 273-277.

Krumbach, A. W. (1960). The effect of freezing and thawing on soil moisture, bulk density, and shear strength under open and forest conditions. Ph.D. Thesis, Michigan State Univ., East Lansing, Michigan, 185 p.

Mackay, J. R. (1974). Reticulate ice veins in permafrost, northern Canada. Canadian Geotechnical Journal, Vol. 11, pp. 230-237.

McRoberts, E. C., and N. R. Morgenstern (1973). A study of landslides in the vicinity of the Mackenzie River, Mile 205 to 660. Environmental Social Committee, Northern Pipelines Task Force on Northern Oil Development, Report No. 73-75, 96 p.

McRoberts, E. C., and N. R. Morgenstern (1974). The stability of thawing slopes. Canadian Geotechnical Journal, Vol. 11, pp. 447-469.

McRoberts, E. C., and J. F. Nixon (1975). Reticulate ice veins in permafrost, northern Canada: Discussion. Canadian Geotechnical Journal, Vol. 12, pp. 159-166.

Vallejo, L. E. (1980). A new approach to the stability analysis of thawing slopes. Canadian Geotechnical Journal, Vol. 17, pp. 607-612.

Vallejo, L. E. (1981). Stability analysis of mudflows on natural slopes. Proceedings of the Tenth Int. Conf. on Soil Mechanics and Foundation Eng., Stockholm, Sweden, Vol, 3, pp. 541-544.

Vallejo, L. E., and T. B. Edil (1981). Stability of thawing slopes: field and theoretical investigations. Proceedings of the Tenth Int. Conf. on Soil Mechanics and Foundation Eng., Stockholm, Sweden, Vol. 3, pp. 545-548

Van Vliet, B., and V. R. Langohr (1981). Correlation between fragipans and permafrost with special reference to silty Weichselian deposits in Belgium and northern France. Catena, Vol. 8, pp. 137-154.

Williams, P. J. (1967). The nature of freezing soil and its behaviour. Norwegian Geotechnical Institute, Publication No. 72, pp. 91-119.

Wood, J. (1976). Influence of repetitious freeze-thaw on structure and shear strength of Leda Clay. Ph.D. Thesis, Clarkson College of Technology, Potsdam, New York, 181 p.